



Space engineering

Structural materials handbook - Part 2: Design calculation methods and general design aspects

NOTE:

This pdf-file does not contain automatic cross-references. To make use of the cross-references please use the MS Word version of this document.

Foreword

This Handbook is one document of the series of ECSS Documents intended to be used as supporting material for ECSS Standards in space projects and applications. ECSS is a cooperative effort of the European Space Agency, national space agencies and European industry associations for the purpose of developing and maintaining common standards.

This handbook has been prepared by the ECSS-E-HB-32-30 Working Group, reviewed by the ECSS Executive Secretariat and approved by the ECSS Technical Authority.

Disclaimer

ECSS does not provide any warranty whatsoever, whether expressed, implied, or statutory, including, but not limited to, any warranty of merchantability or fitness for a particular purpose or any warranty that the contents of the item are error-free. In no respect shall ECSS incur any liability for any damages, including, but not limited to, direct, indirect, special, or consequential damages arising out of, resulting from, or in any way connected to the use of this document, whether or not based upon warranty, business agreement, tort, or otherwise; whether or not injury was sustained by persons or property or otherwise; and whether or not loss was sustained from, or arose out of, the results of, the item, or any services that may be provided by ECSS.

Published by: ESA Requirements and Standards Division
ESTEC, P.O. Box 299,
2200 AG Noordwijk
The Netherlands

Copyright: 2011 © by the European Space Agency for the members of ECSS

Change log

ECSS-E-HB-32-20 Part 2A 20 March 2011	First issue
--	-------------

Table of contents

Change log	3
Introduction	27
10 Stress-strain relationships	28
10.1 Introduction.....	28
10.2 Elastic property prediction for UD ply from constituent properties.....	28
10.3 Analytical notation for elastic constant methods.....	30
10.4 Calculation methods for elastic constants of UD ply.....	30
10.5 Longitudinal modulus.....	32
10.6 Longitudinal Poisson's ratio	34
10.7 Transverse modulus	35
10.7.1 General.....	35
10.7.2 Jones method.....	35
10.7.3 Förster/Knappe method.....	35
10.7.4 Schneider method	36
10.7.5 Puck method.....	36
10.7.6 Tsai method.....	36
10.7.7 HSB method	37
10.7.8 Graphs.....	37
10.8 Transverse Poisson's ratio	40
10.9 Transverse shear modulus	40
10.9.1 General.....	40
10.9.2 Jones method.....	40
10.9.3 Förster/Knappe method.....	40
10.9.4 Schneider method	40
10.9.5 Puck method.....	41
10.9.6 Tsai method.....	41
10.9.7 HSB method	41
10.9.8 Graphs.....	42
10.10 In-plane stress calculation methods	44

10.11	Analytical notation for in-plane methods.....	44
10.12	Stress-strain relations for unidirectional plies	46
10.12.1	Fibre-oriented co-ordinate system.....	46
10.13	On axis stress strain relations.....	46
10.13.1	General.....	46
10.13.2	Compliance matrix.....	47
10.13.3	Modulus matrix	47
10.13.4	Symmetry of compliance and modulus matrices	47
10.14	Stress-strain relations for a ply of arbitrary orientation	47
10.14.1	General.....	47
10.14.2	Off axis stiffness of a unidirectional ply	49
10.15	Stiffness matrix for a laminate	50
10.15.1	General laminates	50
10.15.2	Symmetric laminates	52
10.15.3	Flow chart.....	53
10.16	Calculation methods with interlaminar stresses and strains	54
10.16.1	Calculation with free-edge stresses.....	54
10.17	Qualitative evaluation of interlaminar strength for design purposes.....	56
10.17.1	General.....	56
10.17.2	Variation of fibre direction within a $[\pm\phi^\circ, 0^\circ, \pm\phi^\circ]$ laminate	58
10.17.3	Variation of the thickness of the 0° layer within the $[\pm 30^\circ, 0n^\circ, \pm 30^\circ]$ laminate.....	58
10.17.4	Variation of the sequence of layers	59
10.18	References	59
10.18.1	General.....	59
11	Strength prediction and failure criteria.....	61
11.1	Introduction.....	61
11.1.1	Micro-mechanical strength models.....	61
11.1.2	Lamina failure models	61
11.1.3	Failure criteria studies	62
11.1.4	Summary of World Wide Failure Exercise (WWFE)	63
11.2	Tensile strength of UD composites in fibre direction	65
11.2.1	General.....	65
11.2.2	Weakest-link failure model	65
11.2.3	Cumulative weakening failure model.....	65
11.2.4	Fibre break propagation model.....	67
11.2.5	Cumulative group mode failure model.....	67

11.2.6	Status of models.....	67
11.3	Compressive strength of UD composites in fibre direction.....	67
11.3.1	General.....	67
11.3.2	Extension mode buckling.....	68
11.3.3	Shear mode buckling.....	68
11.3.4	Analysis of compression failure.....	69
11.4	Transverse tensile strength of UD composites.....	71
11.4.1	General.....	71
11.4.2	Prediction of transverse tensile strength.....	72
11.4.3	Empirical analysis.....	72
11.5	Static strength criteria for composites.....	73
11.6	Analytical notation for static strength criteria for composites.....	73
11.6.1	Co-ordinate system.....	73
11.6.2	Formulae.....	74
11.7	Different types of failure criteria.....	75
11.7.1	General.....	75
11.7.2	Evaluation studies.....	76
11.8	Overview - Failure criteria.....	76
11.8.1	Introduction.....	76
11.8.2	Independent conditions.....	77
11.8.3	Interactive conditions – Pure interpolative conditions.....	78
11.8.4	Interactive conditions - Physical considerations.....	80
11.9	Comparison between test data and various failure criteria.....	88
11.9.1	Effects on failure mode.....	88
11.10	Description of failure modes.....	92
11.10.1	Laminates.....	92
11.10.2	Failure.....	92
11.11	Fatigue strength of composites.....	97
11.11.1	Background.....	97
11.11.2	Analytical notation.....	98
11.11.3	Approximation of fatigue life.....	98
11.12	References.....	100
11.12.1	General.....	100
12	Calculation of thermal stress and displacement.....	104
12.1	Introduction.....	104
12.1.1	General.....	104
12.1.2	Longitudinal CTE.....	104

12.1.3	Transverse CTE	104
12.2	Analytical notation for thermal stress calculations	105
12.3	Calculation of CTE from constituents	106
12.3.1	CTE in fibre direction	106
12.3.2	CTE perpendicular to fibre direction	106
12.4	CTE for a laminate	107
12.5	Thermal stresses within laminate layers	109
12.5.1	General	109
12.5.2	Residual curing stresses	109
12.6	Stress strain temperature relation	110
12.6.1	General	110
12.6.2	Mechanical strains	110
12.6.3	Incremental strain theory	110
12.7	Microstress analysis	112
12.7.1	General	112
12.7.2	Microstresses on fibre axis	112
12.7.3	Microstresses normal to fibre axis	112
12.8	References	112
12.8.1	General	112
13	Moisture effects on composite properties	114
13.1	Introduction	114
13.1.1	General	114
13.1.2	Moisture penetration	114
13.1.3	Moisture effects	114
13.2	Analytical notation for moisture effects	115
13.3	Typical effects of moisture	116
13.3.1	General	116
13.3.2	Sample data: Effects of moisture	116
13.4	Approximate method for calculation of strength and modulus retention of [0°/90°] laminates	121
13.4.1	General	121
13.4.2	Modulus retention	121
13.4.3	Strength retention	123
13.5	Moisture content	124
13.5.1	Fick's law	124
13.5.2	Determination of moisture content	125
13.5.3	Maximum moisture content	126

13.5.4	Experimental determination of the diffusion coefficient	127
13.6	Calculation of swelling coefficient from constituents.....	129
13.6.1	General.....	129
13.6.2	Swelling coefficient β_1 in fibre direction	129
13.6.3	Swelling coefficient β_2 transverse to fibres	129
13.6.4	Swelling coefficient for a laminate	130
13.7	Coefficient of moisture expansion (CME)	132
13.7.1	Resin behaviour.....	132
13.7.2	Composite behaviour.....	134
13.8	References	134
13.8.1	General.....	134
14	Stress concentrations and fracture	136
14.1	Introduction.....	136
14.1.1	General.....	136
14.1.2	Fracture mechanics models	136
14.2	Analytical notation for stress concentrations	137
14.3	Summary of fracture models.....	137
14.4	Evaluation of fracture models	138
14.5	WEK fracture model.....	139
14.5.1	General.....	139
14.5.2	Circular holes.....	139
14.5.3	Straight crack.....	142
14.6	WN fracture model.....	145
14.6.1	General.....	145
14.6.2	Failure criteria.....	145
14.6.3	Characteristics of WN fracture model.....	147
14.6.4	Circular holes.....	148
14.6.5	Straight cracks.....	152
14.6.6	Point stress criteria.....	153
14.6.7	Average stress criterion.....	154
14.7	Finite plate models.....	158
14.8	Finite width correction (FWC)	158
14.8.1	General.....	158
14.8.2	Circular holes.....	160
14.8.3	Centre crack	161
14.9	Calculated stress concentration factor at circular holes	161
14.9.1	NASA results	161

14.9.2	Finite width correction (FWC)	163
14.9.3	MBB/ERNO study.....	163
14.10	Stress distribution around circular holes.....	168
14.10.1	General.....	168
14.10.2	Stress concentration due to tensile load.....	168
14.10.3	Stress concentration due to shear load.....	169
14.11	Interlaminar fracture mechanics	171
14.11.1	Nomenclature	171
14.11.2	Delamination and fracture mechanics overview	171
14.11.3	Standard test methods (static and fatigue).....	175
14.11.4	Calculation of strain energy release rate in structural analysis	179
14.12	References	185
14.12.1	General.....	185
15	Prediction of dynamic characteristics	189
15.1	Introduction.....	189
15.2	Definition of damping terms.....	189
15.2.1	General terms.....	189
15.2.2	Complex modulus model.....	191
15.3	Prediction methods for damping.....	192
15.4	Determination of damping characteristics.....	193
15.4.1	Unidirectional characteristics.....	193
15.4.2	Off axis characteristics	193
15.4.3	Laminate characteristics.....	194
15.5	Approximate data on damping.....	194
15.6	References	195
15.6.1	General.....	195
16	Computer analysis of composites	196
16.1	Introduction.....	196
16.2	Computer programs: Analysis of composites	196
16.2.1	General.....	196
16.2.2	Finite element programs.....	198
16.2.3	Laminate analysis programs.....	199
16.2.4	Special applications programs.....	201
16.3	ESDU data for composite analysis	203
16.3.1	General.....	203
16.3.2	ESDU data items.....	203
16.3.3	ESDUpac.....	205

16.4	Buckling of orthotropic plates.....	205
16.4.1	Title.....	205
16.4.2	Usage and scope.....	205
16.4.3	Analysis	205
16.4.4	ESDUpac A7303	205
16.4.5	Notes	206
16.5	Flexural stiffness of flat strips	206
16.5.1	Title.....	206
16.5.2	Usage and scope.....	206
16.5.3	Analysis	206
16.6	Metallic skin stiffeners reinforced by composite - local buckling.....	207
16.6.1	Title.....	207
16.6.2	Usage and scope.....	207
16.6.3	Analysis and data	207
16.7	Laminate stress analysis	208
16.7.1	Title.....	208
16.7.2	Usage and scope.....	208
16.7.3	Analysis	208
16.8	Plate stiffnesses (In-plane)	209
16.8.1	Title.....	209
16.8.2	Usage and scope.....	209
16.8.3	Analysis and methods	209
16.9	Bonded joints - 1.....	210
16.9.1	Title.....	210
16.9.2	Usage and scope.....	210
16.9.3	Analysis and data	210
16.10	Bonded joints - 2.....	211
16.10.1	Title.....	211
16.10.2	Usage and scope.....	211
16.10.3	Analysis and data	211
16.10.4	ESDUpac A7916	212
16.11	Bonded joints - 3.....	212
16.11.1	Title.....	212
16.11.2	Usage and scope.....	212
16.11.3	Analysis and data	213
16.12	Buckling of rectangular specially orthotropic plates.....	213
16.12.1	Title.....	213

16.12.2	Usage and scope.....	213
16.12.3	Analysis and data	213
16.13	Bonded joints - 4.....	214
16.13.1	Title.....	214
16.13.2	Usage and scope.....	214
16.13.3	Analysis and data	214
16.13.4	ESDUpac A8039	215
16.14	Bonded joints - 5.....	215
16.14.1	Title.....	215
16.14.2	Usage and scope.....	215
16.14.3	Information and guidance	215
16.15	Buckling of orthotropic plates.....	216
16.15.1	Title.....	216
16.15.2	Usage and scope.....	216
16.15.3	Analysis and data	216
16.15.4	ESDUpac A8147	216
16.16	Lay-up arrangements for special orthotropy	217
16.16.1	Title.....	217
16.16.2	Usage and scope.....	217
16.16.3	Analysis and data	217
16.17	Failure modes of laminated composites	218
16.17.1	Title.....	218
16.17.2	Usage and scope.....	218
16.17.3	Analysis and failure modes.....	218
16.18	Failure criteria for layers of a laminated composite	219
16.18.1	Title.....	219
16.18.2	Usage and scope.....	219
16.18.3	Analysis and data	219
16.19	Plate stiffnesses and apparent elastic properties	219
16.19.1	Title.....	219
16.19.2	Usage and scope.....	219
16.19.3	Analysis for stiffnesses and elastic properties.....	220
16.19.4	ESDUpac A8335	220
16.20	Natural frequencies of laminated flat plates.....	220
16.20.1	Title.....	220
16.20.2	Usage and scope.....	221
16.20.3	Calculation of natural frequencies	221

16.20.4	ESDUpac A8336	221
16.21	Strain in skin panels under acoustic loading.....	222
16.21.1	Title.....	222
16.21.2	Usage and scope.....	222
16.21.3	Calculation of surface strains	222
16.21.4	ESDUpac A8408	222
16.22	Failure analysis.....	223
16.22.1	Title.....	223
16.22.2	Usage and scope.....	223
16.22.3	Analysis	223
16.22.4	ESDUpac A8418	224
16.23	Endurance under acoustic loading	225
16.23.1	Title.....	225
16.23.2	Usage and scope.....	225
16.24	Stress and strain around circular holes	226
16.24.1	Title.....	226
16.24.2	Usage and scope.....	226
16.24.3	Analysis	226
16.24.4	ESDUpac A8501	226
16.25	Damping in composite plates.....	227
16.25.1	Title.....	227
16.25.2	Usage and scope.....	227
16.25.3	Calculation of damping.....	227
16.25.4	ESDUpac 8512.....	228
16.26	Sandwich panel natural frequencies.....	228
16.26.1	Title.....	228
16.26.2	Usage and scope.....	228
16.26.3	Calculation of natural frequencies	229
16.26.4	ESDUpac A8537	229
16.27	Selection of reinforcement around circular holes.....	229
16.28	Buckling of unbalanced composite plates.....	230
16.28.1	Title.....	230
16.28.2	Usage and scope.....	230
16.28.3	Analysis and data	231
16.28.4	ESDUpac A8620	231
16.29	Sandwich panel response to acoustic loading.....	231
16.29.1	Title.....	231

16.29.2	Usage and scope.....	232
16.29.3	Calculation of natural frequencies and surface strains.....	232
16.29.4	ESDUpac A8624	232
16.30	Sandwich column and beam face plate wrinkling.....	233
16.30.1	Title.....	233
16.30.2	Usage and scope.....	233
16.30.3	Analysis	233
16.30.4	ESDUpac A8713	234
16.31	Buckling of curved composite panels	234
16.31.1	Title.....	234
16.31.2	Usage and scope.....	234
16.31.3	Analysis and data	234
16.31.4	ESDUpac A8725	235
16.32	Sandwich panel face plate wrinkling.....	235
16.32.1	Title.....	235
16.32.2	Usage and scope.....	236
16.32.3	Analysis	236
16.32.4	ESDUpac A8815	236
16.33	Vibration of singly-curved laminated plates	237
16.33.1	Title.....	237
16.33.2	Usage and scope.....	237
16.33.3	Calculation of natural frequencies	237
16.33.4	ESDUpac A8911	237
16.34	Plate through-the-thickness shear stiffnesses.....	238
16.34.1	Title.....	238
16.34.2	Usage and scope.....	238
16.34.3	Analysis	238
16.34.4	ESDUpac A8913	239
16.34.5	Notes	239
16.35	Vibration of plates with in-plane loading	239
16.35.1	Title.....	239
16.35.2	Usage and scope.....	239
16.35.3	Calculation of natural frequencies	240
16.35.4	ESDUpac A9016	240
16.36	Delamination and free edge stresses	240
16.36.1	Title.....	240
16.36.2	Usage and scope.....	241

16.36.3	Analysis	241
16.36.4	ESDUpac A9021	241
16.36.5	Notes	242
16.37	Delamination at termination of plies.....	242
16.37.1	Title.....	242
16.37.2	Usage and scope.....	242
16.37.3	Analysis	242
16.37.4	ESDUpac A9103	243
16.38	Thickness selection to meet a loading combination	243
16.38.1	Title.....	243
16.38.2	Usage and scope.....	243
16.38.3	Analysis	244
16.38.4	ESDUpac A9233	244
16.39	ESAComp.....	245
17	Composite adequate design.....	246
17.1	Introduction.....	246
17.2	Anisotropy of composites.....	246
17.3	Stress-strain relationships	248
17.3.1	Reinforcing fibres.....	248
17.3.2	Stress concentrations	248
17.4	Fibre strength and stiffness	250
17.4.1	General.....	250
17.4.2	High stiffness applications	251
17.5	Basic design rules.....	252
17.5.1	General.....	252
17.5.2	Aspects of construction	252
17.5.3	Aspects of laminate lay up.....	255
17.5.4	Fabrication aspects	258
17.6	First steps in designing a composite.....	261
17.6.1	General.....	261
17.6.2	Carpet plots	261
17.6.3	Use of carpet plots.....	263
17.7	References	264
17.7.1	General.....	264
18	Curing stresses: Effects and prediction.....	266
18.1	Introduction.....	266
18.2	Cure process	266

18.2.1	Composite materials.....	266
18.2.2	Cure parameters.....	267
18.3	Analytical notation for residual stress	268
18.4	Residual stresses	268
18.4.1	General.....	268
18.4.2	Types of residual stresses.....	268
18.5	Calculation of curing stresses.....	269
18.5.1	Residual stresses after curing	269
18.6	Reduction of thermal stresses and distortions.....	271
18.6.1	General.....	271
18.6.2	Stress relieving.....	272
18.7	References	272
18.7.1	General.....	272
19	Manufacturing faults and service damage	274
19.1	Introduction.....	274
19.2	Manufacturing defects in composite materials.....	276
19.2.1	General.....	276
19.2.2	Description of manufacturing defects	277
19.2.3	Detection of defects.....	281
19.3	Service threats for composite structures	281
19.4	Impact behaviour of laminates and sandwich constructions.....	282
19.4.1	General.....	282
19.4.2	Laminates	283
19.4.3	Sandwich panels	286
19.5	Impact behaviour	286
19.5.1	General.....	286
19.5.2	BVID	287
19.5.3	Impact tests	289
19.5.4	Compression after impact (CAI)	290
19.6	Detection of defects	290
19.6.1	Damage detection techniques.....	290
19.6.2	Laboratory and production based NDT	290
19.6.3	Other techniques	290
19.7	References	291
19.7.1	General.....	291
19.7.2	ASTM standards.....	291
20	Environmental aspects of design	292

20.1	Introduction.....	292
20.2	Description of environments.....	292
20.2.1	Earth environment.....	292
20.2.2	Space environment.....	293
20.2.3	Composite structures.....	297
20.3	Low earth orbit (LEO).....	298
20.4	Geostationary orbit (GEO).....	299
20.5	Deep space exploration.....	299
20.6	Galvanic corrosion.....	300
20.6.1	General.....	300
20.6.2	Physical basis of galvanic corrosion.....	300
20.6.3	Prevention of galvanic corrosion in space structures.....	302
20.7	Effects of moisture on composites.....	302
20.7.1	General.....	302
20.7.2	Modification of CTE by outgassing.....	302
20.7.3	Low coefficient of moisture expansion (CME) resins.....	303
20.7.4	Hot/wet performance.....	303
20.8	LDEF in LEO.....	304
20.8.1	Mission.....	304
20.8.2	Materials and experiments.....	304
20.8.3	Variations in exposure conditions.....	305
20.8.4	Composite materials aboard LDEF.....	307
20.8.5	LDEF experiments M0003-9/10.....	309
20.8.6	LDEF experiment AO 171.....	311
20.8.7	LDEF experiment AO 180.....	313
20.8.8	Surface characterisation of eroded composites.....	313
20.8.9	Overall conclusions on LDEF.....	314
20.8.10	Non-polymeric composites on LDEF.....	314
20.8.11	Polymer films on LDEF.....	314
20.8.12	Lubricants, adhesives and seals on LDEF.....	314
20.9	Thermal cycling.....	315
20.9.1	Conditions.....	315
20.9.2	Damage mechanisms.....	316
20.10	Vacuum.....	319
20.10.1	Effects of vacuum.....	319
20.11	Radiation.....	320
20.11.1	Radiation spectra.....	320

20.11.2	T300/934 in GEO.....	323
20.12	Damage by combined environmental factors	324
20.12.1	General.....	324
20.12.2	P75/930 in GEO	324
20.12.3	UHM CFRP in GEO and LEO.....	328
20.12.4	PEI CFRP in LEO and GEO	331
20.13	Atomic oxygen	333
20.13.1	Effects of atomic oxygen	333
20.14	Siloxanes and silicon polymers.....	335
20.14.1	Protection methods against ATOX	335
20.14.2	Protection of polymer films	336
20.14.3	Protection of composites	336
20.15	Protective coatings	338
20.15.1	Surface coatings.....	338
20.16	Debris	339
20.16.1	Classification of debris.....	339
20.16.2	Damage to LDEF.....	340
20.16.3	Damage to composites.....	340
20.16.4	Damage to aluminium alloys	341
20.16.5	Damage to thermal control materials.....	341
20.16.6	Significance of impact events	342
20.16.7	Protective shielding	342
20.17	References	343
20.17.1	General.....	343
20.17.2	ECSS documents	347
21	Bonded joints.....	349
21.1	Introduction	349
21.2	Adhesives	349
21.2.1	General.....	349
21.2.2	Types of adhesives.....	349
21.2.3	Adhesives for joining different materials.....	352
21.3	Design of bonded joints	354
21.3.1	Basic considerations.....	354
21.3.2	Basic guidelines.....	354
21.3.3	Failure modes.....	354
21.3.4	Features	355
21.4	Joint configuration.....	357

21.4.1	Basic configurations	357
21.4.2	Orientation of surface fibres	360
21.5	Environmental factors for bonded joints	361
21.5.1	General.....	361
21.5.2	Effect of moisture.....	361
21.5.3	Effect of temperature	364
21.5.4	Combined moisture and temperature	364
21.6	Bonding defects.....	365
21.6.1	General.....	365
21.6.2	Description of bonding defects	365
21.6.3	Inspection of bonded joints.....	372
21.7	Bonded joint failure modes	374
21.7.1	Typical failure modes.....	374
21.7.2	Loading modes.....	374
21.8	Calculation of bonded joint strength	375
21.9	Analysis of joint configurations	376
21.9.1	Analytical notation	376
21.9.2	Single lap shear joint	376
21.9.3	Double lap shear joint.....	380
21.9.4	Double-lap shear joint under mechanical and temperature loads	382
21.9.5	Single taper scarf joint.....	390
21.9.6	Double taper scarf joint.....	391
21.9.7	Stepped lap joint.....	392
21.10	Bonded joint design curves and test data.....	394
21.10.1	General.....	394
21.11	Acoustic fatigue of bonded configurations	405
21.12	References	407
21.12.1	General.....	407
21.12.2	ECSS documents	408
22	Mechanically fastened joints	409
22.1	Introduction.....	409
22.2	Basic considerations for design	409
22.2.1	Advantages.....	409
22.2.2	Disadvantages.....	409
22.3	Factors affecting design.....	410
22.3.1	General.....	410
22.3.2	Material parameters.....	411

22.3.3	Fastener parameters	413
22.3.4	Design parameters	413
22.4	Bolted joints	418
22.4.1	Material parameters.....	418
22.4.2	Fastener parameters	418
22.4.3	Design parameters	420
22.5	Bolted joint: Analysis.....	420
22.5.1	General.....	420
22.5.2	Analytical methods	420
22.5.3	Stress distribution.....	420
22.5.4	Failure prediction.....	423
22.5.5	Experimental data.....	425
22.6	Riveted joints	429
22.6.1	General.....	429
22.6.2	Installation damage of riveted joints	429
22.6.3	Pull through strength	430
22.6.4	Fasteners used in composite structures.....	431
22.7	References	433
22.7.1	General.....	433
22.7.2	ECSS standards.....	434

Figures

Figure 10.2-1	- Derivation of macro-mechanical properties for the analysis of laminates.....	29
Figure 10.5-1	- Longitudinal modulus (E_1) of glass/epoxy.....	32
Figure 10.5-2	- Longitudinal modulus (E_1) of carbon (HT)/epoxy	33
Figure 10.5-3	- Longitudinal modulus (E_1) of carbon (HM)/epoxy	33
Figure 10.5-4	- Longitudinal modulus (E_1) of aramid/epoxy	34
Figure 10.7-1	- Transverse modulus (E_2) of glass/epoxy composites	38
Figure 10.7-2	- Transverse modulus (E_2) of carbon (HT)/epoxy composites	38
Figure 10.7-3	- Transverse modulus (E_2) of carbon (HM)/epoxy composites	39
Figure 10.7-4	- Transverse modulus (E_2) of aramid/epoxy composites	39
Figure 10.9-1	- Shear modulus (G_{12}) of glass/epoxy composites.....	42
Figure 10.9-2	- Shear modulus (G_{12}) of carbon (HT)/epoxy composites.....	43
Figure 10.9-3	- Shear modulus (G_{12}) of carbon (HM)/epoxy composites	43
Figure 10.9-4	- Shear modulus (G_{12}) of aramid/epoxy composites	44
Figure 10.12-1	- Definition of the co-ordinate system for the analysis of unidirectional plies	46

Figure 10.14-1 - Definition of axes	48
Figure 10.14-2 - Transformation of stiffness and compliance matrix	50
Figure 10.15-1 - In plane forces and moments	51
Figure 10.15-2 - Geometry of an n -layered laminate	52
Figure 10.15-3 - Calculation of a laminate	53
Figure 10.16-1 - Uniaxial loading of a composite	54
Figure 10.16-2 - Typical decrease of interlaminar stresses with high peaks near the edges	55
Figure 10.17-1 - External load on a composite plate.....	56
Figure 10.17-2 - Determination of the critical fibre direction.....	58
Figure 11.2-1 - Fibre reinforced composite: Tensile failure model	66
Figure 11.3-1 - Buckling modes of fibres under compression	68
Figure 11.3-2 - Comparison of predicted and experimental values of longitudinal compressive strength.....	70
Figure 11.6-1 - Analytical notation: Co-ordinate system	74
Figure 11.8-1 – Cuntze failure criteria - Schematic diagram of failure modes in transversely-isotropic UD material.....	84
Figure 11.8-2 – Cuntze failure criteria – Notation and formulae for fabric failure conditions.....	87
Figure 11.8-3 – Comparison between predicted failure curves for C-C/SiC composites with experimental data.....	88
Figure 11.9-1 - Test results: Effect of thickness variation on static failure	89
Figure 11.9-2 - Test results: Effect of static and dynamic loading.....	90
Figure 11.9-3 - Comparison: Failure theories applied to static strength result-.....	91
Figure 12.3-1 - CTE of unidirectional composites	106
Figure 12.3-2 - CTE for T300/914 $0^\circ/\pm 45^\circ/90^\circ$ laminates.....	107
Figure 13.3-1 - Stress/strain curves of Fibredux 914 (neat resin) for different moisture contents tested at RT.....	117
Figure 13.3-2 - Swelling strain, transverse (UD laminate).....	118
Figure 13.3-3 - Influence of temperature and time on weight gain.....	118
Figure 13.3-4 - Test results: Moisture absorption versus time	119
Figure 13.3-5 - Transverse tensile strength	119
Figure 13.3-6 - Transverse modulus of elasticity	120
Figure 13.3-7 - Influence of temperature and moisture on fatigue strength of unidirectional 0° laminates.....	120
Figure 13.4-1 - Moisture: Comparison of calculated and experimental results of strength and stiffness of $[0^\circ/90^\circ]$ GFRP laminates	122
Figure 13.4-2 - Moisture: Comparison of calculated and experimental results of strength and stiffness $[0^\circ/90^\circ]$ CFRP laminates.....	123
Figure 13.5-1 - Notation: Definition of axes.....	124

Figure 13.5-2 - Illustration of change of moisture content with square root of time.....	127
Figure 13.5-3 - Variation of maximum moisture content with relative humidity for a T300/1034 composite	128
Figure 13.6-1 - Moisture: Coefficient of swelling for unidirectional composites.....	130
Figure 13.6-2 - Moisture: Definition of swelling coefficient β_2 for orthotropic material (unidirectional laminate).....	131
Figure 13.6-3 - Moisture: Swelling coefficients for T300/914 $[0^\circ/\pm 45^\circ/90^\circ]$ s laminates.....	132
Figure 14.4-1 - Strength ratio versus hole diameter: Crack length for WN fracture model - 'Average stress criterion'	139
Figure 14.5-1 - Notation: Infinite isotropic plate with circular hole.....	140
Figure 14.5-2 - Comparison between experiment and prediction by WEK model.....	142
Figure 14.5-3 - Notation: Infinite plate with straight crack	143
Figure 14.5-4 - Comparison between experiment and prediction by WEK model.....	144
Figure 14.5-5 - Determination of a_c for various laminates	145
Figure 14.6-1 - Notation: Point stress criterion diagram.....	146
Figure 14.6-2 - Notation: Average stress criterion diagram.....	147
Figure 14.6-3 - Notation: Infinite orthotropic plate with circular hole	148
Figure 14.6-4 - Comparison between experiments and predictions of WN model.....	150
Figure 14.6-5 - Effects of stacking sequence on notch sensitivity.....	151
Figure 14.6-6 - Effects of fibre angle on notch sensitivity.....	151
Figure 14.6-7 - Infinite orthotropic plate with straight crack.....	152
Figure 14.6-8 - Comparison between experiments and predictions of WN model.....	155
Figure 14.6-9 - Critical stress intensity factor K_{Ic}	155
Figure 14.6-10 - Determination of a_0 for various laminates, applying 'Average stress criterion'	156
Figure 14.6-11 - Characteristic dimensions as a function of half crack length	157
Figure 14.6-12 - Effect of stacking sequence.....	157
Figure 14.8-1 - Anisotropy factor versus net section reduction for centre cracked angle ply CFRP specimens	159
Figure 14.8-2 - Anisotropy factor versus net section reduction for centre cracked CFRP specimens.....	160
Figure 14.9-1 - Stress concentration factor (K_{Tn}) for orthotropic CFRP laminates with a circular hole, $2 \leq L/W \leq 10$	162
Figure 14.9-2 - Stress distribution at a hole for $0^\circ/0^\circ$ laminates	164
Figure 14.9-3 - Stress distribution at a hole for $\pm 32.5^\circ/0^\circ/\pm 32.5^\circ$ laminates.....	165
Figure 14.9-4 - Stress distribution at a hole for laminates.....	166
Figure 14.9-5 - Stress distribution at a hole for laminates.....	167
Figure 14.10-1 - Stress concentration due to tensile load.....	168
Figure 14.10-2 - Stress concentration due to shear load	170

Figure 14.11-1 - Fracture modes: opening, shearing, and tearing	172
Figure 14.11-2 - Outline of no-damage-growth methodology.....	173
Figure 14.11-3 - Fracture mechanics life prediction methodology	175
Figure 14.11-4 - DCB and ENF specimens.....	177
Figure 14.11-5 - Representative $G-N_{onset}$ data	179
Figure 14.11-6 - Node definitions for 2D VCCT	181
Figure 14.11-7 - Node definitions for 3D VCCT	183
Figure 14.11-8 - $G-a$ curve for a stiffener debond	184
Figure 14.11-9 - Schematics of possible $G-a$ curves	184
Figure 15.5-1 - Summary of loss factors for various fibres / epoxy composites.....	194
Figure 17.2-1 - Anisotropic behaviour of carbon fibre reinforced plastic	247
Figure 17.3-1 - Stress-strain response of CFRP (in tension and compression).....	249
Figure 17.3-2 - Fatigue strength of notched and un-notched aluminium and carbon fibre reinforced plastic.....	250
Figure 17.4-1 - Specific tensile strength and modulus properties of reinforcing fibres.....	251
Figure 17.5-1 - Shaping changes in thickness	252
Figure 17.5-2 - Design of shapes	253
Figure 17.5-3 - Need for radii on corners	253
Figure 17.5-4 - Cut outs: Bad and good practice	254
Figure 17.5-5 - Directionality of tensile strength of various semi-product forms: Preferred loading direction.....	256
Figure 17.5-6 - Symmetrical lay-up: Avoids warpage and minimises loading the resin matrix	257
Figure 17.5-7 - Split design technique.....	257
Figure 17.5-8 - Dimensional change for various materials due to a temperature change of 100°	258
Figure 17.5-9 - Fabrication costs for a CFRP structure.....	259
Figure 17.5-10 - Comparison of costs: Metallic and CFRP	260
Figure 17.6-1 - Carpet plot curves of modulus for 0°/±45°/90° laminates	262
Figure 17.6-2 - Carpet plot curves of strength for 0°/±45°/90° laminates.....	262
Figure 18.2-1 - Typical cure cycle for CFRP	267
Figure 18.5-1 - Residual stresses after curing	270
Figure 18.6-1 - Normalised maximum curing stresses in [±θ°]s laminates.....	271
Figure 18.6-2 - Through thickness tensor polynomial distributions for curing stresses and stresses at first failure in [±θ°]s laminates.....	272
Figure 19.1-1 - Examples of defects in composite materials.....	275
Figure 19.4-1 - The primary failure modes of composite laminates under impact loading ...	284
Figure 19.5-1 - Multiple delaminations in a [(0 ₂ , ±45) ₂]s CFRP laminate caused by drop weight impact.....	287

Figure 19.5-2 - Impact damage in a 64-ply CFRP laminate caused by high velocity impact	288
Figure 20.2-1 - Space environment effects: Vacuum	294
Figure 20.2-2 - Space environment effects: Radiation	294
Figure 20.2-3 - Space environment effects: Temperature.....	295
Figure 20.2-4 - Space environment effects: Micrometeoroids and debris.....	295
Figure 20.2-5 - Space environment effects: Atomic oxygen (ATOX)	296
Figure 20.2-6 - Space environment effects: Re-entry	296
Figure 20.6-1 - Galvanic corrosion: Potential in 3.5 % NaCl solution.....	301
Figure 20.8-1 – LDEF: Experiment locations (M0003-10).....	307
Figure 20.8-2 - LDEF: Estimated AO erosion depth versus fibre content for various epoxy CFRP materials.....	309
Figure 20.9-1 - Ratio of residual tensile strength to the initial strength versus number of thermal cycles (-160 to +95°C): $[\pm 45^\circ]_{2S}$ specimen tensile tested at RT and 100°C.....	317
Figure 20.9-2 - Degradation of stiffness of various materials due to thermal cycling (-160°C to +95°C): $[\pm 45^\circ]_{2S}$ specimen tensile tested at RT and 100°C.....	318
Figure 20.11-1 - UV radiation: Effects on tensile moduli of carbon/epoxy composites	321
Figure 20.11-2 - Effects of total radiation dose on microcrack formation in composite specimens subjected to 100 thermal cycles (-150°C to +80°C).....	322
Figure 20.11-3 - Effects of total radiation dose on the coefficient of thermal expansion of a toughened composite system (-150°C to -73°C)	323
Figure 20.12-1 - Effect of cure temperature and electron radiation exposure on the Tg of P75/930 in GEO.....	326
Figure 20.12-2 - Effects of cure temperature and electron radiation exposure on the shear strength of P75/930 in GEO.....	327
Figure 20.12-3 - Step simulation of 7 years in GEO.....	329
Figure 20.12-4 - Effect of ATOX erosion on different CFRP composites	331
Figure 20.12-5 - Irradiation and thermal cycling: Changes in mechanical properties for C6000/PEI	333
Figure 21.2-1 - Adhesives for bonding different materials.....	353
Figure 21.4-1 - Bonded joints: Basic configurations.....	359
Figure 21.4-2 - Bonded joints: Orientation of surface fibre.....	360
Figure 21.5-1 - Effect of moisture on stress distributions in adhesive bonded joints	362
Figure 21.5-2 - Influence of moisture absorption/desorption on peak adhesive shear strains	363
Figure 21.5-3 - Effect of progressive moisture absorption on bond strain.....	364
Figure 21.6-1 - Bonded joints: Examples of acceptable bond flaw sizes	366
Figure 21.6-2 - Typical quality zoning for bonded joints.....	367
Figure 21.6-3 - Adhesive shear stresses in bonded joints	368
Figure 21.6-4 - Adhesive stresses in flawed bonded joints.....	368

Figure 21.6-5 - Adhesive stresses in flawed bonded joints	369
Figure 21.6-6 - Adhesive stresses in flawed bonded joints	369
Figure 21.6-7 - Adhesive bonded joints: Effect of debond flaws on flexibility.....	370
Figure 21.6-8 - Variation of peak induced adhesive stress with thickness of adhesive at ends of overlap	371
Figure 21.7-1 - Components of bonded joint strength.....	374
Figure 21.7-2 - Bonded joints: Loading modes or types of stresses	375
Figure 21.9-1 - Analysis: Notation for symmetrical single-lap shear joint.....	377
Figure 21.9-2 - Analysis: Notation for single-lap joint R -degree peeling	378
Figure 21.9-3 - θ -degree peeling strength	379
Figure 21.9-4 - Analysis: Notation for double-lap shear joint	380
Figure 21.9-5 - Analysis: Notation for double lap joint (standard overlap length).....	382
Figure 21.9-6 - Shear stress distribution versus the adhesive length ($E_1t_1 = E_2t_2$) for single lap joint without eccentricity.....	382
Figure 21.9-7 - Stress concentration factor f_2 as a function of K_2 with parameter ω_2	384
Figure 21.9-8 - Shear stress distribution for large overlap lengths.....	386
Figure 21.9-9 - Stress concentration factor for large overlap lengths	387
Figure 21.9-10 - Shear stress distribution versus the normalised bonding length x/L for a bonded joint between CFRP-HT unidirectional (60 vol. %) and aluminium, titanium, GFRP quasi-isotropic, and GFRP unidirectional materials	388
Figure 21.9-11 - Shear stress distribution versus the normalised bonding length x/L for a bonded joint between CFRP HT quasi isotropic (60 vol. %) and aluminium, titanium, GFRP quasi isotropic, and GFRP unidirectional materials	389
Figure 21.9-12 - Analysis: Notation for single taper scarf joint.....	390
Figure 21.9-13 - Analysis: Notation for symmetrical double tapered scarf joint	391
Figure 21.9-14 - Analysis: Notation for stepped lap joint (recessed and simple)	392
Figure 21.9-15 - Analysis: Notation for recessed and simple scarf joints (four or more steps)	393
Figure 21.10-1 - Design curve: Single lap shear joint	395
Figure 21.10-2 - Design curve: Single lap shear joint	396
Figure 21.10-3 - Design curve: Single lap shear joint	397
Figure 21.10-4 - Design curve: Lower bond tension single lap shear joint strength versus lap length.....	397
Figure 21.10-5 - Design curve: Lower bond tension single lap shear joint strength versus lap length.....	398
Figure 21.10-6 - Design curve: Lower bond tension single lap compression loaded joint strength versus lap length.....	398
Figure 21.10-7 - Design curve: Single lap tension fatigue S-N curve.....	399
Figure 21.10-8 - Design curve: Single-lap shear joint tension fatigue S-N curve.....	399

Figure 21.10-9 - Design curve: Double lap shear joint	400
Figure 21.10-10 - Design curve: Symmetrical double scarf joint strength	401
Figure 21.10-11 - Design curve: Symmetrical double scarf joint strength	402
Figure 21.10-12 - Design curve: Symmetrical double scarf joint, tension fatigue S-N curve	403
Figure 21.10-13 - Design curve: Symmetrical double scarf joint tension fatigue S-N curve	404
Figure 21.10-14 - Design curve: Symmetrical double scarf joint tension fatigue S-N curve	405
Figure 21.11-1 - Bonded joint configurations in Hercules AS 4/3501-6	406
Figure 22.3-1 - Bolted joints: Bearing stresses for various CFRP ply configurations	412
Figure 22.3-2 - Mechanically fastened joints: Examples of configurations	413
Figure 22.3-3 - Mechanically fastened joints: Definition of joint geometry	415
Figure 22.3-4 - Bolted joints: Failure modes	417
Figure 22.3-5 - Local reinforcements for bolted joints	418
Figure 22.4-1 - Bearing strength of bolted carbon fibre reinforced laminates	419
Figure 22.5-1 – Stress σ_2 along the x_1 -axis in an isotropic infinite plate containing an unloaded circular hole	421
Figure 22.5-2 - Stress σ_2 along the x_1 -axis in an orthotropic infinite plate $[0^\circ/90^\circ]$ containing an unloaded circular hole	422
Figure 22.5-3 - Stress σ_2 along the x_1 -axis in an isotropic plate of finite width containing a loaded hole	423
Figure 22.5-4 - Whitney/Nuismer failure hypothesis: Characteristic curve	424
Figure 22.5-5 - Bolted joints: Test device and configuration for in- plane face sheet loading	426
Figure 22.5-6 - Bolted joints: Bearing stress at failure point of CFRP facings with different lay-ups	428
Figure 22.6-1 - Rivets: Improvement in pull-through strength by larger flush head diameter and footprint	430
Figure 22.6-2 - Types of rivets for aerospace materials	432

Tables

Table 10.4-1 - Elastic property data for comparison	31
Table 10.4-2 - Basis of calculation methods for different authors	31
Table 10.17-1 - Intralaminar stresses and strains: κ value for various stacking sequences	59
Table 10.17-2 - Intralaminar stresses and strains: κ value at interface for various stacking sequences	59
Table 11.10-1 - Failure modes of unidirectional laminates	93
Table 11.10-2 - Failure modes of multidirectional laminates	95
Table 11.10-3 - Examples of some failure modes	96

Table 13.5-1 - Summary of constants for the determination of the maximum moisture content, \hat{M}	126
Table 13.7-1 - Moisture absorption: Cyanate ester Fiberite 954 composites.....	133
Table 14.1-1 - Intrinsic and extrinsic variables relevant for stress intensity factors	136
Table 14.3-1 - Some fracture models and their authors.....	137
Table 14.9-1 - HT carbon/epoxy.....	161
Table 14.9-2 - K_T^∞ for various laminates, $w/d \rightarrow \infty$	162
Table 14.9-3 - Material data	163
Table 14.11-1 - Standard test methods.....	177
Table 16.2-1 - Commonly available software for the analysis of composites.....	197
Table 16.2-2 - Computer programs for finite element analysis	198
Table 16.2-3 - Computer programs for laminate analysis	199
Table 16.2-4 - Computer programs for special composite applications	201
Table 16.3-1 - ESDU data sheets for composite analysis.....	204
Table 17.5-1 - Minimum radii for fibres and laminates	254
Table 17.5-2 - Basic and semi-product forms	255
Table 17.5-3 - Composite manufacturing methods	261
Table 19.2-1 - Types of defects in composite materials.....	277
Table 20.8-1 – LDEF: Polymer composites.....	306
Table 20.8-2 - LDEF: Exposure levels	307
Table 20.8-3 - LDEF: Composite material classifications.....	308
Table 20.8-4 - LDEF experiment AO 171: Tensile properties of composites	312
Table 20.9-1 - Coefficient of thermal expansion for $\pm 45^\circ$	316
Table 20.12-1 - Microcrack densities in $[0_2/90_2]_s$ CFRP laminates	330
Table 20.12-2 - GEO and LEO effects: Mechanical properties of C6000/PEI composites ..	332
Table 20.13-1 - Reaction efficiencies for some selected composite polymers and organic films: Determined by ~40 hours of LEO exposure in space.....	334
Table 20.13-2 - Effects of short-term LEO exposure on coefficient of thermal expansion for T300/934 carbon/epoxy laminates (RT to $+82^\circ\text{C}$)	335
Table 21.2-1 - Adhesives: Common types	350
Table 21.2-2 - Adhesives: Typical characteristics	351
Table 21.6-1 - Bonded joints: Description of NDT methods	372
Table 21.6-2 - Bonded joints: Detection methods for various defects.....	373
Table 21.10-1 - Bonded joints: Summary of data curves	394
Table 22.5-1 - Bolted joints: Results of static test on material 914C T300.....	427
Table 22.5-2 - Bolted joints: Results of static test on material 914C – HM	428
Table 22.6-1 - Types of fasteners used to join aerospace materials.....	431

Introduction

The Structural materials handbook, ECSS-E-HB-32-20, is published in 8 Parts.

A glossary of terms, definitions and abbreviated terms for these handbooks is contained in Part 8.

The parts are as follows:

Part 1	Overview and material properties and applications	Clauses 1 - 9
Part 2	Design calculation methods and general design aspects	Clauses 10 - 22
Part 3	Load transfer and design of joints and design of structures	Clauses 23 - 32
Part 4	Integrity control, verification guidelines and manufacturing	Clauses 33 - 45
Part 5	New advanced materials, advanced metallic materials, general design aspects and load transfer and design of joints	Clauses 46 - 63
Part 6	Fracture and material modelling, case studies and design and integrity control and inspection	Clauses 64 - 81
Part 7	Thermal and environmental integrity, manufacturing aspects, in-orbit and health monitoring, soft materials, hybrid materials and nanotechnologies	Clauses 82 - 107
Part 8	Glossary	

10

Stress-strain relationships

10.1 Introduction

The many analytical and practically derived methods developed for predicting the stress-strain behaviour of composite materials are reviewed.

Calculation methods are given for:

- Behaviour prediction from constituent properties, [See:10.2].
- The calculation of intra-ply, [See: 10.10].
- Interlaminar stress-strains, [See: 16.16].

10.2 Elastic property prediction for UD ply from constituent properties

UD ply properties can be predicted by the procedures of micro-mechanics and be measured by physical means. These can then be used in a macro-mechanical analysis of the structure.

Micro-mechanical analysis has inherent limitations. Fibre properties cannot easily be measured, so they are determined from measurements of UD by applying inverse homogenisation formulae. The transverse and shear properties are particularly inaccurate.

In addition, a perfect bond between fibres and matrix is a common assumption for analysis, which is not always true for some composites. Imperfect bonds give a material with poorer properties than those of the micro-mechanical analysis. So, the analysis should be proven by careful experimental work. The derivation of macro-mechanical properties is summarised in Figure 10.2-1.

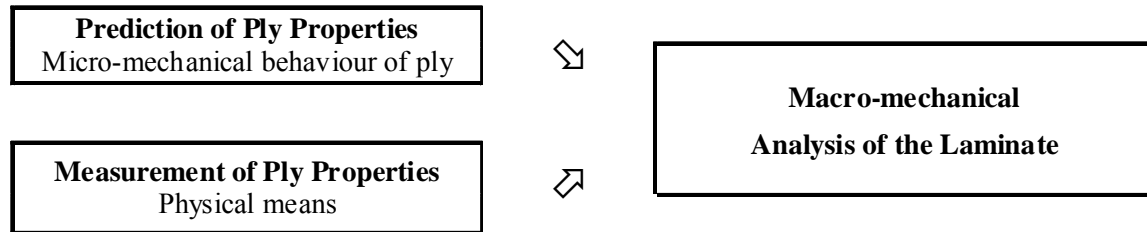


Figure 10.2-1 - Derivation of macro-mechanical properties for the analysis of laminates

The objective of the micro-mechanical approach is to determine the elastic moduli of a composite material in terms of the moduli of the constituent materials. This is also often referred to as the stiffness or compliance.

The additional and complementary objective of the micro-mechanical approach is to determine the strengths of the composite material in terms of the strengths of the constituent materials.

The basic assumptions for the analytical treatment of a composite material are:

- UD ply:
 - Macroscopically homogeneous
 - Linearly elastic
 - Macroscopically orthotropic
 - Initially stress-free
 - Perfect bond between fibres and matrix
- Fibre:
 - Homogeneous
 - Linearly elastic
 - Orthotropic
 - Regularly spaced
 - Perfectly aligned
- Matrix:
 - Homogeneous
 - Linearly elastic
 - Isotropic

Material characteristics of matrices and fibres, along with the fibre volume fraction, can significantly affect the macro-mechanical properties and therefore need careful evaluation.

10.3 Analytical notation for elastic constant methods

Formulae:

E	Young's modulus
ν	Poisson's ratio
G	Shear modulus
V	Volume ratio
E_1	Young's modulus of a ply in the fibre direction
E_2	Young's modulus of a ply in the direction transverse to the fibre
ν_x	Poisson's ratio of the ply when loaded in x -direction
G_{12}	In-plane shear modulus of the ply
η	Stress partitioning parameter

Subscripts:

f	Fibre
m	Matrix
1	Fibre direction
2	Transverse to fibre
12	Shear (in-plane)

10.4 Calculation methods for elastic constants of UD ply

Various authors have expressed analytically the elastic constants of an orthotropic layer dependent upon the Young's moduli, Poisson's ratio and shear moduli of the fibre and matrix according to their volume ratio.

The equations presented have been developed in each case for one specific material system, i.e. glass/epoxy or carbon/epoxy. To verify each equation with respect to commonly used composites, they are depicted together graphically, with test results. Where no test results are given, the diagrams can be used for preliminary design purposes only.

Data used for comparison are given in Table 10.4-1. The basis of the approach used by each author, as referenced, is shown in Table 10.4-2.

Table 10.4-1 - Elastic property data for comparison

	E_1 (kN/mm ²)	E_2 (kN/mm ²)	G_{12} (kN/mm ²)	ν_{12} (%)	Ref. [X] (Key)
Epoxy (1)	3.5	3.5	1.3	0.35	[10-3]
Cyanate Ester (4)	-	-	-	-	-
Glass, E	73	73	30	0.22	[10-2]
Carbon, HT	230	24	50 9.4(2)	0.28	[10-3]
Carbon, HM	550	6.0	18.0 2.0(2)	0.36	(3)
Aramid	130	7.0	12.0 2.5(2)	0.38	(3)
Key: (1) Epoxy: CY209/HT 972, Fibredux 914 (3) Estimated (2) G_{12} defined, Ref. [10-5] (4) ESA-study					

Table 10.4-2 - Basis of calculation methods for different authors

Author	Ref. [X]	Basis
Jones	[10-1]	Based on "representative volume element" with isotropic fibres.
Förster/Knappe	[10-2]	Semi-empirical approach for glass/epoxy.
Schneider	[10-3]	Semi-empirical approach for carbon (HT)/epoxy.
Puck	[10-4]	Semi-empirical approach for glass/epoxy.
Tsai	[10-5]	Semi-empirical approach including transverse and shear modulus.
HSB	[11-6]	Model of circular fibres with "square packing".

The approach used by each referenced author is presented for:

- Longitudinal modulus, [See:10.5].
- Longitudinal Poisson's ratio, [See: 10.6].
- Transverse modulus, [See: 10.7].
- Transverse Poisson's ratio, [See: 10.8].
- Transverse shear modulus, [See: 10.9].

10.5 Longitudinal modulus

Each of the referenced authors, [See: Table 10.4.2], uses the same approach to derive a relationship for longitudinal modulus. This is the 'method of mixtures', i.e.:

$$E_1 = E_f V_f + E_m (1 - V_f) \quad [10.5-1]$$

[See: 10.3 for notation]

The predicted relationship between fibre volume fraction and longitudinal modulus along with test results, where available, are shown for:

- glass/epoxy in Figure 10.5-1.
- carbon high strength HT/epoxy in Figure 10.5-2.
- carbon high modulus HM/epoxy in Figure 10.5-3.
- aramid/epoxy in Figure 10.5-4.

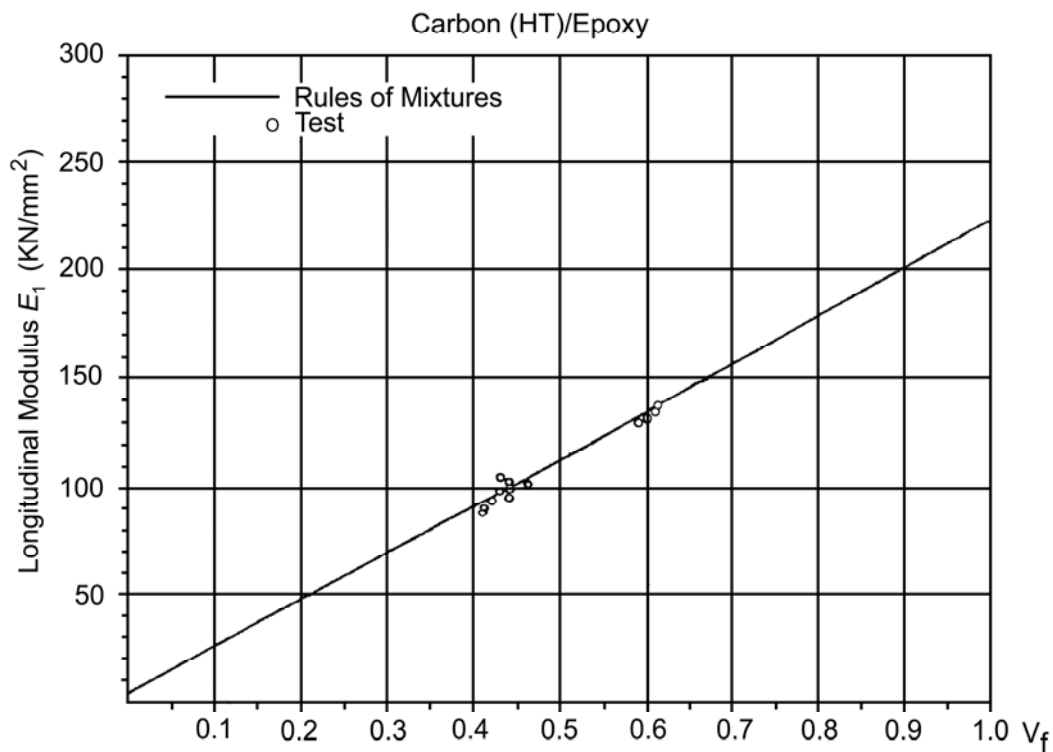


Figure 10.5-1 - Longitudinal modulus (E_1) of glass/epoxy

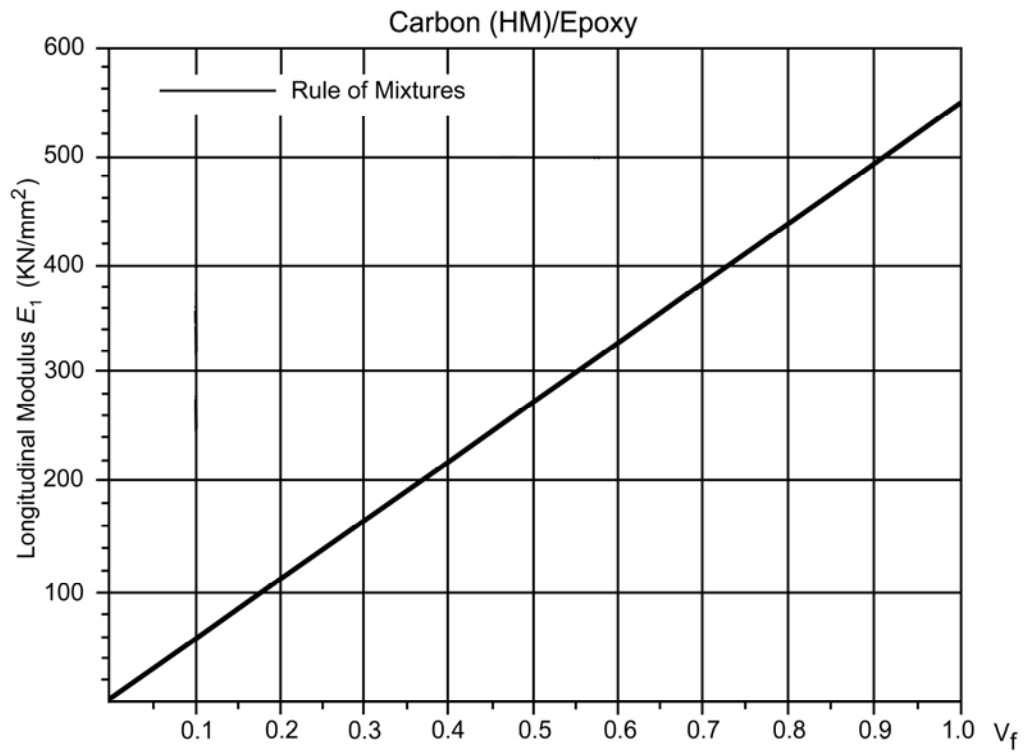


Figure 10.5-2 - Longitudinal modulus (E_1) of carbon (HT)/epoxy

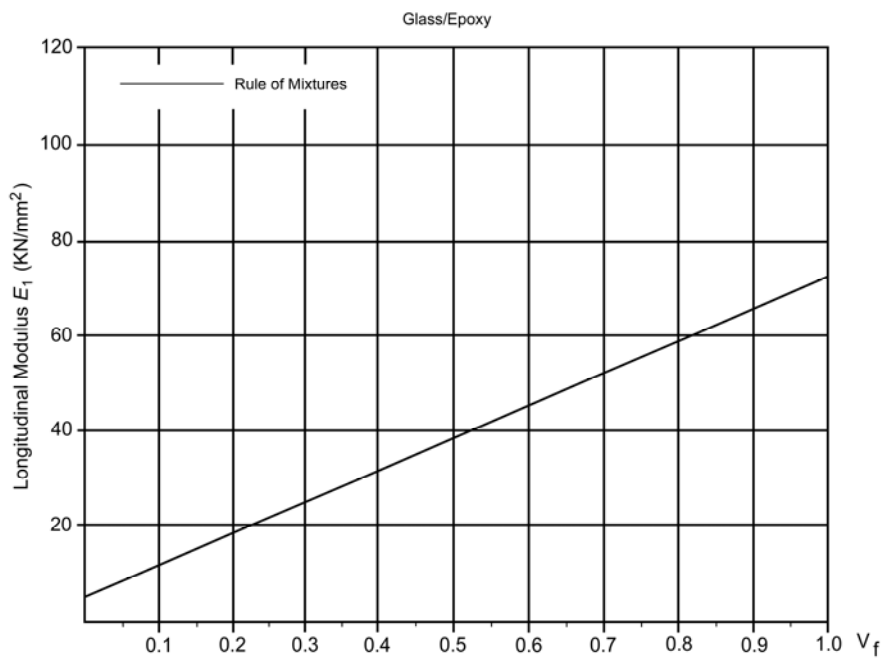


Figure 10.5-3 - Longitudinal modulus (E_1) of carbon (HM)/epoxy

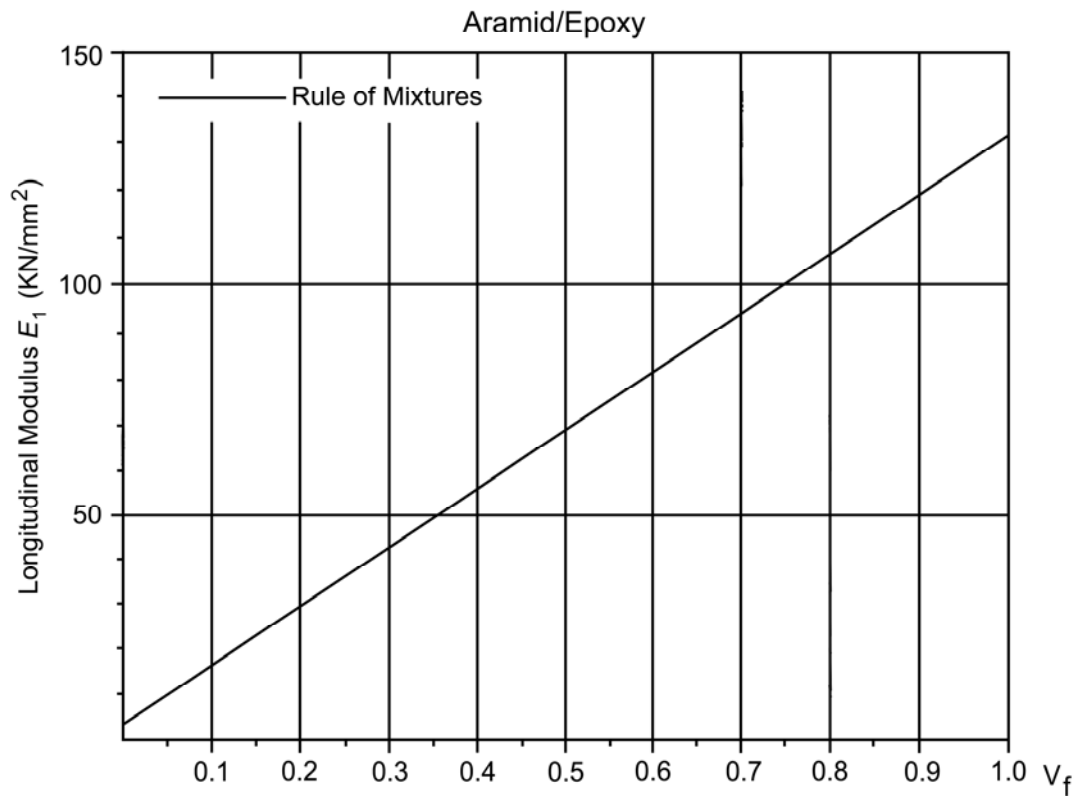


Figure 10.5-4 - Longitudinal modulus (E_1) of aramid/epoxy

10.6 Longitudinal Poisson's ratio

Each of the referenced authors, [See: Table 10.4-2], uses the same 'method of mixtures' to derive a relationship for longitudinal Poisson's ratio:

$$\nu_{12} = \nu_f V_f + \nu_m (1 - V_f) \quad [10.6-1]$$

10.7 Transverse modulus

10.7.1 General

The methods used by each referenced author, [See: Table 10.4-2] are given along with their predictions for transverse modulus:

- Jones method.
- Förster/Knappe method.
- Schneider method.
- Puck method.
- Tsai method.
- HSB method.

[See: 10.3 for notation]

The homogenisation formulas of Jones, Förster/Knappe, Schneider and Puck are suitable for isotropic fibres only and cannot be applied to carbon or aramid fibres, which are not isotropic.

10.7.2 Jones method

$$E_2 = \frac{E_m}{(1 - V_f) + E_m V_f / E_f} \quad [10.7-1]$$

10.7.3 Förster/Knappe method

$$E_2 = \frac{E_m^0}{(1 - V_f)^{1.45} + V_f E_m^0 / E_f} \quad [10.7-2]$$

Where: $E_m^0 = \frac{E_m}{(1 - V_m^2)}$

10.7.4 Schneider method

$$E_2 = \frac{E_m^0 (1 - V_f^3)}{(1 - V_f)^{0.75} + 6V_f E_m^0 / E_f} \quad [10.7-3]$$

Where: $E_m^0 = \frac{E_m}{(1 - V_m^2)}$

10.7.5 Puck method

$$E_2 = \frac{E_m^0 (1 + 0.85V_f^2)}{(1 - V_f)^{1.25} + V_f E_m^0 / E_f} \quad [10.7-4]$$

Where: $E_m^0 = \frac{E_m}{(1 - V_m^2)}$

10.7.6 Tsai method

$$E_2 = \frac{4k_y G_y}{k_y + mG_y} \quad [10.7-5]$$

Where: $m = 1 + \frac{4V_x^2 k_y}{E_x}$

$$\frac{1}{k_y} = \frac{1}{V_f + \eta_k V_m} \left[\frac{V_f}{k_{fy}} + \eta_k \frac{V_m}{k_m} \right]$$

$$V_m = 1 - V_f$$

$$\frac{1}{G_y} = \frac{1}{V_f + \eta_G V_m} \left[\frac{V_f}{G_{fy}} + \eta_G \frac{V_m}{G_m} \right]$$

$$\eta_k = \frac{1}{2(1 - V_m)} \left[2 - 4V_m + \frac{G_m}{G_{fy}} \right]$$

$$\eta_G = \frac{1}{4(1 - V_m)} \left[3 - 4V_m + \frac{G_m}{G_{fy}} \right]$$

$$k_{fy} = \frac{G_{fy}}{1 - 2\nu_f}$$

$$k_m = \frac{G_m}{1 - 2\nu_m}$$

10.7.7 HSB method

$$E_2 = k_y E_m \left[\left(1 - 2\sqrt{\frac{V_f}{\pi}}\right) - \frac{\pi}{2(1 - E_m/E_{fy})} + \dots \right]$$

$$\left[\dots \frac{2}{(1 - E_m/E_{fy})\sqrt{1 - 4V_f/\pi(1 - E_m/E_{fy})^2}} \dots \right]$$

$$\left[\dots \arctan \sqrt{\frac{1 + 2\sqrt{V_f/\pi}(1 - E_m/E_{fy})}{1 - 2\sqrt{V_f/\pi}(1 - E_m/E_{fy})}} \dots \right] \quad [10.7-6]$$

k_y = Correction factor; Ideal laminate $k_y = 1$

10.7.8 Graphs

The predicted relationship between fibre volume fraction and transverse modulus along with test results, where available, are shown for:

- Isotropic fibre: Glass/epoxy in Figure 10.7-1.
- Anisotropic fibres:
- Carbon high strength HT/epoxy in Figure 10.7-2.
 - Carbon high modulus HM/epoxy in Figure 10.7-3.
 - Aramid/epoxy in Figure 10.7-4.

The data presented for anisotropic fibres, derived from the homogenisation formulas of Jones, Förster/Knappe, Schneider and Puck can be ignored in Figure 10.7-1 to Figure 10.7-4, inclusive.

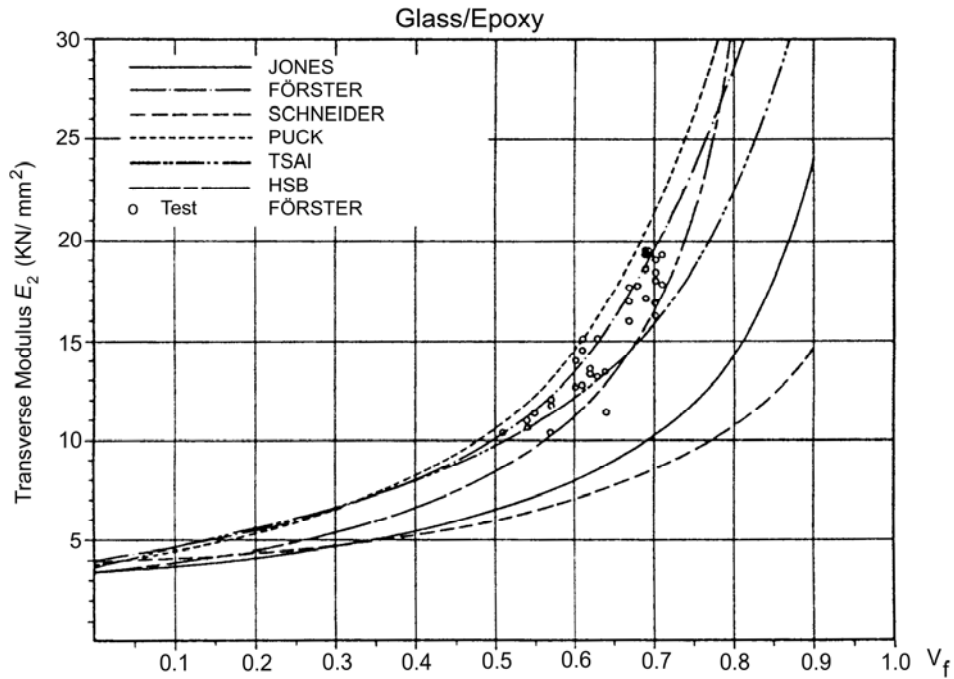
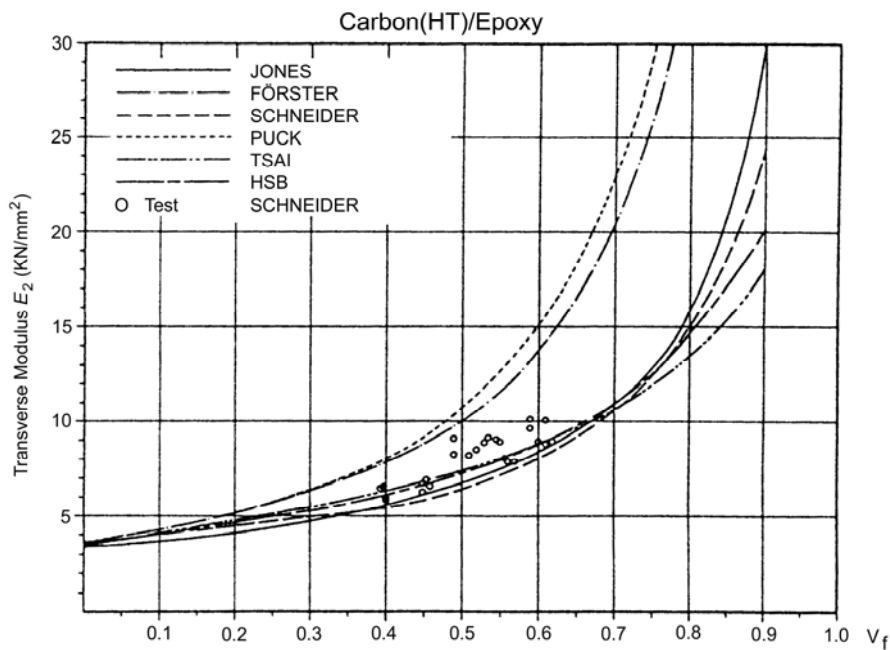
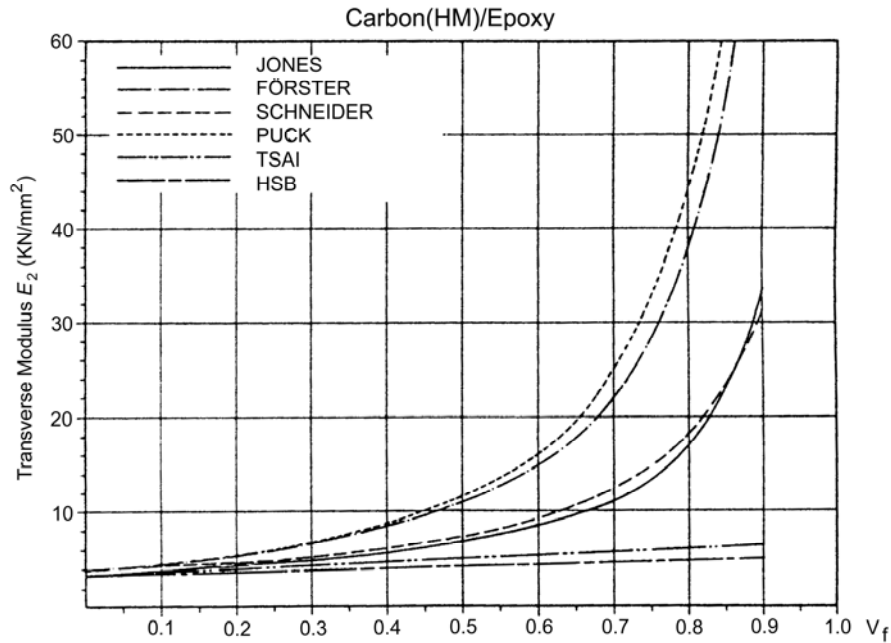


Figure 10.7-1 - Transverse modulus (E_2) of glass/epoxy composites



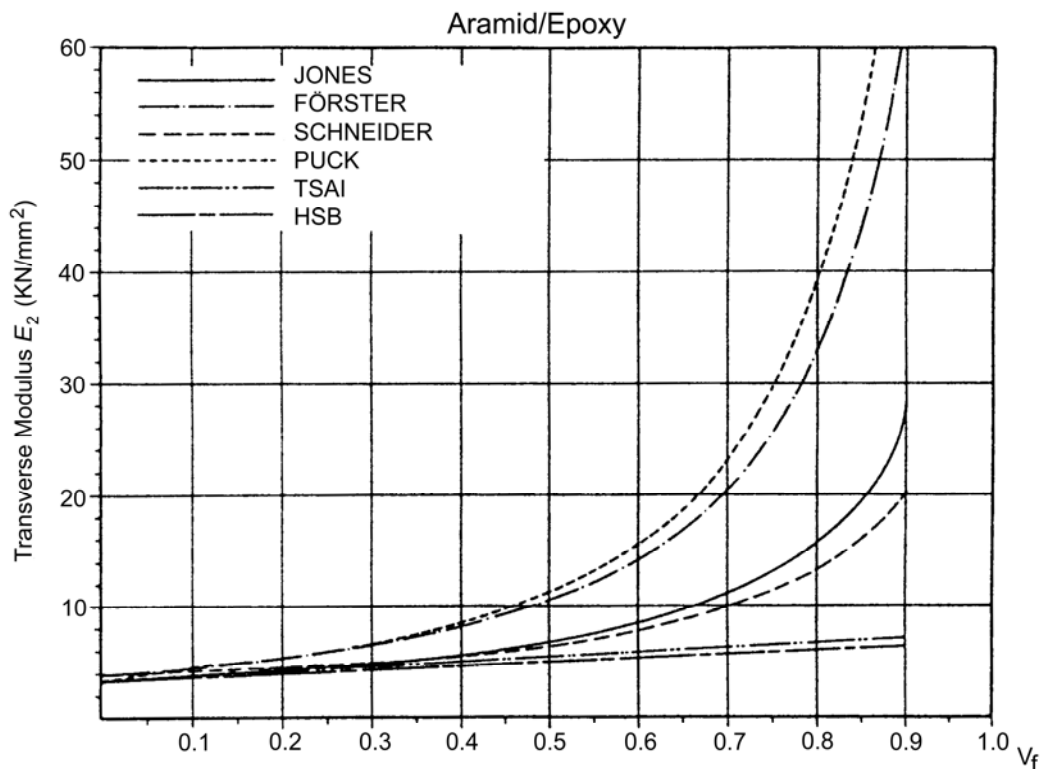
Carbon fibres are anisotropic. Data derived from the homogenisation formulas of Jones, Förster/Knappe, Schneider and Puck can be ignored.

Figure 10.7-2 - Transverse modulus (E_2) of carbon (HT)/epoxy composites



Carbon fibres are anisotropic. Data derived from the homogenisation formulas of Jones, Förster/Knappe, Schneider and Puck can be ignored.

Figure 10.7-3 - Transverse modulus (E_2) of carbon (HM)/epoxy composites



Aramid fibres are anisotropic. Data derived from the homogenisation formulas of Jones, Förster/Knappe, Schneider and Puck can be ignored.

Figure 10.7-4 - Transverse modulus (E_2) of aramid/epoxy composites

10.8 Transverse Poisson's ratio

Each of the referenced authors, [See: Table 10.4-2] uses the same method to derive a relationship for transverse Poisson's ratio:

$$V_{21} = V_{12} \frac{E_2}{E_1} \quad [10.8-1]$$

[See: 10.3 for notation]

The transverse Poisson's ratio is the Poisson's ratio of the ply when loaded in y-direction.

10.9 Transverse shear modulus

10.9.1 General

The methods used by each referenced author, [See: Table 10.4.2] are given along with their predictions for transverse shear modulus.

[See: 10.3 for notation]

10.9.2 Jones method

$$G_{12} = \frac{G_m}{(1 - V_f) + V_f G_m / G_f} \quad [10.9-1]$$

10.9.3 Förster/Knappe method

$$G_{12} = G_m \frac{1 + 0.4 \sqrt{V_f}}{(1 - V_f)^{1.45} + V_f G_m / G_f} \quad [10.9-2]$$

10.9.4 Schneider method

$$G_{12} = \frac{G_m (1 + 0.25 \sqrt{V_f})}{(1 - V_f)^{1.25} + 1.25 V_f G_m / G_f} \quad [10.9-3]$$

10.9.5 Puck method

$$G_{12} = G_m \frac{1 + 0.6\sqrt{V_f}}{(1 - V_f)^{1.25} + V_f G_m / G_f} \quad [10.9-4]$$

10.9.6 Tsai method

$$G_{12} = G_m \frac{1 + 0.6\sqrt{V_f}}{(1 - V_f)^{1.25} + V_f G_m / G_f} \quad [10.9-5]$$

Where: $\eta_{12} = \frac{1}{2} \left[1 + \frac{V_m}{G_f} \right]$

10.9.7 HSB method

$$G_{12} = k_{12} G_m \left[\left(1 - 2\sqrt{\frac{V_f}{\pi}} \right) - \frac{\pi}{2(1 - G_m / G_f)} + \dots \right]$$

$$\left[\dots \frac{2}{(1 - G_m / G_f) \sqrt{1 - 4V_f / \pi (1 - G_m / G_f)^2}} \dots \right]$$

$$\left[\dots \arctan \sqrt{\frac{1 + 2\sqrt{V_f / \pi} (1 - G_m / G_f)}{1 - 2\sqrt{V_f / \pi} (1 - G_m / G_f)}} \right] \quad [10.9-6]$$

k_{12} = Correction factor. For an ideal laminate $k_{12} = 1$

10.9.8 Graphs

The predicted relationship between fibre volume fraction and transverse shear modulus along with test results, where available, are shown for:

- Glass/epoxy in Figure 10.9.1.
- Carbon high strength HT/epoxy in Figure 10.9.2.
- Carbon high modulus HM/epoxy in Figure 10.9.3.
- Aramid/epoxy in Figure 10.9.4.

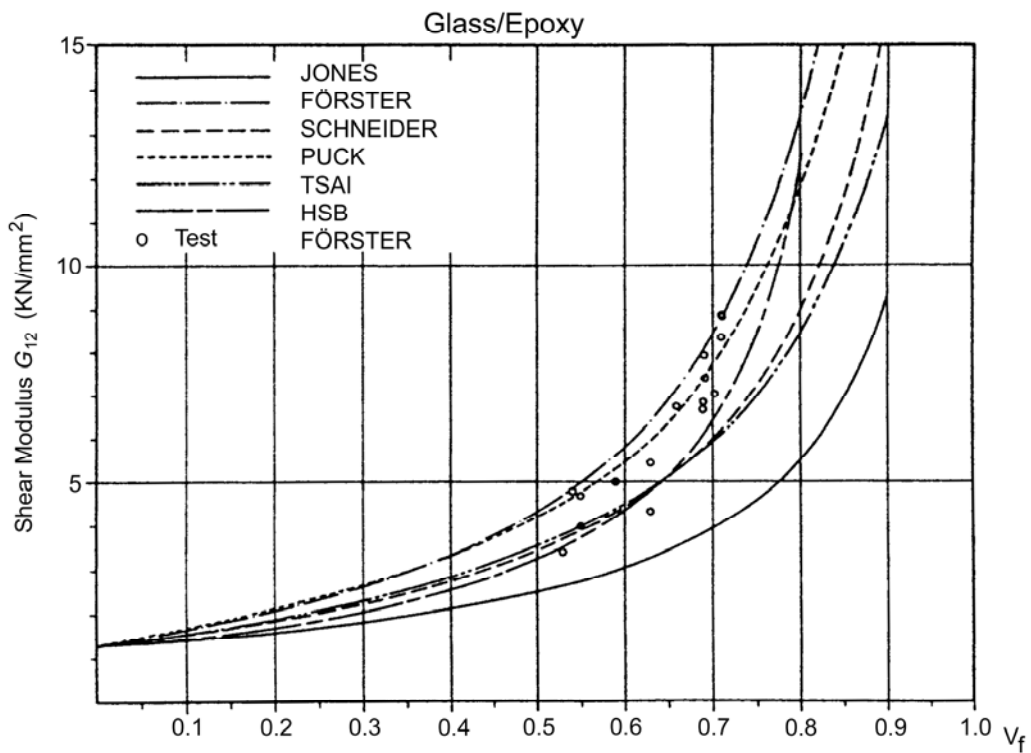


Figure 10.9-1 - Shear modulus (G_{12}) of glass/epoxy composites

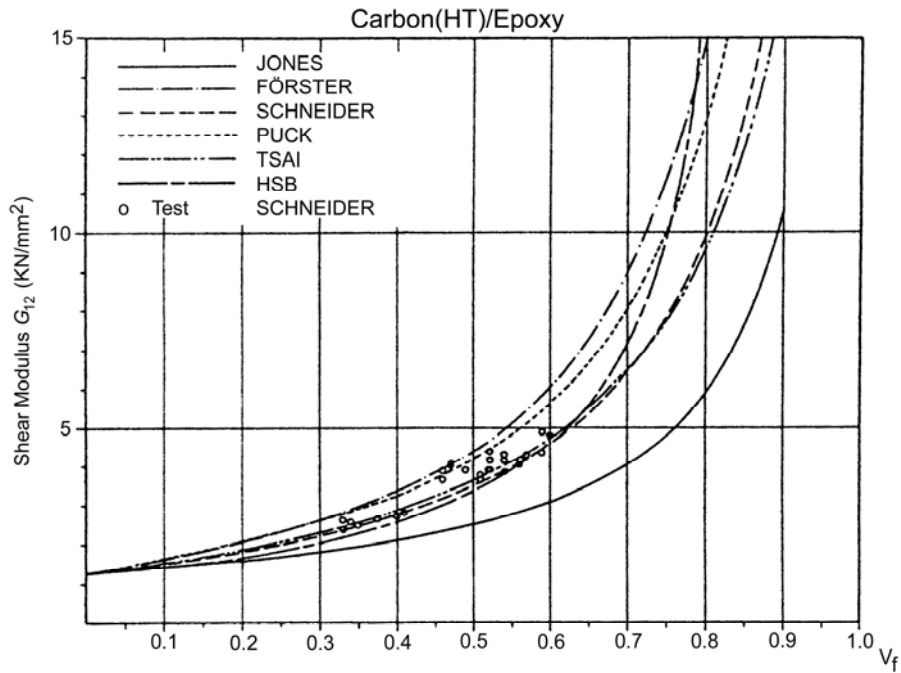


Figure 10.9-2 - Shear modulus (G_{12}) of carbon (HT)/epoxy composites

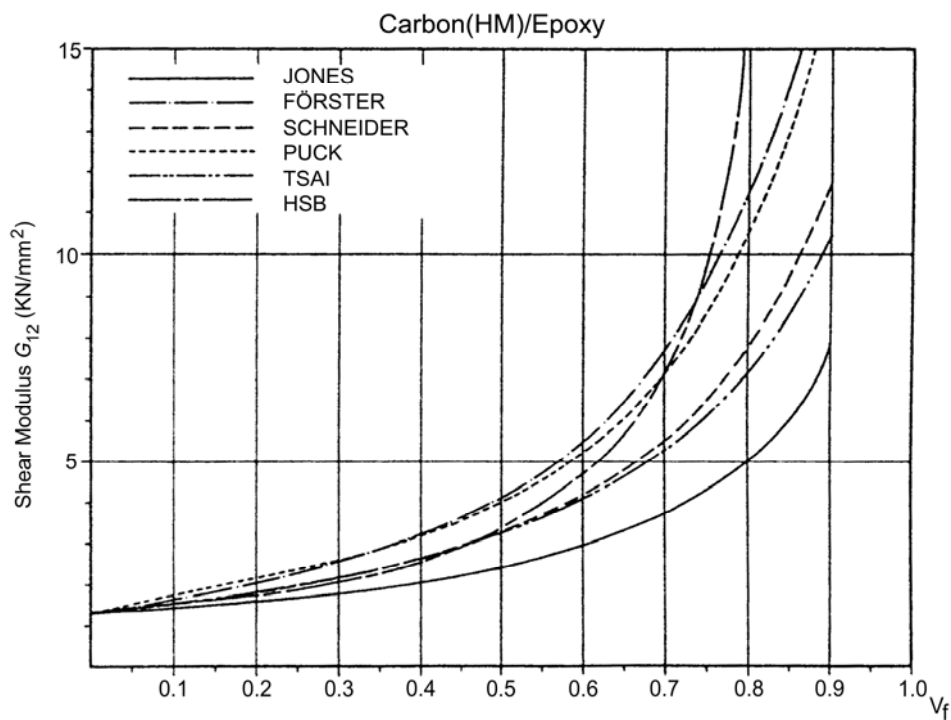


Figure 10.9-3 - Shear modulus (G_{12}) of carbon (HM)/epoxy composites

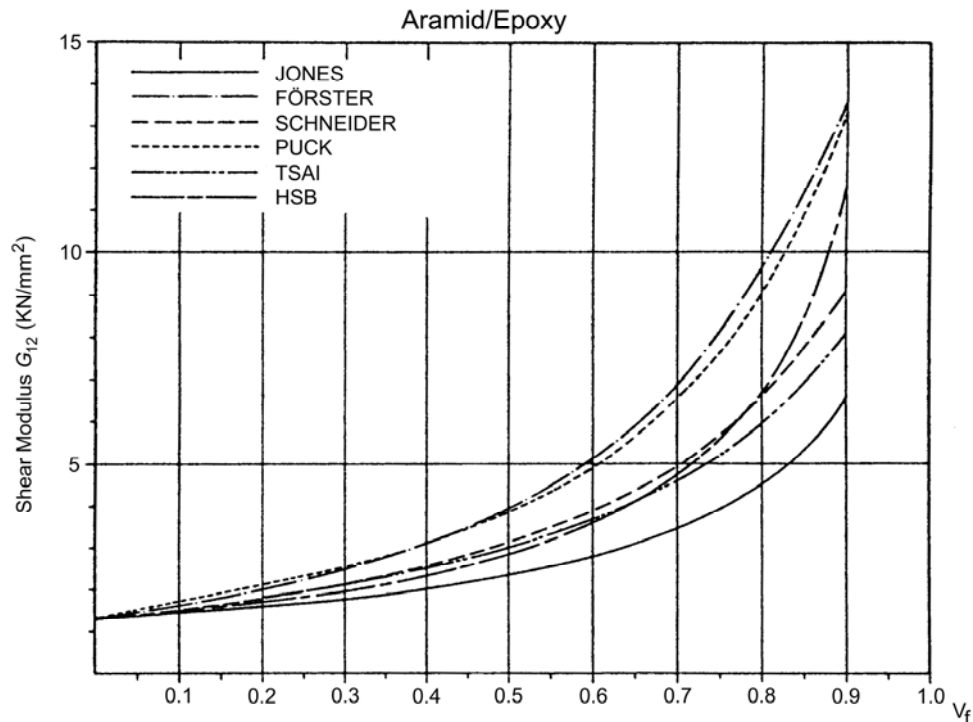


Figure 10.9-4 - Shear modulus (G_{12}) of aramid/epoxy composites

10.10 In-plane stress calculation methods

The stiffness of a unidirectional fibre reinforced layer, like any other structural material, is defined by appropriate stress-strain relations and is coupled to the stress-strain relation of a thin laminate plate according to the arbitrary orientation and thickness of each ply.

[See: 10.12 for unidirectional plies; 10.13 for on-axis relationship; 10.14 for ply orientation]

10.11 Analytical notation for in-plane methods

System of reference axes:

- (1,2,3) Ply reference axes (on-axis). Principal axes of orthotropy of a ply.
- (x, y, z) (x, y, z) Structural axes (off-axis). Plate reference axes.

Strains:

$$\boldsymbol{\varepsilon}_k = \begin{bmatrix} \varepsilon_1 \\ \varepsilon_2 \\ \gamma_{12,k} \end{bmatrix} \quad \text{Column matrix of direct and shear strains referred to } (1,2) \text{ co-ordinates for } k\text{-th layer.}$$

$$\boldsymbol{\varepsilon}_k = \begin{bmatrix} \varepsilon_x \\ \varepsilon_y \\ \gamma_{xy,k} \end{bmatrix} \quad \text{Column matrix of direct and shear strains referred to } (x,y) \text{ co-ordinates for } k\text{-th layer.}$$

System of reference axes:

Stresses:

$$\begin{bmatrix} \sigma_1 \\ \sigma_2 \\ \tau_{12} \end{bmatrix}_k$$
 Column matrix of direct and shear stresses referred to (1,2) co-ordinates for k -th layer.

$$\bar{\sigma}_k = \begin{bmatrix} \sigma_x \\ \sigma_y \\ \tau_{xy} \end{bmatrix}_k$$
 Column matrix of direct and shear stresses referred to (x,y) co-ordinates for k -th layer.

Plate curvatures:

W Deflection of plate in z-direction.

$$K = \begin{bmatrix} K_x \\ K_y \\ K_{xy} \end{bmatrix}_k$$
 Column matrix of curvature components of plate.

ε Column matrix of strains components of plate.

Plate loading intensities:

$$\begin{bmatrix} N_x \\ N_y \\ N_{xy} \end{bmatrix}$$
 Column matrix of direct and shear load intensities referred to (x,y) co-ordinates.

$$\begin{bmatrix} M_x \\ M_y \\ M_{xy} \end{bmatrix}$$
 Column matrix of bending moment intensities acting in xz and yz planes and twisting moment intensity acting about x and y axes, respectively.

Plate stiffnesses:

A In plane stiffness matrix for plate.

B Coupled in plane and flexural stiffness matrix for plate.

D Flexural stiffness matrix for plate.

Q_k Matrix relating stress and strain in (1,2) co-ordinates for k -th layer.

\bar{Q}_k Matrix relating stress and strain in (x,y) co-ordinates for k -th layer.

Ply properties:

E_1, E_2 Moduli of elasticity of a ply in 1- and 2-directions, respectively.

G_{12} Shear stiffness of a ply in (1, 2) direction.

p $1 / \left(1 - \nu_1 \times \nu_1 \times \frac{E_2}{E_1} \right)$ for a ply.

Geometry:

n	Number of plies in plate.
h_k	Thickness of k -th layer.
θ_k	Angle of principal axis of orthotropy, x , of k -th layer measured from plate reference axis, 1.
m_n	Number of groups of layers having identical orientations.

10.12 Stress-strain relations for unidirectional plies

10.12.1 Fibre-oriented co-ordinate system

As the thickness of layers is small, they are assumed to be thin plates in a plane stress state.

The co-ordinate system is defined by the principal material directions, as shown in Figure 10.12.1.

Axes, 1-2, coincide with the longitudinal and transverse directions. This material symmetry is called 'orthotropic' and 'on axis'.

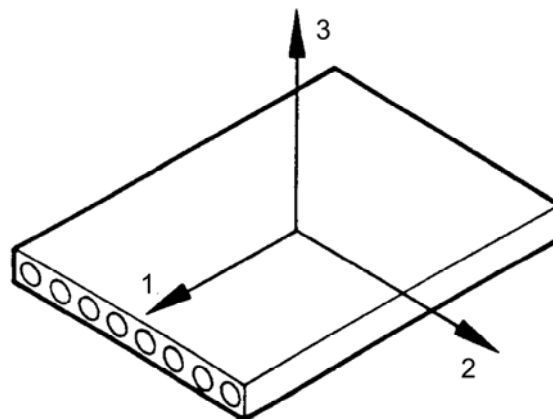


Figure 10.12-1 - Definition of the co-ordinate system for the analysis of unidirectional plies

10.13 On axis stress strain relations

10.13.1 General

The elastic properties of an orthotropic ply are defined, using matrix notation, by equations giving the compliance and modulus matrices.

[See also: 10.11 for notation]

10.13.2 Compliance matrix

$$\{\varepsilon_k\} = [S_k]\{\sigma\}_k \rightarrow \begin{bmatrix} \varepsilon_1 \\ \varepsilon_2 \\ \gamma_{12}_k \end{bmatrix} = \begin{bmatrix} S_{11} & S_{12} & 0 \\ S_{12} & S_{22} & 0 \\ 0 & 0 & S_{66}_k \end{bmatrix} \begin{bmatrix} \sigma_1 \\ \sigma_2 \\ \tau_{12}_k \end{bmatrix} \quad [10.13-1]$$

[Compliance matrix]

Where:

γ_{12} (shear strain) is determined by $(\partial u/\partial y + \partial v/\partial x)$.

$$S_{11} = \frac{1}{E_1}; S_{22} = \frac{1}{E_2}; S_{66} = \frac{1}{G_{12}}; S_{12} = -\frac{\nu_{12}}{E_1}$$

10.13.3 Modulus matrix

$$\{\sigma_k\} = [Q_k]\{\varepsilon\}_k \rightarrow \begin{bmatrix} \sigma_1 \\ \sigma_2 \\ \tau_{12}_k \end{bmatrix} = \begin{bmatrix} Q_{11} & Q_{12} & 0 \\ Q_{12} & Q_{22} & 0 \\ 0 & 0 & Q_{66}_k \end{bmatrix} \begin{bmatrix} \varepsilon_1 \\ \varepsilon_2 \\ \gamma_{12}_k \end{bmatrix} \quad [10.13-2]$$

[Modulus matrix]

Where:

$$Q_{11} = pE_1; Q_{22} = pE_2; Q_{66} = G_{12}; Q_{12} = p\nu_{12}E_2$$

10.13.4 Symmetry of compliance and modulus matrices

There are four independent elastic constants used to describe the behaviour of a thin UD layer. These constants are determined by experiment or from fibre and matrix properties using micromechanical formulae, [See: 10.4].

10.14 Stress-strain relations for a ply of arbitrary orientation

10.14.1 General

A UD unidirectional ply with principal material axes X and Y is defined with respect to an arbitrary system of axes 1 and 2 by the angle 1:X, as shown in Figure 10.14.1.

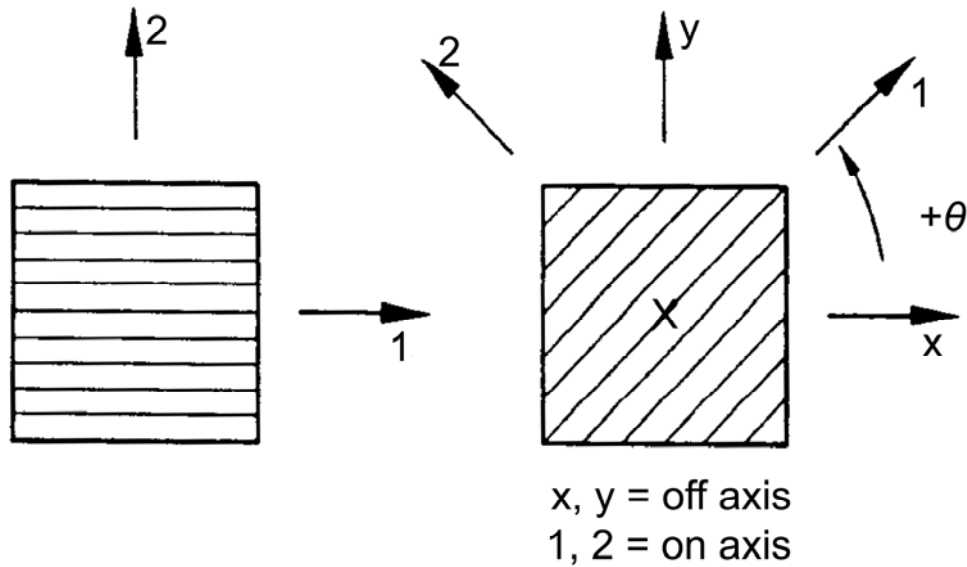


Figure 10.14-1 - Definition of axes

From elementary mechanics of materials, the transformation equations for stresses and strains are known to be:

$$\{\bar{\sigma}\}_k = [M]_k \{\sigma\}_k$$

$$\{\bar{\varepsilon}\}_k = ([M]^{-1})_k^T \{\varepsilon\}_k$$

$$[\bar{Q}]_k = [M]_k [Q]_k [M]_k^T$$

Where:

$$[M] = \begin{bmatrix} m^2 & n^2 & -2mn \\ n^2 & m^2 & 2mn \\ mn & -mn & m^2 - n^2 \end{bmatrix}$$

$$([M]^{-1})^T = \begin{bmatrix} m^2 & n^2 & -mn \\ n^2 & m^2 & mn \\ 2mn & -2mn & m^2 - n^2 \end{bmatrix}$$

With: $m = \cos \theta$; $n = \sin \theta$

10.14.2 Off axis stiffness of a unidirectional ply

The off axis stress strain relation is:

$$\{\bar{\sigma}\}_k = [\bar{Q}]_k \{\bar{\varepsilon}\}_k \rightarrow \begin{bmatrix} \sigma_x \\ \sigma_y \\ \tau_{xy} \end{bmatrix} = \begin{bmatrix} Q_{xx} & Q_{xy} & Q_{xS} \\ Q_{xy} & Q_{yy} & Q_{yS} \\ Q_{xS} & Q_{yS} & Q_{SS} \end{bmatrix} \begin{bmatrix} \varepsilon_x \\ \varepsilon_y \\ \gamma_{xy} \end{bmatrix} \quad [10.14-1]$$

The relationship between the components of the on axis and off axis stiffness matrix is:

$$\begin{bmatrix} Q_{xx} \\ Q_{yy} \\ Q_{xy} \\ Q_{SS} \\ Q_{xS} \\ Q_{yS} \end{bmatrix} = \begin{bmatrix} m^4 & n^4 & 2m^2n^2 & 4m^2n^2 \\ n^4 & m^4 & 2m^2n^2 & 4m^2n^2 \\ m^2n^2 & m^2n^2 & m^4+n^4 & -4m^2n^2 \\ m^2n^2 & m^2n^2 & -2m^2n^2 & (m^2-n^2)^2 \\ mn^3 & -mn^3 & mn^3-m^3n & 2(mn^3-m^3n) \\ mn^3 & -m^3n & m^3n-mn^3 & 2(m^3n-mn^3) \end{bmatrix} \begin{bmatrix} Q_{11} \\ Q_{22} \\ Q_{12} \\ Q_{66} \end{bmatrix} \quad [10.14-2]$$

These relationships are limited to transformation from the on axis orthotropic where shear coupling components are zero.

The off axis stress strain relation in terms of compliance is:

$$\begin{bmatrix} \varepsilon_x \\ \varepsilon_y \\ \varepsilon_s \end{bmatrix} = \begin{bmatrix} S_{11} & S_{12} & S_{1S} \\ S_{12} & S_{22} & S_{2S} \\ S_{1S} & S_{2S} & S_{SS} \end{bmatrix} \begin{bmatrix} \sigma_x \\ \sigma_y \\ \sigma_s \end{bmatrix} \quad [10.14-3]$$

Engineering constants are determined for on-axis load-displacement relationships only and not for off-axis.

In terms of compliance, applying the same steps gives:

$$\begin{bmatrix} S_{xx} \\ S_{yy} \\ S_{xy} \\ S_{ss} \\ S_{xs} \\ S_{ys} \end{bmatrix} = \begin{bmatrix} m^4 & n^4 & 2m^2n^2 & m^2n^2 \\ n^4 & m^4 & 2m^2n^2 & m^2n^2 \\ m^2n^2 & m^2n^2 & m^4+n^4 & -m^2n^2 \\ 4m^2n^2 & 4m^2n^2 & -8m^2n^2 & (m^2-n^2)^2 \\ 2m^3n & -2mn^3 & 2(mn^3-m^3n) & mn^3-m^3n \\ 2mn^3 & -2m^3n & 2(m^3n-mn^3) & m^3n-mn^3 \end{bmatrix} \begin{bmatrix} S_{11} \\ S_{22} \\ S_{12} \\ S_{66} \end{bmatrix} \quad [10.14-4]$$

All of the processes described up to this point are summarised as shown in Figure 10.14.2.

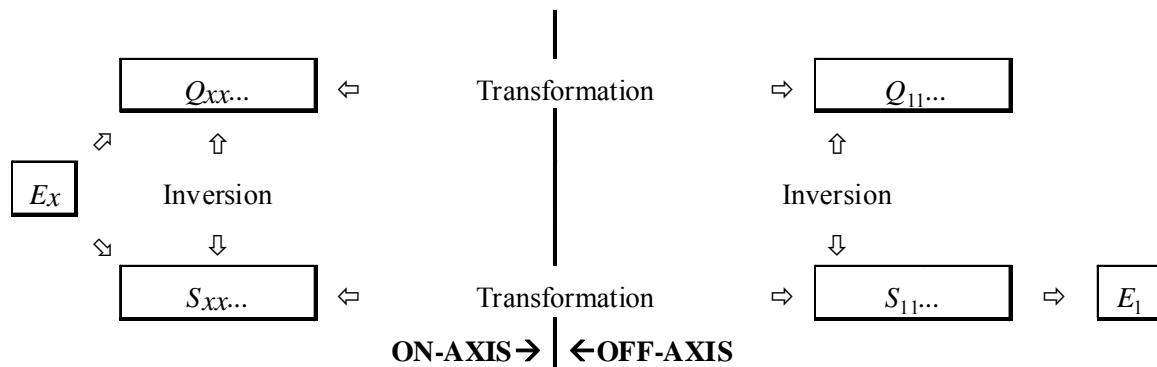


Figure 10.14-2 - Transformation of stiffness and compliance matrix

10.15 Stiffness matrix for a laminate

10.15.1 General laminates

The laminate is considered to be a thin structure of constant thickness t , consisting of n plies of thickness h_k ($k = 1, 2, \dots, n$).

Assuming that the elastic constants of a ply are not influenced by adjacent plies in the laminate, the stress strain relation for the k -th ply is:

$$\{\bar{\sigma}\}_k = [\bar{Q}]_k \{\bar{\varepsilon}\}_k \quad [10.15-1]$$

As usual in the theory of plates, forces and moments per unit length of the cross section of the laminate are shown in Figure 10.15.1 and defined by:

$$\begin{bmatrix} N_x \\ N_y \\ N_s \end{bmatrix} = \int_{-t/2}^{t/2} \begin{bmatrix} \sigma_x \\ \sigma_y \\ \sigma_s \end{bmatrix}_k dz = \sum_{k=1}^n \int_{z_{k-1}}^{z_k} \begin{bmatrix} \sigma_x \\ \sigma_y \\ \sigma_s \end{bmatrix}_k dz \quad [10.15-2]$$

And:

$$\begin{bmatrix} M_x \\ M_y \\ M_s \end{bmatrix} = \int_{-t/2}^{t/2} \begin{bmatrix} \sigma_x \\ \sigma_y \\ \sigma_s \end{bmatrix}_k z dz = \sum_{k=1}^n \int_{z_{k-1}}^{z_k} \begin{bmatrix} \sigma_x \\ \sigma_y \\ \sigma_s \end{bmatrix}_k z dz \quad [10.15-3]$$

$M_{xy} = M_s$ and $N_{xy} = N_s$ (given in Eq [10.15-2] and Eq [10.15-3])

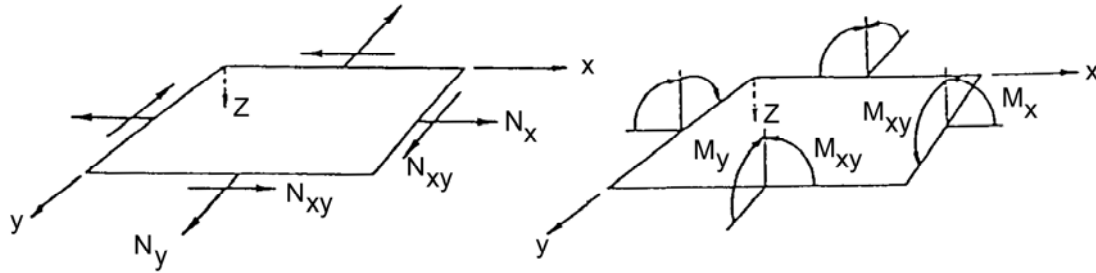


Figure 10.15-1 - In plane forces and moments

It is assumed that the plies are perfectly bonded; in consequence, discontinuities in the in-plane strains are not permitted at the interface of the plies.

The stress strain relationships for a laminate are:

$$\begin{bmatrix} N_x \\ N_y \\ N_{xy} \\ M_x \\ M_y \\ M_{xy} \end{bmatrix} \begin{bmatrix} A_{11} & A_{12} & A_{13} & B_{11} & B_{12} & B_{13} \\ & A_{22} & A_{23} & B_{12} & B_{22} & B_{23} \\ & & A_{33} & B_{13} & B_{23} & B_{33} \\ \hline & & & D_{11} & D_{12} & D_{13} \\ & & & & D_{22} & D_{23} \\ & & & & & D_{33} \end{bmatrix} = \begin{bmatrix} \varepsilon_1 \\ \varepsilon_2 \\ \varepsilon_s \\ \kappa_1 \\ \kappa_2 \\ \kappa_s \end{bmatrix} \quad \text{or} \quad \begin{bmatrix} N \\ M \end{bmatrix} = \begin{bmatrix} A & B \\ B & D \end{bmatrix} \begin{bmatrix} \varepsilon \\ \kappa \end{bmatrix} \quad [10.15-4]$$

Matrices A, B and D are defined by:

$$[A] = \sum_{k=1}^n [\bar{Q}]_k (z_k - z_{k-1})$$

Matrix of extensional stiffness

$$[B] = 1/2 \sum_{k=1}^n [\bar{Q}]_k (z_k^2 - z_{k-1}^2)$$

Matrix of coupling stiffness

$$[D] = 1/3 \sum_{k=1}^n [\bar{Q}]_k (z_k^3 - z_{k-1}^3)$$

Matrix of flexural stiffness

Where:

z_k is the higher level of k-th layer, and z_{k-1} the lower one, as shown in Figure 10.15.2.

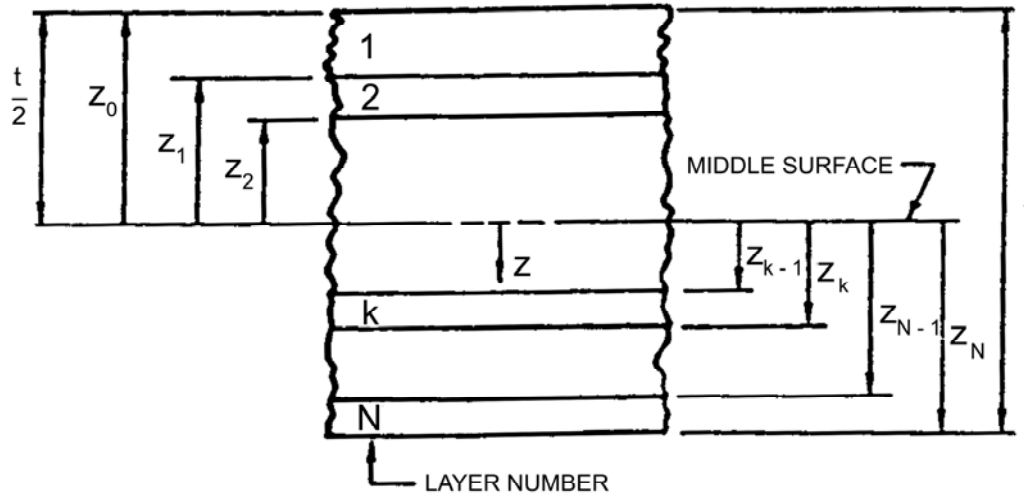


Figure 10.15-2 - Geometry of an n -layered laminate

10.15.2 Symmetric laminates

Bending and stretching problems can only be treated separately in the case of laminates which are symmetric in geometry and material properties; in that case $[B] = [0]$.

The stresses and strains in a laminate ply can be obtained by:

$$\begin{aligned} \{\bar{\varepsilon}\}_k &= \{\varepsilon\} + z\{\kappa\} & ; & \quad \{\varepsilon\}_k = [M]_k^T \{\bar{\varepsilon}\}_k \\ \{\bar{\sigma}\}_k &= [\bar{Q}]_k (\{\varepsilon\} + z\{\kappa\}) & ; & \quad \{\sigma\}_k = [M]_k^{-1} \{\bar{\sigma}\}_k \end{aligned}$$

10.15.3 Flow chart

Figure 10.15.3 shows a flow chart which summarises the steps taken in determining laminate properties.

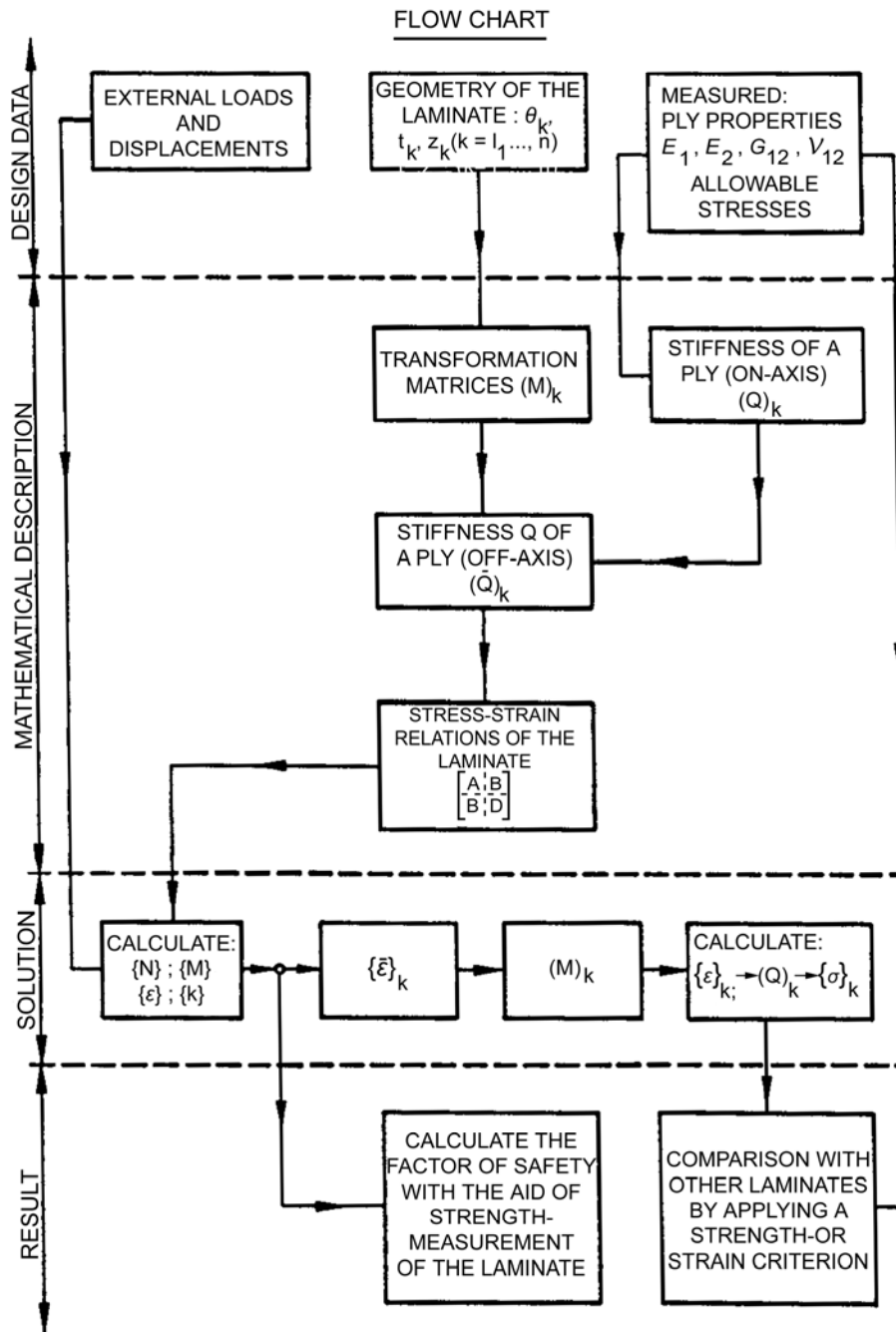


Figure 10.15-3 - Calculation of a laminate

10.16 Calculation methods with interlaminar stresses and strains

10.16.1 Calculation with free-edge stresses

Composites failure produces a large amount of interlaminar separation. Delamination between adjacent layers is induced by interlaminar stresses which can occur at free edges, such as borders, holes or cracks.

Figure 10.16.1 shows that, even in the case of uniaxial loading, individual layers show biaxial stressing. This arises from variations in stiffness, and transverse contraction of layers with different fibre directions. At the free edges of the composite, stress normal to the edge vanishes (to maintain equilibrium conditions). As a result, interlaminar stresses occur within the interface layers.

Figure 10.16.2 shows an example of interlaminar stresses and their decay between the different layers of a laminate. However, the stresses at the free edge are not realistic and cannot be applied in a failure criterion.

Analytical investigations have shown that the decrease of interlaminar stresses is significantly influenced by the stacking sequence. Therefore it can be useful to have criteria that enable the evaluation of the interlaminar strength of composites with different stacking sequences.

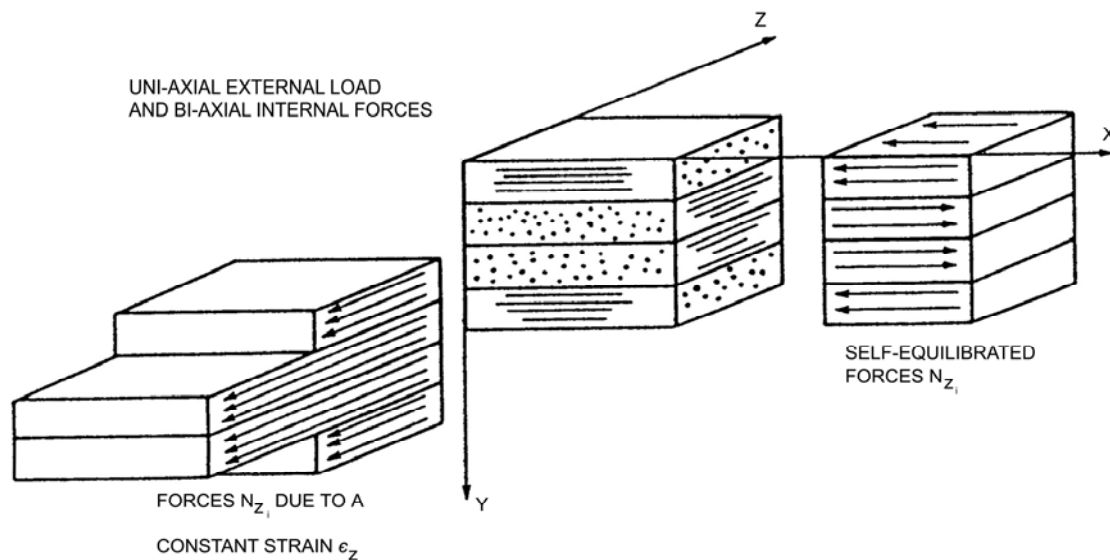


Figure 10.16-1 - Uniaxial loading of a composite

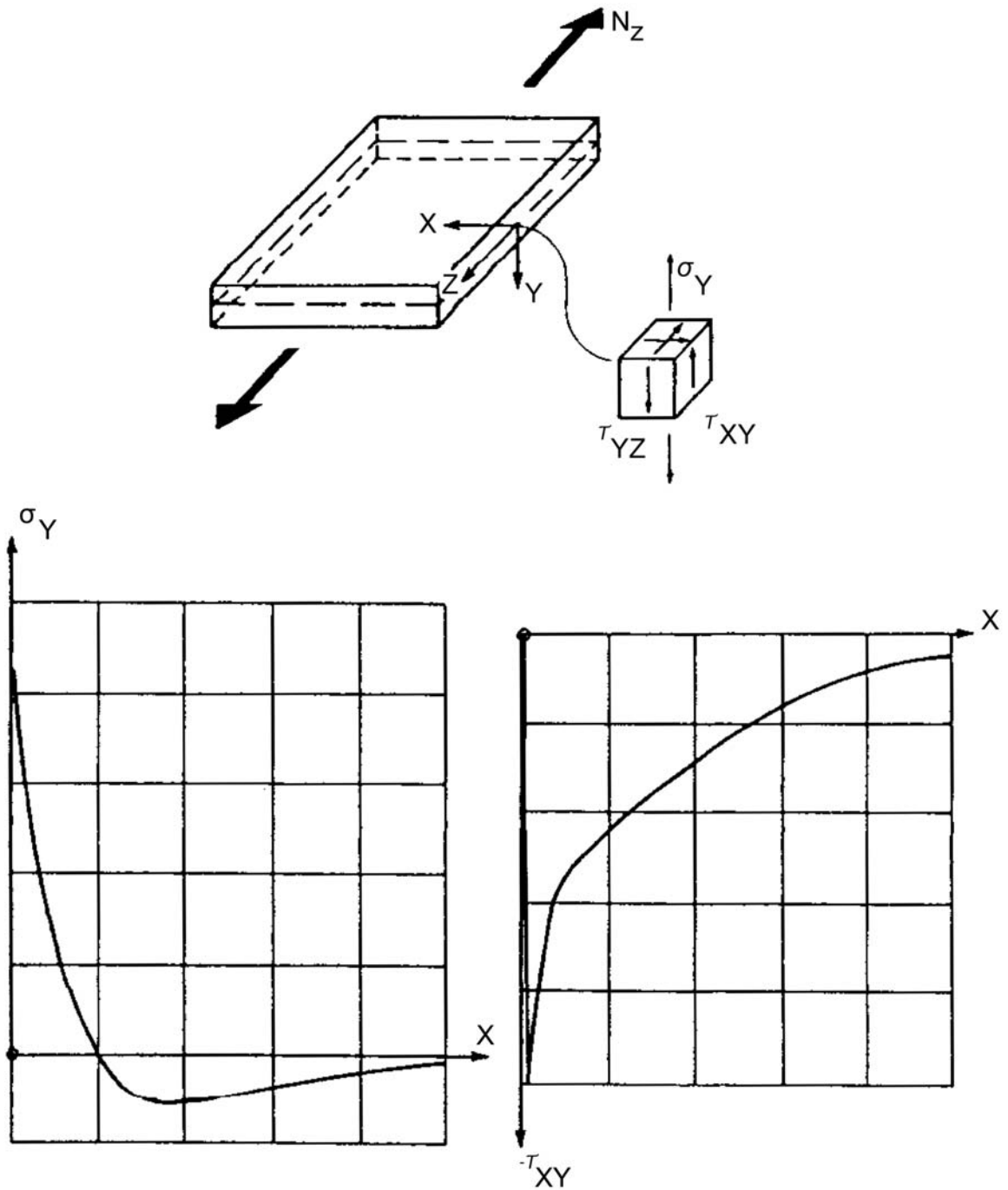


Figure 10.16-2 - Typical decrease of interlaminar stresses with high peaks near the edges

10.17 Qualitative evaluation of interlaminar strength for design purposes

10.17.1 General

Currently, no valid and verified failure criterion for interlaminar stresses exists. Therefore it is helpful to have data that enable the qualitative comparison of laminated plates with different stacking sequences in order to minimise the risk of delamination. Such data for the uniaxial load case are included from Ref. [10-9]. Figure 10.17.1 defines the load and fibre directions.

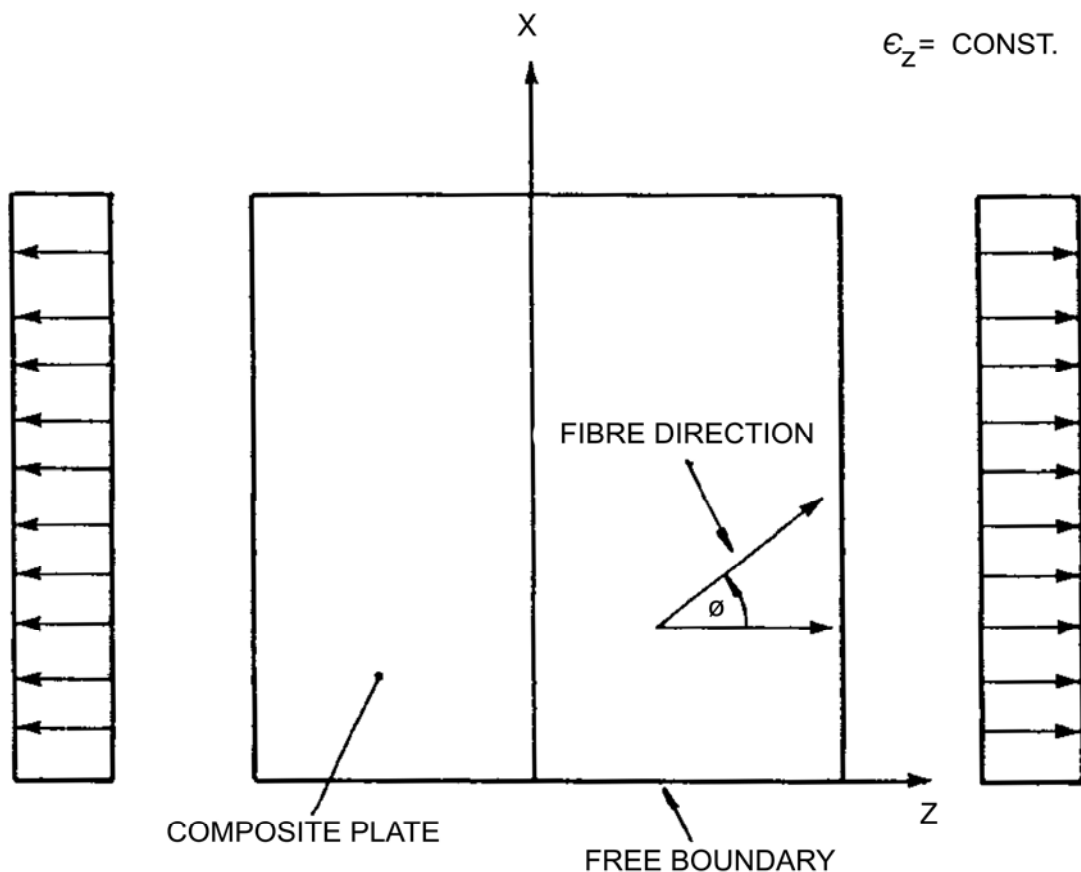


Figure 10.17-1 - External load on a composite plate

Characteristic data of the loaded laminate are combined as a parameter κ that is considered to be a relevant value for evaluation of strength:

$$\kappa = \frac{\Delta N f}{\ell} \frac{1}{E_1 \varepsilon_z} \quad [10.17-1]$$

Where the individual factors are defined as:

- f ; a factor taking into account the interaction between the three relevant interlaminar stresses, thus:

$$f = 1 + \left(\frac{\tau_{yz}}{\tau_{xy}} \right)^2 + \left(\frac{\sigma_y}{\sqrt{3}\tau_{xy}} \right)^2$$

at the location x_f , where x_f is defined by the relation:

$$\int_0^{x_f} \tau_{xy} dx = 0.5\Delta N$$

- ΔN ; the force flow is given by:

$$\int_0^{x \rightarrow \infty} \tau_{xy} dx = \Delta N$$

(τ_{xy} , τ_{yx} and σ_y are calculated by means of a finite element method or the transfer matrix model).

- $\bar{\ell}$; termed the characteristic decay length, with:

$$\int_0^{\bar{\ell}} \tau_{xy} dx = 0.9\Delta N$$

- $(E_1 \varepsilon_z)$ is the reference stress in order to form the non-dimensional parameter κ , where:
 - E_1 is the Young's modulus of a 0° layer in longitudinal direction.
 - ε_z the applied strain in load direction.
 - The term $(E_1 \varepsilon_z)$ is roughly the stress within the 0° layer of the laminate.

The function κ enables one to choose from several considered composites, those with favourable stacking sequences, i.e. those laminates which give low interlaminar stresses and reduce the risk of delamination.

A high value of κ relates to a high interlaminar loading, a small value implies small risk of delamination.

The calculation gives three groups of laminated plates that are investigated for their parameter κ , [See: Table 10.17.1]. UD material data are typical values for a 914 C/T300 laminate:

$$\frac{E_1}{E_2} = 15$$

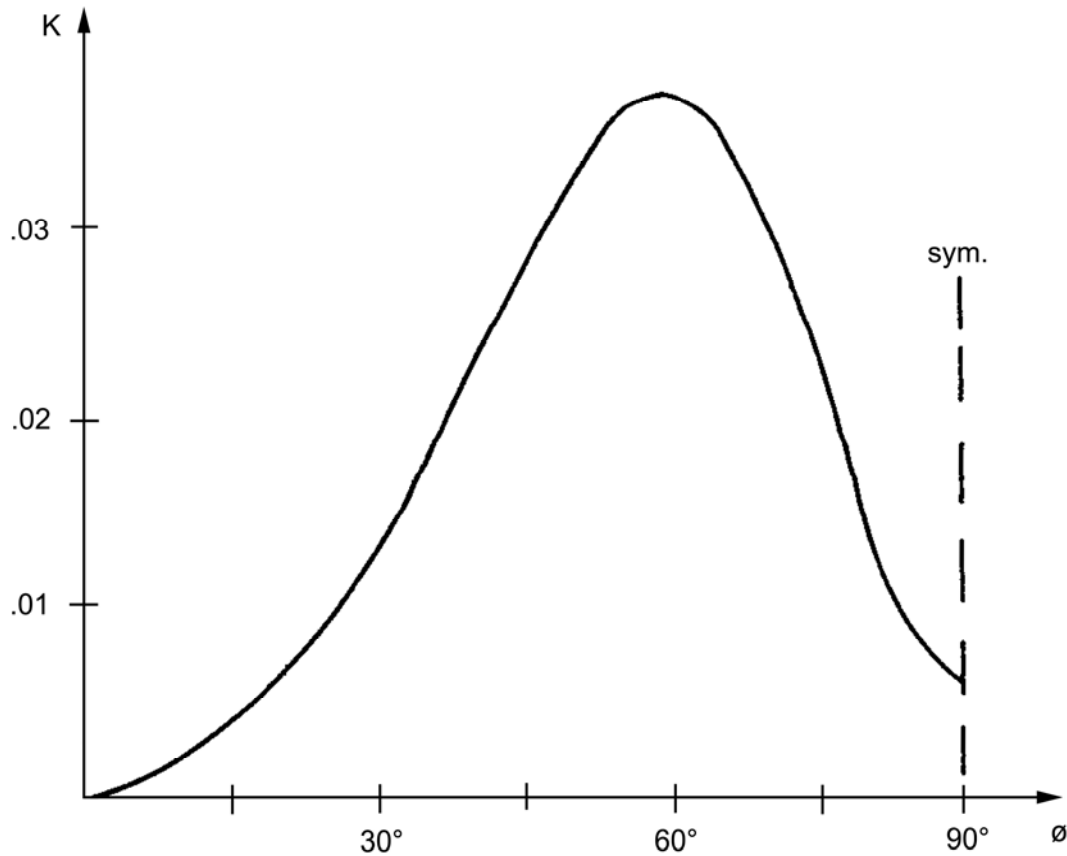
$$\frac{E_1}{G_{12}} = 25$$

$$\nu_{12} = 0.28$$

NOTE 1 = longitudinal, 2 = transverse.

10.17.2 Variation of fibre direction within a $[\pm\phi^\circ, 0^\circ, \pm\phi^\circ]$ laminate

The results for $\kappa = f(\phi)$ are given in Figure 10.17.2. The critical interfaces are those between the ϕ layer and a 0° layer.



Material: 914 C / T300

Figure 10.17-2 - Determination of the critical fibre direction

The results indicate that the most critical case for interlaminar separation occurs for $\phi = 60^\circ$ in a $[\pm\phi^\circ, 0^\circ, \pm\phi^\circ]$ laminate.

Interlaminar effects do not occur if $\phi = 0^\circ$ because the moduli are the same in each layer. The decay in the factor κ for $\phi > 60^\circ$ is mainly a result of decreasing induced forces ΔN . The maximum interaction factor f is 1.09. This suggests that the main stress that occurs as a result of uniaxial loading is the shear stress τ_{xy} within the plane transverse to load direction.

10.17.3 Variation of the thickness of the 0° layer within the $[\pm 30^\circ, 0n^\circ, \pm 30^\circ]$ laminate

Table 10.17.1 shows that this calculation gives three different laminates with the relating value κ between a 30° and a 0° layer:

Table 10.17-1 - Intralaminar stresses and strains: κ value for various stacking sequences

Stacking Sequence	κ
$[\pm 30^\circ, 0^\circ, \pm 30^\circ]$	0.0125
$[\pm 30^\circ, 0_2^\circ, \pm 30^\circ]$	0.0134
$[\pm 30^\circ, 0_3^\circ, \pm 30^\circ]$	0.0136

Owing to increasing ΔN and $\bar{\ell}$ with increasing number of 0° layers, the value of κ remains nearly constant. This result indicates that the risk of delamination does not become significantly greater if the number of 0° layers within this laminate changes.

10.17.4 Variation of the sequence of layers

A symmetric laminate with four 30° and two 0° layers enables three different stacking sequences, as shown in Table 10.17.2.

Table 10.17-2 - Intralaminar stresses and strains: κ value at interface for various stacking sequences

Stacking Sequence	κ at interface " \downarrow "
$[\pm 30^\circ, \downarrow 0^\circ]_s$	0.013
$[0^\circ, \downarrow \pm 30^\circ]_s$	-0.013
$[+ 30^\circ, 0^\circ, \downarrow - 30^\circ]_s$	-0.015

NOTE The minus sign of κ indicates a change in the direction of τ_{xy} and is not relevant for strength.

The results show the $[+30^\circ, 0^\circ, -30^\circ]_s$ laminate to be the most critical case.

10.18 References

10.18.1 General

- [10-1] R.M. Jones
'Mechanics of Composite Materials'
McGraw Hill, 1975
- [10-2] R. Förster & W. Knappe
'Experimentelle und theoretische Untersuchungen zur
Rißbildungsgrenze an zweischichtigen Wickelrohren aus GFK unter
Innendruck'
Kunststoffe, 61(8), 1971

-
- [10-3] H. Schneider
'Experimentelle und theoretische Betrachtungen zur Ermittlung von Elastizitätskenngrößen von CFK Laminaten'
DGLR Vortrag Nr. 81 058, Aachen, Mai 1981
- [10-4] A. Puck
'Zur Beanspruchung und Verformung von GFK - Mehrschichtenverbund Bauelementen'
Kunststoffe, 57(4), 1967
- [10-5] S. W. Tsai & H. T. Hahn
'Introduction to Composite Materials'
Technomic, 1980
- [10-6] Luftfahrttechnisches Handbuch
Handbuch Strukturberechnung (HSB)
Publisher: IABG Ottobrunn, Germany
- [10-7] J.E. Ashton, J.C. Halpin & P.H. Petit
'Primer on Composite Materials: Analysis'
Technomic, 1969
- [10-8] B. D. Agarwal & L. J. Broutman
'Analysis and Performance of Fibre Composites'
John Wiley and Sons, 1980
- [10-9] MBB/ERNO
Previously unpublished work by S. Dieker
Department RB514, 1984

11

Strength prediction and failure criteria

11.1 Introduction

11.1.1 Micro-mechanical strength models

11.1.1.1 Fibres

Similar fibres under load do not all have the same fracture strength neither do they fracture in the same place. A statistical analysis is necessary to rationally define the strength of a composite.

11.1.1.2 UD composites

Based on experimental observations of UD composite failure, statistical strength models have been developed for tension and compression in the fibre direction as well as for tension in the transverse direction, [See: 11.2; 11.3; 11.4].

The methods described are not yet adequate for definitive quantitative strength prediction, but they can be useful for an assessment of the relative merits of different materials, [See also: WWFE].

11.1.1.3 Laminate

The strength design verification (stability is another issue) for a laminate this is performed at different levels:

- Stress: at a local point in a material, by strength,
- Stress concentration: stress peak at a notch or a joint, by notched strength (Neuber),
- Stress intensity: at a delamination site, by fracture toughness.

11.1.2 Lamina failure models

11.1.2.1 Complex stressing

Design values for the ultimate strength in the axial and transverse directions, together with shear, are determined experimentally. However, experimental information of this type is not sufficient for the strength characterisation of single UD lamina because in most structural applications the material is subjected to complex stresses, i.e. stress components acting simultaneously in more than one direction. The stress components are described by three mutually perpendicular normal stresses and three shear stresses acting on an element. The problem for the designer is to predict failure under complex stresses using conventional uniaxial strength data.

11.1.2.2 Failure theories

Failure theories are mathematical functions that connect such strength data with the actual state of stress or strain to predict the failure of a structure under complex loading conditions. Numerous theories have been proposed, [See also: 11.8]. Also, reference is made to an extensive assessment initiated by Soden and Hinton, Ref. [11-16].

In a study lasting for 12 years, 'WWFE - worldwide failure exercise' considers 3D failure theories that include: failure conditions to assess multi-axial states of stress, non-linear stress-strain curves of UD material as input, and non-linear code in the structural analysis of the laminate.

The non-linear stress-strain curves have a hardening branch (from testing of 'isolated' test specimens, which break due to weakest-link behaviour) and a softening branch (due to the redundancy incorporating in-situ effects of the lamina material 'embedded' in the laminate).

Although issues of whether a model is right or wrong, true or untrue are considered to be outside the WWFE remit, guidelines for designers (from WWFE I) illustrate how some 'robust' models could be sufficient to describe all of the conditions that the 1st study considered, Ref. [11-37]. However, the results from WWFE I are only part of the overall story. The robustness of models is under continual assessment and evolution. An overview of the entire WWFE study is described, Ref. [11-38].

11.1.3 Failure criteria studies

11.1.3.1 ESA failure criteria study

An ESA-funded study provided detailed guidelines for the proper use of failure criteria during the different stages of design of spacecraft composite structures, for composites made of fibre-reinforced polymer or CMC ceramic materials, Ref. [11-18], [11-22].

[See: 64.5]

11.1.3.2 WWFE worldwide failure exercise

As part of WWFE, 19 theories were evaluated and a comparison made between accuracy and performance of predictions using several example cases. Advice is also provided on the use of various theories for engineering design, Ref. [11-17], [11-37]. The failure criteria employed in WWFE are intended to represent design methodologies capable of describing the modes of failure, failure locations, ultimate strengths and deformations up to ultimate fracture, Ref. [11-38].

11.1.4 Summary of World Wide Failure Exercise (WWFE)

11.1.4.1 WWFE I

Completed in 2004, WWFE I considered, Ref. [11-38]:

- Use of micro-mechanics for property prediction.
- Prediction of biaxial failure of a lamina in isolation.
- Prediction of 2D modes of failure.
- Prediction of failure envelopes for whole laminates.
- Matrix failure in tension, shear and compression.
- Material non-linearity.
- Post failure modelling under 2D stresses.
- Prediction of fibre failure.

Some of the conclusions of WWFE I, which instigated WWFE II and III, were, Ref. [11-37], [11-38]:

- Improvements in theories by identifying weaknesses:
 - 50% of theories were modified.
 - Theories, adopted for 40 years, modified for the first time.

Guidelines for designers on the accuracy and bounds of applicability for current failure theories.

Many modified theories now embedded in numerical software packages.

Revised definitions of failure, creating new insights.

Bringing together key members of the world community for discussion and argument to advance the science.

Ideas for designers and academics to further improve theoretical and practical areas.

Highlighting of gaps in experimental results.

Highlighting of some areas where a lack of fundamental knowledge exists.

11.1.4.2 WWFE II

WWFE II aims to, Ref. [11-38]:

- Extend the philosophy used previously to include 3D failure criteria.
- Resolve the gaps identified in WWFE I.
- Identify main workers on 3D failure criteria.
- Validate and benchmark their models.
- Identify any gaps in the current models.
- Identify specific shortfalls in experimental data or test results.
- Stimulate the composites community to provide better tools.
- Provide designers with guidance for predicting accurate strengths in 3D stress states.

It considers the particular points, Ref. [11-38]:

- Applicability of composite failure criteria for isotropic materials.
- Effects of pressure on shear strength and deformation of UD lamina.
- Failure of unidirectional lamina under hydrostatic pressure.
- Effect of through-thickness stress on biaxial failure of UD lamina.
- Effects of 3D stresses on the failure of multi-directional laminates.
- Deformation of laminates under hydrostatic pressure.
- 3D elastic constants of multidirectional laminates.
- Effects of lay-up on through-thickness strength of laminates.
- Failure of laminates under combined through-thickness and shear.

11.1.4.3 WWFE III

WWFE III is concerned with damage, fracture and continuum mechanics of composites and aims to, Ref. [11-38]:

- Extend the philosophy used previously to include damage, fracture and continuum mechanics models for composites.
- Solve the gaps identified in the first WWFE.
- Identify main workers on damage and fracture criteria.
- Validate and benchmark their models.
- Identify any gaps in the current models.
- Identify specific shortfalls in experimental data or test results.
- Stimulate the composites community to provide better tools.
- Provide designers with guidance for predicting damage, fracture and deformation in composites.

The specific issues covered include, Ref. [11-38]:

- Damage initiation and evolution.
- Matrix crack initiation and crack density evolution.
- Delamination initiation and propagation.
- Effects of ply thickness and constraints.
- Effects of ply stacking sequence.
- Cracking under thermal loading.
- Monotonic loading, unloading and reloading.
- Failure at stress concentrations (e.g. open hole).
- Statistical and probabilistic nature of failure.
- Leakage prediction.

11.2 Tensile strength of UD composites in fibre direction

11.2.1 General

The statistical tensile failure model takes into account the:

- Length strength relationship,
- Statistical variation of fibre strength, and
- Difference between the strength of the bundle and an average strength of the fibres.

Thus these models predict the strength of the composite by taking into consideration the in-situ fibre strength.

A Weibull distribution provides a good fit to experimental data:

$$f(\sigma) = La\beta\sigma^{(\beta-1)}e^{(-La\sigma^\beta)} \quad [11.2-1]$$

Where:

α and β are parameters to fit the experimental fibre tensile strength data, and L is the fibre length.

A summary is presented of some recent models, Ref. [11-19].

11.2.2 Weakest-link failure model

The weakest-link failure model assumes that the breakage of a single fibre results in localised stress concentrations, which cause fracture of adjacent fibres. In turn the failure of these fibres can affect further fibres and eventually leads to an overall failure. This model leads to a realistic failure prediction only in the case of small samples with fibres of a narrow dispersion of strength.

For practical materials in realistic structures, the strength predicted by the weakest-link failure model is too low.

11.2.3 Cumulative weakening failure model

If failure does not occur at the breakage of the weakest link, then the broken fibre causes a redistribution of stresses near the fracture, giving rise to the 'cumulative weakening failure model'.

Stress transfers from one end of the broken fibre, past the break, to the other. This stress transfer is achieved by high shear stresses in the matrix near the fibre break; as shown in Figure 11.2.1, Ref. [11-1].

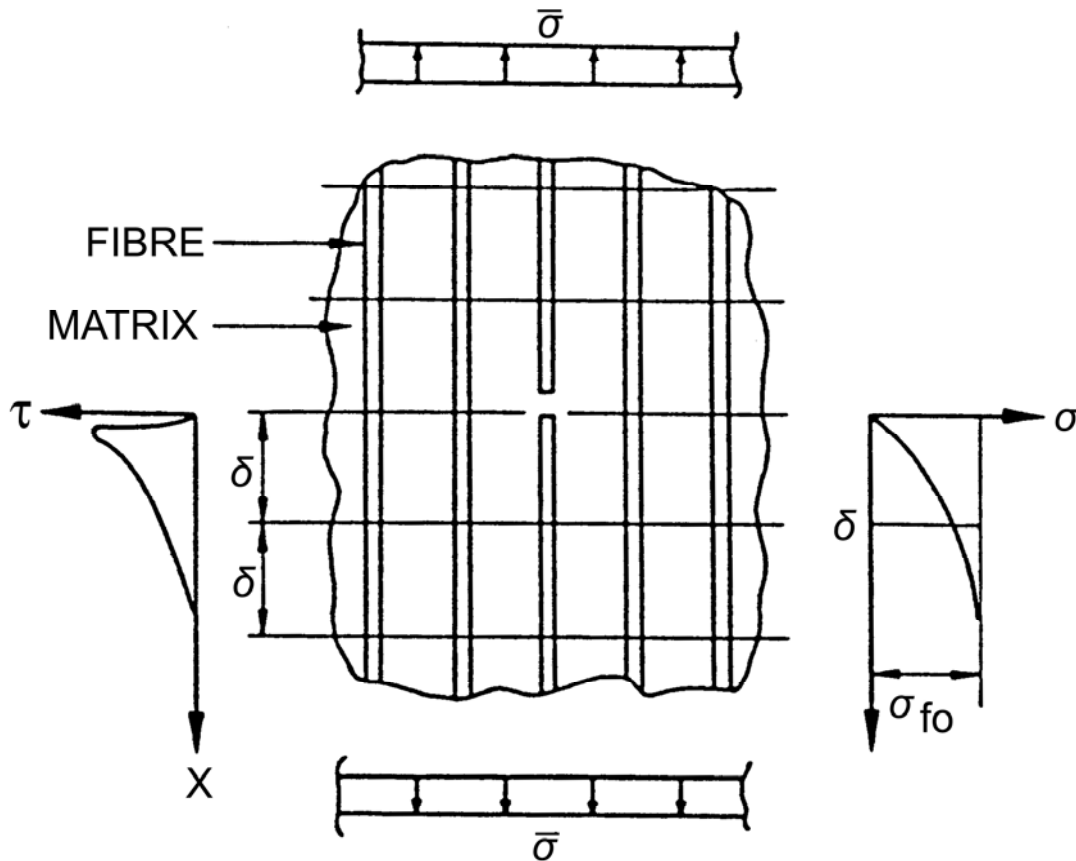


Figure 11.2-1 - Fibre reinforced composite: Tensile failure model

For an elastic fibre and a perfectly plastic matrix an estimate of the ineffective length δ is obtained by:

$$\delta = \sigma_f \frac{d_f}{4\tau_y} \quad [11.2-2]$$

Where:

σ_f is the fibre tensile strength, d_f is the fibre diameter, and τ_y is the matrix shear yield strength.

For fibres having a strength distribution as given in Eq [11.2-1], the cumulative weakening failure model estimates the composite tensile strength based on fibre area as:

$$\sigma^* = (\alpha\delta\beta e)^{(-1/\beta)} \quad [11.2-3]$$

11.2.4 Fibre break propagation model

The load concentration in fibres adjacent to a broken one increases the probability that one or more of them will also break. That leads to the 'fibre break propagation failure model', which states that the propagation of fibre breaks as the mechanism of failure.

The occurrence of the first fracture of an overstressed fibre is used as a failure criterion. This can provide good correlation with experimental data for small specimens, but it gives rather low strength values for large volumes of materials.

11.2.5 Cumulative group mode failure model

The 'cumulative group mode failure model' incorporates three effects:

- Variability of fibre strength results in distributed fractures well below the composite strength.
- Load concentrations in fibres adjacent to broken fibres influence the growth of the crack region to include additional fibres (fibre break propagation).
- High shear stresses in the vicinity of broken fibres cause matrix shear failure, which has a crack arresting effect. This can lead to groups of broken fibres.

This model can be viewed as a generalisation of the 'Cumulated Weakening Failure' model with chains of bundles instead of single fibres. For practical application the model is complicated by bundles of various sizes, where both the number of broken fibres in a bundle and the ineffective length of that bundle vary. Consequently, statistical parameters to describe the model are difficult to obtain.

11.2.6 Status of models

Although the statistical models described are not yet adequate for definite quantitative strength prediction, they can be useful to assess relative merits of different materials.

Equation [11.2-3] can be applied in connection with the ineffective length of Equation [11.2-2] to estimate the actual strength and to indicate the role of the properties of each constituent.

11.3 Compressive strength of UD composites in fibre direction

11.3.1 General

When fibre reinforced composites are subjected to compressive loads, the mode of failure appears to be fibre buckling.

In composites with very low fibre volume content, fibre buckling can occur even when the matrix stresses are in the elastic range. However, at practical volume fractions, ($V_f > 0.40$), fibre buckling is generally preceded by matrix yield and/or constituent debonding and matrix microcracking, Ref. [11-19].

Fibre buckling can also result from shrinkage stresses developed during curing of the composite. These are generated by the differential thermal coefficient of expansion of the matrix and fibres, [See: Chapter 12].

Two fibre buckling modes are possible, as shown in Figure 11.3.1.

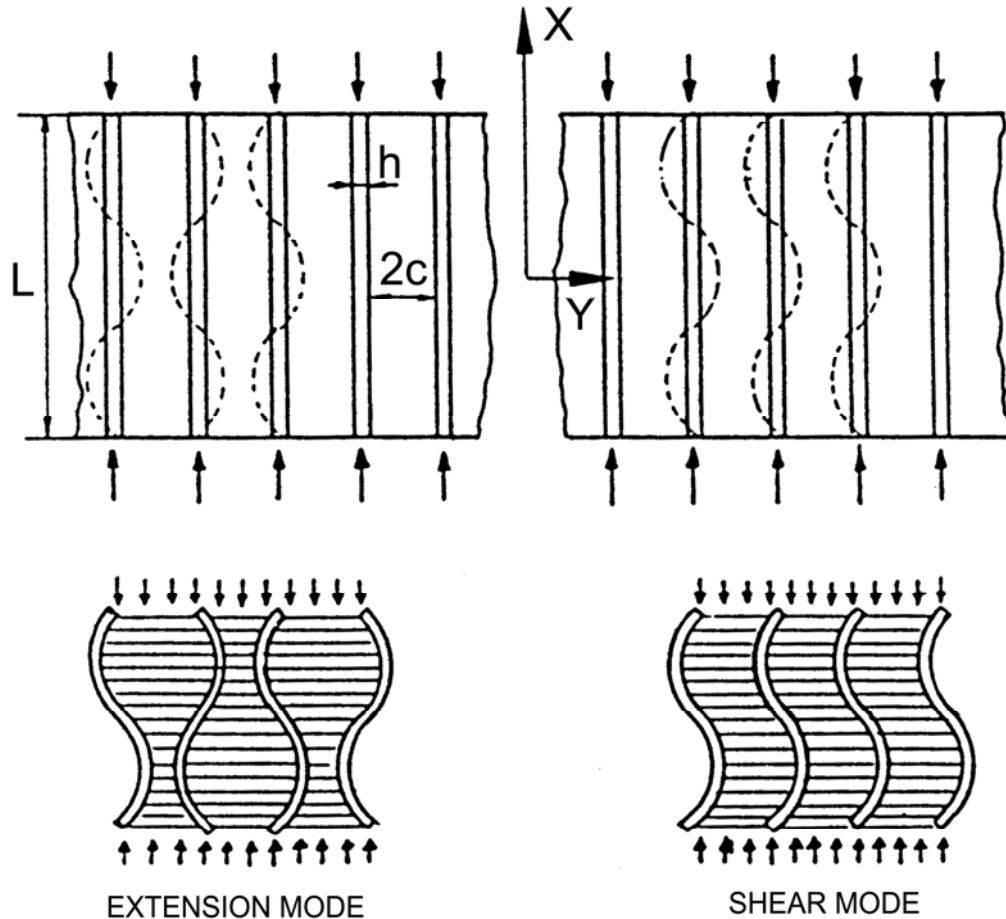


Figure 11.3-1 - Buckling modes of fibres under compression

11.3.2 Extension mode buckling

The adjacent fibres in a composite can buckle independently and out of phase relative to each other. The resulting strains in the matrix are predominantly extensional. The matrix alternately deforms in extension and compression, transverse to the fibres. This is called 'extension mode buckling', and is only possible when the inter-fibre distance is quite large, i.e. when the fibre volume fraction is very low.

11.3.3 Shear mode buckling

This buckling mode is more common and occurs at most practical fibre volume fractions. In this case the transverse deformation of adjacent fibres is in phase. The resulting strains in the matrix are predominantly shear strains; so therefore called 'shear mode buckling'.

11.3.4 Analysis of compression failure

11.3.4.1 General

For both buckling modes, the fibres are regarded as plates with thickness h separated by matrix $2c$ wide. Each fibre is subjected to a compressive load P and is of length L . The fibres are also regarded as being much stiffer than the matrix, i.e. $G_f \gg G_m$; so that fibre shearing deformations are negligible.

The analysis to determine the fibre buckling load in each mode is based on the Rosen theory. This equates the change in strain energy for the fibre and matrix to the work done by the fibre force during deformation to a buckled state.

11.3.4.2 Extension mode buckling

For extension mode buckling, the critical stress in the composite is:

$$\sigma_{c \max} = 2V_f \sqrt{\frac{V_f E_m E_f}{3(1-V_f)}} \quad [11.3-1]$$

11.3.4.3 Shear mode buckling

For shear mode buckling, the maximum composite stress is:

$$\sigma_{c \max} = \frac{G_m}{1-V_f} \quad [11.3-2]$$

Both of the composite stress expressions are shown in Figure 11.3.2 for a glass/epoxy composite, Ref. [11-3].

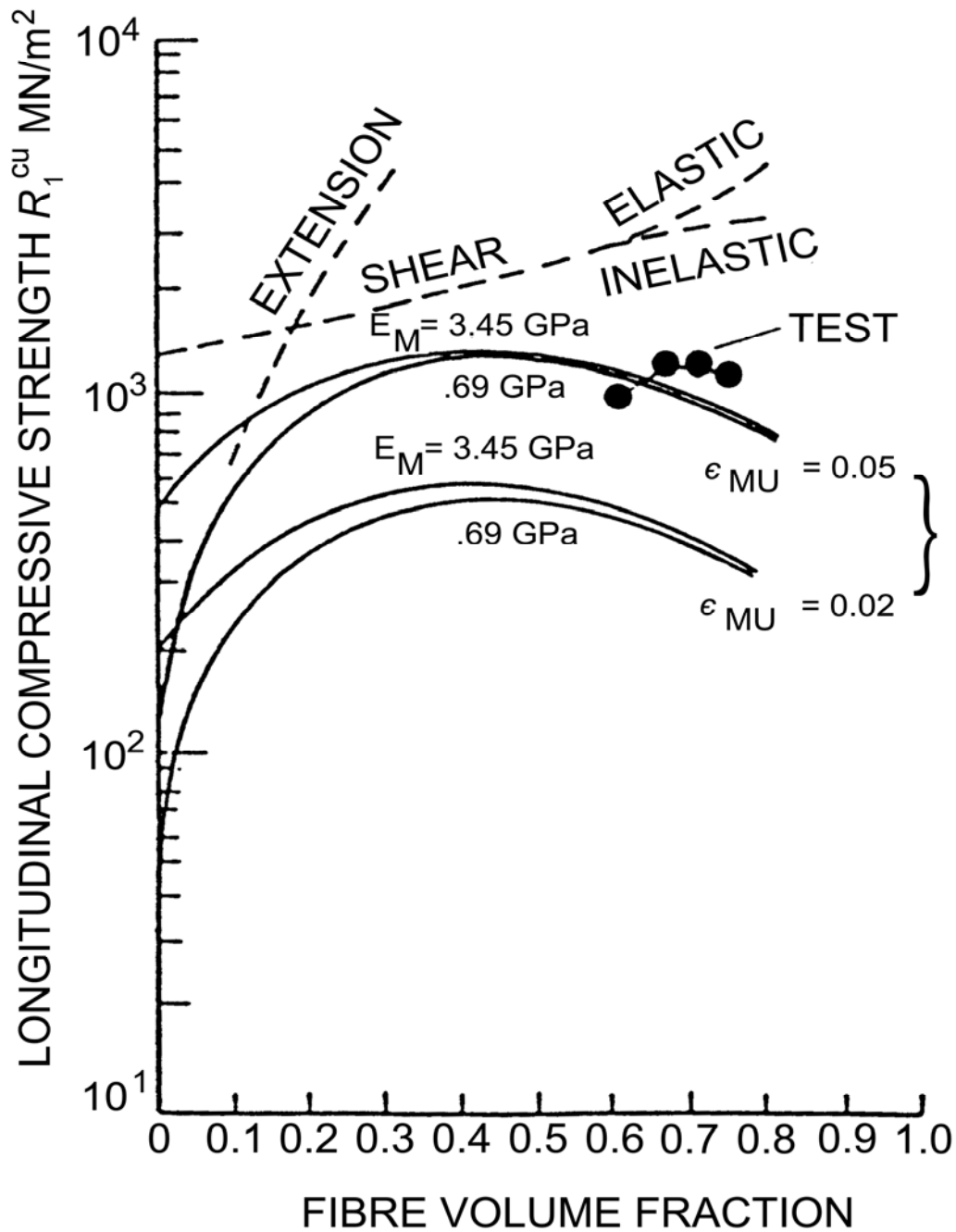


Figure 11.3-2 - Comparison of predicted and experimental values of longitudinal compressive strength

Eq [11.3-2] holds for a linear elastic matrix material. A more general result is obtained by modelling the matrix as an elastic, perfectly plastic material, Ref. [11-19]. The secant modulus value at each strain level can be assumed to govern the instability. These assumptions lead to:

$$\sigma_{c \max} = \sqrt{\frac{V_f E_f \sigma_y}{3(1-V_f)}} \quad [11.3-3]$$

where: σ_y is the matrix yield stress.

Shear mode buckling gives the lowest strength for composites over a wide range of fibre volume fractions (actual composites); transverse or extensional mode governs the composite strength for low fibre volume fractions only. However, Eq [11.3-2] predicts values much greater than those measured in practice. Initial fibre misalignment can be identified as a major reason for the discrepancy. This is taken care of by:

$$\sigma_{c \max} = \left(\frac{G_m}{1 + \Phi_0 / \gamma_y} \right) \quad [11.3-4]$$

where: Φ_0 is the fibre misalignment; γ_y is the composite shear yield strain.

In the literature the values given for Φ_0 are usually 2 to 3 degrees, and the compressive strengths predicted by means of Eq [11.3-3] agree well with experimental results, Ref. [11-20].

11.3.4.4 Debonding

The observation that transverse splitting or debonding is a possible initiating event can be formulated as a simple theoretical expression. This gives the maximum composite strength as:

$$\sigma_{c \max} = \frac{(E_f V_f + E_m V_m)(1 - V_f^{1/3}) \epsilon_{mu}}{V_f V_f + V_m V_m} \quad [11.3-5]$$

Where: ϵ_{mu} is the matrix ultimate strain.

The predicted strength is greatly influenced by the matrix ultimate strain and is also a maximum at a given fibre volume fraction.

11.4 Transverse tensile strength of UD composites

11.4.1 General

The longitudinal strength and stiffness are good because of the dominant role played by the fibres in this direction. Load is shared between the fibres and the matrix. However, because of their higher strength and stiffness, fibres carry a major portion of the load.

No such load sharing takes place when the composite is subjected to transverse loading. Instead, the matrix carries the load whilst the fibres act as stress concentrators, and composite failure occurs at a much lower strain than that of the unrestrained matrix. Therefore, unlike longitudinal strength and stiffness, and transverse modulus, the transverse strength is reduced by the presence of the fibres.

11.4.2 Prediction of transverse tensile strength

The transverse tensile strength of the composite, R_2^{tu} , is predicted on the assumption that it is controlled by the matrix ultimate strength σ_m^u . It is further assumed that the composite strength is lower than the matrix strength by a factor, S , known as the strength reduction factor.

Thus the composite transverse strength can be written as:

$$R_2^{tu} = \frac{\sigma_m^u}{S}, \text{ in terms of stresses,}$$

And:

$$\epsilon_2^{tu} = \frac{\epsilon_m^u}{S^1}, \text{ in terms of strains}$$

Where: S^1 is the strain magnification factor.

When Poisson's ratio effects are neglected, the equations for S and S^1 take the simplified forms:

$$S = \frac{1 - V_f \left[1 - \left(\frac{E_m}{E_f} \right) \right]}{1 - \left(4V_f / \pi \right)^{1/2} \left[1 - \left(\frac{E_m}{E_f} \right) \right]} \quad [11.4-1]$$

$$S^1 = \frac{1}{1 - \left(4V_f / \pi \right)^{1/2} \left[1 - \left(\frac{E_m}{E_f} \right) \right]} \quad [11.4-2]$$

Thus once S or S^1 is known, the transverse strength in terms of stresses or strains can be calculated.

11.4.3 Empirical analysis

A further empirical approach for the prediction of transverse tensile strength of fibrous composites is described by Nielsen, Ref. [11-4]. The composite strain to failure can be approximated as:

$$\epsilon_2^{tu} = \epsilon_{mB} \left(1 - V_f^{1/3} \right) \quad [11.4-3]$$

Where:

ϵ_2^{tu} ϵ_{cB} is the breaking strain of the composite transverse to the fibres.
 ϵ_{mB} is the matrix breaking strain.

If the matrix and composite have linear elastic stress strain curves, the Eq [11.4-3] can be stated, in terms of stress, as:

$$R_2^{tu} = \sigma_{mB} \frac{E_2}{E_m} (1 - V_f^{1/3}) \quad [11.4-4]$$

Where:

E_2 = transverse modulus of the composite.

E_m = matrix modulus.

Both Eq [11.4-3] and Eq [11.4-4] assume perfect adhesion between phases, with failure occurring by matrix fracture at or near the interface.

11.5 Static strength criteria for composites

Static strength criteria for composites use uniaxial strength data to specify the failure envelope under a complex state of stress.

A large number of criteria have been proposed, which in certain cases predict very different failure strengths. Only limited experimental data is available to judge the suitability of criteria, especially true for the compression-compression region, where the criteria show the largest differences. In this region experiments are extremely difficult to perform and available data should be used with caution.

The extensive WWFE assessment, Ref. [11-17], gives some indication of the strengths and weaknesses of a number of criteria. The WWFE I guidelines give useful information to designers when selecting an appropriate criterion in a given situation (only within the constraints of WWFE-I), Ref. [11-37]. It also makes obvious that none of the criteria is right or wrong, but are more or less suitable.

[See also: 11.1 for WWFE]

11.6 Analytical notation for static strength criteria for composites

11.6.1 Co-ordinate system

Figure 11.6.1 defines the notation co-ordinate system.

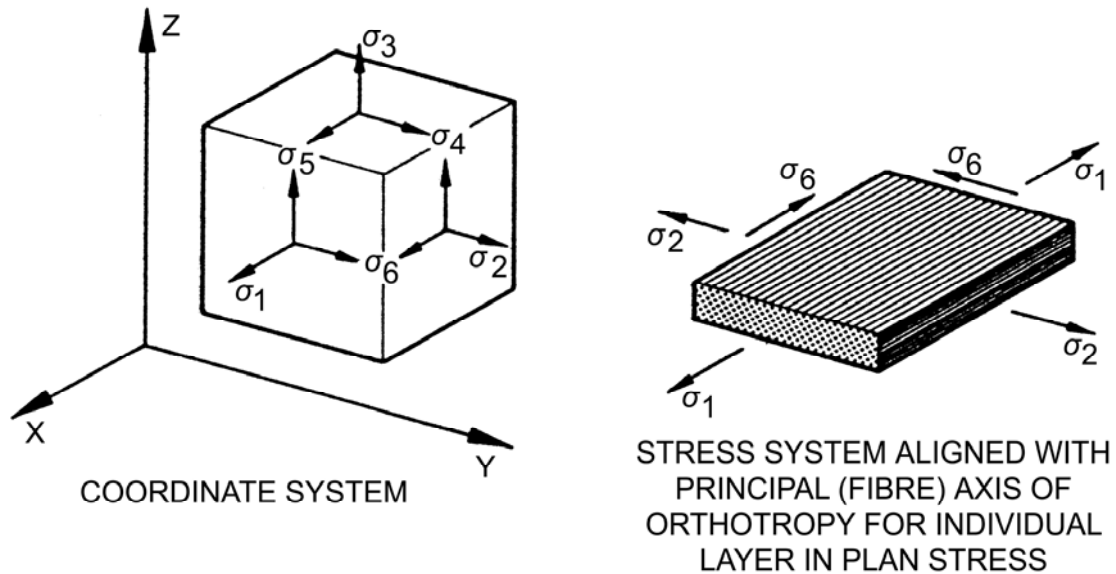


Figure 11.6-1 - Analytical notation: Co-ordinate system

11.6.2 Formulae

E_1, E_2 modulus of elasticity in 1- and 2-directions, respectively

$$E_1 = \frac{1}{S_{11}} \quad \text{and} \quad E_2 = \frac{1}{S_{22}}$$

G_{12} shear modulus, $G_{12} = \frac{1}{S_{66}}$

$S_{11}, S_{22}, S_{12}, S_{21}, S_{66}$, compliance of layer material. Note that $S_{12} = S_{21}$

R_{12}^{su} shear stress to failure of layer in 12-plane

R_1'' direct stress to failure in fibre direction

R_2'' direct stress to failure normal to fibre (in-plane)

ε strain

γ_{12}'' direct strain to failure in 12-plane

ε_1'' direct strain to failure in fibre direction

ε_2'' direct strain to failure normal to fibre (in-plane)

ν_{12} longitudinal Poisson's ratio, ratio of transverse (in plane) strain to longitudinal (fibre direction) strain due to an applied

longitudinal direct stress: $\nu_{12} = -\frac{S_{12}}{S_{11}}$

σ stress

σ_1	direct stress in fibre direction
σ_2	direct stress normal to fibre (in-plane)
τ_{12}	shear stress in 12-plane
1, 2, 3	co-ordinate notation, [See: Figure 11.6.1].

Subscripts:

c	compression
t	tension
s	shear
1, 2, 3	refer to co-ordinate system, [See: Figure 11.6.1].

Direct failure stresses are always positive, in tension as well as in compression.

11.7 Different types of failure criteria

11.7.1 General

A great many failure criteria for UD composites can be found in the open literature. In the context of this handbook, [See: 11.8], they are grouped as, Ref. [11-35]:

- Independent conditions:
 - Maximum stress.
 - Maximum strain.
- Interactive conditions – Pure interpolative conditions:
 - Tensor criteria.
 - Consideration of maximum strength in fibre direction.
- Interactive conditions - Physical considerations:
 - Hashin's failure criterion.
 - Puck's action plane failure criterion.
 - Simplified parabolic model.
 - Cuntze FMC-based UD failure criterion, Ref. [11-36].
 - Zinoviev's failure criterion (not described here).
 - Bogetti's failure criterion (not described here).
 - Tsai's failure criterion (not described here).

Topic 11.8 presents an up-to-date perspective of failure criteria compiled from more recent work, Ref. [11-17], [11-21], [11-35], [11-36], [11-37].

11.7.2 Evaluation studies

An ESTEC-funded study considered failure criteria for non-metallic materials; both FRP and CMC, Ref. [11-22].

[See also: 64.5]

In WWFE-I, the intention was to validate failure criteria at the 2D level, Ref [11-17], [11-37].

In the WWFE-II a test data platform is provided to validate 3D UD criteria. Various test cases are planned with carbon- and glass-fibre reinforced composites having different epoxy matrices and stacking sequences. The loading conditions include uni- and bi-axial tension and compression, torsion, shear and hydrostatic loading, and combinations thereof.

Note should also be taken of the reduced properties in the thickness direction, Ref. [11-36].

[See also: 11.1 - WWFE]

11.8 Overview - Failure criteria

11.8.1 Introduction

This overview was prepared by DLR in 2005, Ref. [11-35], to reflect the state of the art in failure criteria together with points arising from the on-going WWFE 'World-Wide Failure Exercise', Ref. [11-17], [11-37]. Cuntze's failure criterion was added in 2009, Ref. [11-36].

The criteria are limited to UD layers having ideal straight fibres. Misalignment and ondulation are not taken into account.

Some of the failure criteria in open literature are based on fracture mechanics aspects whereas others evaluate the local state of stress or strain; only the latter type is considered here.

These can be grouped further into:

- Independent conditions where single stress/strain components are checked against failure.
- Interactive conditions where several stress/strain components contribute to the effort to reach failure.

Within each group are a number of criteria, i.e.

- Independent conditions:
 - Maximum stress.
 - Maximum strain.
- Interactive conditions - Pure interpolative conditions:
 - Tensor criteria.
 - Consideration of maximum strength in fibre direction.

- Interactive conditions - Physical considerations:
 - Hashin's failure criterion.
 - Puck's action plane failure criterion.
 - Simplified parabolic model.
 - Cuntze's failure criterion.
 - Zinoviev's failure criterion (not described here).
 - Bogetti's failure criterion (not described here).
 - Tsai's failure criterion (not described here).

11.8.2 Independent conditions

11.8.2.1 Maximum stress

The criterion states that failure occurs as soon as a stress component in the principal material direction reaches the respective strength. In the case of plane stress, this is:

$$\begin{aligned}
 & \sigma_1 = X_t \text{ or } -X_c \\
 \text{or } & \sigma_2 = Y_t \text{ or } -Y_c \\
 \text{or } & |\sigma_6| = Q
 \end{aligned}
 \tag{11.8-1}$$

11.8.2.2 Maximum strain

The criterion is similar to the maximum stress criterion, except that strains are limited rather than stresses, with:

$\varepsilon_{X_t} (\varepsilon_{X_c})$ = maximum tensile (compressive) direct strain in fibre direction

$\varepsilon_{Y_t} (\varepsilon_{Y_c})$ = maximum tensile (compressive) direct strain in transverse direction

ε_Q = maximum shear strain in the 1-2 plane

Failure is predicted if:

$$\begin{aligned}
 & \varepsilon_1 = \varepsilon_{X_t} \text{ or } -\varepsilon_{X_c} \\
 \text{or } & \varepsilon_2 = \varepsilon_{Y_t} \text{ or } -\varepsilon_{Y_c} \\
 \text{or } & |\varepsilon_6| = \varepsilon_Q
 \end{aligned}
 \tag{11.8-2}$$

This is not identical to the maximum stress criterion. For linear elasticity and a plane state of stress the criterion can be reformulated in terms of stresses, resulting in:

$$\begin{aligned}
 & \sigma_1 - \nu_{12}\sigma_2 = X_t \text{ or } -X_c \\
 \text{or } & \sigma_2 - \nu_{12}\sigma_1 = Y_t \text{ or } -Y_c \\
 \text{or } & |\sigma_6| = Q
 \end{aligned}
 \tag{11.8-3}$$

11.8.3 Interactive conditions – Pure interpolative conditions

11.8.3.1 General

In most cases the state of stress in a structure consists of more than just one component. Interpolative conditions assume that there is an interaction between the stress components at the analysed point, contributing in some way to the effort to reach failure.

11.8.3.2 Tensor criteria

A general criterion for anisotropic material is a tensor polynomial written in stresses, usually truncated after the quadratic term:

$$\sum_{i=1}^6 \left[B_i \sigma_i + \sum_{j=1}^6 A_{ij} \sigma_i \sigma_j \right] = 1
 \tag{11.8-4}$$

Where A_{ij} and B_i are material constants.

For a plane state of stress aligned with the principal axes of orthotropy, the general expression is reduced to:

$$A_{11}\sigma_1^2 + 2A_{12}\sigma_1\sigma_2 + A_{22}\sigma_2^2 + A_{66}\sigma_6^2 + B_1\sigma_1 + B_2\sigma_2 = 1
 \tag{11.8-5}$$

Terms containing shear stresses linearly are omitted since shear stress reversal does not affect the strength. With special assumptions and additional conditions Equation [11.8-3] produces many of the established criteria. Substituting the direct and shear failure stresses produces five linear equations:

$$\begin{aligned}
 A_{11} &= \frac{1}{X_t X_c} & B_1 &= \frac{1}{X_t} - \frac{1}{X_c} \\
 A_{22} &= \frac{1}{Y_t Y_c} & B_2 &= \frac{1}{Y_t} - \frac{1}{Y_c} \\
 A_{66} &= \frac{1}{Q^2}
 \end{aligned}
 \tag{11.8-6}$$

Additional biaxial tests are needed for determining the remaining interaction term A_{12} . Since they are difficult to perform, various values have been proposed instead.

Among these are:

$$A_{12} = \frac{-0.5}{X_t X_c} \quad (\text{Hoffman})$$

$$A_{12} = \frac{-0.25}{X_t X_c} \quad (\text{DeTeresa/Larsen, Ref. [11-23]})$$

$$A_{12} = \frac{-0.5}{\sqrt{X_t X_c Y_t Y_c}} \quad (\text{Tsai/Hahn})$$

$$A_{12} = 0 \quad (\text{Tsai/Wu})$$

11.8.3.3 Consideration of maximum strength in fibre direction

With $A_{12} \neq 0$ the tensor criterion predicts strength values which can be much higher than X_t or X_c , respectively. In order to avoid such unrealistic results Ref. [11-24] limits the tensor criterion by the conditions for fibre failure:

$$\sigma_1^2 = X_t^2 \quad \sigma_1^2 = X_c^2 \tag{11.8-7}$$

By differentiating between fibre failure and inter-fibre failure, a more physically based criterion is derived.

11.8.4 Interactive conditions - Physical considerations

11.8.4.1 Hashin's failure criterion

For UD material the failure criterion should be invariant under any rotation around the fibre direction. Based on this, Hashin, Ref. [11-25], uses four stress invariants to determine failure limits that are different in tension and compression, in the fibre direction as well as the transverse direction. Under plane stress conditions, these are:

Tensile fibre mode ($\sigma_1 > 0$)

$$\frac{\sigma_1^2}{X_t^2} + \frac{\sigma_6^2}{Q^2} = 1$$

Compressive fibre mode ($\sigma_1 < 0$)

$$\frac{\sigma_1^2}{X_c^2} = 1$$

Tensile matrix mode ($\sigma_2 > 0$)

$$\frac{\sigma_2^2}{Y_t^2} + \frac{\sigma_6^2}{Q^2} = 1$$

Compressive matrix mode ($\sigma_2 < 0$)

$$\left(\frac{Y_c^2}{4Q_{23}^2} - 1 \right) \frac{\sigma_2^2}{Y_c^2} + \frac{\sigma_2^2}{4Q_{23}^2} + \frac{\sigma_6^2}{Q^2} = 1$$

Where Q_{23} is the shear stress to failure in the 23 direction.

11.8.4.2 Puck's action plane failure criterion

In recent publications in connection with the WWFE 'World-Wide Failure Exercise', Puck and Schürmann, Ref. [11-26], proposed conditions for fibre failure (FF) and for inter-fibre failure (IFF).

The FF criterion is based on the assumption that the fibre stress σ_{f1} at failure is the same for a uniaxial as well as for a plane state of stress:

$$\frac{1}{X_t} \left(\sigma_1 - \nu_{12} \sigma_2 + \nu_{f12} \frac{E_1}{E_{f1}} m_{of} \sigma_2 \right) = 1 \quad \text{for } (...) > 0$$

$$\frac{1}{X_c} \left(\sigma_1 - \nu_{12} \sigma_2 + \nu_{f12} \frac{E_1}{E_{f1}} m_{of} \sigma_2 \right) = -1 \quad \text{for } (...) < 0$$

Where:

E_{f1} = Young's modulus of the fibre;

ν_{f1} = Poisson's ratio of the fibre.

The factor m_{of} accounts for slightly higher stresses σ_2 in the fibres than in the matrix (glass fibres $m_{of} \approx 1.3$; carbon fibres $m_{of} \approx 1.1$).

IFF is caused by σ_2 and σ_6 alone. The criterion distinguishes three different failure modes:

Mode A:

$$\sqrt{\left(\frac{1}{Y_t} - \frac{p_{\perp}^{(+)}}{Q} \right)^2 \sigma_2^2 + \frac{\sigma_6^2}{Q^2} + p_{\perp}^{(+)} \frac{\sigma_2}{Q}} = f_w$$

for $\sigma_2 \geq 0$; fracture plane angle $\theta_{fp} = 0^\circ$

Mode B:

$$\frac{1}{Q} \sqrt{\sigma_6^2 + \left(p_{\perp}^{(-)} \sigma_2 \right)^2} + p_{\perp}^{(-)} \sigma_2 = f_w$$

for $\sigma_2 < 0$ and $0 \leq \left| \frac{\sigma_2}{\sigma_6} \right| \leq \frac{R_{\perp}^A}{|\sigma_{6c}|}$; fracture plane angle $\theta_{fp} = 0^\circ$

Mode C:

$$\left[\left(\frac{\sigma_6}{2(1+p_{\perp\perp}^{(-)})Q} \right)^2 + \left(\frac{\sigma_2}{Y_c} \right)^2 \right] \frac{Y_c}{(-\sigma_2)} = f_w$$

$$\text{for } \sigma_2 < 0 \text{ and } 0 \leq \frac{|\sigma_6|}{\sigma_2} \leq \frac{|\sigma_{6c}|}{R_{\perp\perp}^A}; \text{ fracture plane angle } \theta_{fp} = \sqrt{\frac{f_w R_{\perp\perp}^A}{(-\sigma_2)}}$$

Evaluating these conditions needs the two tangents to the (σ_2, σ_6) -curve at $\sigma_2 = 0$:

$$p_{\perp\perp}^{(+)} = - \left(\frac{d\sigma_6}{d\sigma_2} \right)_{\sigma_2=0} \quad \text{for } \sigma_2 \geq 0 \quad \text{and} \quad p_{\perp\perp}^{(-)} = - \left(\frac{d\sigma_6}{d\sigma_2} \right)_{\sigma_2=0} \quad \text{for } \sigma_2 \leq 0.$$

These inclination parameters are determined from fracture curves for different load combinations. Typical values for thermosetting matrix as provided by Puck et al, Ref. [11-27], are:

$$\text{For GFRP:} \quad p_{\perp\perp}^{(+)} = 0.3 \quad p_{\perp\perp}^{(-)} = 0.25$$

$$\text{For CFRP:} \quad p_{\perp\perp}^{(+)} = 0.35; \quad p_{\perp\perp}^{(-)} = 0.3$$

$$R_{\perp\perp}^A = \frac{Q}{2p_{\perp\perp}^{(-)}} \left(\sqrt{1 + 2p_{\perp\perp}^{(-)} \frac{Y_c}{Q}} - 1 \right)$$

$$p_{\perp\perp}^{(-)} = p_{\perp\perp}^{(-)} \frac{R_{\perp\perp}^A}{Q}$$

$$\sigma_{6c} = Q \sqrt{1 + 2p_{\perp\perp}^{(-)}}$$

The weakening factor f_w takes care of the reduced IFF strength due to premature breakage of single fibres. If test results are missing, the expression used is:

$$f_w = 1 - \left(\frac{\sigma_1}{\sigma_{1d}} \right)^n$$

where $\sigma_{1d} \approx 1.1X_t$ or $-1.1X_c$ for tensile or compressive stresses respectively and $n = 8$ or $n = 6$ for matrices with high or low fracture strain.

11.8.4.3 Simplified parabolic model

Puck's model can be simplified by specifying only one inclination parameter, p , which has some stability advantages. A corresponding criterion based on the work of Jeltsch-Fricker, Ref. [11-28], was presented by Cuntze et al, Ref. [11-29].

11.8.4.4 Cuntze FMC-based UD failure criterion

A global failure condition, i.e. $F(\{\sigma\}, \{R\}) = 1$, has a single condition representing the failure surface for all failure modes, hence the interaction between several failure modes is mathematically fixed. Mode failure conditions, $F(\{\sigma\}, R^{mode}) = 1$, have a separate failure condition for each mode (as used in the Cuntze FMC 'Failure Mode Concept').

a. For UD material the 3D ply stress vector is:

$$\{\sigma\} = (\sigma_1, \sigma_2, \sigma_3, \tau_{23}, \tau_{31}, \tau_{21})^T$$

and the strength vector:

b. With average strength properties applied in the stress-strain analysis and strength design allowables (minimum values according to MIL-HDBK 5, no bar over R), for strength analysis (design verification):

$$R'_{\parallel} (= X^t), R^c_{\parallel} (= X^c), R'_{\perp} (= Y^t), R^c_{\perp} (= Y^c), R_{\perp\parallel} (= S)$$

This notation is in accordance with the German guideline VDI 2014, Ref. [11-33].

Stress-strain analysis gives the average (typical) structural response which is best when utilising 50% values. Therefore, average physical properties are used, including an average stress-strain curve and a \bar{R} value.

According to material symmetry requirements, transversely-isotropic UD material has 5 elasticity properties, 5 strengths, and 5 failure modes. Each failure mode is dominated by one strength.

For generally orthotropic fabric material this number is 9. If the warp reinforcement equals the fill (weft) reinforcement the reduced number of failure modes is 6.

Therefore, the FMC employs 5 failure modes in the UD material case and either 9 or 6 failure modes in the orthotropic case. Whether the ply can be modelled as a transversely-isotropic material or as an orthotropic material should be established.

For UD material, the 5 (brittle fracture) failure modes consist of 2 FF (Fibre-Failure) and 3 IFF (Inter-Fibre-Failure) modes.

These failure conditions are defined in Figure 11.8.1. The superscripts σ and τ indicate either normal or shear stress dominated failure. Strength and elasticity properties are shown as symbols to avoid confusion.

$$\text{FF1} \rightarrow F_{\parallel}^{\sigma}$$

$$\text{FF2} \rightarrow F_{\parallel}^{\tau}$$

$$\text{IFF1} \rightarrow F_{\perp}^{\sigma}$$

$$\text{IFF2} \rightarrow F_{\perp}^{\tau}$$

$$\text{IFF3} \rightarrow F_{\perp\parallel}$$

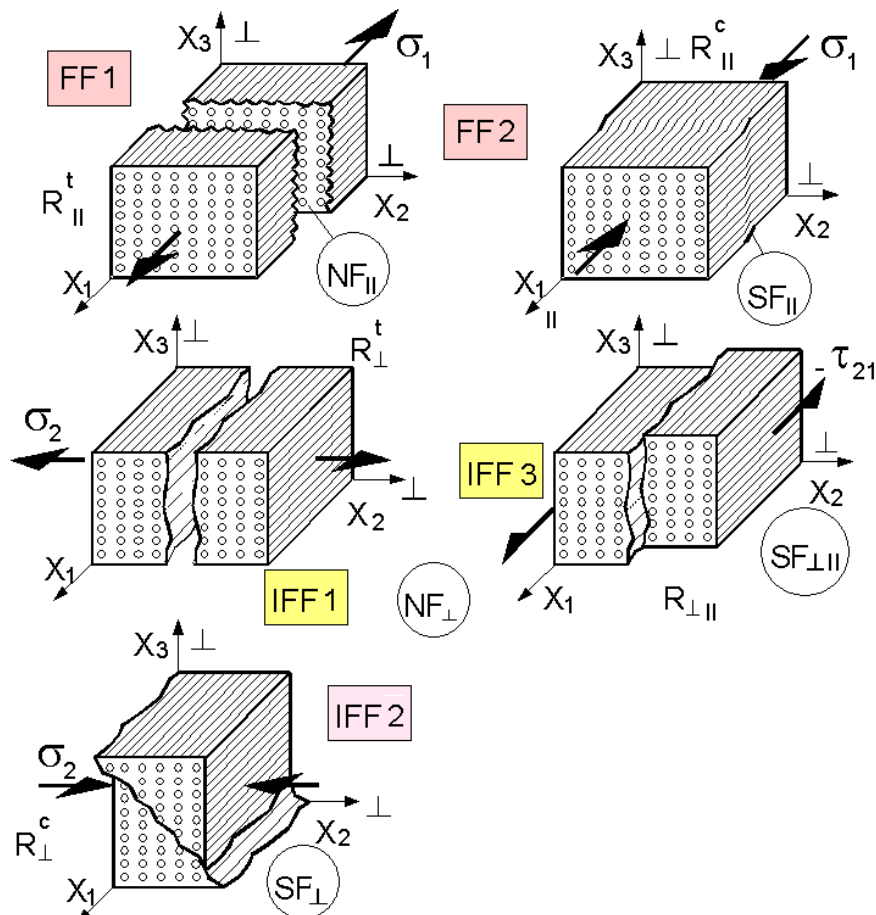


Figure 11.8-1 – Cuntze failure criteria - Schematic diagram of failure modes in transversely-isotropic UD material

Each failure mode is characterised by one strength and therefore, for a non-isotropic material, an equivalent stress exists for each of the 5 failure modes:

$$\{\sigma_{eq}^{mod e}\} = (\sigma_{eq}^{\parallel\sigma}, \sigma_{eq}^{\parallel\tau}, \sigma_{eq}^{\perp\sigma}, \sigma_{eq}^{\perp\tau}, \sigma_{eq}^{\perp\perp})^T$$

In practice ‘Material Stress Effort’ gives a better estimate of the remaining load-carrying capacity of the ply material. This is linked to the equivalent mode stress:

$$Eff^{mode} = \sigma_{eq}^{mode} / R^{mode}$$

Only ‘Material Stress Effort’ is applicable in non-linear strength analysis, not the material reserve factor (this is permitted only for linear analysis where stress is proportional to load, [See also: Puck’s criterion]).

FF1 (tension) and FF2 (compression) are more accurately termed ‘filament modes’ because in the case of bi-axially lateral compression the filament can break in tension due to the Poisson’s effect without any applied axial stress. Replacing σ_1 in the 3D case, shown below, enables FEA macro-stress level to be used instead of micro-mechanical filament stress.

The IFF modes, also termed ‘matrix modes’, IFF1 (lateral tension) and IFF3 (shear) are relatively benign failure modes. However, the σ_2 -dependent wedge failure IFF2 (lateral compression) of an embedded lamina can also lead directly to final failure, Ref. [11-39], [11-40], [11-41], because it can cause delamination of the stacked laminate.

3D case UD mode failure conditions

Where: $Eff^{mode} = 100\% = 1$ for mode failure

$$FF1 \quad Eff^{\parallel\sigma} = \sigma_1 / \bar{R}_{\parallel}^t = \sigma_{eq}^{\parallel\sigma} / R_{\parallel}^t \quad \text{with} \quad \sigma_1 \cong \varepsilon_1^t E_{\parallel}$$

$$FF2 \quad Eff^{\parallel\tau} = -\sigma_1 / \bar{R}_{\parallel}^c = +\sigma_{eq}^{\parallel\tau} / \bar{R}_{\parallel}^c \quad \text{with} \quad \sigma_1 \cong \varepsilon_1^c E_{\parallel},$$

$$IFF1 \quad Eff^{\perp\sigma} = [(\sigma_2 + \sigma_3) + \sqrt{\sigma_2^2 - 2\sigma_2\sigma_3 + \sigma_3^2 + 4\tau_{23}^2}] / 2\bar{R}_{\perp}^t = \sigma_{eq}^{\perp\sigma} / \bar{R}_{\perp}^t,$$

$$IFF2 \quad Eff^{\perp\tau} = [(b_{\perp}^{\tau} - 1)(\sigma_2 + \sigma_3) + b_{\perp}^{\tau} \sqrt{\sigma_2^2 - 2\sigma_2\sigma_3 + \sigma_3^2 + 4\tau_{23}^2}] / \bar{R}_{\perp}^c = +\sigma_{eq}^{\perp\tau} / \bar{R}_{\perp}^c,$$

$$IFF3 \quad Eff^{\perp\parallel} = \{ [b_{\perp\parallel} I_{23-5} + (\sqrt{b_{\perp\parallel}^2 I_{23-5}^2 + 4\bar{R}_{\perp\parallel}^2 (\tau_{31}^2 + \tau_{21}^2)}) / (2\bar{R}_{\perp\parallel}^3)] \}^{0.5}$$

$$\text{With: } I_{23-5} = 2\sigma_2\tau_{21}^2 + 2\sigma_3\tau_{31}^2 + 4\tau_{23}\tau_{31}\tau_{21}.$$

These stresses include the non-linearly load-dependent stresses $\{\sigma\}_L$ and the equally non-linear residual stresses $\{\sigma\}_R$. Curing of a thick wall generally results in higher residual stresses than thin walls. Delamination conditions are also taken into account in these equations.

Determination of the two FMC-based friction parameters from test results is demonstrated in Ref. [11-31]. Bounds for typical epoxy-based GFRP, CFRP and AFRP are: $0.1 < b_{\perp\parallel} < 0.45$ and $1.0 < b_{\perp}^{\tau} < 1.6$.

For pre-dimensioning, a value of $(b_{\perp}^{\tau} - 1) = 0$ is advisable.

2D case UD mode failure conditions:

$$Eff_{\parallel}^{\sigma} = \frac{\sigma_1}{\bar{R}_{\parallel}^{\sigma}}$$

$$Eff_{\parallel}^{\tau} = \frac{-\sigma_1}{\bar{R}_{\parallel}^{\tau}}$$

$$Eff_{\perp}^{\sigma} = \frac{\sigma_2}{\bar{R}_{\perp}^{\sigma}}$$

$$Eff_{\perp}^{\tau} = \frac{-\sigma_2}{\bar{R}_{\perp}^{\tau}}$$

$$Eff_{\perp\parallel} = \frac{|\tau_{21}|}{\bar{R}_{\perp\parallel} - \mu_{\perp\parallel} \sigma_2}$$

The friction coefficient $\mu_{\perp\parallel}$ in the simplified 2D Mohr-Coulomb formula corresponds to $b_{\perp\parallel}$, Ref. [11-31]. It can be estimated from a typical fracture point according to:

$$\mu_{\perp\parallel} = (\bar{R}_{\perp\parallel} - \tau_{21}^{fracture}) / \sigma_2^{fracture}$$

Failure mode interaction

Where: Eff = 100% = 1 for pseudo-global failure.

The FMC generates a phenomenological 3D lamina stress-based engineering approach for the derivation of failure conditions. It addresses the mechanics (physics) in the pure failure mode domains and applies simple probabilistic methods in the transition (interaction) zones of the failure modes, hence again producing a relationship which appears as a 'global failure surface'.

The probabilistic, theory-based, rounding-off of the failure modes in the transition domains uses a series failure system model:

$$Eff^m = (Eff^{\text{mode } 1})^m + (Eff^{\text{mode } 2})^m + \dots = 1$$

with the (global) stress effort Eff and the mode material stress efforts Eff^{mode} contributing each participating failure mode, representing the actual portion of the 'load'-carrying capacity of the material, and with the (Weibull-related) interaction coefficient m .

In practice a maximum of 3 of the 5 failure modes interact. The interaction formula is:

$$Eff^m = (Eff_{\parallel}^{\sigma})^m + (Eff_{\parallel}^{\tau})^m + (Eff_{\perp}^{\sigma})^m + (Eff_{\perp}^{\tau})^m + (Eff_{\perp\parallel})^m = 1$$

showing again a single failure equation with an interaction exponent:

$2.5 < m < 3$ (the lower value being safer)

Remarks on applicability

- The application of Cuntze FMC to transversely-isotropic UD material was successful. The validation of the failure conditions by the WWFE-I test data was satisfied after re-evaluation of the provided (sometimes contradictory) static test data base.
- If the z-thread density is not too high and if the fibres remain straight, the UD failure conditions above can also be applied to non-crimp fabrics and axially weft-knitted composites.
- A good mapping of CFRP, GFRP and UD-tape based C/C materials, Ref. [11-34], was achieved
- In contrast to global criteria, the utilised interaction procedure does not take into account that a change in one independent (pure) failure mode regime has an effect on another mode.
- The application of Cuntze FMC to orthotropic fabrics is possible, as shown Figure 11.8.2, for predicted failure curves of CMC (C-C/SiC) laminae.

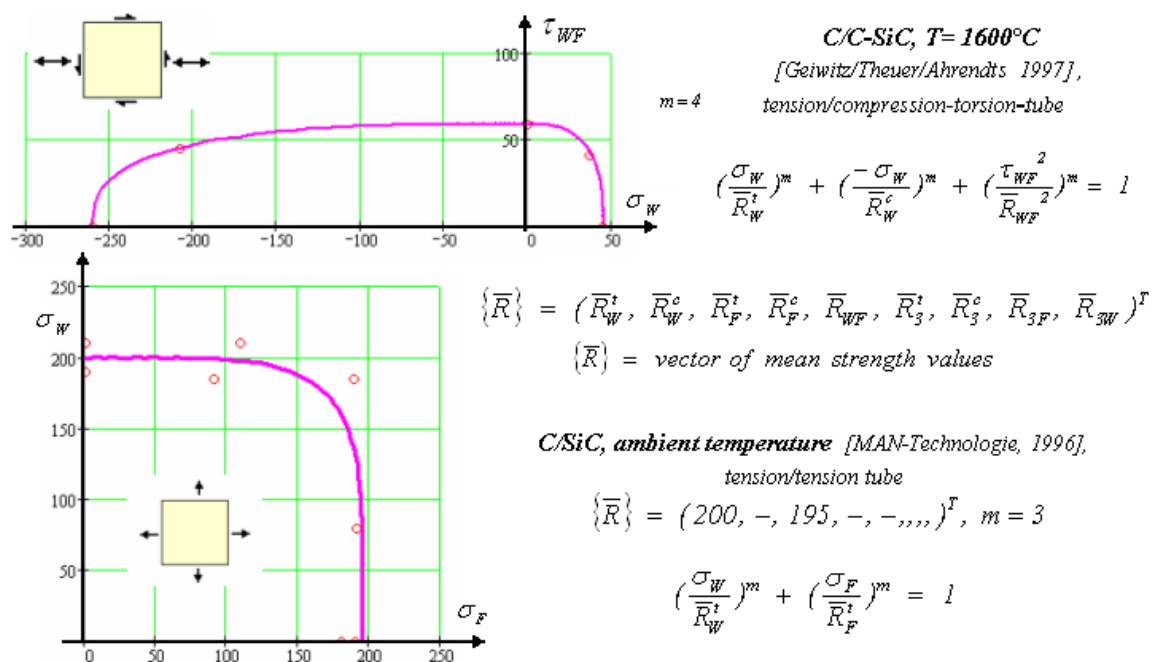


Figure 11.8-2 – Cuntze failure criteria – Notation and formulae for fabric failure conditions

11.8.4.5 Other failure criterion

According to the WWFE ‘World-Wide Failure Exercise’, Ref. [11-17], [11-38], criteria that also provide good results are:

- Zinoviev’s failure criterion.
- Bogetti’s failure criterion.
- Tsai’s failure criterion.

[See also: 64.5 for failure criteria for CMC’s]

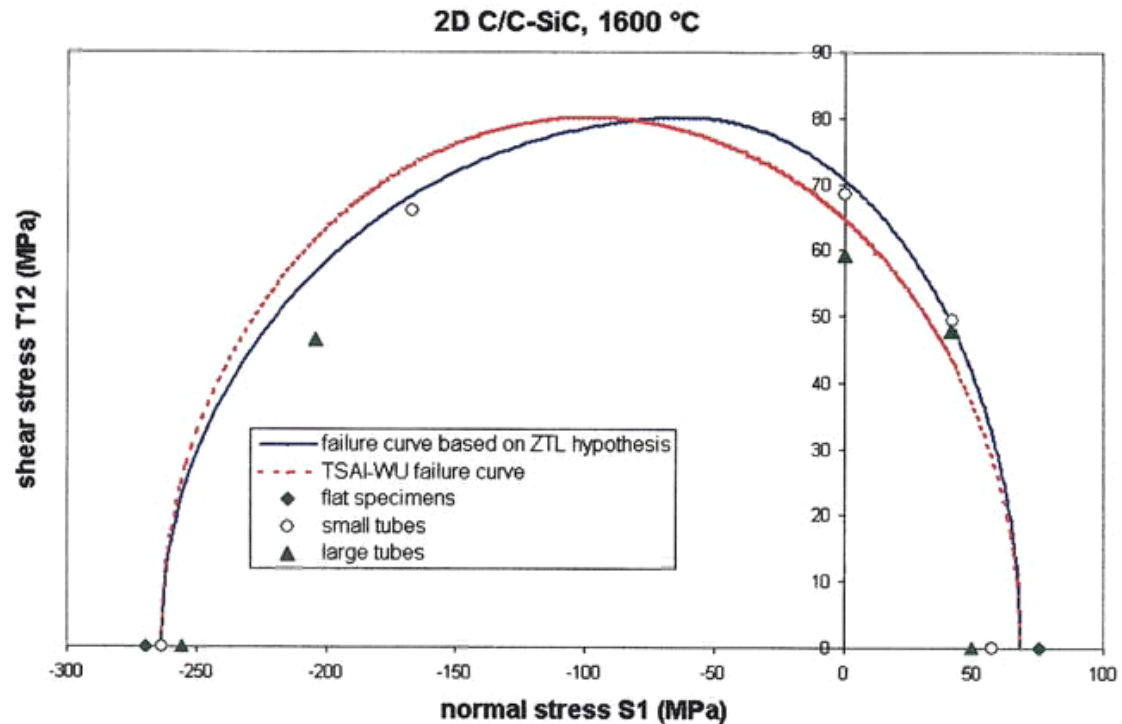


Figure 11.8-3 – Comparison between predicted failure curves for C-C/SiC composites with experimental data

11.9 Comparison between test data and various failure criteria

11.9.1 Effects on failure mode

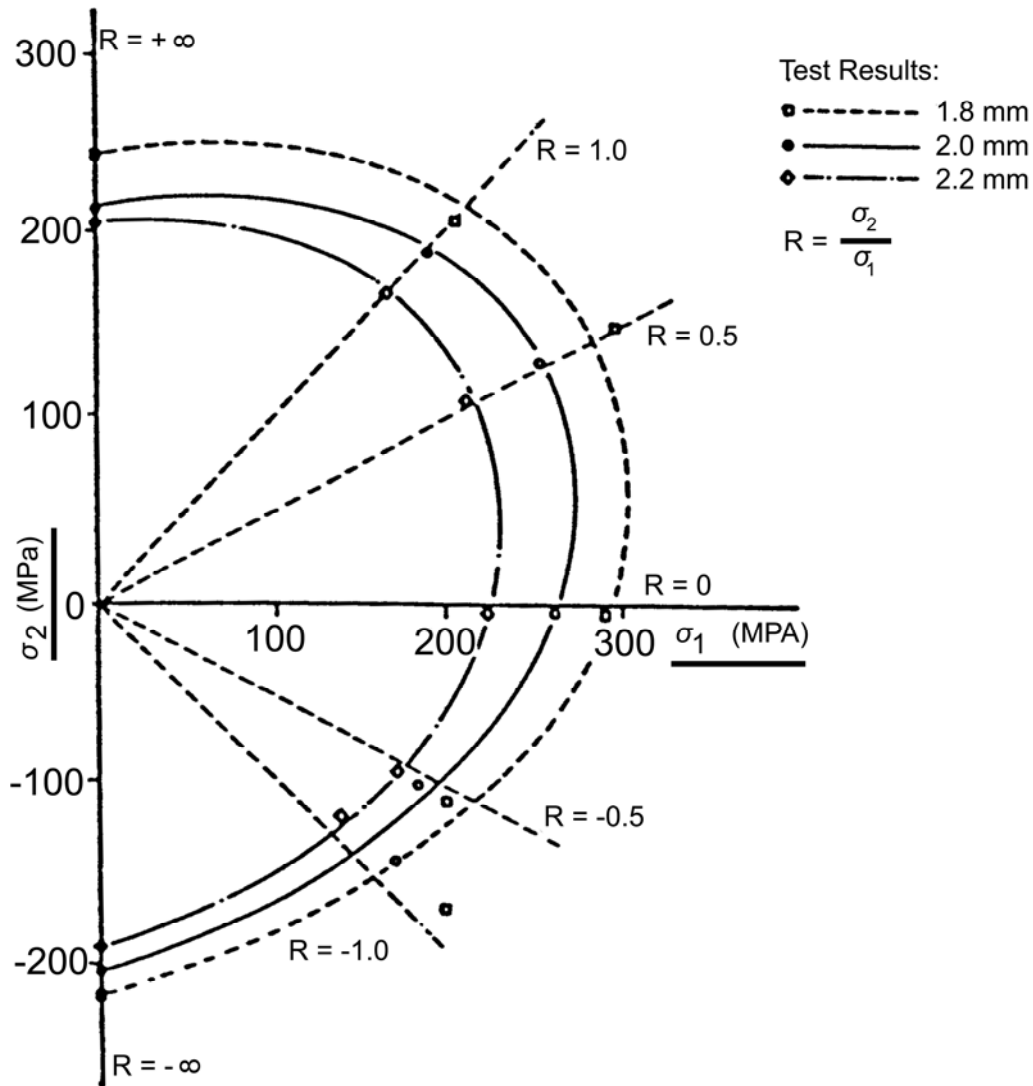
The results of tube tests using glass fabric-reinforced polyester resins are shown for, Ref. [11-7]:

- Variations in thickness in Figure 11.9.1
- Static and dynamic loading in Figure 11.9.2
- Static strength in Figure 11.9.3

These illustrate the various effects on failure mode, Ref. [11-7].

It can be shown that the failure mode depends on the:

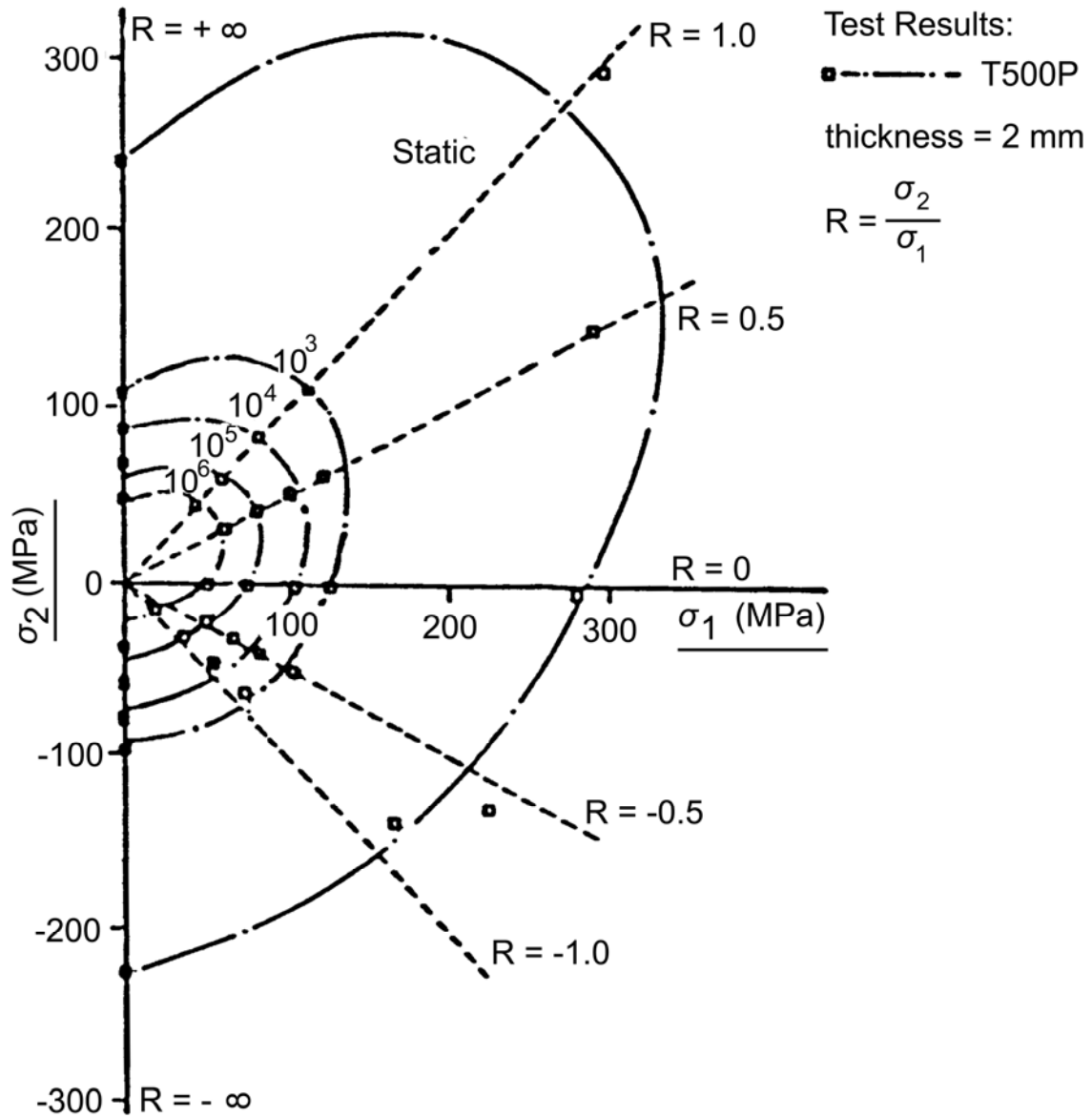
- Biaxial stress ratio,
- Fatigue life, and
- Material combination.



The fit of failure theories to test data tends to deteriorate with increasing fatigue life, Ref. [11-7].

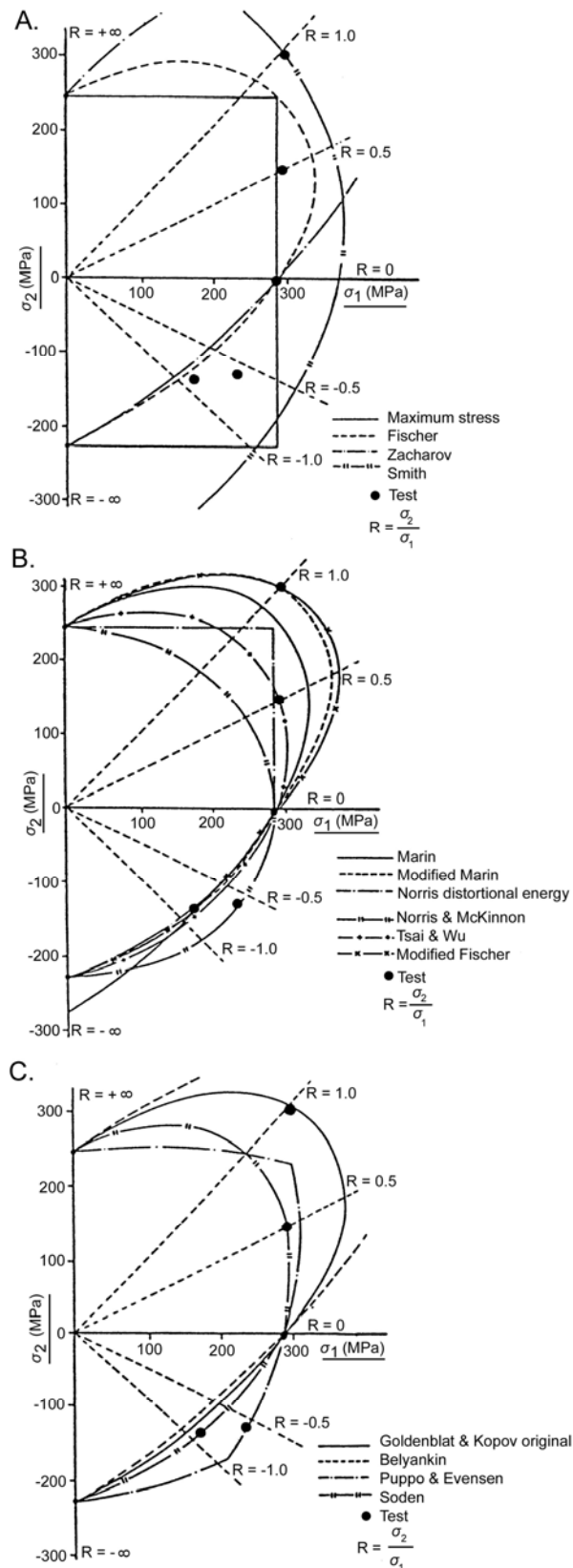
Example: Y449/T500 - glass fabric.

Figure 11.9-1 - Test results: Effect of thickness variation on static failure



Test results for biaxial strength Y449/T500P from Ref. [11-7].

Figure 11.9-2 - Test results: Effect of static and dynamic loading



For Y449/T500 glass fabric, $t = 2.0$ mm, Ref. [11-7].

Figure 11.9-3 - Comparison: Failure theories applied to static strength result-

11.10 Description of failure modes

11.10.1 Laminates

11.10.1.1 General

Failure modes of fibre-reinforced laminates are described in which the individual layers consist of continuous fibres that are strong and stiff along their length, within a more flexible matrix.

The fibres and matrix are designed to perform complementary functions and therefore react to the various loading conditions in different ways.

11.10.1.2 Role of fibres

In each layer of a laminate the principal function of the fibre is to transmit loads in its longitudinal direction, although it also transmits transverse and shear loads.

11.10.1.3 Role of matrix

The resin matrix connects the fibres, maintaining their relative position while distributing the load among the fibres and ensuring continuity of transverse and shear loading in the laminate.

11.10.1.4 Loading

The laminate can be subjected to any combination of loading, though the layers are most efficient under in plane, longitudinal direct load.

11.10.1.5 Fibre orientation

The orientation of the fibres normally varies from layer to layer through the laminate thickness. Consequently there are many more potential failure modes for these laminates than for conventional metallic materials.

11.10.2 Failure

The principal ways of considering the failure of laminates are based on the:

- Behaviour of the individual layers and the interfaces between them.
- Laminate as a whole.

Table 11.10.1 gives failure modes for UD unidirectional laminates and Table 11.10.2 for MD multidirectional laminates.

Table 11.10-1 - Failure modes of unidirectional laminates

	Mode of Failure	Nature of Loading		Primary Factors (see: Key)		Secondary Factors
1	Fibre failure transmitted laterally (brittle failure).	Longitudinal Tension	- - + +	Fibre tensile strength. Fibre volume fraction. Matrix stiffness and strength. Interface bond strength.	-	Cure shrinkage stress.
2	Fibre failure transmitted longitudinally and laterally (brushing).		- - - - +	Fibre tensile strength. Fibre volume fraction. Matrix stiffness and strength. Interface bond strength. Cure shrinkage stresses.	+	Fibre strength variability.
3	Brittle fibre failure (inclined shear).	Longitudinal Compression	- + -	Fibre strength and volume fraction. Local and overall stability. Local distortion/eccentricity.		
4	Kink band failure (timber like).		- + -	Matrix shear stiffness. Local distortion/eccentricity. Fibre diameter.	- - +	Fibre shear stiffness. Fibre volume fraction. Moisture and temperature (matrix).
5	Fibre microbuckling.		- - -	Matrix transverse stiffness. Fibre diameter and volume fraction. Fibre Young's Modulus.	+	Moisture and temperature (matrix).
6	Locally originated delamination.		+ - -	Local distortion/eccentricity. Fibre diameter and modulus. Matrix tensile strength.	- +	Matrix shear stiffness. Moisture and temperature (matrix).
						(continued...)

	Mode of Failure	Nature of Loading		Primary Factors (see: Key)		Secondary Factors
7	Matrix/bondline tension fracture.	Transverse Tension	- - +	Matrix/fibre average failure strain. Fibre/matrix bond strength. Cure shrinkage stresses.	+ - + +	Disparity between fibre and matrix stiffnesses. Matrix strength. Fibre distribution irregularity. Fibre volume fraction.
	As above. (delamination possible)	Short Transverse Tension (normal)	+	As above. Curved laminate bonding.		As above.
8	Matrix/bondline fracture(inclined shear).	Transverse Compression		As for Mode 7.		As for Mode 7.
9	Transverse layer buckling.		- -	Matrix/fibre transverse modulus. Matrix/fibre shear modulus.	+	Fibre volume fraction.
10	Shear in matrix, fibre/matrix debonding, interlaminar shear in laminate.	Longitudinal Short Transverse Shear	- - +	Matrix shear strength. Fibre matrix adhesion. Moisture and temperature (resin).	+ +	Fibre volume fraction. Cure shrinkage stresses.
11	Shear in matrix, interlaminar shear in laminate.	Longitudinal/Transverse Shear	-	Matrix shear strength.	+ +	Cure shrinkage stresses. Moisture and temperature (matrix).
12	Shear in matrix (cross-fibre shear), interlaminar shear in laminate.	Transverse/Short Transverse Shear		As for Mode 10.		As for Mode 10.
Key: <ul style="list-style-type: none"> + The greater the quantity, the more likely the failure. - The lower the quantity, the more likely the failure. For exhaustive description, see Ref. [11-6] .						

Table 11.10-2 - Failure modes of multidirectional laminates

Mode of Failure	Nature of Loading on Laminate		Primary Factors (See: Key)	Secondary Factors
Layer transverse tension cracking (regularly spaced crack through independent layers).	Tension Shear Compression	+ +	Transverse tensile strain components in layer, crack frequency increases with strain. Cure shrinkage stresses.	Some effective transverse and shear stiffness retained initially via uncracked zones.
Layer longitudinal tensile fracture.			See: Table 11.10.1 - unidirectional longitudinal tensile. + Stress concentration from adjacent cracked layers.	Laminate lay-up and stacking sequence. + Cure shrinkage stresses.
Delamination from free edges or notches.		- +	Inter-layer shear strength. + Moisture and temperature (resin matrix). Varies with lay-up and stacking sequence.	In tension or shear, delamination often local to stress raisers. Usually catastrophic in compression.
Delamination/layer buckling.		+ + - -	Local layer distortion. + Layer thickness. - Longitudinal layer modulus. - Matrix tensile strength.	- Matrix shear stiffness. + Moisture and temperature (resin matrix).
Interlaminar shear.	Short Transverse Shear (normal).		See: Table 11.10.1 - Modes 10 and 12. Will vary with stacking sequence.	See: Table 11.10.1 - Modes 10 and 12.
Interlaminar tension.	Normal Tension		See: Table 11.10.1 - Mode 7. Will vary with stacking sequence.	See: Table 11.10.1 - Mode 7.
Key: + The greater the quantity, the more likely the failure. - The lower the quantity, the more likely the failure. For exhaustive description, see Ref. [11-6] .				

The laminate strength can be influenced by:

- Cracking of the matrix.
- Voids, affecting the stresses in the laminate, can also be present as a result of imperfect manufacturing processes.
- Environmental conditions, where the temperature and moisture content significantly affect the matrix behaviour, and consequently those failure modes that are heavily matrix dependent.

Examples of some failure modes are shown in [Table 11.10.3](#).

Table 11.10-3 - Examples of some failure modes

Mode 3		<p>Fibre Microbuckling Initially similar to the out-of-phase buckling shown here.</p>
Mode 4		<p>Fibre Microbuckling The in-phase fibre buckling shown here often precedes "Kink-band" failure.</p>
Mode 10		<p>Longitudinal/Short Transverse Shear Failure</p>
Mode 11		<p>Longitudinal/Transverse Shear Failure</p>
Mode 12		<p>Transverse/Short Transverse Shear Failure</p>

11.11 Fatigue strength of composites

11.11.1 Background

11.11.1.1 General

In the first investigations of the fatigue behaviour of CFRP composites, emphasis was placed on the cyclic tension/tension loading of unidirectional laminates. In contrast to what is known about the behaviour of metals, no single through-crack was found to nucleate and grow.

From such observations, it has often been concluded that composites exhibit better fatigue properties than metals and even that they are insensitive to fatigue. However, such a conclusion is not justified in the case of multidirectional laminates.

11.11.1.2 Factors influencing residual strength

Various parameters have a strong influence on the residual strength of a specimen when it is fatigue loaded, [See: 4.7]. These include the:

- Type of loading (load ratio R).
- Laminate lay-up.
- Environmental conditions.
- Discontinuities, e.g. open holes, delamination, flaws, and cracks.

11.11.1.3 Analysis

Although there are a number of analytical descriptions of the fatigue behaviour of metallic materials, the literature contains very little information on the subject of composites. Some preliminary information (estimates) on ways of investigating the behaviour of composites under fatigue loading is provided.

11.11.2 Analytical notation

D_{11}	flexural stiffness of delaminated plies
K	stress-intensity factor
K_b	buckling coefficient
N	load cycles
N_{cr}	load cycles to failure
N_s	load cycles related to a specific residual strength
N_x	load per unit width
a	length of delamination
a_{cr}	critical length of delamination at failure
a_s	length of delamination related to specific residual strength
l_{cr}	critical delamination length (buckling)
t	thickness of delaminated plies
σ	stress in undisturbed cross section
σ_{cr}	static ultimate compression strength
σ_c	compression strength
σ_{cs}	residual compression strength
σ_{min}	minimum stress limit of last compression load cycle

11.11.3 Approximation of fatigue life

Crack propagation (propagation of delaminations) in composite materials induced by cyclic loading can be described by fracture mechanics formulation, Ref. [11-9], where the increase in crack length, da , with increasing number of load cycles, dN , is expressed as:

$$\frac{da}{dN} = C \cdot (\Delta K)^n = c \cdot \Delta \sigma^n a^m \quad [11.11-1]$$

Where the stress intensity factor $\Delta K = \Delta \sigma \sqrt{\pi a}$ and c , n and m are constants that should be determined experimentally.

Integrating Equation [11.11-1], one gets the number of cycles related to a specific delamination length:

$$N_s = \frac{a_s^{(1-m)} - a_0^{(1-m)}}{(1-m) \cdot c \cdot \sigma^n} \quad [11.11-2]$$

Failure of the specimen occurs when the length of the delamination is equal to the critical buckling length $a = l_{cr}$ and the remaining cross section of the specimen is not able to withstand the loads.

The further assumptions made are:

$$\text{at: } N = 0 \rightarrow l_{cr} = a_0; \sigma_c = \sigma_{cr}$$

$$\text{at: } N = N_{cr} \rightarrow l_{cr} = a_{cr}; \sigma_c = \sigma_{\min}$$

For given loading cycles, N_s , residual compression strength $\sigma_{cr} = \sigma_{cs}$ is related to the critical delamination length $l_{cr} = a_s$.

Ref. [11-9] presents an approximation for the critical delamination length based on the buckling of thin plates; see also Ref. [11-2]:

$$N_x = K_b \frac{\pi^2 D_{11}}{a^2} \quad [11.11-3]$$

$$\text{With: } N_x = \sigma_x t_b$$

From Equation [11.11-3]:

$$a_{cr} = \sqrt{K_b \frac{\pi^2 D_{11}}{N_x}} \quad [11.11-4]$$

Introducing Equation [11.11-4] into Equation [11.11-2] gives a formula representing the relationship between the load cycles and the residual strength of a laminate:

$$N_s = \frac{\left(\frac{K_b \cdot \pi^2 \cdot D_{11}}{t \cdot \sigma_{cs}} \right)^{\frac{1-m}{2}} - \left(\frac{K_b \cdot \pi^2 \cdot D_{11}}{t \cdot \sigma_{cr}} \right)^{\frac{1-m}{2}}}{(1-m) \cdot c \cdot \Delta \sigma^n} \quad [11.11-5]$$

The number of cycles to failure is given by a similar equation:

$$N_{cr} = \frac{\left(\frac{K_b \cdot \pi^2 \cdot D_{11}}{t \cdot \sigma_{\min}} \right)^{\frac{1-m}{2}} - \left(\frac{K_b \cdot \pi^2 \cdot D_{11}}{t \cdot \sigma_{cr}} \right)^{\frac{1-m}{2}}}{(1-m) \cdot c \cdot \Delta \sigma^n} \quad [11.11-6]$$

11.12 References

11.12.1 General

- [11-1] N. F. Dow & Walter B. Rosen
'Evaluation of Filament Reinforced Composites for Aerospace Structural Applications'
NASA CR 207, April 1965
- [11-2] R.M. Jones
'Mechanics of Composite Material'
McGraw Hill, 1975
- [11-3] B. D. Agarwal & L. Y. Broutman
'Analysis and Performance of Fibre Composite'
John Wiley and Sons, 1980
- [11-4] L.E. Nielsen
'Mechanical Properties of Polymers and Composites'
Vol. 2, Marcel Dekker, New York, 1974
- [11-5] ESDU 83014
'Failure Criteria for an Individual Layer of a Fibre Reinforced Composite Laminate under In Plane Loading'
- [11-6] ESDU 82025
'Failure Modes of Fibre Reinforced Laminates'
- [11-7] ASTM STP 787
'Biaxial Strength Behaviour of Glass Reinforced Polyester Resins'
- [11-8] S. W. Tsai & H.T. Hahn
'Introduction to Composite Materials'
Technomic Publishing Co., Inc. 1980
- [11-9] DFVLR-Mitteilung 87-08
'Schadensmechanik kohlenstoffaseverstärkter Kunststoffe bei Schwingbelastung'
- [11-10] Not stated
- [11-11] Not stated
- [11-12] Not stated
- [11-13] Not stated
- [11-14] Not stated
- [11-15] Not stated

- [11-16] Soden and Hinton
Composite Science and Technology Vol. 58 (1998)
Composite Science and Technology Vol. 62 (2002).
- [11-17] M. Hinton et al.: DERA (UK)/UMIST (UK)/QinetiQ Ltd, (UK)
'Failure Criteria in Fibre-reinforced-Polymer Composites'
[Elsevier](#), ISBN: 0-08-044475-X (2004)
- [11-18] C. Kaiser et al: HPS/Kayser Threde/DLR, (D)/ESTEC (NL)
'Failure Criteria in Fibre-reinforced-Polymer Composites'
European Conference on Spacecraft Structures, Materials and
Mechanical Testing, ESTEC (NL). 10-12 May 2005.
ESA-SP-581 (August 2005) CDROM
- [11-19] B.W. Rosen and Z. Hashin.
'Analysis of Material Properties'
Reinhardt, T.D. et al. (Eds.): Engineered Materials Handbook, Vol. 1,
Composites. Metals Park, Ohio; ASM International, 1989, pages 185-
205.
- [11-20] S. Goutianos et al
'Mechanisms of stress transfer and interface integrity in carbon/epoxy
composites under compression loading, Part I: Experimental
investigation'
International Journal of Solids and Structures 39 (2002) p.3217-3231
- [11-21] K. Rohwer: DLR (D)
'Draft for discussion - Failure criteria'
Structural Materials Handbook Working Group (April 2004)
- [11-22] C. Kaiser et al: HPS/DLR/Kayser Threde/ESTEC
'Failure criteria for FRP and CMC: Theory, Experiments and
Guidelines'
Proceedings of the European Conference on Spacecraft Structures,
Materials and Mechanical Testing, ESTEC, Noordwijk, NL 10-12 May
2005
ESA-SP-581 (August 2005) CDROM
- [11-23] S.J. DeTeresa & G.J. Larsen
Reduction in the Number of Independent Parameters for the Tsai-Wu
Tensor Polynomial Theory of Strength for Composite Materials.
Journal of Composite Materials, Vol. 37, No. 19 (2003), 1769-1785.
- [11-24] Kröber
Bruchhypothese und Reservefaktoren für unidirektionale
Einzelschichten in Faserverbunden. Handbuch für
Strukturberechnung, 51301-01, 1982.
- [11-25] Z. Hashin
Failure Criteria for Unidirectional Fiber Composites. Journal of
Applied Mechanics, Transactions of the ASME, Vol. 47 (1980), 329-334.

- [11-26] A. Puck & H. Schürmann:
Failure analysis of FRP laminates by means of physically based
phenological models. *Composites Science and Technology* 58 (1998)
1045-1067 and *Composites Science and Technology* 62 (2002) 1633-
1662.
- [11-27] A. Puck, J. Kopp & M. Knops
Guidelines for the determination of the parameters in Puck's action
plane strength criterion. *Composites Science and Technology* 62 (2002)
371-378.
- [11-28] R. Jeltsch-Fricker
Bruchbedingungen vom Mohrschen Typ für transversal-isotrope
Werkstoffe am Beispiel der Faser-Kunststoff-Verbunde. *ZAMM Vol.*
76 (1996), No. 9, 505-520.
- [11-29] R. G. Cuntze et al.:
Neue Bruchkriterien und Festigkeitsnachweise für unidirektionalen
Faserkunststoffverbund unter mehrachsiger Beanspruchung –
Modellbildung und Experimente. *Fortschrittberichte VDI, Reihe 5:*
Grund- und Werkstoffe, No. 506, Düsseldorf: VDI-Verlag, 1997, p.198
- [11-30] M. Hinton et al.: DERA (UK)/UMIST (UK)/QinetiQ Ltd, (UK)
'Failure Criteria in Fibre-reinforced-Polymer Composites'
Elsevier, ISBN: 0-08-044475-X (2004)
- [11-31] R.G. Cuntze
'The Predictive Capability of Failure Mode Concept-based Strength
Conditions for Laminates composed of UD Laminae under static tri-
axial stress states'
WWFE-II, Part A, issue in *Composites Science and Technology* 2009
(planned)
- [11-32] R.G. Cuntze
'The Predictive Capability of Failure Mode Concept-based Strength
Criteria for Multidirectional Laminates'
WWFE-I, Part B, *Composites Science and Technology* 64 (2004), 487-
516
- [11-33] VDI 2014: German Guideline, Sheet 3 "Development of Fibre-
Reinforced Plastic Components, Analysis". Beuth Verlag, 2006. (in
German and English)
- [11-34] R.G. Cuntze
'Strength Prediction for Multi-axially Loaded CMC-Materials. 3rd
European Workshop on thermal Protection Systems'
ESA-ESTEC: Noordwijk, March 1998, WP P141
- [11-35] Klaus Rohwer: DLR (D)
'Overview of Failure Criteria'
ECSS Working Group (2005)

-
- [11-36] Ralf Cuntze: formerly MAN Technologie AG, Augsburg (D)
'Cuntze's FMC-based Failure Conditions'
ECSS Working Group (2009)
- [11-37] M.J. Hinton, A.S. Kaddour, P.D. Soden
'A further assessment of the predictive capabilities of current failure theories for composite laminates: comparison with experimental evidence'.
Composites Science & Technology 64 (2004) p549–588.
- [11-38] Dr. A S Kaddour, QinetiQ (UK)
'None of the criteria is right or wrong, but more or less suitable'
Discussions by email between Dr.Ing K.Rohwer, Dr Ing Cuntze, QinetiQ, (August 2009)
- [11-39] A. Puck
'Festigkeitsanalyse von Faser-Matrix-Laminaten – Modelle für die Praxis', Hanser, 1996
- [11-40] R.G. Cuntze et al
'Neue Bruchkriterien und Festigkeitsnachweise für uni-direktionalen Faserkunststoffverbund unter mehrachsiger Beanspruchung – Modellbildung und Experimente'
VDI-Fortschrittbericht, Reihe 5, Nr. 506 (1997), 250 pages (in German)
New fracture criteria (Hashin-Puck action plane criteria) and Strength Design Verifications for Uni-directional FRPs subjected to Multiaxial States of Stress – Model development and experiments'
- [11-41] R.G. Cuntze et al

12

Calculation of thermal stress and displacement

12.1 Introduction

12.1.1 General

As with most other properties of unidirectional composites, the coefficient of thermal expansion CTE in the longitudinal direction is different from that in the transverse direction.

12.1.2 Longitudinal CTE

The longitudinal coefficient α_1 is generally small because the fibres themselves usually have a smaller coefficient than the matrix resin and impose a mechanical restraint on the matrix material.

12.1.3 Transverse CTE

The transverse coefficient α_2 is larger. At low fibre volume fraction it can be even greater than that of the neat resin, because the matrix is prevented from expanding in the longitudinal direction, so is forced to expand more in the transverse direction.

12.2 Analytical notation for thermal stress calculations

Formulae:

A	In-plane stiffness
B	Coupling stiffness
D	Bending stiffness
E	E -Modulus
G	G -Modulus
N	In-plane forces
M	Bending moments
S	Stress - strain matrix
T	Temperature
X, Y, Z	Laminate co-ordinate system
h	Laminate thickness
α	Coefficient of thermal expansion, CTE
ϵ	Strain
κ	Curvature
ν	Poisson's ratio
σ	Stress
V_f	Fibre volume ratio

Subscripts:

m	Matrix
f	Fibre
1	Parallel to fibre direction
2	Perpendicular to fibre direction

Superscripts:

M	Mechanical
T	Thermal

12.3 Calculation of CTE from constituents

12.3.1 CTE in fibre direction

The coefficient of thermal expansion for a UD layer parallel to the fibre direction is given by the simple mixing rule:

$$\alpha_1 = \frac{E_{f1} V_f \alpha_{f1} + E_m (1 - V_f) \alpha_m}{E_1} \quad [12.3-1]$$

where E_1 is given by:

$$E_1 = [E_{f1} V_f + E_m (1 - V_f)]$$

12.3.2 CTE perpendicular to fibre direction

12.3.2.1 Calculation Methods

Some methods for the calculation of the transverse CTE are given in references 12-1 and 12-2.

Figure 12.3.2 provides an example of CTE for various unidirectional composites and their dependence on fibre volume content.

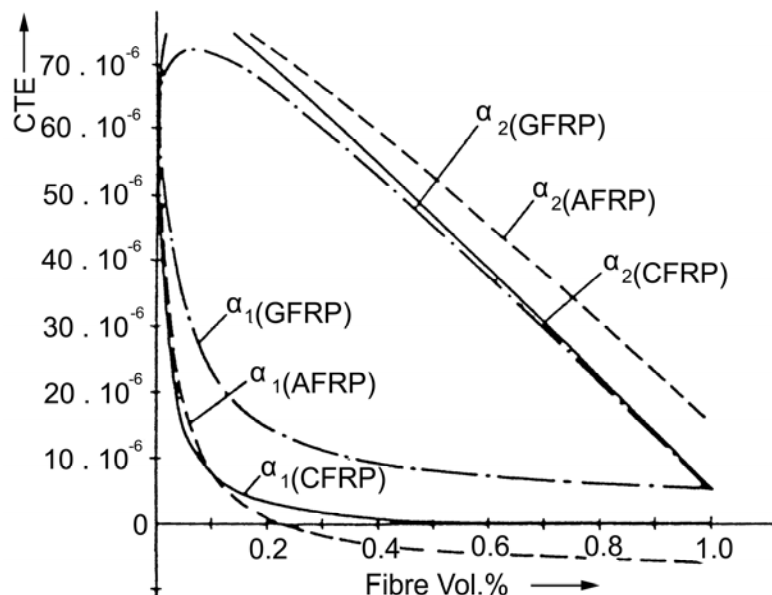


Figure 12.3-1 - CTE of unidirectional composites

The CTE for T300/914 0°/±45°/90° laminates is shown in Figure 12.3.3.

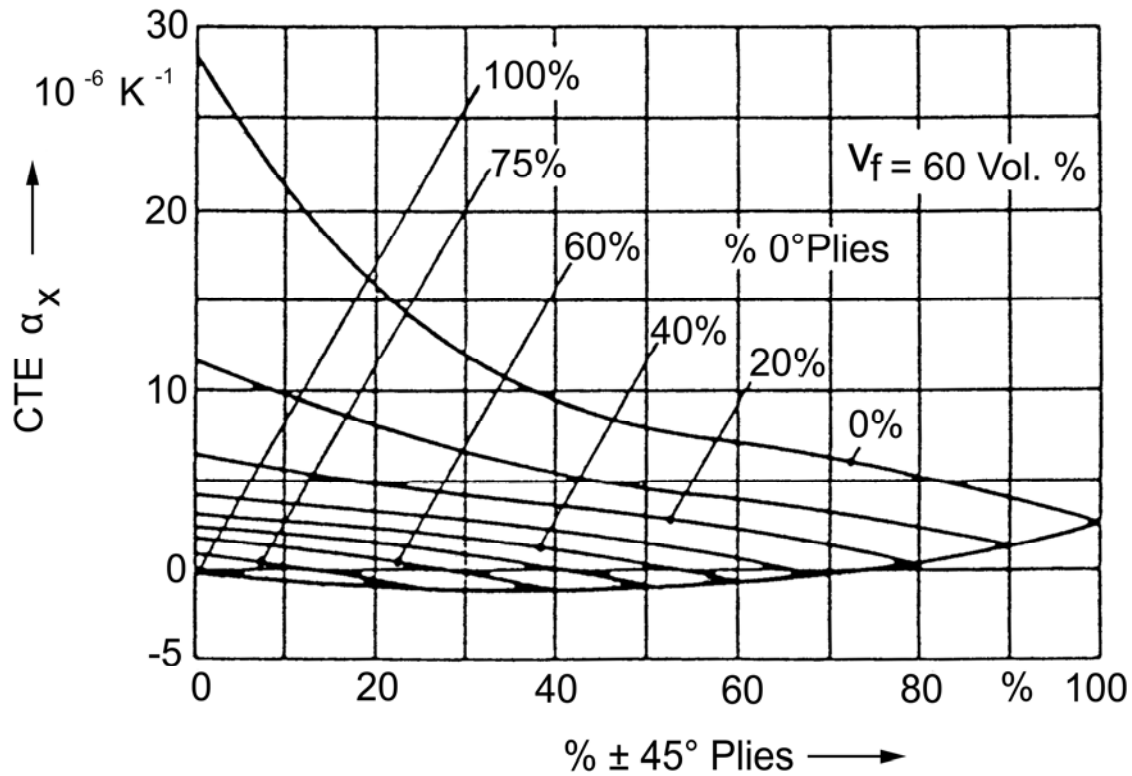


Figure 12.3-2 - CTE for T300/914 0°/±45°/90° laminates

12.4 CTE for a laminate

The constitutive equation relates the stress resultants (in plane forces and bending moments) to the in plane strains and curvatures:

$$\begin{aligned} \{\bar{N}\} &= [A]\{\mathcal{E}^0\} + [B]\{\kappa\} \\ \{\bar{M}\} &= [B]\{\mathcal{E}^0\} + [D]\{\kappa\} \end{aligned} \quad [12.4-1]$$

The overall stress resultants $\{N\}$ and $\{M\}$ are given by:

$$\begin{aligned} \{N\} &= \{\bar{N}\}\{N^T\} \\ \{M\} &= \{\bar{M}\}\{M^T\} \end{aligned} \quad [12.4-2]$$

Where the equivalent thermal forces and moments can be written as:

$$\{N^T\} = \int_{-h/2}^{+h/2} [S]\{\mathcal{E}^T\} dz \quad [12.4-3]$$

$$\{M^T\} = \int_{-h/2}^{+h/2} [S] \{\epsilon^T\} z dz \quad [12.4-4]$$

In this analysis it is assumed that Hooke's Law for orthotropic material applies to each layer and that the layers are in a state of plane stress, which is true only away from the edge of the laminate.

The stress-strain matrix is given by:

$$[S]^i = \begin{bmatrix} \frac{E_1}{1-\nu_{12}\nu_{21}} & \frac{\nu_{12}E_1}{1-\nu_{12}\nu_{21}} & 0 \\ \text{SYMM.} & \frac{E_2}{1-\nu_{12}\nu_{21}} & 0 \\ & & G_{12} \end{bmatrix} \quad [12.4-5]$$

and from the definition of stress resultants one obtains the in plane, bending and coupling stiffness of the laminated composite:

$$\{A\} = \int_{-h/2}^{+h/2} [S'] dz \quad [12.4-6]$$

$$\{D\} = \int_{-h/2}^{+h/2} [S'] z^2 dz \quad [12.4-7]$$

$$\{B\} = \int_{-h/2}^{+h/2} [S'] z dz \quad [12.4-8]$$

Where: h denotes the thickness of the laminated plate and $[S]^i$ is the transformed stress strain matrix in laminate co-ordinates x-y. The stresses in the i -th layer are then given by:

$$\{\sigma\}^i = [S]^i \left[\{\epsilon^0\} + Z\{\kappa\} - \{\epsilon^T\}^i \right] \quad [12.4-9]$$

Where the thermal strains can be written as:

$$\{\boldsymbol{\varepsilon}^T\}^i = \{\boldsymbol{\alpha}\}^i \Delta T^i \quad [12.4-10]$$

Dividing the thermal strains and curvatures by the temperature differences ΔT , one obtains the coefficients of thermal expansion for the laminate.

$$\{\boldsymbol{\alpha}^c\} = \frac{1}{\Delta T} \{\boldsymbol{\varepsilon}\} \quad [12.4-11]$$

Where $\{\boldsymbol{\alpha}^c\}$ is a 6×1 vector.

With the constitutive expressions Eq [12.4-1], Eq [12.4-3], Eq [12.4-4] and Eq [12.4-10], and assuming that the overall stress resultants are equal to zero, the vector $\{\boldsymbol{\alpha}^c\}$ can be written as:

$$\{\boldsymbol{\alpha}^c\} = \begin{bmatrix} [A] & [B] \\ [B] & [D] \end{bmatrix}^{-1} \sum_{i=1}^n \begin{bmatrix} [A] & [B] \\ [B] & [D] \end{bmatrix}_i \begin{bmatrix} \boldsymbol{\alpha} \\ 0 \end{bmatrix}_i \quad [12.4-12]$$

Where α^i are the CTEs of the i -th layer.

In the case of a symmetrical laminate, the coupling stiffness $[B]$ vanishes and only the first three coefficients of $\{\boldsymbol{\alpha}^c\}$ are non-zero. For an unsymmetrical laminate, thermally-induced curvatures occur and the vector $\{\boldsymbol{\alpha}^c\}$ is fully populated.

12.5 Thermal stresses within laminate layers

12.5.1 General

The behaviour of the resin matrix, determines the extent to which the mechanical and thermal properties of CFRP are temperature dependent. Consequently, the Young's moduli parallel and perpendicular to the fibre direction, the shear modulus, Poisson's ratio and the coefficients of thermal expansion of an unidirectional laminate are functions of temperature in an unrestricted manner. As a result the total stiffness matrix, the thermal stress resultants and the vector of coefficients of thermal expansion for a multidirectional laminate are likewise temperature dependent.

12.5.2 Residual curing stresses

The anisotropic thermal expansion characteristic of the fibres, together with that of the resin matrix which is isotropic, lead to residual stresses in the laminate after curing.

12.6 Stress strain temperature relation

12.6.1 General

The resulting strains in an unidirectional layer of a laminate, which is subjected to a temperature load and stresses, are obtained from the sum of mechanical and thermal strains.

12.6.2 Mechanical strains

The mechanical strains depend on the temperature, because the compliance is a function of temperature, while the thermal strains are independent of the stresses. Hence, even at the same stress level the mechanical strains are influenced by the temperature.

$$\varepsilon_i = \varepsilon_i^M(\sigma_i, T) + \varepsilon_i^T(T) \quad [12.6-1]$$

When the mechanical strains are linearly dependent on the stresses σ_i , a simplified form of Eq [12.6-1] is obtained:

$$\varepsilon_i^M = S_{ij}(T)\sigma_i \quad [12.6-2]$$

Where: $S_{ij}(T)$ denotes the temperature dependent compliance.

From Eq [12.6-1] one can now calculate the change of strain due to an infinitesimal change of stress and temperature:

$$d\varepsilon_i = S_{ij}(T)d\sigma_i + \left(\frac{\delta\varepsilon_i^M}{\delta T} + \frac{\delta\varepsilon_i^T}{\delta T} \right) dT \quad [12.6-3]$$

Where: $\delta\varepsilon_i^M/\delta T$ is the coupling coefficient.

12.6.3 Incremental strain theory

In incremental strain theory, where the thermal strain and stress-strain relations are only of interest at the final temperature, the coupling term, $\delta\varepsilon_i^M/\delta T$, is omitted. This is correct only when the compliance is temperature independent. In some cases this omission can result in as much as 35 % difference in the curing stress prediction, Ref. [12-1].

The stepwise evaluation of thermal strains and stresses is performed assuming that:

- The overall stress resultants are equal to zero.
- Temperature-dependent material properties are given in a table with constant temperature difference steps ΔT .
- The upper temperature bound is the curing temperature, where the laminate is in a stress free state.

The thermal strains in a layer j at present temperature T_N are given by:

$$\{\boldsymbol{\varepsilon}^T(\mathbf{T}_N)\}_j = \sum \frac{1}{2} (\{\boldsymbol{\alpha}(\mathbf{T}_i)\}_j + \{\boldsymbol{\alpha}(\mathbf{T}_{i-1})\}_j) \Delta T \quad [12.6-4]$$

And the total thermal strains in the laminate at T_N are given by:

$$\begin{bmatrix} \{\boldsymbol{\varepsilon}^0(\mathbf{T}_N)\} \\ \{\boldsymbol{\kappa}(\mathbf{T}_N)\} \end{bmatrix} = \begin{bmatrix} [A[\mathbf{T}_N]] & [B[\mathbf{T}_N]] \\ [B[\mathbf{T}_N]] & [D[\mathbf{T}_N]] \end{bmatrix}^{-1} \begin{bmatrix} \{\mathbf{N}^T(\mathbf{T}_N)\} \\ \{\mathbf{M}^T(\mathbf{T}_N)\} \end{bmatrix} \quad [12.6-5]$$

With the thermal stress resultants:

$$\{\mathbf{N}^T(\mathbf{T}_N)\} = \int_{-h/2}^{+h/2} [S(\mathbf{T}_N)] \{\boldsymbol{\varepsilon}^T(\mathbf{T}_N)\} dz \quad [12.6-6]$$

And:

$$\{\mathbf{M}^T(\mathbf{T}_N)\} = \int_{-h/2}^{+h/2} [S(\mathbf{T}_N)] \{\boldsymbol{\varepsilon}^T(\mathbf{T}_N)\} z dz \quad [12.6-7]$$

Where: h denotes the laminate thickness.

From the total thermal strains, the coefficients of thermal expansion for the laminate at $(T_N + T_{N-1})/2$ are:

$$\{\boldsymbol{\alpha}_c\} = \frac{\begin{bmatrix} \{\boldsymbol{\varepsilon}^0(\mathbf{T}_N)\} - \{\boldsymbol{\varepsilon}^0(\mathbf{T}_{N-1})\} \\ \{\boldsymbol{\kappa}(\mathbf{T}_N)\} - \{\boldsymbol{\kappa}(\mathbf{T}_{N-1})\} \end{bmatrix}}{\Delta T} \quad [12.6-8]$$

and finally the single layer thermal stresses are given in layer j by:

$$\{\boldsymbol{\sigma}\}_j = [S(\mathbf{T}_N)]_j (\{\boldsymbol{\varepsilon}^0(\mathbf{T}_N)\} + z_j \{\boldsymbol{\kappa}(\mathbf{T}_N)\} - \{\boldsymbol{\varepsilon}^T(\mathbf{T}_N)\}_j) \quad [12.6-9]$$

12.7 Microstress analysis

12.7.1 General

Microstresses arise due to the difference between:

- curing temperature and the temperature at use, and
- the coefficients of thermal expansion of fibres and matrix.

There are stresses both along and perpendicular to the fibre direction.

12.7.2 Microstresses on fibre axis

Along the fibre axis the higher coefficient of thermal expansion of the resin produces a tensile stress in the resin when the composite is cooled from curing to working temperature.

The tensile stress in the resin can be evaluated by:

$$\sigma_m = \frac{(\alpha_m - \alpha_{f_x}) \Delta T E_m}{1 + \frac{E_m}{E_{f_x}}} \quad [12.7-1]$$

where the assumption is that there is a perfect bond at the resin-to-fibre interface, Ref. [12-4].

12.7.3 Microstresses normal to fibre axis

The microstresses perpendicular to the fibre direction are of more interest, because this is the more critical direction of a single layer with respect to the strength and stiffness properties.

To evaluate the internal stresses in fibre and matrix perpendicular to the fibres a finite element program should be used, Ref. [12-1].

12.8 References

12.8.1 General

- [12-1] ESTEC Contract No. 2930/76/NL/PP(SC)
'Final report for a study on evaluation of in built stresses during manufacture of elements made of carbon fibre reinforced plastics'

- [12-2] R.A. Schapery
'Thermal expansion coefficients of composite materials based on energy principles'
J. Composite Material 2 (3), 1968

- [12-3] S.W. Tsai & H.T. Hahn
'Introduction to Composite Materials'
Technomic, 1980

- [12-4] R.C. Novak & M.A. de Crescente
'Fabrication stresses in graphite/resin composites'
ASME Paper No. 70 GT 84, 1970

13

Moisture effects on composite properties

13.1 Introduction

13.1.1 General

The properties of composite materials are susceptible to changes induced by the absorption of moisture. Such effects should be considered because moisture is likely to be present in the atmosphere during the production of components and launch of a spacecraft. The subsequent desorption occurring in the operational space vacuum also need consideration.

13.1.2 Moisture penetration

Moisture penetrates the organic resin material (and also aramid fibres) by a diffusion-controlled process. Additional heat can increase the moisture-retention capacity of the material. Such moisture acts like a plasticiser, which softens the matrix and lowers the glass transition temperature. Such processes are often reversible. The process can, however, lead to modification of residual strain and microcracks within the resin system. Thermal cycling can cause some permanent changes in the coefficient of thermal expansion and possibly also in mechanical properties. Such effects should be avoided in structures that have to be very stable, either dimensionally or optically, [See: Chapter 28].

13.1.3 Moisture effects

13.1.3.1 Swelling

An important effect of the absorption of moisture by composites is swelling of the resin matrix. This can lead to a modification of the pre-existing residual-stress conditions, which can result in the production of microcracks both in the matrix and at the interface with the fibres. In certain cases, swelling due to moisture absorption can cause a reduction in the thermally-induced stresses.

13.1.3.2 Mechanical properties

The mechanical properties of the composites that are altered by moisture absorption are those governed by the behaviour of the matrix, [See: 13.3].

The properties affected include the:

- Interlaminar shear strength (ILSS),
- In-plane shear strength,
- Compression strength, and
- Coefficient of thermal expansion (CTE).

These alterations become more evident at high temperatures, owing to the depression of the glass transition point, T_g .

13.1.3.3 Prediction of moisture effects

Analytical methods have been developed to predict the changes in material properties brought about by the presence of moisture. Methods are presented for determination of the:

- Moisture distribution, [See: 13.5].
- Final moisture content, [See: 13.5].
- Swelling coefficient of unidirectional plies, [See: 13.6].
- Swelling coefficient for the laminate, [See: 13.6].

13.2 Analytical notation for moisture effects

a, b	constants
d	thickness of specimen
D	state of diffusion
D_1	diffusion coefficient parallel to the fibres
D_2	diffusion coefficient transverse to the fibres
D_m	diffusion coefficient of the matrix
D_z	diffusion coefficient normal to the surface
E	Young's modulus
E_2	transverse modulus of elasticity (Young's modulus transverse to unidirectional plies, here in tensile)
F	force
G	time dependent parameter, [See: Equation 13.5-4].
H	thickness
ΔL	swelling strain transverse to unidirectional plies
M	moisture content (percentage weight gain)
M_i	initial moisture content
\hat{M}	maximum moisture content
N	number of cycles
$R_2^m \sigma_{22}$	transverse tensile strength of unidirectional plies
S	equivalent thickness

T	temperature
T	time
V_f	volume fraction of fibres
V_r	volume fraction of resin
α	angle between surface plane and the normal x -axis ($\alpha = 90^\circ$ fibres are in a plane parallel to the surface)
β	swelling coefficient
ε	tensile strain
ε_m	swelling strain
ϕ	relative humidity
ν	Poisson's ratio
σ	fatigue strength of unidirectional plies
σ_t	tensile strength of neat resin
ψ_r	weight fraction of resin

Subscripts:

c	composite
f	fibre
m	matrix
1	fibre direction
2	transverse to fibre direction
i	i -th layer of a laminate

13.3 Typical effects of moisture

13.3.1 General

In general, moisture absorption by the matrix of a composite:

- changes the chemical structure (softens matrix)
- causes swelling of the matrix

13.3.2 Sample data: Effects of moisture

13.3.2.1 General

The rate of diffusion of moisture determines the extent to which moisture influences the softening or swelling effects.

Sample data are presented for:

- Matrix plasticising in Figure 13.3.1, Ref. [13-4].
- Matrix swelling in Figure 13.3.2
- Temperature-time dependence of moisture absorption in Figure 13.3.3 and Figure 13.3.4.

The effects of moisture on mechanical properties are shown for:

- Changes in strength in Figure 13.3.5, Ref. [13-4].
- Changes in moduli in Figure 13.3.6, Ref. [13-4].
- Changes in fatigue behaviour in Figure 13.3.7, Ref. [13-4].

[See also: 4.5 for further data on hygrothermal effects on mechanical and physical properties]

13.3.2.2 Matrix plasticising

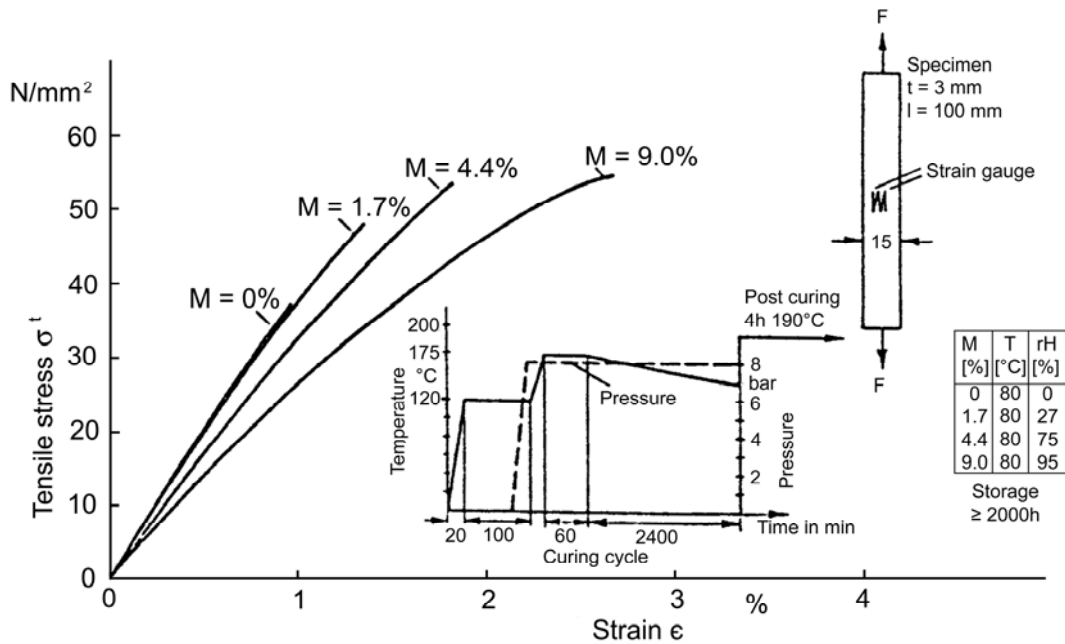


Figure 13.3-1 - Stress/strain curves of Fibredux 914 (neat resin) for different moisture contents tested at RT

13.3.2.3 Matrix swelling

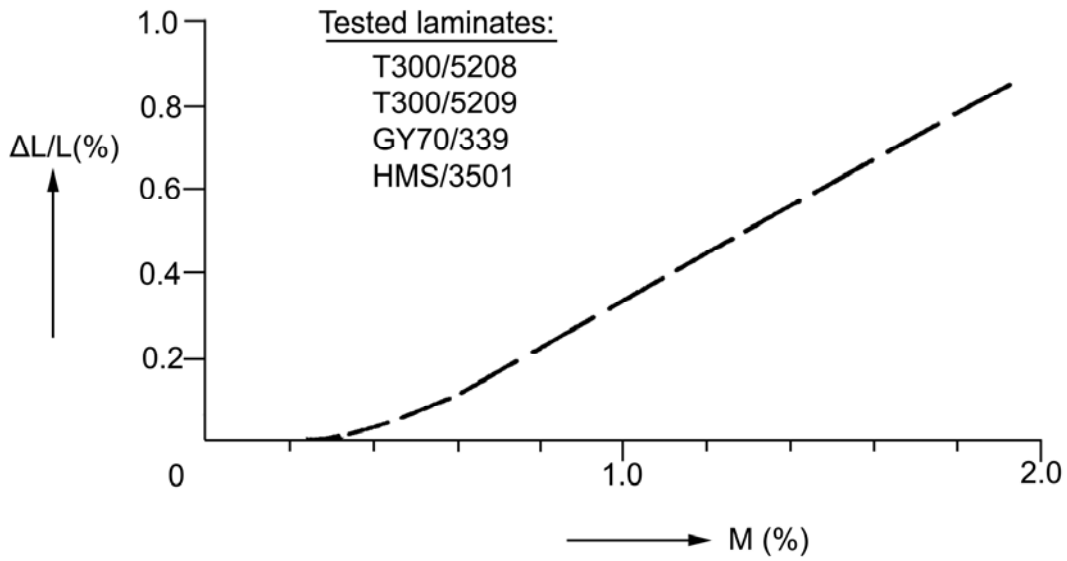


Figure 13.3-2 - Swelling strain, transverse (UD laminate)

13.3.2.4 Temperature-time dependence of moisture absorption

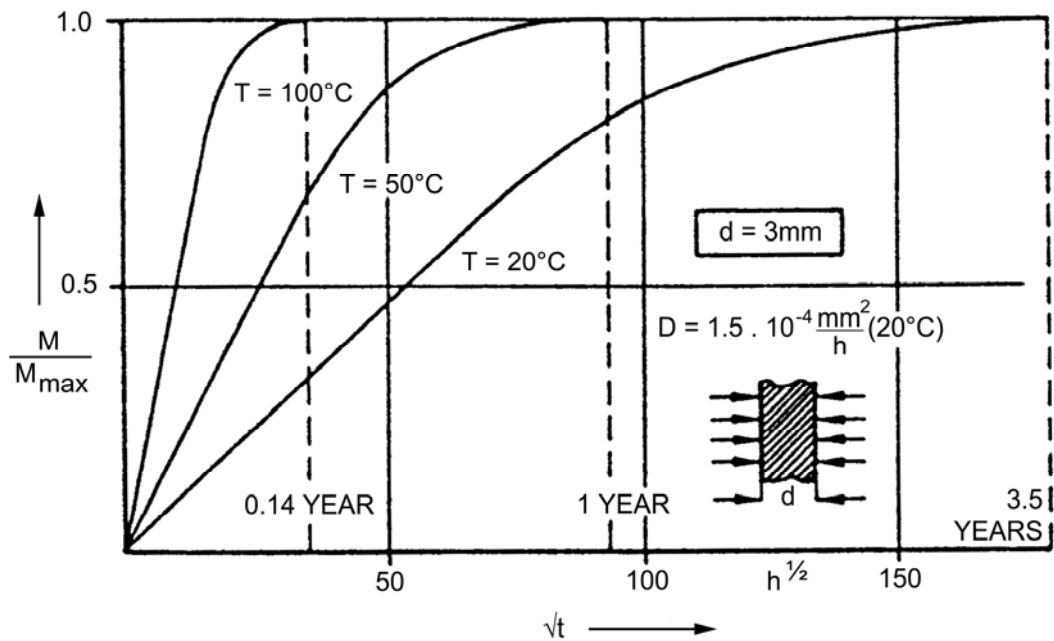


Figure 13.3-3 - Influence of temperature and time on weight gain

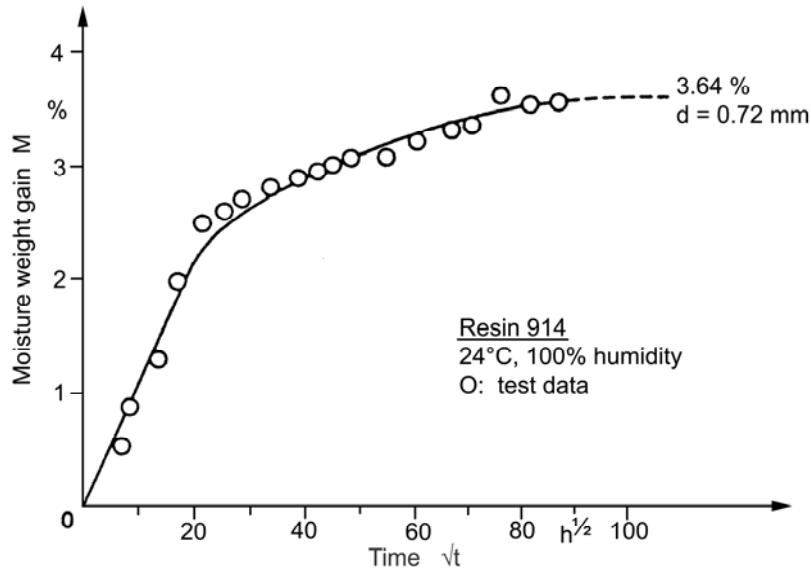
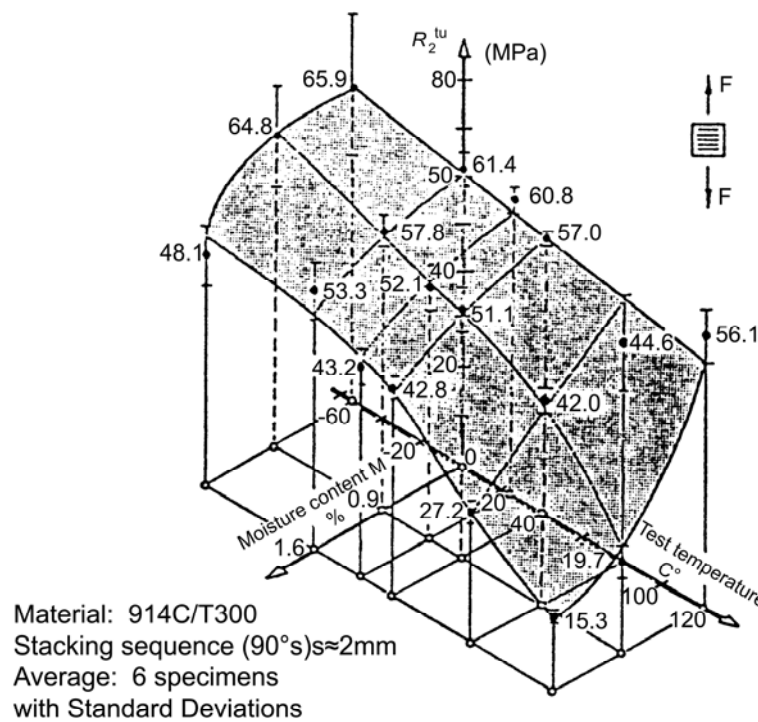


Figure 13.3-4 - Test results: Moisture absorption versus time

13.3.2.5 Changes in strength



13.3.2.6 Changes in moduli

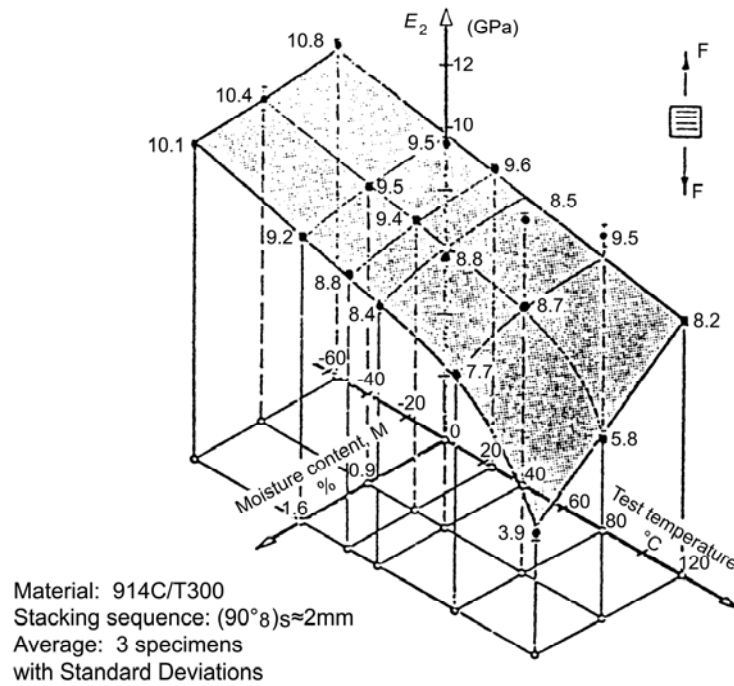


Figure 13.3-6 - Transverse modulus of elasticity

13.3.2.7 Changes in fatigue behaviour

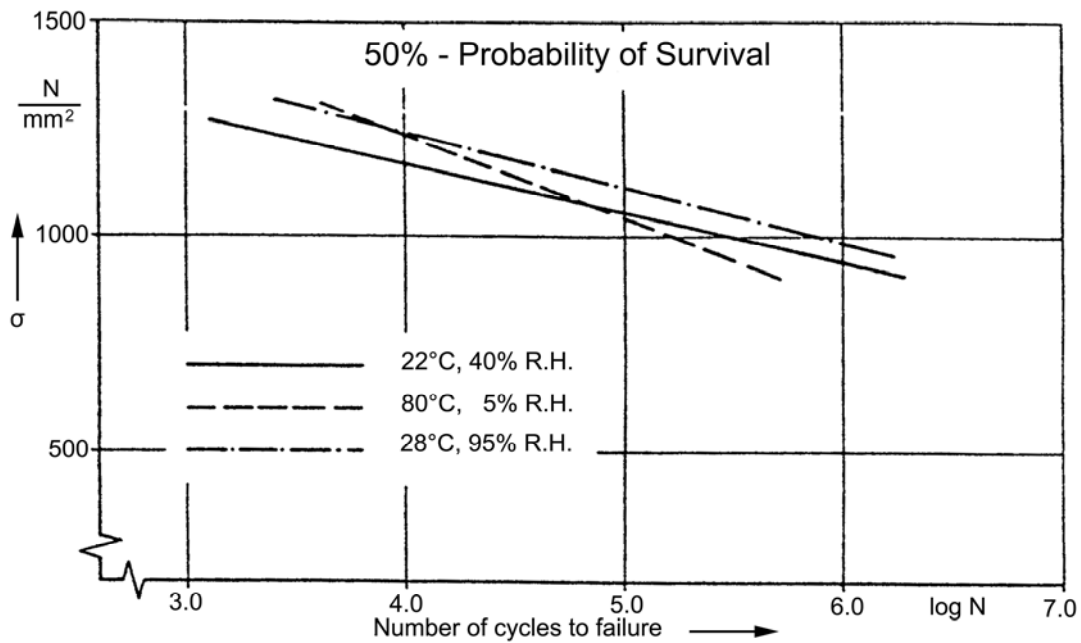


Figure 13.3-7 - Influence of temperature and moisture on fatigue strength of unidirectional 0° laminates

13.4 Approximate method for calculation of strength and modulus retention of [0°/90°] laminates

13.4.1 General

The absorbed water in epoxy composites not only produces changes of chemical and physical nature but also causes a degradation of the mechanical properties.

The reduction of strength and stiffness is the result of softening of the fibre, the matrix and their interface.

The level of degradation depends on the moisture content in the composite; it varies with the structural components and the quality of composite and cannot be ignored.

[See: [13.2](#) for analytical notation]

13.4.2 Modulus retention

Because the degradation in resin properties results in a parallel degradation in composite properties, the simple rule of mixtures can be used as a basis for calculating the moduli of [UD](#) composites, [See: [10.4](#)].

$$E_c = V_f E_f + V_m E_m \quad [13.4-1]$$

Where the subscripts c , f and m refer to the composite, fibre and resin respectively; V is the volume fraction, and E is the elastic modulus.

E_c decreases when E_m is reduced by moisture, which affects the interfacial bonding strength of the composite and causes a loss of efficiency of stress transfer between fibres.

According to Ref. [13-3], Equation [13.4-1] is modified to:

$$E'_c = V_f E_f + V_m E'_m - \alpha E_f V_f W_c \quad [13.4-2]$$

Where:

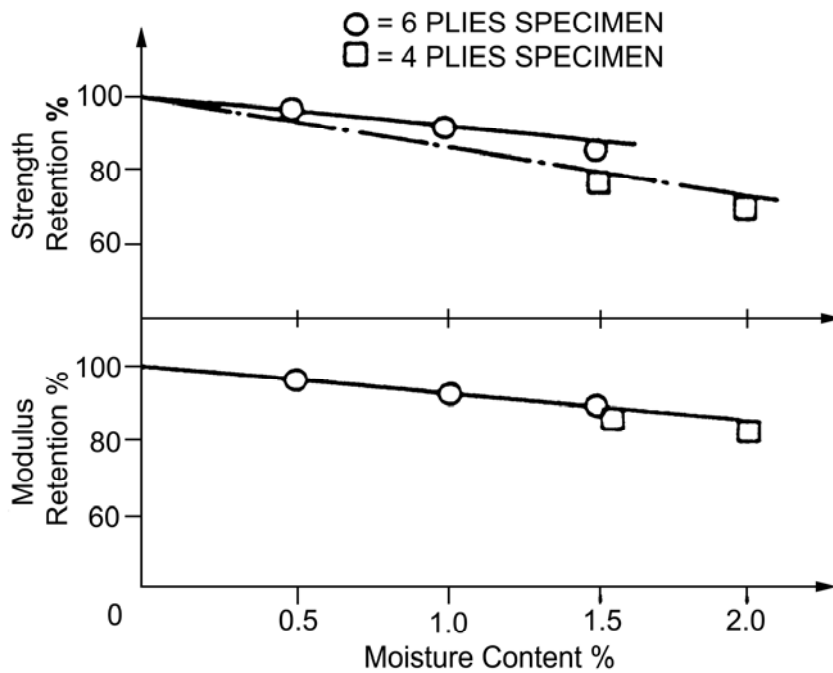
- α is an empirical constant for a fixed type of reinforcement and coupling agent.
- E'_c, E'_m are the moduli of composite and resin matrix after moisture absorption, E'_m can be obtained from test results.
- W_c is the moisture content by weight of the composite.

For a [0°/90°] laminate, Eq [13.4-2] can be approximated as:

$$E'_c = \frac{V_f}{2} E_f + V_m E'_m - \alpha E_f V_f W_c \quad [13.4-3]$$

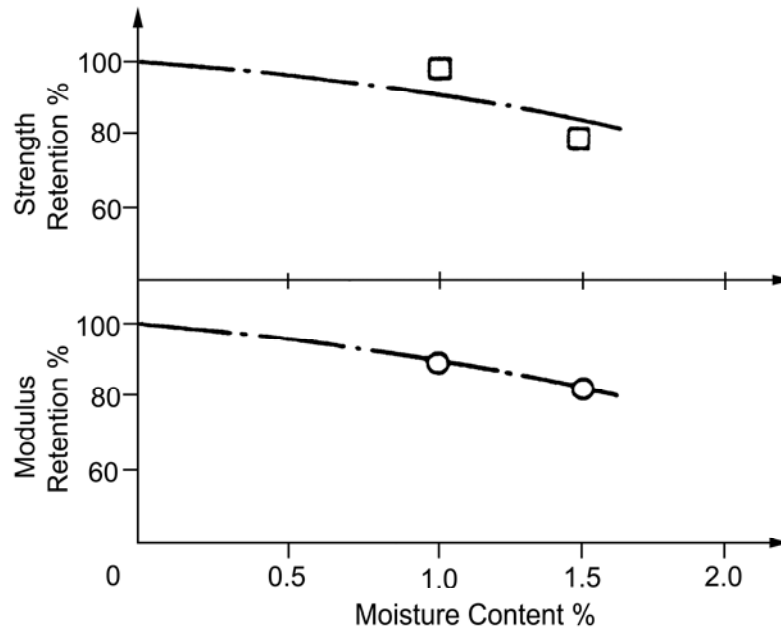
This equation correlates very closely with the experimental results for both glass and carbon composites; when $\alpha = 2$ for glass and $\alpha = 3$ for carbon.

Figure 13.4.1 shows a comparison of calculated and measured results for GFRP and Figure 13.4.2 for CFRP, Ref. [13-3].



Material: Araldite - 507/HY 956, glass - ASA H, MS 252 fabric and woven rovings

Figure 13.4-1 - Moisture: Comparison of calculated and experimental results of strength and stiffness of $[0^\circ/90^\circ]$ GFRP laminates



Material: Araldite - 507/HY 956, carbon - Carborundum GSG C2

Figure 13.4-2 - Moisture: Comparison of calculated and experimental results of strength and stiffness [0°/90°] CFRP laminates

13.4.3 Strength retention

According to the general engineering equation for strength of UD composites, [See: 11.2], including the effects of moisture on composite material and its components, an approximate calculation can be used to determine the strength of [0°/90°] composite laminate after absorption of moisture:

$$R_c^u = R_f^u \left[\frac{V_f}{2} + V_m \beta \frac{E'_m}{E_f} \right] - \alpha R_f^u V_f W_c \quad [13.4-4]$$

Where:

β is an empirical constant for a fixed type of reinforcement and coupling agent.

R_c^u strength of composite.

R_f^u strength of fibre.

[See also: Figure 13.4.1 for GFRP; Figure 13.4.2 for CFRP, Ref.[13-3]]

13.5 Moisture content

13.5.1 Fick's law

The basis for the calculation of the diffusion of moisture into composite materials is Fick's Law:

$$\frac{\partial c}{\partial t} = \frac{\partial}{\partial x} D_x \frac{\partial c}{\partial x} \quad [13.5-1]$$

This is valid for an infinite plate where the moisture content varies only in the x-direction, as defined in Figure 13.5.1.

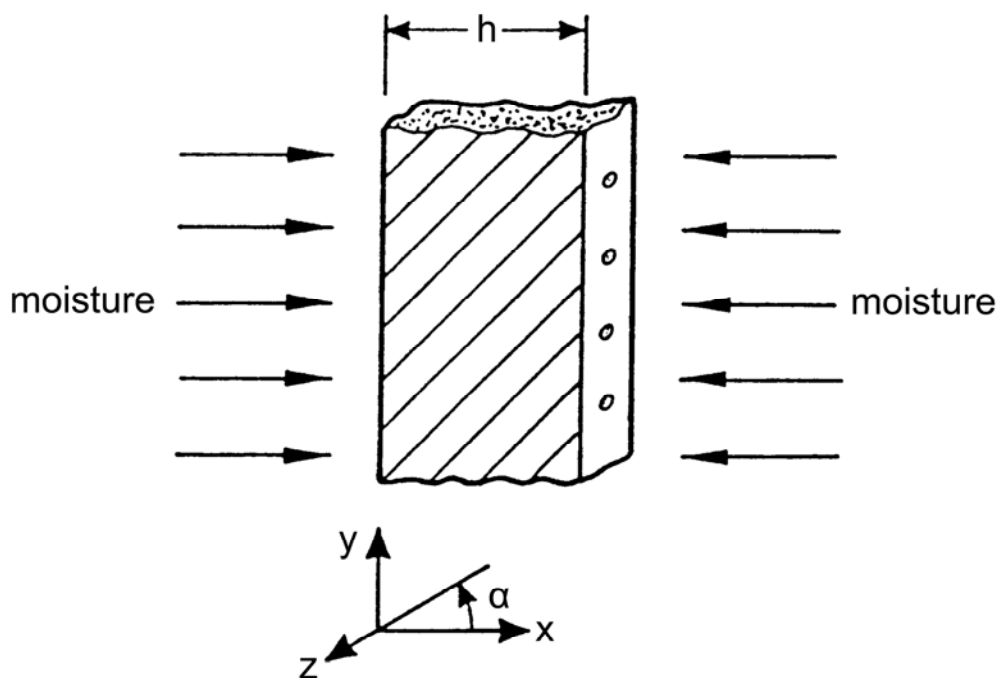


Figure 13.5-1 - Notation: Definition of axes

Additional assumptions for the definition of a Fickian process are, Ref. [13-5]:

- The environmental conditions (temperature, moisture) on both sides of the plate are constant.
- The temperature inside the material approaches equilibrium much faster than the moisture concentration, i.e. the temperature inside is equal to the environmental conditions.
- The temperature distribution inside the material is homogeneous.
- The diffusion coefficient depends only on temperature and is independent of moisture concentration or of the stress levels inside the material.

13.5.2 Determination of moisture content

Depending on the environmental conditions and the condition of the material itself, moisture is either absorbed or dried out. This weight gain or weight loss is described as the percentage moisture content M of the material as a function of time t , Ref. [13-5], defined as:

$$M = M_{(t)} = \frac{\text{weight wet material} - \text{weight dry material}}{\text{weight dry material}} \times 100 \quad [13.5-2]$$

If the process is assumed to be Fickian, [See: Fick's Law], the percentage moisture content during absorption or desorption is:

$$M = G(M_m - M_i) + M_i \quad [13.5-3]$$

The time-dependent parameter G is given in Ref. [13-5] as:

$$G = 1 - \frac{8}{\pi^2} \sum_{j=0}^{\infty} \frac{\exp\left[-(2j+1)^2 \pi^2 D_x t/s^2\right]}{(2j+1)^2} \quad [13.5-4]$$

According to Ref. [13-5], Eq [13.5-4] can be approximated by the expression, [See: Figure 13.5.2]:

$$G = 1 - \exp\left[-7.3(D_x t/s^2)^{0.75}\right] \quad [13.5-5]$$

NOTE Eq [13.5-3] is only valid for time periods greater than one day.

If the material is exposed only on one side, i.e. the material is insulated on one side; the equivalent thickness s is equal to twice the thickness h ($s = 2h$), otherwise $s = h$.

The diffusion coefficient D_x (normal to the surface) can be expressed for a unidirectional laminate as:

$$D_x = D_1 \cos^2 \alpha + D_2 \sin^2 \alpha \quad [13.5-6]$$

Generally, the diffusion of moisture in the fibres is small compared with that in the matrix (D_r). Consequently, the diffusion parallel to the fibres, D_1 , and that transverse to the fibres, D_2 , can be written as:

$$D_1 = (1 - V_f) D_m \quad [13.5-7]$$

$$D_2 = \left(1 - 2\sqrt{V_f/\pi}\right) D_m \quad [13.5-8]$$

Substituting Eq [13.5-7] and Eq [13.5-8] in Eq [13.5-6] gives:

$$D_x = D_m \left[(1 - V_f) \cos^2 \alpha + (1 - 2\sqrt{V_f/\pi}) \sin^2 \alpha \right] \quad [13.5-9]$$

13.5.3 Maximum moisture content

It has been observed from experiment that the maximum moisture content within the laminate is not sensitive to temperature, but does depend on the moisture content of the environment to which the material has been exposed.

According to Ref. [13-5], the maximum moisture content can be related to the relative humidity ϕ by the expression:

$$\hat{M} = a\phi^b \quad [13.5-10]$$

Where: a and b are material constants.

Table 13.5.1 gives a and b values for various materials, Ref. [13-5].

Table 13.5-1 - Summary of constants for the determination of the maximum moisture content, \hat{M}

$\hat{M} = a\phi^b [\%]$			
Material		a	b
Narmco	T300/5208 (70 vol. %)	1.5	1
Fiberite	T300/1034 (65 vol. %)	1.7	1
Hercules	AS/3501-5 (65 vol. %)	1.8	1
Resin Narmco	5208	6.7	1.32
Resin Fiberite	934	6.3	1.77
Resin Hercules	3501-1	6.3	1.46

There are variations in the reported values of these material constants, probably owing to differences in the curing processes. The value of b can be approximated by unity.

The maximum moisture content of the composite can also be estimated from the maximum moisture content of the neat resin, \hat{M}_m . The basis for this is the assumption that the fibres do not absorb any moisture. The assumption is only valid for carbon and glass fibres, aramid fibres do absorb moisture.

$$\hat{M} = \hat{M}_m \psi_m \quad [13.5-11]$$

Where: ψ_m is the weight fraction (percent) of resin in the composite.

13.5.4 Experimental determination of the diffusion coefficient

From Ref. [13-5], the material constants a and b in Eq [13.5-10] and the diffusion coefficient of a composite should be determined experimentally. If the diffusion coefficient of the resin is known, D_x can also be calculated using Eq [13.5-9] provided that:

- The specimen is completely dried in a desiccator and its dry weight is measured.
- The specimen is placed in a constant temperature, constant moisture environment and its weight is recorded as a function of time.
- The moisture content (percent weight gain) is plotted against the square root of t , as shown in Figure 13.5.2, to determine the diffusion coefficient and against the relative humidity ϕ , as shown in Figure 13.5.3, to determine the material constants a and b .

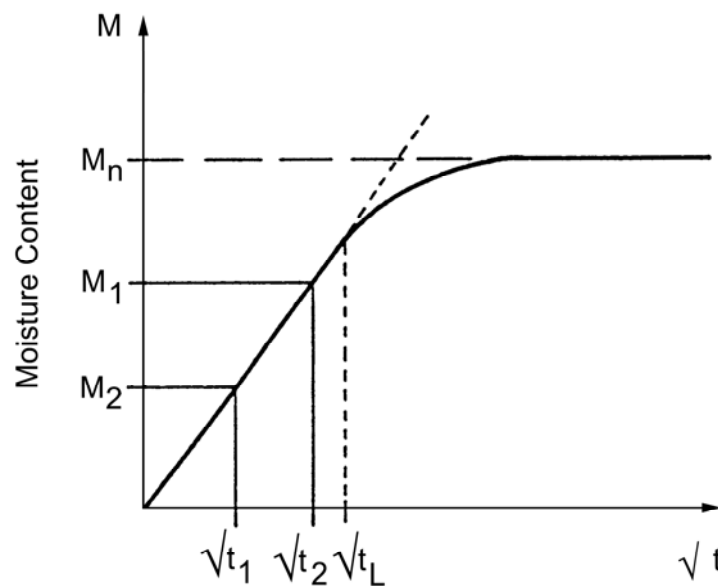


Figure 13.5-2 - Illustration of change of moisture content with square root of time

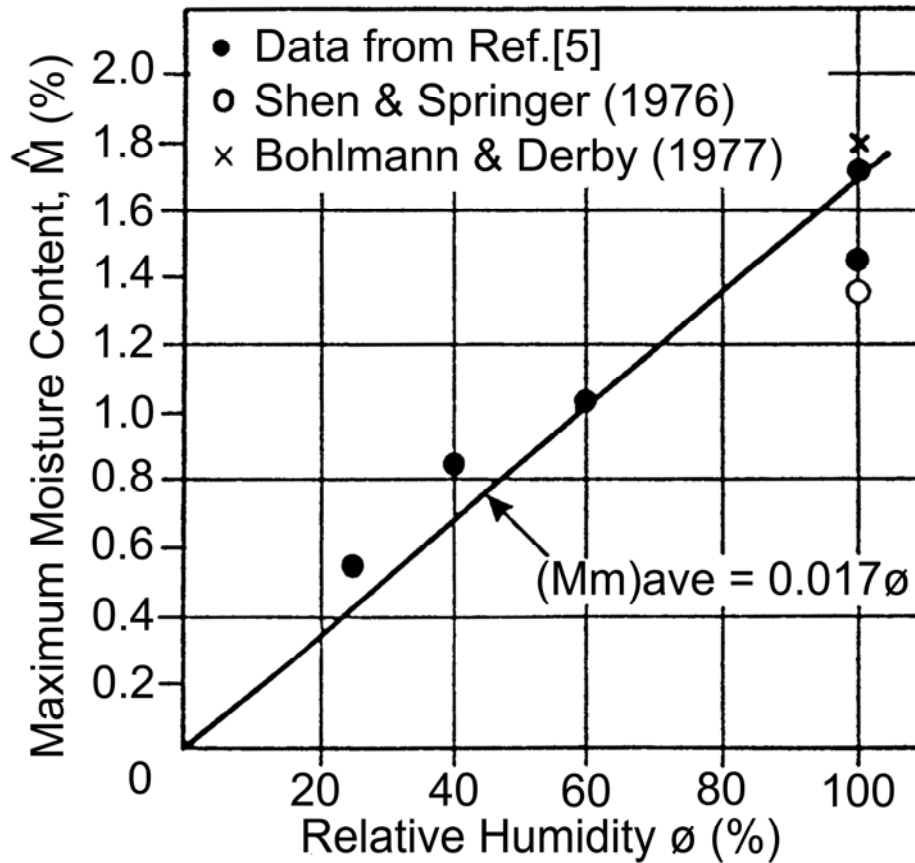


Figure 13.5-3 - Variation of maximum moisture content with relative humidity for a T300/1034 composite

The diffusion coefficient, D , is obtained from [Figure 13.5.2](#) from the initial slope $t < t_L$ of the \hat{M} versus \sqrt{t} curve.

$$D = \pi \left(\frac{h}{4\hat{M}} \right)^2 \left(\frac{M_2 - M_1}{\sqrt{t_2} - \sqrt{t_1}} \right)^2 \quad [13.5-12]$$

If all the fibres are parallel to the surface through which the moisture diffuses, the edges can be neglected:

$$D_x = D \quad [13.5-13]$$

If edge effects cannot be neglected, the method outlined in Ref. [13-5] should be used.

13.6 Calculation of swelling coefficient from constituents

13.6.1 General

Like the coefficient of thermal expansion, the swelling coefficient, β , for a unidirectional composite is not the same in the longitudinal and transverse directions. The longitudinal coefficient β_1 is generally small because fibres themselves usually do not absorb moisture. [Aramid](#) fibres are the exception because they do absorb moisture.

As swelling is predominantly caused by the matrix, the transverse coefficient of swelling β_2 is of more interest.

The two coefficients can be calculated in the same way as the coefficient of thermal expansion, as can the coefficients for the laminate as a whole.

A method for calculating the unidirectional swelling coefficients from the constituents is summarised from that provided in Ref. [\[13-6\]](#).

13.6.2 Swelling coefficient β_1 in fibre direction

$$\beta_1 = \frac{\beta_{f1} + \beta_m \left(\frac{1-V_f}{V_f} \right) E_m E_{f1}}{1 + \left(\frac{1-V_f}{V_f} \right) E_m E_{f1}} \quad [13.6-1]$$

The swelling coefficient β_1 can be approximated by:

$$\beta_1 \cong \beta_{f1} \quad [13.6-2]$$

but is normally neglected.

13.6.3 Swelling coefficient β_2 transverse to fibres

$$\beta_2 = \beta_{f1} V_f + \beta_m (1-V_f) - \frac{(1-V_f)(\nu_{f12} E_m / E_{f1} - \nu_m)}{1 + \left(\frac{1-V_f}{V_f} \right) E_m / E_{f1}} (\beta_m - \beta_{f1}) \quad [13.6-3]$$

Eq [13.6-3] can be approximated by:

$$\beta_2 = \beta_{f1} V_f + \beta_m (1 + \nu_m) - \beta_{f1} \nu_m (1 - V_f) \quad [13.6-4]$$

The variation of the swelling coefficients with fibre volume fraction is shown in Figure 13.6.1.

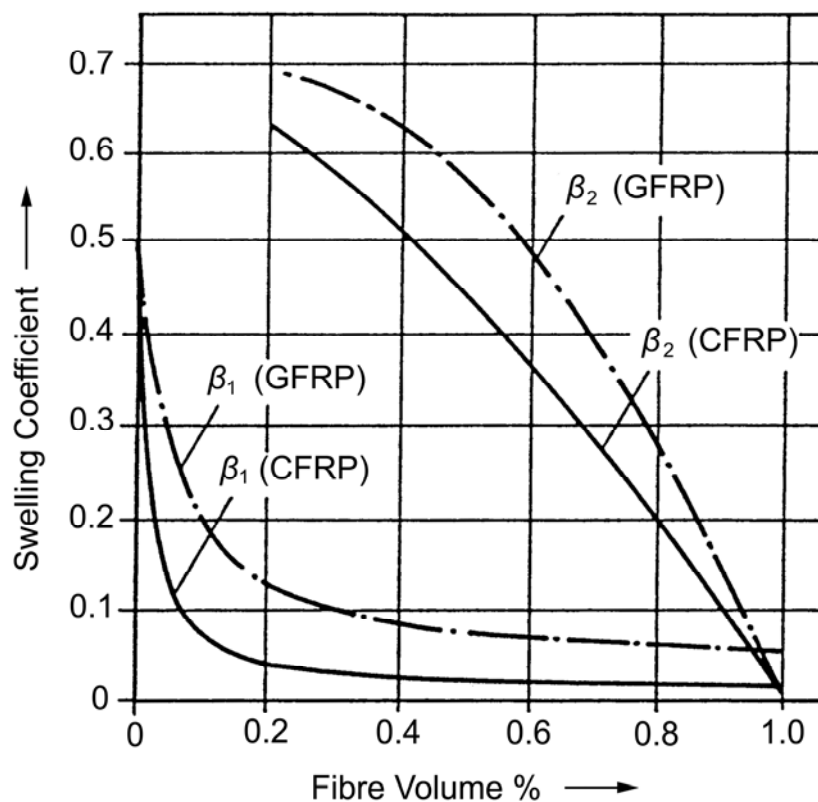


Figure 13.6-1 - Moisture: Coefficient of swelling for unidirectional composites

13.6.4 Swelling coefficient for a laminate

A change in the moisture content of a composite produces a change in its dimensions which is proportional to the change in moisture content and its initial dimensions. Thus, swelling strains develop in the composites as a result of changes in moisture content.

The swelling strain ϵ_m is given by:

$$\{\epsilon_m\}_i = \{\beta\}_i \Delta M_i \quad [13.6-5]$$

Dividing the swelling strains by the changes in moisture content ΔM , gives the coefficient of swelling, [See: Figure 13.6.2]:

$$\{\beta\}_i = \frac{1}{\Delta M_i} \{\epsilon_m\}_i \quad [13.6-6]$$

Where: β_i denotes the coefficients of the i -th layer of a composite.

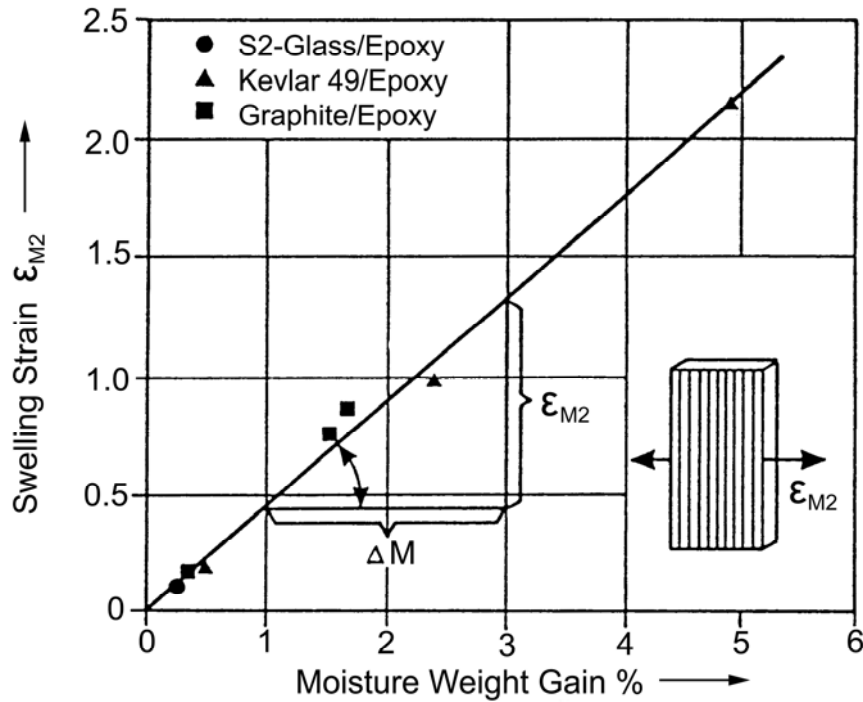


Figure 13.6-2 - Moisture: Definition of swelling coefficient β_2 for orthotropic material (unidirectional laminate)

Calculation of the swelling coefficient of a laminate is analogous to that of the coefficient of thermal expansion, [See: 12.4] and makes use of the expression:

$$\{\beta\} = \begin{bmatrix} [A] & [B] \\ [B] & [D] \end{bmatrix}^{-1} \sum_{i=1}^n \begin{bmatrix} [A] & [B] \\ [B] & [D] \end{bmatrix}_i \begin{Bmatrix} \beta \\ 0 \end{Bmatrix}_i \quad [13.6-7]$$

With:

$$[A] = \int_{-h/s}^{+h/2} [c']_i dz$$

$$[B] = \int_{-h/s}^{+h/2} [c']_i z dz$$

$$[D] = \int_{-h/s}^{+h/2} [c']_i z^2 dz$$

Where:

h is the thickness of the composite,

$[c']$ denotes the transformed stiffness matrix in the laminate coordinates x - y .

Figure 13.6.3 is an example of the calculated swelling coefficient of $[0^\circ/\pm 45^\circ/90^\circ]_s$ laminates for T300/914 composite.

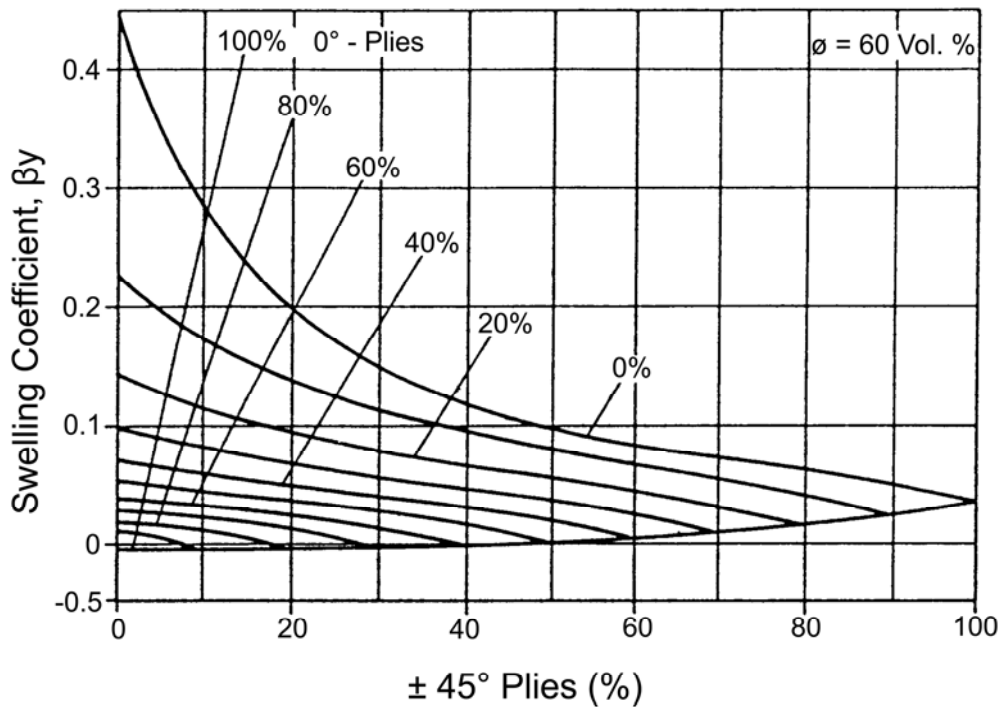


Figure 13.6-3 - Moisture: Swelling coefficients for T300/914 [0°/ ±45°/90°]s laminates

13.7 Coefficient of moisture expansion (CME)

13.7.1 Resin behaviour

13.7.1.1 General

The expansion characteristics of a composite are of interest for dimensionally stable structures, [See: Chapter 28].

[See also: 2.4 for matrix systems; 4.5 for hygrothermal effects]

13.7.1.2 In-plane

The coefficient of moisture expansion is principally a fibre-dominated characteristic, [See also: 5.3].

13.7.1.3 Through-thickness (transverse)

Expansion is both positive and large, reflecting the contribution of both resin and fibre. In this direction any swelling of the resin due to moisture absorption is directly conferred on the composite. The coefficient of moisture expansion (CME) of the resin is therefore an important parameter.

13.7.1.4 Measurement of CME

For the base resin, CME is measured as an increase in specimen dimension (strain) accompanying a weight gain by moisture absorption, often by:

$$\varepsilon^s = \beta C \quad [13.7-1]$$

Where:

ε = strain by swelling

β = CME

C = moisture content

This value describes the resin behaviour in the saturated state for a particular relative humidity and temperature. Ideally both moisture uptake and change in strain are small. The relationship between the two parameters need not be linear with respect to changes in relative humidity (RH) or temperature.

The moisture absorbency of resins differ enormously and can span a range up to 6% by weight in the fully saturated condition at elevated temperatures and high RH.

Moving from the first generation epoxies to toughened epoxies, cyanate esters and thermoplastics, the level of moisture absorption and hence expansion has reduced significantly. This is shown in Table 13.7.1 for UHM composites made with Fiberite 954-3 cyanate ester resin. The information is advisory only as the materials were not necessarily tested under the same conditions. The level of moisture take up is dependent on the fibre type, lay-up, cure temperature, temperature and RH.

[See also: Table 6.35.1 for data on RS3 cyanate ester resin alone]

Table 13.7-1 - Moisture absorption: Cyanate ester Fiberite 954 composites

	Fiberite® 954 Cyanate Resin Systems		
	954-3	954-2	934
Hygrostrain (ppm)	18.9	29.2	108.5
Water Absorption (%)	0.18†	0.17‡	0.70‡
CME <i>f</i> (ppm/%)	105	172	155
Lay-up	(0,+60,-60) _{XS}	(0,30,60,90,120,150) _S	
Key:	†: 55% RH/EQ ‡: 50% RH/EQ <i>f</i> : CME: Coefficient of moisture expansion = hygrostrain/%M Pseudo-isotropic P75 laminates; 30% RC		

13.7.2 Composite behaviour

13.7.2.1 General

The volume fraction of resin present in composites is typically 30% to 35% with the remainder as non-moisture absorbing fibre. The exception is aramid fibres which can absorb large quantities of moisture.

The amount of moisture absorbed by UHM CFRP composites can be as low as 0.2% with the newer resins.

13.7.2.2 CFRP composites

The magnitude of moisture expansion in CFRP caused by moisture uptake by the resin is dependent on the:

- Total amount of moisture absorbed (under specific saturation conditions)
- Resin expansion due to moisture (CME),
- Carbon fibre modulus,
- Fibre volume fraction.

This indicates that comparisons between different composites can be difficult if neither the resin nor the fibre is common.

To provide a means of comparison a theoretical calculation can be undertaken which normalises on a specific moisture weight gain and enables the difference in composite modulus to be taken into account. The value of such calculations is debatable unless the resins are radically different in their moisture absorption behaviours.

13.8 References

13.8.1 General

- [13-1] C.H. Shen & G.S. Springer
'Moisture absorption and desorption of composite materials'
Journal of Composite Materials, 10(1), 1976
- [13-2] P.E. McMahon & L. Ying
'Effects of fiber/matrix interactions on the properties of
graphite/epoxy composites'
NASA CR 3607, 1982
- [13-3] D.P. Bashford: Fulmer Research Ltd., UK
'Review of moisture absorption/desorption and its effects on residual
stresses in carbon fibre reinforced plastics for space applications'
- [13-4] DFVLR
'Development of fracture mechanics maps for composite materials'
ESA CR(P)-2017, January 1985

- [13-5] G.S. Springer
'Environmental Effects on Composite Materials'
Technomic Publishing Company Inc. 1981

- [13-6] G. Niederstadt et al
'Leichtbau mit kohlenstoffaserverstärkten Kunststoffen'
Kontakt & Studium, Bd. 167
Expert-Verlag, 1985

14

Stress concentrations and fracture

14.1 Introduction

14.1.1 General

Under steadily increasing test loads, failure of notched CFRP specimens is initiated in individual plies, long before the maximum load capability is reached. This occurs along or transverse to the fibres and also between certain plies. The partial damage in or between the plies, leads to a redistribution of the local stresses resulting in a complex failure.

14.1.2 Fracture mechanics models

Based upon the experience gained with brittle metallic materials, the linear elastic fracture mechanics, LEFM, approach was applied to describe the brittle fracture behaviour of CFRP materials.

Research directed towards the application of LEFM to composites indicates that it can only be applied in a limited number of cases because the approach based on metallic materials is physically wrong for composites.

Consequently, several modified fracture models have been proposed to overcome the shortcomings of LEFM for composite materials, [See: 14.3]. Primarily, these compare the critical stress intensity factor with that of metals.

Such fracture models also seek to predict the notch strength of composites, but it has to be emphasised that the semi empirical fracture models presented here do not directly address the micro and macro-failure associated with the crack extension process at the crack tip damage zone.

The failure process, type of damage and its progression (parameters associated with the different fracture models) strongly depend upon a variety of intrinsic and extrinsic variables, as summarised in Table 14.1.1, Ref. [14-1].

Table 14.1-1 - Intrinsic and extrinsic variables relevant for stress intensity factors

Intrinsic Variables	Extrinsic Variables
Laminate Configuration	Loading Function
Stacking Sequence	Loading Rate
Properties of Constituents	Specimen Geometry
Fibre Volume Fraction	Shape of Discontinuity
Fibre Matrix Interface	Test Temperature
Fabrication Procedure	Moisture Control

14.2 Analytical notation for stress concentrations

Formulae:

E_x, E_y	Young's modulus of the laminate
G_{xy}	shear modulus of the laminate
K_t	concentration factor (tensile)
K_s	concentration factor (shear)
ν_{xy}	Poisson's ratio
σ	tensile stress
τ	shear stress

Subscripts:

A	point on the circumference of the hole for which the tangential stresses are of interest
x, y	orthotropic axes of the laminate
α	angle in relation to the orthotropic axis
θ	circumferential angle at the hole
∞	undisturbed area (infinity)

14.3 Summary of fracture models

Table 14.3.1 summarises some of the fracture models applied to composites, with comments on their scope and authors, Ref. [14-1].

Table 14.3-1 - Some fracture models and their authors

Model Abbr.	Fracture Criterion	Application		Authors	[Reference]
		Hole	Crack		
WEK	Linear Elastic Fracture Mechanics (LEFM) [See: 14.5]	✓	✓	Waddoups, M.E. Eisenmann, J.R. Kaminski, B.E.	Ref. [14-3]
WN	Point Stress Average Stress [See: 14.6]	✓	✓	Whitney, J.M. Nuismer, R.Y.	Ref. [14-4] , [14-5]
K	Point Stress	✓		Karlak, R.F.	Ref. [14-6]
PWG	Point Stress	✓	✓	Pipes, R.B. Wetherhold, R.C. Gillespie, J.W.	Ref. [14-7] , [14-8] , [14-9]
ML	$N \neq -0.5$	✓	✓	Mar, J.W. Lin, K.Y.	Ref. [14-10] , [14-11]
PS	Strain	✓		Poe, C.C. Sova, J.A.	Ref. [14-12]

14.4 Evaluation of fracture models

Based on the research of Awerbuch, Ref. [14-1], some general comments on fracture models for composites includes:

- Good agreement between all fracture models and all experimental results, [See: Table 14.3.1].
- All fracture models are semi empirical, i.e. they can be applied providing that at least two or three (depending on the fracture model) notched strength data are known.
- The fracture models include certain parameters assumed to be material constants. i.e. independent of specimen geometry:
 - These parameters strongly depend on laminate configuration and material system as well as on the variety of intrinsic and extrinsic variables, [See: Table 14.1.1].
 - These parameters should be determined experimentally for each laminate lay-up and material system independently
- The number of tests to be conducted in determining the fracture model's parameters depends on the model itself and the level of accuracy required.
- In all fracture models the actual pattern and details of the notch tip damage are by passed by assuming an 'effective' notch tip damage zone which grows in a self similar manner.
- Most CFRP laminates are highly notch sensitive. For many cases, the notched strength is reduced by as much as 50% for notch length to width ratios of 0.2 to 0.3, as shown in Figure 14.4.1.

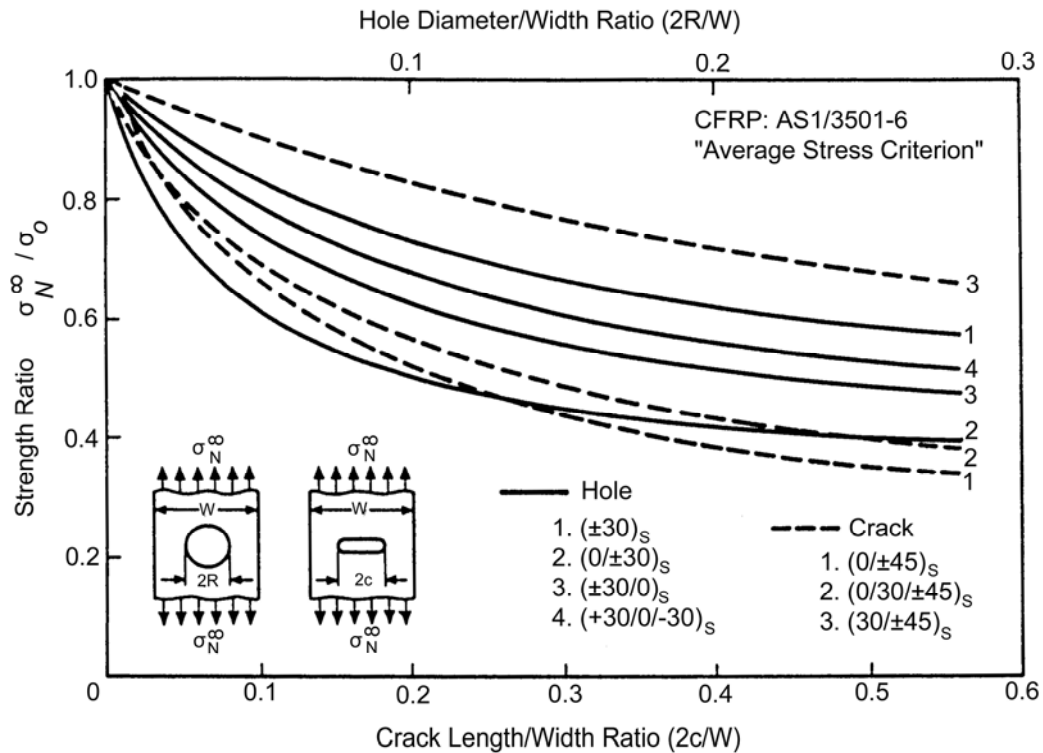


Figure 14.4-1 - Strength ratio versus hole diameter: Crack length for WN fracture model - 'Average stress criterion'

14.5 WEK fracture model

14.5.1 General

The basic assumptions for the Waddoups, Eisenmann and Kaminski (WEK) model, Ref. [14-3], are based upon the LEFM linear elastic fracture mechanics approach, which can be directly applied to anisotropic materials given that the conditions are, Ref. [14-2]:

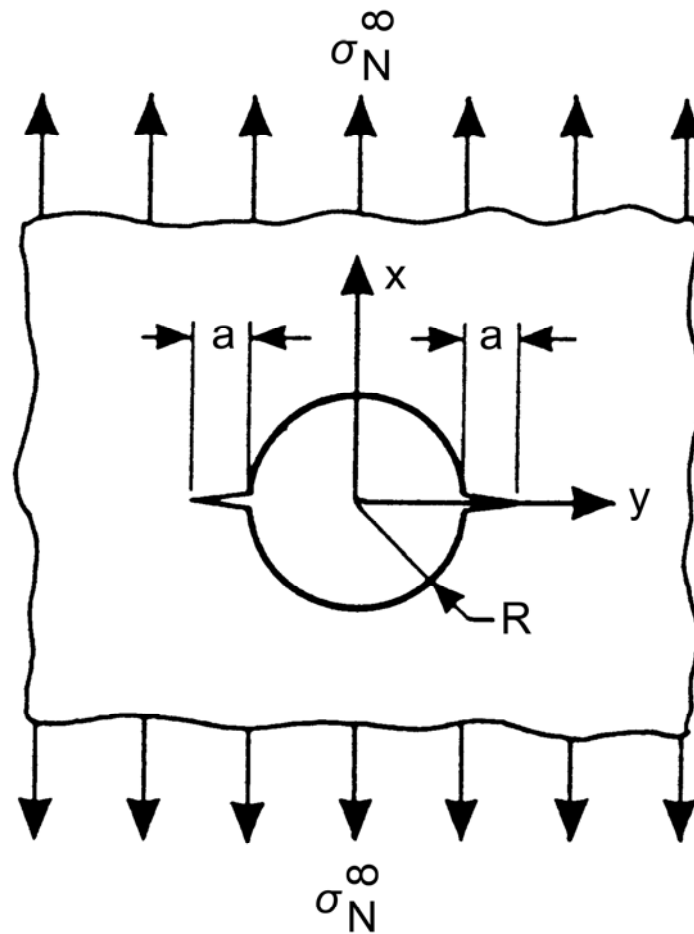
- The orientation of the flaw (notch) with respect to the main axis of symmetry is fixed.
- The stress intensity factor defined for anisotropic cases is consistent with the isotropic case in stress distribution and in crack displacement models.
- The critical orientation coincides with one of the main directions of elastic symmetry.

Dependent upon material parameters, an equivalent damage tip zone is defined. The total defect is considered the superposition of the defect initially present (before loading) and the damage tip zone. The stress intensity factor and the equivalent damage tip zone are assumed to be material constants.

14.5.2 Circular holes

Bowie, Ref. [14-13], provides a stress intensity factor for symmetrical cracks emanating from a circular hole in an infinite isotropic plate, as defined in Figure 14.5.1, with the result:

$$K_I = \sigma_N^\infty \sqrt{\pi a} f(a/R) \quad [14.5-1]$$



a = Characteristic Dimension of the Intense Energy Region

Figure 14.5-1 - Notation: Infinite isotropic plate with circular hole

Failure occurs when the applied stress reaches σ_N^∞ :

$$\sigma_N^\infty = \frac{K_{IC}}{\sqrt{\pi a} f(a/R)} \quad [14.5-2]$$

In the case of an infinite plate without a hole:

$$R = 0$$

$$a/R = \infty$$

And, from Ref. [14-1]:

$$f(a/R) = 1$$

The unnotched strength σ_0 is defined as:

$$\sigma_0 = \frac{K_{IC}}{\sqrt{\pi a}} \quad [14.5-3]$$

Thus the notch sensitivity becomes:

$$\sigma_N^\infty / \sigma_0 = \frac{1}{f(a/R)} \quad [14.5-4]$$

It is assumed that a is independent of the hole radius. Thus, Eq [14.5-4] predicts the notch strength to be a function of absolute hole size.

An approximation for the function $f(a/R)$ is given by:

$$f(a/R) = \frac{C_1}{C_2 + a/R} + C_3 \quad [14.5-5]$$

With: $C^1 = 0.6866$
 $C^2 = 0.2772$
 $C^3 = 0.9439$

The equivalent damage zone size, a , can now be adapted such that the equations for notched and unnotched conditions are fulfilled best. Using Equation [14.5-5] a value a_c is given as:

$$a_c = R \left[\frac{C_1}{\sigma_0 / \sigma_N^\infty - C_3} - C_2 \right] \quad [14.5-6]$$

The notch sensitivity $\sigma_N^\infty / \sigma_0$ represented by this single parameter is shown for a $[\pm 45^\circ/0^\circ]_s$ CFRP laminate in Figure 14.5.2, Ref. [14-1].

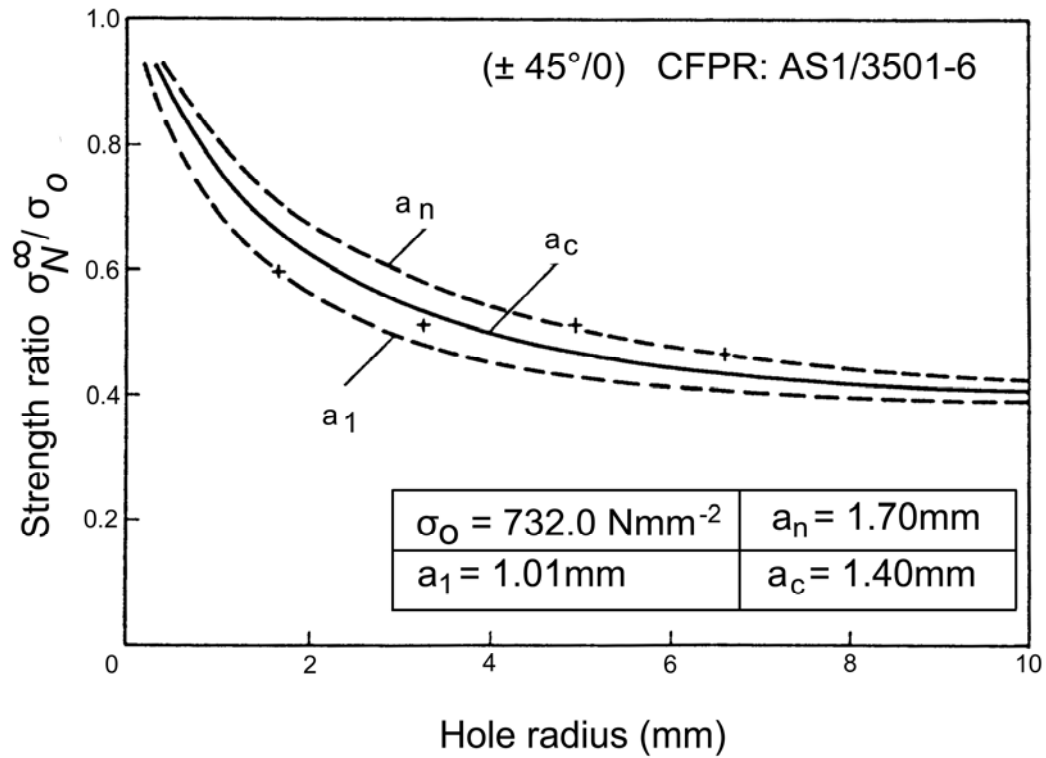


Figure 14.5-2 - Comparison between experiment and prediction by WEK model

14.5.3 Straight crack

Figure 14.5.3 shows the notation for a straight crack.

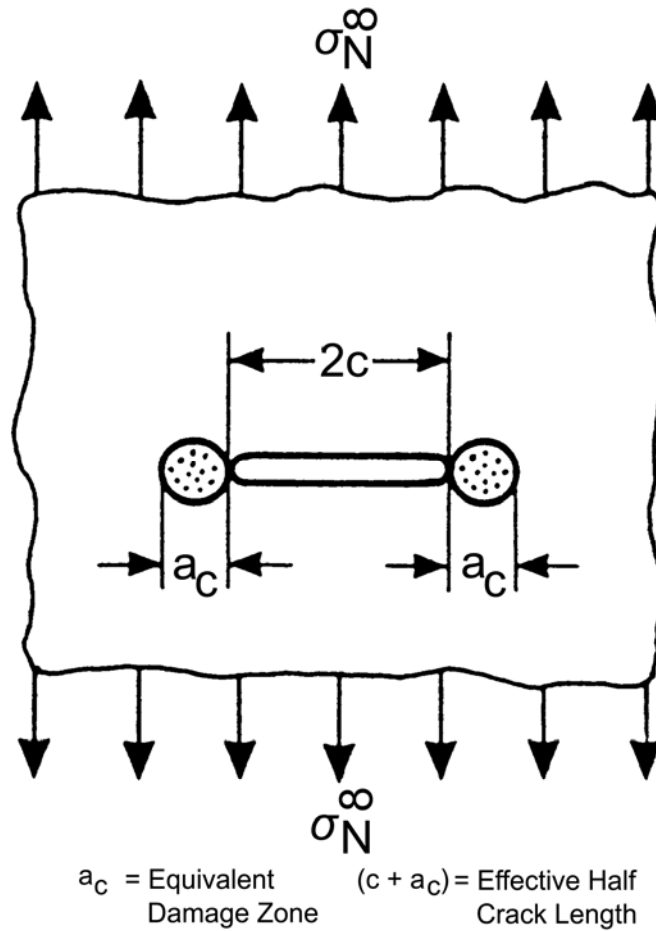


Figure 14.5-3 - Notation: Infinite plate with straight crack

In a similar way to the plastic zone correction, Ref. [14-14], the stress intensity is defined as:

$$K_{IC} = \sigma_N^{\infty} \sqrt{\pi(c + a_c)} \quad [14.5-7]$$

In the unnotched condition:

$$c = 0$$

$$\sigma_N^{\infty} = \sigma_0$$

Therefore:

$$K_{IC} = \sigma_0 \sqrt{\pi a_c} \quad [14.5-8]$$

Hence the notch sensitivity becomes:

$$\frac{\sigma_N^\infty}{\sigma_0} = \sqrt{\frac{a_c}{c+a_c}} \quad [14.5-9]$$

An example of the strength ratio versus half crack length for a $[0/90/\pm 45]_S$ CFRP laminate is given in Figure 14.5.4.

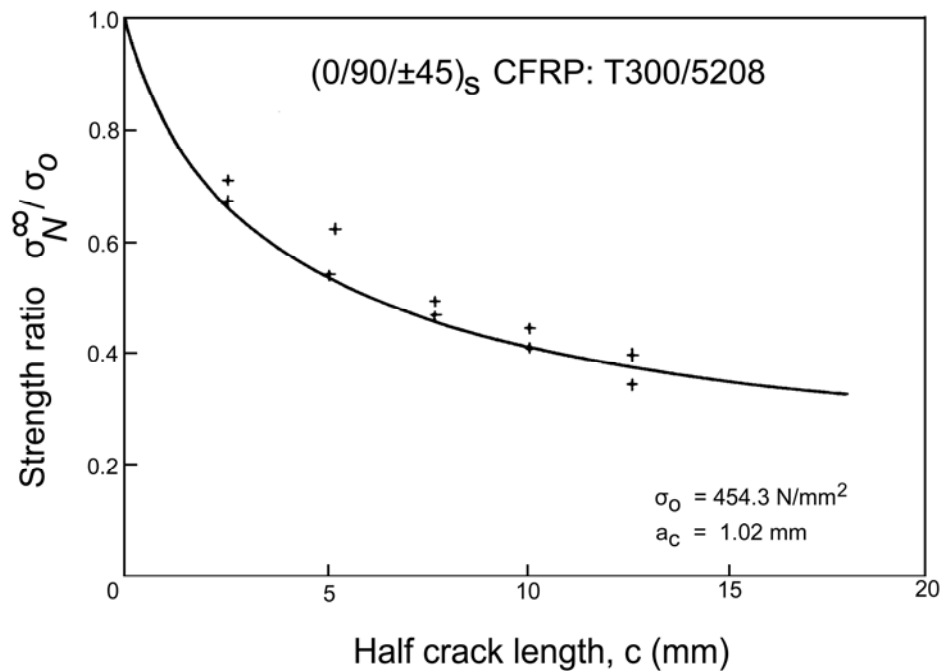


Figure 14.5-4 - Comparison between experiment and prediction by WEK model

If the equivalent damage zone a_c is assumed to be independent of the crack length c , a_c can be calculated with σ_0 and σ_N^∞ derived from tests and different crack length c , using Equation [14.5-10].

$$a_c = \frac{c}{\left[\left(\frac{\sigma_0}{\sigma_N^\infty} \right)^2 - 1 \right]} \quad [14.5-10]$$

Best fit curves from tests are shown in Figure 14.5.5, Ref. [14-1].

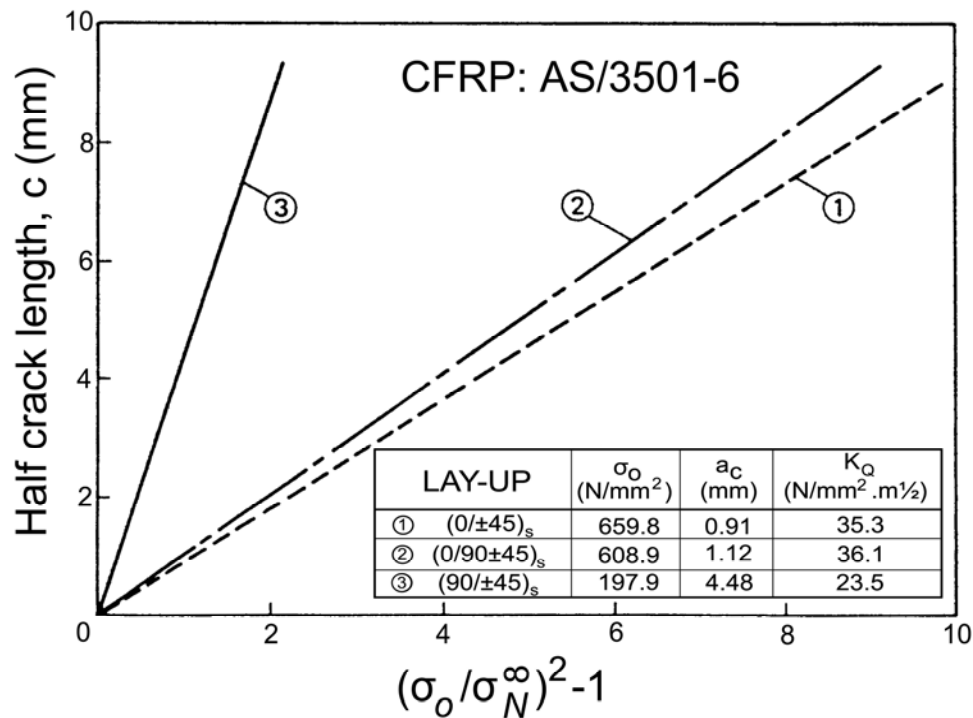


Figure 14.5-5 - Determination of ac for various laminates

14.6 WN fracture model

14.6.1 General

The WN model predicts that final fracture of a notched multi angle laminate occurs when the stress in a certain zone exceeds the ultimate strength of the unnotched material.

The different failure criteria formulated are:

- Point stress criterion.
- Average stress criterion.

14.6.2 Failure criteria

14.6.2.1 Point stress criterion

The point stress criterion, notation shown in [Figure 14.6.1](#), assumes that failure occurs when the stress, σ_x , over some distance, d_0 , away from the discontinuity is equal to or greater than the strength of the unnotched laminate, Ref. [\[14-4\]](#):

$$\sigma_x(0, y) = \sigma_0 \quad [14.6-1]$$

at:

$$y = R + d_0$$

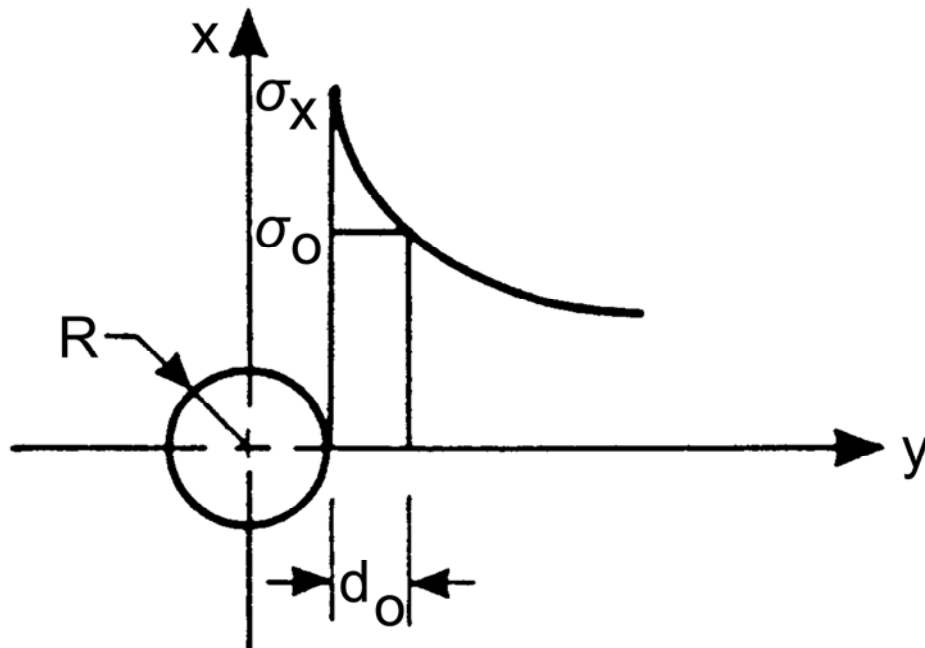


Figure 14.6-1 - Notation: Point stress criterion diagram

14.6.2.2 Average stress criterion

The average stress criterion, notation given in Figure 14.6.2, assumes that failure occurs when the average stress, σ_x , over some distance, a_0 , equals the unnotched laminate strength, Ref. [14-4]:

$$\sigma_0 = \frac{1}{a_0} \int_R^{R+a_0} \sigma_x(0, y) dy \quad [14.6-2]$$

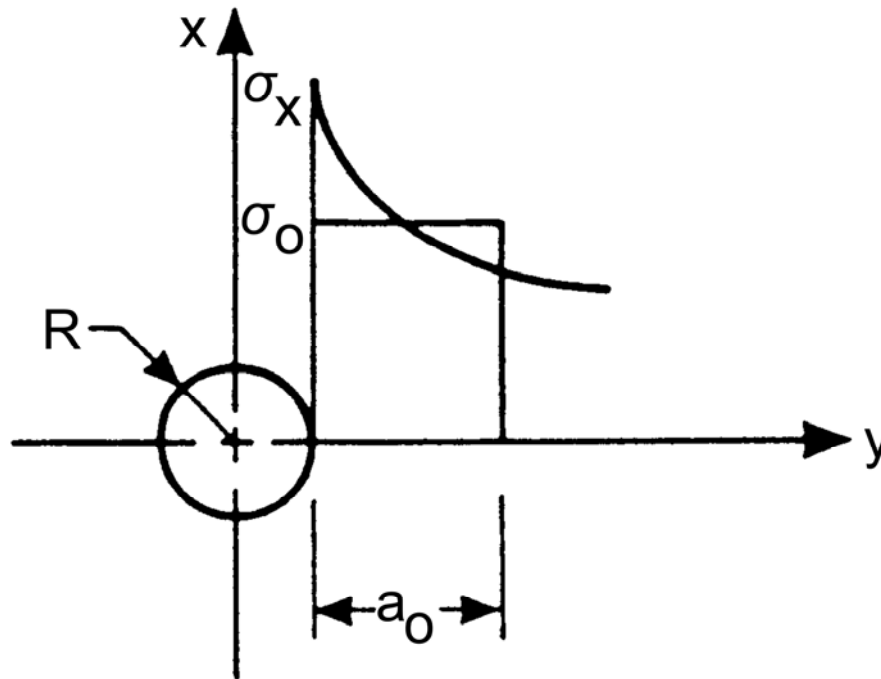


Figure 14.6-2 - Notation: Average stress criterion diagram

14.6.3 Characteristics of WN fracture model

Features of the WN fracture model are:

- Both stress failure criteria are two parameter fracture models: σ_x and d_0 or a_0
- For any material system they can be determined experimentally from testing unnotched and notched specimens.
- It is recommended at least two tests to be performed, normally more tests are performed to take into account a scatter in test results.
- The characteristic distances d_0 and a_0 depend on the type of laminate and are assumed to be material constants.
- The characteristic distances are determined experimentally for each material system and laminate lay-up independently.
- When d_0 and a_0 are determined, both failure criteria can be applied to predict the trend for the notch strength and the critical stress intensity factor.
- Excellent agreement with experiments when d_0 and a_0 are properly determined; illustrated in Figure 14.6.8 and Figure 14.6.9.
- Results obtained by Awerbuch, Ref. [14-1], indicate that d_0 and a_0 are independent of notch size; shown in Figure 14.6.11.
- In contrast to the WEK model, [See: 14.5], $KIC = KQ$ is not a material constant.

14.6.4 Circular holes

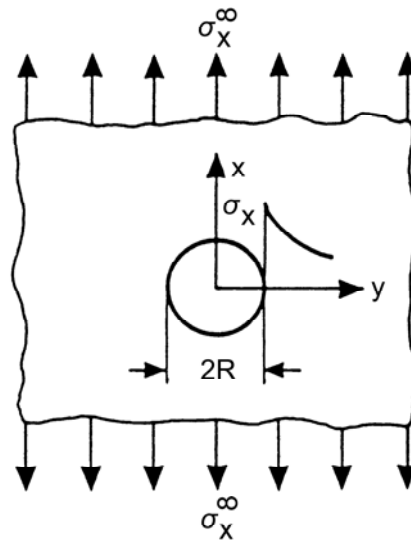


[Figure 14.6.3](#) shows a diagrammatic representation of an infinite orthotropic plate with circular hole.

Figure 14.6-3 - Notation: Infinite orthotropic plate with circular hole

For an infinite orthotropic plate subject to a uniform stress, σ_x^∞ , applied parallel to the x -axis at infinity, the normal stress, σ_x along the y -axis ahead of the hole can be expressed as:

$$\sigma_x(0, y) = \frac{\sigma_x^\infty}{2} \left\{ 2 + \left(\frac{R}{y}\right)^2 + 3\left(\frac{R}{y}\right)^4 - (K_T^\infty - 3) \left[5\left(\frac{R}{y}\right)^6 - 7\left(\frac{R}{y}\right)^8 \right] \right\} \quad [14.6-3]$$

with the orthotropic stress concentration factor for infinite plates:

$$K_T^\infty = 1 + \left\{ 2 \left[(E_1/E_2)^{1/2} - \nu_{12} + 0.5 E_1/G_{12} \right] \right\}^{1/2} \quad [14.6-4]$$

E_1 , E_2 , ν_{12} and G_{12} are the effective elastic moduli of an orthotropic laminate, [See: [Figure 14.6.3](#) for notation].

Using Eq [\[14.6-3\]](#) in conjunction with the [point stress criterion](#):

$$\frac{\sigma_N^\infty}{\sigma_0} = \frac{2}{2 + \phi_1^2 + 3\phi_1^4 - (K_N^\infty - 3) (5\phi_1^6 - 7\phi_1^8)} \quad [14.6-5]$$

with:

$$\phi_1 = \frac{R}{R+d_0} \quad [14.6-6]$$

When $R \rightarrow \infty$ (large holes, $\phi_1 = 1$): $\sigma_N^\infty / \sigma_0 = 1 / K_T^\infty$

When $R \rightarrow 0$ (small holes, $\phi_1 = 0$): $\sigma_N^\infty / \sigma_0 = 1.00$

For quasi isotropic materials $K_T = 3.0$:

$$\sigma_N^\infty / \sigma_0 = \left\{ \frac{2}{2 + \phi_1^2 + 3\phi_1^4} \right\} \quad [14.6-7]$$

When $R \rightarrow \infty$ (large holes, $\phi_1 = 1$): $\sigma_N^\infty / \sigma_0 = 1/3$

When $R \rightarrow 0$ (small holes, $\phi_1 = 0$): $\sigma_N^\infty / \sigma_0 = 1.00$

Applying the average stress criterion to Eq [14.6-3]:

$$\sigma_N^\infty / \sigma_0 = \frac{2(1-\phi_2)}{2 - \phi_2^2 - \phi_2^4 + (K_T^\infty - 3)(\phi_2^6 - \phi_2^8)} \quad [14.6-8]$$

With:

$$\sigma_2 = \frac{R}{R+a_0} \quad [14.6-9]$$

When $R \rightarrow \infty$ (large holes, $\phi_2 = 1$): $\sigma_N^\infty / \sigma_0 = 1 / K_T^\infty$

When $R \rightarrow 0$ (small holes, $\phi_2 = 0$): $\sigma_N^\infty / \sigma_0 = 1.00$

When $K_T = 3.0$ (quasi-isotropic materials):

$$\sigma_N^\infty / \sigma_0 = \frac{2(1-\phi_2)}{(2-\phi_2^2-\phi_2^4)} \quad [14.6-10]$$

When $R \rightarrow \infty$ (large holes, $\phi_2 = 1$): $\sigma_N^\infty / \sigma_0 = 1/3$

When $R \rightarrow 0$ (small holes, $\phi_2 = 0$): $\sigma_N^\infty / \sigma_0 = 1.00$

A comparison of analytical results for point stress criterion and average stress criterion with experiment is given in Figure 14.6.4, Ref. [14-1].

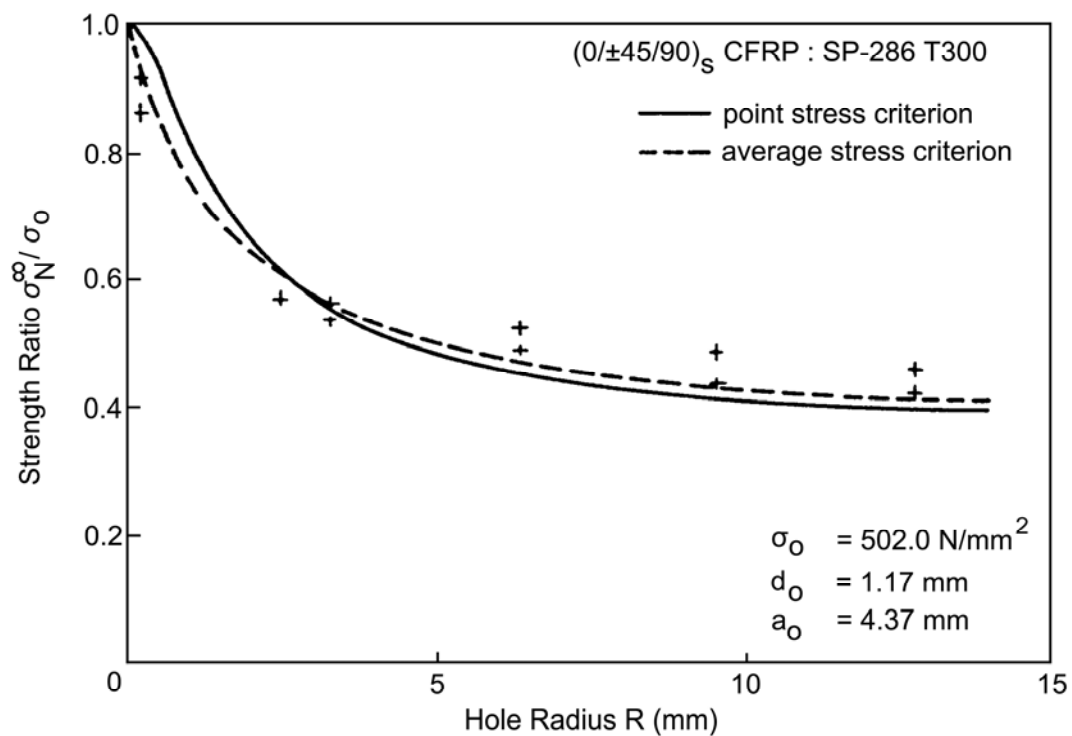


Figure 14.6-4 - Comparison between experiments and predictions of WN model

The effects of the stacking sequence of a laminate on the notch sensitivity are shown in Figure 14.6.5, Ref. [14-1].

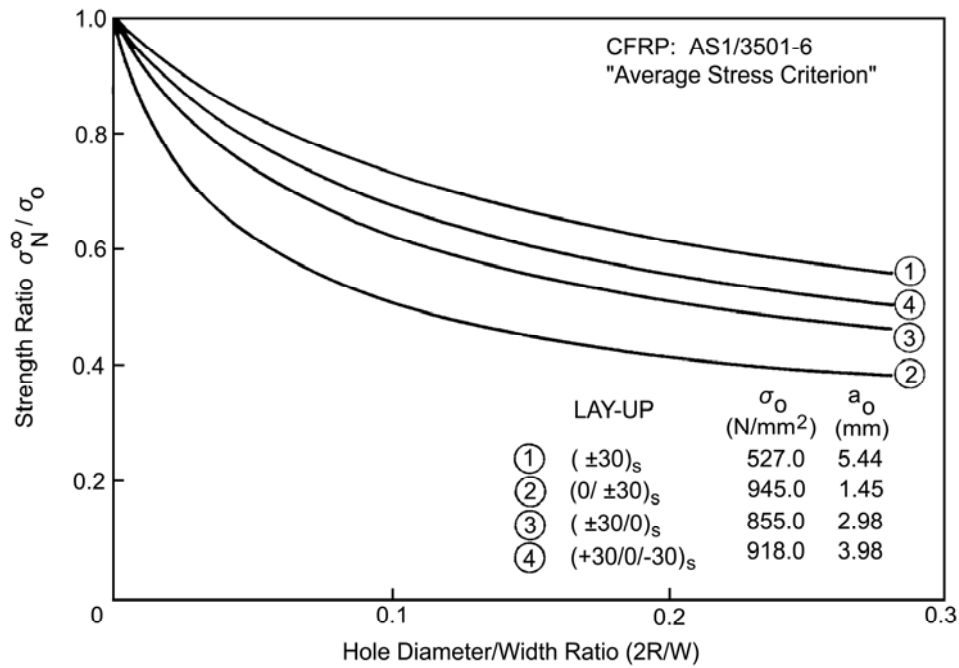


Figure 14.6-5 - Effects of stacking sequence on notch sensitivity

The effects of fibre angle variation of a laminate on the notch sensitivity are shown in Figure 14.6.6, Ref. [14-1].

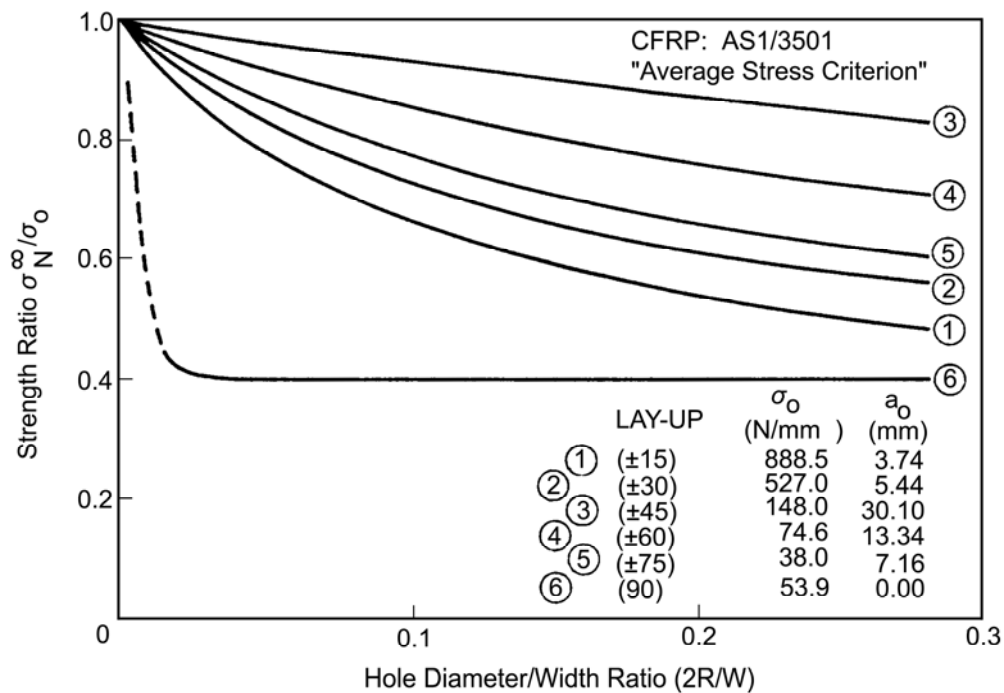


Figure 14.6-6 - Effects of fibre angle on notch sensitivity

14.6.5 Straight cracks

Figure 14.06.7 shows a diagrammatic representation of an infinite orthotropic plate with straight crack.

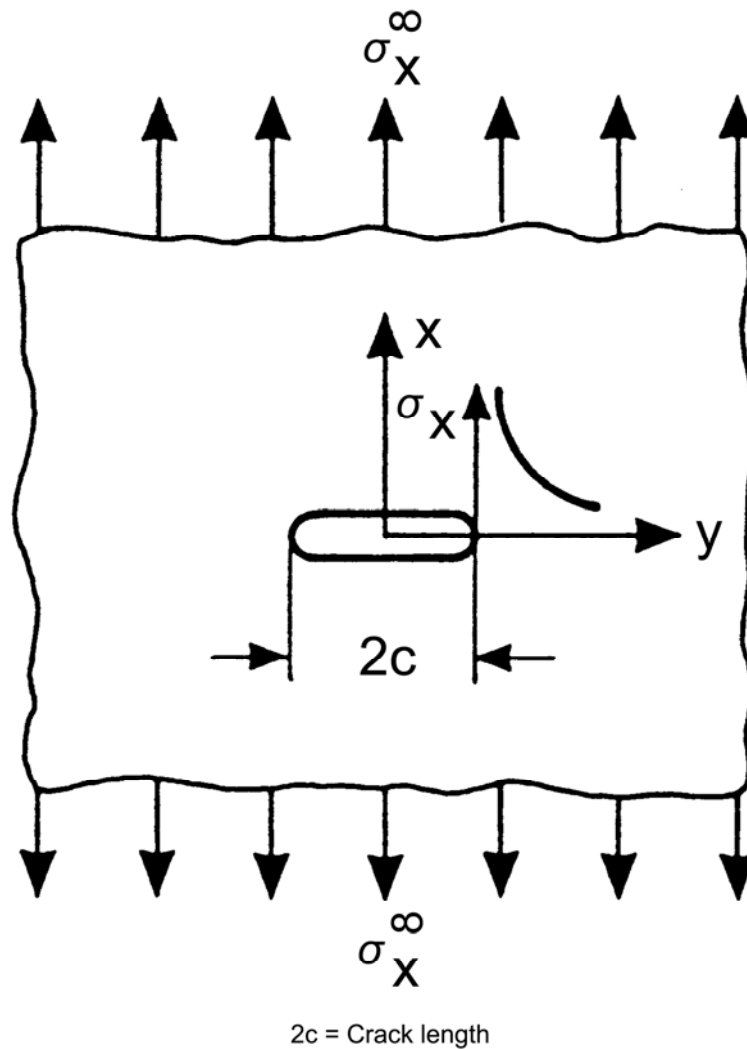


Figure 14.6-7 - Infinite orthotropic plate with straight crack

The stress in the vicinity of a crack in an orthotropic laminate of infinite width under uniaxial loading, σ_x^∞ , yields a singularity at the crack tip.

The exact expression for the stress ahead of the crack can be written, after Ref. [14-15], as:

$$\sigma_x(0, y) = \frac{\sigma_x^\infty y}{\sqrt{y^2 - c^2}} \quad y > c \quad [14.6-11]$$

This is independent of material properties.

Because of the singularity of the crack tip the concept of a stress concentration factor is replaced by a stress intensity factor.

For uniaxial tension (Mode I) this factor is defined as:

$$K_I = \sigma_x^\infty \sqrt{\pi c} \quad [14.6-12]$$

The stress distribution, Eq [14.6-11], in terms of the stress intensity factor is given by:

$$\sigma_x(0, y) = \frac{K_I y}{\sqrt{\pi c (y^2 - c^2)}} \quad y > c \quad [14.6-13]$$

For large cracks, the approximate expression is:

$$\sigma_x(0, y) = \frac{K_I}{\sqrt{2\pi(y-c)}} = \sigma_x^\infty \sqrt{\frac{c}{2(y-c)}} \quad [14.6-14]$$

This gives predictions close to the exact solutions of Eq [14.6-11] and Eq [14.6-13]. For smaller cracks Eq [14.6-11] or [14.6-13] can be applied.

14.6.6 Point stress criteria

Applying the point stress criterion in conjunction with Eq [14.6-11] or Eq [14.6-13], the notch sensitivity of an infinite laminate plate with a centre crack becomes:

$$\sigma_N / \sigma_0 = \sqrt{1 - \phi_3^2} \quad [14.6-15]$$

With:

$$\phi_3 = \frac{c}{c + d_0} \quad [14.6-16]$$

The critical stress intensity factor K_{IQ} becomes:

$$K_{IQ} = \sigma_0 \sqrt{\pi c (1 - \phi_3^2)} \quad [14.6-17]$$

Using Eq 14.06.14 gives:

$$K_Q = \sigma_0 \sqrt{2\pi d_0} = \text{const} \quad [14.6-18]$$

14.6.7 Average stress criterion

Applying the average stress criterion in conjunction with Eq [14.6-11] or Eq [14.6-13], the notch sensitivity ratio gives:

$$\sigma_N^\infty / \sigma_0 = \sqrt{\frac{1-\phi_4}{1+\phi_4}} \quad [14.6-19]$$

With:

$$\phi_4 = \frac{c}{c+a_0} \quad [14.6-20]$$

And:

$$a_0 = \frac{2c}{\sigma_0 / \sigma_N^\infty - 1} \quad [14.6-21]$$

The critical stress intensity factor becomes:

$$K_Q = \sigma_0 \sqrt{\pi c (1-\phi_4)(1+\phi_4)} \quad [14.6-22]$$

Using Eq [14.6-14]:

$$K_Q = \sigma_0 \sqrt{\pi a_0 / 2} = \text{const} \quad [14.6-23]$$

From Eq [14.6-19] and Eq [14.6-20]:

$$\sigma_N^\infty / \sigma_0 = \sqrt{(a_0/2)/(c+a_0/2)} \quad [14.6-24]$$

This is similar to [WEK](#) fracture model, [See: [14.5](#) (Eq [\[14.5-9\]](#))] with $a_0 = 2a_c$.

Figure 14.06.8 shows a good correlation between the analytical results for both criteria with tests, while Figure 14.06.9 shows the correlation of calculated stress intensity factors with tests, Ref. [14-1].

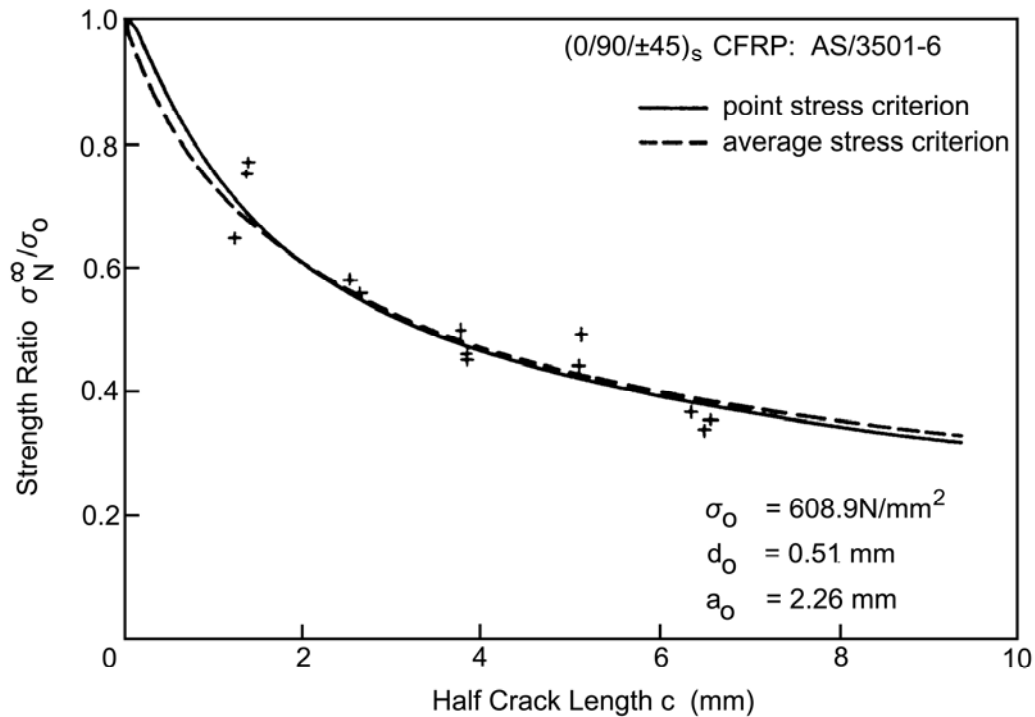


Figure 14.6-8 - Comparison between experiments and predictions of WN model

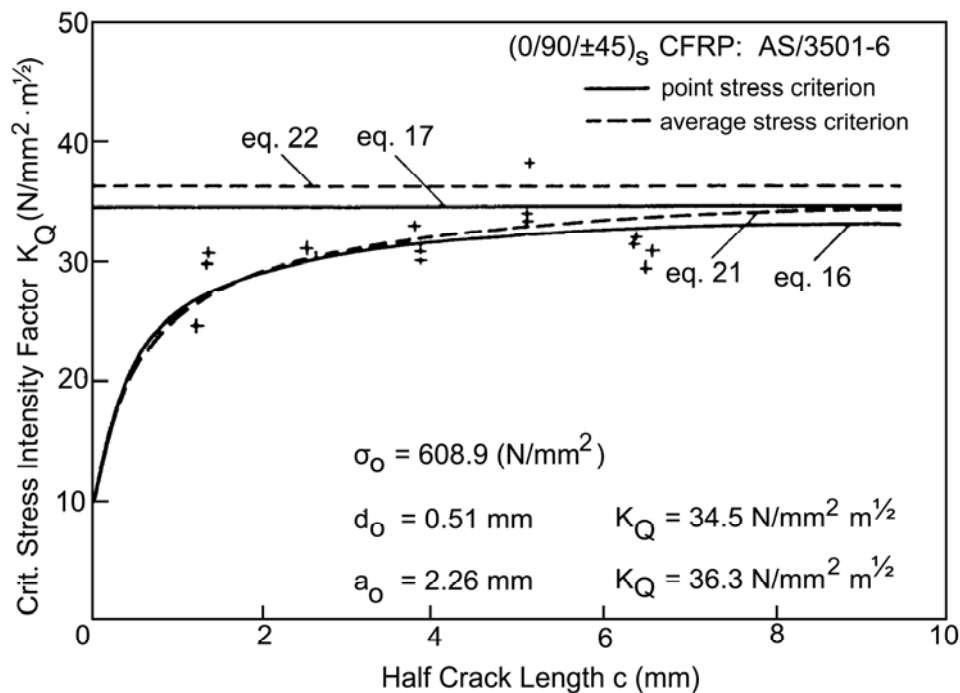


Figure 14.6-9 - Critical stress intensity factor K_Q

Best fit curves for the determination of a_0 from test are shown in [Figure 14.06.10](#) for different laminates, Ref. [\[14-1\]](#).

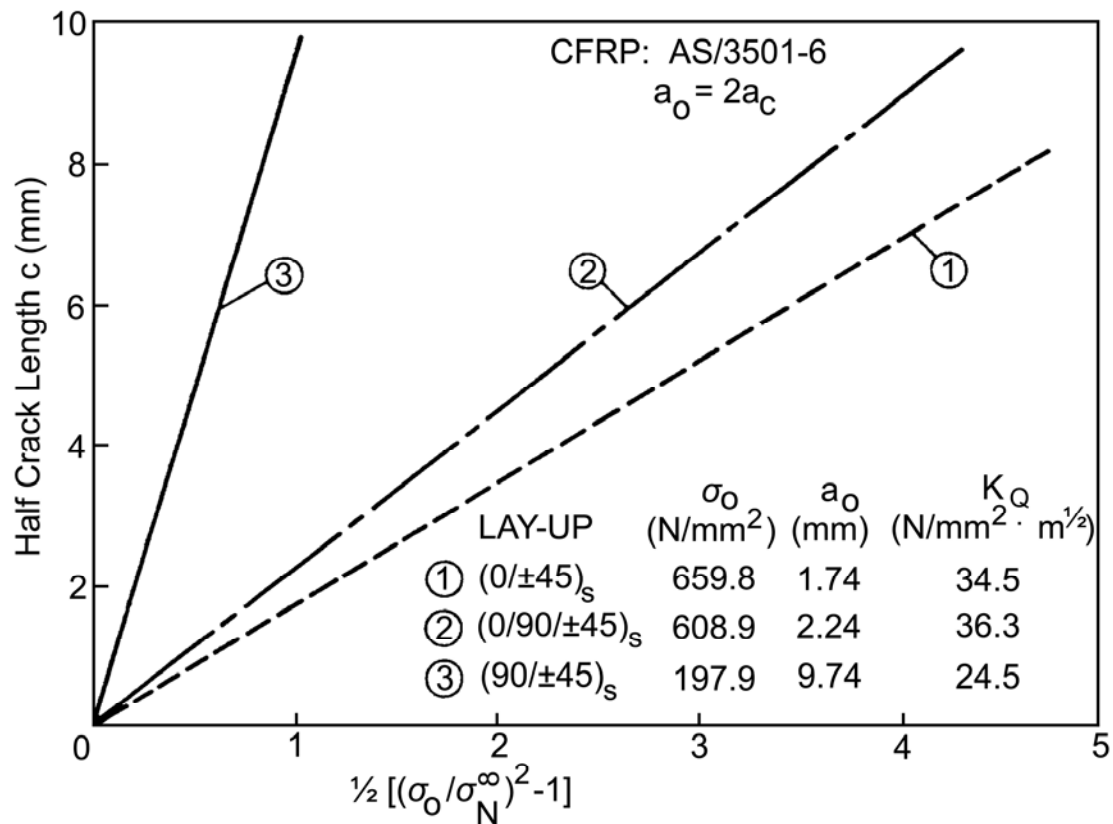


Figure 14.6-10 - Determination of a_0 for various laminates, applying 'Average stress criterion'

The agreement with results from the [WEK](#) model is fairly good, [See: [Figure 14.05.4](#)].

The [WN](#) model assumes that the characteristic lengths d_0 and a_0 are material constants and are independent of crack length.

From [Figure 14.06.11](#), Ref. [\[14-1\]](#), it can be deduced that this can be true for d_0 (point stress criterion) to a greater extent than for a_0 (average stress criterion).

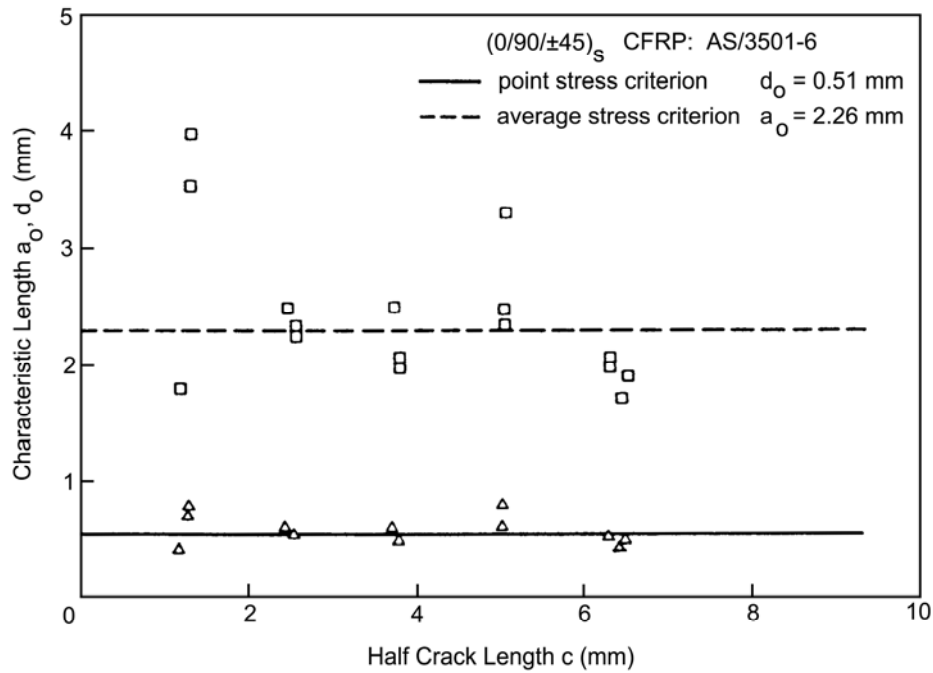


Figure 14.6-11 - Characteristic dimensions as a function of half crack length

The effect of the laminate lay up on notch sensitivity is shown in Figure 14.06.12, Ref. [14-1].

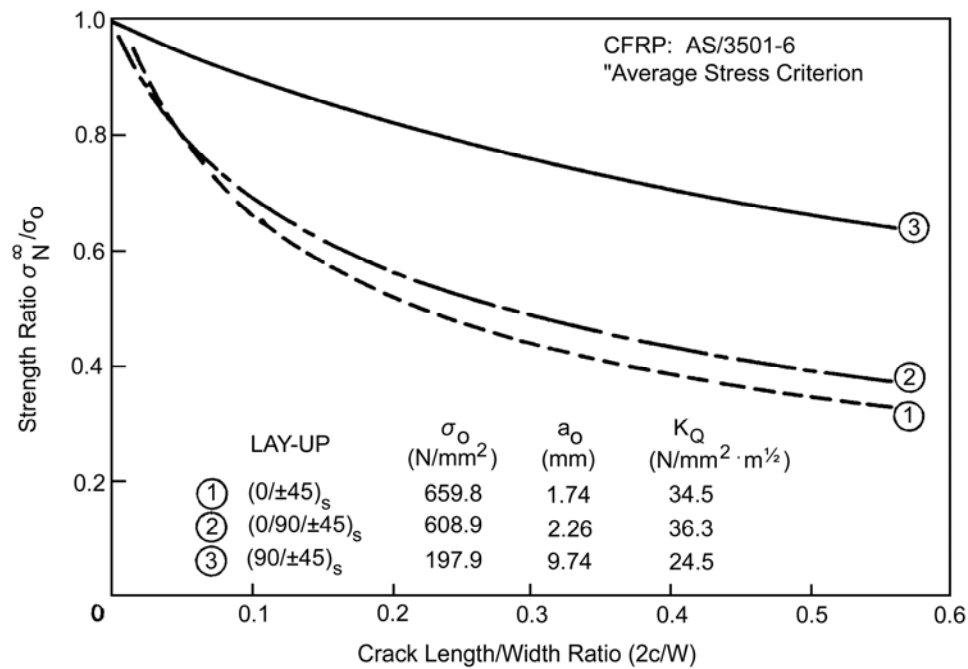


Figure 14.6-12 - Effect of stacking sequence

14.7 Finite plate models

The WEK, [See: 14.5] and WN, [See: 14.6], fracture models were formulated assuming plates of infinite width.

For a real application consisting of finite plates, it is necessary to add a correction factor. There are several analytical methods, including finite element methods, to determine the finite width correction, FWC, factor, Ref. [14-1].

For orthotropic materials, no closed form solutions are available; therefore the closed form expressions for isotropic materials are often used.

The applicability of the isotropic FWC factor to orthotropic materials is justified for the cases having, Ref. [14-1]:

- Large length-to-width ratios, where $L/W > 3.0$.
- Large 'free edge distances', where $2c/w$ or $d/w < 0.5$.

[See: 14.8 for numerical results for finite width correction; 14.9 for results from calculated stress concentration factors at circular holes]

14.8 Finite width correction (FWC)

14.8.1 General

To use isotropic FWC on orthotropic materials, an anisotropy factor, H , is added which depends on the specimen geometry, lay-up and material properties:

$$H = Y/Y_{iso} \quad [14.8-1]$$

Where: H approaches unity.

Values of H for various CFRP laminate lay-ups are given in Figure 14.08.1 and Figure 14.08.2, Ref. [14-1].

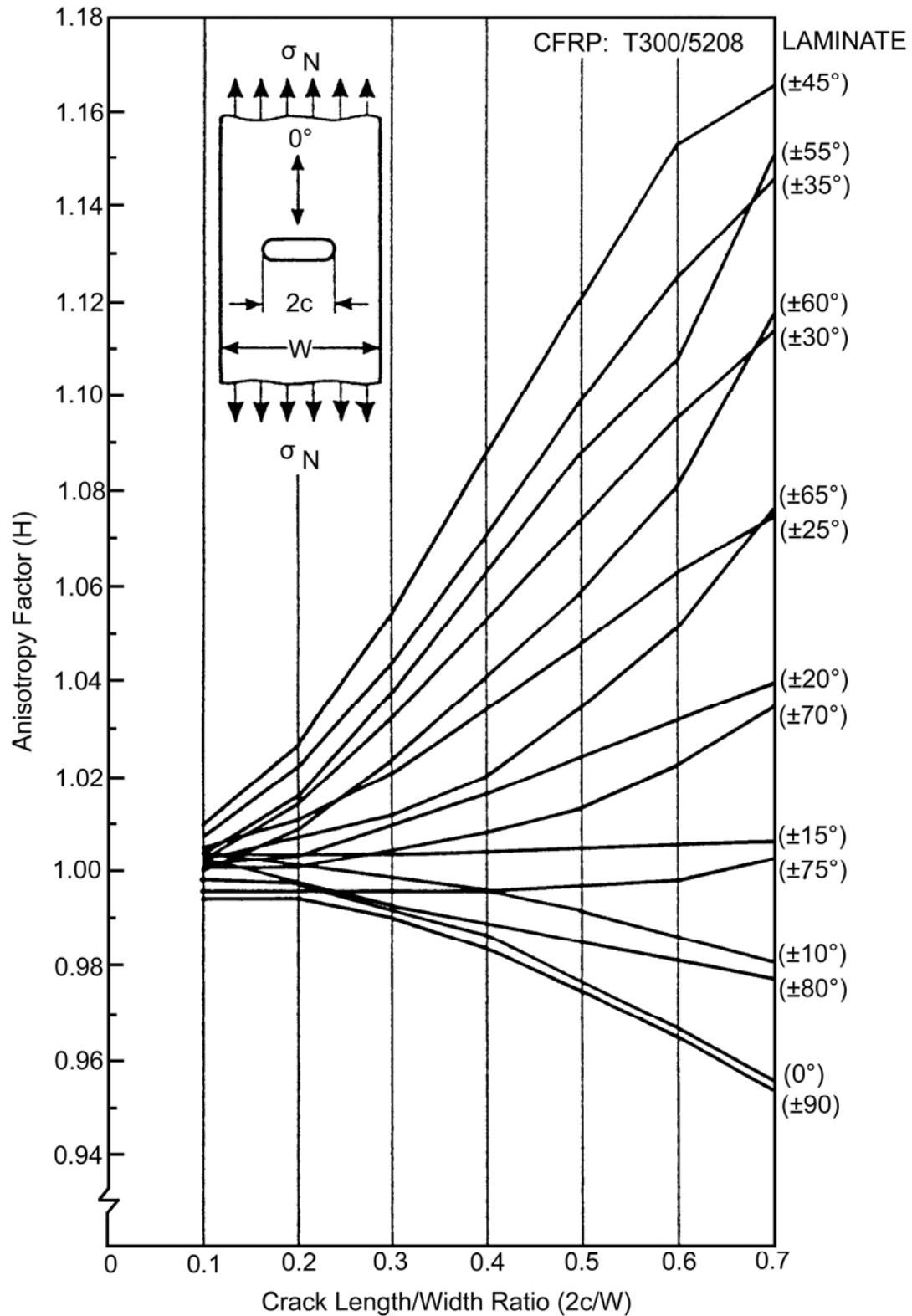


Figure 14.8-1 - Anisotropy factor versus net section reduction for centre cracked angle ply CFRP specimens

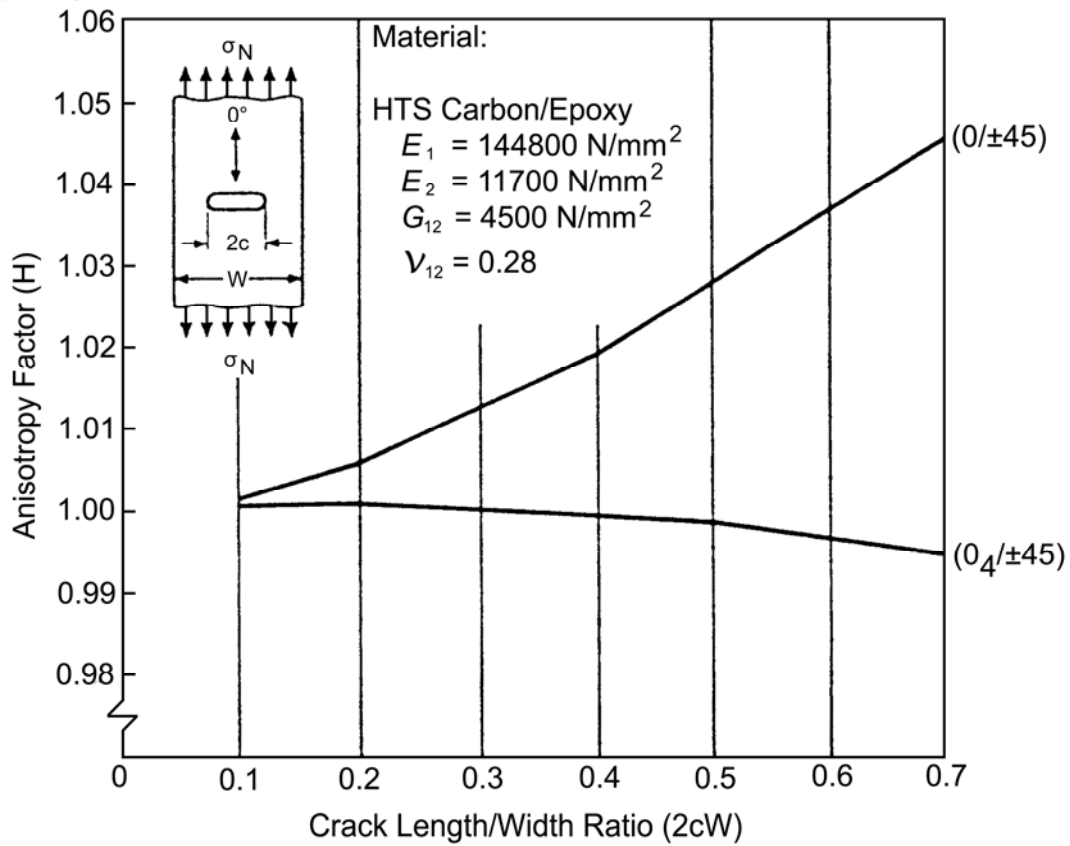


Figure 14.8-2 - Anisotropy factor versus net section reduction for centre cracked CFRP specimens

Definition of the FWC factor, Y_{iso} , as given in Eq [14.8-3] or Eq [14.8-4], Ref. [14-16], [14-17], gives:

$$\sigma_N^\infty = Y \sigma_N \quad [14.8-2]$$

and: $K_Q = Y \sigma_N$

enabling a comparison between experimental results and predictions.

14.8.2 Circular holes

For plates containing holes, Ref. [14-16] recommends the FWC:

$$Y_{iso} = \frac{2 + (1 - 2R/W)^3}{3(1 - 2R/W)} \quad [14.8-3]$$

14.8.3 Centre crack

For plates containing cracks, Ref. [14-17] recommends the [FWC](#):

$$Y_{iso} = 1 + 0.1282 \left(\frac{2c}{W} \right) - 0.2881 \left(\frac{2c}{W} \right)^2 + 1.5254 \left(\frac{2c}{W} \right)^3 \quad [14.8-4]$$

14.9 Calculated stress concentration factor at circular holes

14.9.1 NASA results

In Ref. [14-18], stresses are calculated for finite-width orthotropic laminates under uniaxial tension load. A two-dimensional finite element, FE, analysis was used.

Table 14.09.1 summarises the HT carbon/epoxy laminate configurations and elastic constants, Ref. [14-18]

Table 14.9-1 - HT carbon/epoxy

Laminate	Elastic Constants			
	E_x (MPa)	E_y (MPa)	G_{xy} (MPa)	ν_{xy}
Quasi-isotropic $[0^\circ/\pm 45^\circ/90^\circ]_S$	57,890	57,890	22,090	0.310
0°	146,900	10,890	6,412	0.380
90°	10,890	146,900	6,412	0.028
$[0^\circ/90^\circ]_S$	79,500	79,500	6,412	0.052
$[\pm 45^\circ]_S$	22,250	22,250	37,770	0.735

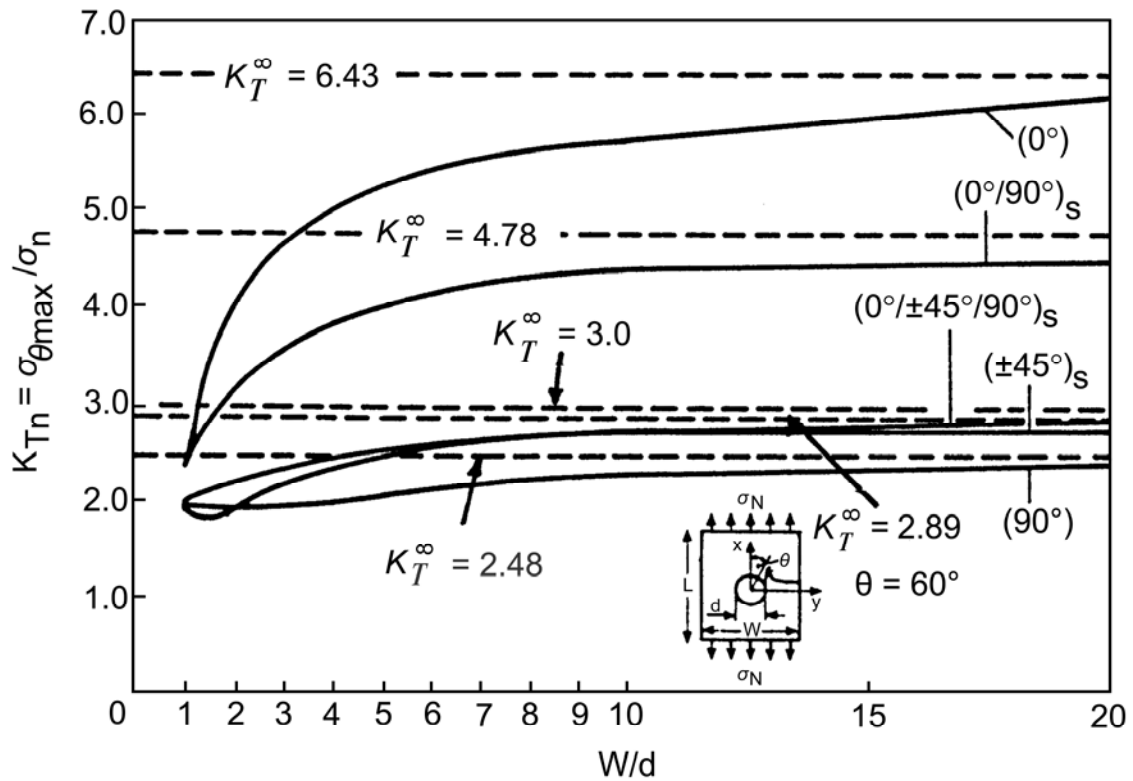


Figure 14.9-1 - Stress concentration factor (K_{Tn}) for orthotropic CFRP laminates with a circular hole, $2 \leq L/W \leq 10$

Figure 14.9.1 shows that anisotropy has a strong influence on the stress concentration factor (K_{Tn}) for long strips with large w/d values.

K_{Tn} is defined as the ratio of $\sigma_{\theta_{max}}$ at the edge to the tensile net section stress σ_n where:

$$\sigma_n = \frac{\sigma_N W}{W - d}$$

Where: σ_N is the gross section tensile stress applied across the laminate.

For $w/d \rightarrow \infty$, Table 14.9.2 gives values of K_T^∞ , [See also: Table 14.9.1 for laminate properties].

Table 14.9-2 - K_T^∞ for various laminates, $w/d \rightarrow \infty$

Laminate	K_T^∞	θ
[0°]	6.43	90°
[90°]	2.48	90°
[±45°] _s	2.89	60°
[0°/90°] _s	4.78	90°
[0°/±45°/90°] _s	3.0	90°

Values of K_T^∞ in Table 14.9.2 can be easily calculated by using Eq [14.6-2], [See: 14.6].

14.9.2 Finite width correction (FWC)

Ref. [14-18] notes that for sufficiently large L/W ($L/W = 10$) and $w/d > 3$ the [FWC](#) can be approximated by using the quasi-isotropic case, [See: [14.8](#)].

14.9.3 MBB/ERNO study

The stress distribution at holes in an infinite plate can be calculated according to Ref. [14-6]. The results of these calculations for some CFRP HT and HM laminates are given for:

- $0^\circ/0^\circ$ laminates in Figure 14.9.2.
- $\pm 32.5^\circ/0^\circ/\pm 32.5^\circ$ laminates in Figure 14.9.3.
- $+30^\circ/0^\circ/-30^\circ$ (HM) and $+45^\circ/0^\circ/-45^\circ/90^\circ$ (HT) laminates in Figure 14.9.4.
- $+30^\circ/0^\circ/-30^\circ$ (HM) and $90^\circ/90^\circ$ (HT) laminates in Figure 14.9.5.

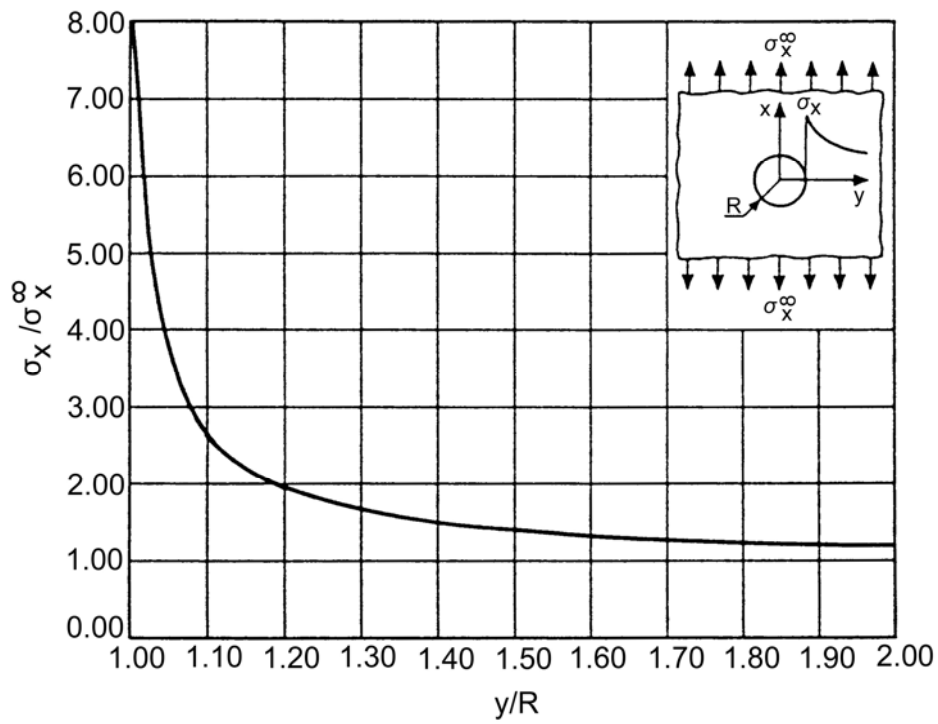
The material data is given in Table 14.9.3.

Table 14.9-3 - Material data

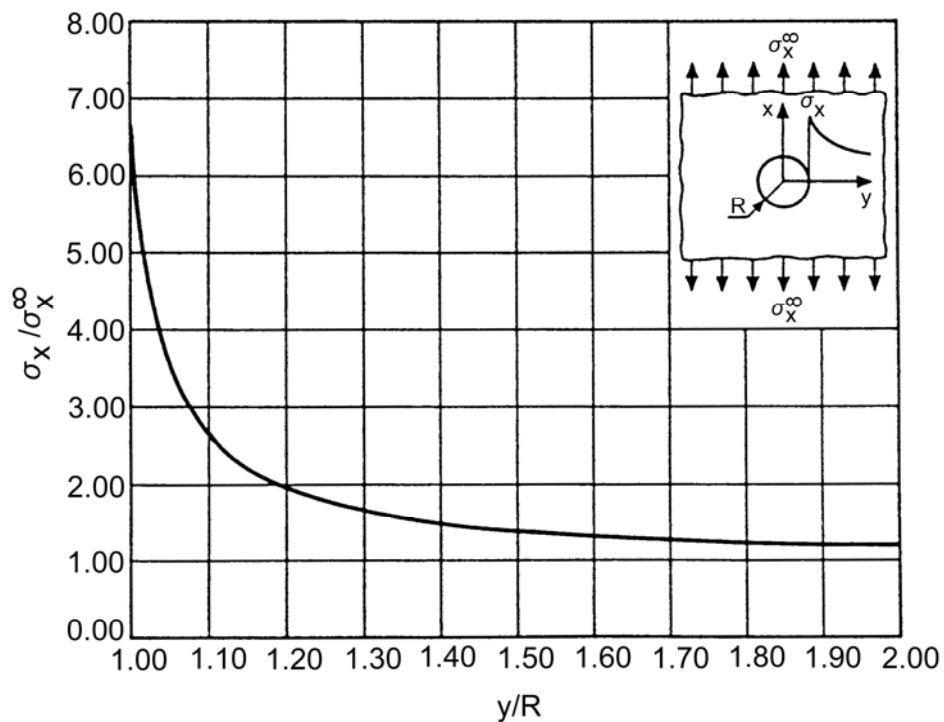
Material/ Stacking Sequence	E_x	E_y	G_{xy}	ν_{xy}	K_T^∞
(a) 914C-MS-4-40					
(High-Modulus CFRP = HM)					
$0^\circ/0^\circ$	221000	7300	5300	0.330	8.21
$+30^\circ/0^\circ/-30^\circ$	116956	12874	30686	1.572	3.59
$\pm 32.5^\circ/0^\circ/\pm 32.5^\circ$	84413	14279	38663	1.523	3.00
$+45^\circ/0^\circ/-45^\circ/90^\circ$	80507	80507	30686	0.312	3.00
$+30^\circ/-30^\circ$	58376	10260	43379	1.771	2.60
$90^\circ/90^\circ$	7300	221000	5300	0.011	2.31
(b) 914C-TS-4-40					
(High-Tension CFRP = HT)					
$0^\circ/0^\circ$	128000	8850	5400	0.300	6.54
$\pm 32.5^\circ/0^\circ/\pm 32.5^\circ$	59248	13148	23596	1.134	3.12

[See: Figure 14.9.2, Figure 14.9.3, Figure 14.9.4, and Figure 14.9.5]

a) HM - CFRP



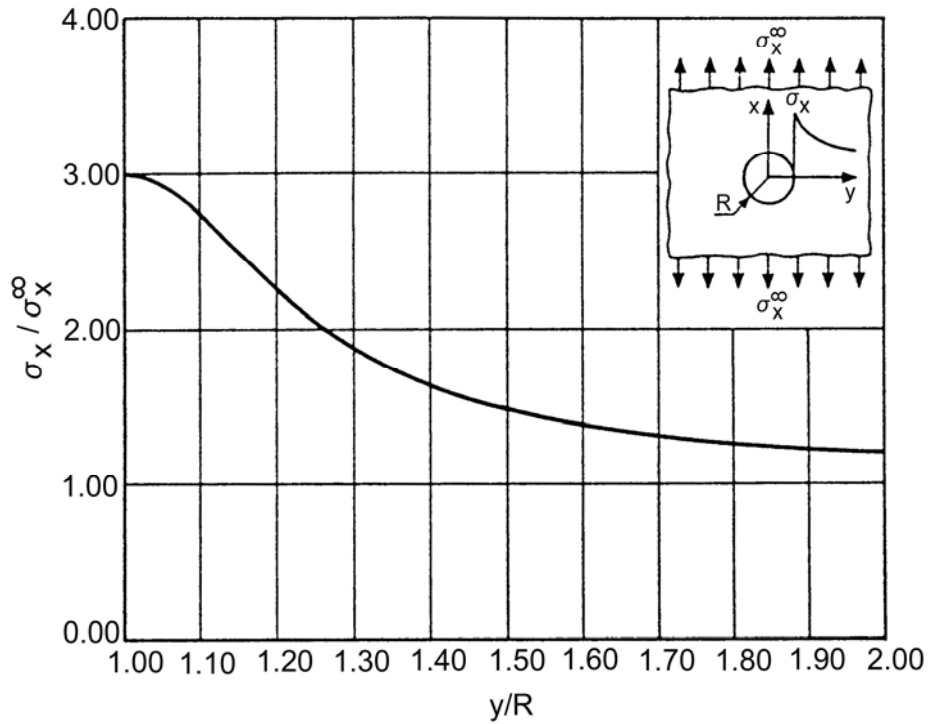
b) HT - CFRP



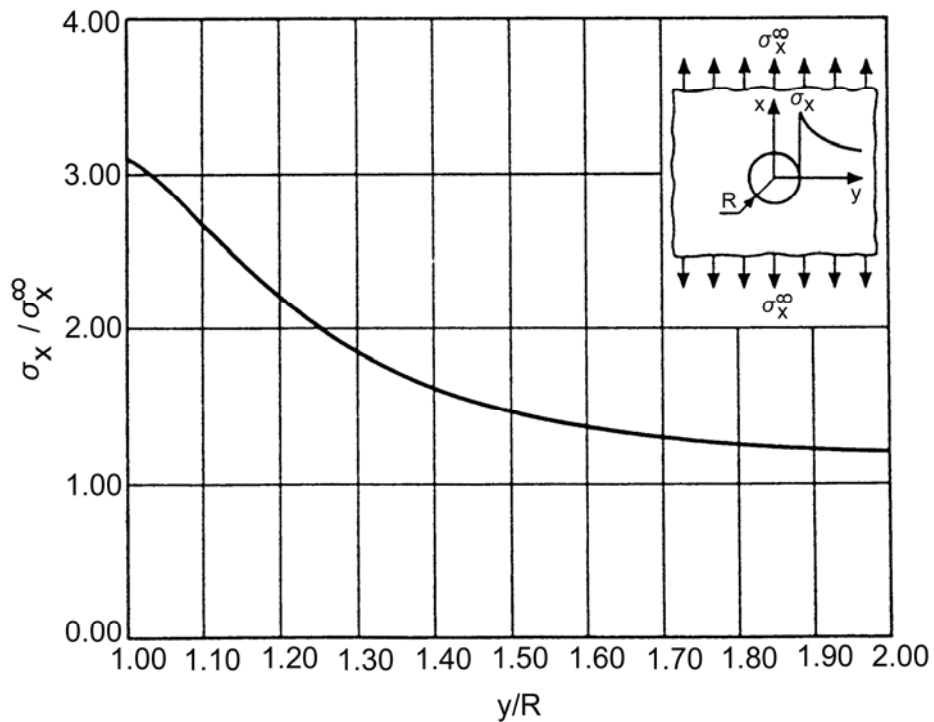
[See: [Table 14.9.3](#) for material data]

Figure 14.9-2 - Stress distribution at a hole for 0°/0° laminates

a) HM - CFRP



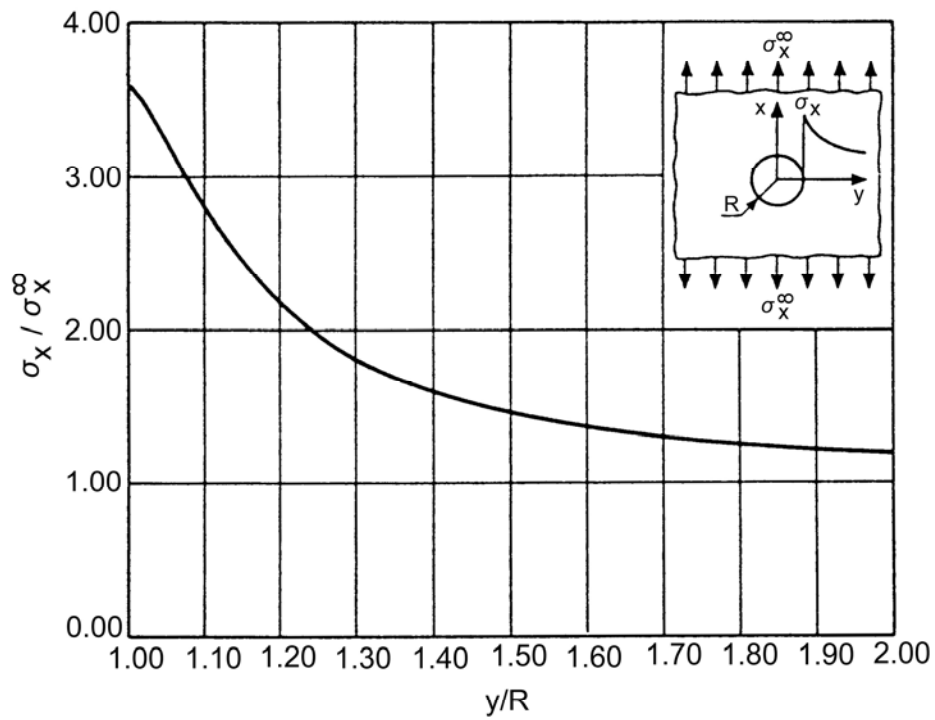
b) HT - CFRP



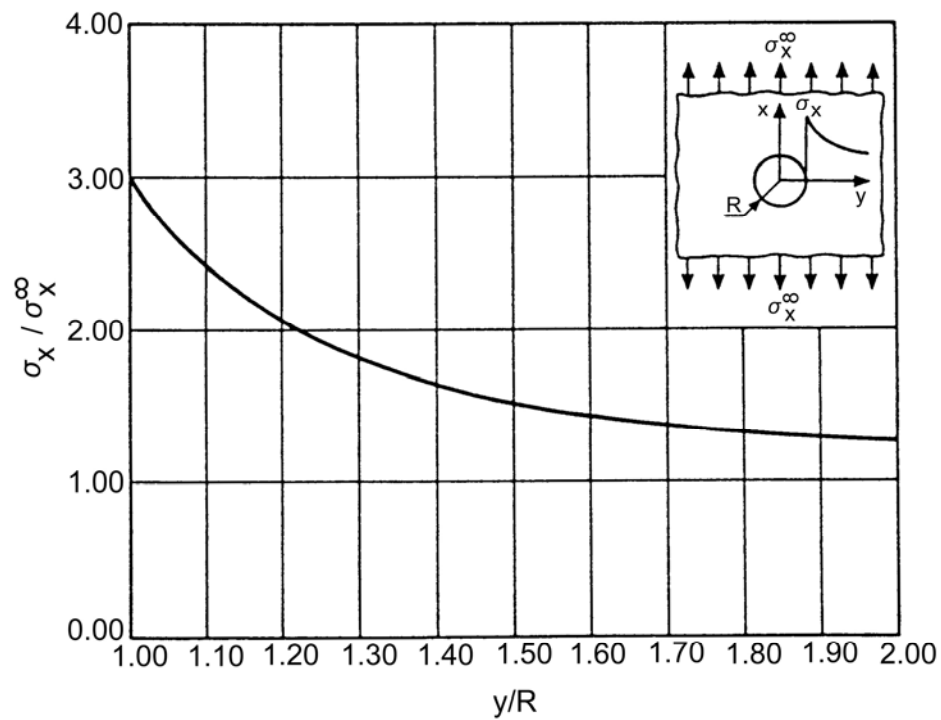
[See: [Table 14.9.3](#) for material data]

Figure 14.9-3 - Stress distribution at a hole for $\pm 32.5^\circ/0^\circ/\pm 32.5^\circ$ laminates

a) +30°/0°/-30° HM - CFRP



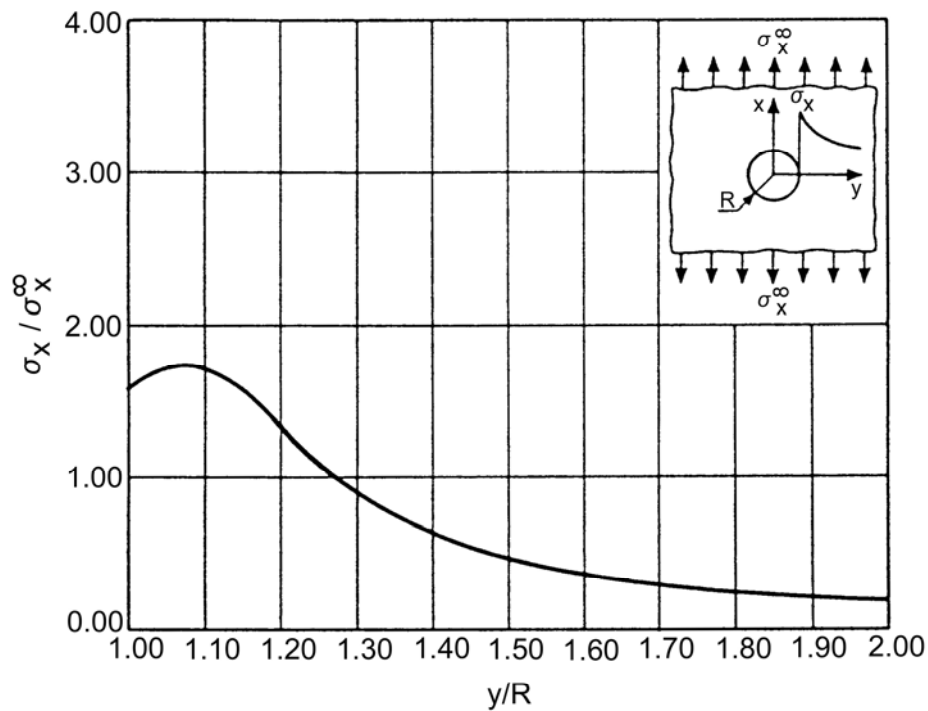
b) +45°/0°/-45°/90° HM - CFRP



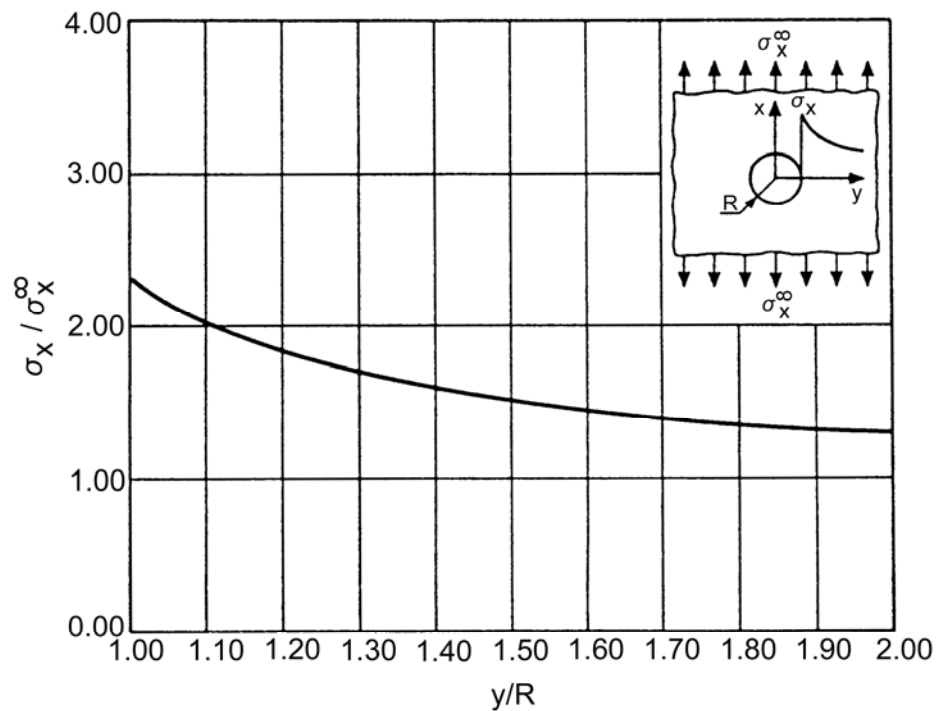
[See: [Table 14.9.3](#) for material data]

Figure 14.9-4 - Stress distribution at a hole for laminates

a) +30°/-30° HM - CFRP



b) 90°/90° HM - CFRP



[See: [Table 14.9.3](#) for material data]

Figure 14.9-5 - Stress distribution at a hole for laminates

The point of intersection of the stress curve with the ordinate indicates the stress concentration factor K_T^∞ .

For distances $y \geq 2R$, the net section stress, σ_x , becomes:

$$\sigma_x \geq 1.2\sigma_x^\infty$$

Finite width correction can be applied when necessary, [See: [14.8](#)].

14.10 Stress distribution around circular holes

14.10.1 General

The strength of composite plates with holes is less sensitive to stress concentration than those for isotropic materials. A number of authors have investigated the problem of the stress concentrations around holes in orthotropic plates, Ref. [14-1], [14-5], [14-21], [14-22], [14-23].

The results presented here are based on the work of Lekhnitski, Ref. [14-15], and are given for plates containing circular holes subjected to tensile or shear loading.

The analysis is based on the assumptions that the

- Plate width is much greater than the diameter of the hole,
- Behaviour of the material is linear elastic,
- Hole is open and unloaded,
- Laminate is orthotropic.

14.10.2 Stress concentration due to tensile load

[Figure 14.10.1](#) shows the notation for tensile load case.

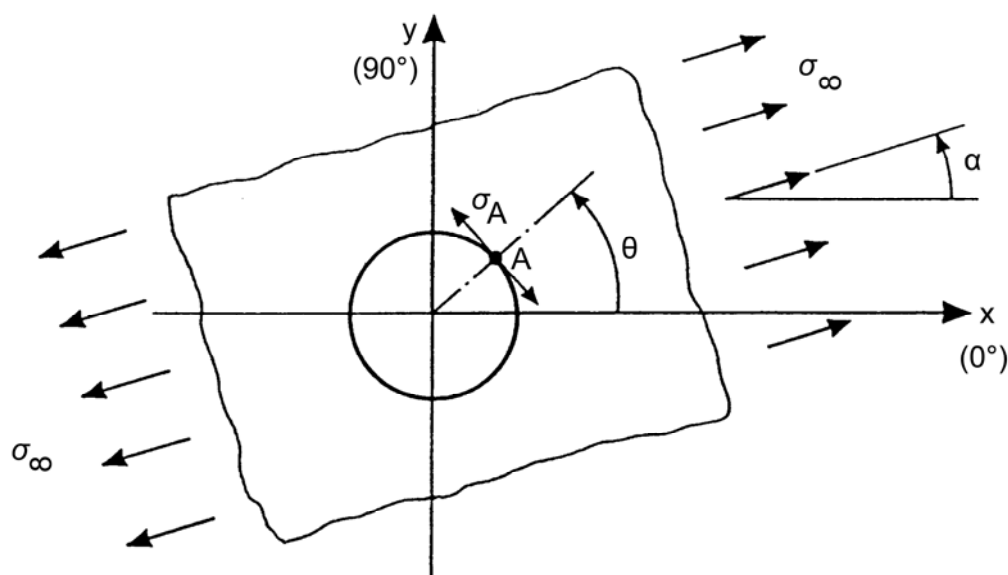


Figure 14.10-1 - Stress concentration due to tensile load

On the basis of the assumptions, the tangential stress σ_A is defined by:

$$\sigma_A = \sigma_\infty \frac{E_\theta}{E_x} \left\{ \begin{array}{l} [-\cos^2 \alpha + (m+n)\sin^2 \alpha] m \cos^2 \theta + [(1+n)\cos^2 \alpha - m \sin^2 \alpha] \\ \sin^2 \theta - n(1+m+n)\sin \alpha \cos \alpha \sin \theta \cos \theta \end{array} \right\} \quad [14.10-1]$$

With:

$$\frac{1}{E_\theta} = \frac{\sin^4 \theta}{E_x} + \left(\frac{1}{G_{xy}} - \frac{2\nu_{xy}}{E_x} \right) \sin^2 \theta \cos^2 \theta + \frac{\cos^4 \theta}{E_y}$$

$$m = \sqrt{\frac{E_x}{E_y}}$$

$$n = \sqrt{2 \left(\sqrt{\frac{E_x}{E_y}} - \nu_{xy} \right) + \frac{E_x}{G_{xy}}}$$

The maximum tangential stress ($\theta = 90^\circ$) gives, for $\alpha = 0^\circ$, the concentration factor K_t :

$$K_t = \frac{\sigma_A(\theta = 90^\circ)}{\sigma_\infty}$$

$$K_t = 1 + \sqrt{2 \left(\sqrt{\frac{E_x}{E_y}} - \nu_{xy} \right) + \frac{E_x}{G_{xy}}}$$

14.10.3 Stress concentration due to shear load

[Figure 14.10.2](#) shows the notation for shear load case.

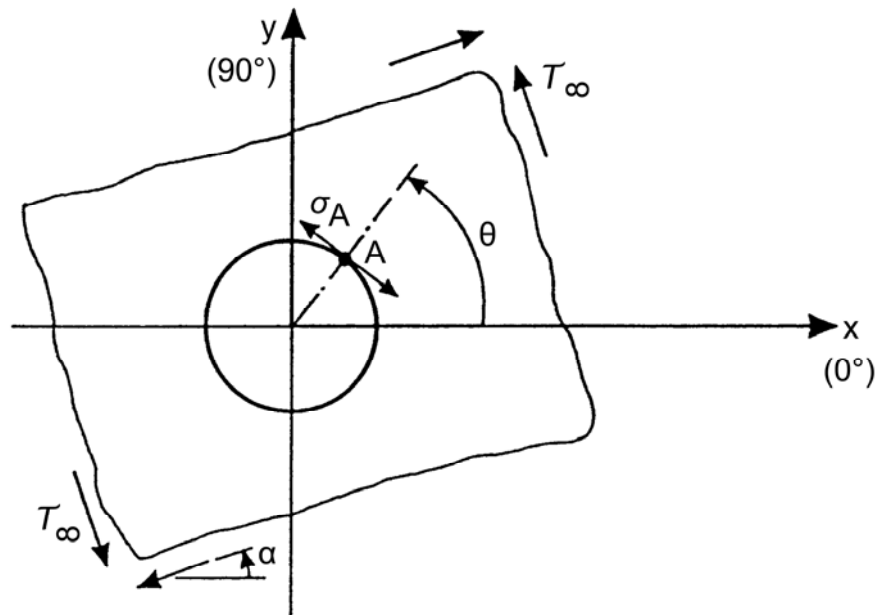


Figure 14.10-2 - Stress concentration due to shear load

Using the same basic assumptions as for tensile loading, the tangential stress σ_A is defined by:

$$\sigma_A = \tau_\infty \frac{E_\theta}{2E_x} (1+m+n) \cdot \{-n \cos 2\alpha \sin 2\alpha + [(1+m) \cos 2\theta + m-1] \sin 2\theta\}$$

With:

$$m = \sqrt{\frac{E_x}{E_y}}$$

$$n = \sqrt{2 \left(\sqrt{\frac{E_x}{E_y} - \nu_{xy}} \right) + \frac{E_x}{G_{xy}}}$$

In contrast to the tensile load case, the location of the maximum tangential stress for shear loading depends on the lay-up.

For $\alpha = 0^\circ$, the concentration factor becomes:

$$K_s = \left| \frac{\max(\sigma_A)}{\tau_\infty} \right|$$

14.11 Interlaminar fracture mechanics

14.11.1 Nomenclature

a	delamination length
A	delamination area, and constant in delamination growth expression
B, D_1, D_2	exponent in delamination growth rate expression
G	strain energy release rate
G_{init}	strain energy releaser rate to initiate a delamination
G_I, G_{II}, G_{III}	individual modes of strain energy release rate
G_{Ic}, G_{IIc}, G_c	mode I, mode II and total interlaminar fracture toughness
G_{max}	maximum cyclic strain energy release rate
G_R	values of fracture toughness when an R-curve is present
G_{th}	cyclic threshold of strain energy release rate
G_{tot}	total strain energy release rate
ΔG	amplitude of cyclic strain energy release rate
N	elapsed fatigue cycles
N_{init}	fatigue cycles to delamination initiation
U	strain energy

14.11.2 Delamination and fracture mechanics overview

14.11.2.1 Delamination initiation and growth

Delamination, or interlaminar cracking, is a common type of damage in composite materials. Delaminations are debonds in the resin rich regions between the laminated plies of a composite. Delamination can be a source of primary failure in composite structures.

Delaminations can arise from interlaminar stresses due to geometric or material discontinuities at design features, such as edges, holes, joints or dropped plies. They can also occur from matrix cracks or from interlaminar stresses caused by structural loading, such as in a curved laminate, or by foreign body impacts.

It is also possible to inadvertently introduce delaminations into structures at the manufacturing stage. The delamination, once initiated, extends under fatigue loading. During delamination growth, the structural loads can be redistributed such that other delaminations occur elsewhere. The delaminations then continue to grow and accumulate until a structural failure occurs, such as buckling or fibre failure. Individual delaminations can cease to grow due to changes in overall stress distribution.

The progressive damage can result in final structural failure, which is dependent on the local loading. If the loading is compressive, sub-laminate buckling can occur, or tensile fibre failure if the loading is tension.

Mechanical loading is often the main cause of failure. However, the effects of environment, including temperature and fluid exposure under normal operating conditions, also need to be accounted for. Generally, a hostile environment has a negative effect, reducing the fatigue life of the structure. The effects of mechanical and environmental load act together and cannot be investigated in isolation.

14.11.2.2 Linear elastic fracture mechanics and the strain energy release rate approach

Efforts to predict the initiation and growth of delamination have focused on interlaminar fracture mechanics. For this, the change in strain energy per unit area of delamination growth; known as the strain energy release rate, G , can be calculated using the formula:

$$G = -\frac{\partial U}{\partial A} \quad [14.11-1]$$

where:

U : strain energy of the body,

A : the crack surface area

Calculated values of G for a delamination in a structure, are compared with the critical values obtained from materials tests to determine whether the delamination is likely to grow. The critical values of G depend upon the way loading is applied. The total strain energy release rate is considered in terms of three components called fracture modes, as shown in Figure 14.11.1.

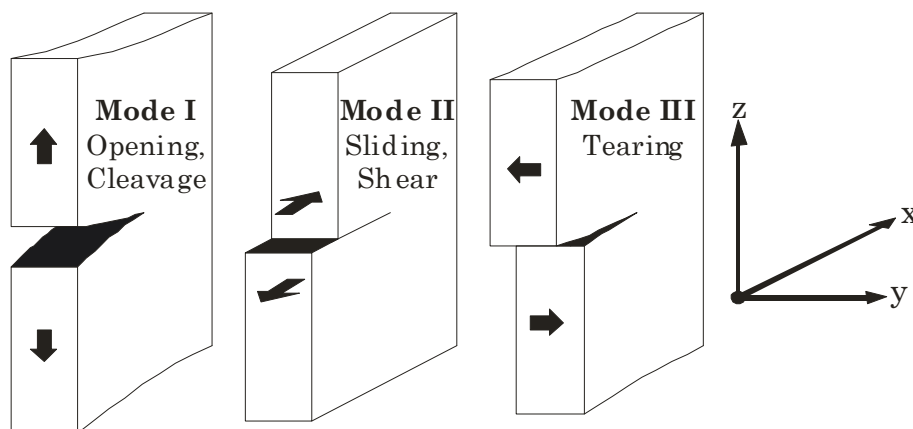


Figure 14.11-1 - Fracture modes: opening, shearing, and tearing

The fracture toughness modes are described as:

Mode I - opening, cleavage,

Mode II - sliding, shear,

Mode III - tearing.

The total strain energy release rate is given by sum of the components:

$$G_T = G_I + G_{II} + G_{III}$$

The critical value of G , in pure Mode I is called G_{Ic} . The critical value of G in pure Mode II is called G_{IIc} . The critical value of G in pure Mode III is called G_{IIIc} . The three components of loading are normally applied in combination creating a mixed-mode loading condition.

Coupon tests have been developed to measure fracture toughness in both pure and combined modes.

Strain energy release rate (SERR) can be calculated for a given delamination using finite element analysis (FEA) of a composite structure. The principal method used for calculation of SERR using FEA is the virtual crack closure (VCCT) method.

14.11.2.3 Using fracture mechanics to identify the critical delamination location

A flow diagram showing the overall framework for modelling damage using interlaminar fracture mechanics with respect to structural integrity is given in Figure 14.11.2.

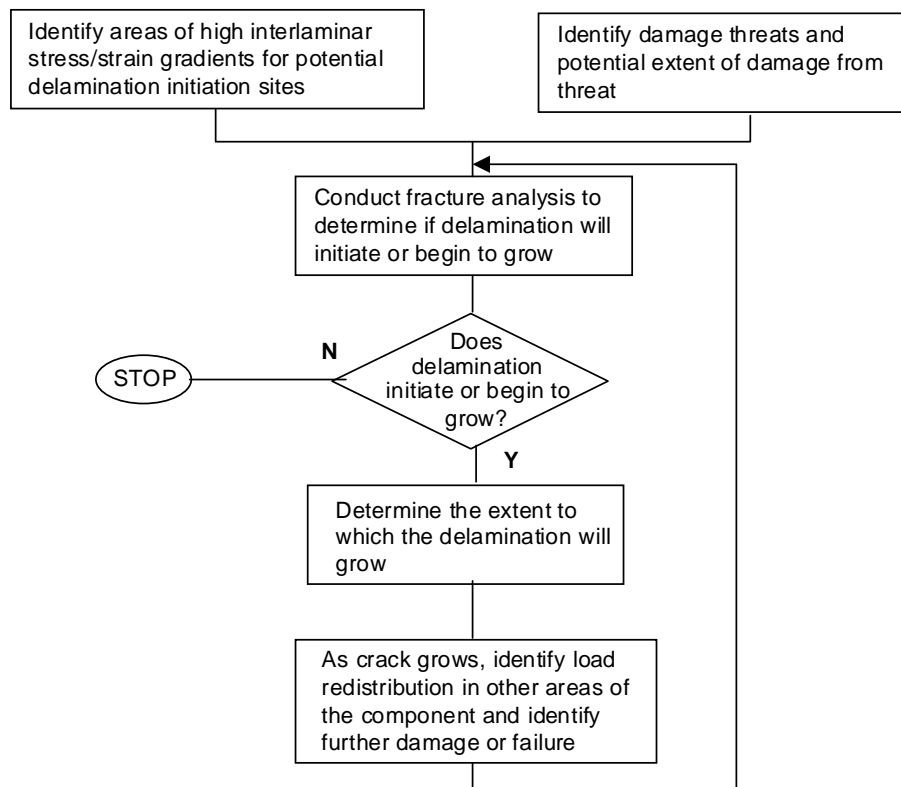


Figure 14.11-2 - Outline of no-damage-growth methodology

The methodology begins by investigating “areas of concern” or “hotspots” with high interlaminar stresses and strains that result in the matrix being highly loaded. These interlaminar stresses can arise from geometry or from damage threats.

Once identified, a fracture analysis is conducted to determine whether a delamination initiates and grows. If a delamination does grow, the analysis continues to assess how far it grows and if that growth is likely to lead to structural failure. Component failure is dependent on the loading in the area of interest, hence this needs to be defined. In many situations a significant reduction in the stiffness of the component could be deemed to define failure.

If component failure does not occur, then the analysis can be stopped, or another potential delamination site examined. If the delamination arises from a structural discontinuity, then that local area can be redesigned to prevent initiation at that site. If the delamination grows in a stable, predictable, manner, then inspection intervals can be established to ensure that the delamination has not grown beyond that expected.

Identification of interlaminar stresses and fracture properties need accurate modelling of through-thickness properties. Often these models are a local model of the area of concern with either idealised boundary conditions applied, or the actual boundary conditions from the global model using global-local modelling techniques. Selection of the “area of concern” is often done by engineering judgement, especially if global finite element models include 2-D shell elements which do not identify areas of high interlaminar stress.

The stress outputs from the local models enable the identification of interlaminar stresses away from any stress singularities associated with geometric discontinuities. These stresses or strains can be used with suitable failure criteria, such as maximum strain-stress or interaction criteria, or with the other fracture criteria described in this chapter. If an interlaminar failure occurs, it does so as a delamination and the extent to which it grows is determined using interlaminar fracture mechanics. If a delamination is not predicted to initiate, then other structural discontinuities are examined. The stresses at these locations are FEA mesh size dependent and, hence, are indefinite. Thus, the numerical values are not used to predict failure in or near these locations. However, the trend of the data is important. Delaminations primarily occur when the interlaminar tension stresses are high. They can also grow where there is a high interlaminar shear stress. Therefore, these areas are identified for fracture analysis. In a damaged structure, invariably, the damage region is where further delaminations can grow. For a damaged component and for a component where delamination is expected to initiate, a fracture analysis is conducted for delaminations growing either from the damage or from the potential initiation site.

14.11.2.4 Fracture mechanics prediction procedure

Interlaminar fracture mechanics analysis, uses values of the strain energy release rate for a given load at different delamination lengths. These values are then compared with the material’s interlaminar fracture toughness and fatigue crack growth properties.

The fracture mechanics prediction procedure is summarised in Figure 14.11.3.

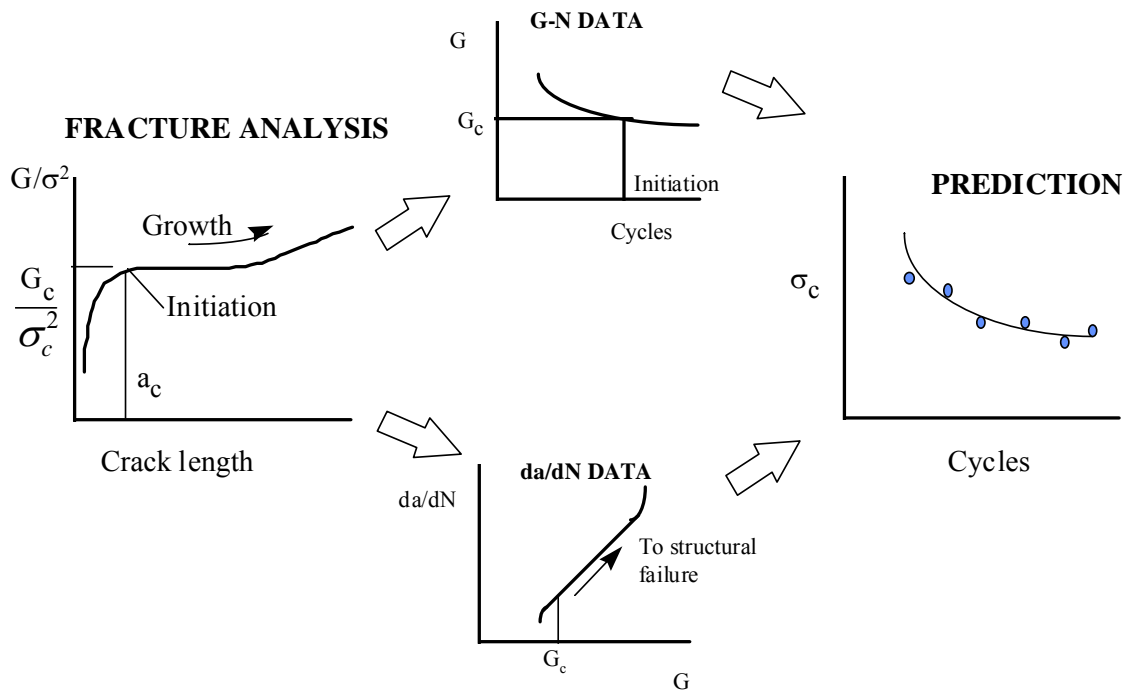


Figure 14.11-3 - Fracture mechanics life prediction methodology

The first step is to analyse the model to obtain a relationship between strain energy release rate, G and delamination length, a , for a given stress or strain. For an initial delamination length, a critical value, G_c is obtained. The G_c analytical value is compared with the material delamination data to give static failure load and location and the number of cycles necessary to initiate the delamination.

From this value of G_c , the delamination growth rate, da/dN is obtained using the material fatigue data. For an incremental number of cycles, the increment in delamination length is determined. This provides a new value of G from the G - a relationship and a new value of da/dN for each increment. This continues until either the delamination grows to a critical length or stops growing, so providing the fatigue life at the given load.

14.11.3 Standard test methods (static and fatigue)

14.11.3.1 General

The discussion of interlaminar fracture toughness testing methods given here is more detailed than the overview of test methods for composites, [See: Chapter 7].

14.11.3.2 Interlaminar fracture toughness testing

Coupon tests are used to measure the interlaminar fracture toughness. The majority of the tests developed to date are designed to individually measure Mode I, Mode II or Mode III fracture toughness. However, to use fracture toughness data for delamination initiation and growth studies, it needs to be determined using representative loading conditions for a delamination in the composite structure. Fracture toughness changes with the loading mode.

It is likely that the delamination will be subject to mixed-mode loading in a real structural situation. The mixture of modes could also change as the delamination grows. No single test method has been developed to measure an arbitrary mixture of Mode I, Mode II and Mode III.

Mixtures of Mode I and Mode II are the most common loading conditions seen at delamination fronts in composite structures. Test methods are available to measure arbitrary mixtures of Mode I and Mode II, most notably the MMB mixed-mode bending test.

There are limitations on how fracture toughness tests can be used, such as the limitations on unidirectional lay-ups and fibre bridging. For most of the tests, initiation and pre-crack data can be measured and a crack growth resistance (*R*-curve) obtained. The initiation data often provides the most conservative value for use in fracture mechanics based design studies.

14.11.3.3 Types of test methods

Various test methods have been devised to assess fracture behaviour. These include:

- DCB double cantilever beam, used for Mode I, as shown in Figure 14.11.4.
- CN centre notch for Mode I.
- DT double torsion for Mode I.
- ENF end notch flexure for Mode II, shown in Figure 14.11.4.
- 4ENF 4 point bend end notch flexure for Mode II.
- ENS end loaded split for Mode II used for thin laminates.
- ELS end lap shear for Mode II.
- ENCB end notched cantilever beam used for thick laminates.
- CBEN cantilever beam enclosed notch for Mode II.
- EDT edge delamination tension test for mixed Modes I and II.
- CLS cracked lap shear for mixed Modes I and II. This was developed for assessing adhesives.
- DSDCB double split double cantilever beam for Mode III.
- Arcan test arrangement for mixed Mode I and II.
- ECT edge crack torsion test for Mode III
- MMB mixed mode bending for Modes I and II

Some of these tests are more widely accepted than others. The most commonly used test methods are given in Table 14.11.1.

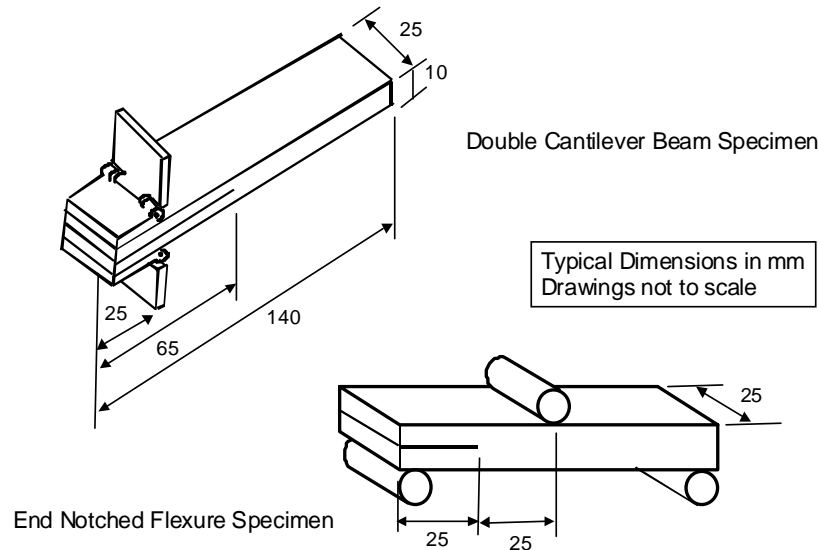


Figure 14.11-4 - DCB and ENF specimens

Table 14.11-1 - Standard test methods

Test method (Standard)	Comments
ISO/CD 13,586	Mode I assessment based on ESIS document from USA. (Mode II being studied in VAMAS lead project).
ASTM D 5528 - 94a:	Double cantilever beam - Mode I
ASTM D 6671	Mixed mode bending - Mode I + II
Airbus prEN 6033	Determination of Mode I (G_{Ic}) for CFRP
Airbus prEN 6034	Determination of Mode II (G_{IIc}) for CFRP

14.11.3.4 Fatigue delamination characterisation

There are essentially two approaches for characterising fatigue delamination. These methods are the delamination initiation method and the delamination growth method. Both methods are needed in order to accurately predict the structural integrity of a component.

The DCB and ENF specimens, as shown in [Figure 14.11.4](#), have been used to characterise fatigue delamination by monitoring the delamination growth per fatigue cycle, da/dN .

Alternatively, a 4ENF, Ref. [\[14-24\]](#), specimen (four-point-bend end-notched-flexure specimen) can be used to determine G_{IIIc} . The 4ENF has a decreasing crack growth rate with crack length.

Expressions relating the applied cyclic strain energy release rate (G_{max} or ΔG) with da/dN as a power law are given in Equation [\[14.11-2\]](#). This equation can be further extended to incorporate the acceleration of delamination growth as G approaches the quasi-static value and the deceleration as the delamination growth rate reaches a threshold value, giving Equation [\[14.11-3\]](#).

$$\frac{da}{dN} = A(G_{\max})^B \quad [14.11-2]$$

$$\frac{da}{dN} = A(G_{\max})^B \frac{\left[1 - \left(\frac{G_{th}}{G_{\max}} \right)^{D_1} \right]}{\left[1 - \left(\frac{G_{\max}}{G_c} \right)^{D_1} \right]} \quad [14.11-3]$$

For composites however, the values of the exponent B in these power laws are generally high. They can range from approximate values of 3 to in excess of 15. Thus, using only the fatigue growth part of the curve, any small deviation from the anticipated service load can lead to large errors in the predicted delamination growth rate. This is because G is proportional to the square of the load and hence the delamination growth rate is proportional to the load to the power of $2B$. This potential error, and the high rates of delamination growth, have led to the adoption of a 'no growth' approach to design and damage tolerance characterisation of composite structures in fatigue. The 'no growth' approach needs the threshold value of strain energy release rate, G_{th} to be determined. Then, if a delamination is present, and the strain energy release rate is below the G_{th} value, the delamination does not grow.

For high cycle fatigue issues, the value of G_{th} is evaluated for crack growth rates in the order of 10-8 mm/cycle so that threshold values are guaranteed to be below 10-8 mm/cycle or 1mm in 108 cycles. This criteria is confirmed with the allowable damage in the application.

In generating the da/dN data, the delamination needs to be grown during the fatigue test. Fibre bridging can occur during this growth giving artificially high values of G_{th} and exponent B . Therefore, for more representative values, the G data, is normalised by the R -curve. This is achieved by determining G_{Imax}/G_{IR} for each of the fatigue data points where G_{IR} is the value of the static fracture toughness at the corresponding delamination length of that fatigue data point.

Owing to fast delamination growth, emphasis is often placed only on the cycles to produce delamination initiation, delamination growth is not determined. A conservative approach is to assume that once a delamination has initiated, it grows to its full extent, on a given path, in the next load cycle. A complete $G-N$ delamination onset characterisation can be obtained for a given mode mix.

Hence, by testing mode I, mixed mode and mode II specimens, a complete $G-N$ characterisation can be developed for all modes, as shown in [Figure 14.11.5](#). By choosing an appropriate number of cycles for the application, N_a , such as the number of cycles between inspections, or the fatigue life, a design value of G can be specified such that the delamination does not grow within those cycles.

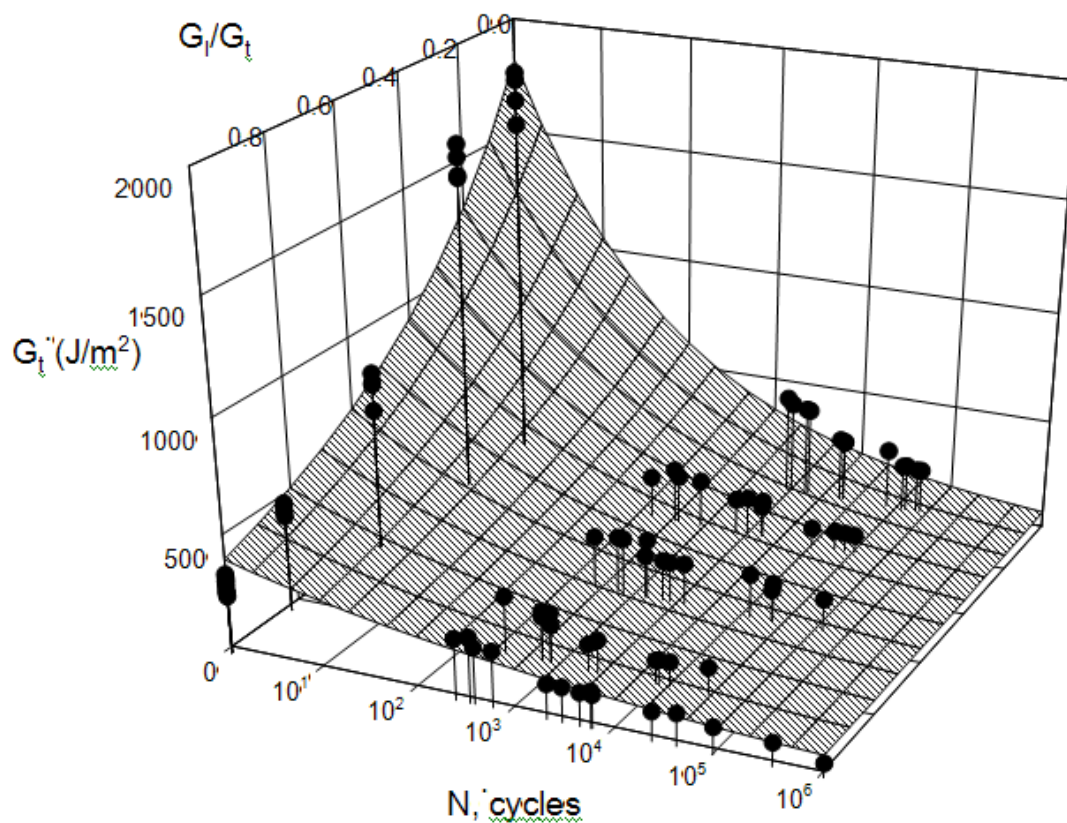


Figure 14.11-5 - Representative $G-N_{onset}$ data

14.11.4 Calculation of strain energy release rate in structural analysis

14.11.4.1 Global energy comparisons

Strain energy release rate, G can be calculated using a global energy balance between two finite element analysis solutions of different delamination areas (A_i and A_{i+1}):

$$G = - \frac{dU}{dA} = - \frac{U_{a_{i+1}} - U_{a_i}}{A_{a_{i+1}} - A_{a_i}} \quad [14.11-4]$$

Where: U is the strain energy and A is the delamination area for the i -th solution

This gives a value for the total strain energy release rate, G_{tot} . The limitation to this approach, however, is that the component parts, G_I , G_{II} , and G_{III} cannot be determined using this method. Other methods are available for calculation of G such as:

- Virtual crack closure technique (VCCT)
- J-integral method
- Crack tip element method

14.11.4.2 Virtual crack closure technique (VCCT)

The virtual crack closure technique is used to calculate strain energy release rate in a mixed mode for composite materials. It is easy to implement in FEA packages, Ref. [14-25]. The technique is based on the work done to close the crack tip. An assumption can be made which allows values of G can be calculated from the results of one finite element solution rather than two. If the increment of delamination growth, Δa , is small in comparison with the overall delamination length, then the forces ahead of the delamination can be assumed to be similar to those when the delamination has grown.

G values are plotted at the existing delamination length. Generally, the global change in energy and VCCT approaches give similar results. If they do not, and there is no error, then either there was a significant change of geometry between the two delamination lengths used to calculate dU/dA , or the delamination length is short and the VCCT assumption of Δa being small compared with the overall delamination length, has been violated.

Owing to the numerical oscillatory nature of the stresses at the delamination tip between different materials, or plies of different orientation, the mode ratio is dependent on the size of the elements at the delamination front, Ref. [14-26], [14-27]. When the element size is reduced, the G_I/G_{tot} ratio changes and the values do not converge with continued decrease in element size. One solution to this problem is to incorporate a resin layer between the plies and to grow the delamination within this. The disadvantage of this method is that the modeling can become intensive because of the small thickness of the resin layer. In addition, it is not always possible to determine the size of the resin layer between plies and, hence, an assumption on its thickness is often applied.

An alternative method to determine the mode mix ratio is to modify one of the material properties (normally a Poisson's ratio) to a fictitious value in order to force the bi-material constant in the near crack tip stress field equation to zero, Ref. [14-27], [14-28].

14.11.4.3 2D VCCT

In 2D using 4-noded quadrilateral elements the values of G_I and G_{II} are calculated by using the equations:

$$G_I = \frac{1}{2\Delta A} F_y^F (V^B - V^C) \quad [14.11-5]$$

$$G_{II} = \frac{1}{2\Delta A} F_x^F (U^B - U^C) \quad [14.11-6]$$

In 2D using 8-noded quadrilateral elements the values of G_I and G_{II} are calculated by using the equations:

$$G_I = \frac{1}{2\Delta A} [F_y^F (V^B - V^C) + F_y^G (V^D - V^E)] \quad [14.11-7]$$

$$G_{II} = \frac{1}{2\Delta A} [F_x^F (U^B - U^C) + F_x^G (U^D - U^E)] \quad [14.11-8]$$

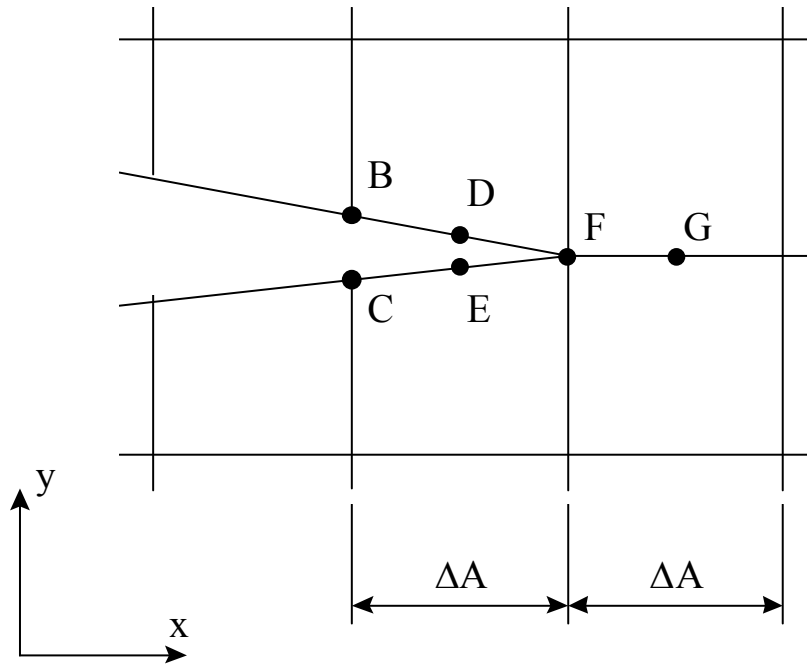
Where:

ΔA is the element length

$F_x^F, F_x^G, F_y^F, F_y^G$ are x and y components of force at nodes F and G

U^B, U^C, U^D, U^E are x components of displacement at nodes B, C, D and E

V^B, V^C, V^D, V^E are y components of displacement at nodes B, C, D and E



The x - y directions are in a local co-ordinate system. The locations of nodes B to D relative to the crack tip are shown in [Figure 14.11.6](#).

Figure 14.11-6 - Node definitions for 2D VCCT

14.11.4.4 3D VCCT

In 3D, values of G are calculated along the entire crack front. The equations used to calculate the components of G using VCCT for both 8-noded and 20-noded brick elements are:

For an 8-noded brick element:

$$G_I = \frac{1}{2\Delta A} F_z^H (W^B - W^E) \quad [14.11-9]$$

$$G_{II} = \frac{1}{2\Delta A} F_x^H (U^B - U^E) \quad [14.11-10]$$

$$G_{III} = \frac{1}{2\Delta A} F_y^H (V^B - V^E) \quad [14.11-11]$$

For a 20-noded brick element:

$$G_I = \frac{1}{2\Delta A} \left[F_z^H (W^B - W^E) + F_z^\gamma (W^\alpha - W^\beta) + \frac{F_z^G}{2} (W^A - W^D) \frac{F_z^J}{2} (W^C - W^F) \right] \quad [14.11-12]$$

$$G_{II} = \frac{1}{2\Delta A} \left[F_x^H (U^B - U^E) + F_x^\gamma (U^\alpha - U^\beta) + \frac{F_x^G}{2} (U^A - U^D) \frac{F_x^J}{2} (U^C - U^F) \right] \quad [14.11-13]$$

$$G_{III} = \frac{1}{2\Delta A} \left[F_y^H (V^B - V^E) + F_y^\gamma (V^\alpha - V^\beta) + \frac{F_y^G}{2} (V^A - V^D) \frac{F_y^J}{2} (V^C - V^F) \right] \quad [14.11-14]$$

Where:

ΔA	is the crack area associated with the G calculation
F_{xi}^{Ai}	is the component of force for $xi = x, y, z$ and $Ai =$ nodes G, H, J, \dots
U^{Ai}	is the x component of displacement for $Ai =$ nodes $A, B, C, D, E, F, \alpha, \beta$
V^{Ai}	is the y component of displacement for $Ai =$ nodes $A, B, C, D, E, F, \alpha, \beta$
W^{Ai}	is the z component of displacement for $Ai =$ nodes $A, B, C, D, E, F, \alpha, \beta$

The definition of the nodes relative to the crack front position at which G is calculated is shown in [Figure 14.11.7](#).

For the 8-noded brick case, nodes $A, C, D, F, G, J, \alpha, \beta$ and γ do not exist. Also, for the case of the 20-noded element where the crack is at a free edge, there are only four elements surrounding node H (instead of eight) and hence the terms involving nodes C, F and J are ignored.

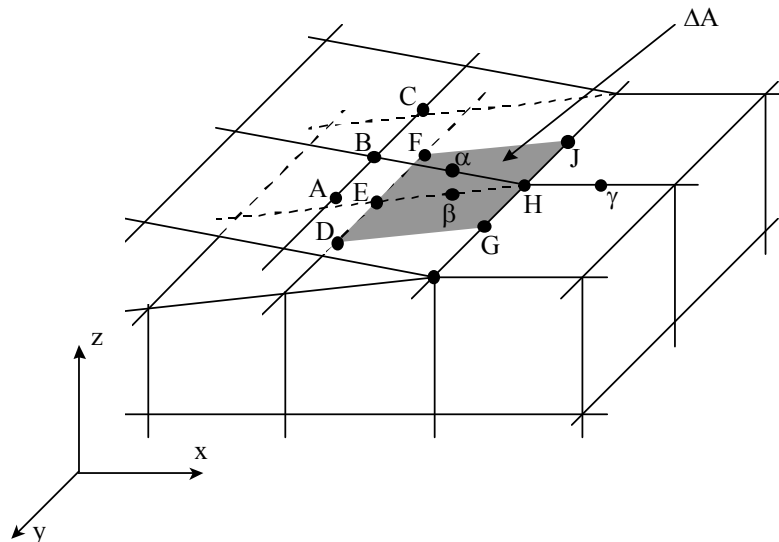


Figure 14.11-7 - Node definitions for 3D VCCT

14.11.4.5 Using interlaminar fracture mechanics in design

An example of a G - a plot for a delamination under a stiffener is described in Ref. [14-29] and shown in Figure 14.11.8.

The plot shows G_{tot} calculated using Equation [14.11-4] and G_I and G_{II} using VCCT in a 2D plane strain model and a 3D model using plate elements. This type of plot gives three pieces of information that help predict delamination initiation and delamination extent in the component. Firstly, the value of G_{tot} contains approximately 60% G_I . In most materials, the mode I interlaminar fracture toughness, G_{Ic} , is significantly less than the mode II interlaminar fracture toughness, G_{IIc} . For brittle epoxies, this difference can be as high as an order of magnitude. Significant differences can also be seen in fatigue initiation and crack growth testing. Hence, if the geometry of the part, the lay-up, or the material can be altered in the design to have a lower G_I component, the panel becomes more damage resistant and damage tolerant.

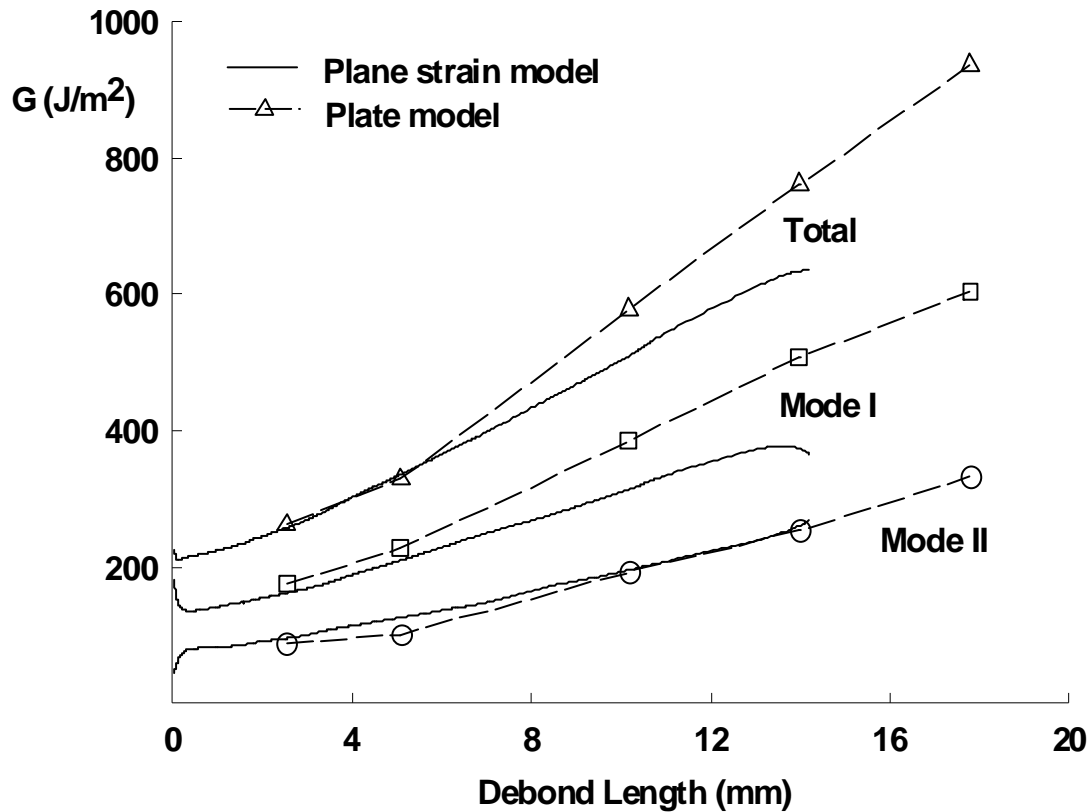


Figure 14.11-8 - G - a curve for a stiffener debond

The second piece of information from [Figure 14.11.8](#), is the general slope of the G - a plot. For all delamination lengths the slope is positive, indicating that delamination growth is unstable under quasi-static loading, or the fatigue delamination growth rate increases with delamination growth.

Schematics for other types of G - a plots are shown in [Figure 14.11.9](#).

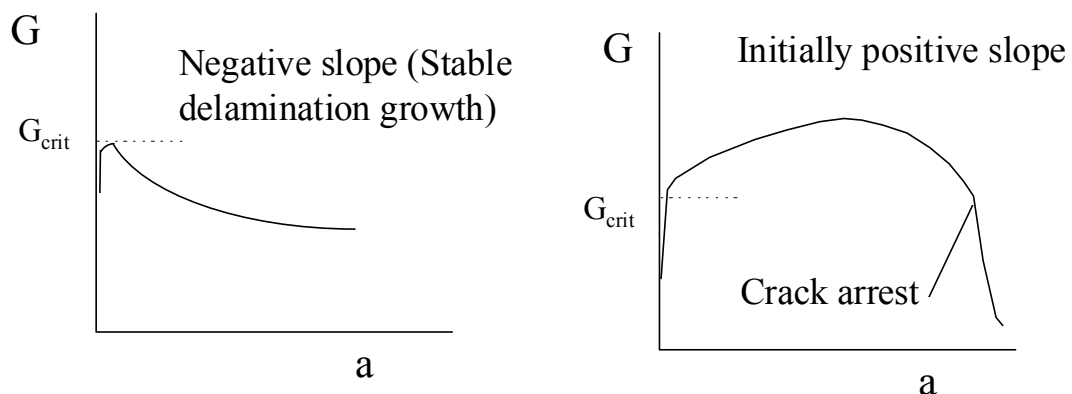


Figure 14.11-9 - Schematics of possible G - a curves

In [Figure 14.11.9a](#), the slope of the G - a plot is always negative, thus under quasi-static loading more load is needed to grow the delamination further. In fatigue, the delamination growth rate decreases until the delamination eventually stops growing.

In [Figure 14.11.9b](#), the slope of the G - a plot is initially positive but then becomes negative. This indicates that the delamination growth is unstable at first and then stops. This behaviour can be used in structural design geometries.

The third piece of information from [Figure 14.11.8](#) is the value of G necessary to initiate the delamination. A stress singularity exists because there is a sudden termination of the delamination at the start of the crack. In the close vicinity of the stress singularity, the G - a curve probably turns sharply towards zero. However, if the G - a curve is extrapolated to a zero crack length ignoring this sharp turn, it is possible to use the extrapolated value of G to compare with the interlaminar fracture toughness, G_c , of the material. Again, local design optimisation can increase the analytical value of G , giving a more durable part.

This methodology has been validated against many different configurations, including: Edge delamination in a flat multidirectional laminate, Ref. [\[14-30\]](#), a tapered laminate, Ref. [\[14-31\]](#) and a curved laminate, Ref. [\[14-32\]](#).

14.12 References

14.12.1 General

- [14-1] J. Awerbuch
'Notched Strength of Composite Laminates'
Internal Report IB 131-85/04, DFVLR (Germany)
ESA CR(P)-2017 (Vol. 4, Appendix H), January 1985
- [14-2] E.M. Wu
'Fracture Mechanics of Anisotropic Plates'
Composite Materials Workshop, Technomic Pub. Co., Inc. Stamford,
Conn., 1968
- [14-3] M.E. Waddoups, J.R. Eisenmann & B.E. Kaminski
'Macroscopic Fracture Mechanics of Advanced Composite Materials'
J. Composite Materials, Vol. 5, 1971
- [14-4] J.M. Whitney & R.J. Nuismer
'Stress Fracture Criteria for Laminated Composites Containing Stress
Concentrations'
J. Composite Materials, Vol. 8, 1974
- [14-5] J.M. Whitney & R.J. Nuismer
'Uniaxial Failure of Composite Laminates Containing Stress
Concentrations'
Fracture Mechanics of Composites, ASTM STP 593
American Society of Testing and Materials, 1975
- [14-6] R.F. Karlak
'Hole Effects in a Related Series of Symmetrical Laminates'
Proceedings of Failure Modes in Composites, IV
The Metallurgical Society of EIME, Chicago, 1977
- [14-7] R.B. Pipes, R.V. Wetherhold & J.W. Gillespie, Jr.
'Notched Strength of Composite Materials'
J. Composite Materials, Vol. 12, 1979

- [14-8] R.B. Pipes, J.W. Gillespie, Jr., & R.V. Wetherhold
'Superposition of the Notched Strength of Composite Laminates'
Polymer Engineering and Science, Vol. 19, No. 16, 1979
- [14-9] R.B. Pipes, R.V. Wetherhold & J.W. Gillespie, Jr.
'Macroscopic Fracture of Fibrous Composites'
Materials Science and Engineering, Vol. 45, 1980
- [14-10] K.Y. Lin
'Fracture of Filamentary Composite Materials'
Ph. D. Dissertation, Department of Aeronautics and Astronautics
M.I.T., Cambridge, Mass., January 1976
- [14-11] J.W. Mar & K.Y. Lin
'Fracture Mechanics Correlation for Tensile Failure of Filamentary
Composites with Holes'
J. of Aircraft, Vol. 14, No. 7, July 1977
- [14-12] C.C. Poe, Jr. & J.A. Sova
'Fracture Toughness of Boron/Aluminium Laminates with Various
Proportions of 0° and ±45° Plies'
NASA Technical Paper 1707, November 1980
- [14-13] O.L. Bowie
'Analysis of an Infinite Plate Containing Radial Cracks Originating
from the Boundary of an Internal Circular Hole'
Journal of Mathematics and Physics, Vol. 35, 1956
- [14-14] G.R. Irwin
'Fracture Dynamics'
Fracture of Metals, A.S.M., Cleveland, 1948
- [14-15] S.G. Lekhnitski
'Anisotropic Plates'
Science Publishers, New York, 1968
- [14-16] R.E. Peterson
'Stress Concentration Factors'
John Wiley & Sons, New York, 1974
- [14-17] W.F. Brown, Jr. & J.E. Srawley
'Plane Strain Crack Toughness Testing of High Strength Metallic
Materials'
ASTM STP 410, American Society of Testing and Materials, 1966
- [14-18] C.S. Hong & J.H. Crew Jr.
'Stress Concentration Factors for Finite Orthotropic Laminates with a
Circular Hole and Uniaxial Loading'
NASA TP 1469, May 1979
- [14-19] S.G. Lekhnitski
'Theory of Elasticity of Anisotropic Elastic Body'

- Holden Day, Inc. (San Francisco), 1963
- [14-20] MBB/ERNO Final Report
'Integrity Control of Carbon Fibre Reinforced Plastics Structural Elements'
ESA Contract 4442/80/NL/AK(SC), 1985
- [14-21] S.P. Garbo & J.M. Ogonowski
'Strength Predictions of Composite Laminates with Unloaded Fastener Holes'
AIAA Journal, Vol. 18, No 5, May 1980
- [14-22] L.B. Greszczuk
'Stress Concentrations and Failure Criteria for Orthotropic and Anisotropic Plates with Circular Openings'
ASTM STP 497, 1972
- [14-23] ESDU Data Sheets, 85001, Nov. 1985
- [14-24] R.H. Martin & B.D. Davidson
'Mode II fracture toughness evaluation using a four point bend end notched flexure test'
4th International Conference on Deformation and Fracture of Composites, March 24-26, 1997, Manchester
- [14-25] K.N. Shivakumar, P.W. Tan & J.C. Newman Jr.
'A virtual crack-closure technique for calculating stress intensity factors for cracked three dimensional bodies'
International Journal of Fracture, Vol. 36, 1988, pp. R43 R50
- [14-26] C.T. Sun & C.J. Jih
'On the strain energy release rates for interfacial cracks in bi-material media'
Engineering Fracture Mechanics, 28:13 27, 1987
- [14-27] R.H. Martin, P. Sriram & S.J. Hooper
'Using a mixed mode fatigue delamination criterion'
Presented at the 12th ASTM Symposium on Composite Materials: Testing and Design, Montreal, Canada, May 1994
- [14-28] B.D. Davidson
'Prediction of energy release rate for edge delamination using a crack tip element'
Composite Materials: Fatigue and Fracture, (Fifth Volume), ASTM STP 1230, R.H. Martin, Ed., ASTM, Philadelphia, 1995, pp.155-175
- [14-29] R.H. Martin
'Local fracture mechanics analysis of stringer pull-off and delamination in a post-buckled compression panel'
Proceedings of the ICCM-10, Whistler, British Columbia, August 14-18 1995 VI-253

- [14-30] T.K. O'Brien
'Mixed-mode strain energy-release rate effects on edge delamination of composites'
Effects of Defects in Composite Materials, ASTM STP 836, D.J. Wilkins, Ed., ASTM, Philadelphia, 1984, pp. 125-142
- [14-31] G.B. Murri, S.A. Salpekar, and T.K. O'Brien
'Fatigue delamination onset prediction in tapered composite laminates'
Composite Materials: Fatigue and Fracture (3rd Volume), ASTM STP 1110, T.K. O'Brien, Ed., ASTM, Philadelphia, 1991, pp. 312-339
- [14-32] R.H. Martin & W.C. Jackson
'Damage prediction in cross-ply curved composite laminates'
Composite Materials: Fatigue and Fracture, Fourth Volume, ASTM STP 1156, W.W. Stinchcomb, N.E. Ashbaugh, Eds., ASTM, Philadelphia, 1993, pp.105-126.

15

Prediction of dynamic characteristics

15.1 Introduction

The important distinction between material and structural damping is often not appreciated and consequent misinterpretation of data results in errors. It is therefore necessary to clarify this matter and show the correct application of prediction methods for damping, [See: 15.3; 15.4 and 15.5].

Definitions of the most widely used damping expressions and their interrelationships, Ref. [15-5], are also given, [See: 15.2].

A rigorous analytical treatment of the theory of damping is given in Ref. [15-1], [15-2], [15-3].

15.2 Definition of damping terms

15.2.1 General terms

15.2.1.1 Specific energy

Damping can be expressed quantitatively on either an absolute or a relative energy basis. In absolute terms, the specific energy ΔU is the energy dissipated per unit volume of material during one cycle of vibration at a given stress amplitude.

The behaviour of many materials can be represented approximately by the relationship:

$$\Delta U = J \sigma^n \quad [15.2-1]$$

Where: J and n are material constants, Ref. [15-2].

The energy dissipated by damping is represented by the area within the stress/strain hysteresis loop.

15.2.1.2 Loss factors

A well established fundamental ratio with which to assess damping on a relative energy basis is the loss factor η , where:

$$\eta = \frac{1}{2\pi} \frac{\text{Energy dissipated during one cycle}}{\text{Maximum strain energy stored during cycle}}$$

$$= \frac{1}{2\pi} \frac{\Delta U}{U} \quad [15.2-2]$$

For a uniform block of material subjected to a uniaxial simple harmonic stress of amplitude σ , η_m is the material loss factor, where:

$$\eta_m = \frac{1}{2\pi} \frac{J\sigma^n}{\sigma^2/2E} = \frac{JE\sigma^{n-2}}{\pi} \quad [15.2-3]$$

If the material has linear material damping, i.e., $n = 2$, η_m is constant:

$$\eta_m = \frac{JE}{\pi} \quad [15.2-4]$$

For the general situation, a member having a non uniform stress distribution, the structural loss factor is determined by:

$$\eta_s = \frac{JE \int_V \sigma(V)^n dv}{\pi \int_V \sigma(V)^2 dv} \quad [15.2-5]$$

Or, in terms of strain:

$$\eta_s = \frac{JE^{n-1} \int_V \varepsilon(V)^n dv}{\pi \int_V \varepsilon(V)^2 dv} \quad [15.2-6]$$

And, in shear:

$$\beta_s = \frac{J^1 G_1^{n-1} \int_V \gamma(V)^n dv}{\pi \int_V \gamma(V)^2 dv} \quad [15.2-7]$$

Therefore, loss factors determined from experiments on specimens having a non-uniform stress distributions are structural loss factors.

If the material has linear damping, i.e. $n = 2$, the structural loss factor is equal to the material loss factor and is independent of structural geometry or stress distribution.

15.2.2 Complex modulus model

15.2.2.1 General

Experimental evidence suggests that the damping of composite materials is linear at small amplitudes. Although this approach has numerous deficiencies, Ref. [15-3], the most widely used model of linear damping in structural dynamics is the complex modulus model. This model, which has the advantage of incorporating stiffness and damping properties in a complex modulus, is used throughout this review, Ref. [15-4].

15.2.2.2 Energy dissipation under steady state sinusoidal excitation

This is usually defined in terms of the specific damping capacity ψ , which is the ratio of the energy dissipated, U_d , in a unit volume per cycle to the maximum strain energy stored per unit volume, U , i.e.:

$$\psi = \frac{U_d}{U} = \eta 2\pi \quad [15.2-8]$$

15.2.2.3 Bandwidth of half power points in steady state sinusoidal excitation

One method of specifying this is in terms of the dimensionless damping ratio, ξ , which is defined in terms of the ratio of the actual to critical damping coefficients, Ref. [15-1]. ξ can be calculated from:

$$\xi = \frac{(\omega_2 - \omega_1)}{2\omega_n} \quad [15.2-9]$$

where ω_1 and ω_2 are the frequencies at which the energy dissipated in the system is one half of that at resonance ω_n .

15.2.2.4 Quality factor

$$Q = 2\xi - 1 \quad [15.2-10]$$

15.2.2.5 Loss tangent under sinusoidal excitation

Applying the complex stiffness approach to the material stiffness (elastic modulus):

$$E = E_R + iE_I = E_R(1 + ig) \quad [15.2-11]$$

Where E is the complex modulus, E_R and E_I , are the real and imaginary components of E respectively and g is the loss tangent:

$$g = \frac{E_R}{E_I}$$

Where E_R and E_I are usually called storage and loss moduli respectively.

15.2.2.6 Decay of free vibration

The most common measure of this phenomenon is the logarithmic decrement, defined as:

$$\delta = \ln \frac{a_i}{a_{i+1}} \quad [15.2-12]$$

Where a_i is the amplitude of the i -th cycle, i is an integer.

For most materials, at least at relatively small amplitudes, δ is small and independent of amplitude. A more practical method of calculating δ from experimental data is then:

$$\delta = \frac{1}{n} \ln \frac{a_n}{a_{n+1}} \quad [15.2-13]$$

where n is an arbitrary integer.

15.2.2.7 Interrelationships

The interrelationships between the parameters can be assumed for low damping complex modulus materials:

$$\eta = g = 2\xi = \psi / 2\pi = \frac{1}{Q} = \frac{\delta}{\pi} \quad [15.2-14]$$

15.3 Prediction methods for damping

If composites are to be used in primary load-bearing structures, it is essential that their responses to static and dynamic loads are predicted accurately. Such predictions involve the use of not only stiffness and strength properties but also damping characteristics. Indeed, damping is the parameter which governs resonant response, a crucial consideration in structures subjected to acoustic loads.

Some simple first approximation theories can be applied to predict the damping of a composite material from the dynamic properties of its constituents and their configuration. Such theories, [See: 15.4], are based on the assumptions that, Ref. [15-5]:

- No significant macroscopic or interfacial slip occurs.
- Fibres and matrix are characterised by their elastic behaviour and associated loss coefficients, Ref. [15-4].

[See also: 15.2 for a compilation of definitions of damping terms; 15.5 for data on damping properties]

15.4 Determination of damping characteristics

15.4.1 Unidirectional characteristics

According to Hashin, Ref. [15-6]:

$$\eta_c = \eta_m V_m \left[\frac{E_m}{E_c} \right] \quad [15.4-1]$$

Where:

η_c = flexural loss factor of the composite in fibre direction

η_m = flexural loss factor of the matrix

V_m = volume fraction of the matrix

E_m = modulus of the matrix

E_c = composite modulus; determined using the 'law of mixtures'

15.4.2 Off axis characteristics

This analysis is based on the strain energy in the ply, Ref. [15-8]. The energy dissipated in the ply is calculated from the compliance matrix of the ply, the stress in the ply, and the specific damping capacities of the ply relative to the fibre axis, as functions of stress. This complex method, involving extensive numerical integration, can be avoided by assuming linear damping.

The complex moduli of the ply relative to the fibre direction can be substituted into modulus transformation equations for a ply of arbitrary orientation, Ref. [15-9], providing ply complex moduli, from which the damping can then be calculated, i.e.:

$$\frac{1}{E_x^*} = \frac{1}{E_1^*} \cos^4 \theta + \left(\frac{1}{G_{12}^*} - \frac{2\nu_{12}^*}{E_1^*} \right) \sin^2 \theta \cos^2 \theta - \frac{1}{E_2^*} \sin^4 \theta \quad [15.4-2]$$

$$\frac{1}{E_y^*} = \frac{1}{E_1^*} \sin^4 \theta + \left(\frac{1}{G_{12}^*} - \frac{2\nu_{12}^*}{E_1^*} \right) \sin^2 \theta \cos^2 \theta - \frac{1}{E_2^*} \cos^4 \theta \quad [15.4-3]$$

$$\frac{1}{G_{xy}^*} = 2 \left(\frac{2}{E_1^*} + \frac{2}{E_2^*} + \frac{4\nu_{12}^*}{E_1^*} - \frac{1}{G_{12}^*} \right) \sin^2 \theta \cos^2 \theta + \frac{1}{G_{12}^*} (\sin^4 \theta + \cos^4 \theta) \quad [15.4-4]$$

$$\nu_{xy}^* = E_x^* \left(\frac{\nu_{12}^*}{E_1^*} (\sin^4 \theta + \cos^4 \theta) - \left(\frac{2}{E_1^*} + \frac{2}{E_2^*} - \frac{1}{G_{12}^*} \right) \sin^2 \theta \cos^2 \theta + \frac{1}{G_{12}^*} \right) \quad [15.4-5]$$

Where:

E_x^* , E_y^* , G_{xy}^* , ν_{xy}^* - are the longitudinal, transverse and shear complex moduli and Poisson's ratio relative to the ply axis

E_1^* , E_2^* , G_{12}^* , ν_{12}^* - are the longitudinal transverse and shear complex moduli and Poisson's ratio relative to the fibre axis

15.4.3 Laminate characteristics

Adams and Bacon, Ref. [15-8], calculated the damping of an FRP laminate by summing the energy dissipated in the individual ply, [See: 'Unidirectional characteristics' and 'Off-axis characteristics'].

The specific damping capacity of the laminate in a specified mode is then calculated by dividing the total energy dissipated by that stored. Again the complexity of the numerical integration makes this method unattractive.

By assuming linear damping, Schultz and Tsai, Ref. [15-10], produced a more attractive method of predicting the damping of CFRP laminates. Essentially, the complex moduli of the laminate are substituted directly into the well-documented transformation equations for laminated composites providing the complex moduli of the laminate. Consequently, the shear or flexural damping of the laminates is found from the real and imaginary parts of the relevant complex moduli.

A computer program, developed by ESDU, can be used to predict the damping of laminates, [See: 16.29].

15.5 Approximate data on damping

To verify the dynamic behaviour of a composite structure at the preliminary design stage, the approximate data on loss factors presented in Figure 15.5.1 can give initial guidance, Ref. [15-5].

[See also: 'References' for more detailed data on damping properties]

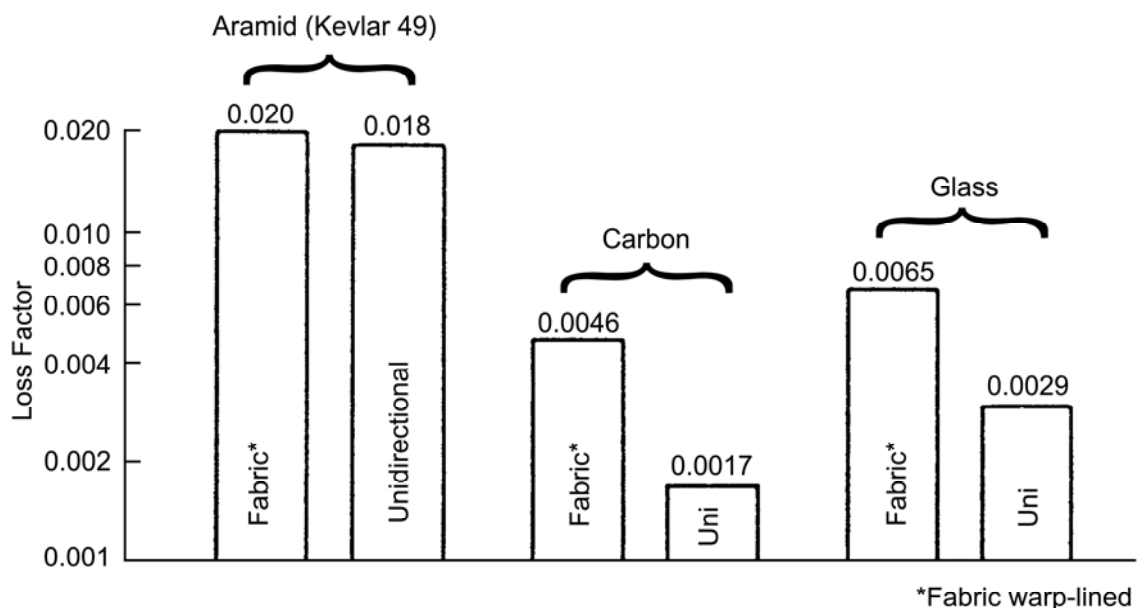


Figure 15.5-1 - Summary of loss factors for various fibres / epoxy composites

15.6 References

15.6.1 General

- [15-1] C.W. Bert
'Material Damping: An introductory Review of Mathematical Models, measures and experimental Techniques'
J. Sound Vib. 29 (2), 1973
- [15-2] B.J. Lazan
'Damping of Materials and Members in Structural Mechanics'
Pergamon Press, 1968
- [15-3] R.E.D. Bishop
'The Treatment of Damping Forces in Vibration Theory'
J. Royal Aero. Soc. 59, 1955
- [15-4] C.W. Bert
'Composite Materials: A Survey of the Damping Capacity of Fibre Reinforced Composites'
Damping Applications for Vibration Control
Proc. Winter Annual Meeting, 1980
- [15-5] T.A. Palmer
'A Design Guide to the Damping of Composite Materials'
SAL Report 1046 for ESTEC, April 1985
- [15-6] Z. Hashin
'Complex Moduli of Viscoelastic Composites: II Fibre Reinforced Materials'
Int. J. Solid Structures, 6, 1970
- [15-7] H.L. Cox
'The Elasticity and Strength of Paper and other Fibrous Materials'
Brit. J. Appl. Phys. 13, 1952
- [15-8] R.D. Adams & D.G.C. Bacon
'Effect of Fibre Orientation and Laminate Geometry on the Dynamic Properties of CFRP'
J. Composite Materials, 7, 1973
- [15-9] R.M. Jones
'Mechanics of Composite Materials'
McGraw Hill, 1975
- [15-10] A.B. Schultz & S.W. Tsai
'Measurements of Complex Dynamic Moduli of Laminated Fibre Reinforced Composites'
J. Composite Materials 3, 1969

16

Computer analysis of composites

16.1 Introduction

An overview of commonly available software products is presented.

NOTE The software packages described are not a comprehensive list of those available. Potential users are advised to contact suppliers for particular details of their software.

The programs are divided into three different types, [See: 16.2]:

- Finite element programs with special composite features included.
- Laminate analysis programs performing laminated plate theory.
- Programs for special applications.

16.2 Computer programs: Analysis of composites

16.2.1 General

Table 16.2.1 lists some commonly available software packages, along with links to supplier's websites. The software is listed by program type.

A summary description for each package is given for:

- Finite element in Table 16.2.2.
- Laminate analysis in Table 16.2.3.
- Special applications in Table 16.2.4.

[See: 16.3 for ESDU; 16.39 for ESAComp]

Table 16.2-1 - Commonly available software for the analysis of composites

Program Name	Supplier (web site link)	Platform	Program Type		
			Finite Element	Laminate Analysis	Special Application
ABAQUS	Abaqus Inc. [Hibbit Karlsson and Sorenson Inc.]		✓		
ACOMAP	C.A.S.A Space Division			✓	
ANSYS	ANSYS Inc. [Swanson Analysis System Inc.]		✓		
ARGUS	Merlin Technologies Inc.		✓		
BEAM	Stanford University *				✓
BOLT					✓
CLASS	Materials Science Corp. : ASM Intl.			✓	
COALA	Cranfield Institute of Technology			✓	
COMPOS	Technical University of Linköping			✓	
COSMOS/M	Structural Research and Analysis Corp.		✓		
CURE	Stanford University *				✓
ESAComp [See: 16.39]	Componeering Inc	PC- Windows; Linux; Unix		✓	✓
ESDU A7916 A8039	ESDU Engineering Data Service [See: 16.03]				✓
ESDU A7303 A8147					✓
ESDU A8335				✓	
ESDU A8418				✓	
ESDU A8501					✓
ESDU A8336					✓
ESDU A8512					✓
GENLAM LAMRANK		S.Tsai; Think Composites			✓
ICAN	COSMIC ‡, University of Georgia			✓	✓
IMPACT	Stanford University *			✓	✓
LAMA	Dornier System ‡			✓	
MSC.NASTRAN	MSC Software †		✓		
NISA	Engineering Mechanics Research Corp.		✓		
SAMCEF	SAMTECH S.A. ; CISI Engineering		✓		
SAP	Computer Software Inc.		✓		
STRESS	Stanford University *				✓
W8GAIN					✓
WIND					✓

16.2.2 Finite element programs

Table 16.2-2 - Computer programs for finite element analysis

Name	Application	Composite Features	Optimise
ABAQUS	<ul style="list-style-type: none"> * General purpose finite element program. * Linear, non-linear and coupled analysis. 	<ul style="list-style-type: none"> * Anisotropic material models in all elements, including non linearity. * 3-D solid elements. 	
ANSYS	<ul style="list-style-type: none"> * General purpose finite element stress and heat transfer analysis program. * Non-linear capabilities, but not generally implemented for composite materials. * Pre- and post-processing. 	<ul style="list-style-type: none"> * 2-D and 3-D plate/shell and solid elements with orthotropic and anisotropic material properties. * Laminated shell elements. * Crack-tip solid elements. * Thick-shell elements. * Max strain, max stress, Tsai-Wu and user defined failure criteria. 	
ARGUS	<ul style="list-style-type: none"> * General purpose finite element program. * Extensive capabilities for non-linear analysis and for composite materials. * Buckling load and mode processor. * Modal analysis processor. * Pre- and post-processing 	<ul style="list-style-type: none"> * 2-D and 3-D plate/shell and solid elements with orthotropic temperature dependent properties. * Layered composite plate/shell and doubly curved elements * Shell element with anisotropic temperature dependent properties. * Biaxial max. stress and max. shear stress failure criteria 	
COSMOS/M	<ul style="list-style-type: none"> * General purpose finite element program. * Linear/non-linear static, linear/non-linear dynamic analysis. * Buckling and heat transfer analysis. * 1-D, 2-D and 3-D structural and thermal models. 	<ul style="list-style-type: none"> * 2-D and 3-D plate/shell and solid elements with orthotropic temperature-dependent properties. * Layered composite shell elements. * Tsai-Hill and mod. Tsai-Wu failure criteria. 	
MSC NASTRAN	<ul style="list-style-type: none"> * General purpose finite element program. * Static, dynamic and thermodynamic analysis. * Non-linear analysis. * Pre- and post-processing by MSC.PATRAN 	<ul style="list-style-type: none"> * Plate/shell elements with orthotropic temperature-dependent properties (input via PCOMP, MAT8 card). * Ply stresses. * Tsai-Hill, Hoffmann and Tsai-Wu failure criteria 	
NISA	<ul style="list-style-type: none"> * General purpose finite element program. * Pre- post-processing (digitiser input of nodal data for 2-D and 3-D structures). 	<ul style="list-style-type: none"> * Solid elements. * Thick-shell elements (material properties may change within an element). * Laminated shell elements. * In-plane and interlaminar stresses. * Max. stress, max. strain, mod. Hill, von Mises, Tsai-Wu and delamination failure criteria 	
SAMCEF	<ul style="list-style-type: none"> * General purpose finite element program * Linear/non-linear stat and dyn. * Thermal analysis * Buckling * Optimisation * Pre-, post-processing 	<ul style="list-style-type: none"> * 2-D and 3-D plate/shell elements * Thick shell elements * Multilayer solid elements * Sandwich modelling * Transverse shear deformation * In-plane and interlaminar stresses * Max. stress, max. strain, Tsai-Hill Tsai-Wu and Sandhu failure criteria 	
SAP	<ul style="list-style-type: none"> * General purpose finite element program * SAP7 has non-linear capability. * Pre- and post-processing. 	<ul style="list-style-type: none"> * Only SAP7 has 2-D and 3-D elements with orthotropic material properties. * Multi-layer plate/shell elements. * Tsai-Hill and Tsai-Wu failure criteria 	

Optimise: software with optimisation routines for laminate elements to be added.

16.2.3 Laminate analysis programs

Table 16.2-3 - Computer programs for laminate analysis

Name	Application	Special Features
ACOMAP	Laminate analysis program based on laminated plate theory	<ul style="list-style-type: none"> * Interactive input/output * Matrix/fibre data: ply properties; hybrid laminates. * Stiffness and compliance matrix. * Engineering constants (membrane) * Mechanical and thermal loads. * Ply stresses in ply co-ordinates. * Ply stresses and strains in laminate co-ordinates. * Max. stress, max. strain and Tsai-Hill failure criteria. * Last ply failure.
CLASS	Laminate analysis program based on laminated plate theory	<ul style="list-style-type: none"> * Matrix/fibre data: ply properties * Stiffness and compliance matrix engineering constants * Thermal expansion coefficient * Ply stresses and strains * First ply/last ply failure
COALA	Laminate analysis program based on laminated plate theory	<ul style="list-style-type: none"> * Input/output files. * Ply properties; hybrid laminates. * Reduced input for symmetric stacking. * Stiffness and compliance matrix * Engineering constants (membrane and bending). * Mechanical and hygrothermal loads. * Variation of hygrothermal loads across the laminate. * Ply stresses and strains in ply co-ordinates. * Ply stresses in laminate co-ordinates. * Stresses and strains at top and bottom of each ply. * Max. stress, max strain, Hoffmann, Tsai-Hill and Tsai-Wu failure criteria * First ply failure. * Index of margin of safety.
COMPOS	Laminate analysis program based on laminated plate theory	<ul style="list-style-type: none"> * Interactive input/output * Ply properties (material data base). * Reduced input for symmetric stacking. * Stiffness and compliance matrix * Engineering constants (membrane anti-bonding). * Mechanical and hygrothermal loads. * Ply stresses and strains in ply and laminate co-ordinates. * Stresses/strains at top and bottom of each ply. * Tsai-Hill and Tsai-Wu failure criteria * First ply failure. * Index of margin of safety.
ESAComp	Analysis and design of composite laminates and laminated structural elements	<ul style="list-style-type: none"> * Fiber/matrix micromechanics * Analyses for constitutive and thermal/moisture expansion behavior of plies * Laminates <ul style="list-style-type: none"> - 2.5D behavior - classical lamination theory (CLT) - laminate strength in principal loading conditions - load response - laminate and layer level response, effects due to thermal/moisture loads - first ply failure (FPF) and degraded laminate failure (DLF) - several commonly used failure criteria and a possibility to add user specified criteria - wrinkling of sandwich face sheets, core shear failure - interlaminar shear failure - constant and variable load approach in determining margins of safety - failure and design envelopes - sensitivity studies for 2.5D behavior and FPF analyses - tolerances for a ply property or layer orientations - notched laminate analysis of circular and elliptic holes - layer drop-off - exterior or embedded drop-off in a solid

Name	Application	Special Features
ESAComp (continued)		laminate or a face sheet of a sandwich - straight free edge analysis using built-in FE solver - laminate through-the-thickness temperature distribution - laminate through-the-thickness moisture distribution and moisture content as a function of time * Plates and stiffened plates - Mindlin plate analysis using built-in FE solver - rectangular plates with any combination of clamped, simply supported, and free edges - load response and failure due to transverse loads (combinations of a point load, line loads, and distributed load), - stability and failure under in-plane loads, natural frequencies * Beams and columns * Bonded joints, [See: Table 16.02.4] * Mechanical joints, [See: Table 16.02.4] Note: Other features include: design tools; FE import/export interfaces; batch run capability (integration with other software); databank.
ESDUpac A8335	Stiffnesses of laminated plates	* Ply properties. * Stiffness and compliance matrix. * Engineering constants.
ESDUpac A8418	Failure of composites based on laminated plate theory	* Ply properties; hybrid laminates * Mechanical and thermal loads. * Damage history up to failure. * Damage caused by constrained unbalanced laminates. * Max stress and mod. Puck failure criteria.
ICAN	Micro-mechanic, macro-mechanic and laminate analysis	* Fibre/matrix and ply properties input from database * Hybrid laminates * Hydrothermal analysis * Stress concentration around holes * Delamination locations around holes * Free edge stresses * Transverse shear stresses * Failure loads based on max. stress * First ply failure by fibre breakage
GENLAM/ LAMRANK	Laminate analysis program and laminate ranking based on laminated plate theory	* Interactive input/output * Ply properties (material data base); hybrid laminates. * Reduced input for symmetric stacking. * Stiffness and compliance matrix. * Engineering constants (membrane and bending). * Mechanical and hygrothermal loads. * Ply stresses and strains in ply and laminate co-ordinates. * Stresses/strains at top and bottom of each ply. * Tsai-Hill and Tsai-Wu failure criteria * First ply failure/ last ply failure. * Index of margin of safety. * Indication of critical load case. * LAMRANK performs a ranking of all possible lay-up for a given load case.
LAMA (continued)	Laminate analysis program based on laminated plate theory	* Interactive input/output ply properties (material data base). * Reduced input for symmetric stacking. * Stiffness matrix (also 3-D). * Engineering constants (membrane). * Stress concentration factor for circular holes. * Optimised stacking sequence with respect to free edge delamination. * Equivalent plate model for symmetric sandwiches. * Mechanical and hygrothermal loads. * Ply stresses and strains in ply and laminate co-ordinates. * Stresses/strains at top and bottom of each ply. * Hashin, Tsai-Hill and Tsai-Wu failure criteria * First ply failure/last ply failure. * Index of margin of safety.

16.2.4 Special applications programs

Table 16.2-4 - Computer programs for special composite applications

Name	Application	Features
ESAComp	Laminates, plates and stiffened panels, beams and columns. [See also: Table 16.02.3].	* Thermal and moisture distribution predictions.
	* Bonded joints * Mechanical joints	* Bonded joints: single and double lap; single and double strap; single and double sided scuffed lap, bonded doubler. Beam and plate models for adherends, linear and nonlinear adhesive models. Combinations of axial, bending, in-plane and out-of-plane shear loads. Joint deflection forces and moments in adherends, adhesive stresses, margins of safety for cohesive failure of adhesive and laminate failure due to in-plane and bending loads. * Mechanical joints: single and double lap joints under axial loads. Fastener and bypass loads, laminate stresses and strains on fastener holes. Margins of safety for failure. Prediction of failure mode.
ESDUpac A7916 A8039	Strength of bonded joints	* Tensile or shear stresses in the adherends. * Inelastic shear stresses or strains in the adhesive of a balanced bonded single or multi-step lap joint. * The adherends may have different material properties. * Program ESDU 2020 does not consider the stresses in the adherend, but the peel stresses.
ESDUpac A7303 A8147	Buckling of rectangular orthotropic plates	* Buckling problems for laminated plates and sandwich panels with composite facings. * Clamped and simply supported edges. * Compression and shear loads (also in combination).
ESDUpac A8501	Stress concentration in composite plates	* Stress/strain distribution around holes in composite plates. * Tensile, compression or shear loads. * Ply properties or laminate stiffnesses.
ESDUpac A8336	Natural frequencies of laminated plates.	* Lower natural frequencies of initially unstressed, specially orthotropic, rectangular, flat or slightly curved plates. * Any combination of simply supported or clamped edges possible.
ESDUpac A8512	Damping of composites	* Material damping in rectangular, multi-layered composites vibrating in one of their lower frequency natural modes. * Only balanced symmetric laminated plates, simply supported or all edges clamped. * Output for the specific damping capacity and viscous damping ratio for each specified mode.

Name	Application	Features
BEAM	Design of composite beams.	<ul style="list-style-type: none"> * Calculation of forces and moments induced on a composite beam by external loads. * Different types of loads and supports. * Output for deflection curvature. * Stresses/strains. * Margin of safety for the plies. * Only symmetric laminates or sandwich with equal face sheets.
BOLT	Design of pin-loaded holes in composites.	<ul style="list-style-type: none"> * Prediction of failure and failure mode. * Three types of bolted joints: <ol style="list-style-type: none"> 1) joints with a single hole 2) joints with two identical holes in a row 3) joints with two identical holes in tandem. * Only uniform tensile loads and symmetric laminates.
CURE	Analysis of curing process of composites.	<ul style="list-style-type: none"> * Calculation of optimal cure cycle. * Influence of material properties and process variables on cure cycle. * Unsymmetric but no hybrid laminates possible.
IMPACT	Calculation of impact damage for composite plates.	<ul style="list-style-type: none"> * Calculation of delamination area induced in a composite plate by a foreign object impact. * Variable characteristics of impactor. * Stress history using transient finite element formulated for a 3-D element mesh.
STRESS	Calculation of hygrothermal stress/strain in composites.	<ul style="list-style-type: none"> * Only hygrothermal loads.
WIND	Analysis of filament winding of composites.	<ul style="list-style-type: none"> * Calculation of: <ul style="list-style-type: none"> - cylinder temperature, - viscosity, - degree of cure, - fibre position, - fibre tension, - residual stresses/strains after curing.
W8GAIN	Calculation of moisture content in a composite.	<ul style="list-style-type: none"> * Moisture content as a function of temperature and time. * Heat conduction and moisture diffusion are described by Fourier and Fick formulae.

16.3 ESDU data for composite analysis

16.3.1 General

ESDU International plc (UK) produces design data and information for engineers working in a range of engineering fields. A number of these documents, referred to as 'Data Items', have particular applicability to design with composites.

A list of the individual 'Data Items' is given in Table 16.3.1, which includes a link to a synopsis of each one, along with details of relevant ESDUpac's.

16.3.2 ESDU data items

In developing ESDU Data Items, a full technical assessment is made of the available data both in terms of the reliability of experimental techniques and by comparison with theoretical predictions. The qualified staff of ESDU work with the guidance and assistance of committees whose members are drawn from industry, research and educational establishments, and include typical users of the data. By this means, the accuracy of the work can be assured, the relevant and practical experience of a number of individuals can be included to supplement the quantitative results and the form of the final presentation can be chosen to suit the typical users.

Table 16.3-1 - ESDU data sheets for composite analysis

SMH Topic	Title	ESDU No.
	Laminated Composites - General analysis	
16.7	Laminate stress analysis	74039
16.8	Plate stiffnesses (in-plane)	75002
16.16	Lay-up arrangements for special orthotropy	82013
16.19	Plate stiffnesses and apparent elastic properties	83035
16.24	Stresses and strains around circular holes	85001
16.27	Selection of reinforcement around circular holes	86003
16.34	Plate through-the-thickness shear stiffnesses	89013
	Buckling of balanced laminated composites	
16.4	Buckling of orthotropic plates	73003
16.5	Flexural stiffness of flat strips	73007
16.6	Metallic skin stiffeners reinforced by composite - local buckling	73015
16.12	Buckling of specially orthotropic composite plates	80023
16.15	Buckling of orthotropic plates	81047
16.31	Buckling of curved composite panels	87025
	Buckling of unbalanced laminated composites	
16.28	Buckling of unbalanced composite plates	86020
	Sandwich panels with composite face plates	
16.30	Sandwich column and beam face plate wrinkling	87013
16.32	Sandwich panel face plate wrinkling	88015
	Bonded joints	
16.9	Bonded joints - 1	78042
16.10	Bonded joints - 2	79016
16.11	Bonded joints - 3	80011
16.12	Bonded joints - 4	80039
16.13	Bonded joints - 5	81022
	Failure criteria	
16.17	Failure modes of laminated composites	82025
16.18	Failure criteria for layers of a laminated composite	83014
16.22	Failure analysis	84018
16.36	Delamination and free edge stresses	90021
16.37	Delamination at termination of plies	91003
	Natural modes of vibration	
16.20	Natural frequencies of laminated flat plates	83036
16.26	Sandwich panel natural frequencies	85037
16.33	Vibration of singly-curved laminated plates	89011
16.35	Vibration of plates with in-plane loading	90016
	Damping and response to acoustic loading	
16.21	Strains in skin panels under acoustic loading	84008
16.23	Endurance under acoustic loading	84027
16.25	Damping in composite plates	85012
16.29	Sandwich panel response to acoustic loading	86024

16.3.3 ESDUpac

Many calculations for fibre-reinforced laminated structures are more conveniently made with the aid of computer programs.

[See: [ESDU International plc](#) website for further details]

16.4 Buckling of orthotropic plates

16.4.1 Title

Buckling of flat rectangular orthotropic plates.

Data Item No. 73003 [See also: ESDU International website].

16.4.2 Usage and scope

Laminated composite plates and sandwich panels faced with laminated composites can be modelled as homogeneous orthotropic plates. For such plates overall buckling is an important condition. Buckling is a function of the plate's in-plane and flexural stiffnesses, its through-the-thickness shear stiffnesses, its shape, boundary conditions and the applied loading. The through-the-thickness shear stiffnesses are of particular importance since, if they are very low, they can dominate buckling.

16.4.3 Analysis

The plate is treated as homogeneous, and can be isotropic or specially orthotropic. The through-the-thickness shear stiffnesses in the principal plane of orthotropy and orthogonally to that plane are included. The elastic buckling load is derived for symmetrical combinations of clamped and simply supported edge conditions for rectangular plate subject to combinations of in-plane compression, tension and shear loading. The solution is presented as a computer program. Buckle wave forms having up to 7 half waves along or across the plate are examined.

16.4.4 ESDUpac A7303

16.4.4.1 General

Previously ESDUpac E1001

The program calculates the elastic overall buckling loads for orthotropic rectangular plates.

16.4.4.2 Input

- Boundary conditions
- All edges clamped.
- All edges simply supported.
- Symmetrical combinations of clamped and simply supported edges.
- Loading (can be tensile)

- Given two of the three in-plane loads determine the remaining cause of buckling.
- Given the ratio of the applied loads determine all their values at buckling.
- Geometry and stiffnesses.
- Plate properties and geometry
- Aspect ratio.
- Parameters derived from flexural and shear stiffnesses of plate. Poisson's ratio.

16.4.4.3 Output

- Buckling loads or ratios of loads and numbers of buckle half wave examined. Statement if applied loads cause buckling alone.

16.4.5 Notes

The accuracy of the calculations is open to variation with the number of iterations in the root solving routines.

[See: [16.3](#) for access to programs and documentation]

16.5 Flexural stiffness of flat strips

16.5.1 Title

Stiffness of loaded flat strips under sinusoidally distributed bending couples at their edges (for use in local buckling calculations).

Data Item No. 73007 [See also: ESDU International website].

16.5.2 Usage and scope

The behaviour of isotropic or specially orthotropic flat strips subject to sinusoidally distributed couples along their edges can be used to provide the local buckling stress of most common structural engineering sections. An example of their use appears in Data Item No. 73015, [See: 16.6].

16.5.3 Analysis

The elastic behaviour of thin strips of specially orthotropic material has been analysed to produce graphs which plot the rotational stiffness at the edges for a range of stiffness values and a range of half wavelengths of the applied sinusoidal couples. Strips with one free edge and a couple acting on the other edge or strips with couples along both edges either opposed or in the same sense, are analysed. Graphs are also provided for calculation of the necessary stiffness values.

[See: [16.3](#) for access to documentation]

16.6 Metallic skin stiffeners reinforced by composite - local buckling

16.6.1 Title

Estimation of the local buckling stress under biaxial compression of an isotropic skin with fibre reinforced integral unflanged stiffeners.

Data Item No. 73015 [See also: ESDU International website].

16.6.2 Usage and scope

Laminated fibre reinforced composite strips can be bonded to stiffeners in metallic (isotropic material) structures to increase their stiffness. The compressive strength of such structures can be limited by local (short wavelength) buckling of the stiffeners coupled to the structure that they stiffen. Where the structure is effectively composed of flat strips, as for example a sheet reinforced by Z-section stiffeners, the stiffness under overall compression with destabilising sinusoidally distributed couples acting along the junctions of the strips can be calculated. This is an unstable condition and the compressive end load where the couples balance and instability, or buckling, occurs without the necessity of externally applying destabilising couples can be found and this represents a buckling condition. The calculation can be repeated for a range of wavelengths and the wavelength yielding the lowest buckling load be ascertained.

16.6.3 Analysis and data

An example of calculation using an integrally machined panel with simple unflanged stiffeners reinforced by carbon fibre bonded to the stiffeners is worked through in detail and the search for the minimum buckling load is set out in tabular form.

The stiffnesses required are obtained from the graphs of Data Item No. 73007, [See: 16.5]. The method involves setting up a simple equation relating the stiffnesses of the strips forming the structure and the formulation of the governing equation is explained.

[See: 16.3 for access to documentation]

16.7 Laminate stress analysis

16.7.1 Title

Stress analysis of laminated flat plates.

Data Item No. 74039 [See also: ESDU International website].

16.7.2 Usage and scope

This item presents the formulae for the elastic analysis of flat laminated plates built up from thin orthotropic layers which can have different material elastic and thermal properties, thicknesses and orientations of their principal axes of orthotropy. Stresses in laminated plates arise either as a result of externally applied loading or as a result of the method of manufacture. Current methods of production of laminated plates usually require the assembly to be cured at a temperature above the working temperature range of the plate. Upon cooling to working temperatures, the different orientations of the layers together with their often different elastic and thermal properties lead to the development of a system of self equilibrating stresses. Similarly, internal stresses can be generated in plates cured at room temperature but which are subjected to a wide range of working temperatures.

16.7.3 Analysis

The formulae presented relate to uniform in-plane stress systems away from the plate boundaries or other geometric discontinuities. No allowance is made for the deformations associated with through-the-thickness shear stiffnesses. The formulae deal with eight cases and provide the stress-strain transformation relationships:

Balanced laminates	Unbalanced laminates
Externally applied loads (no built-in stresses)	Externally applied loads (no built-in stresses)
Built-in stresses (no externally applied loads)	Built-in stresses (no externally applied loads)
Externally applied loads with built-in stresses	Externally applied loads with built-in stresses
	Plate held flat (no other externally applied loads)
	Plate held flat and external in-plane loading applied

Externally applied loads can be direct or shear in-plane loadings or out-of-plane bending or twisting. A fully worked example is provided. It is important that the sign conventions of the stiffnesses and stresses are in accordance. The stiffnesses required for the calculation are set out in Data Item No. 75002, [See: 16.8].

[See: 16.3 for access to documentation]

16.8 Plate stiffnesses (In-plane)

16.8.1 Title

Stiffnesses of laminated flat plates.

Data Item No. 75002 [See also: ESDU International website].

16.8.2 Usage and scope

To correctly analyse laminated composite plates, the in- plane elasticity should also be known so that the following attributes can be determined:

- Stress
- Strain
- Deflection
- Stability
- Vibration

Most structural laminates are composed of highly orthotropic layers and it is important to understand how the arrangement of the layers can influence the stiffnesses. It is also important to understand how the plate stiffnesses relate to the general equation for a solid body. A further knowledge met by the data, is information on the effect of adding layers and their influence on plate symmetry.

16.8.3 Analysis and methods

The fundamental equations used to calculate in-plane stiffness, is set out and the calculation of the stiffnesses for an example laminate is worked through. The effect of layer arrangement is described for the common case where all the layers are specially orthotropic, have the same properties and thickness but are laid up at differing angles to the plate axes. Special cases are identified and then the influence of lay-up arrangement on the direct, bending and coupling terms is explained. The effect of repositioning the plate reference axis (about which the stiffnesses are calculated) is explained and the relevant equations are set out. Tables of the various forms of stiffness matrices that can be constructed are set out together with examples.

[See: 16.3 for access to documentation]

16.9 Bonded joints - 1

16.9.1 Title

Shear stresses in the adhesives in bonded single-step double-lap joints loaded in tension.

Data Item No. 78042 [See also: ESDU International website].

16.9.2 Usage and scope

In order to design bonded lap joints, it is necessary to determine the stress distribution in the adhesive. The shear stresses are one of the major components of the stress distribution and assessment of their maximum value with account of their inelastic behaviour is therefore necessary. This Data Item is complementary to the computer program in Data Item No. 79016, [See: 16.10], and examines the single step joint. A major design objective is that of minimising stresses by careful selection of joint geometry and adhesive, [See: 16.13 for peel or direct normal stresses].

16.9.3 Analysis and data

A shear lag analysis is used to determine the distribution of shear in the adhesive resulting from transmission of the in-plane tension or shear loads from one adherend to the other through the adhesive, taking account of the non-linear stress-strain shear characteristics of the adhesive. It is assumed that the adherends are rigid in flexure and the analysis does not therefore consider the effect on the adhesive or the adherends of normal tensile loads (peel) or bending effects resulting either from the transmission of the load from one adherend to the other or from external bending moments. The adherend is considered to behave elastically. The joint stresses are calculated with the aid of the program in ESDUpac A7916, [See: 16.10], and are presented graphically for three different adhesive materials; with properties stated. The graphs show how the maximum stress is influenced by the geometry and stiffnesses of the joint and aid with the use of the program. Clear trends are discernible and the factors influencing the stresses and their relative sensitivity can be seen.

[See: 16.3 for access to documentation]

16.10 Bonded joints - 2

16.10.1 Title

Inelastic shear stresses and strains in the adhesives bonding lap joints loaded in tension or shear.

Data Item No. 79016 [See also: ESDU International website].

16.10.2 Usage and scope

In order to design bonded lap joints it is necessary to determine the stress distribution in the adhesive. In order to smooth the stress distribution most joints are stepped and details of the stress distribution at each step are calculated. The shear stresses are one of the major stress components of the stress distribution and an assessment of their maximum value with account of the inelastic behaviour of the adhesive material and adherend stiffnesses at each step is therefore necessary. A design objective is to select the combination of step geometries and adhesive stiffness to minimise the shear stresses and so obtain an optimum joint, [See: 16.12 for peel stresses].

16.10.3 Analysis and data

A shear lag analysis is used to determine the distribution of shear in the adhesive, resulting from transmission of the in-plane tension or shear loads, from one adherend to the other through the adhesive, taking account of the non-linear stress-strain shear characteristics of the adhesive. It assumes that the adherends are rigid in flexure and does not therefore consider the effect on the adhesive, or the adherends of normal tensile loads (peel), or bending effects resulting either from the transmission of the load from one adherend to the other, or from external bending moments. The adherend is considered to behave elastically. Each step is divided up into small increments and the stress distribution over each increment is taken to be uniform.

16.10.4 ESDUpac A7916

16.10.4.1 General

Previously ESDUpac E1007.

This program calculates the shear stresses and strains in the adhesives in multi-step lap joints.

16.10.4.2 Input

- Number of steps in joint.
- Geometry and elastic properties of adherends over each step. Elastic shear modulus for adhesive.
- Shear stress in adhesive at elastic limit.
- Shear stress to which adhesive stress/strain curve is asymptotic. Number of increments in each step.
- Requirement for tension or transverse shear loading on joint.

16.10.4.3 Output

- Adhesive shear stresses and strains at each increment on every step.
- Adherend nominal stresses at each increment on every step.
- All input data.

[See: 16.3 for access to program and documentation]

16.11 Bonded joints - 3

16.11.1 Title

Elastic stresses in the adhesive in single-step double-lap bonded joints.

Data Item No. 80011 [See also: ESDU International website].

16.11.2 Usage and scope

In order to design bonded joints it is necessary to determine the stress distribution in the adhesive. The direct (normal through-the-thickness direction) stresses and the shear stresses are the major stresses governing joint design. The direct (normal) stresses peak at the ends of the joints. This Data Item is complementary to the computer program in Data Item No. 80039, [See: 16.12] and examines a single-step joint. A major design objective is minimising the stresses by careful selection of joint geometry and adhesive.

16.11.3 Analysis and data

The data are based on the elastic flexible joint analysis, [See: 16.12]. The joint stresses are calculated with the aid of the program of ESDUpac A8039 and are presented graphically, for a range of non-dimensional parameter ratios of joint component stiffnesses and geometry. The graphs show how the stresses are influenced by the geometry and stiffnesses and therefore aid design of this and more complex types of joints using the program. Clear trends are desirable and the relative sensitivity of stresses to the factors affecting them can be seen.

[See: 16.3 for access to documentation]

16.12 Buckling of rectangular specially orthotropic plates

16.12.1 Title

Buckling of rectangular specially orthotropic plates.

Data Item No. 80023 [See also: ESDU International website].

16.12.2 Usage and scope

Overall flexural buckling of laminated composite plates, subject to biaxial in-plane compressive loading or in-plane shear, can be a design limitation.

For specially orthotropic materials, laminated composite plates in which the lay-up is such that end load and shear, and bending and twisting moments, are all uncoupled, [See also: [16.16](#)], the elastic flexural buckling loads can be ascertained from the boundary conditions and the four flexural stiffnesses. Flexural buckling ignores the through-the-thickness shear stiffness and therefore is an upper limit to the buckling load, [See also: [16.15](#)].

16.12.3 Analysis and data

The elastic analysis of orthotropic plates subject to in-plane loadings and with clamped or simply supported edges shows that, with suitable manipulation, the buckling solutions for isotropic plates can be used if the terms are appropriately modified by the orthotropic properties. By this means solutions are presented graphically for the cases:

Plate loading	Conditions of plate edges
Uniaxial	All sides simply supported
	All sides clamped
	One pair of opposite sides simply supported the other pair clamped against rotation
Biaxial	All sides simply supported
	One pair of opposite sides simply supported the other pair clamped

	Long plates with the long sides simply supported
Shear	All sides simply supported Long plates with the long sides normally supported and elastically restrained against rotation
Shear plus uniaxial	All sides simply supported

[See: [16.3](#) for access to program and documentation]

16.13 Bonded joints - 4

16.13.1 Title

Elastic adhesive stresses in multi-step lap joints loaded in tension.

Data Item No. 80039 [See also: [ESDU International](#) website].

16.13.2 Usage and scope

In order to design bonded joints it is necessary to determine the stress distribution in the adhesive. The direct (normal, through-the-thickness direction) stresses and the shear stresses are the major stresses governing joint design. The direct (normal) stresses peak at the ends of the joint and where steps in the adherend are introduced with the maximum usually occurring at the extreme ends. A design objective is the selection of joint geometry and adhesive to prevent failure under the normal stresses developed.

16.13.3 Analysis and data

The program is based on the elastic flexible joint analysis described here. The analysis determines the distribution of shear and direct normal stresses in the adhesive resulting from the transmission of in-plane tension loads from one adherend to the other through the adhesive, zero external bending moments are assumed.

The assumptions made are:

- Adherend stresses normal to the plane of the joint and adhesive direct stresses in the plane of the joint are neglected.
- Also, the joint and its adjacent sheet are taken to behave according to the theory of cylindrical bending of plates of stepped cross-section and neutral plane.
- The adhesive layer behaves elastically, is negligibly thin and provides a perfect shear connection between the two adherends.

Consequently, at both ends of the bonded length, and the inter-step boundaries, the total joint depth is immediately effective in bending and in tension. This leads to an overestimate of the stress, but has little influence on the stresses in the case of multi-step joints.

16.13.4 ESDUpac A8039

16.13.4.1 General

Previously ESDUpac E1020.

This program calculates the elastic shear and direct (normal) stresses in a bonded lap joint.

16.13.4.2 Input

- Number of steps in the joint and joint configuration type number.
- Elastic properties of adherends.
- Elastic properties of adhesive.
- Geometry and applied loading.

16.13.4.3 Output

- Shear and direct (normal) stress distribution across the joint and their ratios to their average value in the joint.
- Joint geometry and elastic properties of the adhesive and each adherend.
- Applied loading.
- All input data.
-

[See: [16.3](#) for access to program and documentation]

16.14 Bonded joints - 5

16.14.1 Title

Guide to the use of data items in the design of bonded joints.

Data Item No. 81022 [See also: [ESDU International](#) website].

16.14.2 Usage and scope

In order to make the most efficient use of data for the analysis of bonded joints it is necessary to understand their limitations and helpful to know their relationship to the other analytical methods available. The influence of the data on the resulting designs is also of interest. The scope of the data available in ESDU Data Items on bonded joints is addressed together with the available data on joint design, [See also: [16.9](#), [16.10](#), [16.11](#) and [16.12](#)].

16.14.3 Information and guidance

The major theories on analysis of the strength of bonded joints are briefly noted. This is followed by a comparison of the analytical methods and their relevance to joint design. This commences with the joint types and then relates joint failure modes to the data available for assessing failure.

A major factor in designing bonded joints is the availability of the strength and stiffness properties of the adhesive. Where these are not available they should be determined experimentally and suitable test methods are described. Data for fourteen adhesives are listed and shear stress-strain curves presented. The major factors influencing the strength data are discussed and the influence of some, e.g. temperature and humidity, is illustrated.

[See: [16.3](#) for access to documentation]

16.15 Buckling of orthotropic plates

16.15.1 Title

Buckling of flat rectangular orthotropic plates (Application to laminated composite plates).

Data Item No. 81047 [See also: [ESDU International](#) website].

16.15.2 Usage and scope

Laminated composite plates and sandwich panels faced with laminated composites can be modelled as homogeneous orthotropic plates. For such plates overall buckling is an important condition. Buckling is a function of the plate's in-plane and flexural stiffnesses, its through-the-thickness shear stiffnesses, its shape, boundary conditions and the applied loading. The through-the-thickness shear stiffnesses are of particular importance since, if they are very low, they can dominate buckling.

16.15.3 Analysis and data

The plate is treated as homogeneous, and can be isotropic or specially orthotropic. The through-the-thickness shear stiffnesses in the principal plane of orthotropy and orthogonally to that plane are included. The elastic buckling load is derived for symmetrical combinations of clamped and simply supported edge conditions for rectangular plates subject to combinations of in-plane compression, tension and shear loading. The solution is presented as a computer program. Buckle wave forms having up to 7 half waves along or across the plate are examined.

16.15.4 ESDUpac A8147

16.15.4.1 General

Previously ESDUpacs E1001 and E1031.

The program calculates the elastic overall buckling loads for orthotropic rectangular plates from the properties of the layers from which it is constructed and the plate size and boundary conditions. The program of ESDUpac A8147 can deal with any combination of the plate materials, loadings and boundary conditions described.

16.15.4.2 Plate materials

Covers any plate which is specially orthotropic, [See: [16.16](#)]. Some examples of plate types that can be within this limitation and can be dealt with by the program are:

- isotropic materials
- sandwich panels, with isotropic or orthotropic cores and face plates.
- laminated fibre-reinforced plates, composed of layers having different properties, thicknesses or orientations of their principal axes of orthotropy. Such plates can conform exactly to the conditions of special orthotropy if suitable ply stacking sequences are chosen. However, approximate satisfaction is more commonly encountered.

16.15.4.3 Plate loadings

Any combination of direct biaxial loads and shear loading in which any two loads are specified. Also calculations where all three loads are in a fixed ratio to one another.

16.15.4.4 Plate boundary conditions

All edges either clamped or simply supported or an opposite pair of edges clamped and the other pair simply supported.

[See: [16.3](#) for access to program and documentation]

16.16 Lay-up arrangements for special orthotropy

16.16.1 Title

Laminate stacking sequences for special orthotropy (Application to fibre reinforced composites).

Data Item No. 82013 [See also: [ESDU International](#) website].

16.16.2 Usage and scope

In most structural laminates analysis is simplified, stability is maximised, and distortion during manufacture is minimised if stacking sequences are used which ensure that end load and shear, and bending and twisting moments, are all uncoupled. The uncoupled condition is termed special orthotropy. This Data Item provides the definitive list of specially orthotropic stacking sequences for laminates of up to 21 layers. In addition, notes are given on combining the stacking sequences provided and on stacking arrangements for laminates with large numbers of layers.

The provision of tabulated lists of lay-ups that are specially orthotropic enables easy selection of arrangements that meet both direct and flexural loadings.

16.16.3 Analysis and data

A formal definition of special orthotropy is given. Lay-ups are separated into four groups: symmetric laminates with even or odd numbers of layers and anti-symmetric groups with even or odd numbers of layers. For each group the sequences of 0° (or 90°) and angled layers which give special orthotropy for plates of up to 21 layers are listed. Of particular importance is knowledge of the smallest number of layers in each group with which special orthotropy can be achieved. The tables list 48 lay-ups of symmetric (even), 27 lay-ups of symmetric (odd), 380 lay-ups of anti-symmetric (even) and 273 lay-ups of anti-symmetric (odd) all of which are specially orthotropic.

The tables also list coefficients which enable easy calculation of the terms of the flexural stiffness matrix from the stiffness matrix of one of the identical layers from which the plate is composed.

Rules for extending lay-ups beyond the limit of 21 layers listed are provided.

[See: [16.3](#) for access to documentation]

16.17 Failure modes of laminated composites

16.17.1 Title

Failure modes of fibre reinforced laminates.

Data Item No. 82025 [See also: [ESDU International](#) website].

16.17.2 Usage and scope

In long fibre laminated composites, the fibres and matrix are designed to perform complementary functions and therefore react to the various loading conditions in different ways. Additionally, the orientation of the fibres usually varies from layer to layer through the laminate thickness.

Consequently there are many more potential failure modes for such laminates than for metallic materials. There are two principal ways of considering the failure of such laminates based on the:

- a. Behaviour of the individual layers and the interfaces between them.
- b. Laminate as a whole.

Data Item No. 82025 deals with the first of these approaches.

16.17.3 Analysis and failure modes

In each layer of a laminate the principal function of the fibre is to transmit loads in its longitudinal direction, although it also transmits transverse and shear loads. The resin matrix connects the fibres, maintaining their relative positions while distributing the load among the fibres, ensuring continuity of transverse and shear loading in the laminate. The typical laminate is composed of a number of individual layers. The laminate can be subjected to any combination of loading, though the layers are most efficient at taking in-plane longitudinal direct load. The failure modes are best understood by dealing first with the modes for a single layer, under simple loading and then relating these to the modes for more complex configurations.

Twelve different modes of failure of a layer of a laminated plate reinforced by unidirectional fibres are identified, illustrated and discussed. The primary factors and secondary factors affecting each mode are listed.

In addition to the individual layer failures multidirectional laminates can fail in up to 6 further modes. These are listed and described together with the primary and secondary factors affecting them.

[See: [16.3](#) for access to documentation]

16.18 Failure criteria for layers of a laminated composite

16.18.1 Title

Failure criteria for an individual layer of a fibre reinforced composite laminate under in-plane loading. Data Item No. 83014 [See also: [ESDU International](#) website].

16.18.2 Usage and scope

Many different criteria have been developed for predicting the failure of the layers of long fibre laminated composites, subject to the full range of in-plane loadings. Many are identical in some regions and some show discontinuities in their failure envelope, whilst other envelopes are smooth. The provision of the appropriate strength data, and the choice of a suitable criterion are linked and should be considered together. Both aspects are examined in Data Item No. 83014.

16.18.3 Analysis and data

Eight of the commonly used failure criteria are described in detail and the failure envelopes illustrated. The equations for a further three criteria are given. The types of failure criteria are identified and tabulated in a coherent notational system. This highlights the similarities and differences between the criteria. Comparisons of the failure predictions with experimental data are shown for four of the criteria and failure envelopes are compared for all the criteria. The choice of criterion appropriate to the data commonly available is discussed.

Strength test data used in the various criteria are noted together with illustrations of the typical tests that were used to obtain them. References are provided to these standard tests.

[See: [16.3](#) for access to documentation]

16.19 Plate stiffnesses and apparent elastic properties

16.19.1 Title

Estimation of the stiffnesses and apparent elastic properties of laminated flat plates. Data Item No. 83035 [See also: [ESDU International](#) website].

16.19.2 Usage and scope

Stiffnesses and elastic properties, that can be estimated using Item No. 83035, which can be used for strength and stability analyses of structures. The item provides a computer program, referred to as ESDUpac A8335, for the estimation of the stiffness and apparent elastic properties of composite material laminated plates. The plate stiffnesses generated are those required for the strength, or stability, analysis of thin plates and the apparent elastic properties are those required when using orthotropic plate analysis methods. The program is applicable to plates composed of layers having different properties, thicknesses and orientations of the principal axes of orthotropy. Individual layers are assumed to be orthotropic and homogeneous and the bonding between layers is considered to be

perfect. Within the item, approximate relationships are given for lamina elastic properties in terms of individual fibre and matrix properties and their volume fractions. These relationships can also be used to estimate changes in known elastic properties of an individual lamina at different fibre volume fractions.

16.19.3 Analysis for stiffnesses and elastic properties

The plane stress constitutive equation for individual layers is formed using Hooke's law. Then using the strain-displacement relations in the expressions for the stress and moment resultants the constitutive relations yield the in-plane stiffness sub-matrix A, the coupled in-plane flexural stiffness sub-matrix B and flexural stiffness sub-matrix D. The apparent orthotropic plate elastic properties are derived from elements of the in-plane stiffness sub-matrix. These latter values are applicable to multilayered plates having six or more layers.

16.19.4 ESDUpac A8335

16.19.4.1 General

Previously ESDUpac E1038

This program estimates the stiffnesses and apparent elastic properties of laminated flat plates.

16.19.4.2 Input

Lamina elastic properties can be either input or estimated from input values of the constituent matrix and fibre elastic properties and the fibre volume content. Other inputs are the thickness and lay-up angle of each layer and the layer stacking sequence.

16.19.4.3 Output

Any estimated laminae properties are first output followed by the plate lay-up arrangement. A, B and D stiffness matrices are then output followed by the plate apparent elastic properties.

16.19.4.4 Limitations

Maximum of 5 laminae for which elastic properties are calculated and a maximum of 50 layers.

[See: [16.3](#) for access to program and documentation]

16.20 Natural frequencies of laminated flat plates

16.20.1 Title

Natural frequencies of rectangular specially orthotropic laminated plates.

Data Item No. 83036 [See also: [ESDU International](#) website].

16.20.2 Usage and scope

Natural frequencies should be used for dynamic response calculations such as the analysis for acoustic fatigue. The item provides a computer program, referred to as ESDUpac A8336, for the estimation of the natural frequencies for initially unstressed, rectangular, specially orthotropic plates. Specially orthotropic plates are balanced laminates having layers of equal thickness, elastic properties and orientations that are symmetrically arranged about the plate central plane. The program enables the estimation of the natural frequencies of flat plates having any combination of simply supported and clamped edge conditions. The item also provides an approximate procedure for the estimation of the fundamental natural frequency of slightly curved plates having all edges clamped.

16.20.3 Calculation of natural frequencies

For specially orthotropic plates, the in-plane and flexural stiffness sub-matrices are uncoupled so that the flexural stiffness sub-matrix (D-matrix) only is used for the estimation of natural frequencies. The method of analysis is based on the Rayleigh-Ritz method in which the plate displacements are represented by a single beam characteristic function in each of the x, y orthogonal directions. In calculating natural frequencies shear deformation and rotary inertia effects are neglected. Also displacements are assumed to be small relative to the plate thickness, and the plate is assumed to be thin relative to the plate dimensions.

16.20.4 ESDUpac A8336

16.20.4.1 General

Previously ESDUpac E1039

The computer program evaluates natural frequencies for initially unstressed, rectangular, specially orthotropic plates.

16.20.4.2 Input

Elements of the D-matrix can be input or evaluated from the individual layer properties, their relative orientations and lay-up sequence. The plate geometry and the mode numbers of interest are input.

16.20.4.3 Output

Input data are output, and if the elements of the D-matrix are calculated, these are output together with the plate construction. Natural frequencies are output for the mode numbers required.

16.20.4.4 Limitations

If the elements of the D-matrix are calculated, a maximum number of 50 within the plate.

[See: [16.3](#) for access to program and documentation]

16.21 Strain in skin panels under acoustic loading

16.21.1 Title

Estimation of r.m.s. strain in laminated skin panels subjected to random acoustic loading.

Data Item No. 84008 [See also: [ESDU International](#) website].

16.21.2 Usage and scope

Laminated composite plates, on the surface of aerospace vehicles, can be subjected to intense acoustic loading during part, or all, of their normal working cycle. Knowledge of the response of such structures under random acoustic loading is needed in order to assess their acoustic fatigue life. The item provides a computer program, referred to as ESDUpac A8408, for estimating the r.m.s. surface strains in rectangular laminated skin panels subjected to random acoustic loading. The data are applicable to specially orthotropic plates having principal axes of orthotropy parallel to the plate edges. The computer program evaluates r.m.s. strains on the centreline of the plate parallel to the shorter (curved) side at the plate edge and the plate centre.

16.21.3 Calculation of surface strains

The assumption of special orthotropy ensures that the in-plane and flexural stiffnesses are uncoupled and enables the plate bending moments to be simply related to the elements of the plate flexural stiffness sub-matrix (matrix D). This relationship is used to evaluate the ratio of stress at a point on the surface of the plate to the applied static pressure. This ratio is used in a simplified normal mode method which assumes that the predominant form of skin vibration is one in which individual plates within the stiffened panel vibrate independently in their fundamental fixed-edge mode. Further it is assumed that the pressure is uniform and in-plane over the range of frequencies close to the fundamental natural frequency of the panel. Empirically derived correction factors are used to improve the correlation between estimated and measured surface strains.

16.21.4 ESDUpac A8408

16.21.4.1 General

Previously ESDUpac 1042

The computer program evaluates the r.m.s. strain response of thick, quasi-isotropic plates under the action of acoustic loading. The thick criterion is usually satisfied if plates have not less than six layers.

16.21.4.2 Input

Elements of the D-matrix and plate orthotropic elastic properties can be input or evaluated from the individual layer properties, their relative orientations and lay-up sequence. The plate geometry together with the response frequency, damping ratio and sound pressure level are all input.

16.21.4.3 Output

Input data is computed, the plate stiffness sub-matrices and elastic properties are calculated, they are output together with the plate construction and apparent elastic properties. For each set of data the r.m.s. strains are tabulated.

16.21.4.4 Limitations

If plate stiffness sub-matrices and elastic properties are estimated, a maximum number of 50 layers is possible.

[See: [16.3](#) for access to program and documentation]

16.22 Failure analysis

16.22.1 Title

Failure analysis of fibre reinforced composite laminates.

Data Item No. 84018 [See also: [ESDU International](#) website].

16.22.2 Usage and scope

The design of long fibre laminated composites involves an analysis of the failure of the various layers (at their various orientations) under the loading applied to the composite. This is achieved by a stress analysis of the plate and the layers therein and then the application of a failure criterion. The failure of the matrix material supporting a fibre does not necessarily constitute total failure and it is often of value to follow the various matrix failures that occur as the load increases up to the point where collapse occurs. This makes it possible to take account of the fact that minor failure of the matrix material at one load is not complete collapse.

16.22.3 Analysis

The failure assessment is based on a linear elastic layer-by-layer plate analysis of the laminate, in which the stresses in each layer in turn are compared with the Puck Modified Criterion, [See: [16.18](#)], which differentiates between fibre and matrix material failures. If a layer matrix failure occurs, the matrix material properties of that layer are removed by assuming that its transverse direct (in-plane) and shear stiffnesses are zero. It is assumed that when this happens the fibre can still take load in its direction and that the laminate through-the-thickness shear integrity is retained. Therefore, during further analysis, the layer longitudinal (fibre) stiffness properties are retained as is the allowance for the thickness of the layer. Because these layer matrix failures can lead to the progressive failure of other layers their development is traced through the gradual application of a loading system in which matrix material failures are present to provide a damage history under that system. This continues until either total matrix failure has occurred throughout the laminate or a single longitudinal (fibre) layer failure occurs, at which point total laminate failure is assumed.

Analysis is performed by a Fortran computer program. A laminate is analysed under consecutive systems of combined in-plane, moment and thermal loading. The program differentiates between individual layer matrix material failure, termed damaged, an individual layer fibre failure or matrix

material failure of all the layers, both termed laminate failure. The consecutive loading systems can be applied with either the damage of each loading system in turn carried over to the next or with each new loading system applied to the laminate as originally undamaged. If laminate failure does not occur under a particular loading system an assessment of the level at which failure would occur for that system is provided before the analysis returns to the next loading system.

The program applies to balanced or unbalanced laminates that are initially unrestrained but also includes the effect of holding the unloaded laminate flat (for storage), if required. While thermal effects have been included in the analysis moisture effects have not because of the less certain, time-dependent, long-term nature of such effects. However, moisture degradation can be incorporated for each individual layer by providing reduced values of layer material properties and allowable stresses, particularly for the matrix material.

16.22.4 ESDUpac A8418

16.22.4.1 General

Previously ESDUpac E1043

This program traces the in-plane damage history of a laminate through to failure.

16.22.4.2 Input

- Properties of each type of layer used:
 - stiffness
 - Poisson's ratio
 - coefficients of thermal expansion
 - thickness.
- Allowable stresses in tension, compression and shear of each type of layer used.
- Lay-up stacking arrangement and layer orientations.
- Loading conditions:
 - applied loads
 - bending
 - direct
 - shear in orthogonal directions
 - working temperature
 - curing temperature
 - restraints at manufacture
 - indicator for damage to be passed to successive load cases or not.

16.22.4.3 Output options

- Data for layers where chosen fraction of failure criterion is exceeded only.
- Extract output only.

16.22.4.4 Output

- Full output gives stresses in each layer together with the value of the failure criterion at every step of the calculation.
- A statement of damaged layers at every stage.
- All input data.

[See: [16.3](#) for access to program and documentation]

16.23 Endurance under acoustic loading

16.23.1 Title

Endurance of fibre-reinforced composite, laminated structural elements subjected to simulated random acoustic loading.

Data Item No. 84027 [See also: [ESDU International](#) website].

16.23.2 Usage and scope

Often a final requirement from an acoustic fatigue calculation is an assessment of the life of the structure. This can be made from plots of r.m.s. strain against equivalent endurance, taken as half the number of zero crossings to failure of the strain-time function. These data are often referred to as S-N plots. This item gives the results of fatigue tests on fibre-reinforced composite specimens, typical of aircraft structural elements, subject to narrow-band excitation to produce random amplitude responses, with zero mean, to simulate response in a resonant mode to acoustic loading. The results of these tests are plotted as r.m.s. surface strains, at a reference location, against equivalent endurance.

The data presented in this item are intended to be used only for guidance since, in some cases, unusual configurations were tested and not all relevant test data were reported. Endurance data are specific to the types of element tested, the method of testing and the method of failure identification. Test data are within the endurance range 10^3 to 10^8 cycles.

The types of specimen considered are plain specimens and specimens representative of both bonded and riveted skin-rib construction, typical of aircraft structural elements. Both carbon fibre and boron fibre structural elements are considered and details are given of the element tested, the method of testing and the method of failure identification.

Factors that can affect the endurance of fibre-reinforced composite structural elements are discussed.

New data are added to this item as they become available.

[See: [16.3](#) for access to documentation]

16.24 Stress and strain around circular holes

16.24.1 Title

Elastic stress and strain distributions around circular holes in infinite plates of orthotropic material (applicable to fibre reinforced composites).

Data Item No. 85001 Computer program [See also: [ESDU International](#) website].

16.24.2 Usage and scope

A measure of the stresses and strains acting around the perimeter of a hole in a laminated composite subject to a combination of in-plane loads is of interest if failure or edge delamination is to be avoided. The stresses and strains are a function of both the loading applied and the orthotropy of the material and their respective orientations. The points where the stresses are a maximum are not always critical because they can also be the points where the strength is high. It is therefore necessary to survey the perimeter to locate those points where the local stress exceeds the local strength in its direction of action. Because of symmetry, analysis of the stresses over only half the perimeter is necessary and this is provided by the ESDUpac A8501 program described.

16.24.3 Analysis

The equations for the elastic stress field acting around the perimeter of a circular hole in a homogeneous orthotropic plate subject to any combination of in-plane loadings are set out. Additionally the stress-strain relationships in both the circumferential direction and the chosen Cartesian co-ordinates are set out. In application to laminated composites, the analysis is more appropriate to holes whose diameter is greater than about 6 thicknesses.

16.24.4 ESDUpac A8501

16.24.4.1 General

Previously ESDUpac 1048

This program calculates the elastic stresses and strains acting around a circular hole in an orthotropic material.

16.24.4.2 Input

- The in-plane moduli and Poisson's ratio for the layers
- The lay-up arrangement
- The applied loading

Alternatively, the elements of the in-plane direct stiffness matrix or the plate effective moduli can be input.

16.24.4.3 Output

The values given at 5° intervals around 180° of the hole circumference are:

- two direct and shear stresses in the plate axes
- two direct and shear strains in the plate axes
- circumferential and radial and shear stresses
- in-plane stiffness matrix.
- input data.

[See: [16.3](#) for access to program and documentation]

16.25 Damping in composite plates

16.25.1 Title

Estimation of damping in laminated and fibre-reinforced plates.

Data Item No. 85012 [See also: [ESDU International](#) website].

16.25.2 Usage and scope

Knowledge of the damping of the structure in the mode of response is necessary for the estimation of the dynamic response to an applied loading. Fibre-reinforced laminated structures are often constructed with adhesive joints, thus eliminating sources of energy dissipation associated with discrete joint attachments and consequently increasing the material damping contribution to the overall damping. This item provides a computer program, known as ESDUpac A8512, for the estimation of the material damping in a rectangular, multilayered laminate that is vibrating in one of its lower-frequency natural modes.

The estimation procedure is applicable only to plates in which laminae having the same material properties, and orientations of their principal axes of orthotropy, are symmetrically arranged about the plate mid-plane, i.e. balanced symmetric laminates.

The program estimates damping in plates having either all edges simply supported or all edges clamped. Within the item approximate relationships are given for the specific damping capacity of an individual lamina in terms of components in longitudinal flexure, Ψ_L , transverse flexure, Ψ_T , and longitudinal shear, Ψ_{LT} . These damping components are necessary inputs for the program. The item also gives guidance on the factors affecting damping.

16.25.3 Calculation of damping

The total energy dissipated is estimated by summing, over each layer of the plate, the energy dissipated in longitudinal tension-compression, transverse tension-compression and longitudinal shear. The specific damping capacity is then given by the ratio of total energy dissipated to the maximum strain energy stored in the plate.

Beam characteristic functions are used to define the mode shapes and it is assumed that the effect of in-plane force on bending is negligible. Further it is assumed that, if the amplitudes of vibration are small, damping can be considered to be independent of cyclic stress amplitude.

16.25.4 ESDUpac 8512

16.25.4.1 General

Previously ESDUpac E1047

The program estimates the damping in rectangular, multilayered laminates.

16.25.4.2 Input

Elastic properties are input together with the three specific damping capacities Ψ_1 , Ψ_2 and Ψ_{12} for each layer. Other inputs are the thickness and lay-up angle and the layer stacking sequence, the plate geometry and the list of mode numbers to be considered.

16.25.4.3 Output

The plate layer properties and the layer stacking arrangement are output followed by a tabulation of damping values for each mode of vibration considered. Damping is output both in terms of specific damping capacity and viscous damping ratio.

16.25.4.4 Limitations

Maximum of 30 layers and mode numbers less than 6.

[See: [16.3](#) for access to program and documentation]

16.26 Sandwich panel natural frequencies

16.26.1 Title

Natural frequencies of simply supported sandwich panels with laminated face plates.

Data Item No. 85037 [See also: [ESDU International](#) website].

16.26.2 Usage and scope

A knowledge of the natural frequencies of a structure is often required before a dynamic response calculation is made. The item provides a computer program, called ESDUpac A8537, for the estimation of natural frequencies of initially unstressed rectangular sandwich panels having laminated composite face plates. The panels are assumed to be simply supported on all boundaries and can be flat or singly curved with shallow curvature. In practical applications simply supported boundary conditions are seldom achieved, so effective dimensions are used to estimate panel natural frequencies. Guidance on the choice of effective panel dimensions is given in the item. For each pair of mode numbers, the program enables five natural frequencies to be evaluated. These frequencies correspond with modes having predominant deflections in the x-, y- and z-directions (the central

plane of the plate being in the xy -plane) and predominant rotations in the xz - and yx -planes. An option is given to calculate the lowest natural frequency only.

16.26.3 Calculation of natural frequencies

For the calculation of the natural frequencies and associated normalised panel deflections, it is assumed that the face plates are orthotropic and have principal axes of orthotropy parallel to the sides of the panel. The face plates can be made of different materials and thicknesses. It is assumed that bending is carried only by the face plates and transverse shear stresses only by the core. The displacement forms used in the solution of the equations of motion are appropriate for simply supported boundary conditions. The method of analysis is based on linear sandwich panel theory and is applicable to panels having thin face plates and small vibration amplitudes.

16.26.4 ESDUpac A8537

16.26.4.1 General

Previously ESDUpac E1053

The computer program estimates the natural frequencies and mode shapes of flat, or singly curved, sandwich panels having laminated composite face plates.

16.26.4.2 Input

The orthotropic face plate properties can be input or evaluated from the individual layer properties, their relative orientations and lay-up sequence. The core properties, panel geometry and mode numbers of interest are also input.

16.26.4.3 Output

Input data are output and if face plate orthotropic properties are evaluated these are output together with the face plate construction. Natural frequencies are output and mode shapes are tabulated if requested.

16.26.4.4 Limitations

If face plate orthotropic properties are estimated, a maximum of 20 layers is possible in each face plate.

[See: [16.3](#) for access to program and documentation]

16.27 Selection of reinforcement around circular holes

16.27.1.1 Title

Example of the use of Data item No. 85001. Choice of reinforcement for a circular hole in a fibre reinforced laminated plate (Data relating to one particular set of laminate properties).

Data Item No. 86003 [See also: [ESDU International](#) website].

16.27.1.2 Usage and scope

In composite plates, the properties of the material vary with direction. This means that some composites have a high stress at a point around the hole boundary yet this stress is in a direction in which the composite is particularly strong. Alternatively, another composite can give a lower stress but the maximum stress is in a direction in which the material is less strong. The addition of reinforcement is often an option where the strength is poor and a method of deciding the optimum reinforcement is provided. The stresses and strains are obtained from the program of ESDUpac A8501 [See: [16.24](#)].

16.27.1.3 Analysis and data

A graphical technique is described and illustrated, by example, for determining the critical locations around the boundary of an unreinforced hole using data generated by ESDUpac A8501. Where the strength is low, hole reinforcement is considered. The calculation of the reinforcement thickness is described together with its desirable orientation. Strictly, the method only relates to holes well away from edges or other discontinuities. The extent of the reinforcement is discussed and a recommendation made.

[See: [16.3](#) for access to documentation]

16.28 Buckling of unbalanced composite plates

16.28.1 Title

Elastic buckling of unbalanced laminated fibre-reinforced composite plates.

Data Item No. 86020 [See also: [ESDU International](#) website].

(Rectangular plates of *AsBtDs* type, all edges simply supported, under biaxial loading)

16.28.2 Usage and scope

In complex laminated structures, it is often not practical to reduce laminate thickness exactly in line with reducing load and maintain a balanced laminate. Layer continuity over several adjacent panels is often preferred for strength considerations even though it results in unbalanced plates within the structure.

The form of the stiffness matrix for an unbalanced plate can significantly influence the buckling load. Where some choice in the lay-up arrangement is open, it is preferable to select a lay-up such that the in-plane and flexural stiffness matrices are populated in the same way as for a specially orthotropic plate but the coupling stiffness matrix terms are zero except for the terms relating direct and shear loads to curvature and twisting. Plates of that type are preferable because they exhibit bifurcational buckling. (Most other unbalanced forms exhibit out-of-plane bending upon the application of a small in-plane load and thereafter behaviour becomes non-linear.)

Although the result of employing an unbalanced plate that exhibits bifurcational buckling is a reduction in buckling load this is still preferable to the non-linear behaviour of other unbalanced

plates. Reductions upto 30% of the balanced plate value can occur in extreme cases, but reductions of 10% or 20% are more common.

16.28.3 Analysis and data

The solution is based upon elastic thin plate small deflection theory in which the plate is assumed to behave as a homogeneous orthotropic material whose axes of orthotropy are aligned with the edges of the plate. The theory only takes account of direct in-plane, flexural and twisting deformations. No account is taken of through-the-thickness shear deformations. The plate is assumed to be initially flat, rectangular and simply supported along all four sides with the loadings applied in-plane and uniformly along all four edges. The applied loads are assumed to lie in the mid-plane of the plate and this is the plane to which the flexural and coupling stiffnesses are related.

16.28.4 ESDUpac A8620

16.28.4.1 General

Previously ESDUpac E1057

This program calculates the buckling load of a particular class of unbalanced laminated flat plates.

16.28.4.2 Input

- Plate dimensions.
- Transverse load or longitudinal to transverse loading ratio.
- Material properties of each type of layer used in the plate.
- Stacking sequence of layers and their orientations.

16.28.4.3 Output

- Buckling loads with number of buckle half-waves along and across the plate.
- In-plane, flexural and coupling stiffness matrices.
- Plate construction, layer properties and geometry.

[See: [16.3](#) for access to program and documentation]

16.29 Sandwich panel response to acoustic loading

16.29.1 Title

Estimation of r.m.s. strain in laminated face plates of simply supported sandwich panels subjected to random acoustic loading; including a simplified natural frequency prediction method.

Data Item No. 86024 [See also: [ESDU International](#) website].

16.29.2 Usage and scope

Sandwich panels are widely used in the design of lightweight structures for aerospace applications. Where such structures are used in a high-intensity acoustic environment it is necessary to investigate their response to acoustic loading. The item provides a computer program, called ESDUpac A8624, for the estimation of the r.m.s. surface strains in the laminated face plates of sandwich panels subjected to random acoustic loading. The data are applicable to flat, or shallow cylindrically curved, sandwich panels having thin laminated composite face plates. One stage within the analysis procedure is the estimation of natural frequencies of vibration so that the program can be used to estimate the lower natural frequencies of the panel bending modes. The panels are assumed to be simply supported on all edges so that the reference location for surface strains is chosen to be the centre of the panel. In practical applications simply supported boundary conditions are seldom achieved so that effective dimensions are used to estimate panel natural frequencies and strains. Guidance is also given on the choice of effective dimensions.

16.29.3 Calculation of natural frequencies and surface strains

For the calculation of natural frequencies and r.m.s. surface strains of sandwich panels, the face plates are assumed to be orthotropic and to have principal axes of orthotropy parallel to the panel sides. The upper and lower face plates can be different materials and thicknesses and the core is assumed to have zero flexural stiffness. For the estimation of r.m.s. strains, it is assumed that the panel responds only in its fundamental mode and that the loading spectral density is constant over a range of frequencies including the predominant response frequency.

16.29.4 ESDUpac A8624

16.29.4.1 General

Previously ESDUpac E1059

The computer program evaluates the bending mode natural frequencies, and strain response under acoustic loading, of sandwich panels with composite face plates.

16.29.4.2 Input

The elastic properties of the face plates can be input or evaluated from the individual layer properties, their relative orientations and lay-up sequence. The core properties and panel dimensions are also input. For the calculation of natural frequencies the mode numbers of the frequencies of interest should be entered. For r.m.s. strain calculations, the damping and sound pressure levels are input for each case.

16.29.4.3 Output

Input data are output and if face-plate properties are calculated these are output together with the face-plate construction. For each set of data natural frequencies are output (if required) and r.m.s. strains at the panel centre are output for both the upper and lower face plates.

16.29.4.4 Limitations

If face-plate elastic properties are estimated, a maximum of 20 layers is possible in each face plate.

[See: [16.3](#) for access to program and documentation]

16.30 Sandwich column and beam face plate wrinkling

16.30.1 Title

Elastic wrinkling of sandwich columns and beams with unbalanced laminated fibre reinforced plates.

Data Item No. 87013 [See also: [ESDU International](#) website].

16.30.2 Usage and scope

One possible mode of failure of a sandwich column or beam with thin face plates is the localised buckling (wrinkling) of the compression faces. For fibre reinforced face plates made up from a number of thin layers, it is possible that the face plates each form an unbalanced lay-up about their local mid-planes. This lack of balance is further accentuated by the layer of adhesive that is used to bond each face plate to the core material and which can have a significant effect on the wrinkling loads. It is therefore necessary to explore the influence of these factors.

Two forms of wrinkling can occur, symmetrical and anti-symmetrical, and both are to be investigated to determine the minimum buckling loading. Compressive loadings of interest are those applied directly and those occurring as a result of bending.

16.30.3 Analysis

The solution is based upon elastic, thin-plate, small-deflection theory, in which the laminated face plates are assumed to behave as homogeneous orthotropic plates, whose axes of orthotropy are aligned with the edges of the beam or column. For columns, the face plates are assumed to form a balanced lay-up about the central plane of the sandwich. In beams, the tension face plate is assumed to provide a rigid boundary for the core against wrinkling of the compression face plate.

The theory only takes account of direct in-plane and flexural deformations as governed by the direct and flexural terms of the in-plane, flexural and coupling stiffness sub-matrices. No account is taken of through-the-thickness shear deformations of the face plates. The faces are assumed to be initially flat, and to be held flat by the core until they wrinkle. The core is assumed to give continuous support to the faces and the possibility of localised buckling within honeycomb-type cells (often called inter-cell buckling) is not considered. Also, the core is taken to have zero longitudinal stiffness but finite direct and shear stiffnesses in the through-the-thickness direction. These assumptions make the analysis more applicable to honeycomb type cores than to solid-foam cores, but give conservative results for the latter. Half the applied load is assumed to lie in the mid-plane of each face plate (which might include a layer of adhesive) and this is the plane to which the stiffnesses are related.

16.30.4 ESDUpac A8713

16.30.4.1 General

Previously ESDUpac E1065

The program calculates the load on a sandwich column or beam at face plate wrinkling.

16.30.4.2 Input

- Sandwich core compressive and shear stiffnesses.
- Sandwich thickness.
- Stiffnesses, Poisson's ratio of each layer type used in face plates.
- Laminated face plate layer stacking sequence and orientation.

16.30.4.3 Output

- Load at face plate wrinkling in symmetric and anti-symmetric modes, and on bending.
- Wavelengths of wrinkles.
- Faceplate stiffnesses, and effective stiffness terms.
- All input data.

[See: [16.3](#) for access to program and documentation]

16.31 Buckling of curved composite panels

16.31.1 Title

Elastic buckling of cylindrically curved laminated fibre reinforced composite panels with all edges simply supported under biaxial loading.

Data Item No. 87025 [See also: [ESDU International](#) website].

16.31.2 Usage and scope

Curved panels can be subject to buckling under axial compressive loading. Additionally, curved panels are often loaded by pressure on the convex face reacted at the sides parallel to the axis. The resulting buckling behaviour is complex. For relatively short panels, all buckle wavelengths give the same minimum buckling load. For intermediate lengths of panel, usually one of two combinations of wavelengths dominates and, for very long panels, another combination dominates. The buckling load decreases as the length increases for those longer panels. A method investigating all wavelength combinations is therefore necessary to ensure that the minimum buckling load is identified.

16.31.3 Analysis and data

The panels considered are of rectangular form and uniform thickness having cylindrical curvature across the width. All edges of the panel are assumed to be simply supported. The panel is subjected to direct loading applied uniformly to the ends of the panel in the direction of the cylindrical axis, which

can be combined with similar loading along the sides of the panel applied in the circumferential direction in order to exert a pressure on the panel surface.

The analysis is based upon elastic, thin-plate, small-deflection theory in which the panel is assumed to behave as a homogeneous orthotropic material whose axes of orthotropy are aligned with the edges of the plate.

The theory only takes account of direct in-plane, flexural and twisting deformations as governed by the in-plane and flexural stiffness matrices. Through-the-thickness shear deformations are disregarded.

16.31.4 ESDUpac A8725

16.31.4.1 General

Previously ESDUpac E1068

The program calculates the axial buckling load with or without pressure loading applied.

16.31.4.2 Input

- Material properties of each type of layer used.
- Stacking sequence and orientations of each layer.
- Panel geometry.
- Circumferential loading (reacting pressure on the convex face).

16.31.4.3 Output

- Axial buckling load and number of buckle half waves along and across the plate.
- Flexural, direct and coupling stiffness matrices.
- Plate construction, loading and geometry.
- Circumferential loading applied.

[See: [16.3](#) for access to program and documentation]

16.32 Sandwich panel face plate wrinkling

16.32.1 Title

Elastic wrinkling of sandwich panels with laminated fibre reinforced face plates.

Data Item No. 88015 [See also: [ESDU International](#) website].

16.32.2 Usage and scope

A possible mode of failure of a sandwich panel with thin face plates that is subjected to in-plane biaxial loads is the localised buckling (wrinkling) of the faces. For fibre-reinforced face plates made up from a number of thin layers, it is possible that the face plates each form an unbalanced lay-up about their local mid-planes. This lack of balance is further accentuated by the layer of adhesive that is used to bond each face plate to the core material and which can have a significant effect on the wrinkling loads. Two modes of buckling occur, symmetrical and anti-symmetrical forms.

16.32.3 Analysis

The solution is based upon elastic, thin-plate, small-deflection theory, in which the laminate face plates are assumed to behave as homogeneous orthotropic plates whose axes of orthotropy are aligned with the panel loading directions. The face plates are assumed to form a lay-up about the central plane of the sandwich.

No account is taken of through-the-thickness shear deformation of the face plates. The faces are assumed to be initially flat, and to be held flat by the core until they wrinkle. The core is assumed to give continuous support to the faces and the possibility of localised buckling within honeycomb type cells (often called inter-cell buckling) is not considered. Also, the core is taken to have zero stiffness in the x- and y-directions but finite direct and shear stiffnesses through-the-thickness. These assumptions make the analysis more applicable to honeycomb-type cores rather than to solid foam cores, but gives conservative results for the latter. Half the applied load is assumed to lie in the mid-plane of each face plate (which might include a layer of adhesive) and this is the plane to which the stiffnesses are related.

16.32.4 ESDUpac A8815

16.32.4.1 General

The program calculates the loads on a sandwich panel at face plate wrinkling.

16.32.4.2 Input

- Sandwich thickness
- Core shear stiffnesses and through-the-thickness compressive stiffness.
- Face-plate properties can be input as either:
 - properties of individual layers and their thicknesses, lay-up stacking sequence and layer orientations, or
 - the elements of the in-plane, flexural and coupling stiffness matrices for the complete face plate assembly.
- Loading arrangements are:
 - fixed value of transverse load,
 - longitudinal to transverse loading ratio fixed.

16.32.4.3 Output

- Longitudinal load at wrinkling or longitudinal and transverse loads in prescribed ratio at wrinkling.
- Wavelength of wrinkles along and across the panel.
- Calculated or input stiffness matrices.
- All input geometry and materials data.

[See: [16.3](#) for access to program and documentation]

16.33 Vibration of singly-curved laminated plates

16.33.1 Title

Natural frequencies of singly-curved laminated plates with simply supported edges.

Data Item No. 89011 [See also: [ESDU International](#) website].

16.33.2 Usage and scope

Curved laminated composite plates are used in various applications, particularly in the aerospace industry. The item provides a computer program, called ESDUpac A8911, for the estimation of the lower natural frequencies of singly-curved laminated plates. The data are applicable to thin, rectangular plates of shallow curvature having all edges simply supported. Static in-plane forces, uniformly distributed along the plate edges, can be considered but in-plane shear forces are assumed to be zero. Within the item, the effects of both curvature and in-plane loading on composite plate natural frequencies are illustrated.

16.33.3 Calculation of natural frequencies

The method of analysis is applicable to thin laminated plates of shallow cylindrical curvature. The program is not restricted to symmetric laminates but the shear coupling terms within the stiffness matrices are necessarily negligible. The laminated plate constitutive relations are substituted into the equations of motion and, using the strain-displacement and curvature-displacement relationships obtained from classical theory of elasticity, a set of three displacement equations is derived.

Substitution of appropriate displacement relationships into the displacement equations leads to a cubic equation in frequency. The lowest of the three natural frequencies, for which the predominant displacement is normal to the surface of the plate, is evaluated.

16.33.4 ESDUpac A8911

16.33.4.1 General

The computer program estimates the natural frequencies of curved, laminated composite plates having simply supported edge conditions.

16.33.4.2 Input

The elements of the in-plane stiffness sub-matrix (A-matrix), the coupled in-plane flexural stiffness sub-matrix (B-matrix) and the flexural stiffness sub-matrix (D-matrix) are necessary. These matrix elements can be directly input or evaluated from the individual layer properties, their relative orientations and lay-up sequence. The plate geometry, the in-plane applied loads and the mode number list are also input.

16.33.4.3 Output

The input data are output and, if the stiffness sub-matrices are evaluated, the plate construction is output followed by the A-, B- and D-matrices. For each loading case the natural frequencies are listed.

16.33.4.4 Limitations

If the stiffness sub-matrices are evaluated the maximum number of plate layers is 20.

[See: [16.3](#) for access to program and documentation]

16.34 Plate through-the-thickness shear stiffnesses

16.34.1 Title

Transverse (through-the-thickness) shear stiffnesses of fibre reinforced composite laminated plates.

Data Item No. 89013 [See also: [ESDU International](#) website].

16.34.2 Usage and scope

The transverse (through-the-thickness) elastic properties of continuous fibre reinforced composite laminated plates are, to a large extent, dependent upon the properties of the matrix material used to bond the fibres together. For many matrix materials, these properties can be very low compared with those in the direction of the reinforcing fibres, with the result that significant deflections can be caused by through-the-thickness shear stresses which arise in plate bending. It is necessary to obtain values for the shear stiffness terms which relate the transverse shear force resultants to the transverse shear strains. ESDUpac A8913 provides a FORTRAN computer program for the determination of these stiffnesses for laminated plates, without restriction on the type of lay-up. The plates are considered to be built up from thin orthotropic homogeneous layers with perfect bonding between them. The layers can have different material elastic properties, thickness and orientations of their principal axes of orthotropy. The analysis is also applicable to thick sandwich panels.

16.34.3 Analysis

Mindlin's plate theory is applied to orthotropic plates. The assumption implies that the transverse strains are independent of the through-the-thickness dimension, with the result that the corresponding shear stresses are constant in each layer of the laminated plate if they are calculated from the simple shear stress-strain equations. This constant strain-stress approach leads to transverse shear stiffnesses which are usually too high. An improvement is obtained by using the stress equilibrium equations in each layer to evaluate the transverse shear stress distribution (not taken to be

constant in each layer). These stresses are then related to the transverse shear forces per unit width, using the overall plate equations of cylindrical bending. The shear strain energy density is evaluated, using the transverse shear stress-strain equations for each layer. This is used to obtain a flexibility matrix and hence the shear stiffness matrix giving the relation between the transverse shear forces per unit length and the transverse shear strains.

16.34.4 ESDUpac A8913

16.34.4.1 Input

Material properties of each layer type used; moduli and Poisson's ratio for the three orthogonal directions. Thickness and lay-up angle of principal axes. Stacking arrangement of the layers.

16.34.4.2 Output

- Through-the-thickness shear stiffnesses of laminate.
- In-plane, bending and coupling stiffness matrices.
- Input properties and lay-up arrangement.

16.34.4.3 Limitations

Limited to laminates of 500 layers maximum composed of up to 50 different materials or orientations.

16.34.5 Notes

All layers are checked to ensure that the input properties relate to a real material.

[See: [16.3](#) for access to program and documentation]

16.35 Vibration of plates with in-plane loading

16.35.1 Title

Natural frequencies of isotropic and orthotropic rectangular plates under static loading; including shear loading.

Data Item No. 90016 [See also: [ESDU International](#) website].

16.35.2 Usage and scope

Often plates are subjected to static in-plane loading that significantly affects natural frequencies. The item provides a computer program, called ESDUpac A9016, for the estimation of the lower natural frequencies of isotropic, flat rectangular plates under such loading. The static in-plane loading, uniformly distributed along the plate edges, can be any combination of direct and shear loading that does not cause the plate to buckle. The program is applicable to specially orthotropic plates for which the principal axes of orthotropy are parallel to the plate edges. Plates having all combinations of

clamped, simply supported and free boundary conditions can be considered. General guidance is also given on the effect of in-plane loading on natural frequencies of plates.

16.35.3 Calculation of natural frequencies

The Rayleigh-Ritz method of analysis is used in which the plate displacements are represented by a finite series of orthogonal polynomial functions. The set of orthogonal polynomials used are sequentially derived from a starting polynomial function that satisfies the boundary conditions of the plate under consideration. Plates are assumed to be thin and effects of shear deformation and rotary inertia are neglected.

16.35.4 ESDUpac A9016

16.35.4.1 General

The program estimates the natural frequencies, gives a tabulation of associated plate displacements and plots nodal lines of isotropic and orthotropic plates under static loading.

16.35.4.2 Input

The isotropic or orthotropic material properties

Plate geometry

In-plane applied loading

Boundary conditions

The number of frequencies of interest or the maximum frequency of interest can be specified.

16.35.4.3 Output

Input data are calculated for each set of in-plane applied loads, natural frequencies and if requested mode shapes and nodal line plots are output. If the applied loading exceeds the buckling load no modal data are output.

16.35.4.4 Limitations

The maximum number of modes that can be evaluated is controlled by the chosen number of orthogonal functions used to define the mode shapes.

[See: [16.3](#) for access to program and documentation]

16.36 Delamination and free edge stresses

16.36.1 Title

Delamination and free edge stresses in laminated plates subjected to constant uniaxial strain.

Data Item No. 90021 [See also: [ESDU International](#) website].

16.36.2 Usage and scope

At free edge regions, classical plate theory cannot account for the three dimensional nature of the stress field in which the unattached free edge has zero values of direct stress and shear stresses. At free edges the stresses in the through-the-thickness direction can be sufficiently high to cause local delamination. ESDUpac A9021 provides a Fortran computer program for the approximate calculation of these stresses for plates which are subjected to a constant uniaxial strain. Also, a failure criterion is used to predict edge delamination and the interlayer in which it occurs. The plates are built up from thin orthotropic homogeneous layers and these can have different material elastic properties, thicknesses and orientations. The method is capable of analysing plates with a hundred or so different layers. This gives it a major advantage over finite element methods which have difficulty in coping with more than 10 or so layers.

16.36.3 Analysis

The analysis of the free edge stresses is based on linear elastic theory and treats a plate subjected to a constant uniaxial strain parallel to the edge. Under this condition it is assumed that the dependence of the stress components across and through the plate can be separated, and that exponential functions can be used to represent them. The stresses are averaged over a chosen distance from the free edge and then used in a quadratic failure criterion to predict when delamination is likely to occur. Guidance on an appropriate value of the averaging distance is obtained from the available experimental data. Not all the boundary conditions are properly met by analysis. However, those which are not met do not appear to affect significantly the stresses obtained.

16.36.4 ESDUpac A9021

16.36.4.1 Input

- Material properties of each layer type, moduli, Poisson's ratios and interlaminar shear stresses and direct stress at failure.
- Layer thickness and angle of orientation.
- Lay-up arrangement.
- Applied uniform strain parallel to the free edge.
- Averaging distance to be used for edge stresses.

16.36.4.2 Output

- Strain and equivalent load to cause delamination.
- Stresses resulting from applied strain.
- Values of constants in stress equations.
- In-plane direct stiffness matrix.
- All input data.

Layer data can be requested for all interfaces or only those with a failure criterion above a set value or for those with a set number of the highest values of the criterion.

16.36.4.3 Limitations

Plate should be of a balanced arrangement of less than 500 layers composed of less than 50 different materials and orientations.

16.36.5 Notes

All materials are checked to ensure that they relate to a real material. Laminates are checked to ensure that they are balanced.

[See: [16.3](#) for access to program and documentation]

16.37 Delamination at termination of plies

16.37.1 Title

Delamination of tapered composites.

Data Item No. 91003 [See also: [ESDU International](#) website].

16.37.2 Usage and scope

Laminated composite plates can be manufactured with variable thickness by terminating, or dropping-off, some of the plies along the length of the laminate. Thus, discontinuities are introduced in the form of steps, where the plies are terminated, and this gives rise to high local stresses which can cause the dropped plies to delaminate from adjacent plies. ESDUpac A9103 provides a Fortran computer program for the approximate calculation of the axial load to cause delamination in tapered laminated plates, where the load is applied in the direction of the taper.

16.37.3 Analysis

Delamination is predicted using linear elastic fracture mechanics combined with simple strength of materials theory. An equation is obtained for the applied load to cause delamination in terms of the local dropped-ply geometry, the effective elastic moduli, and the critical strain energy release rate. This latter quantity can be obtained from experiment and a test method for obtaining it is discussed. Also, guidelines are given for good design practice.

The fracture mechanics solution is approximate. Although the theoretical predictions agree quite well with the available experimental results, there can be lay-up geometries and materials in which agreement between theory and experiment is not so good. This applies more to asymmetric tapered plates in compression where instability effects can lead to premature failure. Thus, the predicted delamination loads are only used as a guide for initial design purposes. Where possible, verification of final designs involves testing on specimens that are representative of the actual method of manufacture, materials, geometry and loading.

16.37.4 ESDUpac A9103

16.37.4.1 General

This program calculates the load at which delamination is likely at a ply termination point.

16.37.4.2 Input

- Properties of layers used in laminate:
 - stiffnesses
 - Poisson's ratio
 - thickness
 - orientation.
- Termination arrangement:
 - lay-up and stacking sequence of layers each side of the termination point
 - configuration number for termination arrangement.
- Critical strain energy release rate between layers.

16.37.4.3 Output

- Mean delamination stresses and loads under conditions of both zero transverse strain and zero transverse load.
- Effective moduli of plate either side of the termination point.
- All input data.

[See: [16.3](#) for access to program and documentation]

16.38 Thickness selection to meet a loading combination

16.38.1 Title

Thickness selection for laminated plates subject to in-plane and bending moments.

Data Item No. 92033 [See also: [ESDU International](#) website].

16.38.2 Usage and scope

Using classical laminated plate theory, it is relatively straightforward to calculate the separate layer stresses for given layer thicknesses, angles and mechanical properties of laminated plates. However, if the layer thicknesses are not specified at the outset then the problem of finding a set of thicknesses to withstand a given set of loads efficiently is far more difficult.

This procedure is provided for plates which are symmetrical about their mid-plane, with all layers made of the same material, and the layer angles are limited to 0° , 90° , $+45^\circ$ or -45° . Layers at angles $+45^\circ$ and -45° occur as adjacent pairs. Also, all layers of the same angle have the same thickness. A stacking sequence for the layer angles is specified at the beginning, and a design procedure is used to

determine layer thickness for this lay-up. In this procedure, the thickness of layers is increased or reduced according to certain rules based on expectations of how best the layers reinforce each other. These are referred to as heuristic design rules. If requested, the procedure provides alternative lay-ups for comparison with that obtained for the specified lay-up. It can also take into account practical ply thicknesses, where each layer consists of multiples of a specified standard ply thickness.

16.38.3 Analysis

The laminated plate is assigned a particular stacking sequence for the layer angles and an initial set of layer thicknesses is determined using a netting analysis, where only the fibres in certain specified directions are assumed to carry a given set of in-plane loads and moments. The plate is then tested to failure. Depending on the mode of failure and where it occurs, specific heuristic re-design rules are invoked which either increase or reduce the thickness of some layers to a certain extent. This new design is then tested for failure and the process is repeated until the set of thicknesses is such that a layer (or layers) is just on the point of failure at the prescribed loads.

A corresponding design having the same lay-up but with the layer thicknesses rounded up or down (as requested) is then provided. Alternatives having the same number of layers or less than a specified lay-up can also be obtained as can a full layer-by-layer stress and strain analysis for each design.

16.38.4 ESDUpac A9233

16.38.4.1 Input

- Properties of layers used in laminate:
 - stiffnesses,
 - Poisson's ratio,
 - thickness,
 - allowable strain.
- Initial arrangement: lay-up and orientation of layers

16.38.4.2 Output

- All input details
- Plate layer composition of least thickness
- Overall mid-plane strains
- Overall plate curvatures
- Strains at the top and bottom of each layer
- Stresses at the top and bottom of each layer.

[See: [16.3](#) for access to program and documentation]

16.39 ESAComp

[ESAComp](#) is software for the analysis and design of composite laminates and laminated structural elements.

The development work was initiated by the European Space Agency -[ESTEC](#), who envisioned open software which combines all necessary composites analysis and design capabilities under one unified user interface. Although it originated in the aerospace field, ESAComp has been developed as a general tool for people dealing with composites, both in industry and in research.

The core of the ESAComp development work was conducted under an [ESA/ESTEC](#) contract by Helsinki University of Technology, Laboratory of Lightweight Structures and its partners. The first official release of ESAComp was in 1998. In 2000, the development work was transferred to [Componeering](#) Inc. (Finland), which also serves as the software distributor and provider of ESAComp support services.

ESAComp has a vast set of analysis and design capabilities for solid and sandwich laminates and for micromechanical analyses. It also includes analysis tools for structural elements: plates, stiffened panels, beams and columns, bonded and mechanical joints.

[See: [Table 16.2.3](#) for ESAComp analysis features; [Table 16.2.4](#) for special application functions]

Owing to the ability to interface with widely-used finite element software packages, ESAComp fits seamlessly into the design process.

[See also: [Componeering](#) Inc. website for access to program and documentation]

17

Composite adequate design

17.1 Introduction

The application of fibre-reinforced plastics, [FRP](#), offers the possibility to tailor an optimised composite structure to a given set of design requirements. Unfortunately the designed structure is very sensitive to off design conditions or imperfections.

Some basic design rules on how to approach the design of composite structures are provided.

[See: [17.5](#) for basic rules; [17.6](#) for first steps]

17.2 Anisotropy of composites

The behaviour of fibre-reinforced composites is dictated by the different properties in the parallel and perpendicular directions, i.e.:

- Parallel to the fibres, the properties of the fibres dominate.
- Transverse to the fibres, matrix (resin) properties are more important.

For this reason the designer should consider either:

- make use of this [anisotropy](#), by having the strongest material direction in the direction of greatest load, or
- reduce the degree of anisotropy, by laminating the material in varied directions.

An optimised composite structure also should take account of:

- Type of fibres.
- Type of resin.
- [Volume fraction](#) of fibres.
- Thickness of each ply.

Properties influenced by the [anisotropy](#) of a composite are:

- Strength and stresses.
- Elastic behaviour ([Young's modulus](#)).

- [Poisson's ratio](#).
- Coefficient of thermal expansion.
- Moisture conductivity
- Electrical conductivity.
- Thermal conductivity.

Figure 17.2.1 illustrates the anisotropy of CFRP.

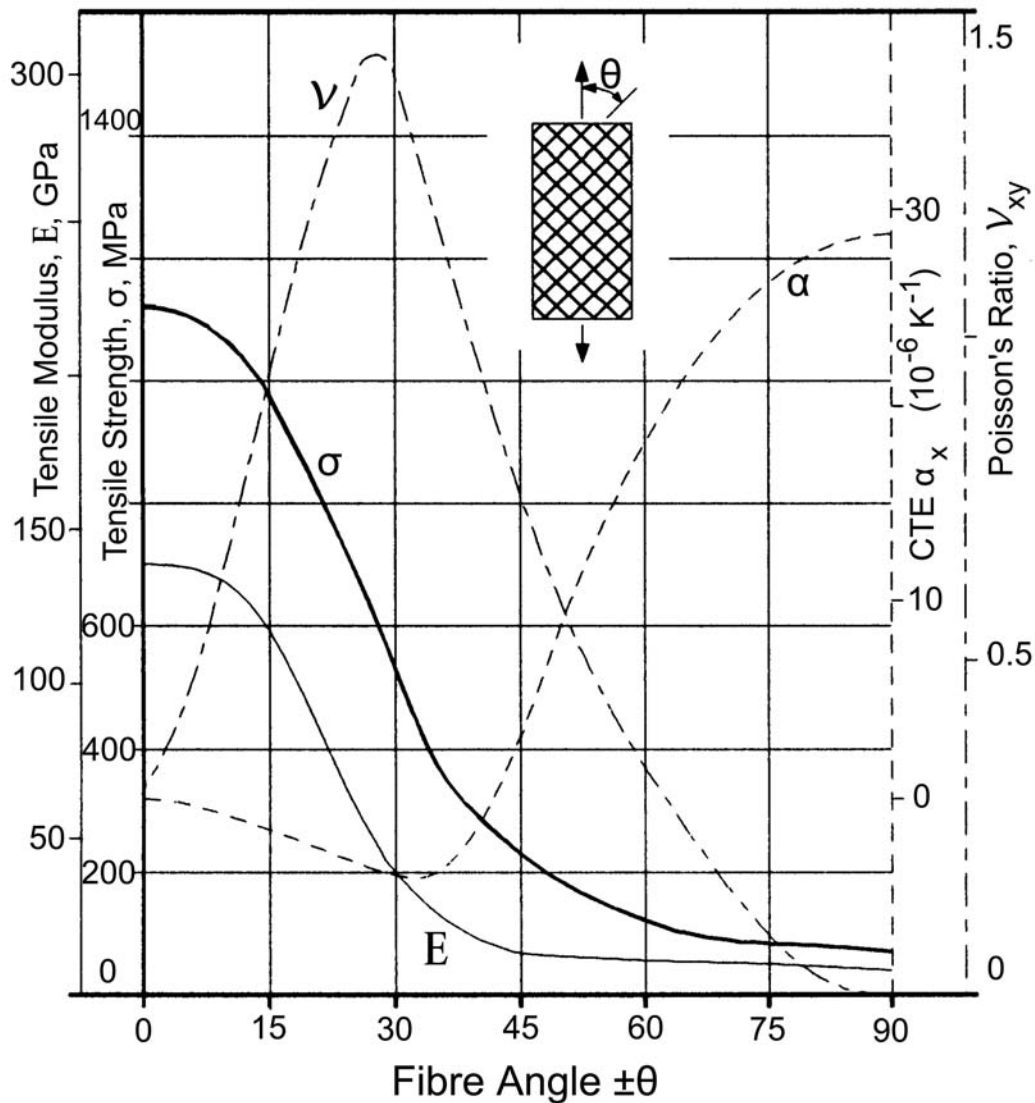


Figure 17.2-1 - Anisotropic behaviour of carbon fibre reinforced plastic

Problems arising from [anisotropy](#) often occur when metallic design concepts are directly translated into composite designs.

17.3 Stress-strain relationships

17.3.1 Reinforcing fibres

Fibres do not have a defined [yield point](#), i.e. they are mostly elastic until fracture, as shown in [Figure 17.3.1](#), Ref. [\[17-1\]](#).

[See also: [17.4](#)]

17.3.2 Stress concentrations

Composites are not able to reduce local stress concentrations by plastic deformation. This leads to:

- high [notch sensitivity](#)
- prevention or limiting [residual stresses](#).

The influence of a notch on aluminium and [CFRP](#) specimens is shown in [Figure 17.3.2](#). The notched CFRP specimens have an important reduction in specific tensile strength, whereas notched aluminium specimens show no significant decrease when statically loaded.

As regards fatigue strength, CFRP test specimens seem to be less affected by notches than aluminium. The [fatigue strength](#) of notched and unnotched CFRP approaches the same level after 10^7 stress cycles.

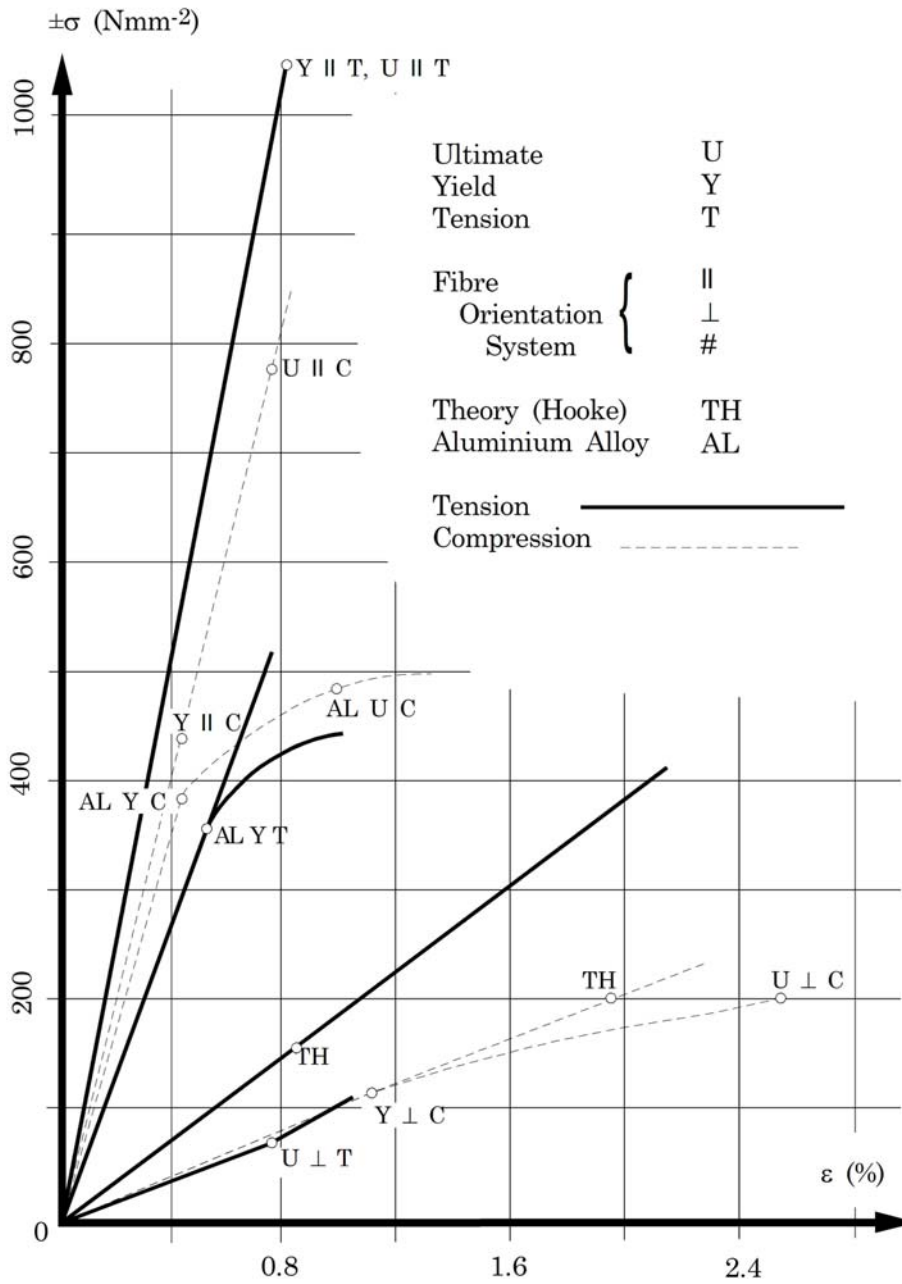


Figure 17.3-1 - Stress-strain response of CFRP (in tension and compression)

The notch sensitivity of composites needs careful consideration during the design of statically-loaded structures. Whereas for dynamic loading, composites appear to be less notch sensitive than [conventional metals](#).

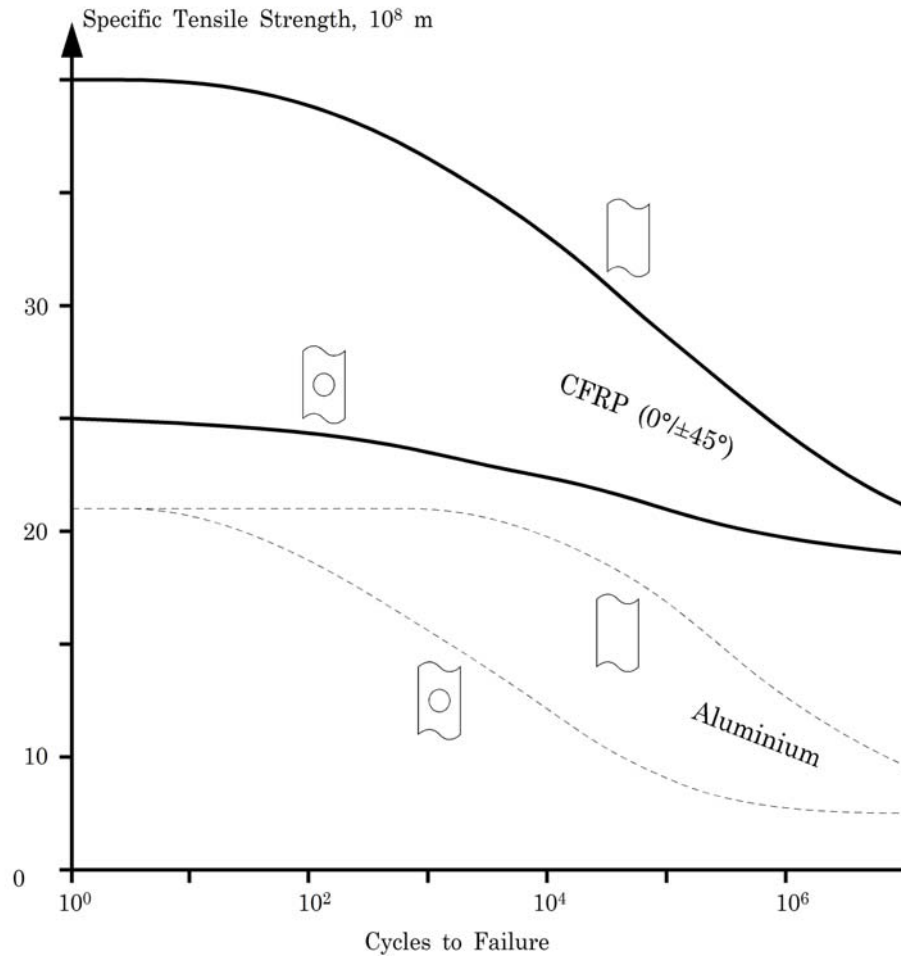


Figure 17.3-2 - Fatigue strength of notched and un-notched aluminium and carbon fibre reinforced plastic

17.4 Fibre strength and stiffness

17.4.1 General

Fibre-reinforced plastic composites cover a wide range of specific tensile strengths and specific tensile modulus, as shown in [Figure 17.4.1](#), Ref. [\[17-2\]](#).

The high strength and stiffness are only available in the fibre direction. Therefore fibres are oriented along load paths to make use of these properties.

Definition of the laminate [lay-up](#) (ply angle, thickness) need careful stress analysis, including the mechanical and thermal strain compatibility between each layer.

In aerospace engineering, comparisons between different materials are often made using specific properties, where:

$$\text{Specific property} = \frac{\text{Property}}{\text{Density}}$$

So giving an indication of the level of property available per unit mass of material.

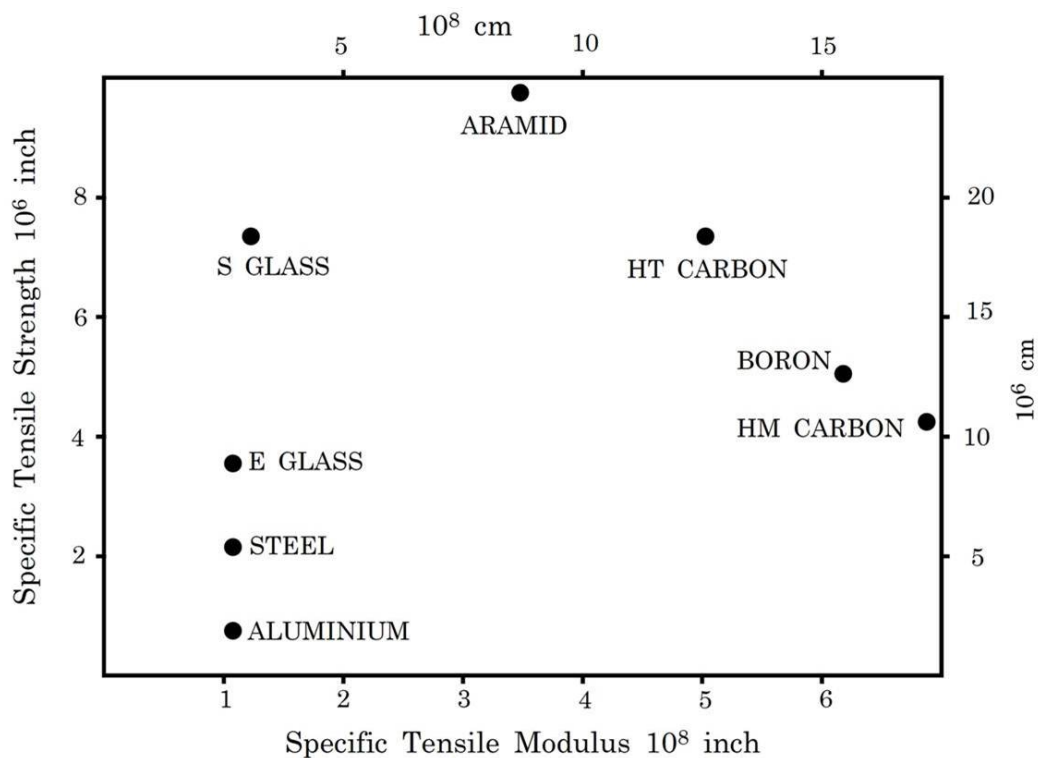


Figure 17.4-1 - Specific tensile strength and modulus properties of reinforcing fibres

17.4.2 High stiffness applications

17.4.2.1 Glass fibres

The frequently used [S-glass](#) and [E-glass](#) fibres have high tensile strengths, but the tensile modulus is comparatively low. Structures where high stiffness is imperative are therefore excluded.

17.4.2.2 Carbon fibres

For high-stiffness applications, carbon fibre-reinforced plastics, especially those with high modulus ([HM](#)) fibres are used.

[See also: [2.3](#), [3.3](#), [6.2](#)]

17.4.2.3 Boron fibres

[Boron](#) fibres are also used for stiff structures, but their handling is difficult and costs of production are high. Their use within various metal matrix composites, [MMCs](#), enables use at operating temperatures above 300°C.

[See also: [46.14](#), [46.15](#)]

17.4.2.4 Aramid fibres

The polyamide fibres, also known as [aramid](#), combine high strength and high modulus but suffer from low compression strength, e.g. Kevlar™ 49 (DuPont) and Twaron HM (Teijin; previously AZKO).

Kevlar is often substituted for glass fibres in reinforced plastics for certain applications.

[See also: [2.3](#), [3.3](#)]

17.5 Basic design rules

17.5.1 General

In principle the design of composites does not differ from that of metal, i.e. most of the rules which are employed for metal structures are also acceptable for composites.

17.5.2 Aspects of construction

17.5.2.1 Changes in thickness

Where variations in thickness of a laminate are necessary (stiffness changes), they are stepped gradually; as shown in [Figure 17.5.1](#).

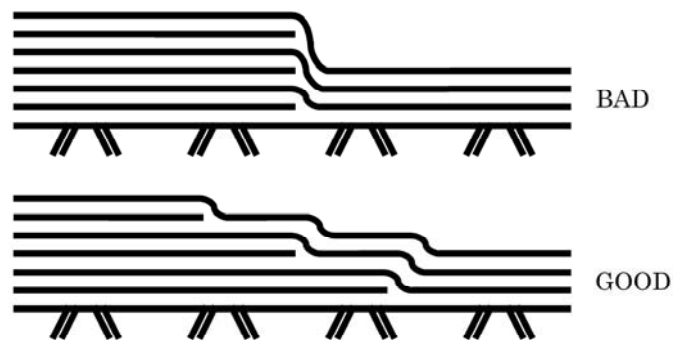


Figure 17.5-1 - Shaping changes in thickness

An abrupt change in the thickness acts as a stress concentration and should be avoided. Such areas are susceptible to [delamination](#) and can result in structural failure.

Equation [\[17.5-1\]](#) is a suggested design rule for shaping thickness changes; illustrated in [Figure 17.5.2](#):

$$l \geq \Delta t \quad [17.5-1]$$

where: $\Delta t = 0.7\text{mm}$

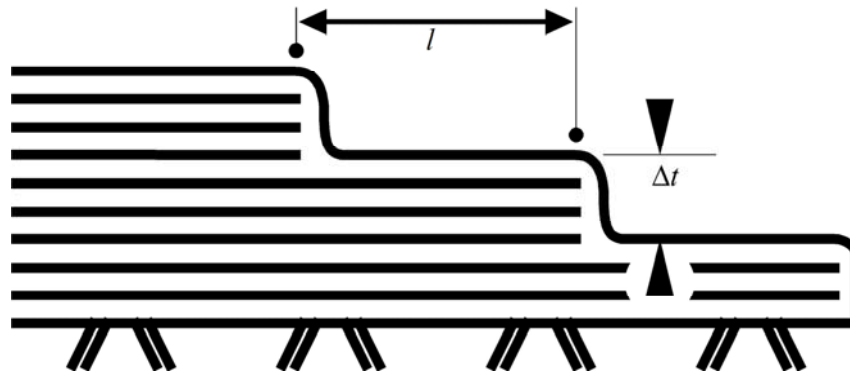


Figure 17.5-2 - Design of shapes

17.5.2.2 Radii, curves and sharp corners

The minimum radius of a single fibre means that [lay-ups](#) are not able to follow a sharp corner, i.e. 90° angle, without a radius.

[Figure 17.5.3](#) shows that the laminate does not fit into the corner, or over the edge.

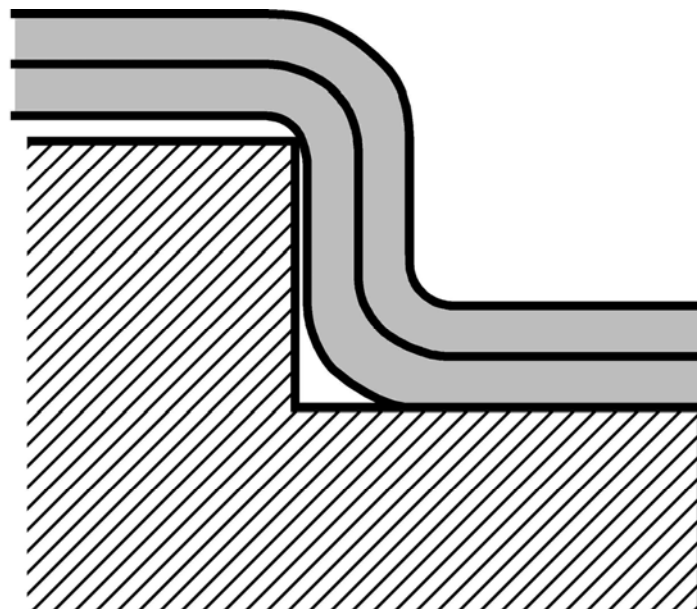


Figure 17.5-3 - Need for radii on corners

Sharp corners lead to stress concentration, [delamination](#) and finally cracking of the laminate.

To avoid this problem, the recommendations include:

- Use large radii. Radii are influenced by:
 - fibre type,
 - fabrication technique, and
 - [curing](#) process.

- Use recommended minimum radius of curvature for fibres and laminate, as shown in [Table 17.5.1](#).

Table 17.5-1 - Minimum radii for fibres and laminates

Fibre	GRP: $r = 0.2$ to 0.5 mm
	CFRP (HT): $r = 0.5$ to 1.0 mm
Laminate	$R_i = 1$ mm + $n \times 0.1$ mm
	$R_i = 4.8$ to 6.4 mm

Key: n : number of plies; r : radius.

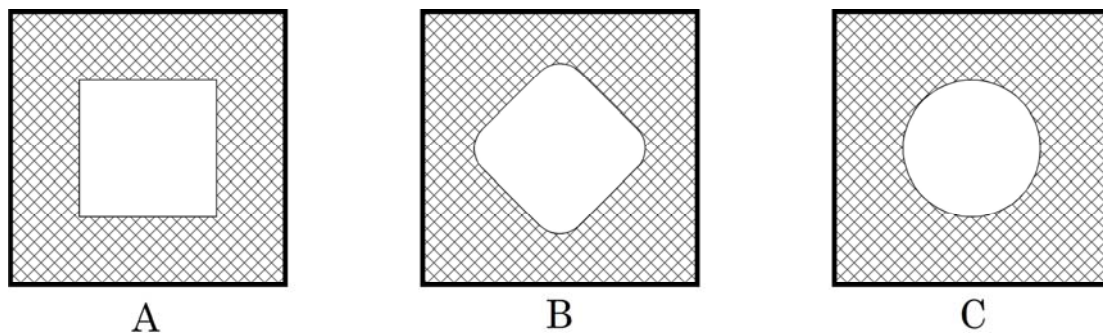
17.5.2.3 Openings

Openings are cut-outs in the structure, for purposes such as:

- wiring,
- fuel pipes, or
- inspection.

Design guidelines for the shape of cut-outs, as shown in [Figure 17.5.4](#), include:

- As far as possible, use round holes for cut-outs (lower stress concentrations).
- Where rectangular holes are unavoidable, all corners are rounded with a large radius to prevent cracks.
- The cut-out is positioned so that only the smallest possible number of fibres are cut, as illustrated in [Figure 17.5.4-B](#).



A = Bad → C = Good

Figure 17.5-4 - Cut outs: Bad and good practice

Cutting out larger areas of a structure means disturbing load paths. Loads disturbance can be avoided around the cut-out by either:

- designing a moulded in flange around the opening, or
- by bonding on a reinforcement.

17.5.2.4 Other design considerations

- Avoid undercuts, but these can be made by using split or rubber moulds.
- Provide draft angle of between 1° and 3° (generally 2°)
- Moulded in holes only for large diameter
- Practical thicknesses:
 - Minimum: 0.6mm to 0.8mm, because handling becomes difficult
 - Maximum: Unlimited, but only 6mm to 8mm per cure, otherwise a critical exothermic reaction takes place.
- No limiting size factor, except mould size and handling considerations.
- If an angle section (or in general open profiles) is designed the spring back resilience of the structure, produced by different properties parallel and perpendicular to fibres, should be considered.
- Load transfer by bolted joints: Use of lugs and avoiding drilled holes prevent edge delamination, stress concentration and early failure.

17.5.3 Aspects of laminate lay up

17.5.3.1 Fibre forms

Different kinds of fibres are available, in various semi-product forms as summarised in [Table 17.5.2](#).

The basic differences between these forms are illustrated in [Figure 17.5.5](#), which shows a sketch of the tensile strength of a single layer for various directions. This determines the preferred loading direction, i.e. maximises the strength obtained from the fibres.

Table 17.5-2 - Basic and semi-product forms

Basic Fibre Form	Semi-product
Continuous rovings	UD prepreg
Woven fabrics and tapes	Bi-directional prepreg
Short fibres	Multi-directional prepreg †
Key: † : Examples: chopped strand mat (CSM), felts; UD : unidirectional	

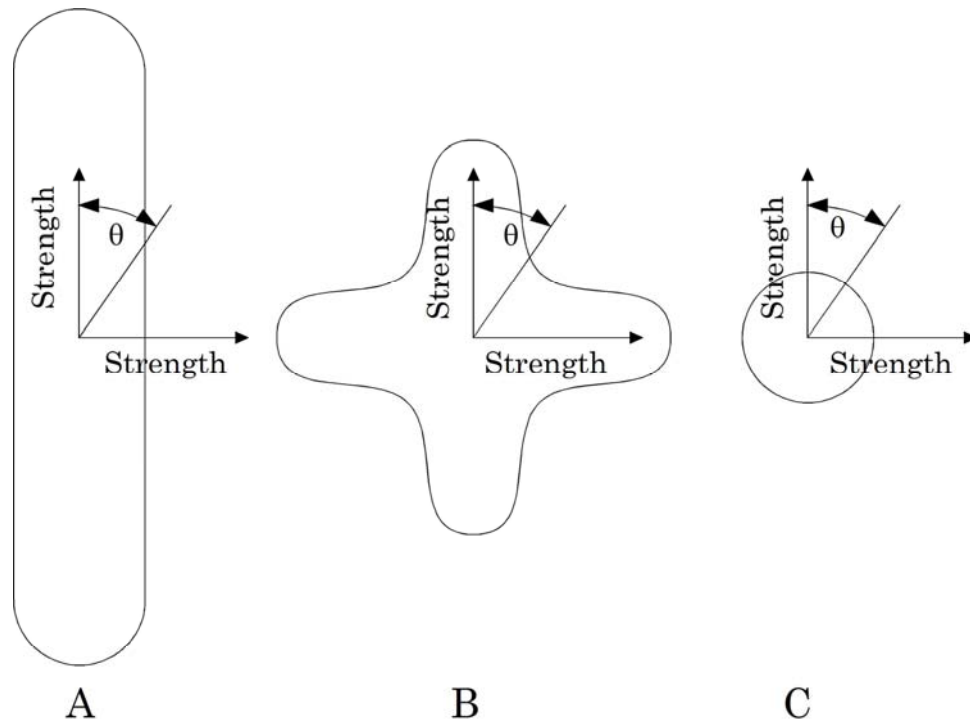


**Figure 17.5-5 - Directionality of tensile strength of various semi-product forms:
Preferred loading direction**

17.5.3.2 Lay up

If a [lay-up](#) is not well designed, [FRP](#) are susceptible to residual stresses. To reach a mechanical and thermal compatibility between the plies and to prevent distortion after curing, the design guidance should include:

- Use a symmetrical stacking of plies and a minimum of three different fibre angles, as shown in [Figure 17.5.6](#). This leads to:
 - non warping structures, and
 - minimum loading of resin matrix.
- The angle between two stacked plies should be as small as possible to prevent interlaminar stresses, e.g.

$0^\circ / +45^\circ / 90^\circ / -45^\circ \mid -45^\circ / 90^\circ / +45^\circ / 0^\circ$

better than

$0^\circ / +45^\circ / -45^\circ / 90^\circ \mid 90^\circ / -45^\circ / +45^\circ / 0^\circ$

- When rivets or bolted joints are involved, a laminate with about 50% $\pm 45^\circ$ layers is necessary to have high bearing strength, [See: Chapter [22](#)].
- Composites of carbon fibres are:
 - thermally [isotropic](#) when only $0^\circ/90^\circ$ plies are used.
 - thermally and elastically isotropic when $0^\circ/\pm 60^\circ$ plies used.
- If possible 'split design' techniques are employed, as shown in [Figure 17.5.7](#). This enables the application of elementary profiles (only a few layers in a simple structure) which are assembled to a more complex product.

- Take into account the different coefficients of thermal expansion when a laminate is placed in or on a metal mould. [Figure 17.5.8](#) summarises dimensional changes for different materials.

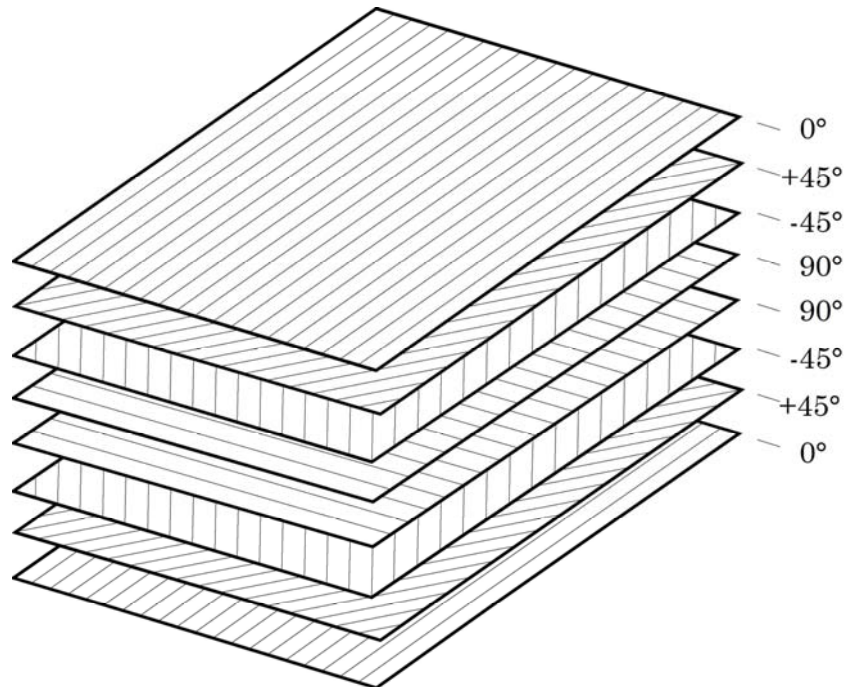


Figure 17.5-6 - Symmetrical lay-up: Avoids warpage and minimises loading the resin matrix

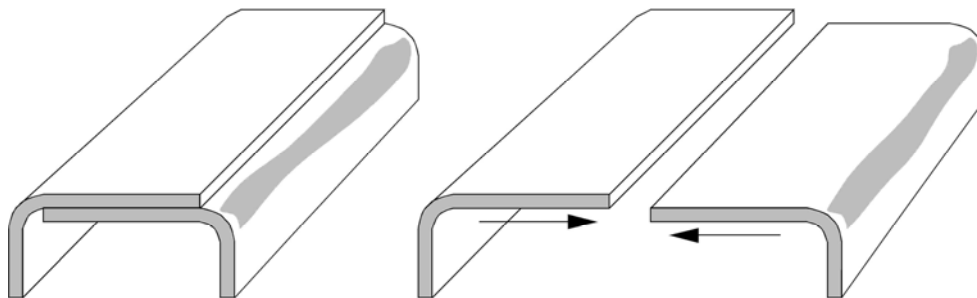


Figure 17.5-7 - Split design technique

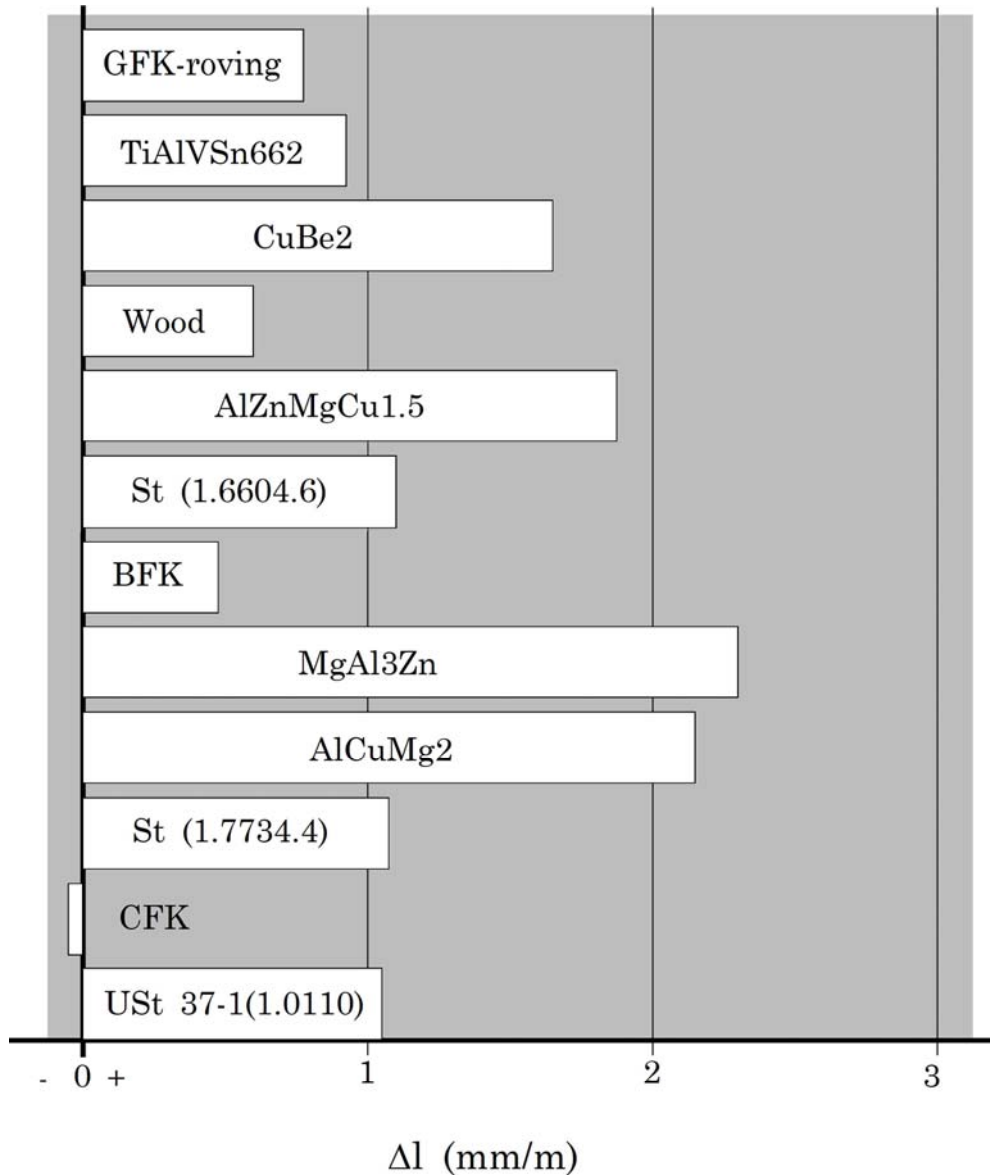


Figure 17.5-8 - Dimensional change for various materials due to a temperature change of 100°

17.5.4 Fabrication aspects

17.5.4.1 Cost effectiveness

Although material prices, especially carbon fibres, have fallen in recent years, the designer of composite structures should consider cost effectiveness.

The main parts of fabrication cost are:

- Material costs,
- Cost of production equipment,
- Cost of assembly,

- Quality control, and
- Waste.

[Figure 17.5.9](#) illustrates the contributing factors to the cost of fabrication, Ref. [\[17-4\]](#).

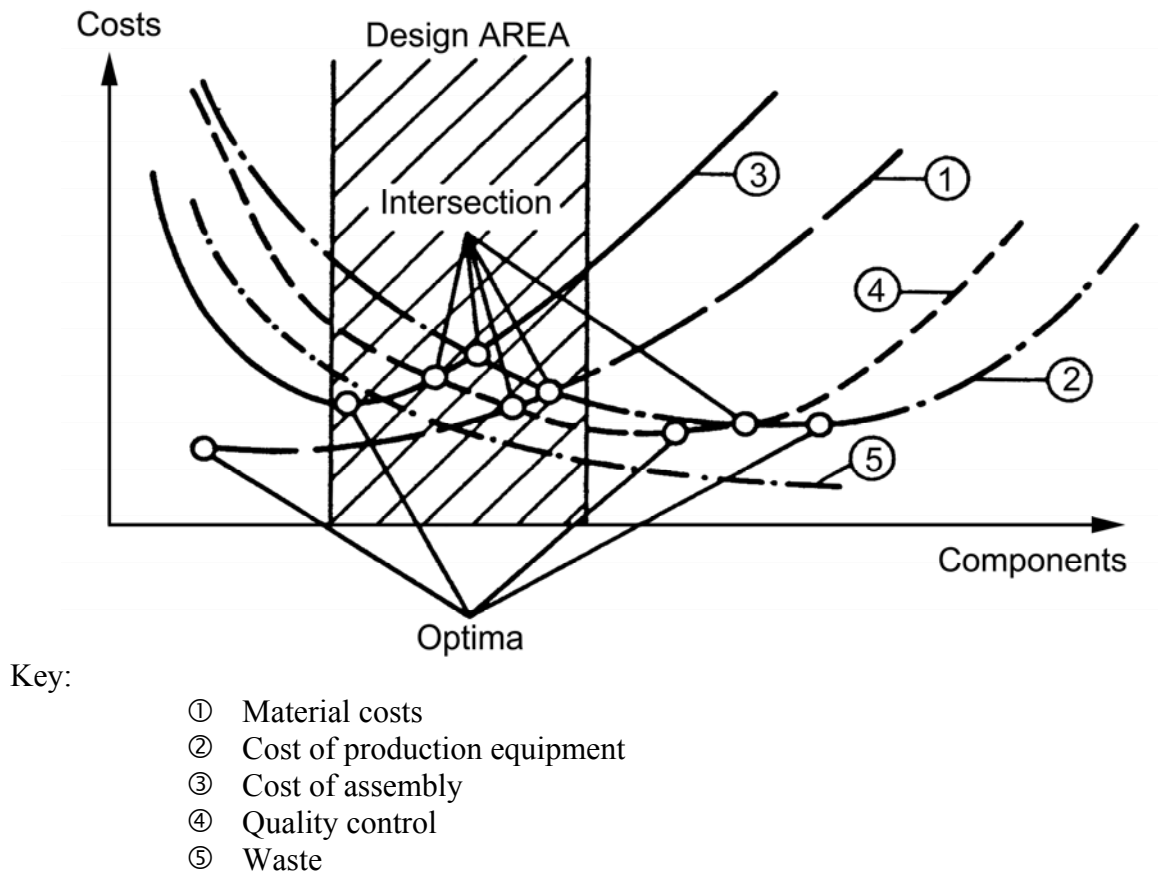


Figure 17.5-9 - Fabrication costs for a CFRP structure

[Figure 17.5.10](#) compares the cost distribution for the fabrication of a typical structural component designed in metal or [CFRP](#), Ref. [\[17-5\]](#).

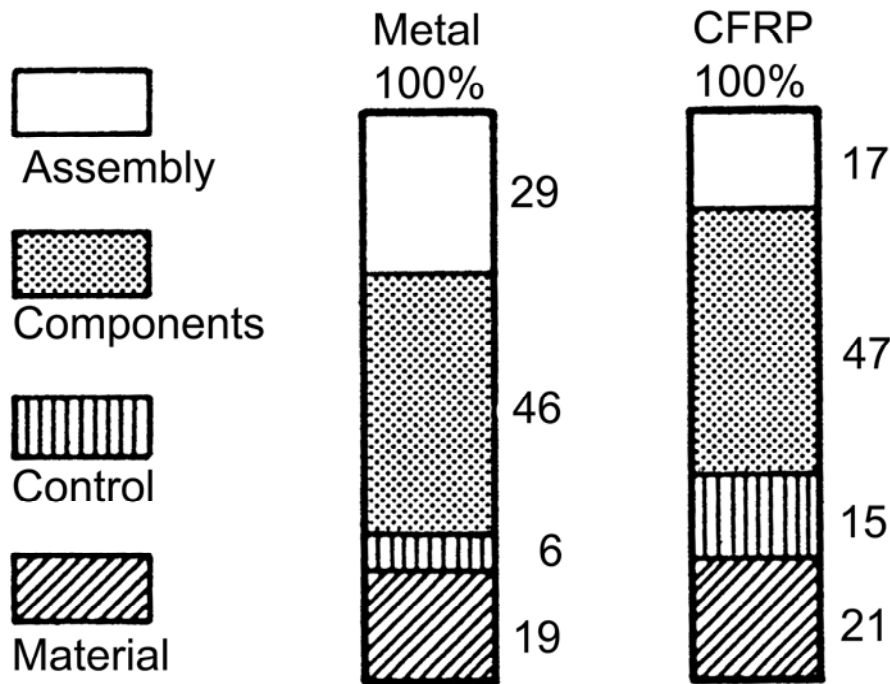


Figure 17.5-10 - Comparison of costs: Metallic and CFRP

17.5.4.2 Criteria for cost effectiveness

General guidelines for cost effectiveness include:

- Construction:
 - Is the structure manufactured by 'one shot' technique, whenever possible? 'Split design' reduces waste but raises assembly costs.
 - Is maximum automation used?
- Material: Reduce material cost by optimum utilisation.
- Fabrication:
 - Is the number of components at a minimum?
 - Has composite adequate design been fully considered?
 - Choose optimum processing techniques to reduce waste.
 - Are assembly costs at minimum? Use as few joints as possible.
- Make quality control simple.

17.5.4.3 Processing technique

Various manufacturing methods are used, as summarised in [Table 17.5.3](#), [See also: Chapter [38](#)].

Table 17.5-3 - Composite manufacturing methods

Moulding Pressure Vacuum bag Autoclave Resin injection	Hand Semi-automatic Automatic lay-up
Filament Winding Weaving Braiding	Automatic lay-up
Pultrusion	

17.6 First steps in designing a composite

17.6.1 General

A typical example for the preliminary design of composites is a '[Carpet Plot](#)'. This is a graphical solution based on the classical lamination theory for $0^\circ/\pm 45^\circ/90^\circ$ laminates and is used for the determination of moduli, strength or thermal expansion coefficients. Carpet plots are only of limited use.

More effective methods were developed by S.W. Tsai, Ref. [\[17-6\]](#); often available in the form of software.

17.6.2 Carpet plots

A simplified design method, where it is assumed that a laminate lay up only consists of $0^\circ/\pm 45^\circ/90^\circ$ plies, is presented in [Figure 17.6.1](#) (modulus) and [Figure 17.6.2](#) (stiffness) for a carbon fibre/epoxy composite, Ref. [\[17-2\]](#).

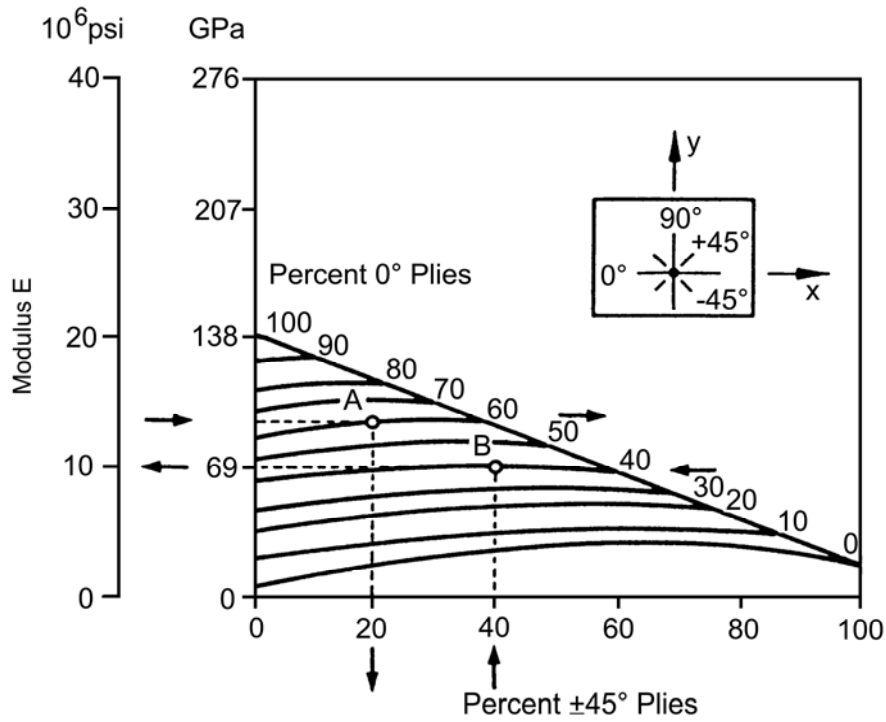


Figure 17.6-1 - Carpet plot curves of modulus for 0°/±45°/90° laminates

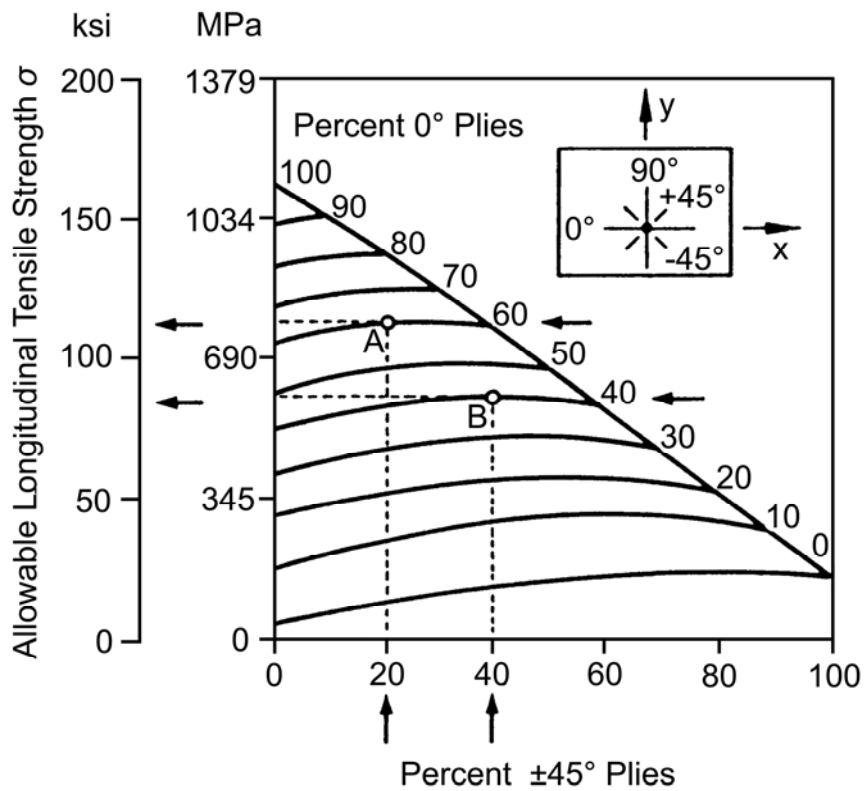


Figure 17.6-2 - Carpet plot curves of strength for 0°/±45°/90° laminates

The basis for the use of these diagrams is that the $0^\circ/\pm 45^\circ/90^\circ$ family is reasonably close to optimum with regard to design, fabrication and weight. The diagrams show how to make a first approximation of stacking order, [See: [Use of carpet plots](#)].

Carpet plots are of limited use because the basis for the calculation is rarely defined. The transition of uniaxial strength from unidirectional to multidirectional laminates is often made by over simplification of theory, i.e. it is assumed that a biaxial state of stress can be resolved in the manner of netting analysis. The kind of failure of the laminate (first or last ply failure) is not always defined.

17.6.3 Use of carpet plots

17.6.3.1 General

There are two different ways of using [Carpet Plots](#):

- Method 1, when the elastic modulus of the composite is known.
- Method 2, when an optimum stacking is assumed.

Carpet Plot use is described by example with [Figure 17.6.1](#) and using [Figure 17.6.2](#).

17.6.3.2 Method 1

This is applied when the elastic modulus of the composite is known:

- Select a percentage share of 0° , $\pm 45^\circ$ and 90° plies:
- For example, [See: [Figure 17.6.1](#)]:
- Modulus $E_x = 90$ GPa (13x106 psi), and as shown in point "A", a percentage stacking of:

$$60\% \rightarrow 0^\circ$$

$$20\% \rightarrow \pm 45^\circ$$

$$20\% \rightarrow 90^\circ$$

is an arbitrary choice.

(To obtain the percentage of 90° plies, simply subtract the percentage of plies at 0° and $\pm 45^\circ$ from 100 %).

- From the stacking choice the allowable longitudinal tensile strength can be determined:

For example, [See: [Figure 17.6.2](#)]:

With the percentage stacking of point "A" an allowable strength $\sigma_x = 724$ MPa (10^5 ksi) results.

- If the strength value is not acceptable, choose a new percentage distribution:

It can be necessary to know optimum stacking, when only modulus E_y is given. If this is true, interchange the x and y co-ordinates and 0° and 90° percentage distributions to obtain the allowable strength σ_y .

17.6.3.3 Method 2

This is applied when an optimum stacking is assumed:

- By which E_x can be determined

For example, [See: [Figure 17.6.1](#)]:

40 % \rightarrow 0°

40 % \rightarrow $\pm 45^\circ$

20 % \rightarrow 90°

A combination is shown by point "B" and leads to a modulus $E_x = 69$ GPa, (10×10^6 psi)

- From the assumed stacking, the allowable longitudinal tensile strength can be determined.

For example, [See: [Figure 17.6.2](#)]:

With the percentage stacking of point "B" an allowable strength $\sigma_x = 586$ MPa (85 ksi) results.

17.6.3.4 Other parameters

Besides determining lay-up, modulus or tensile strength other characteristics can also be determined by a similar procedure, including:

- shear modulus
- compressive strength
- [Poisson's ratio](#)
- coefficient of thermal expansion

These are often in the form of a computer variation program based on the classical lamination theory.

[See also: Chapters [11](#), [12](#), [13](#), [14](#), [15](#) and [16](#)]

17.7 References

17.7.1 General

- [17-1] E. Heinze & S. Roth: Dornier Systems GmbH
'Practical finite element method of failure prediction for composite material structure'. Dornier Internal Report, 1975
- [17-2] L.M. Schwartz
'Composite Material Handbook'
McGraw Hill, 1984
- [17-3] George Lubin (Ed)
'Handbook of Composites'
Von Nostrand Reinhold Company, 1982

- [17-4] M. Flemming: Dornier System GmbH
Lecture Paper at Technical University Berlin, 1980

- [17-5] H. Conen, Kaitatzidis
'Höhenleitwerk aus CFK für den Alpha Jet'
Verarbeiten und Anwenden von Kohlefaser Kunststoffen
VDI Verlag GmbH, Düsseldorf, 1981

- [17-6] S.W. Tsai
'Composite Design 1986'
Think Composites, 1986

18

Curing stresses: Effects and prediction

18.1 Introduction

Composite materials are manufactured by:

- placing fibre and resin into or onto a mould, then
- curing the lay-up.

The fibre and resin are normally combined as a [prepreg](#), although some non-prepreg processing methods are used.

Both the laminate [lay-up](#) and the [cure cycle](#) are selected carefully to minimise [residual stresses](#).

This chapter describes how residual stresses occur, [See: [18.4](#)], how they are calculated, [See: [18.5](#)], and how they can be reduced, [See: [18.6](#)].

18.2 Cure process

18.2.1 Composite materials

18.2.1.1 Thermosetting resin

Composite curing is accomplished by exposing the lay-up for a predetermined length of time to:

- elevated temperature, and
- pressure

It is applicable to all [thermosetting](#) resin systems, although the precise conditions vary between resin types.

18.2.1.2 Thermoplastic composites

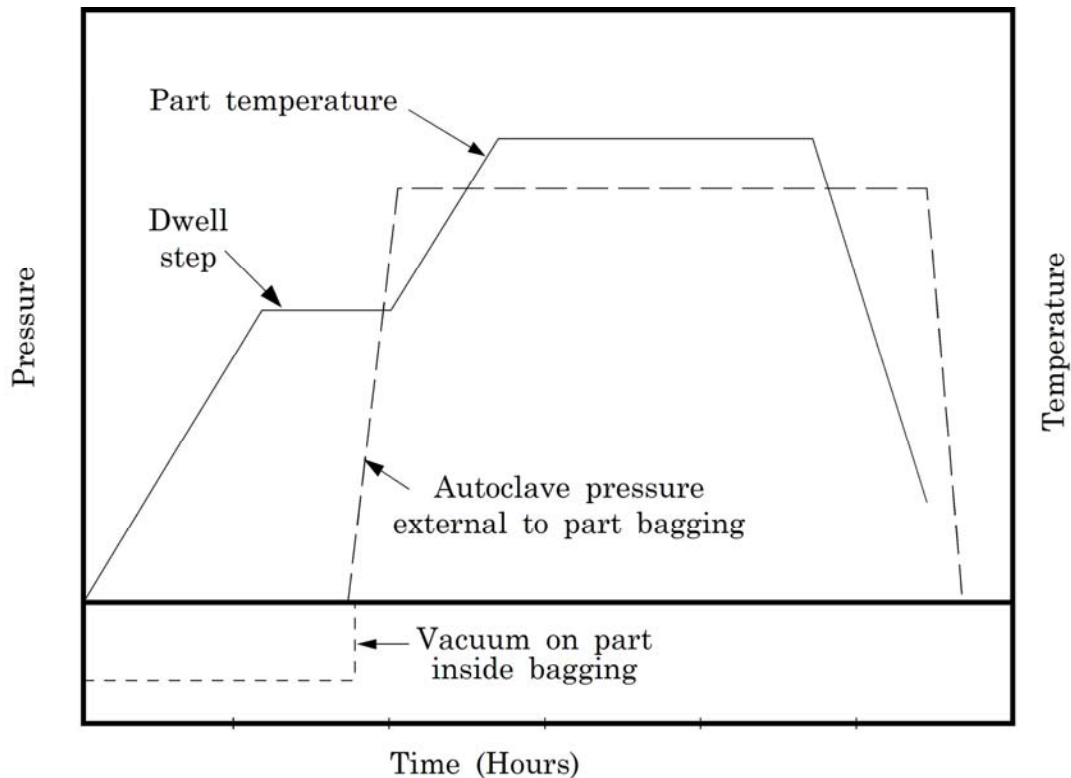
[Thermoplastic](#) polymers do not cure, [See: [6.16](#), [6.17](#)].

18.2.2 Cure parameters

18.2.2.1 General

The magnitude and duration of temperature and cure pressures have a significant affect on the performance of the finished product.

A typical [cure cycle](#) for a [CFRP](#) composite is shown in [Figure 18.2.1](#).



Material: Carbon/Epoxy: T300/914

Figure 18.2-1 - Typical cure cycle for CFRP

18.2.2.2 Temperature

The heat applied during the [cure](#) provides initiation and promotion of the chemical reaction in the resin, which changes the molecular structure by [cross-linking](#).

18.2.2.3 Pressure

The applied pressure provides the force needed to:

- squeeze excess resin out of the laminate,
- consolidate individual plies, and,
- compress vapour bubbles and [voids](#)

18.3 Analytical notation for residual stress

A_{ij}	Laminate stiffness
N_i^T	Equivalent stress resultants (due to thermal strain)
N_k	Load (where subscript k denotes the loading direction)
Q_{ij}	Reduced stiffnesses (at the final temperature)
$x; y$	Loading direction
ε_j°	Mid-plane total strains (measured from the stress-free state)
ε_j^T	Thermal strains (measured from the stress-free state)
σ_i	Ply stresses (i -th ply)
σ_i^R	Residual stresses (i -th ply)

18.4 Residual stresses

18.4.1 General

[Residual stresses](#) in fibre-reinforced plastic composites are produced during processing. The stresses result when the composite cools from the curing temperature because of:

- different coefficients of thermal expansion, [CTE](#), parallel and perpendicular to the fibre, and
- different CTE of the fibres and matrix.

18.4.2 Types of residual stresses

The types of residual stress are:

- [Micro-residual stresses](#).
- [Macro-residual stresses](#).

18.4.2.1 Micro-residual stresses

These are associated with the local geometry within the plies. [Microcracking](#) of the matrix leads to a decrease in residual bending strains (unsymmetrical laminates), reduced deformation and value of [CTE](#). Difficulties also occur when moisture enters microcracks and the structure operates at [cryogenic](#)

temperature. In general, all of these problems depend on the properties of the resin. A bad choice of matrix material can cause catastrophic damage.

18.4.2.2 Macro-residual stresses

These are caused by gross average stress through the cross ply. The parameters which have an effect on the more general distortion of the laminate are:

- variation in thickness.
- [stacking](#) sequence.
- fibre angle orientation.

Without full consideration of these parameters, curvature and warp of the cured structure occurs on cooling, as a result of:

- differences in the conductivity and coefficient of thermal expansion, [CTE](#), between fibre and matrix, and
- different thermal [anisotropic](#) behaviour of the fibre itself; especially carbon fibre.

Other parts processed using a curing process, such as sandwich materials or block inserts, have a major impact on residual stresses. To avoid reaching critical stress or to limit shape changes and spring-back occurring, care is needed to consider fully the effects of such residual stresses.

18.5 Calculation of curing stresses

18.5.1 Residual stresses after curing

18.5.1.1 General

Supposing that the 0° plies and the 90° plies contract unconstrained by each other when cooling down from the [cure](#) temperature, the thermal strains are defined as shown in [Figure 18.5.1](#).

Since ε_x^T and ε_y^T are not equal, there is a geometrical mismatch between the 0° and 90° plies.

To ensure geometric compatibility, the residual stresses σ_x^R and σ_y^R are internally applied to the 0° and 90° plies resulting in final strain ε^{oT} (laminate curing strain) which depends on ε_x^T , ε_y^T and the elastic moduli.

18.5.1.2 Symmetric laminates

Assuming elastic material behaviour and symmetrical [stacking](#), the [ply](#) constitutive relations can be written as, Ref. [\[18-2\]](#), [\[18-3\]](#):

$$\sigma_i^R = Q_{ij} A_{jk}^{-1} N_K^T - Q_{ij} \varepsilon_j^T \quad [18.5-1]$$

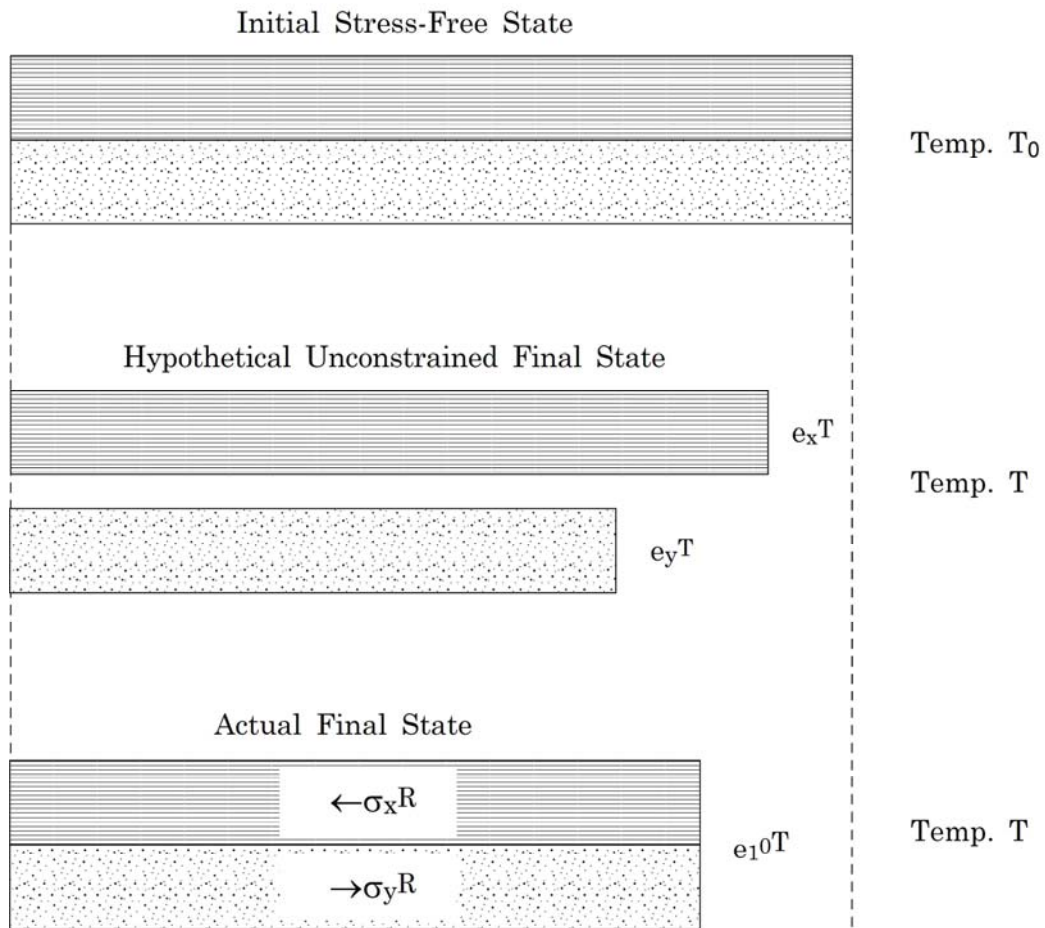


Figure 18.5-1 - Residual stresses after curing

From Eq [18.5-1], the total ply stresses related to the applied laminate resultants, N_i , can be written as:

$$\sigma_i = Q_{ij} A_{jk}^{-1} N_K + \sigma_i^R \quad [18.5-2]$$

The transverse residual stresses in the plies after fabrication are tensile.

18.6 Reduction of thermal stresses and distortions

18.6.1 General

Recommendations to reduce thermal stresses and thermal distortions resulting from [cure cycles](#) include:

- Symmetrical laminate [stacking](#) is the first design rule.
- Evaluate carefully the combination of [CFRP](#) with other materials, e.g. steel, aluminium, because measures like pre strain should be carried out to prevent curvature after fabrication.
- Avoid large variations in thickness because this leads to dissimilar cooling and cracks in the areas of thickness changes.
- Fibre angle orientations influence the residual stresses due to curing. An angle ply laminate using $\pm 45^\circ$ plies only is most susceptible to thermal loading. Such an orientation results in high interlaminar stresses which affect the generation of [microcracks](#), Ref. [\[18-4\]](#).

NOTE The situation is different if mechanical loads are also applied.

[Figure 18.6.1](#) and [Figure 18.6.2](#) show the principal behaviour of various angle ply laminates due to thermal (curing) and mechanical loading, Ref. [\[18-4\]](#).

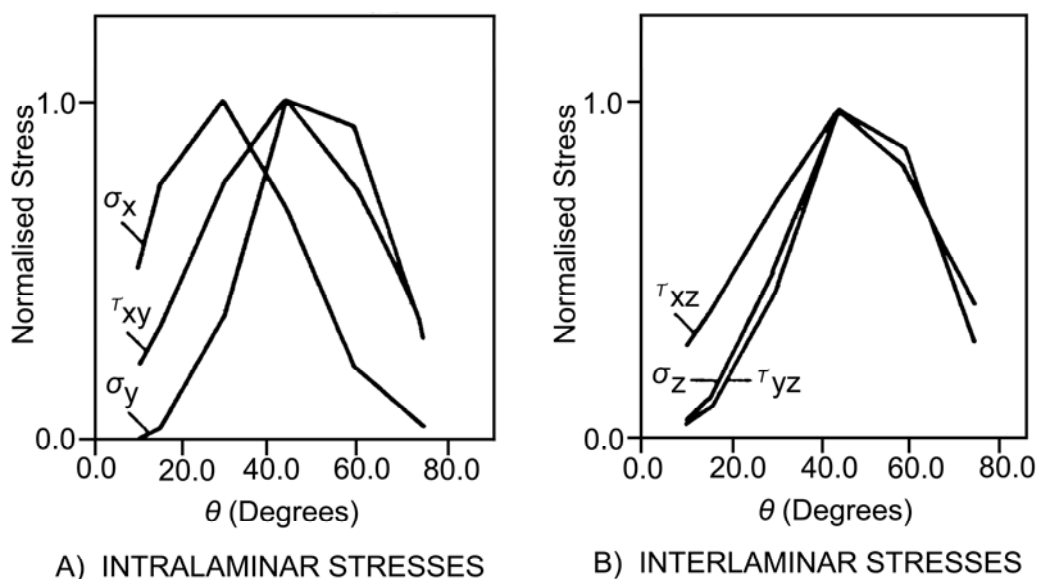


Figure 18.6-1 - Normalised maximum curing stresses in $[\pm\theta]_s$ laminates

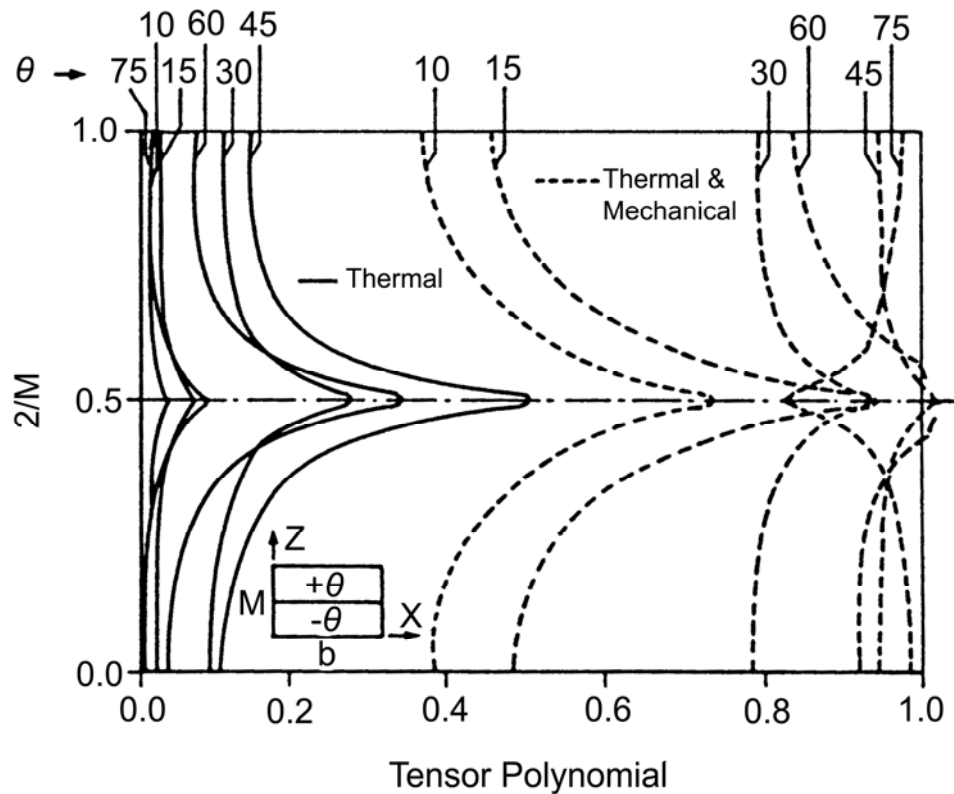


Figure 18.6-2 - Through thickness tensor polynomial distributions for curing stresses and stresses at first failure in $[\pm\theta]_s$ laminates

18.6.2 Stress relieving

18.6.2.1 Annealing

The [annealing](#) of curing stresses through a post cure at the original [cure](#) temperature is not effective.

18.6.2.2 Low temperature thermal cycling

Thermal cycling to a low temperature shows no direct influence on the residual strength of the laminate. However, it leads to a stress relief caused by [microcracking](#) of the resin. Therefore low temperature cycling can be used for unbalanced laminates, e.g. composites with variable resin content within the laminate or more generally distorted laminates after manufacturing.

18.7 References

18.7.1 General

- [18-1] Dornier System GmbH
 'Final report of a study on evaluation of in built stresses during manufacture of elements made of carbon fibre reinforced plastics'

ESTEC Contract 2930/75/NL/PP (SC)

- [18-2] S.W. Tsai & H.T. Hahn
'Introduction to Composite Materials'
Technomic Publication, 1980

- [18-3] R.Y. Kim
'Effect of curing stresses on the first ply failure of composite laminates'
Journal of Composite Materials, Vol. 13, January 1979

- [18-4] C.T. Herakovich
'On failure modes in finite width angle ply laminates'
ICCM 3, 1980, Vol. 1

19

Manufacturing faults and service damage

19.1 Introduction

Composite structures, like many engineering structures, need to be able to function effectively throughout a defined lifetime whilst also meeting safety and economic targets. Structures are exposed to a series of events that include loading, environment, and damage threats. These events, either individually or cumulatively, can cause structural degradation, which can affect the ability of the structure to perform its function.

One of the uncertainties for the user of composite materials is how to determine whether a defect is benign or not. There are two separate types of defect that effect the strength of a composite structure:

- Manufacturing threats: Imperfections or defects from manufacturing of the composite or assembly of the structure.
- Service threats: Damage resulting during handling, installation or in-service use.

Understanding the nature of the defect present enables both the effect of this defect to be ascertained and in some instances a forensic examination of a failed part to be carried out for failure analysis. For every composite part, acceptance/rejection criteria are established to be used during inspection of the part. This combines analysis and testing to help identify the effect of a defect on performance of a composite structure. The approach is very dependent on the purpose of the structure, e.g. the presence of microcracking can be less important for a structural application but more so for a fluid containment application.

Some examples of possible defects are illustrated in [Figure 19.1.1](#).

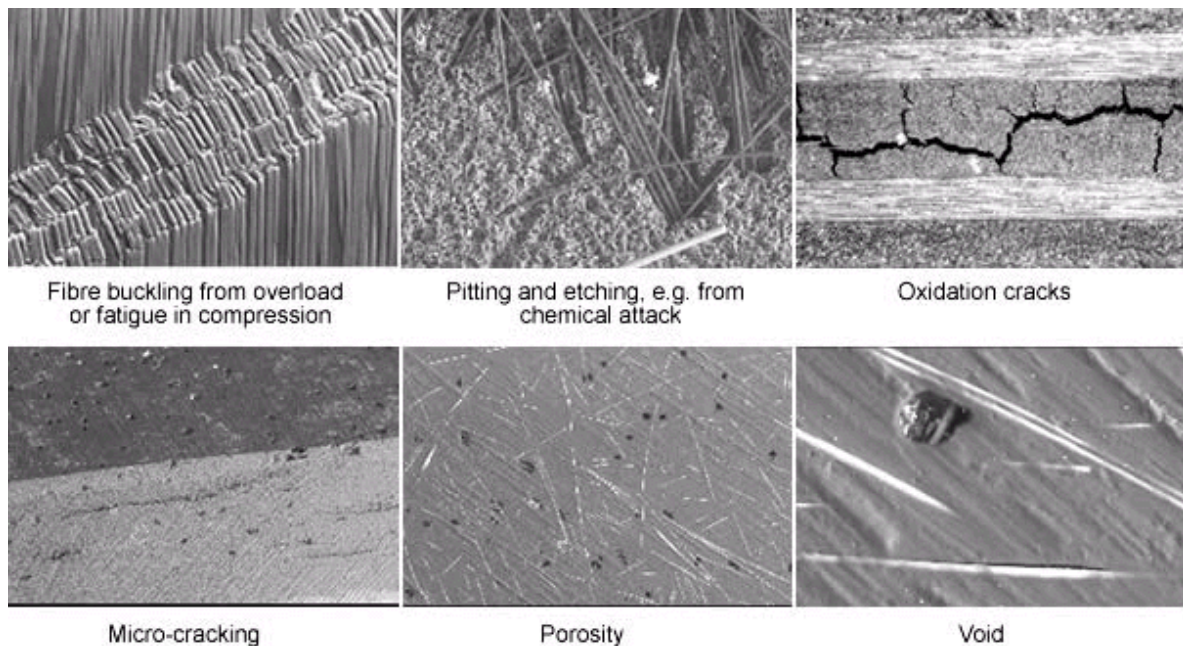


Figure 19.1-1 - Examples of defects in composite materials

The properties of materials and structures can be significantly degraded through manufacturing or in-service damage. In the case of composite materials, the situation is very different from that of metals. Unlike metals, fibre-reinforced composite materials do not undergo plastic deformation under impact. A local blow or impact event therefore either results in elastic deformation or damage. The energy absorbed in an impact event depends on the strength of the fibre-resin bond, amongst other things. If the bonding is strong, a crack can propagate through the material with minimal deviation. Given a weaker bond, the crack path could be much more irregular, leading to extensive interfacial debonding but considerable energy absorption.

The location or severity of manufacturing defects and in-service damage can be difficult to anticipate and detect. Some manufacturing flaws are not easily detectable until the structure is exposed to the service environment, e.g. 'kissing bonds' are not detectable until the joint is loaded in service. The complex loading that a structure experiences in service and the design of the structure can result in load cases that are not predicted during the design phase.

In this chapter a general overview of the manufacturing and in-service defects which can occur in composite materials is presented. Means of preventing or minimising manufacturing faults are discussed and potential in-service damage events are highlighted.

[See also: Chapter [8](#) for effects of manufacturing practices]

19.2 Manufacturing defects in composite materials

19.2.1 General

Manufacturing defects can arise from a number of sources, including:

- Improper cure or processing,
- Improper machining,
- Contamination,
- Mishandling,
- Inadequate tooling,
- Improper drilling,
- Tool drops,
- Mislocation of holes or details,
- Improper sanding,
- Substandard material.

[Table 19.2.1](#) lists [defects](#) that can occur in composite materials, including honeycomb interfaces with a composite. Each defect is also described. The table does not contain quantitative information because the complexity of composite materials produces a highly specific interdependence of:

- composite structure
- component dimensions, and
- defect type, orientation and size.

Consequently, it is impossible to define detection limits.

[See also: Chapter [34](#)]

To avoid defects arising in prepreg material supplied by manufacturers, consult Ref. [\[19-4\]](#).

For inspection and quality assurance [See also: [34.2](#), [34.3](#) and [34.4](#)].

Table 19.2-1 - Types of defects in composite materials

Porosity
Prepreg gaps
Contamination
(solvent, solid, prepreg backing sheet)
Fibre alignment
Lay-up order
State of cure of the matrix
Fibre/resin ratio local variations
Prepreg joints
Inter-ply delaminations
Skin to core debonding
Resin microcracking
Damaged honeycomb core *
Misplaced potting compound *
Edge member/shear connection debond *

Key: * - Interfaced with a composite.

19.2.2 Description of manufacturing defects

19.2.2.1 Porosity

[Porosity](#) is also referred to as resin voids and void content. It usually occurs as a result of the application of pressure too late in the cure [cycle](#), causing entrapment of air or vapour. The resulting porosity usually occurs throughout the [lay-up](#) rather than being confined to a restricted area.

Contamination by dust particles or other foreign objects increases the possibility of void nucleation. Resin-rich zones are also preferred sites for the formation of [voids](#). A high population of voids within the lay-up causes some reduction in the load-transfer capabilities of the lay-up, therefore affecting resin-dominated properties.

Voids act as reservoirs for moisture and can have a marked effect on the moisture-initiated changes in the overall properties of the lay-up. Porosity can occur in filament-wound components when correct procedures are not followed, for example insufficient resin applied to the yarn, over-rapid winding or incorrect curing. The presence of these voids can cause changes in the mechanical and environmental properties of the composite.

19.2.2.2 Prepreg gaps

A sheet of unidirectional [prepreg](#) is produced by rolling and flattening several [bundles](#) of fibres which are then impregnated with resin. Damage or inadequate monitoring of this process can result in gaps in a fibre sheet or, less seriously, disturbances in the fibre direction. These gaps in as-delivered prepreg are identified by quality control procedures both by the producer and the user, so, in practice, tend not to be a major problem.

19.2.2.3 Contamination

A laminate can become contaminated by the incorporation of:

- dust, [See also: Porosity],
- oils or greases,
- solvents, or
- solids.

Such contaminants are normally controlled by strict cleanliness procedures. The two types of contamination that need particular consideration are:

- Sharp solid debris: Such as metal [swarf](#) which could, if incorporated into a laminate, cause significant fibre cutting and local damage.
- Prepreg [backing sheet](#): Small pieces can be left when the prepreg is cut to shape. Where backing sheet is present between plies, no bonding occurs, with a consequent drastic local change in laminate properties.

19.2.2.4 Fibre alignment

During [prepreg](#) manufacture and handling, fibres can become detached from the prepreg and form either into [whorls](#) (during prepreg manufacture) or mis-oriented fibres (during [lay-up](#) or in the prepreg). These affect the local properties of the laminate and introduce stress raisers and resin-rich areas which provide preferential void-formation sites. Whorls are coils of fibre that form in the prepreg sheet. They occur at the end of prepreg production runs and are rarely encountered. Mis-oriented fibres are usually caused by the prepreg 'tack' or stickiness causing fibres to be dragged during lay-up operations.

19.2.2.5 Lay up order

The number of plies and their relative orientations are determined by the stipulated design strength and stiffness of a laminate. The same is true for the number and winding angle of layers in a [filament-wound](#) item. It is possible for a particular layer to be either laid or wound at the incorrect angle to the other layers, or even to be omitted altogether. If either of these faults occurs, the properties of the laminate do not meet those stated in the design.

19.2.2.6 State of cure

State of cure describes the final state of the resin:

- determined by [cure cycle](#), and
- affected by variations in resin chemistry.

Both of these are significant in the final properties of the composite. The cure cycle is rarely the cause of faulty laminate production, because procedures can be readily established and automatically monitored. These procedures come from extensive development programmes using both non-destructive and mechanical testing. Variations of resin chemistry within a single prepreg sheet can be assumed to be very small; although significant variations between [batches](#) have been found for some types of resins. Prepreg properties are usually within the tolerances laid down by the prepreg supplier. Such tolerances are taken into account when designing with the prepreg. Although the chemistry of a resin changes throughout storage - prepreg 'life' - the most rapid changes occur during

the cure cycle. Consequently to obtain a consistent chemistry throughout fabrication, it is necessary to ensure even curing in terms of temperature and pressure distribution.

There is no practical non-destructive means of checking the state of cure. Furthermore, destructive quality control samples taken from peripheral test areas cannot ensure uniformity across a laminated sheet.

19.2.2.7 Local fibre/resin ratio variations

The manufacture of [prepreg](#) uses [tows](#) of fibres that are compounded with the resin. In some cases an uneven distribution of fibres throughout the resin can result. With a sample size of greater than 1 gramme, this variation is usually no greater than $\pm 2\%$ to $\pm 3\%$ of the nominal value.

19.2.2.8 Prepreg joints

The types of prepreg joint that can occur in any given layer are:

- End-to-end joints, where the joint is perpendicular to the fibre direction
- Side-by-side joints, which are parallel to the fibre direction.

End-to-end joints are not advisable, except possibly in the most uncritically stressed area of a component. There is a sharp discontinuity of stress transfer at the joint and the high mechanical properties of the fibre are lost. Joints parallel to the fibre direction are much less serious to the integrity of the fabrication. They are arranged so that the two pieces of prepreg butt exactly together:

- An overlap causes an extra ply to be formed locally with resin rich fillets.
- A gap results in a local lack of fibres and a resin rich area.

19.2.2.9 Inter-ply delaminations

Delamination [defects](#) are defined as the failure, for any reason, of two plies within a laminate to bond together. The most common cause is the inclusion of protective prepreg backing sheet during [lay-up](#), which results in a complete disbond or delamination, [See: Contamination]. Another cause can be entrapped air bubbles formed during lay-up over complex curved surfaces, [See also: Porosity].

[Delaminations](#) are particularly deleterious to a laminate as the:

- Whole basis of the strength and stiffness of the composite structure is modified, particularly with respect to compressive loads.
- Resistance of the laminate to [buckling](#) failure is severely reduced.
- [Fatigue](#) strength of the laminate is likely to be significantly affected; the delamination is a [crack-like](#) fatigue initiator.

In a [CFRP](#)-faced honeycomb structure, a delamination in one face skin locally reduces the interlaminar shear strength to zero. This introduces a degree of asymmetry which affects the stability of the whole sandwich structure.

19.2.2.10 Skin to core debonding

This is a particularly deleterious defect that affects composite-skinned honeycomb sandwich panels. The mechanical properties of the panel are seriously degraded in the region of the disbond, particularly with respect to buckling failure. A [debond](#) can be caused by:

- Contamination of, or damage to, the film adhesive used to join the [face skin](#) laminate to the core
- Contamination of the face skin laminate itself
- Contamination of the bond area of the core
- Mechanical damage to [core](#) cell walls, by crushing or more local damage.

A face skin bonded to a crushed core, such that an indentation is formed in the skin, produces a shift of the neutral axis with consequent changes in stability and bending stiffness.

19.2.2.11 Resin microcracks

Microcracks can be caused during the cure cycle or by subsequent thermal cycling. Resin-rich zones are preferred sites for the nucleation of cracks within the resin but they can be created throughout the whole cured laminate. Owing to the nature of [CFRP](#) composites, a differential stress is inherent in the material and it is believed that [microcracking](#) is the mechanism by which this stress is relieved. As the resin is a plastic, the rate of loading affects the strain at which the resin breaks. Therefore rapid temperature changes are more likely to cause microcracks than slower temperature variations.

Resin starvation can give rise to [microcracking](#) in the direction of the fibres. Whilst resin microcracking is essentially a [defect](#) in the matrix, it can have either beneficial or adverse effects depending on the intended use of the composite. There are instances where the presence of microcracks provides stress relief in the composite, thus providing a beneficial effect, [See: [18.6](#)].

19.2.2.12 Damaged honeycomb core

The types of damage that can occur in the honeycomb core are:

- Crushing damage, where the cell walls are depressed such that there is a depression in the honeycomb surface. The result of such a depression is at best a thickening of the [bond line](#) between the skin and the core and, at worst, a total disbond in which skin, adhesive and core never make contact
- Forming damage, when the honeycomb is shaped over a curved mandrel. The desired gradual curvature sometimes becomes disrupted by the excessive deformation of a single line of cells. This causes a discontinuity in the surface, which again causes bond line thickening or possibly a disbond.

19.2.2.13 Misplaced potting compound

Where fixings are used in a honeycomb sandwich panel, the crushing strength of the panel is locally increased by filling the honeycomb cells with a [potting compound](#). This is normally done before integration of the face skins with the [core](#). It is possible that the potted region can be wrongly positioned such that, in the extreme, the fixing misses the strengthened area altogether. It is therefore necessary to determine the position of the potting before fixing takes place.

19.2.2.14 Edge member debond

There are two types of [edge member](#):

- Structural, and
- Non-structural

Structural edge members are designed to join composite honeycomb sandwich components to other parts of the structure. The joint between the honeycomb sandwich and the edge member can transfer the loads from bolts, rivets or adhesive joints and distribute them throughout the face skins. The shear components of these loads are transferred from the edge member to the honeycomb core by means of an adhesive bond lying parallel to the core cell walls. This bond is usually made by means of a foaming adhesive. Defects in the bond usually involve large voids (or to a lesser extent distributed [porosity](#)) in the adhesive layer. The layer can be several millimetres in thickness and several hundred millimetres in lateral extent. There is thus the possibility for large [voids](#) to occur. The presence of these voids affects the load transfer and stress distribution properties of the composite.

Non-structural edge member are provided for cosmetic and handling protection purposes and are used on free edges only. Commonly known as 'edge-closeouts', they usually consist of vented tape or foamed plastic. They have little effect on the performance of the composite. The tape edge member can reduce surface quality and can have a detrimental effect on a paint finish. The foamed plastic avoids both these problems but does incur a mass penalty.

19.2.3 Detection of defects

Most manufacturing damage is detected by routine quality inspection. Acceptance/rejection criteria are used during inspection of the part to determine whether it is fit for purpose. Damage that is deemed acceptable is included in the test and analysis program of the structure to demonstrate strength and durability with the damage present.

Rogue defects or damage that is smaller than the maximum acceptable limits are not always detected. The possible existence and size of such flaws or damage should be assumed as part of the damage tolerant design process [See: Chapter [33](#)].

19.3 Service threats for composite structures

Besides defects related to manufacturing [See: [19.2](#)], there are always potential risks of damage from:

- handling,
- assembly,
- in-service operation, e.g.:
 - low velocity impact damage from tooling,
 - high velocity impact by micrometeorites or debris,
 - environmental damage in flight,
 - structural overload or overstressing,
 - chemical contamination,
 - thermal and mechanical fatigue.

The most common installation and in-service damage events can be classified under 'impact'. Such risks for composite structures can be numerous with a many variables such as the geometry of the impactor, the energy of the impact event, the frequency of impact events and the environmental conditions. These parameters are often not well defined until service data is collected.

In-service damage often occurs randomly and the type of damage, its location, size, and frequency of occurrence can only be predicted statistically. In-service damage is typically defined as non-detectable (non-visible) or detectable (visible). Components or structures are designed so that non-visible damage can be tolerated for the life of the structure. The most common in-service damage is due to impact events.

High-speed meteoroids and space debris are a growing hazard for orbiting space missions with the possibility of hypervelocity impacts. The combination of these impact risks and the wide use of composites raises concerns for the operational integrity of current spacecraft.

This large number of potential events are further combined with aspects of the structure's status:

- The condition of the structure at the time of the event.
- Material properties, e.g. fibre type, fibre forms, ply orientation, matrix material, laminate configuration.
- The response of the structure to the event.
- The history of the structure.

Together, these can greatly increase costs for validating structural integrity under all potential conditions.

In composites, the main damage features of hypervelocity impacts are matrix and fibres breaking under compressive and tensile loads, together with plies delaminating (or peeling) under shear loads

The detection of damage during launch preparation is more difficult than in manufacturing, so [damage tolerance](#) methodologies should include such events.

[See: Chapter [20](#) for further descriptions of the operating environments for space equipment]

19.4 Impact behaviour of laminates and sandwich constructions

19.4.1 General

Damage of composite components and structures due to impact can vary greatly in severity. The damage mode also varies between laminates and [sandwich](#) constructions.

In laminates, damage can occur in the matrix or fibre up to the level of failed structural elements and the failure of bonded or bolted attachments. The extent of the damage caused by the impact event determines the residual strength and fatigue behaviour and is crucial to [damage tolerance](#).

During the impact of a projectile with a sandwich panel, the panel is subjected to structural deformation as well as localised deformation around the point of impact.

19.4.2 Laminates

19.4.2.1 General

The various forms of impact damage observed in laminates are shown schematically in Figure 19.06.1, Ref. [19-3]. Included are expressions for the energy needed to cause them, typical energy values for 2 mm thick [CFRP](#) and the likely area of damage caused.

It can be seen from the effects of geometry that:

- [Delaminations](#) are more likely with short spans, thick laminates or laminates with low interlaminar shear strength.
- Flexural failures are more likely with large spans or thin skins.
- Penetration is most likely for small projectiles moving at such a high velocity that the laminate cannot respond quickly enough in flexure and hence generating high stresses close to the point of impact.

For laminates, an impact event can cause damage that includes:

- Fibre breakage
- Matrix damage
- Delamination and debonds

CFRP 2mm thick

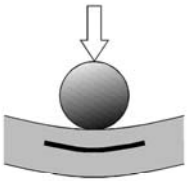
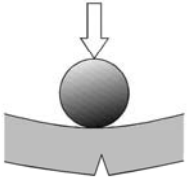
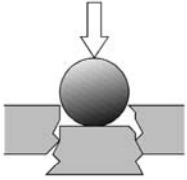
	Energy	Energy	Damage Area
a) Delamination 	$\frac{2}{9} \frac{\tau^2}{E^f} \frac{wl^3}{t}$	0.3J	150 mm ²
b) Flexure 	$\frac{1}{9} \frac{(R^{fu})^2}{E^f} \frac{wtl}{t}$	1.5J	20 mm ²
c) Penetration 	$\pi \gamma t d$	3J	40 mm ²

Figure 19.4-1 - The primary failure modes of composite laminates under impact loading

19.4.2.2 Fibre breakage

Fibre breakage can be a critical failure mode because structures are typically designed to be fibre dominant (i.e. fibres carry most of the loads). In many instances failure is typically limited to an area near the point of impact, and is constrained by the impact object size and energy, Ref. [19-6].

19.4.2.3 Matrix damage

Matrix damage, such as cracking, usually appears at the matrix-to-fibre interface or in the matrix parallel to the fibres. These cracks can reduce mechanical properties but are not usually critical to the structure. They can become critical when the matrix degradation is widespread and the accumulation of cracking causes degradation of matrix-dominated properties.

For fibre dominant laminates, a small reduction in properties is observed when the matrix is severely damaged. However, matrix cracks can significantly reduce characteristics that are dependent on the resin properties or the fibre/resin interface, e.g. interlaminar shear or compression strength. There is always the possibility that matrix imperfections could develop into delaminations, which are a more critical damage type.

19.4.2.4 Delamination and debonds

Delaminations form at the interface between the layers in the laminate and can form from matrix cracks growing into these layers or from low energy impact events.

Debonds can also develop from poor adhesion between two elements during manufacturing, initiating delamination in adjacent laminate layers. Delaminations or debonds can grow under certain conditions when subjected to cyclic loading and can subsequently cause catastrophic failure if the laminate is loaded in compression.

The severity of a delamination or debond depends on:

- Dimensions of the delamination or debond.
- Number of delaminations at a given location.
- Location, including:
 - in the thickness of laminate,
 - in the structure,
 - proximity to free edges,
 - stress concentration,
 - region,
 - geometrical discontinuities.
- Loads – the behaviour of delaminations and debonds depend on the loading type. They have little affect on the response of laminates loaded in tension. Under compression or shear loading however, the sub-laminates adjacent to delaminations or debonded elements can buckle causing load redistribution and leading to structural failure.

19.4.2.5 Combinations of damage

In many instances impact events cause combinations of damage. For example, high-energy impacts by large objects can lead to broken elements and failed attachments. The resulting damage can include significant fibre failure, matrix cracking, delamination, broken fasteners and debonded elements. Damage caused by low-energy impact is more contained, but can also include a combination of broken fibres, matrix cracks and multiple delaminations.

Most types of impact damage affect mechanical properties. This generally includes significant reductions in static strength as well as detrimental effects on fatigue properties and environmental resistance. For load bearing applications, the design requirements are related to the possibility of impact damage and the potential effects on performance. Significant improvements in impact performance are being made through the use of hybrid reinforcements and by modifications to structural designs, amongst other things.

[See: [19.6](#) for descriptions of the impact damage mechanisms and some guidelines on design-relevant features]

At first glance the major damage mechanisms (matrix cracking, debonding and fibre failure) can appear relatively simple when considered in isolation. However, these individual failure modes combine with other features, such as:

- fibre type,
- matrix type,
- laminate lay-up,
- environmental degradation,

- the condition of the fibre to resin bond,
- load conditions.

This creates a complex set of parameters to be taken into account when considering residual strength after impact and potential failure.

19.4.3 Sandwich panels

Impact damage to composite [sandwich](#) structures caused by foreign objects can result in significant reductions in strength, modulus and durability. Hence the [damage tolerance](#) of the system can be compromised by local damage to the facings, core, and core-facing interface.

In general, the material in the core of sandwich constructions largely dominates the impact characteristics. The damage size depends on the properties of the core material and the relationship between the properties of this and those of the facings.

The severity of foreign object impact damage on sandwich composites depends on many factors, including:

- manufacturing processes,
- facing laminate lay-up and thickness,
- core material and thickness,
- strength of the bond between facing and core,
- impact velocity and energy,
- indenter/foreign object shape,
- temperature at time of impact,
- structural loading conditions,
- environmental factors, e.g. thermal history, humidity.

Following impact on [sandwich](#) panels with foamed cores, core-to-facing debonds can occur around the impact site and the core can be permanently deformed. Cracks in the foam core are likely to result from low-energy impacts. In high energy impacts the core is generally compressed under the impact site. An understanding of the core-to-facing mechanical properties is important in order to understand the effect of impact damage on the residual property responses of sandwich composites.

19.5 Impact behaviour

19.5.1 General

Since structures function in environments where they can potentially be damaged by impact events, regular inspections or detection methods should be implemented so that the structure can be repaired before catastrophic structural degradation or failure occurs. The design should where possible use

multiple paths for load bearing paths so that other structural members carry some or all of the load from damaged members. Owing to mass limitations this should be achieved without unnecessary duplication or overdesign of the structure. This subject is discussed in more detail under design allowables [See: 3.9, Chapter 37].

If an impact results in visible damage, this can be seen during inspection. If it occurs on a composite structure, then the appropriate remedial action can be taken.

[See also: Chapter 41 for repairs]

19.5.2 BVID

Of significant concern is the damage that could go undetected or is 'barely visible'. This is often referred to as 'barely visible impact damage' or BVID.

BVID can grow significantly in service through fatigue loading and environmental conditions and can eventually lead to structural failure. In this type of damage, delaminations are often not visible even though there can be significant internal damage to the laminate, as shown in Figure 19.5.1, Ref. [19-3]. The damage is often more severe towards the back face of the laminate, making detection more difficult.

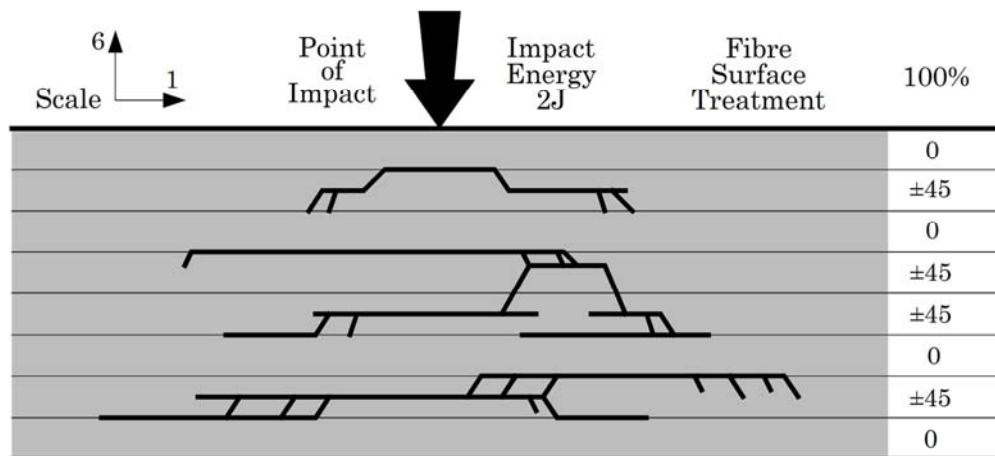


Figure 19.5-1 - Multiple delaminations in a [(0₂, ±45)₂]_s CFRP laminate caused by drop weight impact

Thicker laminates cannot always respond by flexing and impact causes front surface damage, rather like erosion damage by small particles. If the particle has sufficient energy to penetrate a thick laminate, the features are usually:

- Front face damage to a depth of approximately half the thickness, and
- Delamination in the rear half of the laminate, due to flexural response, as shown in Figure 19.6.2, Ref. [19-3].

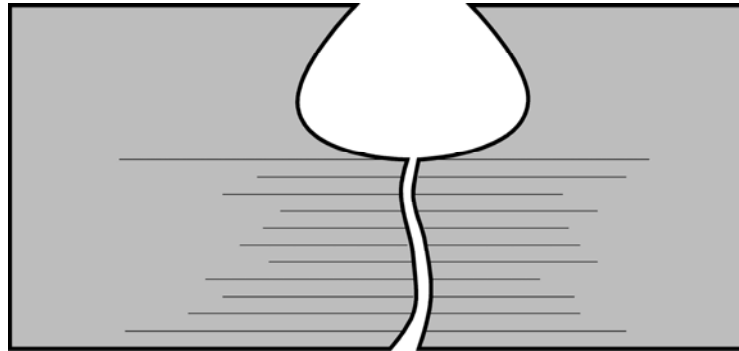


Figure 19.5-2 - Impact damage in a 64-ply CFRP laminate caused by high velocity impact

Impact studies on composite structures incorporating features such as stiffeners showed that:

- Impact on the middle of the bay needed between 30 Joules and 50 Joules of energy to cause BVID because of the relatively large area of material being deformed.
- Near a stiffener, where a flexural response was limited, only a few Joules were needed. Stiffeners also altered the local response of the panel so that the observable damage was sometimes centred to one side of the point of impact or even away from the impact site.

To minimise costs in service, inspection techniques, [See: Chapter [34](#)] analysis should be carried out to calculate inspection intervals for each part of a structure. This needs a clear understanding of:

- damage threats,
- how rapidly damage grows,
- the likelihood of detection of the damage,
- the allowable damage sizes that do not threaten the structure.

In order to avoid the costs associated with unnecessary repairs, inspection methods also need to quantify structural degradation to support strength assessments.

[Damage tolerance](#) is the concept of combining:

- inspection plans,
- knowledge of damage threats,
- damage growth rates,
- residual strength.

[See: Chapter [33](#)]

Cyclic mechanical testing and analytical methods are used in damage tolerance calculations to determine inspection schedules that discover damage before it causes structural failure.

19.5.3 Impact tests

Traditionally, impact tests such Izod and Charpy have been used to indicate the impact toughness of quasi-isotropic materials. They have yielded useful information on notch effects and the ductile-to-brittle transition temperatures. However, owing to the complexity of composite failure processes, such tests are only of limited value for composite materials. They give no indication of residual properties after impact.

The Izod and Charpy impact tests are typically performed on plastic and metallic materials. The Izod test uses a notched rectangular sample. One end of the specimen is held in a clamp as a vertical cantilever, impacted by a weighted pendulum on the same face as the notch at a fixed distance above the notch and clamp. The energy lost by the pendulum during impact is measured and the Izod impact strength is then calculated.

The Charpy test also uses a notched rectangular bar and the specimen is supported as a horizontal simple beam and is broken by the pendulum in three-point loading. The impact site being midway between the supports and directly opposite the notch. The test procedure can be used on test samples with differing notch radii to study the notch sensitivity of the material. The unnotched impact strength of the material can also be assessed.

However, neither the Izod or Charpy tests are particularly appropriate for use with continuously-reinforced composite materials.

Drop weight tests (simulating dropped tools) and ballistic tests (simulating foreign object impact) are more common for composites. Impact using falling weight testing is part of the CAI compression after impact test where a flat panel is impacted at 90° to its surface. Typically a 12.7mm to 25.4mm diameter hemispherical indenter is used. The falling weight used for CAI testing is usually dropped from a few metres giving a relatively low velocity impact and the mass used is typically 5kg to 10kg. Other systems for low velocity tests include pendulum systems and servo-hydraulic actuators. If very low velocity impacts are to be studied, a long fulcrum pendulum can be used to impact the test samples.

The velocities associated with high-speed meteoroids and space debris are not simulated in this type of test. However, test rigs are available that include secondary accelerating mechanisms such as elastic cords, springs or pneumatic systems to obtain higher velocities as well as high-pressure pneumatic systems to obtain ballistic velocities.

Quasi-static indentation tests can also be performed. These typically involve mounting a test sample (usually a flat plate) in a support frame and testing in a universal-testing machine. An example of such a test is given in ASTM D6264. The load and crosshead displacement is typically measured during the test. The test is stopped when a predefined level of damage or crosshead displacement is reached. The depth of the indentation and the extent of the damage are then evaluated.

Other program-specific tests can be included in a test schedule to more closely simulate the actual events expected in the lifetime of the structure.

Whichever impact test method is used, an assessment of the damage is performed after impact and before further testing such as the CAI test.

It is important to understand the nature and size of the impact damage in order to be able to obtain accurate data for [damage tolerance](#) evaluation. Damage assessment can include:

- measurement of the depth of the indentation.
- measurement of the size of the visible damage.
- non-destructive evaluation for internal damage or BVID.

Once this has been evaluated, additional mechanical tests can be performed.

19.5.4 Compression after impact (CAI)

The CAI compression after impact test is an evaluation of the reduction in laminate compressive strength after an impact event. It is often referred to as a '[damage tolerance](#)' test.

The CAI tests were developed to enable candidate composite materials to be assessed for their the damage tolerance [See also: Chapter [32](#)]. The impact event before CAI testing is generally at a relatively low velocity and it is not commonly used to investigate damage tolerance to ballistic events Ref. [\[19-5\]](#).

19.6 Detection of defects

[For repair of defects, See: Chapter [41](#)]

19.6.1 Damage detection techniques

Delaminations can be detected by ultrasonic techniques. C-scans give a silhouette of the damaged areas. A-scans or B-scans provide information on the depth of the damage.

Complex ultrasonic-based inspection systems are used to inspect aerospace structures, such as large subassemblies of the Joint Strike Fighter aircraft, Ref. [\[19-5\]](#).

Useful information on impact damage can also be obtained with X-rays, but the technique uses a radio-opaque dye to penetrate the damaged region, which is not always desirable.

There are now a wide range of inspection systems based on a variety of principles; each performs a different function. In broad terms, the techniques can be grouped as being applicable to:

- laboratory (L) and production (P) environments for the examination of components and assembled structures.
- in-service (S) environments for the examination of fully assembled structures.

[See also: Chapter [34](#)]

19.6.2 Laboratory and production based NDT

For components and assembled structures, the techniques available include:

- Portable conventional and air-coupled ultrasonics, [See: [34.10](#)].
- Eddy currents, [See: [34.18](#)].
- Laser shearography, [See: [34.14](#)].
- Thermography, [See: [34.15](#)].

19.6.3 Other techniques

Techniques that provide a supporting role include:

- Visual inspection, [See: [34.9](#)].
- Coin tapping, [See: [34.9](#)].
- Dye penetrants, [See: [34.9](#)].
- Resonance bond-testers, [See: [34.9](#)].
- Acoustic flaw detectors, [See also: [34.20](#)]
- Acoustic emission, [See: [34.11](#)].

Increased access to compact and powerful computing has encouraged the development of inspection systems that are integrated into structures to provide continual monitoring of thermal and strain responses. These systems are described as 'structural health monitoring', [See: Section XX], and can also be capable of in-service damage detection.

19.7 References

19.7.1 General

- [19-1] Fulmer Research Laboratories (UK)
'Guidelines for non-destructive examination (NDE) of advanced fibre composite materials for space applications'
ESA Contract 4389/80/NL/AU (SC)
- [19-2] R.J. Lee & D.C. Phillips
'The damage tolerance of high performance composites'
Composite Structures 1, Applied Science Publishers, 1981
- [19-3] G. Dorey: RAE (UK)
'Impact damage in composites - development, consequences and prevention'
- [19-4] ESA PSS-03-207: Guidelines for carbon and other advanced fibre prepreg procurement specifications.
Not currently under the ECSS document system.
- [19-5] Private communication (2003)
USL – [Ultrasonic Sciences Ltd.](#) (UK)
- [19-6] MIL HDBK-17

19.7.2 ASTM standards

[See: [ASTM](#) website]

ASTM D6264 Standard test method for measuring the damage resistance of a fiber-reinforced polymer-matrix composite to a concentrated quasi-static indentation force

20

Environmental aspects of design

20.1 Introduction

The Earth and space environments to be experienced by a spacecraft have to be considered fully during the design process.

Space structures are manufactured, stored and transported on Earth prior to launch, hence a controlled environment is necessary to minimise contamination, e.g. by moisture, which can degrade materials or promote [galvanic corrosion](#) between [CFRP](#) and contacting metals.

In space, the conditions experienced can degrade the properties of polymer composites. The extent of property loss depends on the duration of exposure, as well as the severity of the environment. Problems of this type are more significant for long-term deployed structures; especially when the design life extends towards 30 years.

In addition to their widespread use in [GEO](#) - geostationary earth orbit environments, composite structures are increasingly destined for use in [LEO](#) - low earth orbit. Here they are subject to aggressive attack by atomic oxygen ([ATOX](#)). Long-life composite structures can need specific protection against the more aggressive occurrences, e.g. from ATOX, impacts from debris and meteoroids.

The effects of environments on the properties of composite materials are described, [See also: [20.2](#)].

Design guidelines are provided which aim to avoid common environmental-related problems and appropriate materials requirements standards are cited, e.g. [ECSS](#).

For information on materials and process selection for space applications, [See also: [ECSS-Q-ST-70](#); [ECSS-Q-70-71](#)].

20.2 Description of environments

20.2.1 Earth environment

In general, space structures are manufactured and then spend a certain amount of time on Earth before being launched into space to encounter different [space environments](#).

The effects of temperature, moisture and various forms of organic attack can be controlled by appropriate materials selection, adequate design and by ensuring that transportation and storage takes place under well-defined conditions, Ref. [\[20-43\]](#).

Exposure to moisture is possible during storage and integration of the launcher and payload. Moisture contamination can also occur if a launch is aborted.

Materials selection is therefore influenced by the need to control:

- Moisture absorption for dimensionally stable structures,
- Galvanic corrosion in the presence of moisture or fuels,
- Stress corrosion cracking, [SCC](#), of [light alloys](#).

20.2.2 Space environment

After launch, a structure is subjected to a variety of environmental effects, such as, Ref. [\[20-1\]](#):

- temperature,
- vacuum,
- radiation,
- micrometeoroids, and
- debris.

The two most common Earth orbits are:

- [LEO](#) - low Earth orbit, and
- [GEO](#) - geostationary Earth orbit.

It is important to differentiate between LEO and GEO orbits, because the environments differ, [See: [20.3](#); [20.4](#)].

Some of the effects of space environmental factors are summarised in:

- [Figure 20.2.2](#) for radiation, Ref. [\[20-1\]](#).
- [Figure 20.2.3](#) for temperature, Ref. [\[20-1\]](#).
- [Figure 20.2.4](#) for micrometeoroids and debris, Ref. [\[20-1\]](#).
- [Figure 20.2.5](#) for atomic oxygen ([ATOX](#)), Ref. [\[20-1\]](#).
- [Figure 20.2.6](#) for re-entry, Ref. [\[20-1\]](#).

NOTE Not all of these environmental factors relate to composites.

The space environments are not overly aggressive, but materials are evaluated to ensure adequate performance under a variety of combined conditions.

Such data is sparse, so specific testing is necessary. Despite this, reliable configurations for long-duration missions are feasible.

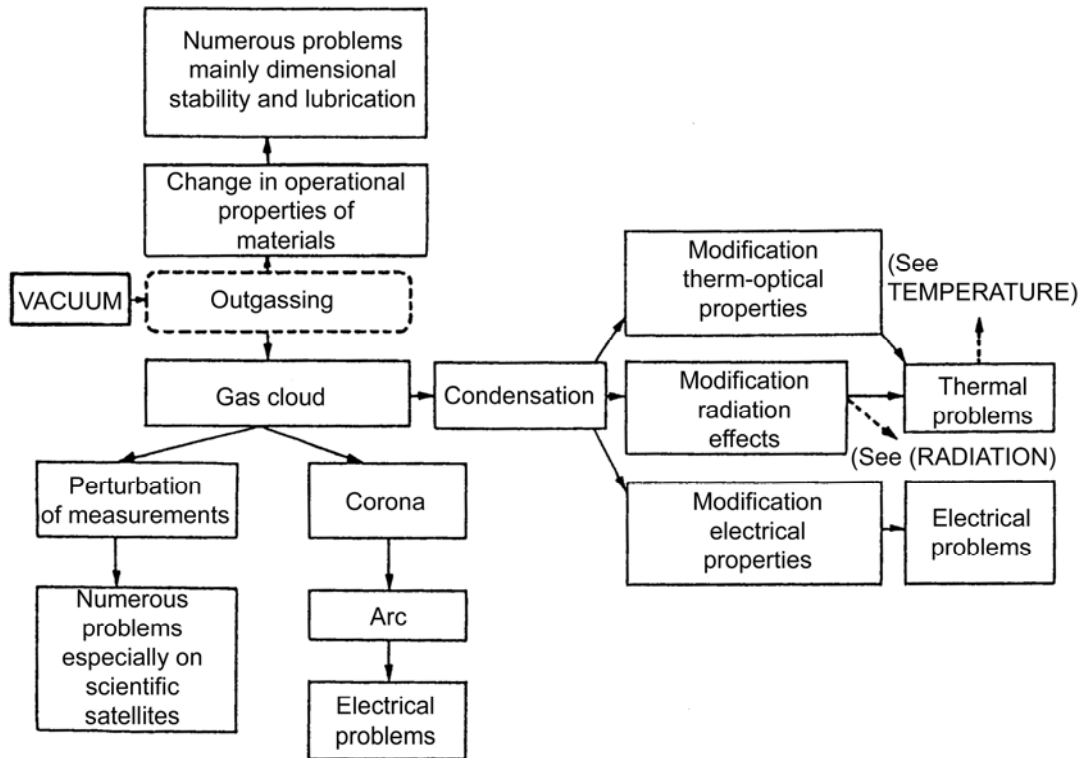


Figure 20.2-1 - Space environment effects: Vacuum

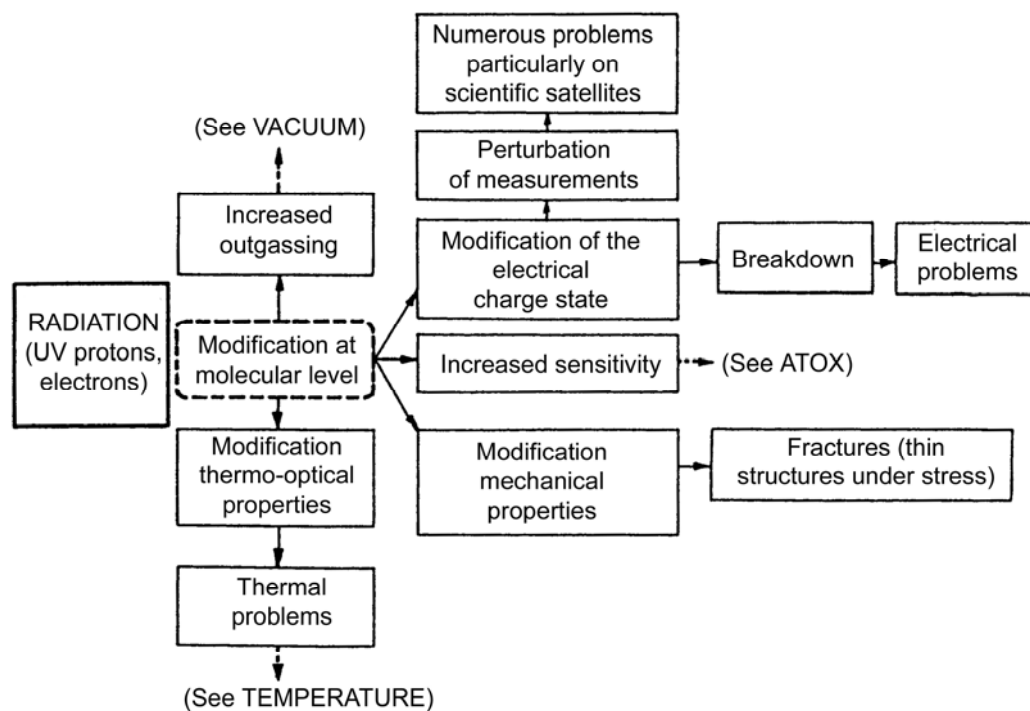


Figure 20.2-2 - Space environment effects: Radiation

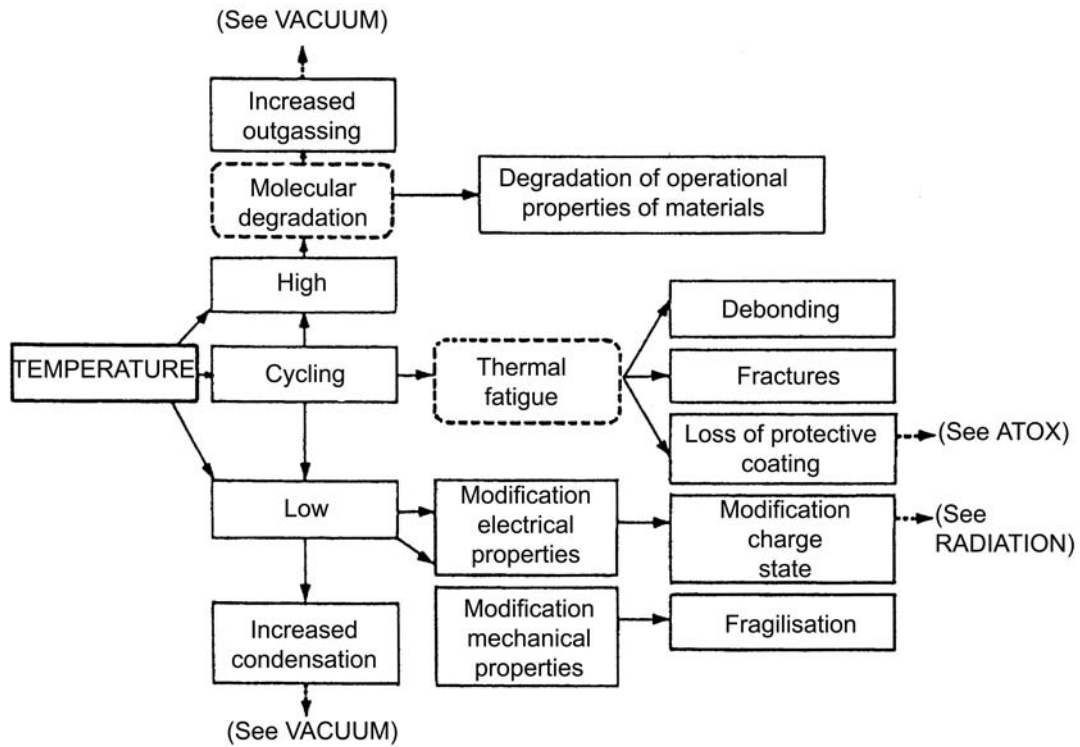


Figure 20.2-3 - Space environment effects: Temperature

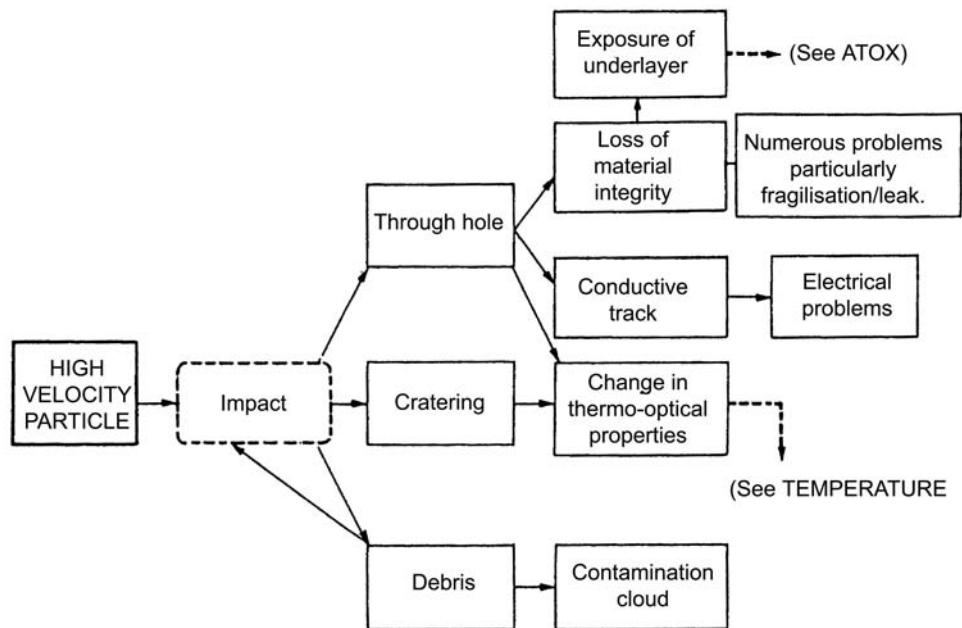


Figure 20.2-4 - Space environment effects: Micrometeoroids and debris

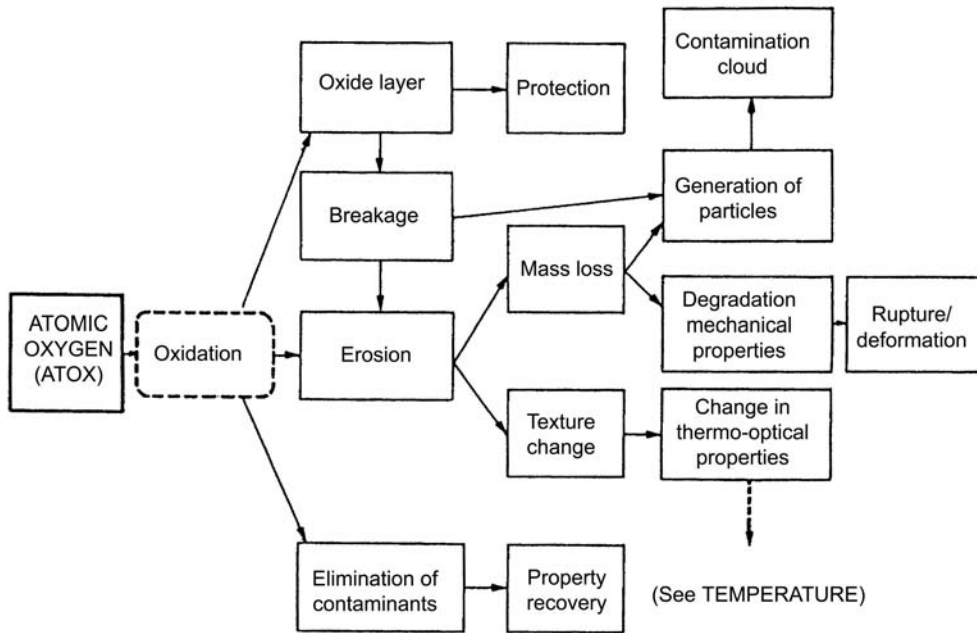


Figure 20.2-5 - Space environment effects: Atomic oxygen (ATOX)

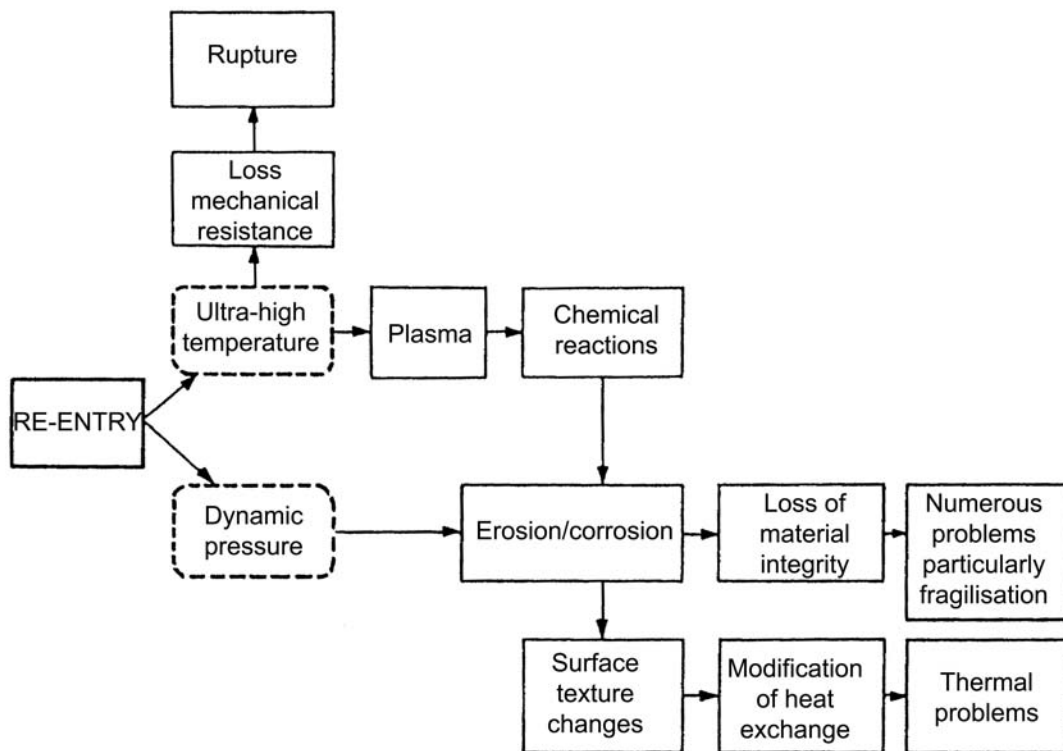


Figure 20.2-6 - Space environment effects: Re-entry

20.2.3 Composite structures

20.2.3.1 General

The significance of the effects of operating environments varies with the function, orbit and design life of different structures. The broad classifications of structures and environmental concerns are:

- Structural load-bearing; guaranteeing the mechanical integrity of the composite, particularly for man-rated structures.
- Dimensionally stable, including the stability of physical properties, e.g. [CTE](#).

[See also: [ECSS-Q-ST-70](#) and [ECSS-Q-70-71](#)]

20.2.3.2 Temperature range

Temperature changes have significant effects on structures because of the wide range typically experienced. This temperature range is more severe in [GEO](#), compared with [LEO](#), although in LEO the cycling is more rapid giving a greater number of cycles in a given period. Additional cooling effects can arise from stored [cryogenic](#) fuels or helium.

Although there are ways of controlling the temperature range experienced by satellites, thermal cycling remains a significant problem, [See also: [20.9](#)].

At low temperatures, the resin matrix can suffer from embrittlement, and at high temperatures the resin can soften and [creep](#). In both cases, strength is reduced and the elastic properties of the composite are changed.

[Microcracking](#) damage, caused by [thermal cycling](#), remains a major problem, as this modifies the thermal expansion ([CTE](#)) characteristics of the composite.

20.2.3.3 Elevated temperature and vacuum

Under these combined conditions, the matrix resin [outgases](#) to some extent, causing:

- condensation of volatile organic species on optical equipment, which can seriously degrade their performance,
- degradation of the mechanical properties of the composite.

These can be controlled by the correct selection of materials, [See also: [20.10](#); [ECSS-Q-ST-70](#) and [ECSS-Q-70-71](#)].

All polymeric composites have a maximum permissible operating temperature, which takes into account the degradation mechanisms that should be avoided or minimised in service.

20.2.3.4 Ultraviolet radiation

[UV](#) radiation affects the physical properties of resins by causing increased [cross-linking](#) in the polymer. This produces a higher strength and stiffness, but also makes the resins more brittle. UV effects are usually insignificant for composites as they are surface effects; the fibres screen the bulk of

the resin matrix. Vacuum ultraviolet ([VUV](#)) degradation is a problem for thin polymeric films and ultra-thin composite sections, [See also: [20.11](#)].

20.2.3.5 Penetrating radiation

The effects of penetrating radiation, i.e. high energy protons and electrons (α - and β -particles), are considered to be largely insignificant for mission durations less than 7 years. It is recognised that a threshold dosage is reached before degradation, in the form of breaking of molecular chains (scission), occurs in a composite matrix. For [GEO](#), in particular, this threshold is reached before 30 years exposure, [See also: [20.11](#)].

20.2.3.6 Meteoroids and debris

General statements on the effects of meteoroids or debris impact are impossible, because they depend on many parameters, including:

- Mission specific factors, e.g. orbit, duration, required safety and orbit height, inclination and eccentricity. The required safety depends on the manned or unmanned rating.
- Impacting particle, e.g. velocity, size, density, impact angle and shape. Sharp, angular projectiles are more damaging than spherical particles. Shape is difficult to account for in impact modelling and design equations.
- Protection provided by the rest of the structure.

Assessment of the damage caused by such impacts is under review. The problem is particularly acute in [LEO](#) and for large, long duration, high-safety (e.g. manned) structures, [See: [20.16](#)].

20.3 Low earth orbit (LEO)

The environmental conditions in [LEO](#) are important to long-life structures, e.g. the [ISS](#) international space station and Columbus.

Vehicles operating in orbits between 400 km and 800 km altitude encounter:

- Temperature changes:
 - typically within the range -90°C to $+90^{\circ}\text{C}$,
 - ~ 16 cycles/day.
- Vacuum: in the range of 10^{-4} torr to 10^{-9} torr.
- Radiation:
 - principally vacuum ultraviolet ([VUV](#)),
 - some particle radiation (98% electron, 2% proton, from Van Allen belts).
- Atomic oxygen ([ATOX](#)).
- Meteoroid or debris impact.

Of these, atomic oxygen and debris impact are potentially the most destructive mechanisms. This was confirmed by experience from the [LDEF](#) programme, [See: [20.8](#)].

For [CFRP](#) composite space structure elements operating in [LEO](#), the polymeric matrix is the degradation-vulnerable phase.

Degradation can lead to significant changes in mechanical properties, [CTE](#) and, possibly, the thermal conductivity of the composite.

20.4 Geostationary orbit (GEO)

The environmental conditions in [GEO](#) are important to long-life telecommunication and Earth resources satellites.

Vehicles operating in orbits around 36000 km altitude encounter:

- Temperature changes:
 - typically -150°C to +120°C.
 - 1 cycle/day.
- Vacuum: in the range of 10^{-9} torr to 10^{-10} torr
- Radiation:
 - Trapped Van Allen belts, which contribute to the total radiation spectrum and are influenced by the magnetic field of the Earth.
 - Additional radiation sources include: galactic radiation, particle radiation from solar flares, but very little ultraviolet.
- Meteoroid or debris impact.

The precise orbit conditions depend on whether a structure is in GEO, [GTO](#) or polar orbit.

Thermal cycling and radiation damage are potentially the most damaging mechanisms for long-duration missions.

20.5 Deep space exploration

Deep space missions have different levels of environmental interaction, although the basic phenomena of temperature change, radiation, vacuum and micrometeoroids remain.

Other mission-specific conditions which can be encountered include:

- Comet debris, e.g. Giotto mission to Halley's comet.
- Planetary atmospheres: e.g. Mars, Saturn, Jupiter.
 - high temperatures, with
 - gaseous reactive chemical species.
- [Cryogenic](#) temperatures in the range of -180°C to -260°C
- Vacuum to 10^{-14} torr:

Where polymer composites are not exposed directly to these environments, i.e. they form part of an underlying structure, a protective shielding can still be necessary.

20.6 Galvanic corrosion

20.6.1 General

Galvanic corrosion can lead to the catastrophic failure of a structure and can occur where carbon fibres are used in mixed material constructions.

Some of the possible locations for galvanic corrosion to occur include:

- [CFRP](#) to metal bolted joints, e.g. aluminium
- Sandwich structures:
 - direct coupling of CFRP to aluminium, e.g. honeycomb [core](#).
 - contact between the [face-skin](#) and core or face-skin to [insert](#).
- Poorly bonded joints between CFRP and metal, e.g. aluminium
- Contact between [dissimilar metals](#).

[See also: Chapter [44](#) for magnesium; Chapter [46](#) for aluminium]

Most of the research into this problem has been carried out under typical aircraft structure environments. Therefore the extent and consequences of galvanic corrosion in the space environment need definition, Ref. [\[20-2\]](#).

[See also: [ECSS-O-ST-70](#) and [ECSS-O-70-71](#)]

20.6.2 Physical basis of galvanic corrosion

Galvanic corrosion occurs when two or more [dissimilar materials](#) are electrically connected, in the presence of a corrosive environment. A galvanic cell is formed, and the more anodic of the materials sacrificially corrodes away, leaving the cathodic material unaffected. The rate of attack can be much higher than that of the single material.

For a given environment the severity of the corrosion is controlled by the galvanic cell strength, which is given by the electrochemical difference between the materials in the galvanic series.

[Figure 20.6.1](#) shows an example of a galvanic series for some common materials in a 3.5% [NaCl](#) solution, Ref. [\[20-2\]](#). The actual electrochemical potential values depend on the details of the corrosive environment.

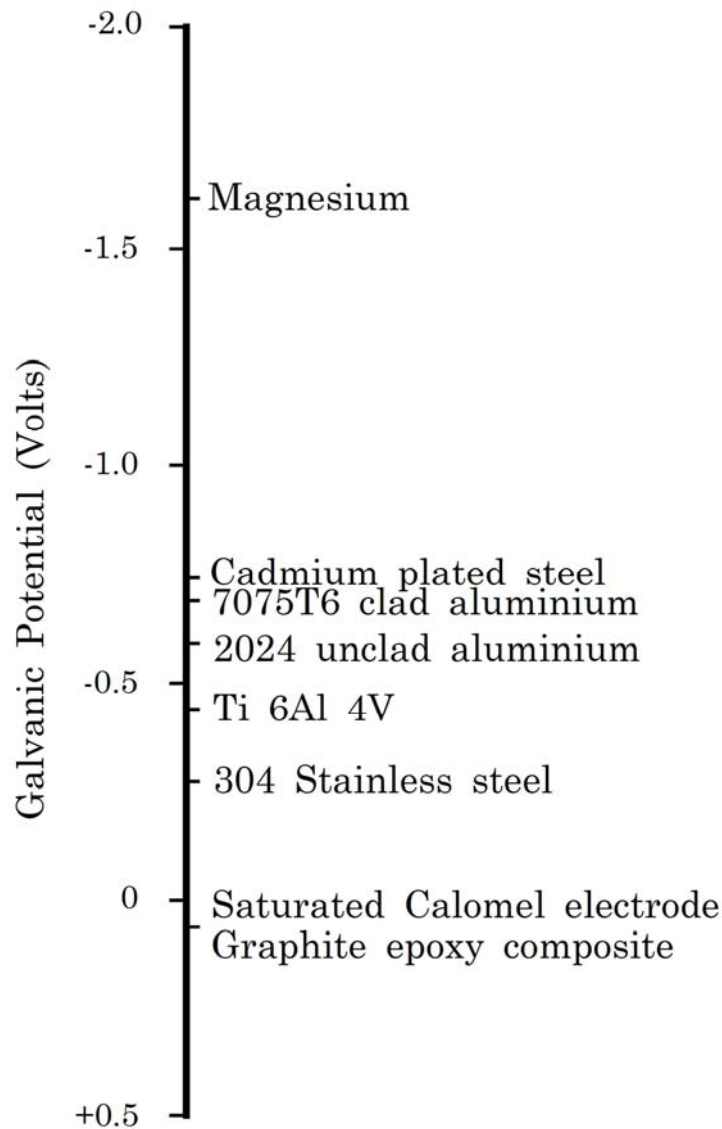


Figure 20.6-1 - Galvanic corrosion: Potential in 3.5 % NaCl solution

EXAMPLE, from [Figure 20.6.1](#):

Potential difference: Carbon fibre - Aluminium $\rightarrow \Delta U = 0.7 \text{ V}$

In practice, a great many physical, chemical and environmental variables play a part in determining the rate of galvanic corrosion for any particular situation.

20.6.2.1 Carbon fibre to metal connections

When carbon fibre composites are in electrical contact with metallic structures, in the presence of an [electrolyte](#), a galvanic cell is created. The highly cathodic nature of carbon, with respect to structural metals, results in carbon becoming the cathode and, for example, aluminium the anode. Under these conditions, the aluminium corrodes.

20.6.3 Prevention of galvanic corrosion in space structures

20.6.3.1 General

No specific studies have been conducted for the space environment, consequently, only general guidelines are given for unmanned structures, [See: [ECSS-Q-ST-70](#) and [ECSS-Q-70-71](#)].

20.6.3.2 Guidelines

Some general guidelines for avoiding galvanic corrosion in unmanned space structures include:

- Maintain a controlled environment (especially with respect to humidity) during manufacture, transportation and storage on Earth. Prevention of the initiation of an electrolytic cell under the special conditions of the space environment ensures that galvanic corrosion does not become a problem.
- After launch, outgassing as a result of [UV](#) radiation and contamination by organic materials (such as hydrazine) can provide the electrolyte for a galvanic cell between carbon fibre and metals.
- Corrosion control factors include:
 - insulation, e.g. special coatings to interrupt the galvanic cell,
 - reduction in cathode area, thus reducing the driving corrosion current,
 - use of corrosion inhibitors,
 - elimination of moisture,
 - minimising differences in galvanic potential between joined elements. Use materials with a minimum potential difference to carbon (less than 0.5V, if possible).

[See also: [ECSS-E-HB-32-23](#) for advice on avoiding galvanic corrosion in mechanically fastened joints]

20.7 Effects of moisture on composites

20.7.1 General

The main factors that influence aspects of design are:

- [Changes to coefficients of thermal expansion \(CTE\)](#) caused by [outgassing](#).
- [Low coefficient of moisture expansion \(CME\)](#) resins.
- [Combined hot/wet performance](#).

[See also: Chapter [13](#) for detailed information on moisture effects in composites]

20.7.2 Modification of CTE by outgassing

Absorbed moisture readily outgases in orbit. Its loss reduces the volume of the matrix and lowers the in-orbit CTE compared with that under controlled storage on Earth.

For many applications, dimensional changes are so small as to be insignificant. However, dimensional changes resulting from moisture content variations can cause problems where a configuration is calibrated on Earth and then placed in orbit. This problem is more severe with [aramid](#) composites than [CFRP](#), because aramid fibres absorb moisture whereas carbon fibres do not.

20.7.3 Low coefficient of moisture expansion (CME) resins

To counter the changes in physical properties caused by moisture absorption, low absorbency resin matrices are being considered for [dimensionally stable](#) structures, Ref. [\[20-3\]](#).

The older generation of resins, such as Fiberite 934 epoxy, are being superseded by resins which have a lower [CME](#) value.

The chemistry-types of low CME matrices are:

- [Thermosetting](#):
 - Epoxy: e.g. Ciba/Brochier M18, Cytec 950-1, Cytec Fiberite Cycom 5555.
 - Cyanate ester, e.g. YLA RS-3 and Fiberite 954-3.
- [Thermoplastics](#), e.g. [PEEK](#), [PEI](#).

Thermoplastics are not widely applied in space structures, largely because of existing investments in thermoset processing technologies and the low volumes of material used in the space industry, [See also: [40.7](#)].

[See also: [2.4](#); [6.35](#) for low CME resins; Chapter [13](#) for moisture effects on polymer composites]

20.7.4 Hot/wet performance

20.7.4.1 Epoxy resins

In aircraft construction, early composites had acceptable thermal performance but the epoxy matrices were brittle. In [prepreg](#) systems (from the mid-1980's), toughening additives were introduced to provide improved impact resistance. The resin formulations also had to retain the upper temperature performance when the cured resin was in a fully saturated state (moisture absorption). Examples of these improved 'hot/wet' epoxy resin systems include Fiberite 977-2 and Fibredux 924.

20.7.4.2 Cyanate ester resins

In addition to epoxies, [cyanate esters](#) are promoted to perform the same 'hot/wet' role, e.g. Fiberite 954-2 and Cycom 785. These systems tend not to be appropriate for use within dimensionally stable structures because they are not available in a prepreg form with [UHM](#) carbon fibres. They can be appropriate for launchers and reusable structures where thermal excursions are within the 130°C to 200°C range.

20.7.4.3 Others

Good 'hot/wet' performance can also be obtained from [bismaleimides](#) and some [thermoplastics](#).

20.8 LDEF in LEO

20.8.1 Mission

Between 1984 and 1990, the 'long duration exposure facility' ([LDEF](#)), a twelve-sided cylindrically shaped spacecraft, was placed in [LEO](#) for 69 months (5.75 years). The craft was built in the USA and was about 9m long, 4.3m in diameter and had a total mass of 10 tonnes. The main structure was made of 6061-T6 aluminium alloy with a mass of 3.6 tonnes. It was placed in orbit and retrieved by Space Shuttle missions. Over 10,000 material samples were carried on the 130m² space-exposed surface. The original mission was for one year but was extended after the loss of Challenger. During the 5.75 years, the orbit decayed from 480km to 340km.

The on-board experiments experienced harsh LEO conditions of combined vacuum, atomic oxygen ([ATOX](#)), ultraviolet radiation ([UV](#)) and [thermal cycling](#). Significantly higher ATOX concentrations were experienced in the last year as the craft neared the Earth's atmosphere; some 80% of the total exposure. Thermal cycles (32,422 at ~16/day) were endured by all materials and experiments.

The LDEF programme used the abbreviation AO to indicate experiments related to atomic oxygen, whereas ATOX is the accepted abbreviation within the European space industry.

[LDEF](#) was retrieved a few months before its decayed orbit resulted in re-entry and burn-up in the Earth's atmosphere.

20.8.2 Materials and experiments

20.8.2.1 General

The prolonged exposure to the [LEO](#) environment has provided extensive data on the ability of materials to withstand the harsh conditions. The materials exposed included:

- Structural materials, i.e. light alloys and composites,
- [MMC](#) materials,
- Polymer films,
- Adhesives,
- Lubricants,
- Seals.

The selection of the materials flown on LDEF was made in the late 1970s and early 1980s. The products chosen were those favoured by NASA and US aerospace companies at that time. Whilst some of these are no longer commercially available, the results reported indicate the performance of generic materials, in particular polymer composites, such as [CFRP](#).

20.8.2.2 Material performance

The detailed evaluation of results from LDEF continued some 5 years after retrieval. However, the overall conclusions indicate that considerable care is necessary when deploying polymers and polymer composites directly in LEO environments because of severe degradation.

The damage mechanisms relate to specific or accumulated degradation arising from:

- Surface erosion by atomic oxygen ([ATOX](#)).
- Prolonged thermal cycling.
- Impact damage from micrometeoroids and debris.
- Embrittlement by radiation.

The material performances observed are significant for intended space station operation. For such a construction, a 30-year design life is typical, i.e. equivalent to 175000 thermal cycles, some 5 times longer than LDEF.

20.8.3 Variations in exposure conditions

The precise location of experiments on [LDEF](#) determined the level of exposure to the principle modes of degradation, i.e.:

- [ATOX](#) flux,
- [VUV](#) dosage, and
- Impact particle flux.

The orientation of the sides of LDEF with respect to forward motion and the angle to incoming radiation means that comparison between different experiments included compensation for the different exposure levels, i.e. position on the craft. That said, the information gained was considerable. The different participating organisations assembled experiments covering a wide range of carbon, glass and boron fibre-reinforced composites with [thermoset](#) and [thermoplastic](#) matrices; as summarised in [Table 20.8.1](#), Ref. [\[20-5\]](#).

Table 20.8-1 – LDEF: Polymer composites

Row No.	Angle off RAM	ATOX flux $\times 10^{21}$ a/cm ²	VUV ESH $\times 10^3$	Experiment No.	Organisation	Materials
9	8	8.32	11.1	AO 134	NASA Langley	5208/T300, 934/T300, P1700/C6000, P1700/C6000, 930/GY70
				M0003-9	Lockheed	CE-339/T300, F263/T50, 934/T50, X904B/T50, E788/T50, 3501-5A/HMS, E788/C6000, 934/HMF176, CE-339/E-glass, F593/P75, 934/P75
				M0003-8	Boeing	934/T300, P1700/T300, PMR15/C6000
10	22	7.78	10.7	AO 054	TRW	Epoxy/E-glass
8	-38	6.63	9.4	AO 171	NASA-MFSC	934/HMS, 934/P75S, P1700/HMF, Epoxy/S-glass
				M0003-10	Lockheed	X904B/GY70, 3501-A/HMS, X904B/E-glass
				M0003-10	General Dynamics	X-30/GY70, CE-339/GY70, CE-339/P75S, 934/P75S, 934/GY70, P1700/W722, V378A/T300
				M0003-10	McDonnell Douglas	5208/T300, P1700/T300, PES/T300, PI/C6000
7	-68	3.16	7.2	M0003-10	Boeing	934/T300, 3501-6/AS, P1700/T300, PMR15/C6000, LaRC 160/Gr
12	82	1.2	6.9	AO 175	Rockwell	F178/T300, PMR15/C6000
				AO 180	University of Toronto	934/T300, 5208/T300, SP288/T300, SP328/K49, SP290/Boron
				AO 019	University of Michigan	5208/T300 interleaved with Kapton
1	112	0.06	7.5	AO 175	Rockwell	934/T300, LaRC 160/C6000
5	-128	0	8.2	P0005	Morton Thiokol	C/C and sundry polymer composites
4	-158	0	10.4	AO 054	TRW	Epoxy/E-glass
3	172	0	11.1	AO 138	Matra Espace	934/GY70, V-108/K49, V108/T300, V108/GY70, V108/G837

Key: AO and ATOX - Atomic Oxygen

VUV - Vacuum Ultra Violet

ESH - Equivalent Sun Hours

Figure 20.8.1 shows how the exposure conditions varied depending on the experiment location, Ref. [20-4]. Table 20.8.2 shows how this translated into exposure levels for selected experiments, Ref. [20-4].

The direction of craft motion (**ram**) is used as a reference direction. The leading edge experienced the highest atomic oxygen ATOX exposure (impacts/cm²). The ATOX exposure diminished with the relative angle of incidence to ram and the (12-sided) angle of craft surface. The trailing edge experienced no ATOX exposure.

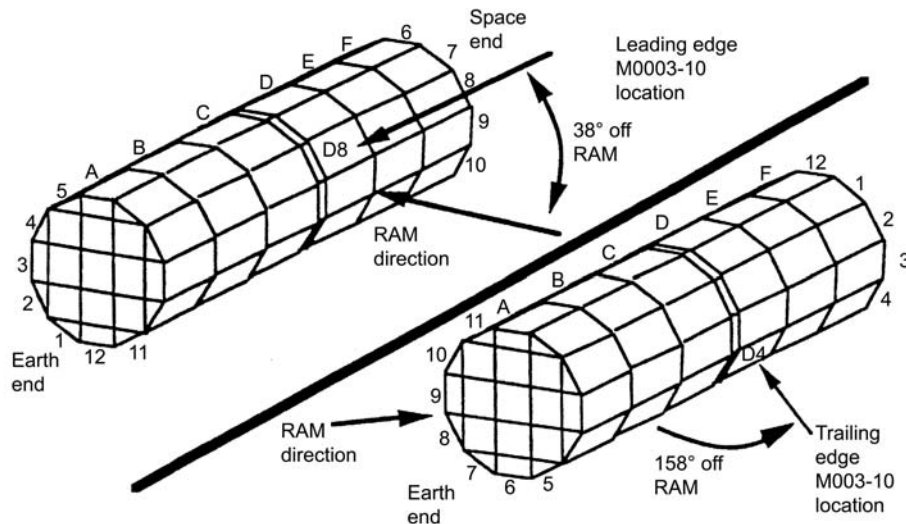


Figure 20.8-1 – LDEF: Experiment locations (M0003-10)

Table 20.8-2 - LDEF: Exposure levels

	Leading Edge “A-Deck” Row 8	Trailing Edge “A-Deck” Row 4	Leading and Trailing Edge “B-Deck”
ATOX Exposure (Impacts/cm ²)	6.93×10^{21}	9.32×10^4	0
Incident Solar and Earth Reflected Radiation (ESH)	9300	10500	0
Thermal cycling (as measured)	-47 to +84°C (32422 cycles)	-33 to +77°C (32422 cycles)	Not known

20.8.4 Composite materials aboard LDEF

A résumé of all of the polymer composites flown on LDEF is given in Table 20.8.3, Ref. [20-5]. The composites were prepared in many different laminate configurations. Composites from Matra Espace (France) were the only European sourced materials included, but were not exposed to ATOX because they were located on the trailing edge.

Table 20.8-3 - LDEF: Composite material classifications

Composite Class	Matrix/Fibre
First generation epoxy CFRP/high strength fibre	<u>5208/T300</u> , <u>934/T300</u> , 3501-6/AS, SP288/T300, V108/T300.
First generation epoxy CFRP/high modulus fibre	934/T50, 3501-5A/HMS, 934/HMS, F263/T50.
First generation epoxy CFRP/ultra high modulus fibre	930/GY70, <u>CE-339/GY70</u> , CE339/P75S, <u>934/P75S</u> , 934/GY70, V108/GY70.
Polysulphone (PS) thermoplastic CFRP	P1700/C6000, P1700/C3000, P1700/T300, P1700/HMF, P1700/W722.
Polyethersulphone (PES) thermoplastic CFRP	PES/T300.
Bismaleimide CFRP	V378A/T300, F178/T300.
Polyimide CFRP	<u>PMR15/C6000</u> , LaRC 160/C6000.
Glass fibre epoxy	CE-339/E-Glass, Epoxy/S-Glass.
Aramid fibre epoxy	SP328/Kevlar, V108/Kevlar.
Boron fibre epoxy	SP290/Boron.
Uncertain	F593/P75, X904B/T50 (Ferro), X904B/GY70, X904B/E-Glass, X-30/GY70, V108/G837, E788/T50.
Resin/fibre combinations shown in <u>bold, underlined</u> text were flown by more than one organisation and at different positions on LDEF.	

[See also: [Table 20.8.1](#) for [LDEF](#) experiment number, exposure conditions and originating organisation]

The general findings from selected [LDEF](#) experiments with respect to [ATOX](#) are discussed:

- [experiments M0003-9/10](#).
- [experiment AO 171](#).
- [experiment AO 180](#).

[See also: [20.9](#) for thermal cycling; [20.11](#) for radiation; [20.13](#) for general comments on atomic oxygen; [20.16](#) for micrometeoroid and debris impact]

20.8.5 LDEF experiments M0003-9/10

20.8.5.1 General

The experiments included over 250 polymer composite samples. The conclusions from the respective contributors are presented, Ref. [\[20-6\]](#).

20.8.5.2 The Aerospace Corporation

The conclusions can be summarised as:

- ATOX erosion depths varied between 38µm and 89µm; based upon mass loss measurements, as shown in Figure 20.08.2, Ref. [\[20-6\]](#).
- ATOX erosion depth is an inverse function of the fibre content of the [CFRP](#).
- Two types of ATOX erosion morphology were observed, probably related to fibre modulus or microstructure.

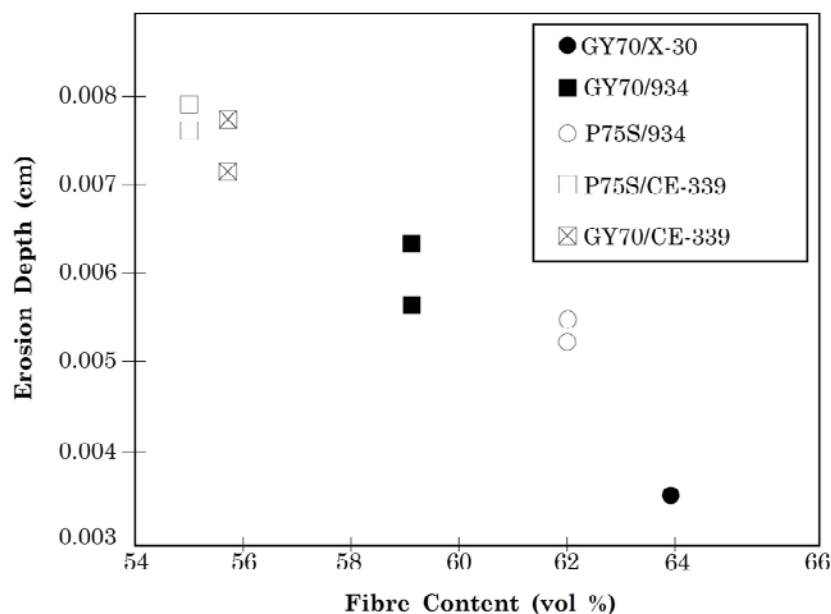


Figure 20.8-2 - LDEF: Estimated AO erosion depth versus fibre content for various epoxy CFRP materials

20.8.5.3 General Dynamics Space Systems Division

The conclusions can be summarised as:

- [ATOX](#) erosion on the leading edge of [LDEF](#) induced a 20% to 30% reduction in the flexural strength and modulus of uncoated (unprotected) epoxy [CFRP](#) composites.
- An uncoated T300/V378A bismaleimide suffered a 60% reduction in flexural strength.
- In general, uncoated CFRP composites suffered a 10% reduction in short beam shear strength ([SBSS](#)).
- Uncoated CFRP composites on the trailing edge of LDEF experienced neither significant changes in flexural strength or modulus nor in short beam shear strength.
- Tin-Indium (Sn-In) coatings applied to some composites provided protection against the effects of ATOX; with no discernible loss in mechanical properties.
- The lap shear strength of spot-welded W-722/P1700 polysulphone thermoplastic composites having [ZnO](#) or [TiO₂](#) coatings were unaffected by exposure on the leading and trailing edges of LDEF.

20.8.5.4 Lockheed Missiles and Space Company

The conclusions can be summarised as:

- No loss of mechanical properties was reported for epoxy matrix composites from trailing edge locations.
- The lap shear strength for an HMF330/934 composite bonded to 2024 aluminium with Hysol 9628 epoxy film adhesive was reduced by ~25% on the trailing edge.
- No loss of shear strength was noted for samples exposed on the leading edge or flight control samples.
- No significant effect on [CTE](#) was seen for [UD](#) GY70/CE-339, T50/F263, T50/934, or T50/X904B epoxy [CFRP](#).
- Epoxy CFRP samples on leading edge locations eroded by 100µm to 150µm, compared with 13µm to 30µm for epoxy glass, Ref. [\[20-7\]](#).

20.8.5.5 Boeing Defence and Space Group

The Boeing portion of M0003-10 exposed materials from both leading and trailing edge locations, [See: [Figure 20.8.1](#)].

The material and laminate constructions evaluated were, Ref. [\[20-4\]](#):

- 934/T300 (0°) 16 ply,
- 3510-6/AS (0°) 16 ply,
- PMR15/C6000 (0°, ±45°, 0°, ±45°)s,
- LaRC 160/Graphite (0°),
- P1700/T300 (0°, 90°) fabric 8 ply.

The observations made on material performance included:

- 934/T300, 3501-6/AS and LaRC 160/Gr showed no significant loss in flexural properties per unit cross-sectional area between the different positions on [LDEF](#) and the ground control. Any mechanical performance reduction was directly attributable to the amount of eroded material all of which was of 0° orientation.
- Ply orientation played a significant role in flexural property behaviour for CFRP with [ATOX](#) exposure.
- PMR15/C6000, with angle ply stacking, showed a significant reduction in flexural strength and modulus due to the near complete loss of the exposed outer 0° ply. This outer ply represented around 25% of primary load bearing capacity; the ±45° orientations contributing very little.
- No modifications to CTE behaviour were detected after LDEF exposure; the test was accurate to approximately 0.001% of relative expansion.
- Examination for [microcracking](#) showed that PMR15/C6000 and P1700/T300 exhibited significant levels of surface intraply cracking (up to 14 cracks/cm). No cracking was seen on any ground control specimens or in any of the other composites.
- Calculations showed that the [ATOX](#) reactivities for the materials, based on mass loss, differed by up to a factor of 4. This did not correspond well with material loss observed by microscopy. It suggested that other factors, e.g. presence of contaminants, were influencing erosion rates.
- Eroded [CFRP](#) surfaces showed a jagged peak like structure with stringy, 'ash-like' material concentrated in clumps around peaks. The level and texture of these features varied between composite types.
- Sodium sulphate was found in the 'ash' from 934 and P1700 composites. It was suggested that the sodium was a residue from the fibres and sulphur from the matrix.
- Silicate contamination was found on all eroded surfaces.

20.8.6 LDEF experiment AO 171

20.8.6.1 NASA Marshall Space Flight Center

The AO 171 exposure conditions are summarised as, Ref. [\[20-8\]](#):

- High vacuum: 10^{-6} to 10^{-7} torr,
- UV radiation: 10471 [ESH](#) (equivalent sun hours),
- Proton flux: 10^9 p+/cm² (0.5MeV to 200MeV),
- Electron flux: 10^{12} to 10^{18} e-/cm² (0.05MeV to 3.0MeV),
- Atomic oxygen: 6.93×10^{21} atoms/cm²,
- Micrometeoroids or space debris: 2 to 5 impacts of less than 1mm diameter per 25 cm².

The conclusions made were:

- Mass loss on [CFRP](#) specimens was consistent with losing approximately 1 ply of the laminate.
- The P1700 polysulphone matrix showed greater erosion than epoxies.
- Organic materials, such as polyimides, silicones and polyurethanes, were found to be luminescent upon exposure to far UV irradiation after flight. Luminescence of composites was not seen.

- Fibrous 'ash' material was observed on eroded CFRP materials.
- Composite surfaces become more diffuse and darker, accompanied by small increases in emissivity and absorption.
- A high density of small (<1 mm) micrometeoroid and space debris impacts was seen on all materials.
- Composite tensile strength decreased approximately in line with thickness loss; as summarised in [Table 20.8.4](#), Ref. [\[20-8\]](#).
- Epoxy matrices became slightly embrittled; probably a result of continued curing under [UV](#) or electron bombardment.
- Changes in the ultimate yield stress of epoxy [CFRP](#) did not correlate with either weave direction or fibre type.
- Synergistic effects were noted, where [ATOX](#) and copious amount of contamination interacted.
- [S-glass](#) reinforced epoxy composites became 'self-protected' when the immediate surface matrix was removed.
- Surface contamination was location specific. This was attributed to discharged spacecraft fluids and interior unbaked polyurethane paints and primer systems.

Table 20.8-4 - LDEF experiment AO 171: Tensile properties of composites

Sample	UTS [MPa]	ϵ [%]	E [GPa]	Poisson's Ratio
P1700/HMF 322 ($\pm 45^\circ$)				
Control	160 \pm 9.7%	-	13.6 \pm 5.3%	-
Flight	139 \pm 3.6%	-	11.8 \pm 0.8%	-
Change	-13.0%	-	-13.2%	-
934/HMS ($\pm 0^\circ$)				
Control	1111 \pm 7.2%	0.52 \pm 8.5%	196 \pm 4.1%	0.24 \pm 4.9%
Flight	883 \pm 17.2%	0.33 \pm 22.3%	193 \pm 2.3%	0.26 \pm 5.9%
Change	-20.8%	-35.4%	-1.75%	+8.1%
934/HMS (90$^\circ$)				
Control	22.7 \pm 9.7%	0.29 \pm 8.5%	7.8 \pm 4.7%	-
Flight	22.8 \pm 17.3%	0.29 \pm 8.5%	8.0 \pm 3.7%	-
Change	+1.3%	-1.7%	+2.7%	-
934/P75S (90$^\circ$)				
Control	18.6 \pm 7.8%	0.28 \pm 8.9%	6.5 \pm 2.8%	-
Flight	12.4 \pm 14.8%	0.18 \pm 14.1%	6.8 \pm 0.9%	-
Change	-34.4%	-36.2%	+3.3%	-
934/P75S (0$^\circ$)				
Control	656 \pm 13.6%	0.31 \pm NA%	225 \pm 5.6%	0.30 \pm NA
Flight	669 \pm 30.6%	NA	247 \pm 8.1%	0.33 \pm 6.9%
Change	+1.9%	NA	+9.8%	+11.1%

20.8.7 LDEF experiment AO 180

20.8.7.1 University of Toronto Institute for Aerospace Studies

The experiment was located at 82° relative to [ram](#). The total [ATOX](#) flux was estimated at $\sim 1.2 \times 10^{21}$ atoms/cm² and the total equivalent sun hours of [VUV](#) radiation was ~ 6900 [ESH](#), Ref. [\[20-9\]](#).

The conclusions were:

- Material erosion was attributed to combined [ATOX](#) and [VUV](#) exposure.
- Boron fibre/epoxy composites show far less erosion than carbon or aramid fibre composites. Whilst surface epoxy was removed, the boron was effective in inhibiting material loss by oxidation
- Kevlar/epoxy composites were significantly eroded, with evidence that material adjacent to aluminium fixtures experienced higher levels of erosion because of reflected [ATOX](#).
- On a 4-ply $\pm 43^\circ$ 934/T300 [CFRP](#) tube, the external layer of epoxy was removed and erosion of the carbon fibres in the outer layer clearly evident. Surface measurement of the eroded CFRP revealed a reduction in C-O content and a large increase in both O and Si content, the latter probably due to contamination.
- Impact damage levels from micrometeoroids or debris were noted on the polymer composites. Some full penetration of 4-ply laminates was seen, with surface damaged areas up to 1.45mm².

20.8.8 Surface characterisation of eroded composites

The presence of chemical species on eroded composite surfaces has an important role in defining the rate of erosion under ATOX flux, Ref. [\[20-10\]](#).

As carbon and hydrogen are stripped away, the surface concentration of non-volatile chemical species increases, often in the form of stable oxides. These species accumulate from:

- residual chemicals from eroded matrix and fibres,
- vapour-phase deposition of contaminants from other sources (excluding physical debris and micrometeoroids).

Characterising the surface of [LDEF](#) materials showed that:

- A common trend for polymer systems, excluding [FEP](#), was an increase in the oxygen and silicon contents with a subsequent decrease in the carbon content.
- Aluminium specimen tray clamps (6061-T6) with thermal control paints, Chemglaze A276 (white) and Z306 (black), were a source of silicon contamination.
- FEP was identified as a source of fluorine contamination. Despite this, the fluorine-containing polymer showed significance resistance to ATOX erosion.
- Levels of contamination were location dependent.
- Higher levels of contamination were found on near-leading or leading edges than on near-trailing or trailing edges of LDEF.

The 'passivating' effect of surface silicon oxides explains the reasoning for siloxane-based coatings and matrices as means of controlling ATOX erosion effects, [See also: [20.14](#)].

20.8.9 Overall conclusions on LDEF

As [LDEF](#) neared re-entry in the later stages of the mission, [ATOX](#) erosion of polymer materials was very severe, Ref. [\[20-11\]](#). In extreme cases, a whole ply was lost from thin [CFRP](#) laminates.

LDEF was in orbit for approaching 6 years compared with the 25 to 30 year design lives of some [LEO](#) projects, such as space stations. An important conclusion is that polymers and polymer composites need surface protection to slow or eliminate surface erosion; particularly in leading-edge ram locations. Also, the effect of accumulated debris damage should be included in the design.

The combined effect of all of the degradation mechanisms depends on the location on the orbiting structure. To be efficient, solutions to combat degradation need to be related to the location and not global to the entire structural design.

20.8.10 Non-polymeric composites on LDEF

The range of materials flown included:

- [MMC](#) metal matrix composites, i.e. Al/C, Mg/C, Al/SiC.
- [GMC](#) glass matrix composites.

These were unaffected by ATOX, but were susceptible to impact damage from debris.

20.8.11 Polymer films on LDEF

20.8.11.1 Silvered Teflon (Ag/FEP)

Ag/[FEP](#) blankets remained functional as a thermal control system over the lifetime of the LDEF, Ref. [\[20-11\]](#). However, the degradation mechanisms observed were:

- ATOX attack reduced the thickness of the film such that its emissivity decreased.
- Solar [UV](#) and [VUV](#) degraded the mechanical properties.
- Delamination zones were observed around debris impact sites.
- The silver layer in the adhesive backed Ag/FEP was cracked during application onto the aluminium substrate, causing 'bleed-through' and subsequent darkening of the adhesive under solar exposure.
- Roughening of the surface texture of the FEP layer dramatically increased the diffuse component of reflectance.

20.8.11.2 Kapton

Up to 250µm of the thickness of polyimide Kapton™ was removed from near-leading edge locations.

20.8.12 Lubricants, adhesives and seals on LDEF

20.8.12.1 General

These were used widely throughout [LDEF](#), but not on external surfaces. Some general comments are provided on their durability, Ref. [\[20-11\]](#), [\[20-12\]](#).

20.8.12.2 Lubricants

Lubricants underwent viscosity changes as organic binders were removed under vacuum. Other than one occasion, where loss of cetyl alcohol lubricant caused severe galling (seizure) of fasteners, the overall behaviour was satisfactory. Other dry-film lubricants, such as molybdenum sulphide, behaved well, as did heat-sink grease (Apiezon H) and graphite-filled polyimide.

The volatiles and contaminants released by lubricants need closer examination as they can affect adjacent materials.

20.8.12.3 Adhesives

Araldite™ adhesives were extensively used, including:

- AV100/HV100.
- AV138/HV998.
- AV138/HW2951.
- AW136/HY994.
- AW2101/HW2951.
- MY750/HY956.

Discolouration from UV exposure was noted.

Experiment M0003 tested two 3M adhesives; AF143 film adhesive and EC2216 RT epoxy, in lap shear specimens with epoxy CFRP-to-CFRP or Ti-to-CFRP [adherends](#). In all cases the LDEF trailing edge exposed joints were stronger than pre-flight controls by 10% to 15%, typically.

Some adhesive bond failures were noted where four solar cells detached. These were bonded to aluminium using an epoxy. Failure occurred at the solar cell interface; such events were random and unexplained. The darkening of adhesives was greatest with solar cells.

Silicone adhesives were successfully used for bonding [FEP](#) and Kapton™ films. Tapes, conformal coatings and potting compounds were also successfully deployed.

20.8.12.4 Seals

The materials included butyl, nitrile, ethylene-propylene and Viton for O-rings, with [EPDM](#), [NBR](#), neoprene and silicones for gaskets.

All seals, both O-ring and compressed sheet, were protected from direct exposure to the space environment. No significant failures were observed.

20.9 Thermal cycling

20.9.1 Conditions

[Thermal cycling](#) of a structure occurs as the spacecraft moves in and out of the Earth's shadow. Typical thermal cycling ranges for the common orbits are:

- [LEO](#) (space station): within -90°C to +90°C, e.g. between -57°C and +38°C for metal coated [CFRP](#) truss tubes, Ref. [\[20-13\]](#).

- [GEO](#):
 - communications satellite between -150°C and +120°C.
 - exceptional conditions from -180°C to +130°C, e.g. Polar Platform.

The number of cycles experienced in each of these orbits is typically:

- LEO: 15.4 cycles/day for 30 years = 169 000 cycles,
- GEO (long duration): can experience 10 950 cycles.

The exact conditions experienced and the number of thermal cycles depends on the details of the mission.

20.9.2 Damage mechanisms

20.9.2.1 General

The relationships identified between thermal cycling, damage mechanisms and thermo-mechanical properties are:

- [Microcracking](#) occurs mainly during the first 103 thermal cycles. If cycling continues beyond this, the growth rate is reduced.
- Strength diminishes as a function of the number of cracks. A reduction of between 3% and 9% was seen in the case of epoxy-based [CFRP](#) composites; as shown in [Figure 20.9.1](#), Ref. [\[20-14\]](#).
- The reduction in stiffness appears to be similar to that for strength, although the tendency for changes to diminish beyond a certain number of cycles cannot generally be expected; as shown in [Figure 20.9.2](#), Ref. [\[20-14\]](#).
- Microcracking causes a reduction in the matrix-dominated properties of composites. These combine to cause changes in the coefficient of thermal expansion. The extent of change of [CTE](#) depends strongly on laminate lay-up and also on the particular fibre/resin combination, as shown in [Table 20.9.1](#), Ref. [\[20-14\]](#). CTE can decrease and show less scatter as the number of cycles increases.

Table 20.9-1 - Coefficient of thermal expansion for ±45°

Material	Laminate Type ±45° Cross Ply			
	Carbon/Epoxy			Carbon/Polyimide
	914C-TS-5	HY-E 1548A/B	LY556/T300	T3TF178
Number of thermal cycles	CTE α_x (10^{-6} K^{-1})			
0	1.9	0.6	1.5	-0.9
1170	-	-	1.7	-
2295	1.9	0.6	2.0	-0.9
3480	2.0	0.6	2.4	-0.8

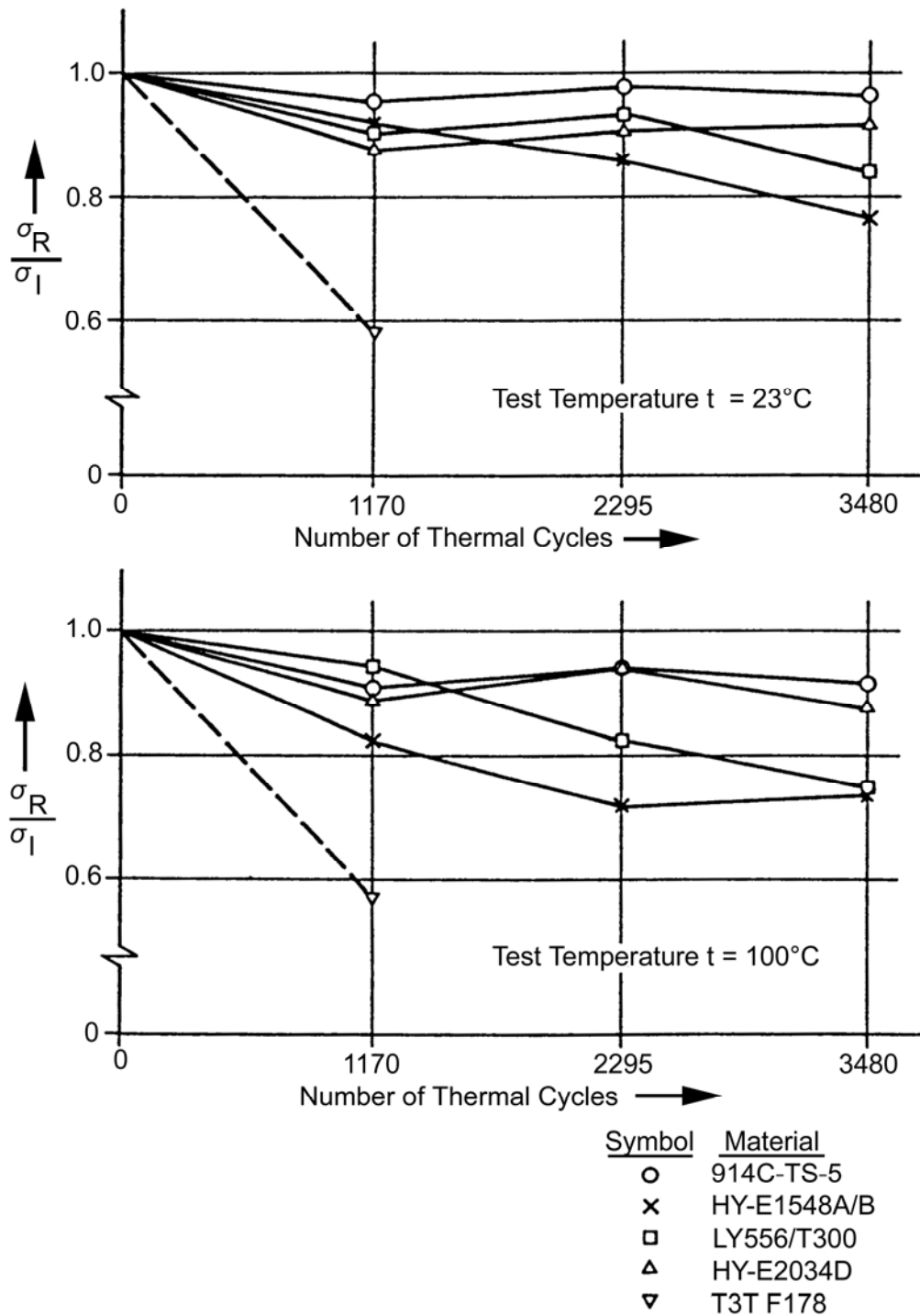
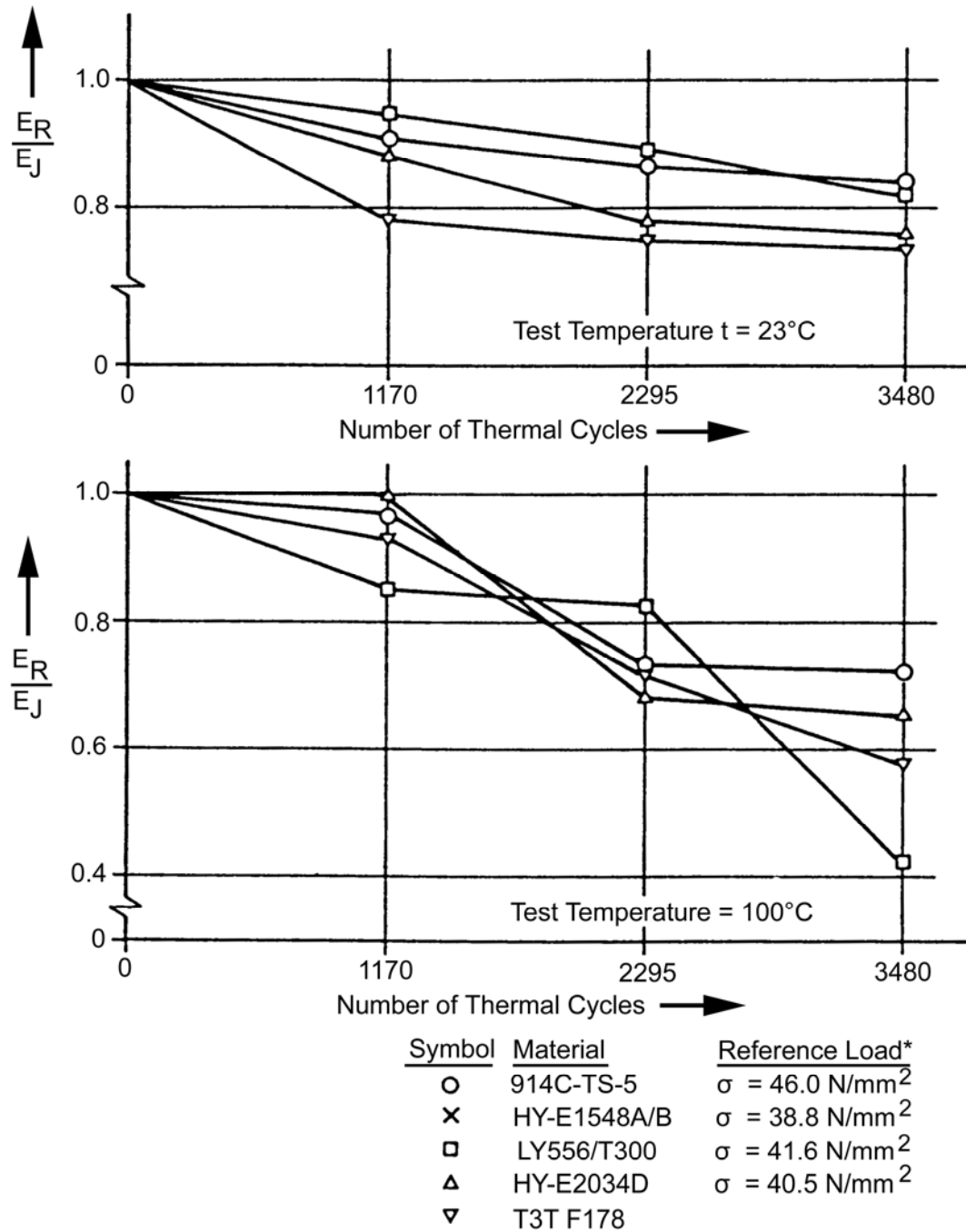


Figure 20.9-1 - Ratio of residual tensile strength to the initial strength versus number of thermal cycles (-160 to +95°C): $[\pm 45^{\circ}]_{2S}$ specimen tensile tested at RT and 100°C



Reference load = Load resulting in elongation of 2 mm/m in a virgin specimen at Room Temperature.

Figure 20.9-2 - Degradation of stiffness of various materials due to thermal cycling (-160°C to +95°C): $[\pm 45^{\circ}]_{2s}$ specimen tensile tested at RT and 100°C

20.9.2.2 Microcracking

An [ESTEC](#)-funded study in 1994 showed that [microcracking](#) can occur at different levels in composites with nominally the same [prepregs](#), Ref. [\[20-15\]](#). This was attributed to space contractors having different preferences as to how the prepregs were consolidated.

The parameters which varied included:

- Use or not of [peel plies](#), e.g. [bleed](#) or no bleed.
- [Dwell](#) periods.
- Mould tool materials.
- Consolidation pressures.

It cannot therefore be automatically assumed that microcracking behaviour is dependent only on materials selection. Laminate lay-up and thickness are additional parameters which affect microcracking behaviour.

20.9.2.3 ECSS requirements

[ECSS-Q-ST-70-04](#) details a thermal cycling test for the screening of space materials and processes.

20.10 Vacuum

20.10.1 Effects of vacuum

20.10.1.1 General

The vacuum of space varies from about 10^{-4} torr (at 100 km) to less than 10^{-10} torr (in excess of 1000 km).

20.10.1.2 Outgassing

The combination of temperature and vacuum encountered by a space structure causes matrix materials to [outgas](#). This, apart from reducing the mechanical properties of the composite, liberates material that can condense on optical equipment and affect the performance.

20.10.1.3 Resin matrix characteristics

For dimensionally stable, and optical structures in particular, there is a progressive move towards matrices with low outgassing characteristics and low moisture absorption. These include:

- thermosets, [See also: [2.4](#); [6.35](#)]:
 - cyanate esters,
 - new low moisture epoxies.
- thermoplastics, [See also: [6.17](#)].
- metals and ceramics, [See also: Chapter [42](#)].

The close proximity of materials to optical devices can be sufficient to dictate the use of very low [outgassing](#) matrices.

[See also: [ESMAT](#) website for outgassing data from the ESTEC Materials and Processes database]

20.10.1.4 Offgassing

For manned vehicles, the [toxicity](#) of offgassed products needs careful consideration.

20.10.1.5 ECSS requirements

In order to minimise the effects of outgassing, the normal ECSS requirements (see ECSS for latest standards), for materials at 10^{-6} torr and space structure temperatures, are:

- a proven maximum recovered mass loss ([RML](#)) < 1%, and
- collected volatile condensed materials ([CVCM](#)) < 0.1%.

[See also: [5.2](#) for comments on outgassing characteristics]

[ECSS-Q-ST-70-02](#) details a thermal vacuum test for the screening of space materials; previously ESA PSS-01-702.

The outgassing values stated in [ECSS-Q-ST-70-02](#) represent the maximum allowable for space use.

Some applications stipulate materials with very low outgassing levels, e.g. for use in close proximity to optical devices.

[ECSS-Q-ST-70-29](#) describes the determination of offgassing products from materials and assembled articles to be used in a manned space vehicle crew compartment; previously ESA PSS-01-729.

20.11 Radiation

20.11.1 Radiation spectra

20.11.1.1 General

In the space environment, polymeric matrix materials can be subject to a wide range of radiation. The effects depend on the molecular structure of the material and the amount of radiation energy absorbed. Initially the production of free radicals and ions within the matrix material gives rise to [cross-linking](#), chain-cracking or chain polymerisation. This is accompanied by a slight increase in the glass transition temperature, [T_g](#). With a very heavy radiation dose, breaking of molecular chains is widespread and the degradation can become acute. This is accompanied by a decrease in [T_g](#). The types of radiation that can be encountered include, Ref. [\[20-16\]](#), [\[20-44\]](#):

- electrons,
- protons,
- ultraviolet,
- solar flares,
- cosmic rays.

The overall levels of radiation are higher in [GEO](#) compared with [LEO](#) and spectra differ. 30 years in GEO is equivalent to ~100 MGray (10,000 Mrad).

Carbon and glass fibres are not affected by radiation in terms of changes to mechanical properties or degradation.

[Aramid](#) fibres degrade, notably by [UV](#), unless shielded by the matrix. Very high doses degrade the polymeric aramid fibres within a composite at the same time as degrading the matrix.

20.11.1.2 UV radiation

[UV](#) radiation does not appear to have much effect on epoxy-based [CFRP](#) composites.

[Figure 20.11.1](#) shows that the stiffness does not change significantly, because UV radiation affects only the surface of the structure, Ref. [\[20-18\]](#). Likewise, CFRP shows no significant change in [CTE](#) when exposed to sun and vacuum.

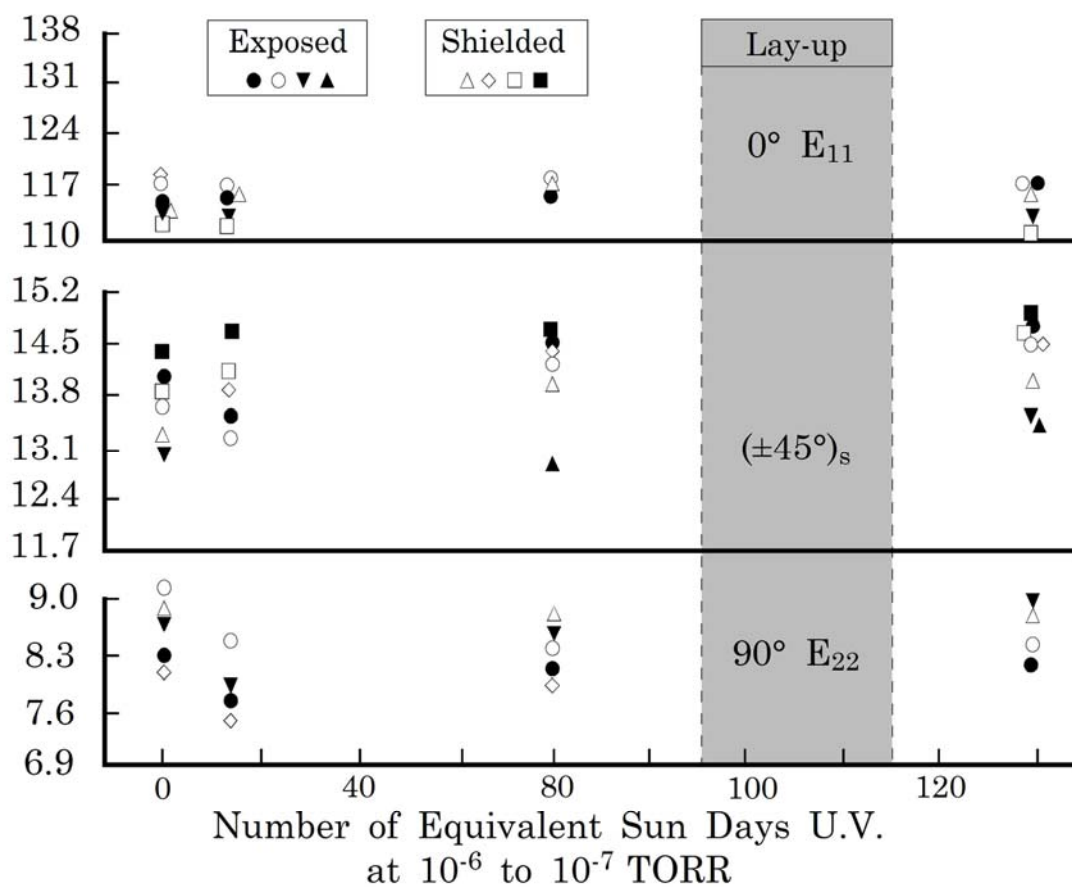


Figure 20.11-1 - UV radiation: Effects on tensile moduli of carbon/epoxy composites

20.11.1.3 Particle radiation

Particle radiation penetrates [CFRP](#) material and causes changes in mechanical properties. Depending on the fibre orientation and dosage (up to 10000 Mrad), a reduction in tensile strength of ~ 25% is noted in some publications; some also report increases in modulus up to 13%, Ref. [\[20-17\]](#).

300 Mrad is equivalent to 1 year in orbit; 10,000 Mrad = 30 years.

The changes in mechanical properties are due to molecular [cross-linking](#) and chain [scission](#) mechanisms. These embrittle the matrix and lead to [microcracking](#) during thermal cycling. As radiation doses increase, chain scission becomes the dominant effect. The coefficient of thermal expansion, [CTE](#), also changes. The effects are material-dependent, but, as shown in [Figure 20.11.2](#), are less pronounced at high dosages; 10000 Mrad, Ref. [\[20-19\]](#).

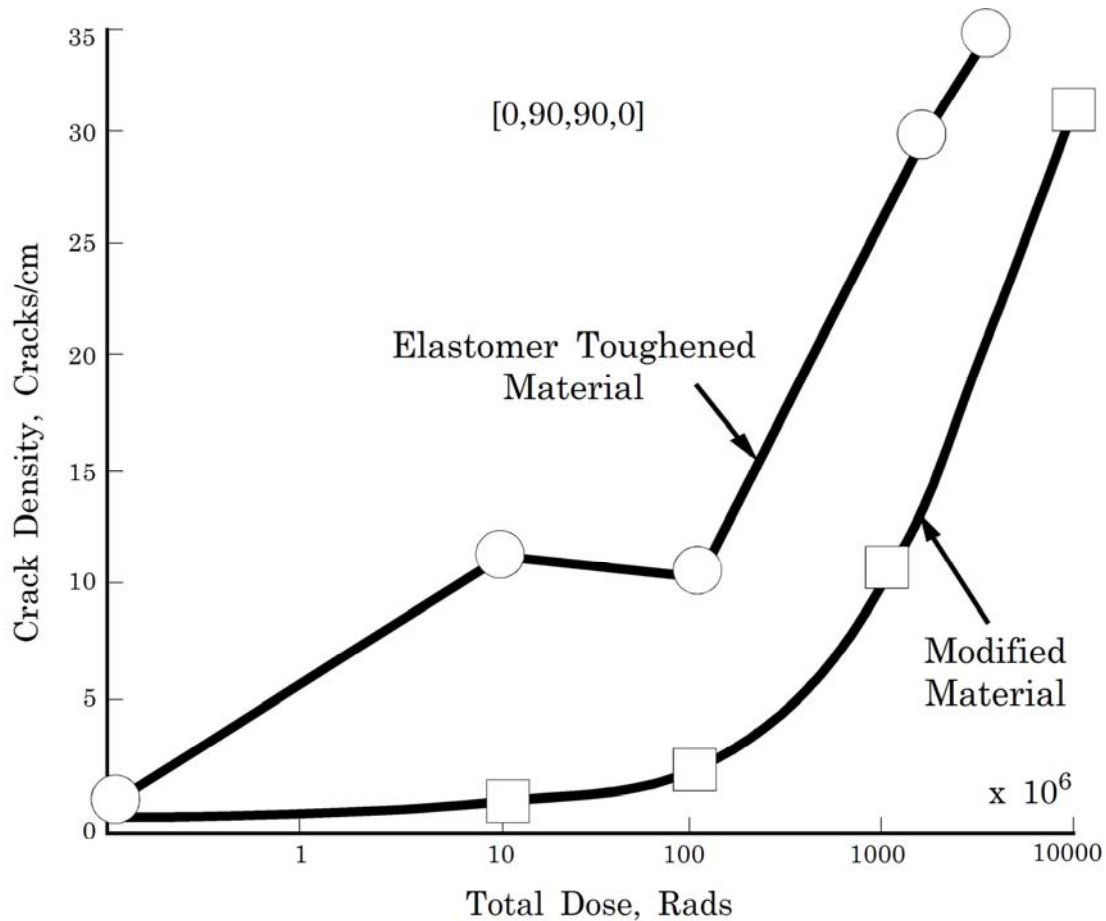


Figure 20.11-2 - Effects of total radiation dose on microcrack formation in composite specimens subjected to 100 thermal cycles (-150°C to +80°C)

[Figure 20.11.3](#) shows small changes in [CTE](#) occur at low doses and an apparent threshold of 108 rad, where a decrease in CTE occurs, Ref. [\[20-19\]](#).

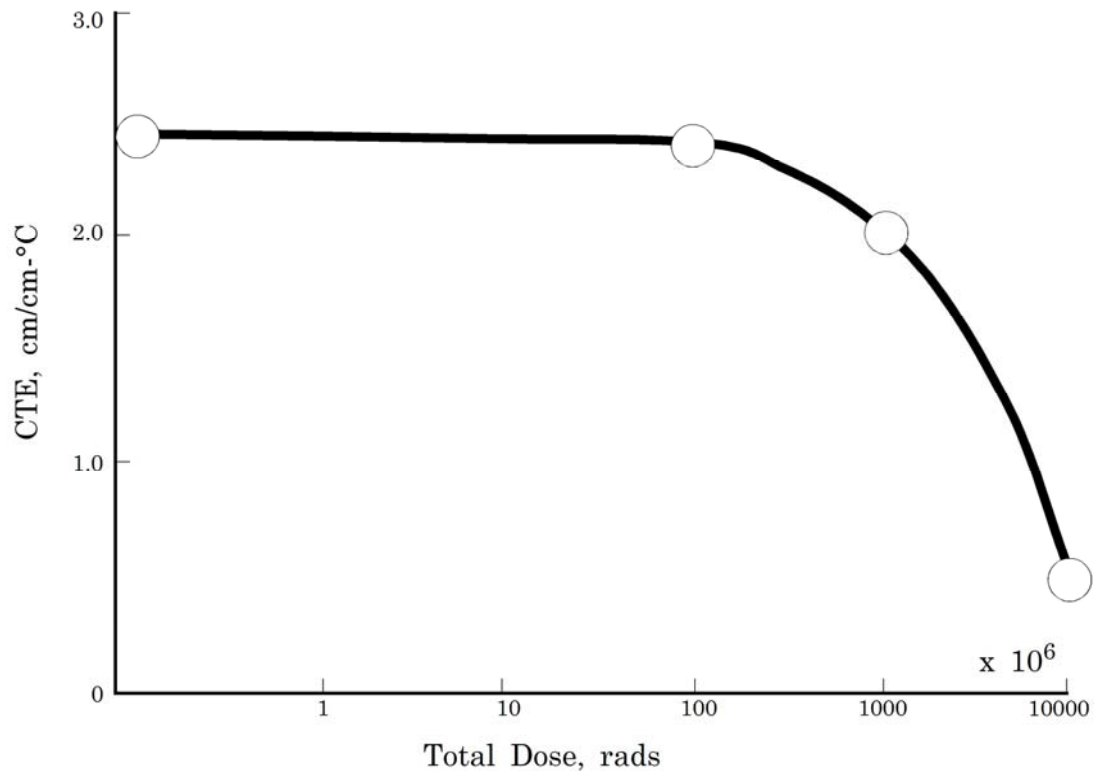


Figure 20.11-3 - Effects of total radiation dose on the coefficient of thermal expansion of a toughened composite system (-150°C to -73°C)

20.11.2 T300/934 in GEO

20.11.2.1 General

[NASA](#) carried out a study on the widely used Fiberite 934 combined with a common first generation, high strength fibre T300, Ref. [\[20-20\]](#).

The principal test parameters were:

- Bulk resin specimens and [UD](#) composites oriented at 0°, 10°, 45° and 90°.
- [Creep](#) behaviour at 20%, 40%, 60% and 80% of ultimate tensile strength, [UTS](#).
- 10000 Mrad exposure to 1 MeV electrons at 35°C.
- Mechanical tests at [RT](#) (23°C) and 121°C.
- Changes in [T_g](#).

The aim of the work was to investigate the [creep](#) behaviour of composites exposed to very high radiation doses, where molecular chain modifications are known to occur.

The conclusions made were:

- Changes in creep behaviour were only observed in off-axis specimens, i.e. non 0°.
- Radiation modification significantly increased creep at 121°C but not at [RT](#).
- The matrix [T_g](#) was lowered from 240°C to 180°C by the total radiation dosage, as a result of molecular chain breaking. This enables increased chain mobility, assisting creep deformation.

- Prolonged exposure at 121°C for ~120 hours promoted a partial recovery in the Tg to 210°C owing to recombination of free radicals, increasing the level of cross linking.
- Greater residual strain was noted in 10° and 45° irradiated specimens at 121°C than the equivalent 90° specimens.

20.11.2.2 ST- requirements

[ECSS-O-ST-70-06](#) describes the particle and UV ultraviolet radiation testing of space materials; previously ESA PSS-01-706.

20.12 Damage by combined environmental factors

20.12.1 General

For orbiting structures in [GEO](#), the typical design life is between 5 years and 7 years. Studies on the effects of thermal cycling and radiation on composites over these periods indicate small changes in mechanical and physical properties. These changes were considered to be largely insignificant for such short-life applications.

With the current goals of extending missions to 30 years in GEO and in [LEO](#), material degradation is being re-evaluated, particularly the possibility of damage from combined space environment factors.

Each orbit has different profiles of degradation mechanism severities. Which need to be considered in studies of prolonged space exposure on materials.

For composites, the dominant mechanisms can be summarised as:

- GEO:
 - high number of severe thermal cycles,
 - high radiation dosages.
- LEO:
 - high atomic oxygen ([ATOX](#)) fluxes,
 - high number of impacts by debris and micrometeoroids.

However, the lesser effects cannot be ignored. Structures in [GEO](#) also experience [outgassing](#) and debris impacts. Likewise, in [LEO](#), a high number of [thermal cycles](#) occur (but with a less severe thermal range than GEO), and also [VUV](#) exposure.

A number of test programmes have been carried out to consider the response of [CFRP](#) materials to GEO- and LEO-type environments. The results of some of these studies are summarised.

20.12.2 P75/930 in GEO

[NASA](#) undertook an evaluation of a carbon/epoxy P75/930 composite system to study the relationship between radiation modification and thermal cycling, and their effect on [microcracking](#) density, Ref. [\[20-21\]](#).

Modifications to the cure schedule were proposed as a means of reducing crack densities.

The principal test parameters were:

- Fiberite 930 epoxy is cured between 135°C and 176°C.
- Reference materials for comparison were T300/934 and P75/934 (177°C cure).
- Thermal cycling between +65°C and -157°C for up to 500 cycles.
- Specimen configurations:
 - (10°)₄ for shear properties,
 - (90°)₄ and (0°, 90°₂, 0°) for microcracking density.
- 10,000 Mrad of 1 MeV electrons in vacuum.

The results and observations that were made included:

- [Figure 20.12.1](#) shows T_g variation with cure temperature and radiation dose, Ref. [\[20-21\]](#).
- For 135°C cure specimens, radiation exposure initially increased the T_g from 110°C to 124°C, followed by a reduction to 93°C after 10,000 Mrad.
- Initial radiation exposure increases [cross-link](#) density, before chain [scission](#) becomes significant at a threshold of 100 Mrad to 1000 Mrad.
- The shear strength of 10° specimens was not significantly dependent on cure temperature; as illustrated in [Figure 20.12.2](#), Ref. [\[20-21\]](#).
- Shear strength was dramatically lowered by radiation dosage, i.e. 80% of 'unexposed' after 100 Mrad, but only 10% after 10,000 Mrad (90% loss).
- As-made P75/930 composites did not have [microcracks](#):
 - After 50 cycles, all non-irradiated materials, irrespective of cure temperature, had significant microcrack densities of 8 to 12 cracks/cm.
 - After 500 cycles, the crack density increased to between 16 and 18 cracks/cm.
- For irradiated samples the microcrack densities peaked at 20 to 22 cracks/cm after 10,000 Mrad and 500 cycles.

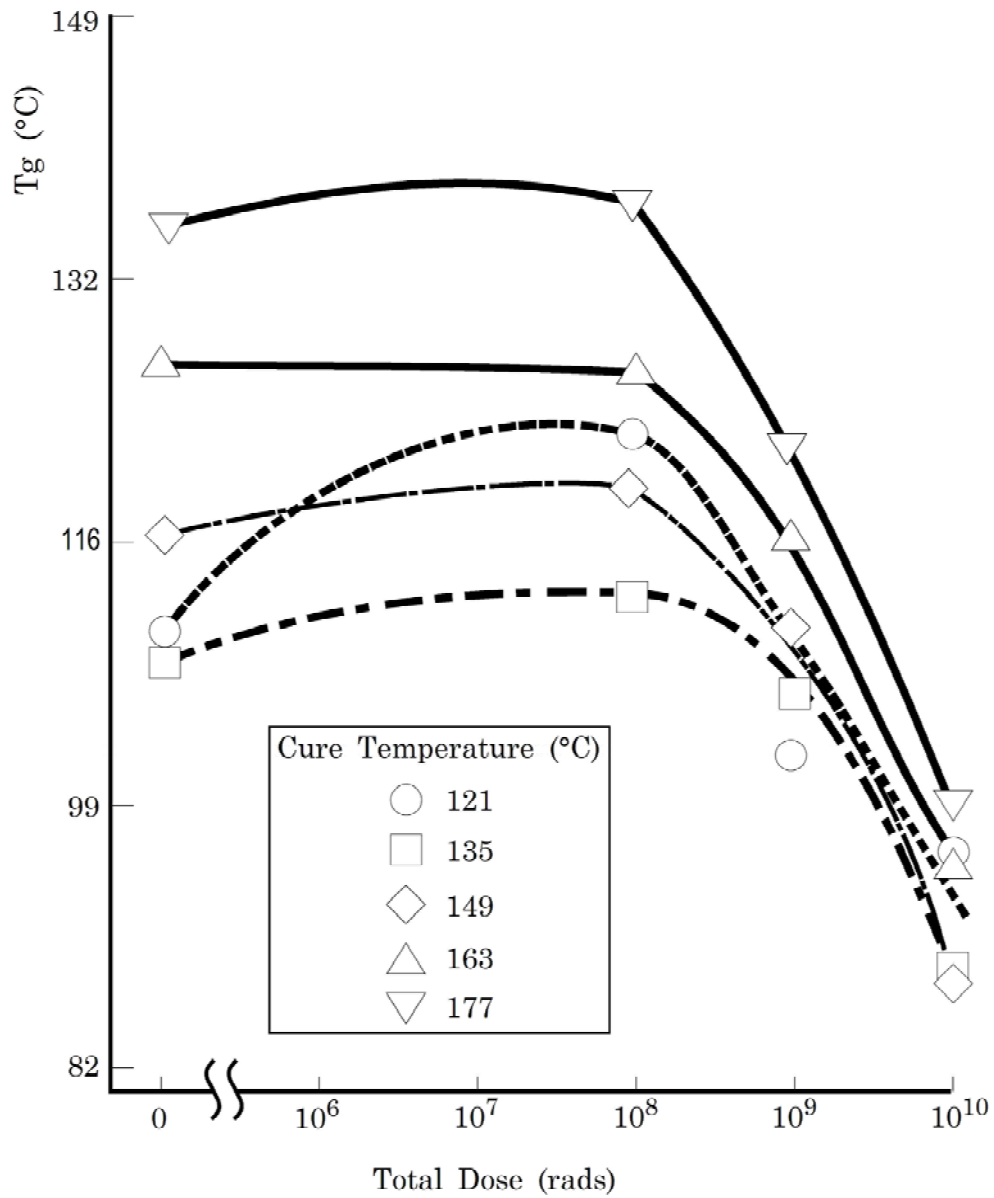


Figure 20.12-1 - Effect of cure temperature and electron radiation exposure on the Tg of P75/930 in GEO

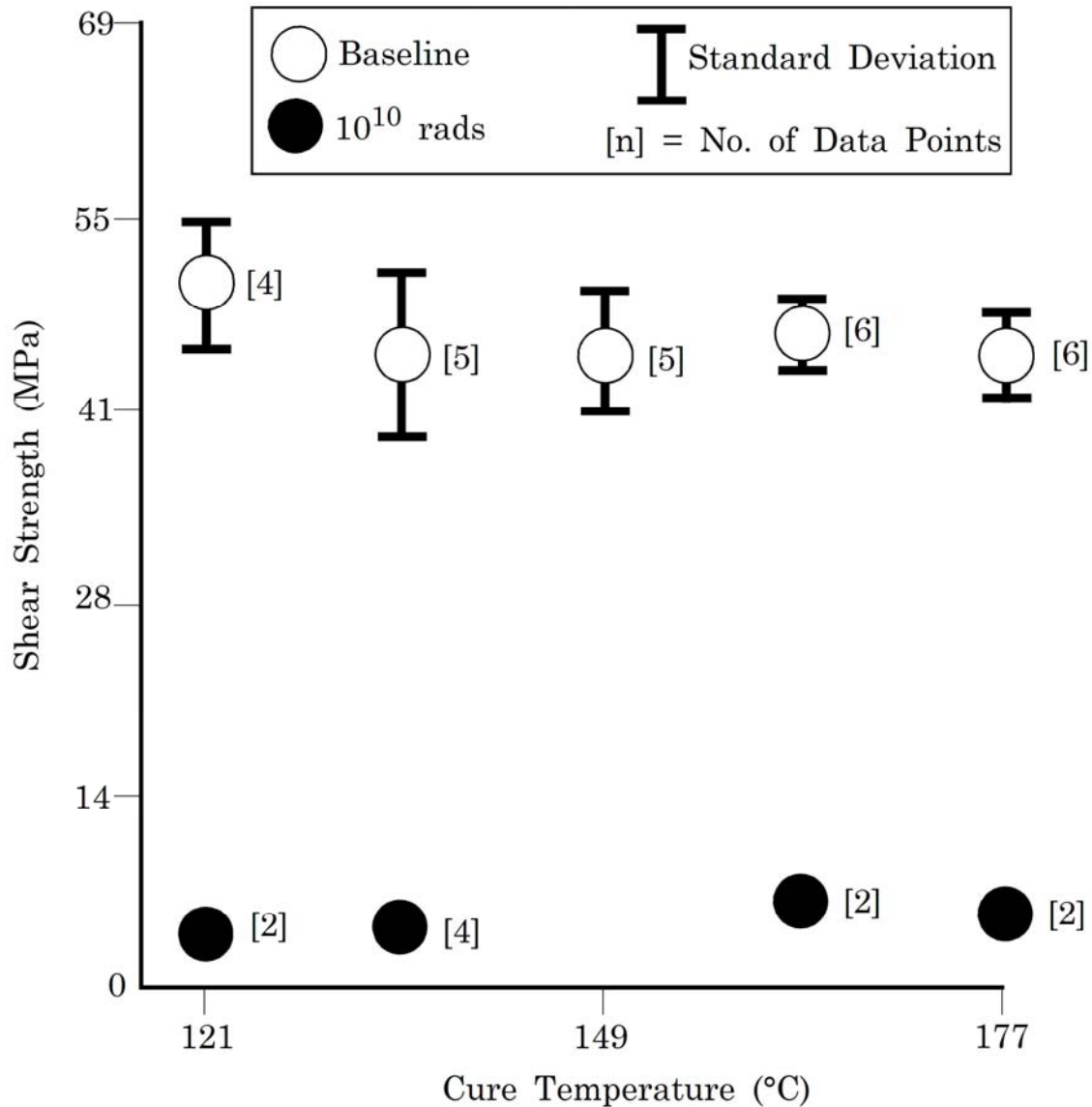


Figure 20.12-2 - Effects of cure temperature and electron radiation exposure on the shear strength of P75/930 in GEO

The results from the [NASA](#) work when compared with those of previous findings for P75/934 showed:

- Both Fiberite 930 and 934 undergo chain [scission](#) at very high radiation dosages. 930 was more susceptible than 934 to changes in [T_g](#).
- Non-irradiated materials:
 - P75/930 started with no [microcracks](#), but attained 18 cracks/cm after 500 cycles.
 - P75/934 started at 5 cracks/cm 'as-made' and stabilised at 11 cracks/cm after 10 cycles.
- Fiberite 930, cured at 135°C, offered no advantages over 934 (the higher temperature curing alternative), when used with P75S fibre.

P75 is a first generation pitch carbon fibre of USA origin. Many organisations consider it to be inadequate for composites experiencing severe thermal cycling because of its poor composite transverse properties, i.e. low fibre/matrix interface strength; hence low 90° ply strength.

20.12.3 UHM CFRP in GEO and LEO

CERT-ONERA (France) examined the behaviour of 4 epoxy-based [CFRP](#) materials, Ref. [\[20-22\]](#).

NOTE GY70 fibre and Amoco ERL1939 resin are no longer commercially available. An [HS](#) carbon fibre was used rather than an [UHM](#).

The principal test parameters were:

- CFRP materials evaluated:
 - GY70/M18,
 - Tenax HTA/M18,
 - GY70/Fiberite 954, and
 - P75/ERL1939.
- Crossply [0₂,90₂]_s laminates.
- In conjunction with thermal cycles (between -100°C and +100°C), a step simulation provided, as shown in [Figure 20.12.3](#), Ref. [\[20-22\]](#), either:
 - asymmetric irradiation, or
 - uniform irradiation.
- Radiation dosages corresponded to 21 years in [GEO](#).
- Asymmetric irradiation reproduces the GEO environment where absorbed energy at 100µm sub-surface is 40 times greater than at 1000µm.
- Electron irradiation with successive electron energies (150 keV, 250 keV and 500 keV) was used to give a dose gradient through the thickness.

NOTE Applied to M18 and ERL1939 laminates.

- Uniform radiation was achieved with more energetic 2 MeV electrons.

NOTE Applied to GY70/M18 laminates only.

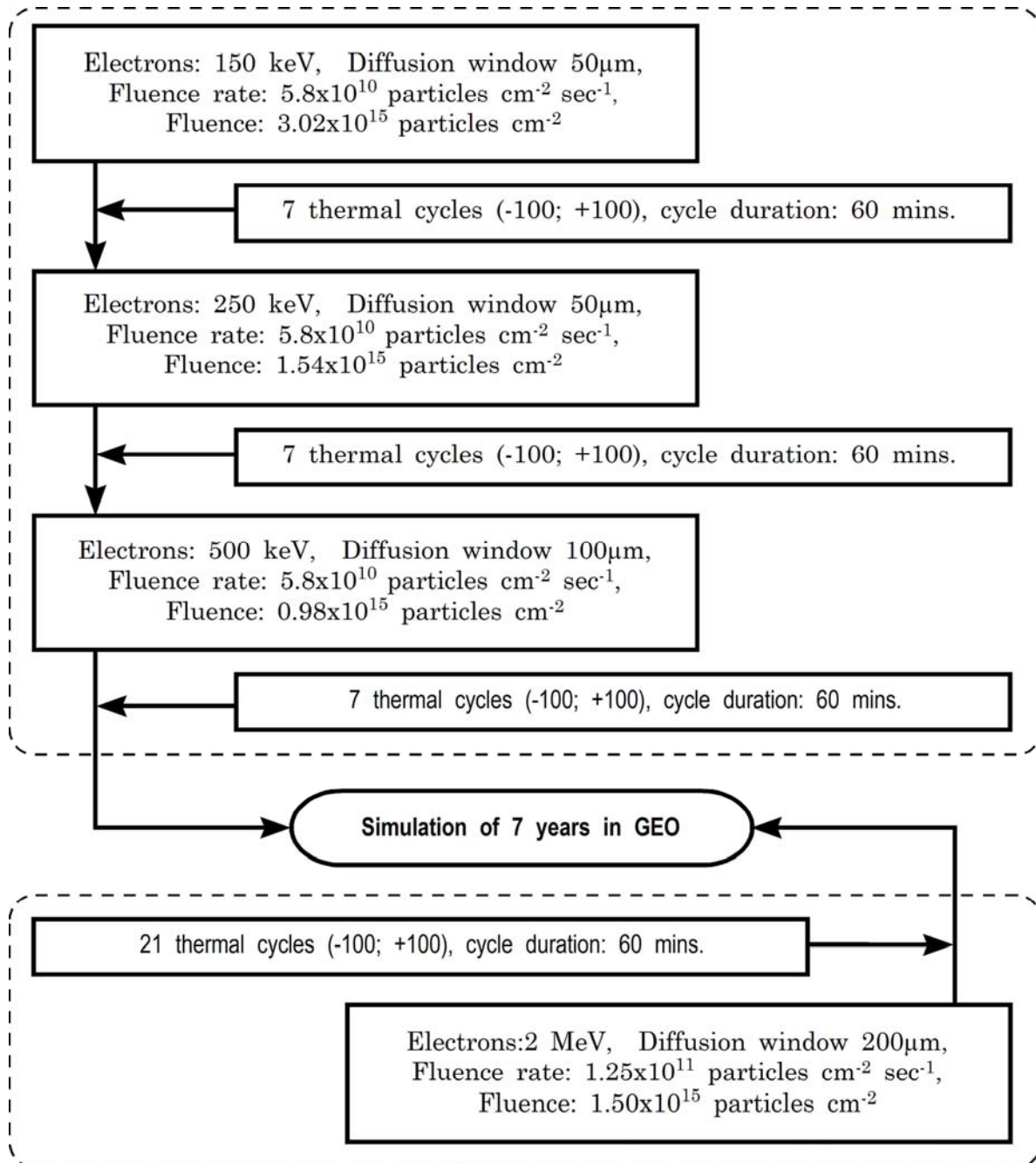


Figure 20.12-3 - Step simulation of 7 years in GEO

Properties studied were:

- Flexural modulus,
- Glass transition temperature [T_g](#),
- [Microcrack](#) densities, and
- Response to atomic oxygen [ATOX](#) erosion.

The observations made were:

- Flexural modulus: The combined effects of radiation and thermal cycling reduced the flexural modulus. The maximum change was a 5% reduction for asymmetrically irradiated GY70/M18.
- Tg: After maximum exposure and thermal cycling, all materials experienced a Tg reduction of ~10°C, e.g. M18 reduced from 200°C to 190°C.
- Microcracking:
 - GY70/M18: An average of 9 cracks/cm was noted in the as-made state. This increased to 13 cracks/cm after irradiation and thermal cycling. Irradiation alone did not increase the crack density; as shown in [Table 20.12.1](#), Ref. [20-22].
 - GY70/954: 7.5 cracks/cm after 63 thermal cycles. The effect of radiation was not studied.
- ATOX erosion:
 - The erosion rate of the composites differed under ATOX erosion up to 1.2×10^{21} atoms/cm²; as shown in [Figure 20.12.4](#), Ref. [20-22].
 - The rate of erosion is primarily a function of the resin, but the fibre type was also seen to have an effect when the different [UHM](#) fibres were compared.

NOTE The maximum dose was approximately 15% of that for ram facing samples on [LDEF](#), [See: [20.8](#)].
 - For the UHM composites, the ATOX erosion accounted for a 4% to 12% reduction in dynamic modulus in bending.

Table 20.12-1 - Microcrack densities in [0₂/90₂]_s CFRP laminates

A) Effect of thermal cycling on microcracking (Cracks/cm)

Composite	Number of Thermal Cycles [-100°C to +100°C]			
	0	21	42	63
M18/GY70	9.7	11.9	12.3	13.8
M18/HTA	<1	<1	<1	<1
954/GY70	1	1.5	2.3	7.5
ERL1939/P75	<1	<1	<1	<1

B) Effect of simulated GEO environment on microcracking (Cracks/cm)

Composite	Equivalent Years in Space			
	0	7	14	21
M18/GY70 †	6.8	10.3	9.1	13.3
M18/GY70 ‡	8.2	8.0	12.2	13.1
HTA/M18 †	<1	<1	<1	<1
ERL1939/P75	<1	2.8	7.7	7.5

Key: †: Uniform irradiation

‡: Asymmetrical radiation

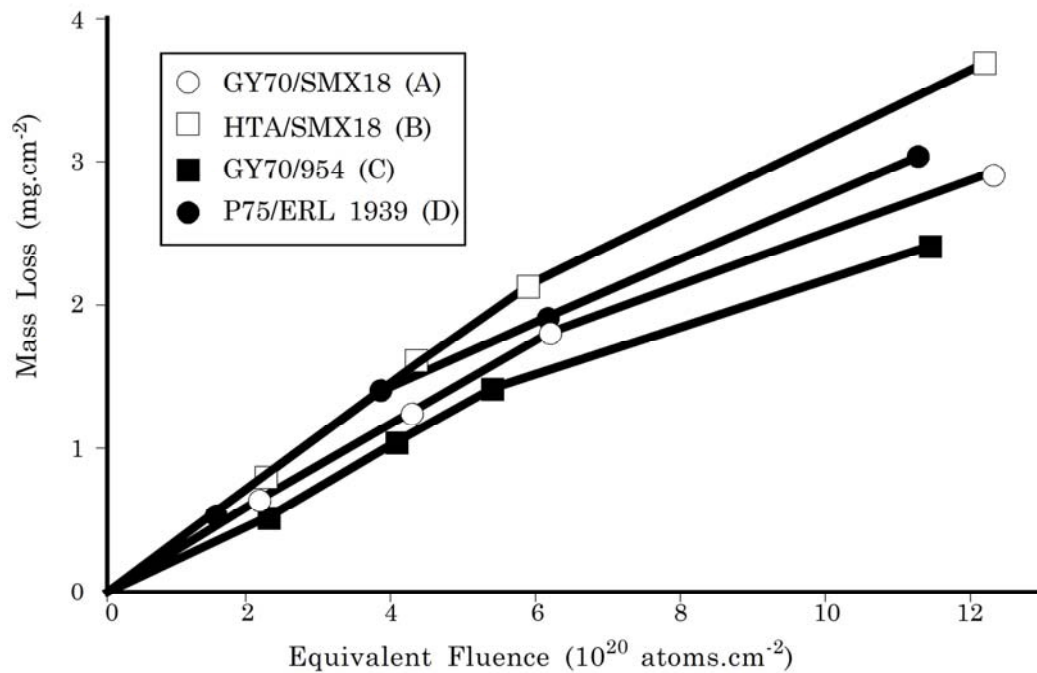


Figure 20.12-4 - Effect of ATOX erosion on different CFRP composites

20.12.4 PEI CFRP in LEO and GEO

NASA investigated the use of thermoplastic polyetherimide, [PEI](#), as a matrix for composite space structures. The effect of high dosage radiation and thermal cycling was studied in conjunction with [ATOX](#) erosion, Ref. [\[20-23\]](#).

The principal parameters of the study were:

- Ultem 1000 PEI/Celanese C6000 composite.
- Non-sized and 2% epoxy-sized laminates.
- 10,000 Mrad by 1 MeV electrons.
- Thermal cycling from -101°C to $+66^{\circ}\text{C}$, up to 1000 cycles.
- ATOX exposure equivalent to 26 days in [LEO](#), e.g. space station levels.
- Flexural properties, interlaminar shear strength [ILSS](#) and [T_g](#) were measured.

The main conclusions of the study were:

- The presence of an epoxy size had a detrimental effect on mechanical properties; as shown in [Table 20.12.2](#), Ref. [\[20-23\]](#).
- The [T_g](#) of [PEI](#) increased by 15°C over the total 10,000 Mrad, but this change did not start until after 7500 Mrad. The change in [T_g](#) was presumably due to [cross-linking](#) effects.
- The relative changes in flexural strength, flexural modulus and flexural strain-to-failure are shown in [Figure 20.12.5](#) for different test conditions, Ref. [\[20-23\]](#).
- The most dramatic changes were seen for transverse properties and not those in the longitudinal direction.

- There was no evidence that thermal cycling alone caused any significant degradation in the composite. Indeed there was evidence that some properties improved.
- The combined effects of thermal cycling and irradiation produced little change in the material.
- [ATOX](#) erosion produced the anticipated loss of material. The effect was more noticeable on transverse rather than longitudinal composites.
- Imide and phenyl groups showed greater resistance to ATOX than ethers and alkane functional groups, or highly branched groups such as isopolypropylene.

Table 20.12-2 - GEO and LEO effects: Mechanical properties of C6000/PEI composites

	Non-Sized Fibres		Sized Fibres	
	T	L	T	L
Flexural strength (MPa)	111±15	2420±110	145±14	2010±170
Flexural modulus (GPa)	8.24±0.42	129±7	7.18±0.60	101±11
Strain to failure (%)	1.4	2.0	1.8	2.0
ILSS (MPa)	-	79±5	-	71±4

Key: T: Transverse

L: Longitudinal

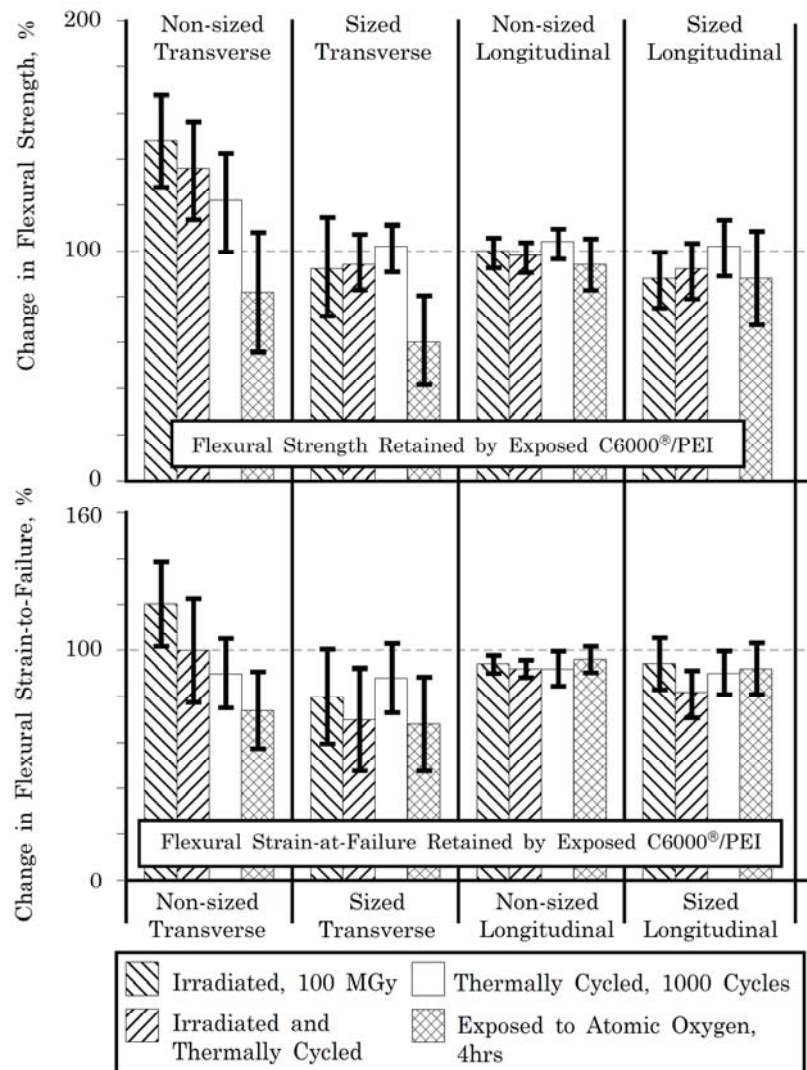


Figure 20.12-5 - Irradiation and thermal cycling: Changes in mechanical properties for C6000/PEI

20.13 Atomic oxygen

20.13.1 Effects of atomic oxygen

20.13.1.1 Typical exposure levels

Spacecraft in [LEO](#) are exposed to a flux of earth-ambient atmospheric species, the most dominant and aggressive of which is atomic oxygen, [ATOX](#).

Although the average density of atoms is only 5×10^8 atoms/cm³, the velocity of spacecraft in orbit (7.6 km/s) leads to a total flux of 10^{15} atoms/cm²/s with a collision energy of about 5 eV.

The level of flux experienced varies with the:

- Altitude of the spacecraft orbit,
- Attitude - maximum for [ram](#), minimum for [wake](#),

- Solar activity, and
- Duration of exposure.

20.13.1.2 Material sensitivity

The reactivity of composite materials is determined by the combination of the reactivities of the matrix and the reinforcement.

Inorganic reinforcing fibres, such as carbon, are initially shielded by the matrix. Eventually the matrix is removed, exposing the fibres. Long-term exposure can lead to degradation of both fibre and matrix system.

The reaction efficiency is the degradation per solar cycle, for a given flux. There are differences in [ATOX](#) reaction efficiencies between hydrocarbon-based matrices depending on the reactive groups and radicals present. Reactivity can be reduced, by orders of magnitude, if silicon or fluorine is present in the molecular structure.

[Table 20.13.1](#) shows the reaction efficiencies for some selected materials, Ref. [\[20-24\]](#). The degradation per solar cycle for the different materials can be predicted, provided that the flux and solar cycle are known.

Table 20.13-1 - Reaction efficiencies for some selected composite polymers and organic films: Determined by ~40 hours of LEO exposure in space

Material	Reaction Efficiency † x 10 ⁻²⁴ (cm ³ atom ⁻¹)
Kapton	3.0
Mylar	3.4
Tedlar	3.2
Polyethylene	3.7
PMMA*	3.1
Polyimide	3.3
Polysulphone	2.4
1034C epoxy	2.1
5028/T300 epoxy	2.6
Teflon, TFE	0.05
Teflon, FEP	0.05

Key: * PMMA: polymethylmethacrylate
 † : Estimated accuracy: 30% to 50%

20.13.1.3 Damage to composites

The damaging effects of atomic oxygen occur by direct oxidation of the organic polymer chains, e.g. epoxy thermoset resin, resulting in the formation and liberation of volatiles with a corresponding loss in mass. On the microscopic level, the surfaces are roughened and ultimately significant quantities of material can be lost.

[See also: [20.8](#) for [ATOX](#) erosion studies conducted as part of the long duration exposure facility programme, [LDEF](#)]

20.13.1.4 Property loss

The oxidation of both matrix and reinforcement produces changes in both mechanical properties and [CTE](#). [Table 20.13.2](#) shows the effect of short exposure time (~40 hours) on CTE, Ref. [\[20-25\]](#).

Significant and continuous changes in CTE can occur when such materials are exposed for up to 30 years.

Table 20.13-2 - Effects of short-term LEO exposure on coefficient of thermal expansion for T300/934 carbon/epoxy laminates (RT to +82°C)

Sample lay-up	CTE x 10 ⁻⁶ °C ⁻¹	
	Control	Flight
±45°	+ 4.61	+ 4.28 to 4.43
0°	+ 1.76 to 1.84	+0.65 to 0.70

20.13.1.5 Protection against ATOX

For satellite surfaces and composites exposed to very high levels of ATOX flux, protection schemes are essential, [See: [20.14](#); [20.15](#)]. Different protection systems are necessary for composites, polymer films, thermal control coatings and solar cells.

20.13.1.6 ECSS requirements

An accurate simulation of [LEO](#) flux is difficult to reproduce on Earth, Ref. [\[20-26\]](#). Test facilities are available at [ESA/ESTEC](#), Ref. [\[20-27\]](#).

No ECSS standard for ATOX testing exists currently.

20.14 Siloxanes and silicon polymers

20.14.1 Protection methods against ATOX

The presence of silicon at the surface of composites has demonstrated its value in forming an oxide barrier to [ATOX](#) erosion. The inclusion of glass fibres (silica) also has a protective effect. However, the possible release of glass fibres, through loss of matrix by erosion, has raised some concerns about this route being an acceptable wide-scale solution, Ref. [\[20-28\]](#). [GFRP](#) is not an efficient structural material, so the cladding of [CFRP](#) as a means of protection has few attractions.

The use of silicon-containing polymers does have merits for passivating the surface. Various techniques have been proposed for increasing the surface silicon content:

- Silicone coatings (paint or fluids), Ref. [\[20-29\]](#),
- Siloxane coatings,
- Siloxane matrix composites,
- Siloxane-modified epoxies, Ref. [\[20-30\]](#),
- Siloxane-modified cyanate esters, Ref. [\[20-31\]](#),
- Anoxic polymers and composites, Ref. [\[20-32\]](#),

- Siloxane molecular composites, Ref. [\[20-32\]](#),
- Sputtered silica coatings, Ref. [\[20-30\]](#).

The questions of particular significance when considering protection against [ATOX](#) flux by these proposed methods are:

- Is there an acceptable process for applying the surface layer to the intended component or structure?
- Does the protective surface coating survive thermal cycling and debris impacts?

20.14.2 Protection of polymer films

Possible solutions for Kapton™ and silver/[FEP](#) films are:

- Sputtered 30nm [SiO₂](#) coating.
- Dow Corning DC 976 and DC 705 silicone fluids applied diluted in solvent.

Coatings for polymer films need to be much thinner than those applied to structural composites.

20.14.3 Protection of composites

20.14.3.1 General

There is a range of possible protection methods because there are many ways of grafting silicon-containing chemical groups onto thermosetting or thermoplastic polymers. For example, if a conventional thermosetting [CFRP](#) composite is used as the primary structural material:

- A siloxane-based coating can be applied to the external surface. Although easily implemented, doubts remain about its adhesion under thermal cycling and debris impact.
- Elastomeric siloxane coatings are flexible and have reasonably high silicon contents, so act as a sacrificial layer to protect the composite substrate.
- The direct incorporation of siloxane groups into the matrix, or even the formation of self-reinforcing molecular composites, is also being studied. A siloxane chain (-Si-O-Si-) with, for example, methyl branches, can be incorporated into a cross-linked molecular arrangement (thermoset) or terminated with a block copolymer (thermoplastic). Examples of the methods under evaluation are:
 - siloxane-modified cyanate ester, and
 - anoxic siloxane molecular composites.

20.14.3.2 Siloxane modified cyanate ester resin

From the early Space Shuttle flights, e.g. STS-8, the benefits of cross-linked polydimethylsiloxanes and poly(siloxane-imide) copolymers were established because they formed stable oxide layers to inhibit [ATOX](#) erosion. By themselves, these polymers are elastomeric in nature and so lack the mechanical properties for structural use.

The cyanate esters have notable advantages as composite matrices, i.e. low moisture absorption and good toughness, adhesion and shear strength, [See also: [6.35](#)].

A combination of siloxanes and cyanate esters, retaining, to some extent, the advantages in a cross-linked structure, was obtained by adding 10% to 20% by weight of siloxane, Ref. [20-19]. The modified resin formulations showed a greater resistance to mass loss by oxygen plasma. In practice this gave a two-fold reduction in mass loss for a [CFRP](#) material prepared with 10% siloxane resin compared with equivalent laminates using epoxy Fiberite 934 and cyanate ester 954-1 matrices.

The addition of the siloxane had a 'softening' effect on the matrices, lowering the shear and flexural moduli. Therefore higher siloxane additions cannot be made without seriously compromising the matrix moduli, on which the shear and compressive integrity of the composite is based. It therefore remains to be proven whether this route provides sufficient protection to prevent carbon fibre loss under prolonged ATOX flux, given its modest surface silicon yield. Composites with silicon-containing matrices have yet to be flown in space.

20.14.3.3 Anoxic siloxane molecular composites

The term '[anoxic](#)' is used to describe materials resistant to thermo-oxidative attack by atomic oxygen, Ref. [20-32].

A '[molecular composite](#)' is the combination of two molecular groups where one rigid phase provides a reinforcing effect. The development of these materials, with support from [ESA/ESTEC](#), includes:

- Molecular composite films (10µm to 30µm), and
- Molecular composite films + carbon fibres = structural composite (work from 1995 onwards).

Molecular composites of polysiloxane-etherimide/polyamide-imide (flexible/rigid) in thin film form were exposed in [LEO](#) on board ESA's [BIOPAN](#) mission.

In addition, test exposures to an oxygen plasma flux of 2.8×10^{20} atoms/cm² demonstrated good erosion resistance. These films are being investigated as solar cell support film for [LEO](#) spacecraft solar arrays to replace Kapton.

NOTE The usual abbreviation for 'polysiloxane-etherimide/ polyamide-imide' is [PSI/PAI molecular composites](#).

The composites are formulated by dissolving both Siltem 1500 PSI and Amoco Torlon 4203 PAI polymers (G E Plastics B.V.), in various proportions in a solvent. These composites are likely to be particularly resistant to [ATOX](#) because of their inherent ability to create a protective surface silica film.

NOTE PSI/PAI molecular composites are likely to conform to the [outgassing](#) requirements in [ECSS-Q-ST-70-02](#).

20.15 Protective coatings

20.15.1 Surface coatings

20.15.1.1 General

The application of coatings to polymer composites is normally considered as a last resort because of the difficulties in obtaining reliable [adhesion](#).

The circumstances which dictate the need to apply protective or surface-modifying coatings include:

- Inhibit moisture absorption, e.g. Sn-In metallic barrier,
- Inhibit [ATOX](#) erosion, e.g. silicon-containing polymer coatings,
- Provide thermal control, e.g. paints,
- Provide a reflective coating, e.g. sputtered metal,
- Provide continuity of electrical conductivity.

[ECSS-O-ST-70](#) and [ECSS-O-70-71](#) provide information on the selection of materials and processes for space applications.

20.15.1.2 Atomic oxygen protection methods for CFRP

Composites and other organic materials intended for long-term deployment in space need protective coatings.

There are several viable ways of providing protection for [CFRP](#) elements. These are mainly based on metals or [perfluorinated](#) polymers.

Candidate protective materials are, Ref. [\[20-25\]](#):

- applied metal foil,
- sputtered metals,
- vapour-deposited metals,
- perfluorinated films, e.g. Teflon™,
- Teflon™-based coatings,
- silicone or siloxane coatings [See: [20.14](#)].

Metals which form stable oxides within space environments can be considered for coatings. The exceptions which have to be avoided are:

- [Osmium](#), which forms a volatile oxide.
- [Titanium](#), which continues to oxidise with a corresponding increase in mass and loss of function.
- [Silver](#), which suffers from cracking and spalling.

Any applied coating needs to be free from scratches and other minor surface damage. Any imperfection in the coating provides sites for oxidation to start and can result in localised penetration of the composite.

20.16 Debris

20.16.1 Classification of debris

20.16.1.1 General

Impacting particles come from two sources:

- [Micrometeoroids](#), and
- Accumulated man-made [debris](#) trapped in orbit.

The impact flux is dependent on the orbit height, craft orientation and velocity, coupled with the impact trajectories.

Flux is not solely a function of a point in space, but depends heavily on the orientation of individual surfaces of the spacecraft.

The [LDEF](#) programme provided the most comprehensive insight into impact events over prolonged exposures in [LEO](#). [See also: [20.8](#)].

20.16.1.2 Micrometeoroids

Micrometeoroids come from natural sources, such as comets, asteroids, the moon and planets. Their characteristics can be summarised as:

- Velocity relative to Earth, from 12 to 72 km/s, typically.
- Impact velocities relative to orbiting satellites, from 4 km/s to 79 km/s, typically.
- Typical velocity range: 10 km/s to 30 km/s (average 19 km/s).
- Comet meteoroids are mainly ice particles, with a density of 0.5 g/cm³, typically.
- Asteroid particles are mainly mineral-based, with densities up to 8g/cm³, typically.
- Most micrometeoroids in the near-Earth environment are in the range of 50µm to 1 mm in diameter.
- Beta meteoroids (interplanetary dust of less than 1 µm diameter) do not cause significant damage.

20.16.1.3 Orbital debris

This consists of a very wide range of man-made [debris](#) resulting from standard launch, deployment and other spacecraft operations.

The general characteristics of debris are:

- Materials, such as:
 - solid rocket-propellant exhaust products, e.g. 10 µm alumina particles, typically.

- paint flakes, and
- structural debris from environmental exposure.
- A wide distribution of particles sizes, with a greater proportion larger than 1 mm than are present in the micrometeoroid flux.
- At 500 km altitude and 28.5° inclination, e.g. Space Station, the relative impact velocity is about 10.7 km/s.
- For highly elliptical orbits, relative velocities range from 0 km/s to 19 km/s; averaging about 8 km/s to 10 km/s relative normal incidence velocity for the majority of impacts at oblique angles.

The increase of in-orbit man-made debris is estimated at 6% per annum. In [LEO](#), 90% of all impacts are caused by man-made debris. Skylab and early Shuttle flights gave the first indications of the impacts that can be experienced in LEO, Ref. [\[20-33\]](#), [\[20-42\]](#).

20.16.2 Damage to LDEF

[LDEF](#) was a large structure orbiting in LEO for nearly six years, [See: [20.8](#)]. It experienced hundreds of thousands, if not millions, of impacts, Ref. [\[20-29\]](#). These included a single impact from a 'large' particle 0.7mm in diameter on the 7m² area exposed in the [ram](#) direction. Such a particle, travelling at 6 km/s, is capable of penetrating a typical 2.5 mm aluminium alloy satellite wall.

[LDEF](#) also experienced ~1 impact/m² on the [ram](#)-exposed surfaces capable of penetrating a typical 1.5 mm thick aluminium electronics box wall. Whilst these impacts can be extremely damaging to internal components, such as electronics, batteries, motors and mechanisms, they are extremely rare.

For all impacts, the damage area is far larger than the diameter of the [debris](#) particle. The shape of the damage area, or crater, is dependent on the angle of incidence to the impacted surface. A low-angle oblique impact produces a significant area of immediate surface damage but lacks the penetration of a high-angle impact. Different structural materials have different responses to impacting high-velocity particles. Whilst individual impacts can be of low structural significance, the accumulated effect of many impacts cannot be underestimated.

20.16.3 Damage to composites

Damage can be characterised as:

- A point of impact with a surrounding spall zone.
- The point of entry shows no sign of melting, but material has been lost and fractured fibres overlap the surface hole.
- A subsurface [delamination](#) zone, larger than the entry hole.
- If through-penetration has occurred, the exit hole can be larger than the entry hole.

The largest impact on [LDEF](#) produced damage which consisted of:

- Surface hole of about 0.5 mm diameter,
- Exit hole of about 1 mm diameter,

- Spall area of several millimetres in size, with cracks in the composite matrix extending for several tens of millimetres.

20.16.4 Damage to aluminium alloys

Damage can be characterised as:

- Formation of a crater, with material displaced from the point of impact.
- Some of the displaced metal is melted by the impact.
- The crater has a rim which stands proud of the surface.
- Some of the molten material is displaced from the crater in the form of droplets which splash on the surrounding area.
- Paint at the point of impact is spalled from the surface to become a contamination source in the environment around the craft.

Impact craters with an angle of incidence normal to the surface are virtually hemispherical in shape. For oblique angle impacts, the main elongated crater can have separate craters within it, presumably resulting from the impacting particle breaking up into smaller pieces.

In general, impact crater diameters average about 5 times the diameter of the impacting particle. The total region experiencing splashed material averages 10 times the diameter of the impactor.

The single large impact to [LDEF](#) struck a structural aluminium 'Z-frame'. The frame was covered with silvered-Teflon adhesively-bonded thermal-control tape, Ref. [\[20-34\]](#).

The impact characteristics were:

- The Z-frame faced the [ram](#) direction with the particle, in an elliptical orbit, striking the space-facing end of LDEF.
- Particle size was estimated at 0.7mm to 0.9mm diameter.
- A very large damage area was observed with delamination at the Teflon-to-silver and Teflon-to-aluminium interfaces.
- Teflon was melted and ejected from the crater.
- The crater diameter was 5.25 mm with severe bulging on the back face of the frame.
- Penetration was prevented by the presence of a backing block of aluminium behind the frame.
- Ejected material was sprayed over a 200 mm wide swath across adjacent areas.

20.16.5 Damage to thermal control materials

20.16.5.1 General

The area of material affected by an impact is larger than that seen for aluminium, mainly because of the delamination of layers that occurs, Ref. [\[20-34\]](#).

20.16.5.2 Thermal blankets

A typical multi-layer thermal control blanket ([MLI](#)) on LDEF consisted of:

- Outer layer of white thermal control paint (Chemglaze A276),
- Mylar layer,
- 22 layers of aluminium foil separated by Dacron mesh,
- Kapton tape,
- Lexan substrate.

These types of constructions not only suffered impact damage, but the subsequent access of [ATOX](#) and [VUV](#) to sub-layers caused further degradation and material break-up.

20.16.5.3 Thermal control painted materials

The thermal control paints suffered ATOX erosion resulting in the removal of the polymer binders, leaving loosely attached pigment particles.

[Debris](#) impact compounded the degradation by causing a 'ring phenomenon'. Here, the impact crater, with its surrounding spall zone, was 'ringed' by a wrinkled and rolled back top layer of paint. The raised rings were outside the spall zone and appeared to be displaced paint or pigment powder. The concern is that a pressure wave effect travels through the paint and induces damage.

20.16.6 Significance of impact events

High-velocity debris can cause damage to a volume of impacted material that far exceeds the particle volume or immediate surface impact crater.

The distribution of impacts over the surface of a satellite depends on many parameters, Ref. [\[20-35\]](#). The parts of the structure that experience the higher impact flux densities can need direct shielding, Ref. [\[20-30\]](#).

As an indication of the level of impacts which can be anticipated, reference can be made to [LDEF](#):

- Immediate surface cratering on LDEF amounted to a total damage area of about 0.1%.
- The 'extended' damage areas due to the combined surface effects of cratering, [spalling](#), [delamination](#) and cracking produced a total damage area of about 3%.

Whilst these do not appear to be particularly high figures, the mission duration was only approximately 6 years. For a 30 year mission, the total surface damage area approaches 15%; ignoring any increase in man-made debris during the years of deployment.

For composites, the damage is not just to the immediate surface, but has a volume effect.

20.16.7 Protective shielding

20.16.7.1 General

The increase in man-made [debris](#) over the years has increased the probability of catastrophic impact by a large particle. This is a very serious possibility for a manned, pressurised spacecraft such as Columbus and [ISS](#).

The critical particle size on which probability theory calculates the likelihood of a critical impact also increases. The implications for structural design are that theory should be used to define the maximum size of particle which is likely to be encountered during a 30-year mission, and adequate protection provided against it. If shielding is required, it has to be lightweight and effective in containing the predicted impact energies, Ref. [\[20-36\]](#), [\[20-37\]](#).

The simulation of impacts can be achieved in test facilities, Ref. [\[20-38\]](#), but with a velocity limitation of 8km/s and centimetre-sized particles; whereas 90% of space debris has a velocity greater than this and are much smaller particles.

20.16.7.2 Columbus bumper shield concepts

To protect the man-rated Columbus structure against large debris, an offset bumper shield arrangement has been proposed, Ref. [\[20-39\]](#), [\[20-40\]](#), [\[20-41\]](#). Such a shield should be orientated to meet a specific ballistic threat, but also needs to be lightweight. Constructions based on aluminium, GLARE™ laminates and Kevlar™ composites have been evaluated, [See also: [46.17](#) for GLARE].

The shield construction has several functions in containing the kinetic energy of the debris particle and subsequent spalled material. An offset arrangement of panels is necessary, fixed at up to 120 mm from the primary structure. The typical areal mass for these types of shield is 13.5 kg/m², which includes the pressure module wall as part of the shield system, Ref. [\[20-41\]](#). Hence the shield has a structural, as well as protective, function.

20.17 References

20.17.1 General

- [20-1] J. Dauphin et al
'Materials for space application'
Metals and Materials, July 1991, p422-430
- [20-2] B.D. Dunn
'Metallurgical Assessment of Spacecraft Parts & Materials'
Published by Ellis Horwood Limited, ISBN-0-7458-0762-3, 1989
- [20-3] B. Fornari & D. Dosio
'Characterisation of a state of the art UHM CFRP prepreg system for satellite application'
Proceedings of the International Symposium on Advanced Materials for Lightweight Structures '94, ESTEC, Noordwijk
March 1994, ESA WPP-070, p569-576
- [20-4] P. George
'Space environmental effects on LDEF low earth orbit exposed graphite reinforced polymer matrix composites'
NASA Conference Publication 3162, Part 2. Proceedings of a Workshop held at H.J.E Reid Conference Centre, NASA Langley Research Centre, 19-22 November 1991, p543-570
- [20-5] R.C. Tennyson et al
'Proposed test program and data base for LDEF polymer matrix composites'

- NASA Conference Publication 3162, Part 2. Proceedings of a Workshop held at H.J.E Reid Conference Centre, NASA Langley Research Centre, 19-22 November 1991, p593-600
- [20-6] G.L. Steckel et al
'Polymer matrix composites LDEF experiments M0003-9 & 10'
NASA Conference Publication 3162, Part 2
Proceedings of a Workshop at H.J.E Reid Conference Centre NASA Langley Research Centre, 19-22 November 1991 p515-542
- [20-7] C. Blair & B.C. Petrie
'Low earth orbit environmental effects on composite materials: results from the long duration exposure facility (LDEF)'
24th International SAMPE Technical Conference, 20-22 October 1992, pT186-T200
- [20-8] 'Property changes induced by the space environment in composite materials on LDEF experiment AO171 (Sample)'
NASA-CR-192572, April 1993, 18 pages
- [20-9] R.C. Tennyson
'Additional results on space environmental effects on polymer matrix composites - experimental AO180'
NASA Conference Publication 3162, Part 2. Proceedings of a Workshop held at H.J.E Reid Conference Centre, NASA Langley Research Centre, 19-22 November 1991, p571-592
- [20-10] J.P. Wightman
'Surface characterisation of LDEF materials'
NASA-CR-194519, October 1993
- [20-11] Discussion Sessions: NASA Conference Publication 3162, Part 2, Proceedings of a Workshop held at H.J.E Reid Conference Centre, NASA Langley Research Centre, 19-22 November 1991.
- Polymers and films (Including Ag/FEP), p707-717
 - Polymer matrix composites, p727-736
 - Lubricants, adhesives, seals, fasteners, solar cells & batteries, p737-747
- [20-12] B. Keough
'Identification and evaluation of lubricants, adhesives & seals used on LDEF'
NASA Conference Publication 3162, Part 2. Proceedings of a Workshop held at H.J.E. Reid Conference Centre, NASA Langley Research Centre, 19-22 November 1991, p603-618
- [20-13] D.F. Thompson & H.W. Babel
'Material applications on the space station - Key issues and the approach to their solution'
SAMPE Quarterly, October 1989, p27-33 & 34th International SAMPE Symposium, 8-11 May 1989, p759-769

- [20-14] W. Hartung
'Influence of thermal cycling on the behaviour of CFRP material for space structures'
ESA SP-225, August 1984
- [20-15] D.P. Bashford
'Microcracking behaviour of epoxy and cyanate ester UHM CFRP composites'
ERA Technology Report 94-0362, Final Report on Work Order No. 34, ESTEC Contract 7090/87/NL/PP, April 1994
- [20-16] ESA PSS-01-609 Issue 1 (May 1993): Radiation design handbook
- [20-17] Matra Espace
Report DM 51.C/CC/FUO138-82
- [20-18] R.C. Tennyson et al
'The effects of combined UV radiation and high energy electrons on the behaviour of polymer matrix composites in hard vacuum'
AGARD-CP 327, September 1982
- [20-19] G.F. Sykes & D.E. Bowles
'Space radiation effects on the dimensional stability of a toughened epoxy graphite composite'
SAMPE Quarterly, July 1986, p39-53
- [20-20] R.N. Yancy et al
'Radiation and thermal effects on the time-dependent response of T300/934 graphite/epoxy'
34th International SAMPE Symposium
8-11 May 1989, p1174-1189
- [20-21] J.G. Funk
'Effects of cure temperature, electron radiation and thermal cycling on P75/930 composites'
NASA Technical Memorandum 102712, Dec. 1990
- [20-22] A. Paillous & C. Pailier
'Degradation of multiply polymer-matrix composites induced by space environment'
Composites, Vol. 25, No. 4, 1994, p287-295
- [20-23] K.T. Kern et al
'Simulated space environmental effects on a polyetherimide at its carbon fibre-reinforced composites'
SAMPE Journal, Vol. 29, No. 3, May/June 1993, p29-44
- [20-24] L.J. Leger et al
'A consideration of atomic oxygen interactions with Space Station'
AIAA-85-0476, January 1985
- [20-25] D.P. Bashford
'A guideline on the response of composite materials to environmental conditions encountered by space structures and launch vehicles'
Fulmer Research Laboratories. ESA Contract: 5497/83

- [20-26] C.R. Stidham et al
'Low earth orbital atomic oxygen environmental simulation facility for space materials evaluation'
38th International SAMPE Symposium
10-13 May 1993, Vol. 1, p649-663
- [20-27] C. Barbier et al
'ATOX: The ESTEC atomic oxygen simulation facility'
Preparing for the Future, Vol. 2, No. 2, June 1992
- [20-28] S.K. Rutledge et al
'Evaluation of atomic oxygen resistant protective coatings for fiberglass-epoxy composites in LEO'
34th International SAMPE Symposium
8-11 May 1989, p1163-1174
- [20-29] J.H. Sanders et al
'Application and performance of silicon-based atomic oxygen protective coatings'
34th International SAMPE Symposium
8-11 May 1989, p1152-1162
- [20-30] S.L. Oldham
'Atomic oxygen resistant, thermally stable epoxies'
21st International SAMPE Technical Symposium, 25-28 September 1989, p984-993
- [20-31] C. Arnold et al
'Siloxane modified cyanate ester resins for space applications'
37th International SAMPE Symposium
9-12 March 1992, p128-136
- [20-32] S. Palsule
'Anoxic molecular composites: The third-generation polymers for aerospace applications'
Proceedings of the International Symposium on Advanced Materials for Lightweight Structures '94, ESTEC, Noordwijk
March 1994, ESA WPP-070, p577-580
- [20-33] C.R. Maag
'Low earth orbit debris effects on materials'
IAF-91-284 Paper from 42nd Congress of the International Astronautical Federation, Montreal, Canada, 5-11 October 1991
- [20-34] M. Allbrooks & D. Atkinson
'The magnitude of impact damage on LDEF materials'
NASA-CR-188258, July 1992
- [20-35] J. Zhang & D. Rex
'The distribution of debris impacts over satellite surfaces with special regard to the long duration exposure facility LDEF'
Z. Flugwiss. Weltraumforsch. 17 (1993), p170-180
- [20-36] M. Lambert
'Shielding against orbital debris - A challenging problem'
Proceedings of an International Symposium on Space Applications of Advanced Structural Materials, ESTEC, Noordwijk
March 1990, ESA SP-303, p319-328

- [20-37] M. Lambert
'Shielding against natural and man-made space debris: A growing challenge'
ESA Journal 1993, Vol. 17, p31-42
- [20-38] E. Schneider & M. Lambert
'Space debris simulation facilities and high speed diagnostic methods'
Proceedings of the International Symposium on Advanced Materials for
Lightweight Structures 94, ESTEC, Noordwijk
March 1994, ESA WPP-070, p385-390
- [20-39] H-G. Reimerdes et al
'Ballistic limit equations for the Columbus-Double Bumper Shield concept'
Proceedings of the First European Conference on Space Debris Darmstadt,
April 1993, ESA SD-01, p433-439
- [20-40] H-G. Reimerdes
'Meteoroid and debris protection study (MDPS) – Executive summary'
ESTEC Contract No. 8732/90/NL/PP, ERNO Raumfahrttechnik GmbH
contractor report CR(P) 3615, October 1992
- [20-41] M. Lambert
'Shielding against orbital debris - A comparison between different shields'
Internal ESTEC Working Paper No. 1740
- [20-42] N.L. Johnson & D.S. McKnight
'Artificial space debris'
Orbit Book Company, Malabar, Florida, USA, 1987
- [20-43] ESA PSS-01-202: Preservation, storage, handling and transportation of
ESA spacecraft hardware
- [20-44] ESA PSS-01-609: Radiation design handbook.

20.17.2 ECSS documents

[See: [ECSS](#) website]

ESA PSS-01-202:	Preservation, storage, handling & transportation of ESA spacecraft hardware.
ESA PSS-01-609:	Radiation design handbook.
ECSS-Q-ST-70	Materials, mechanical parts and processes; previously ESA PSS-01-70.
ECSS-Q-70-71	Data for selection of space materials and processes; previously ESA PSS-01-701.
ECSS-Q-ST-70-02	Thermal vacuum outgassing test for the screening of space materials; previously ESA PSS-01-702
ECSS-Q-ST-70-04	Thermal testing for the evaluation of space materials, processes, mechanical parts and assemblies; previously ESA

	PSS-01-704.
ECSS-Q-ST-70-06	Particle and UV radiation testing for space materials; previously ESA PSS-01-706.
ECSS-Q-ST-70-29	Determination of offgassing products from materials and assembled articles to be used in a manned space vehicle crew compartment; previously ESA PSS-01-729.
ECSS-E-HB-32-23	Threaded fasteners handbook; previously ESA PSS-03-208.
ECSS-E-ST-32-08	Materials

NOTE [ECSS-Q-ST-70](#) and ECSS-Q-70-71 provides information on materials and process selection for space applications.

21

Bonded joints

21.1 Introduction

Design, calculation information and data on adhesively bonded joints are presented. General guidelines on the selection of most practical joint types are also provided.

[See also: [ECSS-E-32-21](#) - Adhesive bonding handbook for advanced structural materials; previously ESA PSS-03-210]

21.2 Adhesives

21.2.1 General

The use of adhesives demands detailed technical specifications. Joint design should be carefully studied, taking into account temperature and area.

In general, adhesives should be able to exhibit several properties, including:

- Strain capability; to accommodate joints between [dissimilar](#) materials.
- [Cure](#) at as low a temperature as practical.
- Coefficients of thermal expansion of adhesives are in the [CTE](#) range of the joint parts.
- minimal Moisture effects .
- Thickness cannot be too large.
- Compatibility with [adherends](#).
- Conform to [outgassing](#) requirements, [See: [ECSS-Q-ST-70-02](#)].

21.2.2 Types of adhesives

21.2.2.1 General

Adhesives are broadly classified as either:

- [Film](#), or
- [Paste](#).

Most suppliers do not provide the information needed to enable the selection of the most appropriate adhesive for design work. This includes the effect of moisture, which should be carefully considered in the selection process.

[Table 21.2.1](#) lists some chemical groups of adhesives that have been used in space applications, Ref. [\[21-1\]](#). Their typical characteristics are shown in [Table 21.2.2](#), Ref. [\[21-1\]](#).

Table 21.2-1 - Adhesives: Common types

Adhesive Type	Maximum Service Temperature (°C)	Shear Strength † (MPa)
Epoxy	90	36
Epoxyphenolic	200	25 - 40
Epoxy polyamide	100	25
Polyimide	400	14 - 18
Silicone	340	14
Phenolic-Polyamide	150	36
Phenolic-Vinyl	100	36
Polyamide	100	40 - 60

Key: † Shear strengths at room temperature

Table 21.2-2 - Adhesives: Typical characteristics

Adhesive Trade Name	Vacuum Outgassing %		Tensile Strength (MPa)	Tensile Modulus (MPa)	Elongation (%)	Thermal Expansion ($10^{-6} \text{ }^{\circ}\text{C}^{-1}$)
	TML	CVCM				
Aerobond 2143	1.22	0	42.7	1240	1	58.9
FM 53	1.6	0.01	44.0	2101	1	88.9
FM 73	1.47	0	52.4	2136	3	74.0
FM 400	0.71	0.02	41.3	7235	1	46.6
A-452	2.24	0.26	57.9	041	3	80.3
C7/W	1.43	0.02	45.5	2019	3	66.4
Plastilock 717A	1.53	0.58	55.1	075	3	75.6
Araldite AV100	1.1	0.07	14.5	2604	-	59.9
Araldite AV138	0.7	0.02	17.7	9164	-	54
Redux 312	1.1	0.05	43.4	-	-	-
Hysol 9309	1.33	0	37.0	2439	3	48.4
Hysol 9601	1.37	0.3	61.3	2556	1	34.4
Epibond 123/945	0.91	0	26.87	5305	1.3	52.4
Epibond 123/931	0.92	0	62.7	965	1	44.5
RTV 566	0.2	0.02	6.89	-	-	648
RTV-S 691	0.2	0.01	6.2	-	-	648-129.6
AF 126	1.59	0.27	22.7	2564	12	78.7
AF 143	1.52	0	40.23	2198	2	84.6
AF 163-2M	1.29	0.26	49.6	2060	6	96.1
AF 163-K	1.65	0.23	37.2	2039	2	86.0
EC 2214	1.02	0.11	50.9	5870	1	57.2
EC 2216	1	0.02	20.7	-	-	-
Metlbond 329	85	0.02	61.3	6856	1.5	78.3
Metlbond 1133	1.67	0	44.1	1915	3	107.3

21.2.2.2 Epoxy

Epoxy resin adhesives are the most common types for space applications. They are obtained as either:

- Two-part mixtures (resin plus hardener) for self-curing at room temperatures, or
- One part (resin) for a heat-curing process.

Epoxy resins without hardeners can be [cured](#) simply by keeping the assembly at the stated temperature for the specified time without an increase in pressure. In this case, the curing temperature can be about 180°C and the curing time is very long.

In order to obtain the maximum strength at elevated service temperature and a very short curing time at low temperature, it is advisable to use a [hardener](#), with or without an [accelerator](#). In this case, the curing time can be as short as 20 minutes at 145°C under a pressure of 0.7 MPa.

'Modified' epoxy resins, i.e. epoxy-phenolic and epoxy-polyamide, adhesives can be cured for about 1 hour between 130°C and 175°C.

21.2.2.3 Polyimides

[Polyimide](#) resin adhesives cure at temperatures between 250°C and 400°C. A [post-cure](#) is necessary to obtain the highest strengths and a range of service temperature of the order of 290°C to 400°C.

21.2.2.4 Fluorocarbon (Viton)

Fluorocarbon polymer resin adhesives are used for special high temperature applications.

21.2.2.5 Polyamides

Polyamide resin in adhesives produces 'modified' epoxy resins and 'phenolic polyamide' resins.

21.2.2.6 Silicones

Silicone adhesives have excellent behaviour at high temperatures but relatively low strength. For this reason they are mixed with other resins to provide high-temperature stability with high mechanical strength. For example, epoxy silicone adhesive can have maximum service temperatures of 340°C (at continuous exposure) and 510°C (at intermittent exposure).

21.2.2.7 Phenolic

Phenolic resin adhesives for space applications are used in mixtures with other resins, including:

- Phenolic-polyamide: Shear strength of the order of 36 MPa and excellent strength at high temperatures, e.g. 1.4 MPa at 150°C.
- Phenolic-vinyl (or vinyl phenolic): Shear strength of the order of 36 MPa, but the range of service temperature is very low and degrades quickly above 100 °C.

21.2.3 Adhesives for joining different materials

[Figure 21.2.1](#) shows the types of adhesives which are applicable for joining different materials.

Where no adhesives are shown, the materials can be bonded with difficulty. Bonding is possible after a surface treatment, which increases the critical surface tension.

Group 1	Metals and Alloys		Ceramics and Glass		Polyurethanes	Phenolics	Epoxies
	E/T	E	PTFE	E/T			
Metals and Alloys	E/T						
Ceramics and Glass	E	-					
PTFE	E/T	-	E/T				
Polyurethanes	E	-	-	E			
Phenolics	E	E	T	-	E		
Epoxies	E	-	E/T	-	E/T	E/T	

Group II	Polyamides	Silicones
	Metals and Alloys	E
Ceramics and Glass	-	
PTFE	-	-
Polyurethanes	-	S
Phenolics	-	-
Epoxies	-	-

Key: E - Epoxies
 T - Thiokol
 S - Silicones
 P - Polyamides

Group III	Polyamides	Silicones
	Polyamides	P
Silicones	-	S

Figure 21.2-1 - Adhesives for bonding different materials

21.3 Design of bonded joints

21.3.1 Basic considerations

21.3.1.1 Adherends

To design a bonded joint, knowledge of the parts to be joined (the [adherends](#)) is necessary, including:

- Ultimate strengths for composites,
- Yield strengths for metals,
- Elasticity moduli,
- Coefficients of thermal expansion,
- Maximum elongation, and
- Chemical composition.

21.3.1.2 Loading

All the possible loading modes that the bonded joint is to withstand during its service life should be considered.

21.3.1.3 Environment

Both the working environment and the exposure duration should be known, e.g. thermal and moisture conditions, and combinations thereof.

21.3.2 Basic guidelines

Fundamental points to be considered before a joint is designed are:

- The whole joint area withstands the loads acting on the joint.
- The loads applied result mainly in shear stresses. [Cleavage](#), [peel](#) stresses and stress concentrations at free ends are either avoided or minimised.
- From experience, the best adhesive bonds have an adhesive layer thickness between 0.1mm and 0.25mm.
- Inspection of the joint during its working life is crucial.

21.3.3 Failure modes

The predominant failure modes depend upon:

- overlap length,
- adhesive thickness, and
- fibre orientation in the layer of composite adjacent to the adhesive.

For example:

- Long lap lengths and a thin adhesive film, giving a length-to-thickness ratio of 50, tend to produce tension or compression failures in the adhesives.
- Length-to-thickness ratios of 25 tend to produce shear failures in the adhesives or interlaminar areas depending on the joint configuration, [See also: [21.4](#) for joint configuration].

21.3.4 Features

21.3.4.1 Polymer composites

Joints between two or more composite layers can be achieved by:

- [Secondary bonding](#), using an adhesive (often a film),
- [Co-curing](#):
 - using the adhesive property of the [prepreg](#),
 - by incorporating an adhesive into a composite assembly prior to curing.

The objective and function of an adhesive joint is to provide load transfer between two adjacent components by the most efficient means. The [anisotropic](#) properties of composites should be taken into account, such as:

- stiffness and stability,
- thermal expansion,
- load bearing requirements.

Bonding is more appropriate for lightly-loaded joints in which its high-efficiency characteristics can be fully utilised.

Damage from drilling or machining makes [orthotropic](#) materials (such as composites) susceptible to:

- interlaminar shear,
- [delamination](#), and
- ply peeling.

Consequently, bonding is usually preferred over mechanically fastened joints between advanced composite components or to metal parts.

Since mechanical loads on joints in spacecraft are often low, the important characteristics are:

- dimensional stability,
- thermal expansion, and
- low weight.

Thermal cycling from -132°C to +121°C can impose high stresses on the bondlines of adhesively bonded joints.

21.3.4.2 Advantages

The main advantages of bonded joints are:

- Load distribution on a large area; avoiding load concentrations.
- High joint efficiency index; relationship of strength and mass of the joint region.
- Low part count.
- No strength degradation of basic laminate by use of cut outs or machining operations.
- Low potential cost.
- Corrosion problems are minimised for bonding [dissimilar](#) materials.

21.3.4.3 Disadvantages

The disadvantages of bonded joints can be summarised as:

- They can be difficult to inspect non-destructively.
- Designs should avoid or minimise [peel](#) loadings.
- Efficient structural bonds rely on accurate mating of [adherends](#).
- They are permanent and cannot be disassembled.
- Thermal cycling and high humidity can affect their strength.
- Special surface preparations are needed prior to bonding.

21.3.4.4 Non-polymer composites

The family of fibre metal laminates [FML](#), i.e. ARALL™ and GLARE™, comprise of fibre-reinforced adhesive layers that are used to bond together sheets of conventional metals, [See: [46.17](#)]. Components made from these 'hybrid' material laminates can also be assembled using adhesive bonding.

Adhesive bonding is widely used in the aerospace industry for the assembly of conventional structural metal alloys, e.g. sheet aluminium components. The structural integrity of honeycomb panels relies on adhesively bonded joints between the face skins and the core, [See also: [26.16](#) and [ECSS-E-HB-32-21](#)].

The potting of inserts and other attachment points into honeycomb panels uses adhesive pastes, often thickened to improve handling characteristics, [See: [ECSS-E-HB-32-22](#)].

Bonding is used to assemble solar panels and also within some electrical and electronic subassemblies, [See: [ECSS-Q-70-71](#)].

[See also: Chapter [58](#) for joint selection factors associated with metal- and ceramic-based advanced materials]

21.4 Joint configuration

21.4.1 Basic configurations

21.4.1.1 General

Examples of each type are shown in [Figure 21.4.1](#), Ref. [\[21-1\]](#).

These are basic configurations and not necessarily practical designs.

21.4.1.2 Single lap joints

Features of single-lap joints can be summarised as:

- It is the simplest bonded joint configuration.
- The highest stress concentrations in this type of joint are at the free ends of the bond.
- The centre of the joint transmits very little load.
- The bevelled and radiused single-lap joints improve on simple joint behaviour, minimising stress concentrations.

21.4.1.3 Double lap joints

Features of double-lap joints are:

- These are more complex than single lap joints.
- They eliminate most of the bending and [peel](#) stresses.
- Numerous applications are possible for joints of this type.

21.4.1.4 Strap joints

Features of strap joints can be summarised as:

- This type of joint is a more sophisticated solution than double-lap, but it is based on the same principle.
- The double-lap advantages are improved by applying special design to each application or problem.

21.4.1.5 Stepped-lap joints

Features of stepped-lap joints can be summarised as:

- They are very difficult to machine.
- They are not applicable to thin adherends.
- Are used to improve the shear strength at joint whose adherends are of very thick section. Nevertheless, the ply stacking sequence - due to different ply orientations - is a great problem since it can result in non 0° oriented fibre areas on the surface, for non uni-directional composite bonding cases.
- They produce very good stress distributions.

- They have a high joint efficiency index (strength-to-weight).

21.4.1.6 Scarf joints

Scarf joints are very similar to stepped lap joints, but are easier to machine.

21.4.1.7 Shim insert joints

Shim insert joints are used to increase joint section, e.g. for [inserts](#).

21.4.1.8 Other configurations

These can be described as designs that provide improvements on the basic configurations for special applications.

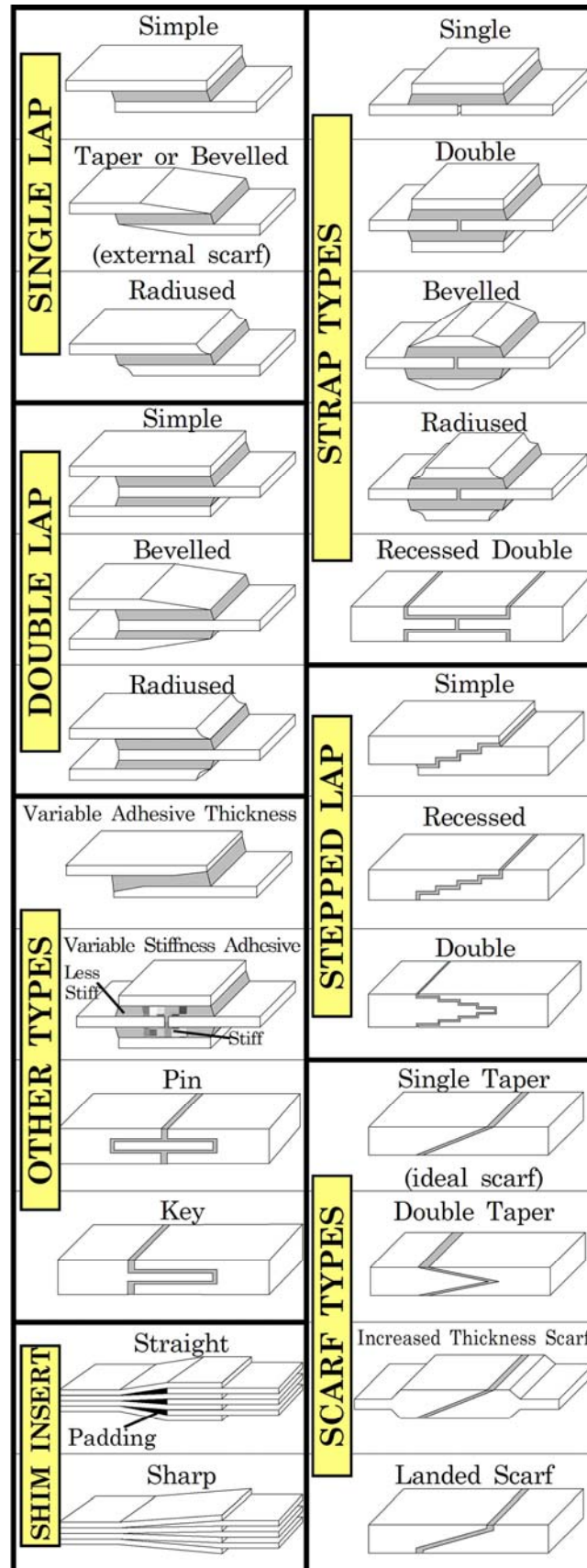


Figure 21.4-1 - Bonded joints: Basic configurations

21.4.2 Orientation of surface fibres

The direction of the surface layer of fibres in a joint is specified in the composite [lay-up](#), so that they are in the direction of the load.

[Figure 21.4.2](#) indicates the fibre orientation according to load directions, Ref. [\[21-3\]](#).

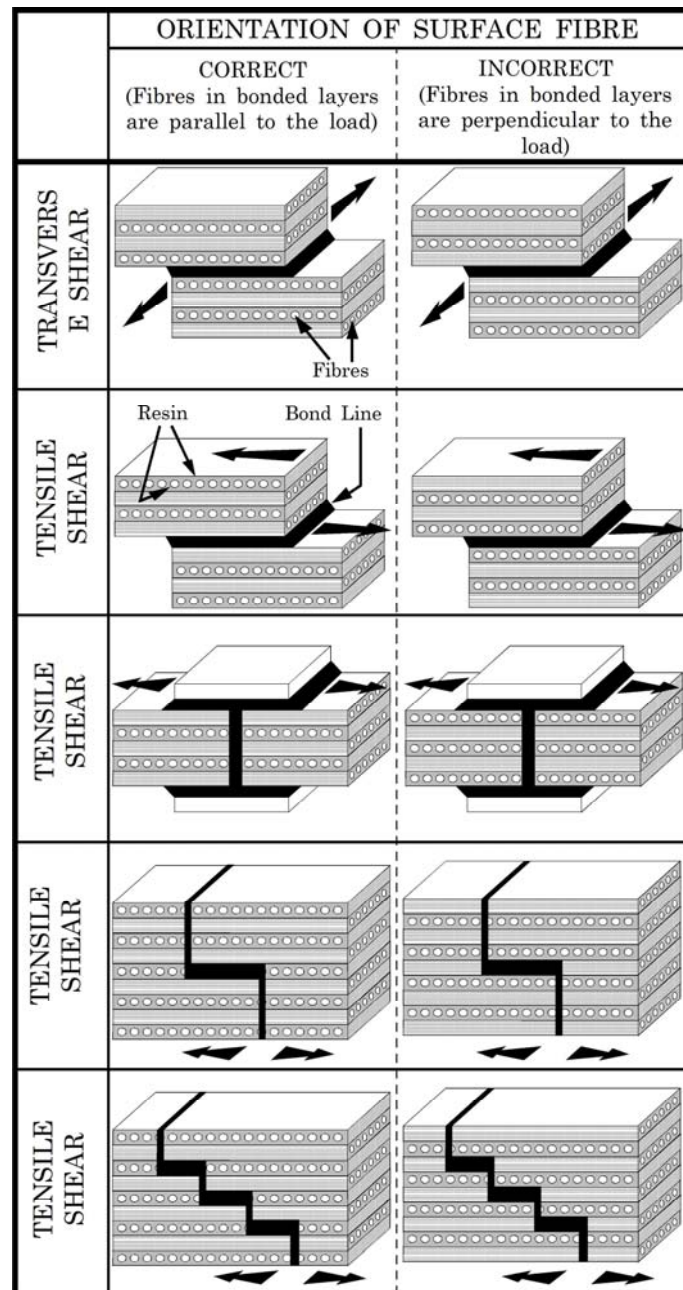


Figure 21.4-2 - Bonded joints: Orientation of surface fibre

21.5 Environmental factors for bonded joints

21.5.1 General

Temperature and moisture are considered in designing composite structures, owing to their influence on composite component properties.

21.5.2 Effect of moisture

Absorbed moisture moves through the adhesive resin by capillary action producing a gradual softening plasticisation, causing:

- [swelling](#), and
- lowering of the glass transition temperature, [T_g](#).

Experimental results indicate that moisture absorption levels in excess of 0.6% can be withstood without any decrease in adhesive strength.

[Figure 21.5.1](#) compares the variation of adhesive shear stress along the joint, due to a constant end load, Ref. [\[21-4\]](#).

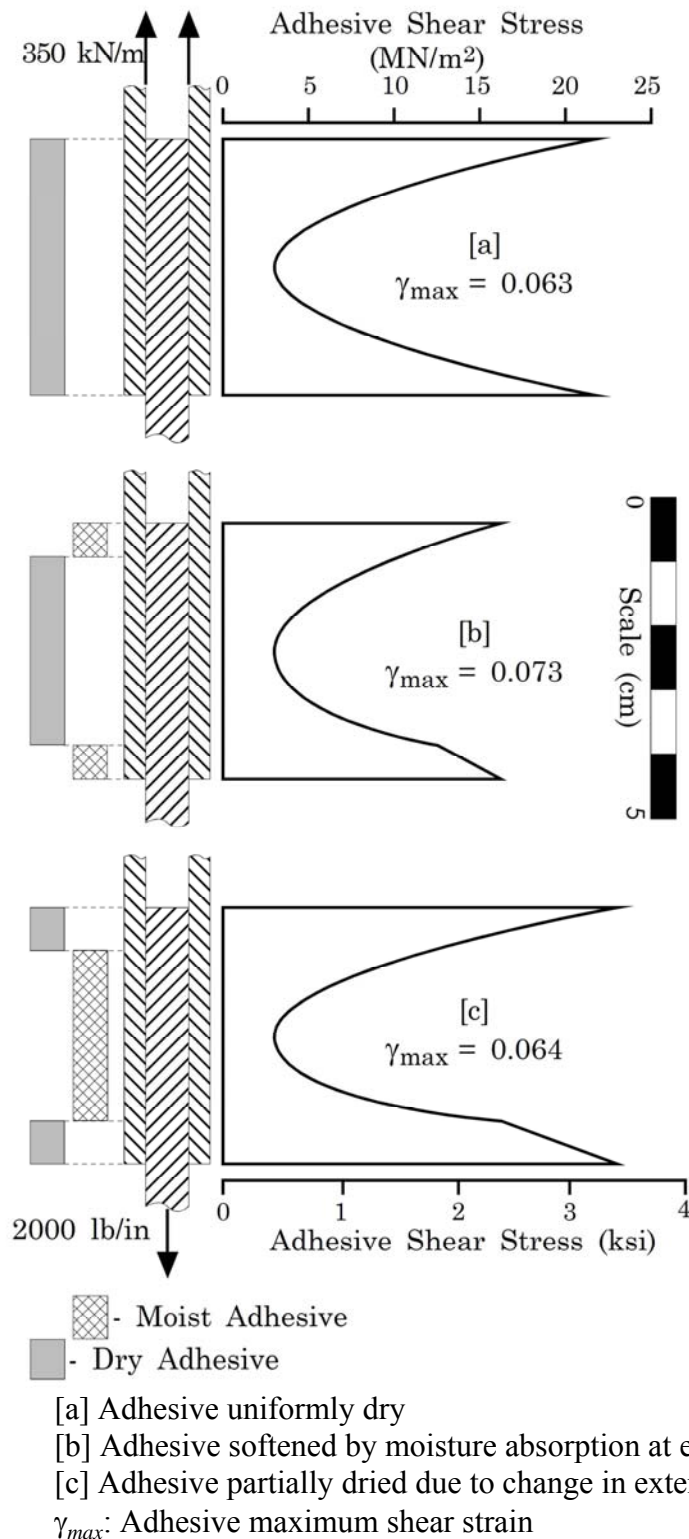
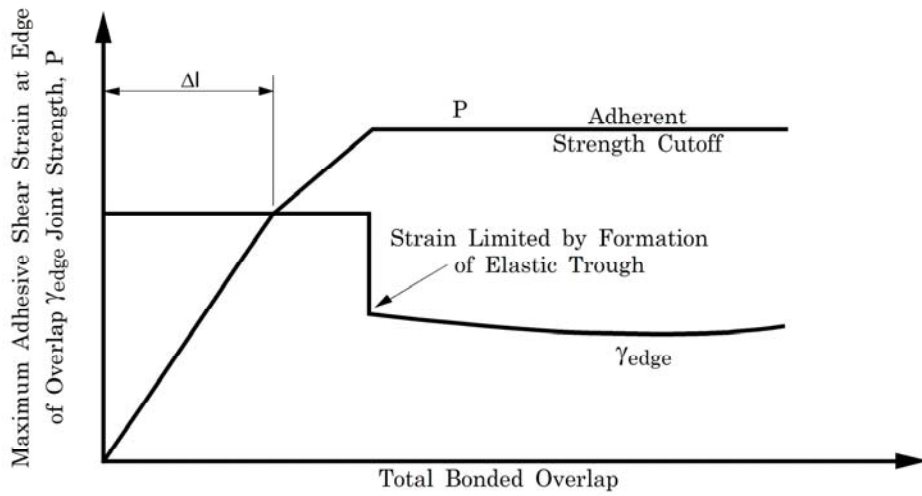
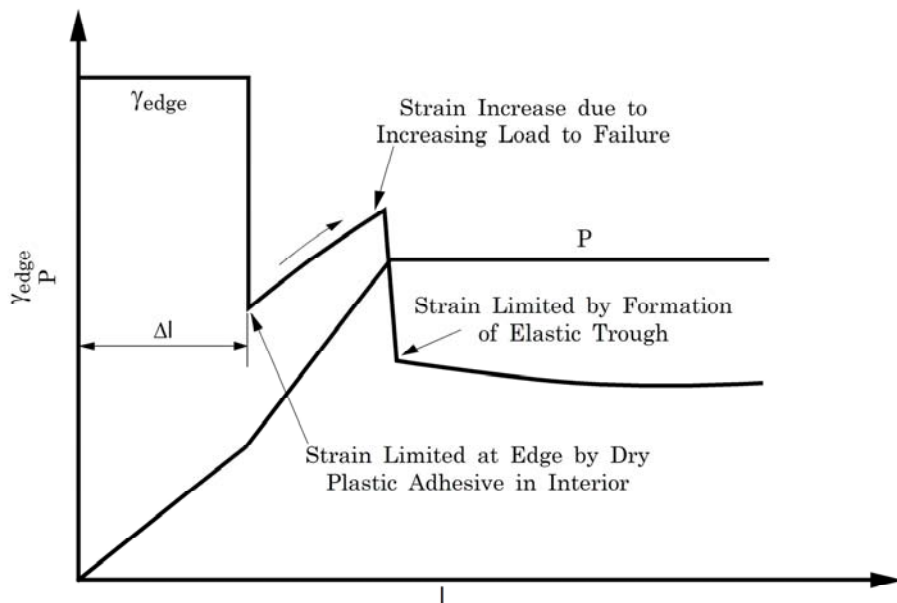


Figure 21.5-1 - Effect of moisture on stress distributions in adhesive bonded joints

[Figure 21.5.2](#) (A) shows a simple transition where there is a dry adhesive on the outside part, in [Figure 21.5.2](#) (B) there are two staggered transitions with a moist adhesive on the outside. In the second case, there are three rather than two adhesive states responsible for defining the outermost adhesive shear strain, Ref. [\[21-4\]](#). These phenomena have been observed for uniform double lap joints.



(A) Adhesive with Dry Exterior $DI/2$ from each end, Interior Moist.



Both illustrations drawn to the same scale

Figure 21.5-2 - Influence of moisture absorption/desorption on peak adhesive shear strains

[Figure 21.5.3](#) shows that, for a bonded doubler or wide overlap joint, continuing penetration of the joint by moisture has little effect on the most critically loaded adhesive near the end of the overlap once the moisture has penetrated past that edge area, Ref. [\[21-4\]](#).

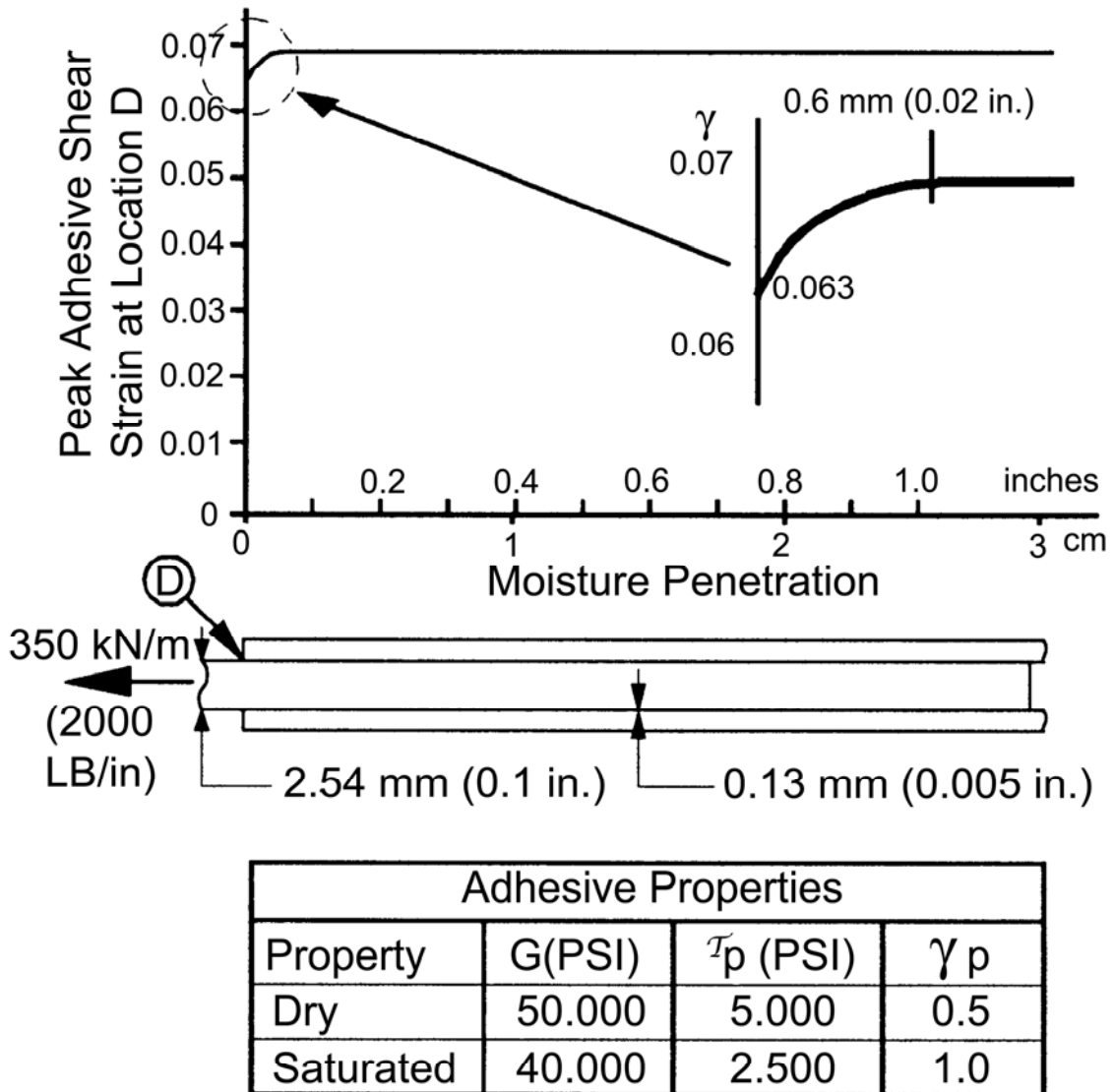


Figure 21.5-3 - Effect of progressive moisture absorption on bond strain

21.5.3 Effect of temperature

Temperature effects by themselves are not important if the adhesive is used within its defined service temperature range.

21.5.4 Combined moisture and temperature

The worst case occurs under the influence of both temperature and moisture, because a high temperature increases the absorption and diffusion of moisture.

Guidelines to avoid the detrimental effects of moisture and temperature are:

- Define accurately the worst case of environmental conditions, which the bonded joint has to withstand.
- Define exactly the service temperature range.

- Select the most adequate type of adhesive resin, e.g. epoxy, polyimide, silicone, taking into account both the worst case conditions and the service temperature range of the particular adhesive.

21.6 Bonding defects

21.6.1 General

The most common bonding defects are:

- [Flaws](#).
- [Porosity](#).

Also important are:

- Variation in thickness,
- Under-curing,
- Variation in resin fraction, and
- Variation in density.

The importance of the defects depends on such factors as:

- The extent to which defects are present.
- Their consequences (critical or not).
- Whether defects are random or locally concentrated.
- Whether defects are indicative of degradation processes or not.
- Whether defects are indicative of material deficiencies or not.

21.6.2 Description of bonding defects

21.6.2.1 Flaws and porosity

Any bonding defects lead to load redistribution through the adhesive film. This idea might suggest an increase in peak stresses at discontinuity points in the adhesive film. However, the actual effect is less than expected and only an imperceptible increase in stress occurs in most cases. This assessment is valid only when the flaw size is proportionally small with respect to joint size.

[Figure 21.6.1](#) gives the possibly acceptable [flaw](#) sizes according to a Zone 1 (critical zone) and a Zone 2 (less critical zone), as classified in Ref. [\[21-4\]](#). It indicates the flaw sizes that are acceptable in primary structures, depending on the zone in which the flaw appears.

The limits for secondary structures in use throughout the aerospace industry are currently more stringent than those given in [Figure 21.6.1](#).

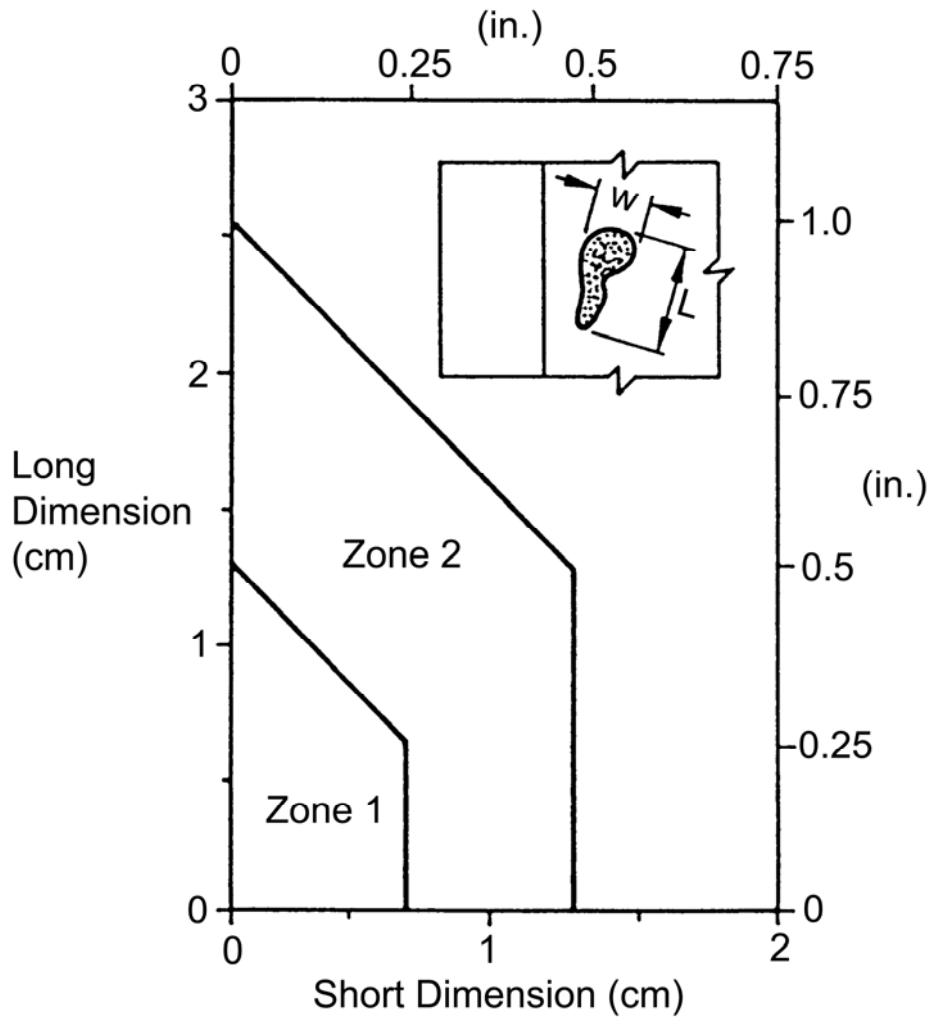
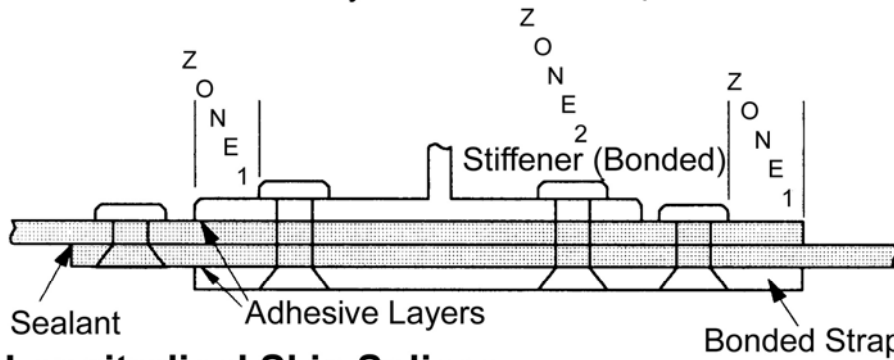
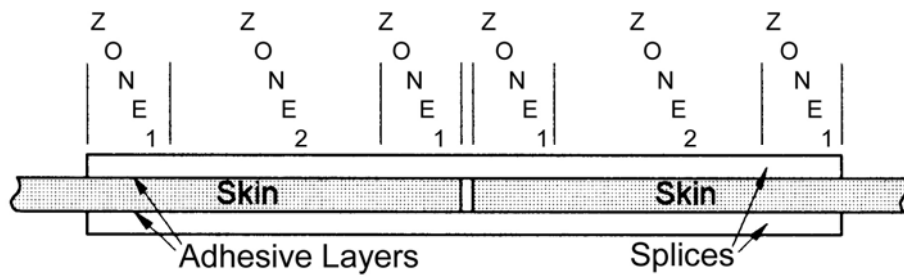
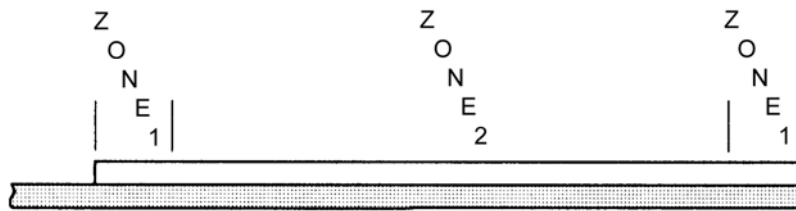


Figure 21.6-1 - Bonded joints: Examples of acceptable bond flaw sizes

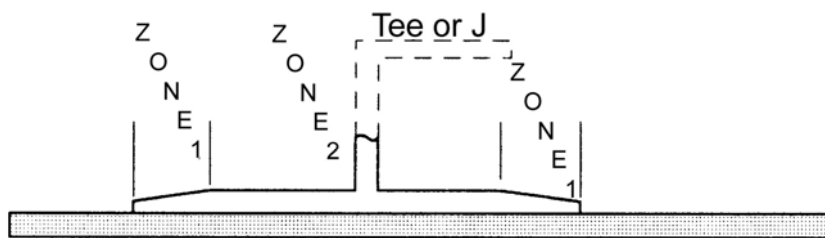
[Figure 21.6.2](#) depicts three different examples of structural joints and their critical zones, Ref. [\[21-4\]](#).



a) Longitudinal Skin Splices



b) Large Area Bonded Doublers



c) Bonded Stiffeners

Key: Zone 1: Critical.
Zone 2: Less critical.

Figure 21.6-2 - Typical quality zoning for bonded joints

Figure 21.6.3 show the normal adhesive shear stress distribution in a defect-free bonded joint.

The joint configuration is the same from Figure 21.6.3 to Figure 21.6.6 inclusive.

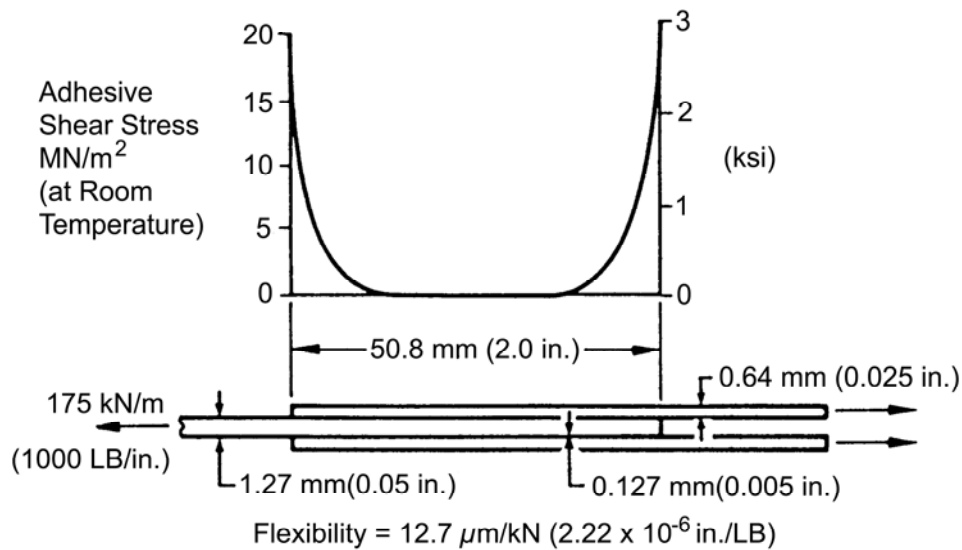


Figure 21.6-3 - Adhesive shear stresses in bonded joints

The effect of an edge [flaw](#) on the shear stress distribution is shown in Figure 21.6.4. When the position of the same sized flaw is changed, the effect on shear stress distribution is shown in Figure 21.03.5.

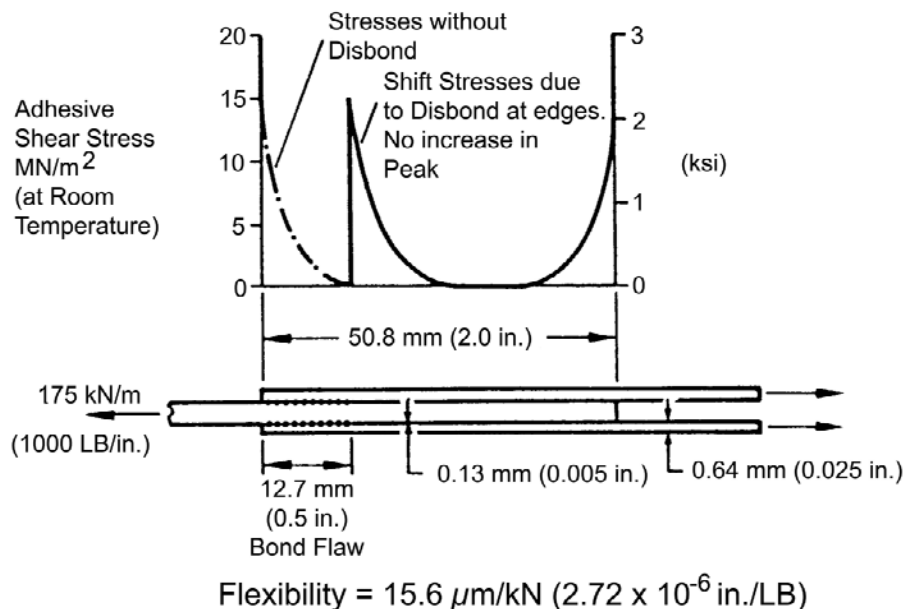


Figure 21.6-4 - Adhesive stresses in flawed bonded joints

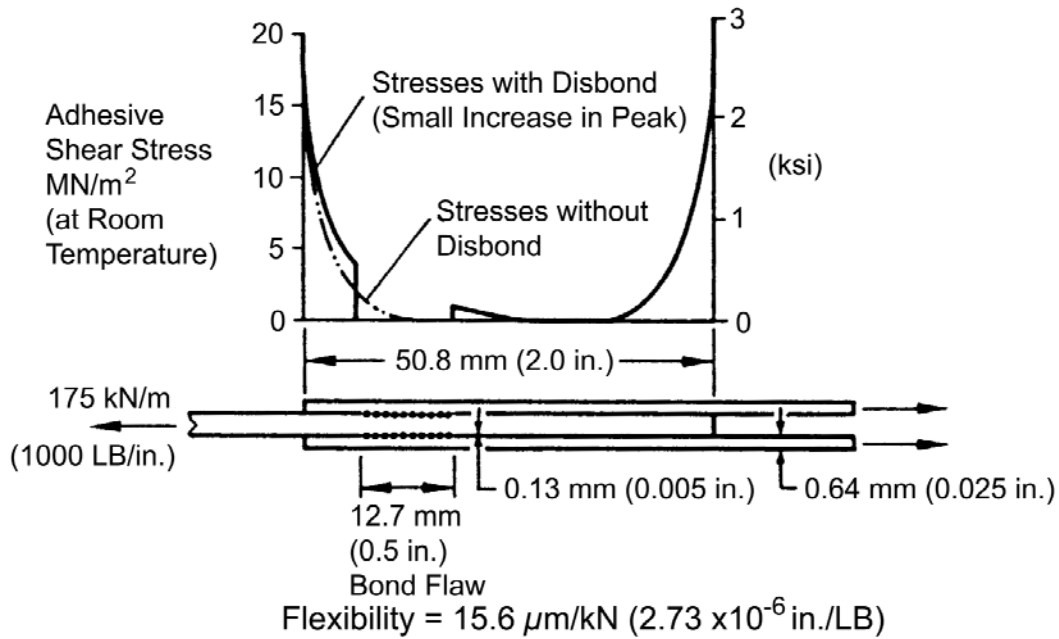


Figure 21.6-5 - Adhesive stresses in flawed bonded joints

Figure 21.6.6 illustrates the effect of a large central [flaw](#) on shear stress distribution.

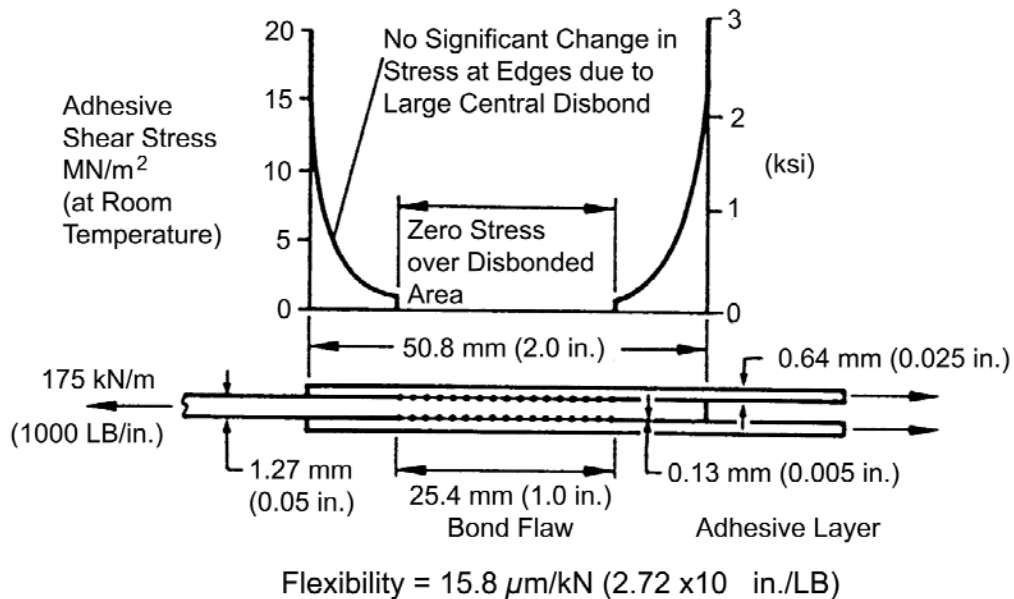


Figure 21.6-6 - Adhesive stresses in flawed bonded joints

In [Figure 21.6.7](#) the effects of [flaws](#) in short and long overlap bonds under the same applied load are compared. Of particular interest is the vertical gradient over which the maximum adhesive shear stress induced is reduced from its failure value to a much lower value, i.e. independent of overlap length.

The effect of flaws is inconsequential, except when total effective overlap is barely sufficient to carry entire load plastically.

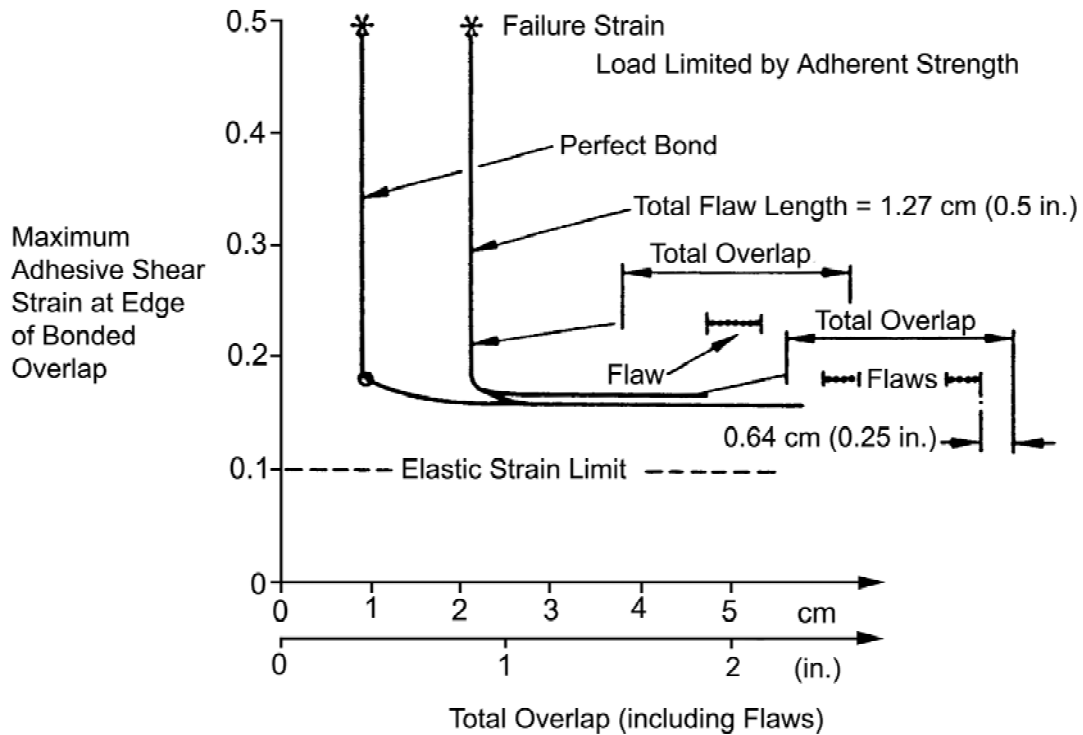


Figure 21.6-7 - Adhesive bonded joints: Effect of debond flaws on flexibility

More detailed analyses are needed to cover the cases in which bond flaws are so large that there is a possibility of complete tearing of the adhesive film. Such analyses need to account for two-dimensional load re-distribution around flaws as well as the one-dimensional re-distribution considered here.

21.6.2.2 Variation in thickness

Experience has shown that the best results in bonding of composites are obtained when the adhesive films have a thickness ranging from 0.12mm to 0.25mm, Ref. [21-4]. In practice this optimum thickness often cannot be achieved. Figure 21.6.8 shows the variation in peak induced adhesive stress with adhesive thickness at the ends of the bond, Ref. [21-4].

[See also: [Variation in resin fraction](#)]

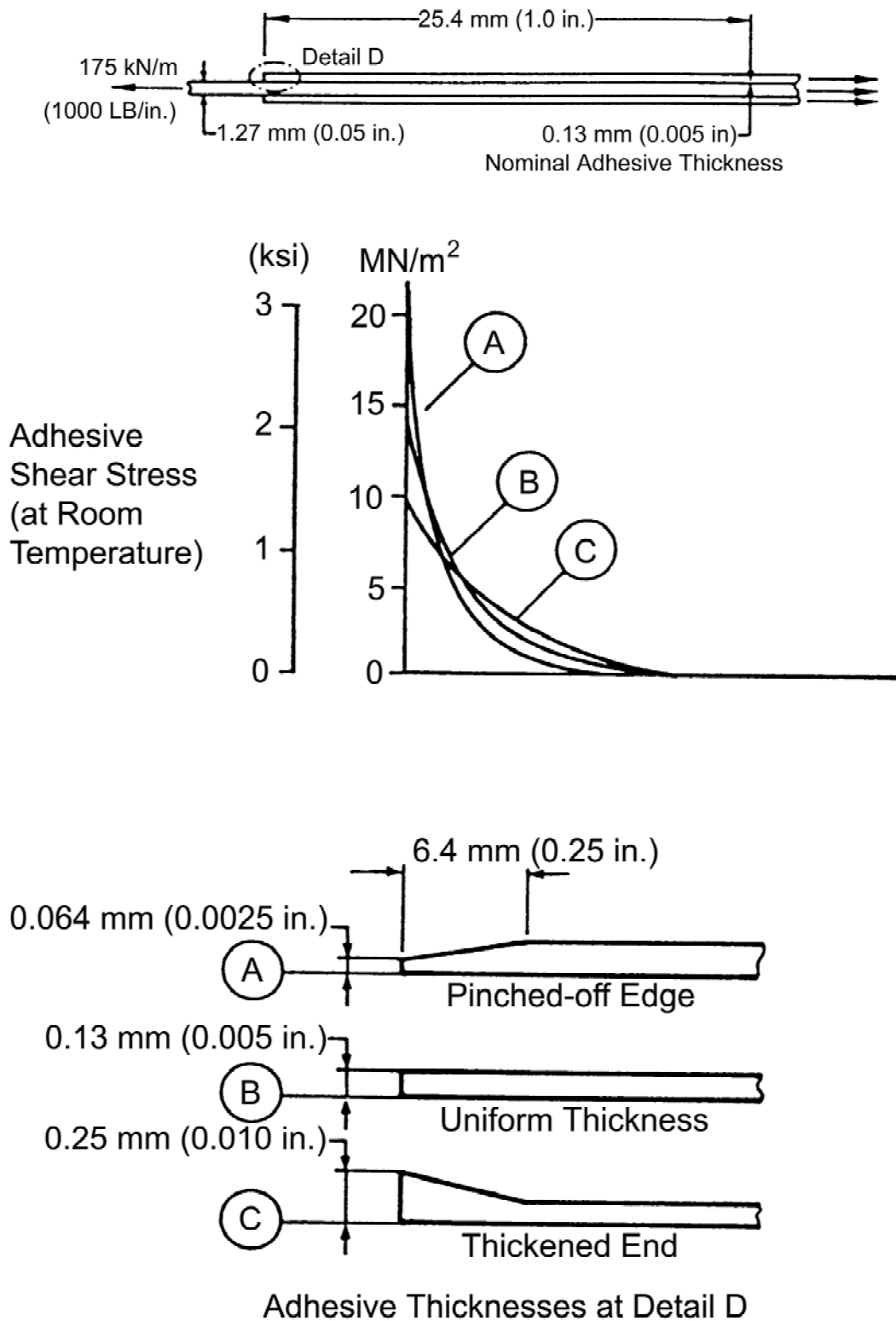


Figure 21.6-8 - Variation of peak induced adhesive stress with thickness of adhesive at ends of overlap

21.6.2.3 Undercuring

[Undercuring](#) occurs due to insufficient time or temperature for adequate curing of the adhesive.

21.6.2.4 Variation in resin fraction

This occurs where there is an uneven distribution of adhesive on the bond surfaces; either an excessive or scant quantity. The defect is usually considered as a variation in thickness.

21.6.2.5 Variation in density

This occurs due to the presence of [flaws](#) and porosity, but also a variation in resin fraction.

21.6.3 Inspection of bonded joints

Non destructive test methods commonly used to detect [defects](#) are described in [Table 21.6.1](#). Some of these methods can be difficult to use in practice.

[Table 21.6.2](#) summarises the possibility of defect detection in bonded joints by various techniques.

[See also: Chapter [34](#) for details of NDT inspection techniques]

Table 21.6-1 - Bonded joints: Description of NDT methods

Method	Description
Radiography (X-ray)	Very effective for examining the uniformity of adhesive joints and intimacy of contact in bonded areas when the adhesives used are not radiation transparent.
Radiography (Neutron)	Used to determine adhesive build up or variation in resin fraction.
Radiation (Gamma)	Used to detect changes in thickness or density of adhesive.
Thermography	Thermochromic or photochromic compounds are added to the adhesive system. Used to determine the degree of adhesive curing.
Ultrasonic	Sound waves ranging in frequency from 1 to 10 MHz are used to find: <ul style="list-style-type: none"> • changes in thickness • detect porosity • delaminations or un-bonded areas. There are three basic ultrasonic systems: <ul style="list-style-type: none"> • Pulse-echo reflector: To detect flaws or/and delaminations. • Transmission: To detect flaws. • Resonant frequency: To detect un-bonded areas.
Acoustic Emission (AE)	Applicable to determine flaws or (through sonic microflows), porosity, undercure or un-bonded areas and variation in density.
Infrared (IR)	Used to find delaminations, un-bonded areas and porosity.
Dye Penetrant	Used to detect flaws, porosity and delaminations.
Induced Current	Used to detect porosity, undercured areas, delamination and variations in thickness.

Table 21.6-2 - Bonded joints: Detection methods for various defects

Defect	Radiography			Thermography	Ultrasonic	AE	IR	Dye Penetrant	Induced Current
	X ray	Neutron	Gamma						
Unbond	✓			✓	✓	✓	✓		
Under Cure				✓	✓	✓			✓
Variation in Resin Fraction		✓							
Density	✓		✓		✓	✓			
Thickness	✓		✓		✓	✓			✓
Porosity	✓		✓		✓	✓	✓	✓	✓
Flaws	✓		✓		✓	✓		✓	
Delamination	✓*		✓	✓	✓	✓	✓	✓	✓

Key: * If delamination is in the same orientation as X-ray beam.

21.7 Bonded joint failure modes

21.7.1 Typical failure modes

The failure behaviour of bonded joints is an important consideration in order to achieve an optimum design.

The failure mode depends upon design parameters, such as, Ref. [21-6]:

- joint configuration
- overlap length
- [adherend](#) thickness, and
- fibre orientation adjacent to the adhesive.

[Figure 21.7.1](#) shows five components of bonded joint strength which, if at fault, produce the typical failure modes.

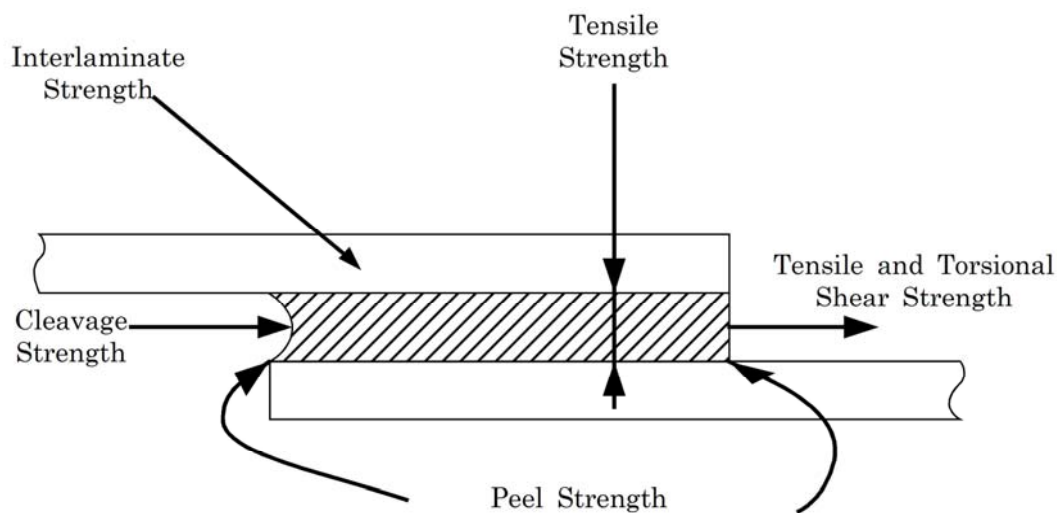


Figure 21.7-1 - Components of bonded joint strength

21.7.2 Loading modes

The loading modes, or types of stress, which a bonded joint can undergo are:

- peel,
- tensile,
- tensile shear,
- torsion,
- cleavage; for thick sections.

[Figure 21.7.2](#) illustrates each of these loading modes.

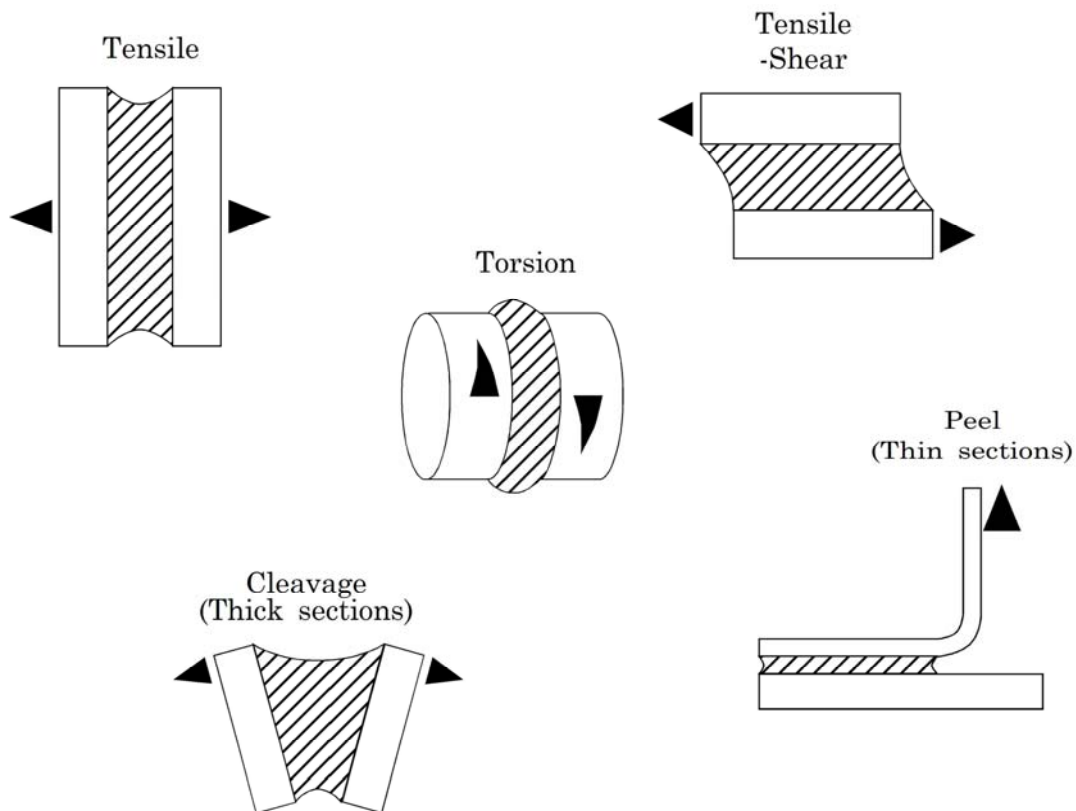


Figure 21.7-2 - Bonded joints: Loading modes or types of stresses

21.8 Calculation of bonded joint strength

The methods given for calculating joint strength, [See: [21.9](#) for analysis of joint configurations], are not closed-form mathematical solutions. Nevertheless, the introduction of various simplifications makes it possible to produce solutions which can readily be used for the various joint configurations, if it is assumed that the behaviour of the [adherend](#) and the adhesive is elastic.

The calculation methods are based mainly on the work of Volkersen, Ref. [\[21-5\]](#) and Goland-Reissner, Ref. [\[21-6\]](#).

Two basic approaches to the study of joints, including plasticity effects, are found in Hart-Smith, Ref. [\[21-7\]](#) or ESDU, Ref. [\[21-8\]](#).

[See also: Chapter [16](#) for information on computer-based joint analysis]

[See: [16.9](#), [16.11](#), [16.13](#), [16.14](#) for ESDU packages; [16.39](#) for ESAComp]

21.9 Analysis of joint configurations

21.9.1 Analytical notation

N	Tensile load
N_{cr}	Critical load
E	Young's Modulus of adherends
G	Adhesive shear modulus
K, α, W, f	Factors
dS	Variation of surface energy
dE	Variation of elastic strain energy
dP	Variation of potential energy of peeling load
l	Length of peeling
L	Length of overlap
b	Width
T	Temperature
t	Thickness of lap sheet
t_a	Thickness of adhesive
ν	Poisson's ratio
τ_m	Average shear stress
τ_{max}	Maximum shear stress
τ	Theoretical shear stress
ω	Stiffness Ratio

[See: [21.8](#) for a description of the methods used]

21.9.2 Single lap shear joint

21.9.2.1 Symmetrical

[Figure 21.9.1](#) defines the analytical notation.

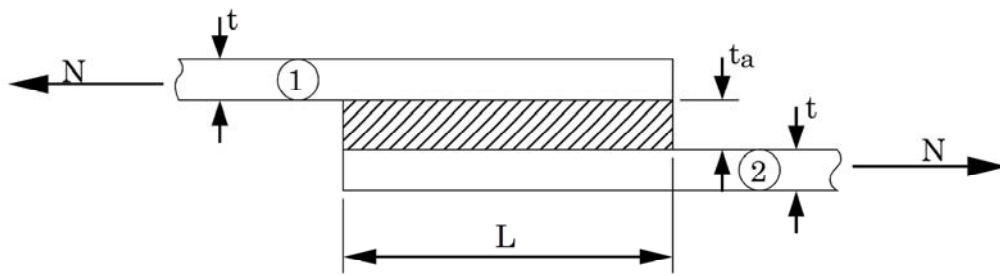


Figure 21.9-1 - Analysis: Notation for symmetrical single-lap shear joint

The tensile load N produces a shear stress τ_m in the adhesive layer.

$$\tau_m = \frac{N}{L} \quad [21.9-1]$$

$$\tau_{max} = K \tau_m \quad [21.9-2]$$

where:

$$K = \frac{1}{4} [WL(1+3\alpha) \coth WL + 3(1-\alpha)] \quad [21.9-3]$$

$$W = \left[\frac{2(1-\lambda_{xy})G}{E t t_a} \right]^{1/2} \quad [21.9-4]$$

$$\alpha = \frac{1}{1 + 2\sqrt{2} \tanh \left[\frac{L}{t} \left[\frac{3(1-\lambda_{xy})N}{2Et} \right]^{1/2} \right]} \quad [21.9-5]$$

$$\lambda_{xy} = \nu_{xy} \nu_{yx} \quad [21.9-6]$$

The relationship between the theoretical and average shear stress is given as:

$$\frac{\tau}{\tau_m} = \frac{1}{4} \left[\left(\frac{2(1 - \lambda_{xy}\lambda_{yx})G}{E t t_a} \right)^{1/2} L(1 + 3\alpha) \frac{\cosh 2WX}{\sinh WL} + 3(1 - \alpha) \right] \quad [21.9-7]$$

The assumptions made are:

- The adhesive flexural rigidity is negligible.
- The behaviour of the laminate and adhesive due to the tensile load N is elastic and isotropic.
- Bending effects can be ignored.
- The normal and shear strains in the transverse direction of the laminate are negligible with respect to those in the adhesive.

21.9.2.2 Analysis of R -degree peeling

[Figure 21.9.2](#) defines the analytical notation.

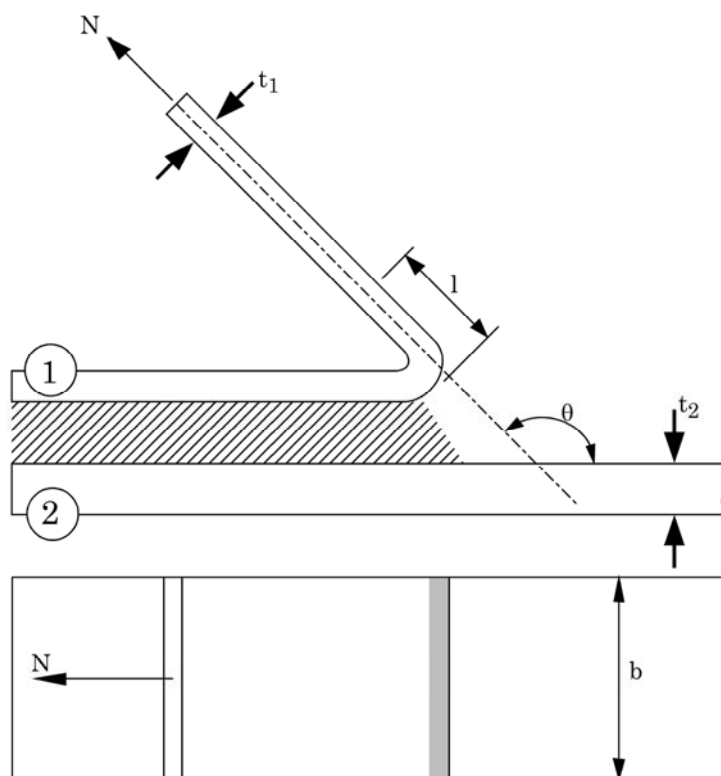


Figure 21.9-2 - Analysis: Notation for single-lap joint R -degree peeling

Figure 21.09.3 shows the θ - degree peeling strength

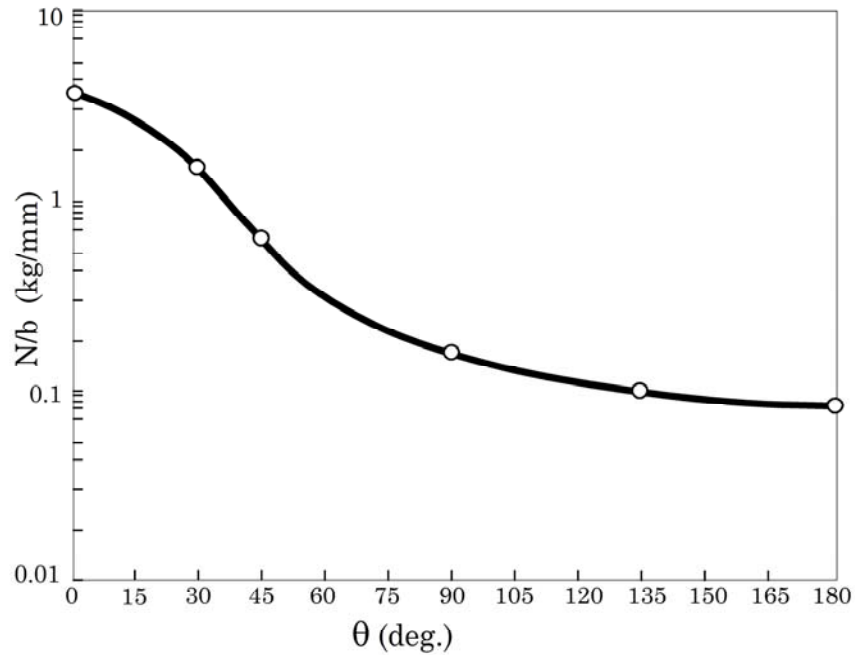


Figure 21.9-3 - θ -degree peeling strength

The critical condition for peeling is:

$$dS + dE + dP = 0 \quad [21.9-8]$$

With γ being the surface energy to cause adhesive fracture, Equation [21.9-9] is obtained from Equation [21.9-1]:

$$N_{cr}^2 \left(\frac{1}{E_1 t_1} + \frac{\cos^2 \theta}{E_2 t_2} \right) + 2bt_1(1 - \cos \theta)N_{cr} - 4\gamma b^2 = 0 \quad [21.9-9]$$

Solving this equation for N_{cr} :

$$N_{cr} = \frac{-2bt_1(1 - \cos \theta) \pm \sqrt{4b^2 t_1^2 (1 - \cos \theta)^2 + 16 \left(\frac{1}{E_1 t_1} + \frac{\cos^2 \theta}{E_2 t_2} \right) \gamma b^2}}{2 \left(\frac{1}{E_1 t_1} + \frac{\cos^2 \theta}{E_2 t_2} \right)} \quad [21.9-10]$$

21.9.3 Double lap shear joint

Figure 21.09.4 defines the analytical notation.

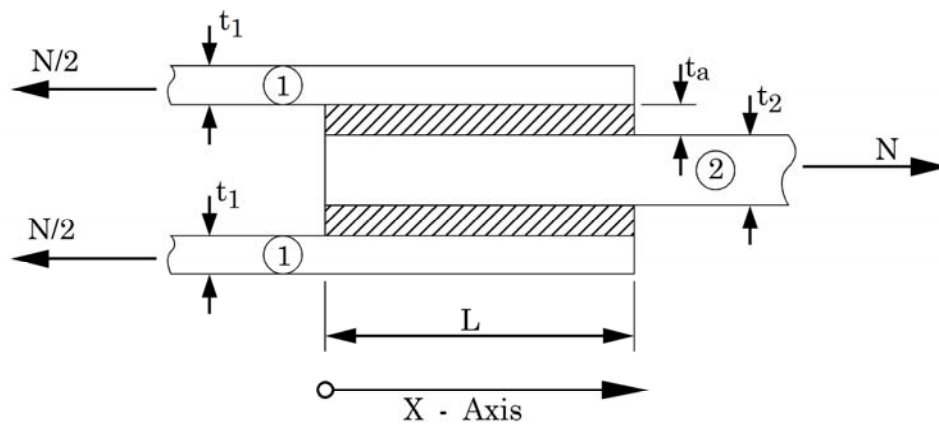


Figure 21.9-4 - Analysis: Notation for double-lap shear joint

The tensile load N produces a shear stress τ_m in each adhesive layer:

$$\tau_m = \frac{N}{2L} \quad [21.9-11]$$

$$\tau_{max} = K t_m \quad [21.9-12]$$

where:

$$K = \frac{(1 - \beta^*) + \beta^* \cosh WL}{\sinh WL} WL \quad [21.9-13]$$

$$W = \left[\frac{2G}{t_a t_2 E_2 \beta} \right]^{1/2} \quad [21.9-14]$$

$$\beta = \frac{1}{1 + \frac{t_2 E_2}{2 t_1 E_1}} \quad [21.9-15]$$

and: β^* the greater of β or $(1 - \beta)$

The relationship between the theoretical and average shear stress is given as:

$$\frac{\tau}{\tau_m} = WL \left[\frac{(1-\beta)\cosh WL + \beta}{\sinh WL} \cosh WX - (1-\beta)\sinh WX \right] \quad [21.9-16]$$

In general, t (thickness) and L (length) values result in $WL < 4$, hence:

$$\tau_{\max} = \beta^* WL \tau_m \quad [21.9-17]$$

When $\frac{L}{t_2} \geq 8$ can be applied, Equation [\[21.9-18\]](#) is obtained:

$$\left(\frac{N}{t_2} \right)_{crit} = K \frac{\sqrt{\beta}}{\beta^*} \quad [21.9-18]$$

where: $K = K_1 K_2$ and K_1, K_2 are defined as:

$$K_1 = \frac{2\gamma\tau_a}{\sqrt{2G}} \sqrt{t_a} \quad [21.9-19]$$

$$K_2 = \sqrt{\frac{E_2}{t_2}} \quad [21.9-20]$$

21.9.4 Double-lap shear joint under mechanical and temperature loads

21.9.4.1 Joint with standard overlap length

Figure 21.9.5 defines the analytical notation.

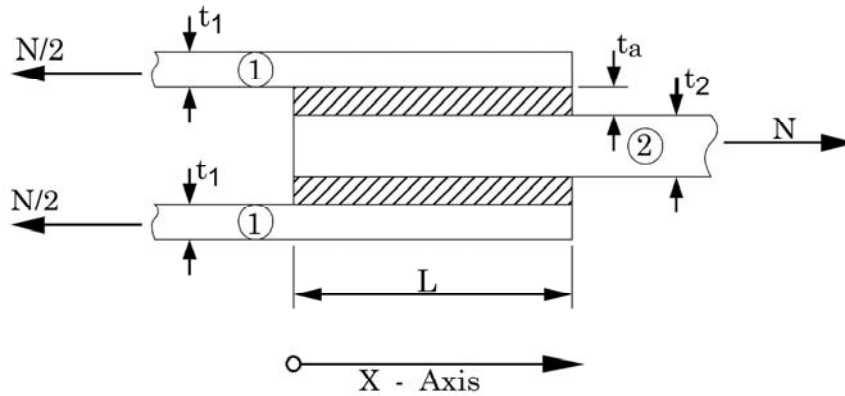


Figure 21.9-5 - Analysis: Notation for double lap joint (standard overlap length)

The distribution of shear stress in the adhesive due to load can be described by the distribution shown in Figure 21.9.6.

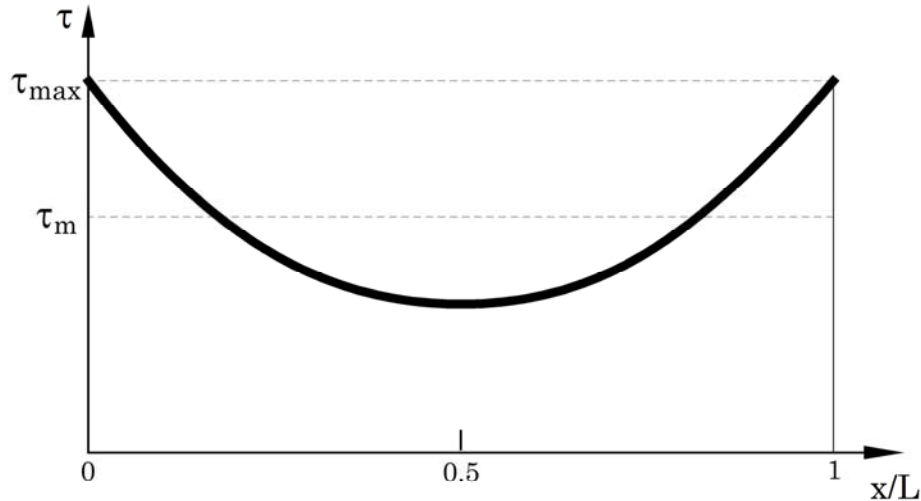


Figure 21.9-6 - Shear stress distribution versus the adhesive length ($E_1 t_1 = E_2 t_2$) for single lap joint without eccentricity

The transfer of force from one flange to the other is concentrated at both edges of the lap joint. This theory leads to peak shear stresses at $x/L = 0$ and $x/L = 1$. As the shear stresses at the edges are zero; the actual shear stress peaks at the edges are smaller.

The shear stress concentration factor, using the maximum shear stress, is defined as:

$$f = \frac{\tau_{\max}}{\tau_m} \quad [21.9-21]$$

where τ_m is defined as:

$$\tau_m = \frac{N/2}{bL} \quad [21.9-22]$$

As given in Ref. [\[21-10\]](#), the factor f is constant for different joints when the correlation factor K is constant.

$$K = \frac{GLb}{Etb} \frac{L}{t_a} = \frac{GL^2}{Ett_a} \quad [21.9-23]$$

The stress peaks at both edges of the bonding can be obtained by means of f_1 and f_2 .

f_2 can be calculated as a function of correlation factor K and the stiffness ratio by:

$$f_2 = \sqrt{\frac{K_2}{\omega_2} \frac{\omega_2^{-1} + \cosh \sqrt{\omega_2 K_2}}{\sinh \sqrt{\omega_2 K_2}}} \quad [21.9-24]$$

with:

$$\omega_2 = \frac{E_1 t_1 + E_2 t_2}{E_1 t_1} \quad [21.9-25]$$

The function $f_2 = f(K_2)$ is shown in [Figure 21.9.7](#) for different stiffness ratios ω_2 .

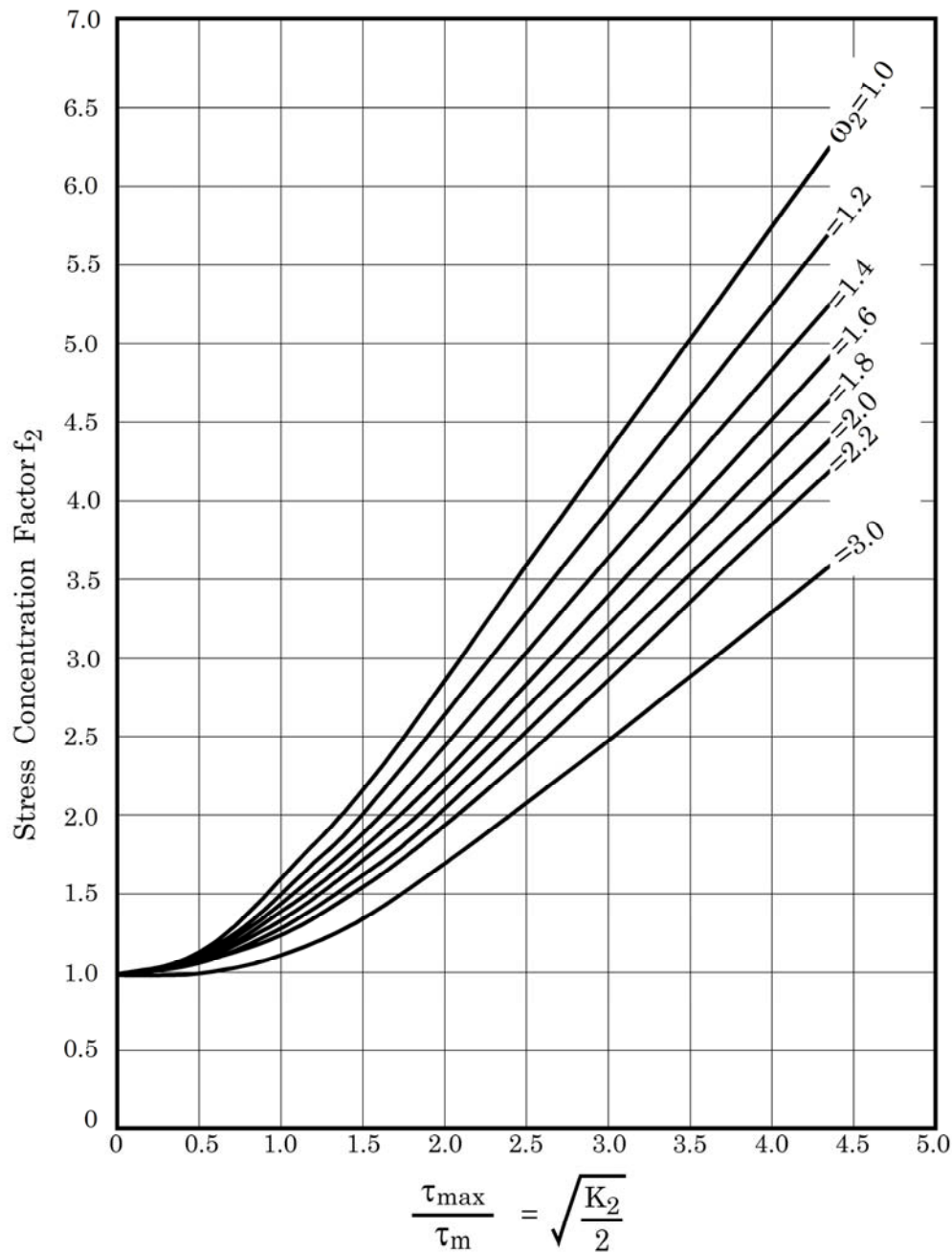


Figure 21.9-7 - Stress concentration factor f_2 as a function of K_2 with parameter ω_2

The peak shear stresses obtained by using the linear elastic theory are reduced when the characteristic shear stress/strain curve is non linear. This reduction is important only when a static analysis is performed. For life endurance calculations only the linear elastic region of the characteristic curve is used.

21.9.4.2 Large overlap length and adherends of the same materials and thicknesses

When lapsheets are of the same material, $E_1 = E_2$, $t_1 = t_2$, therefore:

$$\omega_2 = \frac{E_1 t_1 + E_2 t_2}{E_1 t_1} = 2 \quad [21.9-26]$$

and:

$$\frac{\tau_{max}}{\tau_m} = \sqrt{\frac{K_2}{\omega_2}} \frac{1 + \cosh \sqrt{\omega_2 K_2}}{\sinh \sqrt{\omega_2 K_2}} = \sqrt{\frac{K_2}{2}} \coth \sqrt{\frac{K_2}{2}} \quad [21.9-27]$$

When $K_2 > 10$, the term $\coth \sqrt{\frac{K_2}{2}}$ is approximately 1, resulting in:

$$\frac{\tau_{max}}{\tau_m} = \sqrt{\frac{K_2}{2}} = \sqrt{\frac{GL^2}{2Ett_a}} = L \sqrt{\frac{G}{2Ett_a}} \quad [21.9-28]$$

$$\tau_{max} = L \tau_m \sqrt{\frac{G}{2Ett_a}} \quad [21.9-29]$$

$$\tau_m = \frac{N/2}{Lb} \quad [21.9-30]$$

$$\tau_{max} = \frac{N}{2b} \sqrt{\frac{G}{2Ett_a}} \quad [21.9-31]$$

For long overlap lengths, the maximum shear stress is independent of the length of the joint. Considering that the load transfer is concentrated at the ends of the joint, the shear stress is reduced to zero in the middle part of the overlap zone, as shown in [Figure 21.9.7](#).

As the lap joint length increases, the mean shear stress decreases. This leads to higher shear stress concentration factors. However, for $K > 10$, this behaviour is linear as shown in [Figure 21.9.8](#).



Figure 21.9-8 - Shear stress distribution for large overlap lengths

21.9.4.3 Shear stresses in the adhesive due to temperature

Shear stresses occur in the adhesive due to different coefficients of thermal expansion, α_T , of the adherends.

For this kind of loading it is impossible to define a comparative correlation factor. Thus it seems to be reasonable to formulate the shear stress as a function of the normalised overlap length x/L due to a 100 K temperature increase; as shown in [Figure 21.9.9](#) and [Figure 21.9.10](#).

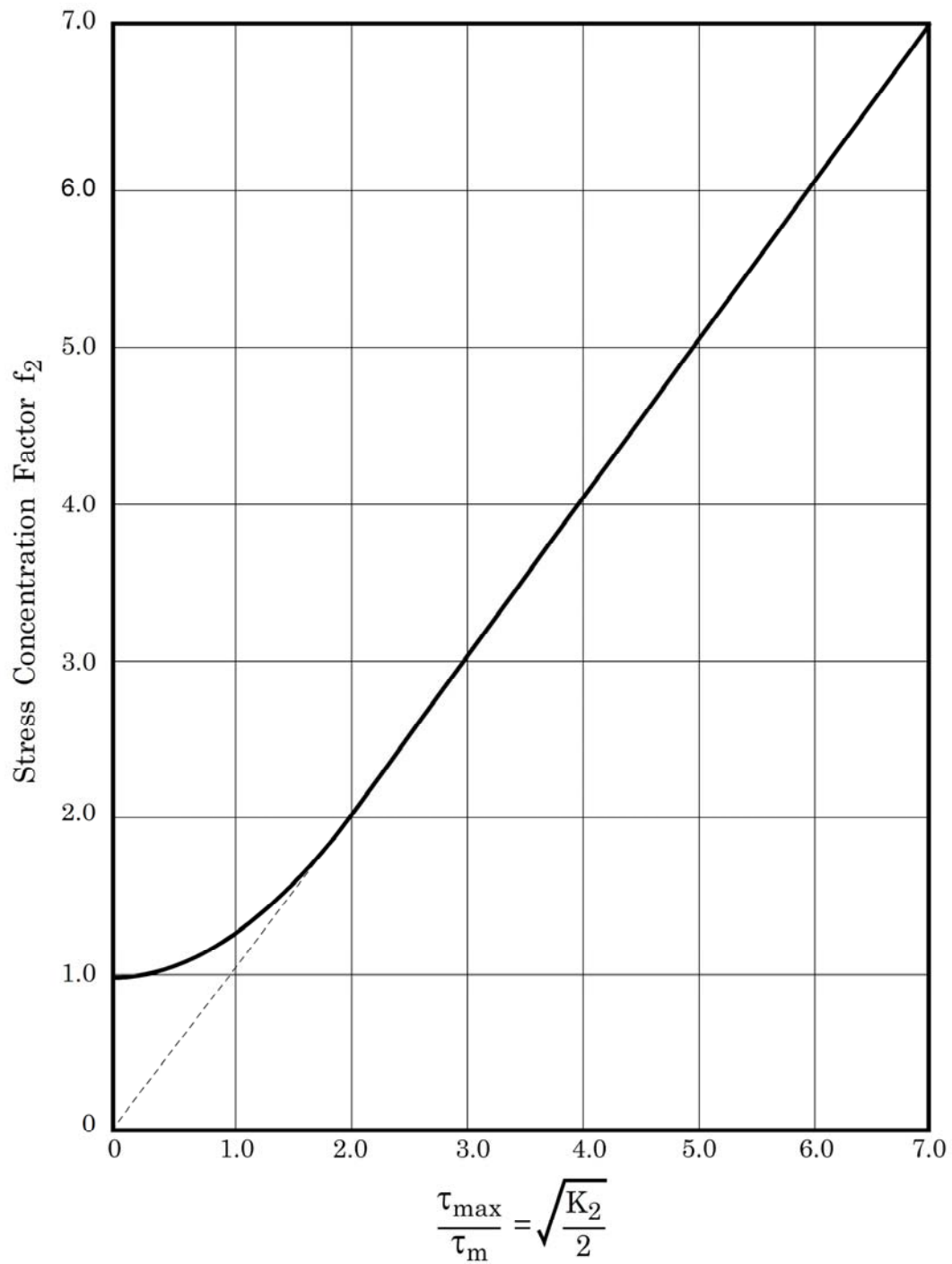


Figure 21.9-9 - Stress concentration factor for large overlap lengths

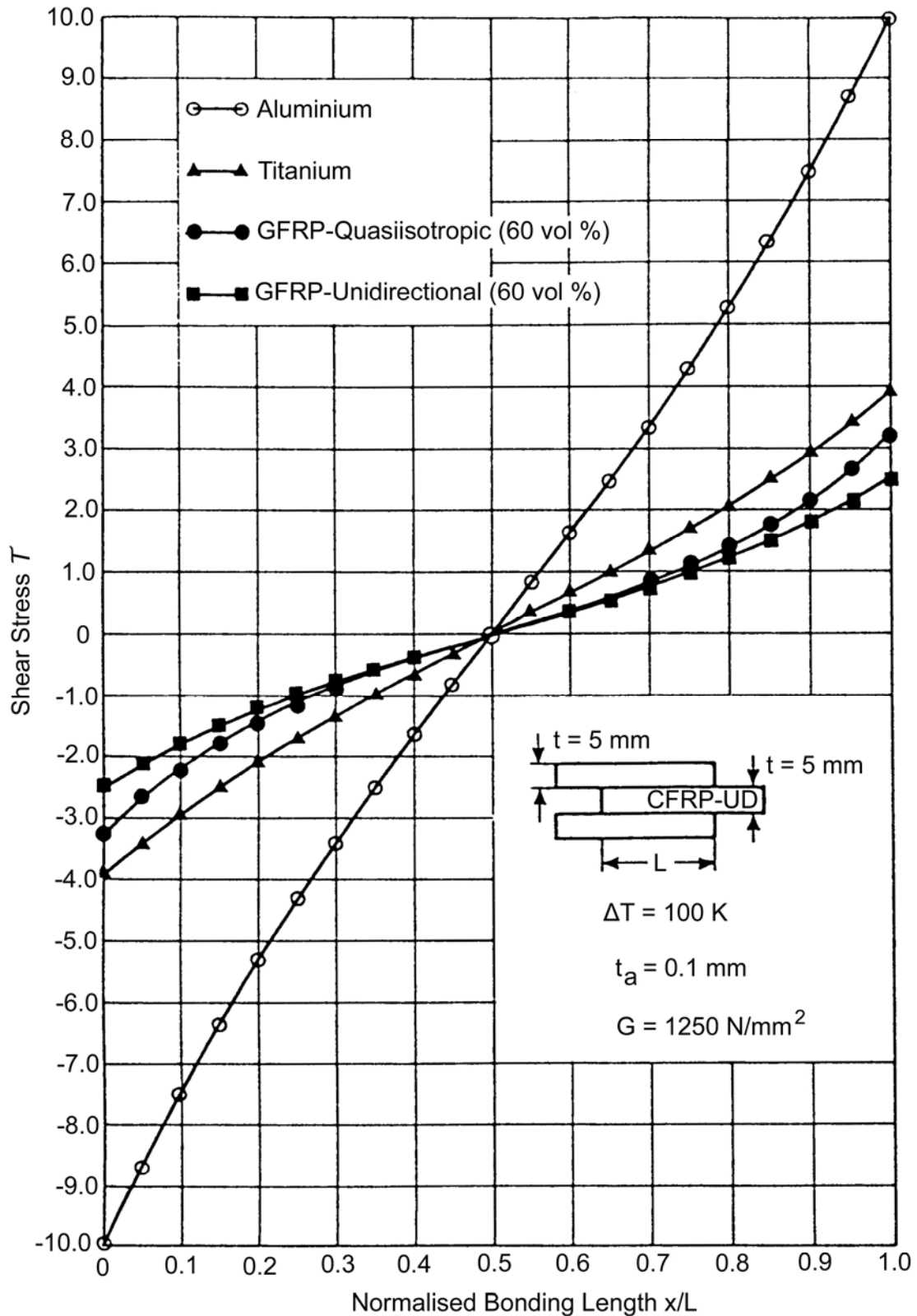


Figure 21.9-10 - Shear stress distribution versus the normalised bonding length x/L for a bonded joint between CFRP-HT unidirectional (60 vol. %) and aluminium, titanium, GFRP quasi-isotropic, and GFRP unidirectional materials

The maximum shear stresses are:

- independent of the overlap length L ,

but:

- directly dependent on the product of the difference in temperature and the difference in the coefficient of thermal expansion of the adherends.

The theory does not consider that the shear stress at $x/L = 0$ and $x/L = 1$ is zero.

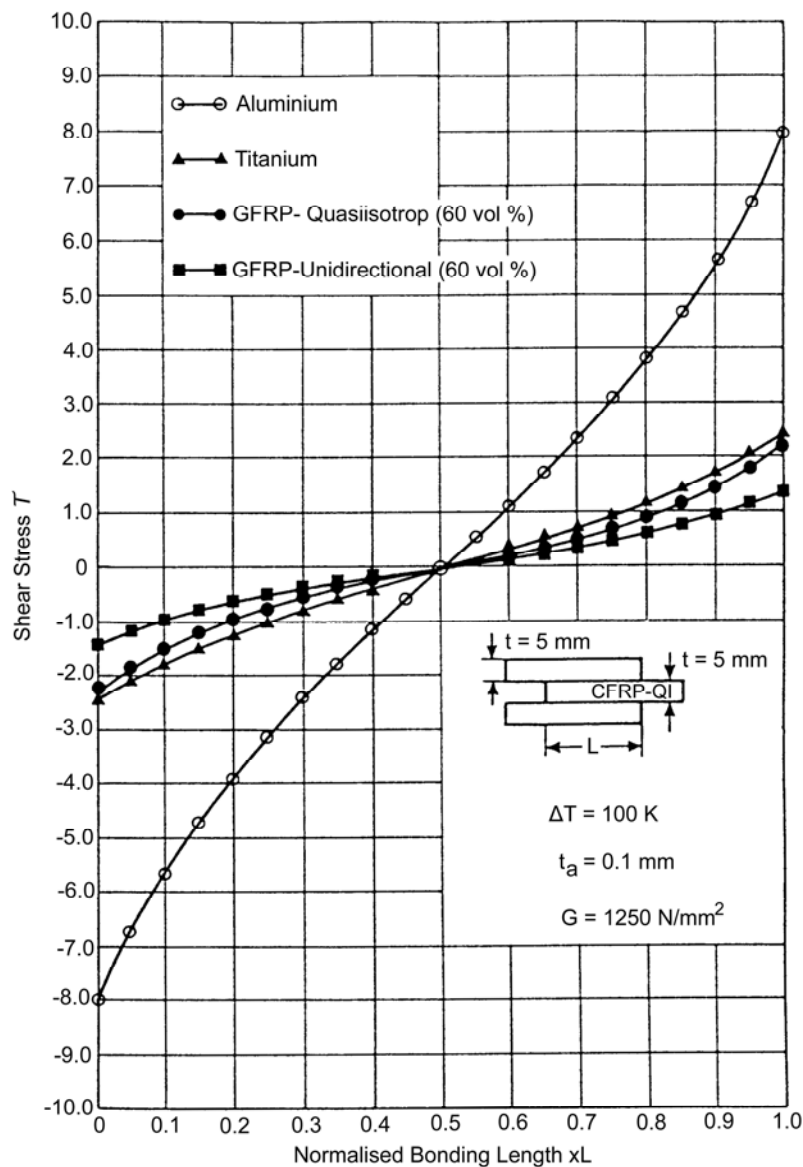


Figure 21.9-11 - Shear stress distribution versus the normalised bonding length x/L for a bonded joint between CFRP HT quasi isotropic (60 vol. %) and aluminium, titanium, GFRP quasi isotropic, and GFRP unidirectional materials

21.9.5 Single taper scarf joint

Figure 21.9.12 defines the analytical notation.

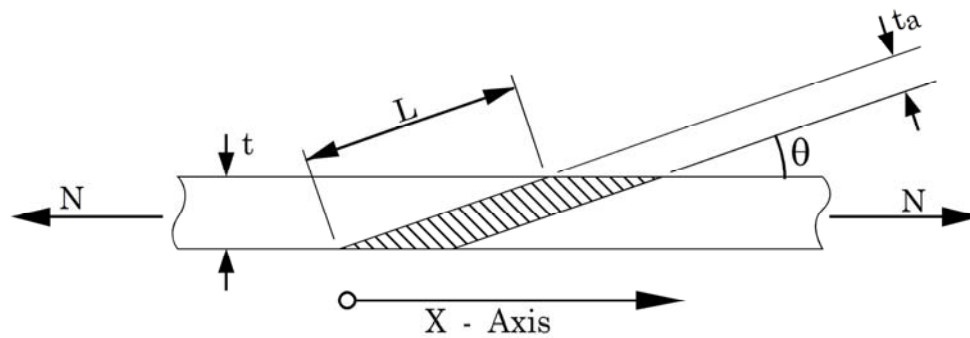


Figure 21.9-12 - Analysis: Notation for single taper scarf joint

The tensile load N produces a shear stress τ_m in the adhesive layer.

$$\tau_m = \frac{N \cos \theta}{L} = \frac{N \cos \theta}{t} \sin \theta \quad [21.9-32]$$

$$\tau_{max} = K \tau_m \quad [21.9-33]$$

where:

$$K = \sqrt{\frac{1}{4} \left[\tan \theta (1 - \psi) - \frac{E_a}{E} \cot \theta \right]^2 + 1} \quad [21.9-34]$$

and:

$$\psi = \nu_a - \nu_{xz} \frac{E_a}{E} \quad [21.9-35]$$

In general, $\theta < 20^\circ$ and $\frac{E_a}{E} \ll 1$

Hence: $K \approx 1$ and $\tau_{max} \approx \tau_m$.

21.9.6 Double taper scarf joint

21.9.6.1 Symmetrical

Figure 21.9.13 defines the analytical notation.

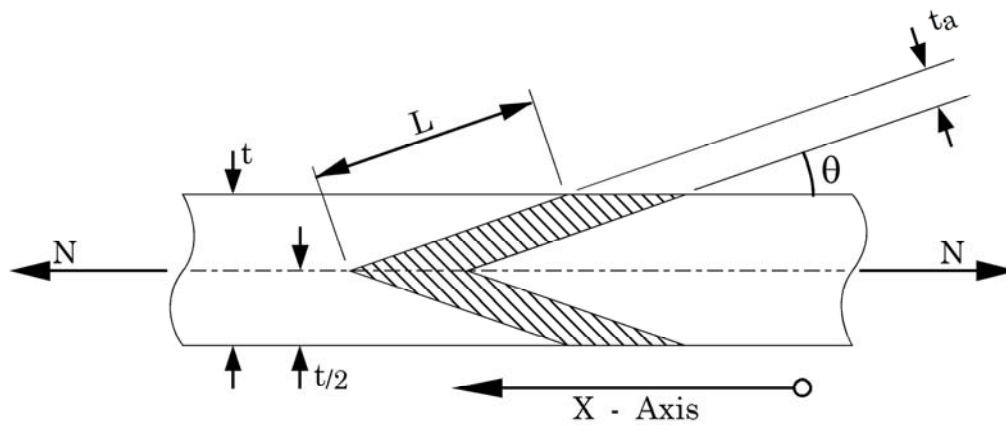


Figure 21.9-13 - Analysis: Notation for symmetrical double tapered scarf joint

The tensile load N produces a shear stress τ_m in the adhesive layer.

$$\tau_m = \frac{N \cos \theta}{2L} = \frac{N \cos \theta}{2t} 2 \sin \theta = \frac{N \cos \theta \sin \theta}{t} \quad [21.9-36]$$

$$\tau_{max} = K \tau_m \quad [21.9-37]$$

where:

$$K = \sqrt{\frac{1}{4} \left[\tan \theta (1 - \psi) - \frac{E_a}{E} \cot \theta \right] + 1} \quad [21.9-38]$$

and:

$$\psi = \nu_a - \nu_{xz} \frac{E_a}{E} \quad [21.9-39]$$

This case is almost the same as the single taper scarf joint with the difference that the necessary bond length is half that of the bond length of double lap shear joint.

21.9.7 Stepped lap joint

21.9.7.1 Recessed and simple

[Figure 21.9.14](#) defines the analytical notation.

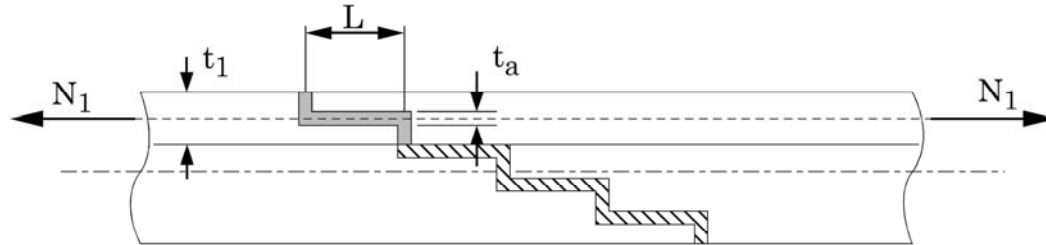


Figure 21.9-14 - Analysis: Notation for stepped lap joint (recessed and simple)

21.9.7.2 Three or fewer steps

For three or fewer steps, this type of joint can be analysed by taking each lap as a single lap of thickness, t .

The recessed and simple configurations are similar, with the only difference that the load transfer (in the case of three or fewer steps) occurs generally about the common midplane. For each step:

$$\tau_m = \frac{N}{L} \quad [21.9-40]$$

$$\tau_{max} = K \tau_m \quad [21.9-41]$$

where:

$$K = \frac{1}{4} [WL(1 + 3\alpha) \coth WL + 3(1 - \alpha)] \quad [21.9-42]$$

$$W = \left[\frac{2(1 - \lambda_{xy})G}{E t t_a} \right]^{1/2} \quad [21.9-43]$$

$$\alpha = \frac{1}{1 + 2\sqrt{2} \tanh \left[\frac{L}{t} \left[\frac{3(1 - \lambda_{xy})N}{2Et} \right]^{1/2} \right]} \quad [21.9-44]$$

$$\lambda_{xy} = \nu_{xy} \nu_{yx} \quad [21.9-45]$$

For each step:

N is N_1 , N_2 or N_3

L is L_1 , L_2 or L_3

t is t_1 , t_2 or t_3

There are stress concentrations in the first case (three or fewer steps).

21.9.7.3 Four or more steps

For four or more steps, the analysis of double lap joints can be carried out by taking the step thickness t_1 and $t_1/2$, [See: Double lap shear joint]. [Figure 21.9.15](#) defines the analytical notation.

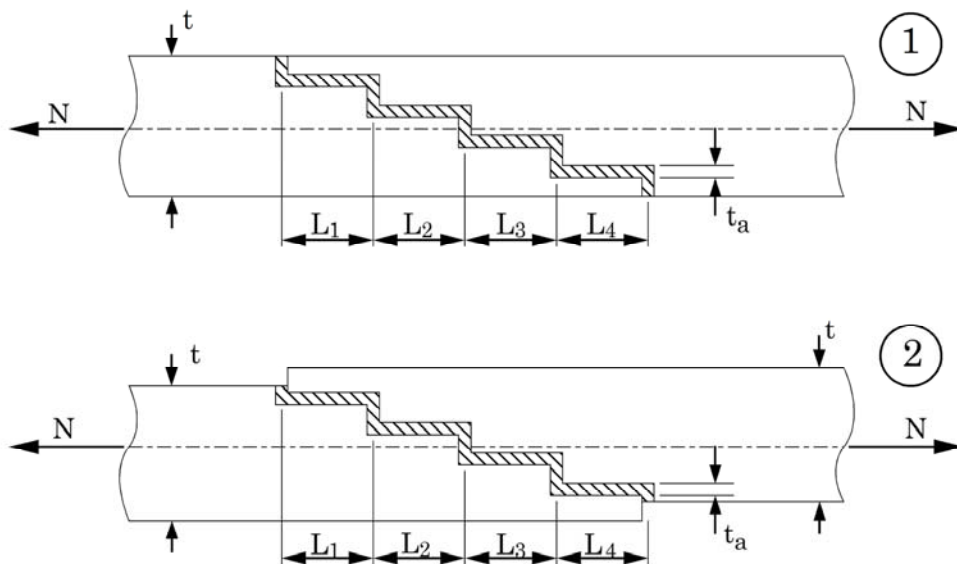


Figure 21.9-15 - Analysis: Notation for recessed and simple scarf joints (four or more steps)

21.10 Bonded joint design curves and test data

21.10.1 General

The design curves present information on the shear stresses to be expected in bonded joints for different geometries, L/t. Static and dynamic loads are considered together with temperature effects.

21.10.1.1 Design curves

The information included on the various joint configurations under static and dynamic loading are summarised in [Table 21.10.1](#), which also serves as an index to the design curves.

Table 21.10-1 - Bonded joints: Summary of data curves

Load	Adherends	Adhesive	Temperature (°C)	See: Figure
Single Lap Joint				
Static	C/E→C/E	High Mod.	RT and 180	Figure 21.10.1
	C/E→St	High Mod.	RT and 180	Figure 21.10.2
	C/E→St	Med. Mod †	RT	Figure 21.10.6
	C/E→St or C/E	Metlbond 329-7	RT and 180	Figure 21.10.4
	C/E→C/E	Metlbond 329-7	RT, 120 and 180	Figure 21.10.5
	C/E→C/E	Metlbond 329-7	RT and 180	Figure 21.10.6
Dynamic	C/E→C/E ‡	Metlbond 329-7	RT	Figure 21.10.8
	C/E→C/E ‡		180	Figure 21.10.9
Double Lap Joint				
Static	C/E→Ti	Med. Mod †	-	Figure 21.10.10
Symmetrical Scarf Joint				
Static	C/E→Ti	Metlbond 329-7	RT and 180	Figure 21.10.11
	C/E→Ti		RT and 180	Figure 21.10.12
Dynamic	C/E ‡ →Ti	Metlbond 329-7	RT and 180	Figure 21.10.13
	C/E ‡ →Ti		RT and 180	Figure 21.10.14

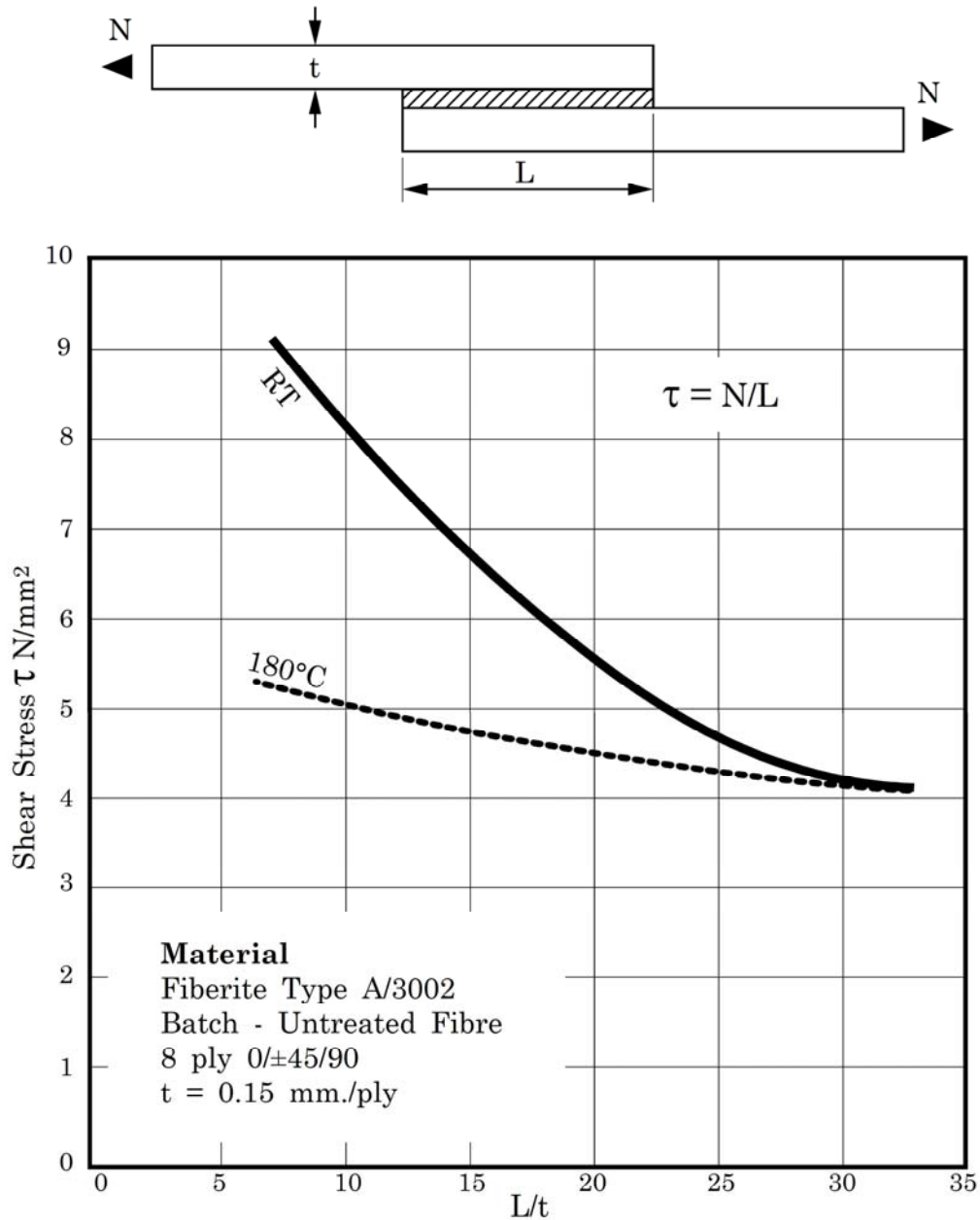
Key: C/E: Carbon/epoxy

†: Shell 951

St: Steel

‡: Intermediate strength

Ti: Titanium

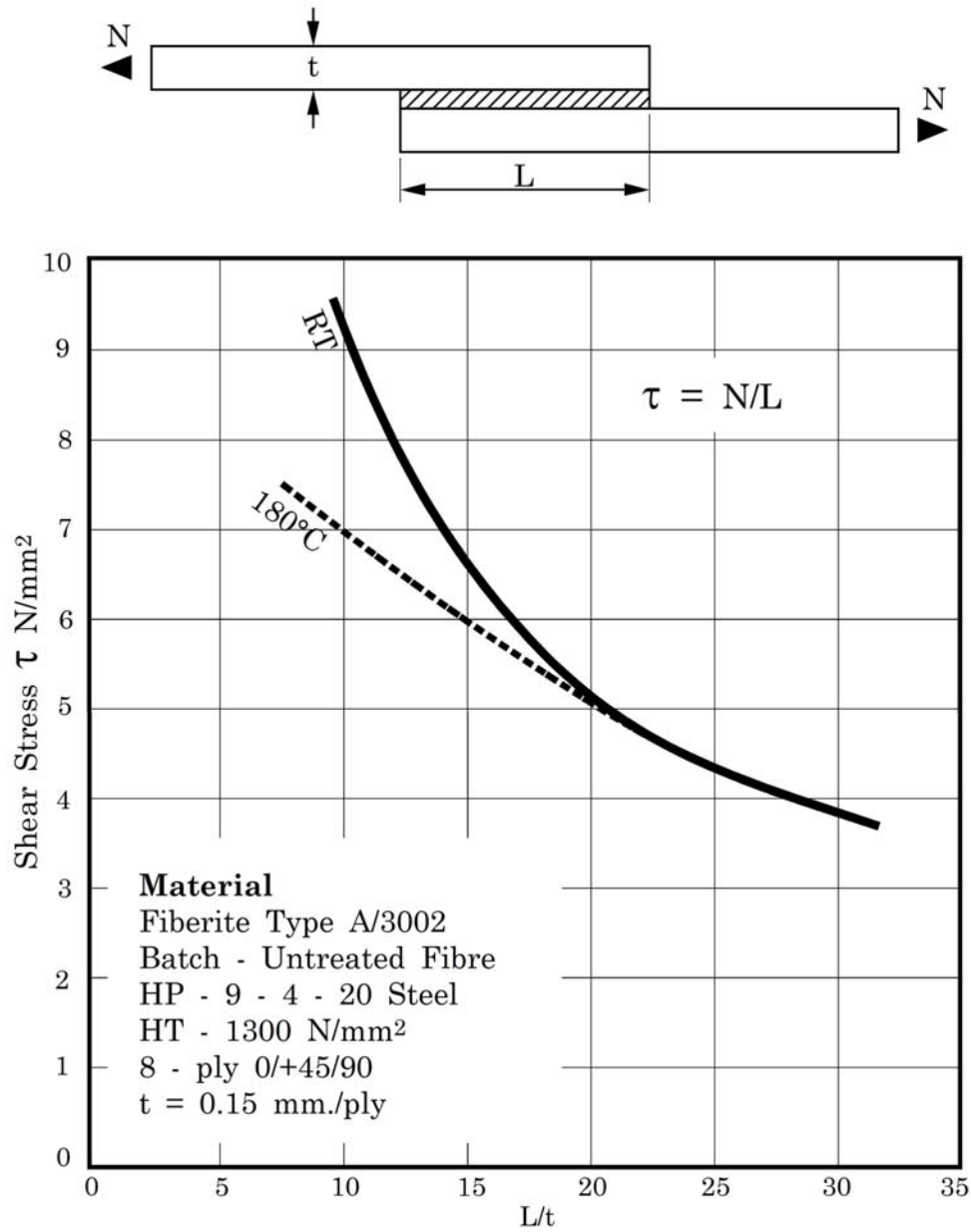


Adherends: Carbon/epoxy to carbon/epoxy

Adhesive: High modulus

Temperature: RT and 180°C

Figure 21.10-1 - Design curve: Single lap shear joint

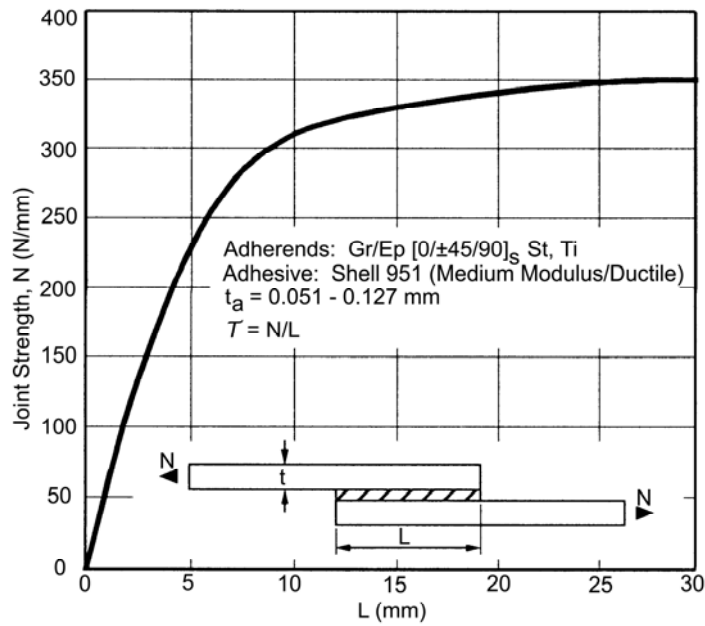


Adherends: Carbon/epoxy to steel

Adhesive: High modulus

Temperature: RT and 180°C

Figure 21.10-2 - Design curve: Single lap shear joint

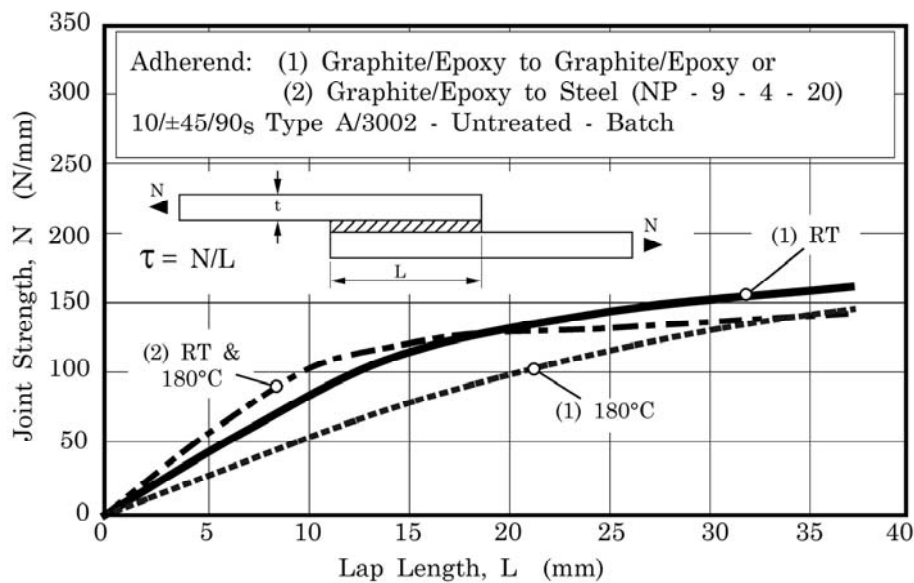


Adherends: Carbon/epoxy to steel

Adhesive: Medium modulus Shell 951.

Temperature: RT

Figure 21.10-3 - Design curve: Single lap shear joint

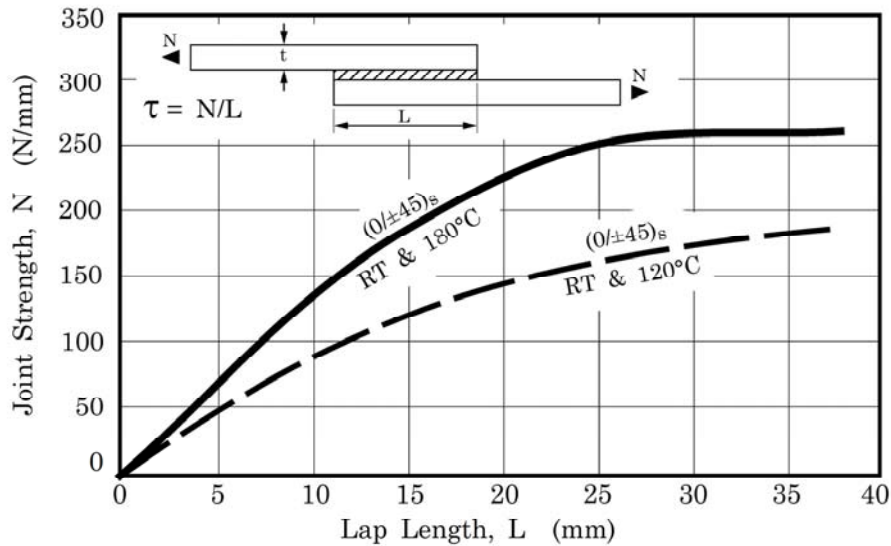


Adherends: Carbon/epoxy to carbon/epoxy

Adhesive: Metlbond 329-7.

Temperature: RT and 180°C

Figure 21.10-4 - Design curve: Lower bond tension single lap shear joint strength versus lap length

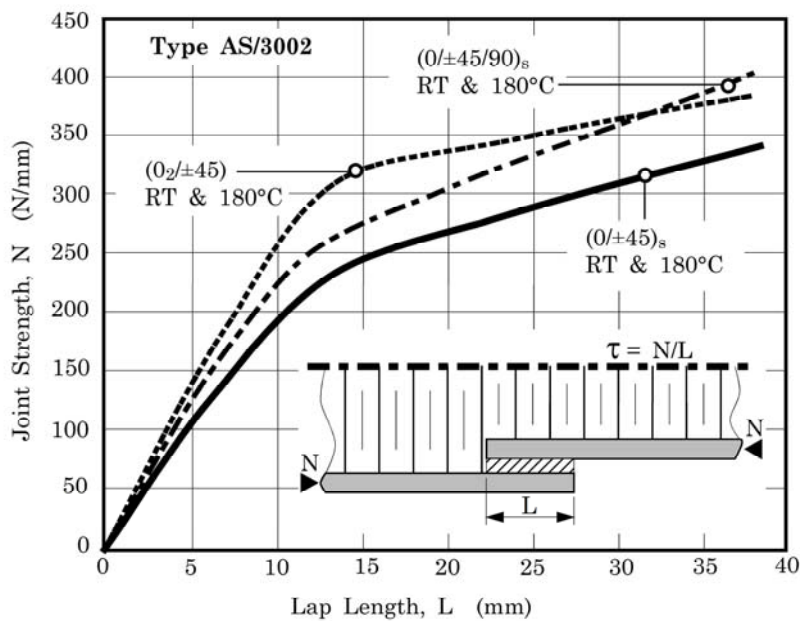


Adherends: Carbon/epoxy to carbon/epoxy

Adhesive: Metlbond 329-7.

Temperature: RT, 120°C and 180°C

Figure 21.10-5 - Design curve: Lower bond tension single lap shear joint strength versus lap length

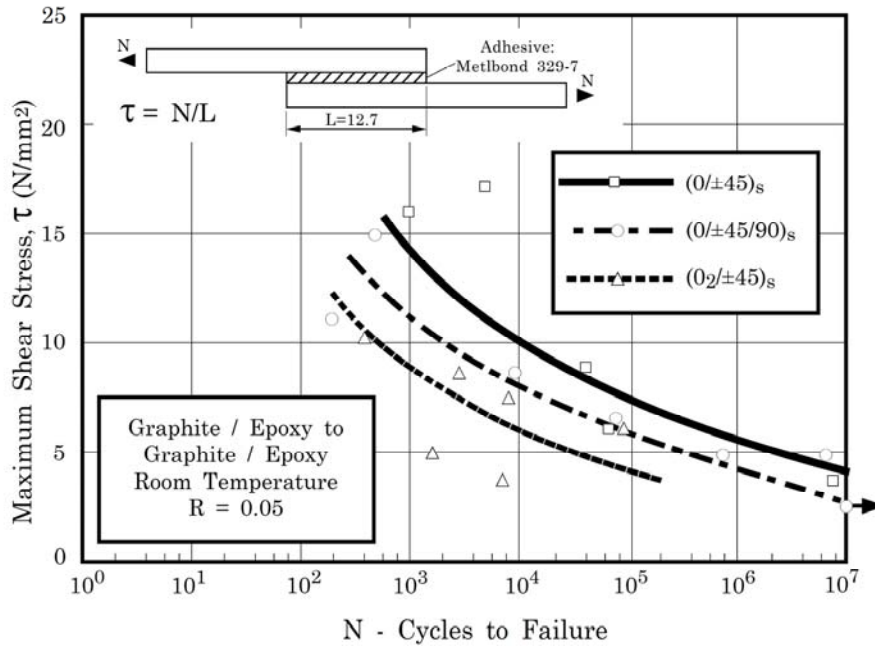


Adherends: Carbon/epoxy to carbon/epoxy

Adhesive: Metlbond 329-7.

Temperature: RT and 180°C

Figure 21.10-6 - Design curve: Lower bond tension single lap compression loaded joint strength versus lap length

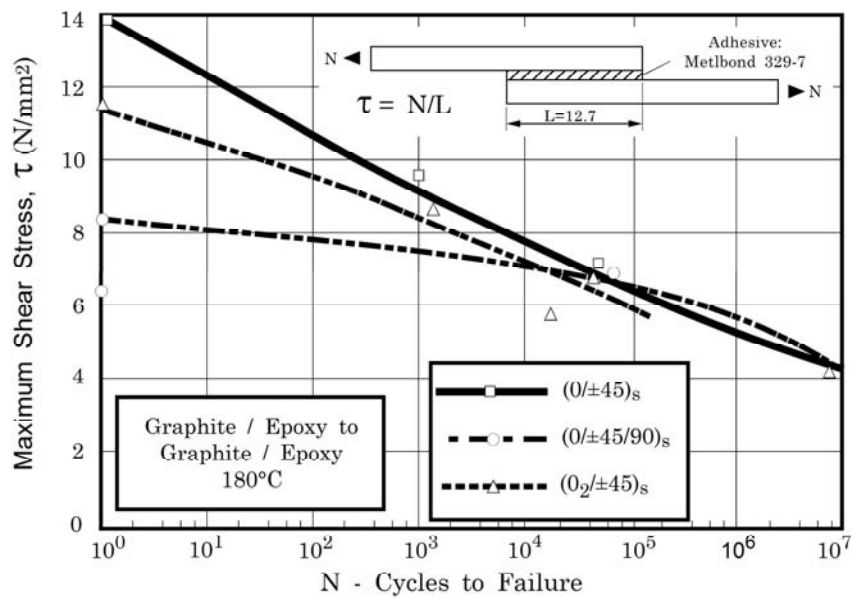


Adherends: Intermediate strength carbon/epoxy to carbon/epoxy

Adhesive: Metlbond 329-7.

Temperature: 180°C

Figure 21.10-7 - Design curve: Single lap tension fatigue S-N curve

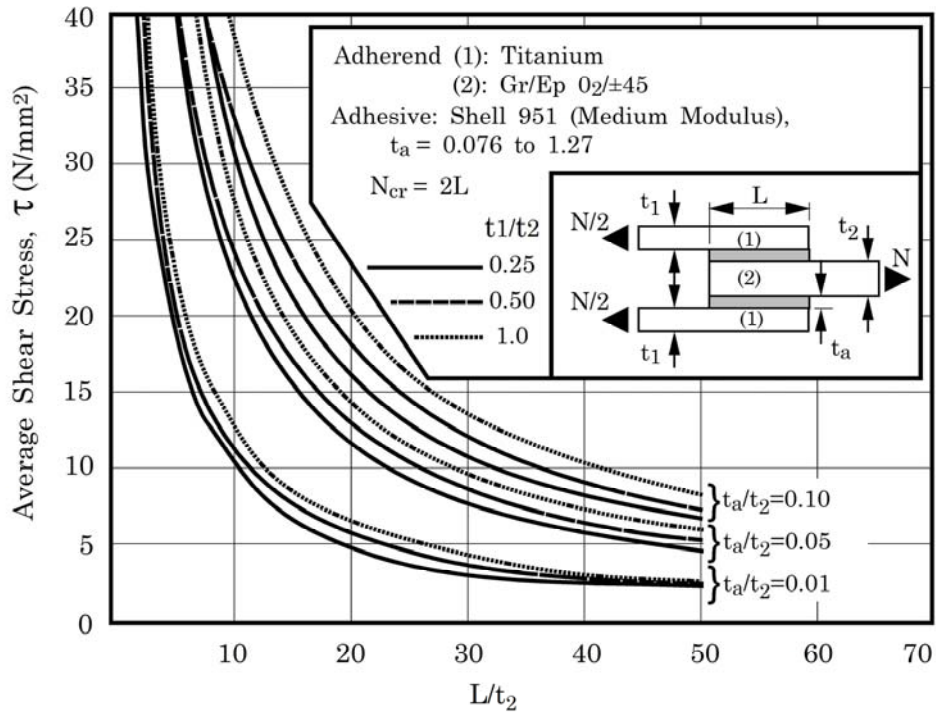


Adherends: Carbon/epoxy to carbon/epoxy

Adhesive: Metlbond 329-7

Temperature: 180°C

Figure 21.10-8 - Design curve: Single-lap shear joint tension fatigue S-N curve

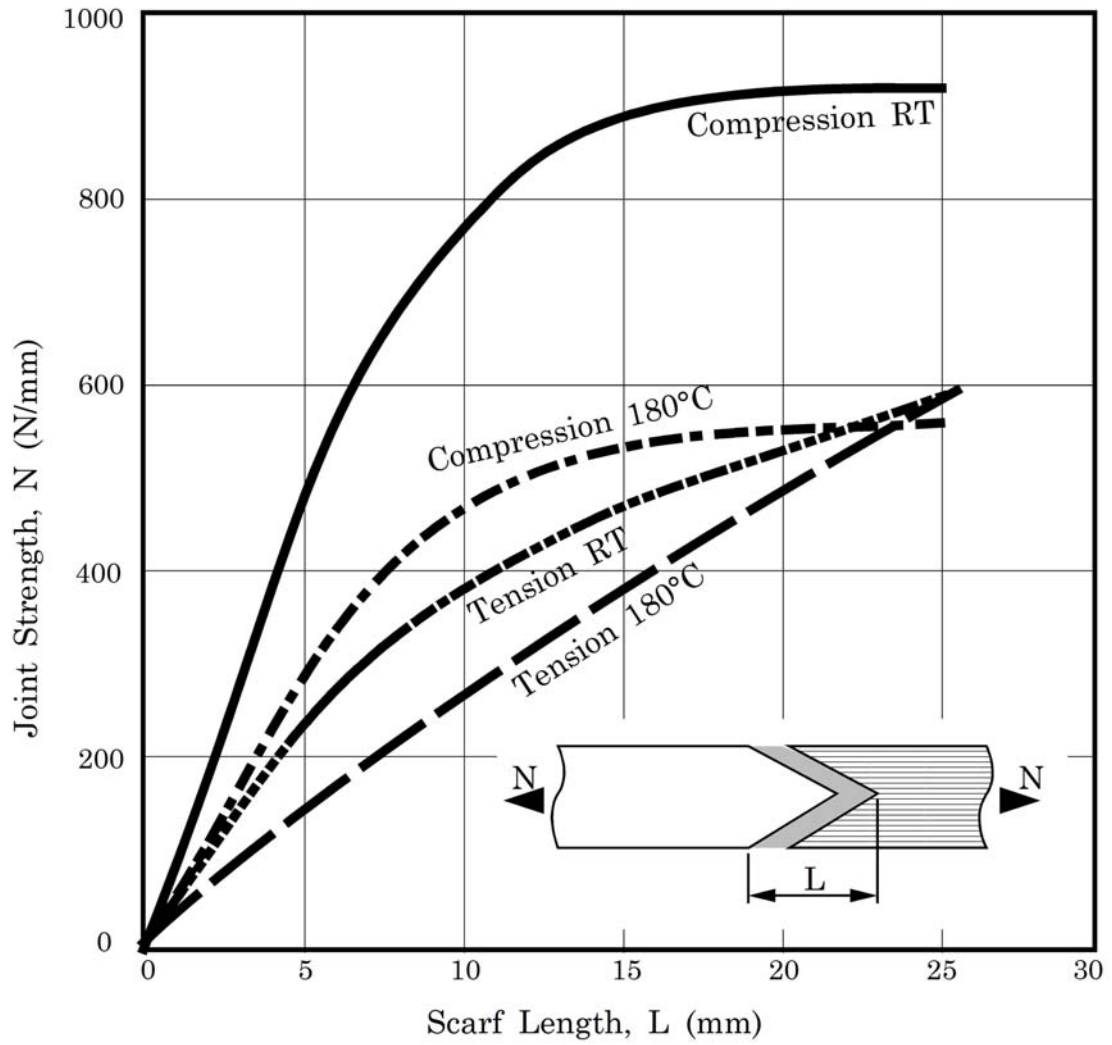


Adherends: Carbon/epoxy to carbon/epoxy or titanium

Adhesive: Shell 951. Medium modulus

Temperature:

Figure 21.10-9 - Design curve: Double lap shear joint

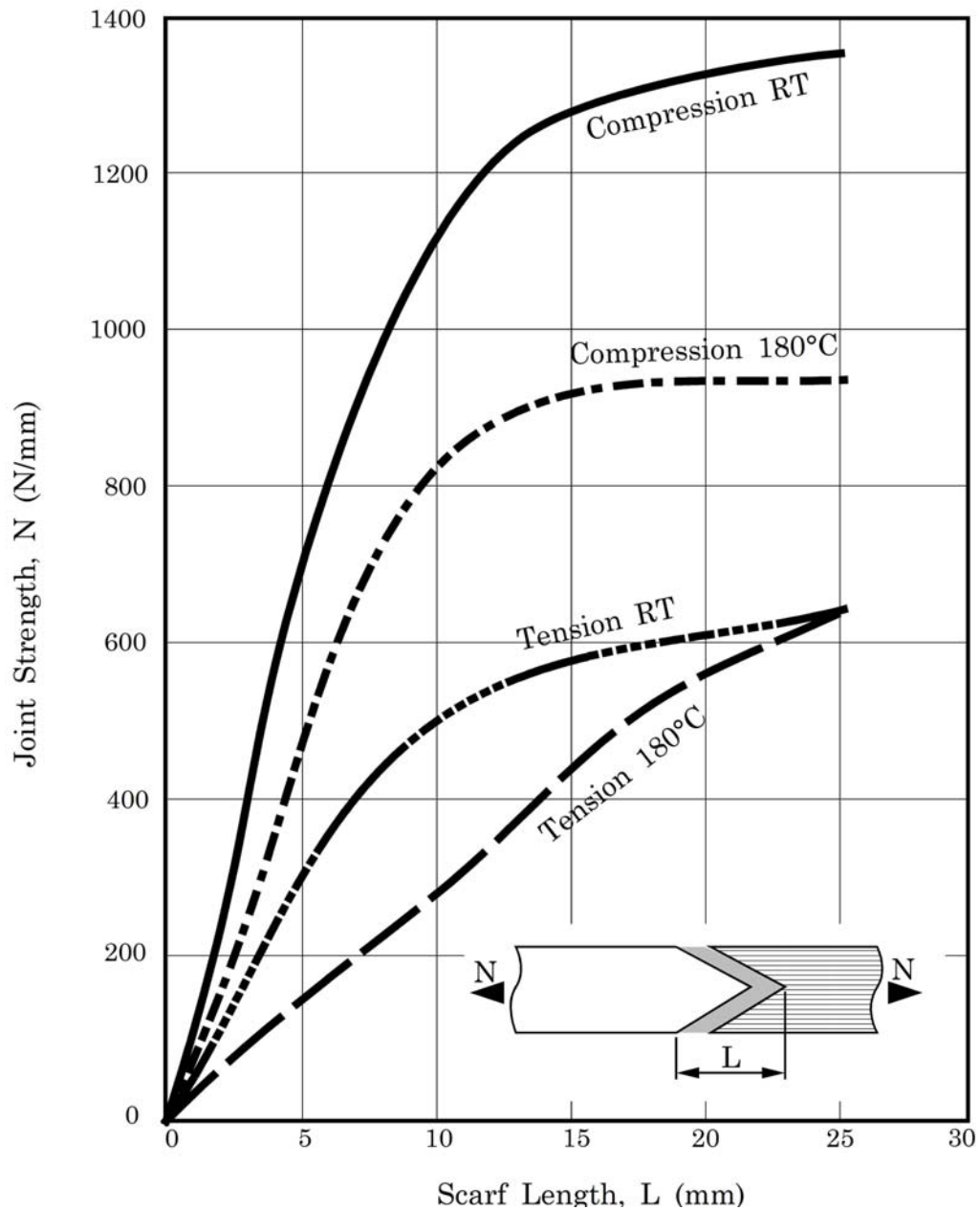


Adherends: Carbon/epoxy to titanium

Adhesive: Metlbond 329-7.

Temperature: RT and 180°C

Figure 21.10-10 - Design curve: Symmetrical double scarf joint strength

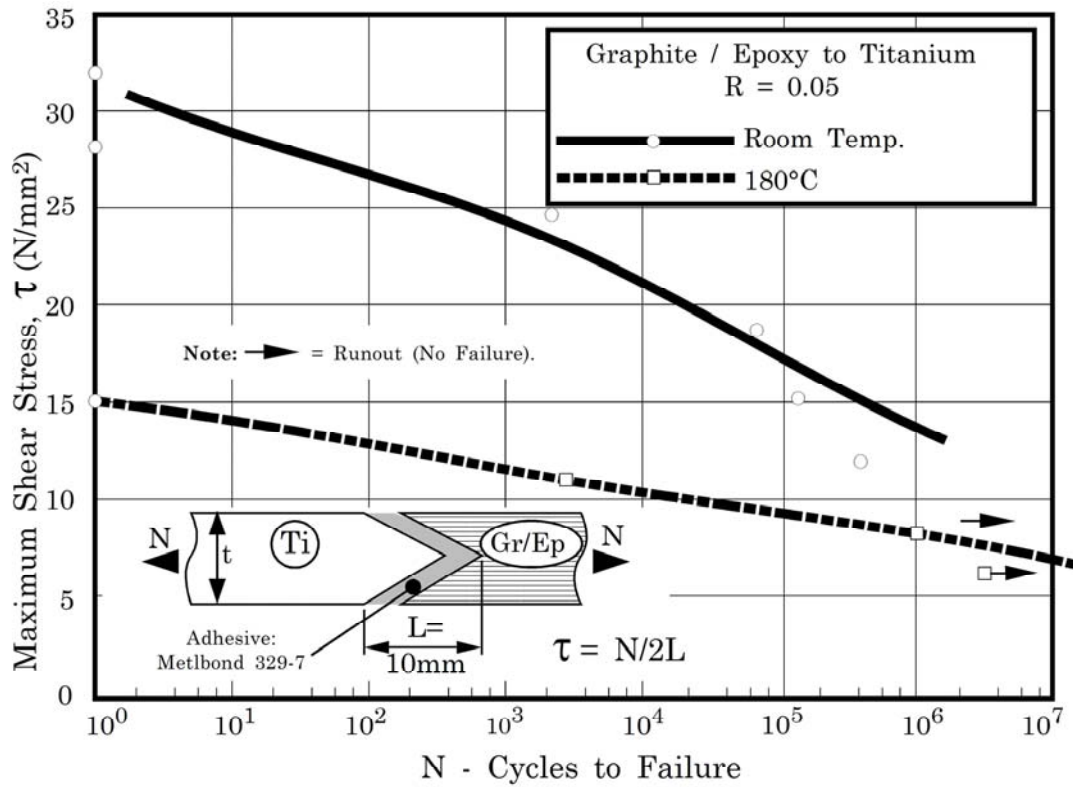


Adherends: Carbon/epoxy to titanium

Adhesive: Metlbond 329-7.

Temperature: RT and 180°C

Figure 21.10-11 - Design curve: Symmetrical double scarf joint strength

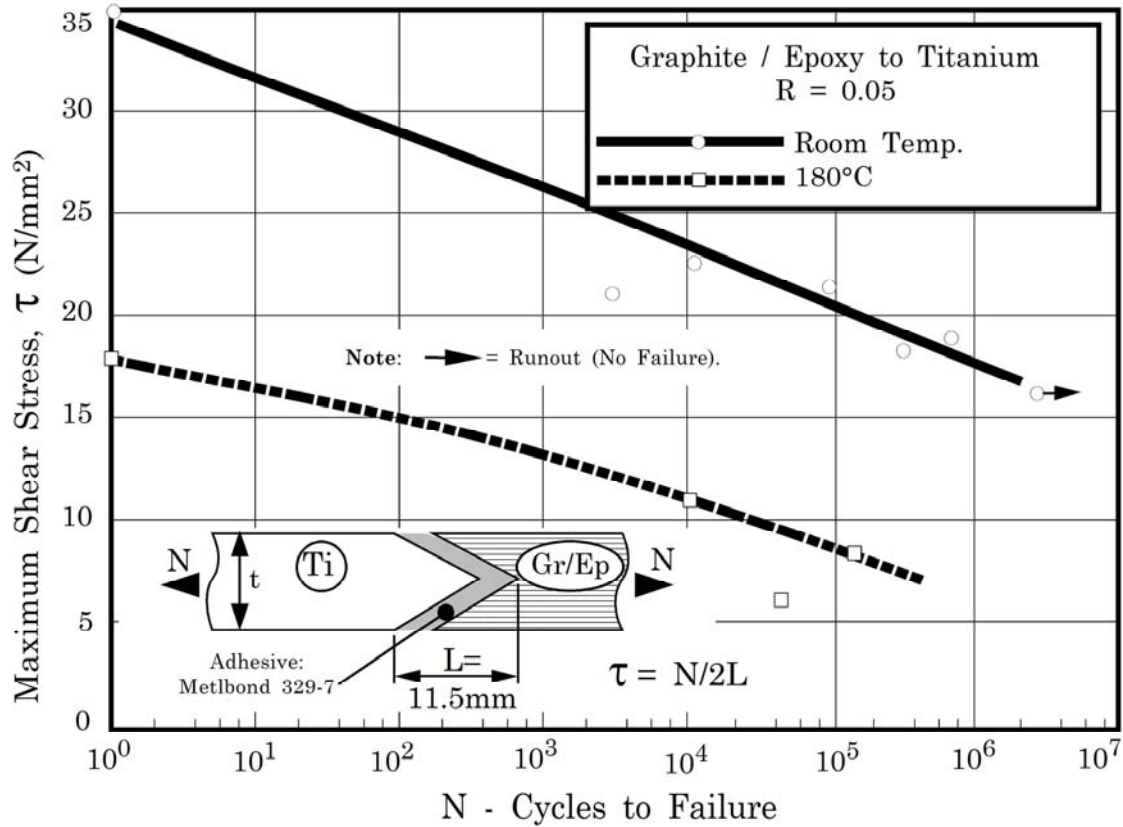


Adherends: Intermediate strength carbon/epoxy to titanium

Adhesive: Metlbond 329-7.

Temperature: RT and 180°C

Figure 21.10-12 - Design curve: Symmetrical double scarf joint, tension fatigue S-N curve

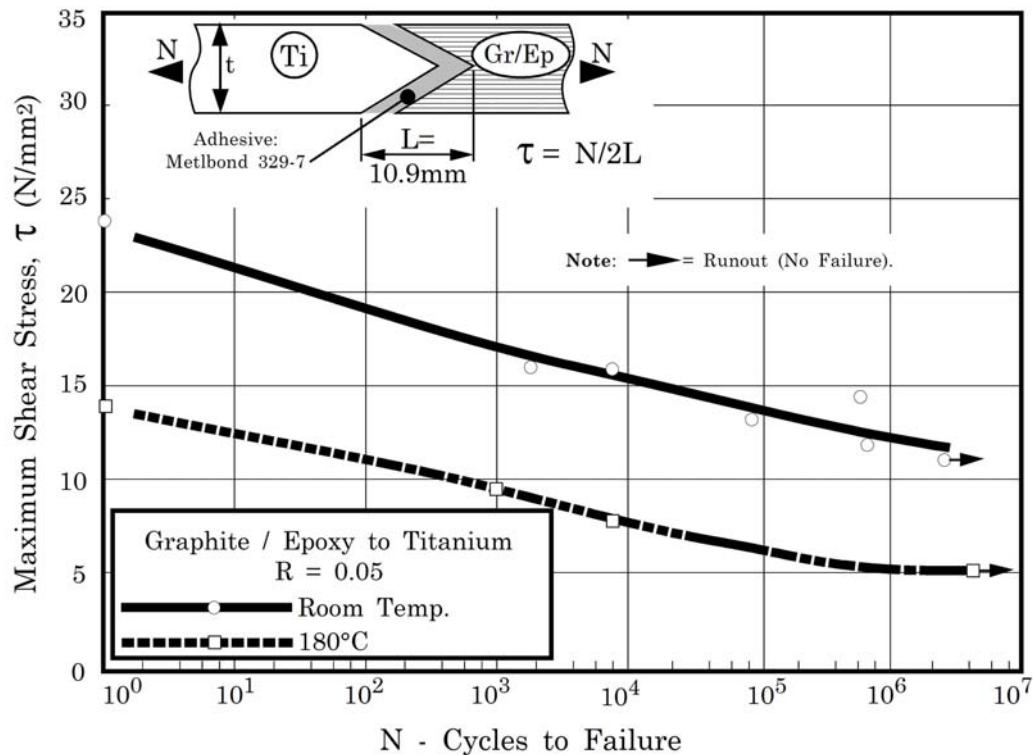


Adherends: Intermediate strength carbon/epoxy to titanium

Adhesive: Metlbond 329-7.

Temperature: RT and 180°C

Figure 21.10-13 - Design curve: Symmetrical double scarf joint tension fatigue S-N curve



Adherends: Intermediate strength carbon/epoxy to titanium

Adhesive: Metlbond 329-7.

Temperature: RT and 180°C

Figure 21.10-14 - Design curve: Symmetrical double scarf joint tension fatigue S-N curve

21.11 Acoustic fatigue of bonded configurations

A study has been made on the response of bonded composite joints to random vibration, Ref. [21-11].

The composite used was Hercules AS4/3501-6 in a balanced multidirectional $0^\circ/90^\circ/\pm 45^\circ$ construction. Bonding was undertaken with epoxy paste adhesive Hysol EA9346-2.

The joint configurations evaluated were:

- Co-cured riser/skin joint
- Bonded rib/skin joint,
- Bonded riveted rib/skin joint,
- Beaded skin (costly construction),
- Integrated riser skin joint.

These are shown in [Figure 21.11.1](#), Ref. [21-11]. Vibration occurred at the natural frequency of each specimen (<300 Hz). The root mean square, [RMS](#), deformation, in μm , was determined for each configuration and failure said to have occurred if the test frequency fell by 5%.

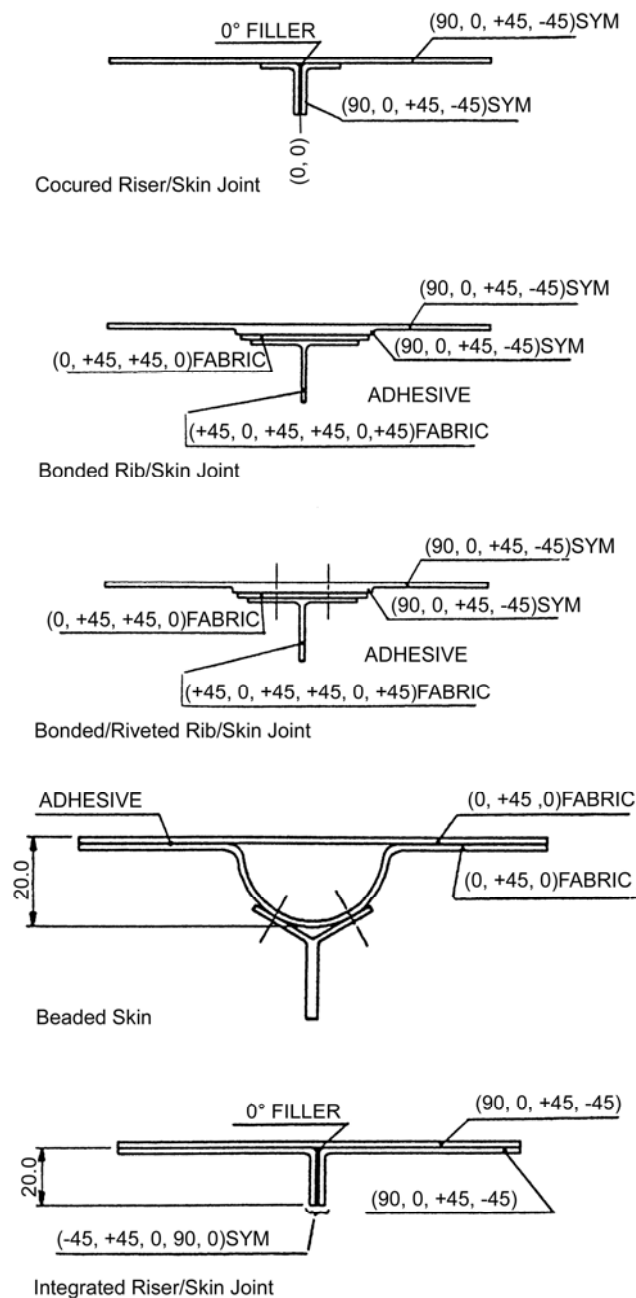


Figure 21.11-1 - Bonded joint configurations in Hercules AS 4/3501-6

The conclusions drawn were that the:

- Integrated skin concept showed little sign of damage after 106 cycles.
- Beaded skin construction exhibited a loss of stiffness after 105 cycles, although little damage was visible.
- Co-cured riser/skin and rib/skin (both riveted and unriveted) joints exhibited peeling before 10⁶ cycles.

Riser/skin joints in bismaleimide Narmco 5250/T300 proved more prone to cracking than the epoxy equivalents.

21.12 References

21.12.1 General

- [21-1] George Lubin
'Handbook of Composites'
Van Nostrand Reinhold. Edition 1982
- [21-2] D.P. Bashford: Fulmer Research Labs. (UK)
'Guidelines on basic aspects of jointing technology for advanced fibre reinforced plastics used in space structures'
September 1984, ESA Contract No. 5497/83/NL/PB (SC)
- [21-3] M.M. Schwartz
'Composite Materials Handbook'
McGraw Hill. Edition 1983
- [21-4] ASTM STP 749
- [21-5] O. Volkersen
Luftfahrtforschung 15, 41; 1938
- [21-6] M. Goland & E. Reissner
J. Appl. Mech., Trans. ASME 66, A17; 1944
- [21-7] L.J. Hart Smith
'Design and analysis of adhesive bonded joints'
McDonnell Douglas Co. Report No. 6059A; 1972
- [21-8] ESDU 79016
'Inelastic shear stresses and strains in the adhesives bonding lap joint loaded in tension or shear', 1979
- [21-9] R. Uhrig
'Elastostatik und Elastokinetik in Matrizenschreibweise'
Springer Verlag, Berlin, 1973
- [21-10] H. Hertel
'Leichtbau'
Springer Verlag, Berlin, 1960
- [21-11] SONACA S.A
'Shaker test results on typical structural CFRP joints under narrow band random fatigue'
Report ESTEC/TP01/BE/R/M1, 7 July 1992
Work undertaken on Work Order No. 21
ESTEC Contract 7090/87/NL/PP

21.12.2 ECSS documents

[See: [ECSS website](#)]

ECSS-Q-70-71	Data for selection of space materials and processes; previously ESA PSS-01-701.
ECSS-Q-ST-70-02	Thermal vacuum outgassing test for the screening of space materials; previously ESA PSS-01-702.
ECSS-Q-ST-70-29	Determination of offgassing products from materials and assembled articles to be used in manned space vehicle crew compartments; previously ESA PSS-01-729.
ECSS-E-HB-32-21	Adhesive bonding handbook; previously ESA PSS-03-210.
ECSS-E-HB-32-22	Insert design handbook; previously ESA PSS-03-1202.

22

Mechanically fastened joints

22.1 Introduction

Composites, like other structural materials, are joined to create useful larger structures. The function of joint elements is to connect two or more parts together in order to transfer load between them. The manner in which these processes are performed is a determining factor in the efficiency and suitability of such components.

The efficiency of a joint can be assessed in relation to its strength, mass and cost of manufacture. A compromise is invariably necessary because maximising strength usually leads to increased mass or increased fabrication costs.

The designer should consider the joint in relation to the whole structure, including dimensional stability, and the loading conditions imposed on the joint.

The [anisotropic](#) nature of composites means it is necessary to design joints very carefully in order to avoid interlaminar or shear failure.

[See also: [ECSS-E-HB-32-23](#) - Threaded fastener handbook for further information on design; previously ESA PSS-03-208; [ECSS-Q-ST-70-46](#) for procurement of threaded fasteners]

22.2 Basic considerations for design

22.2.1 Advantages

The main advantages of mechanical joints are that:

- No special surface preparation or ultra-clean handling operations are necessary.
- No adverse or irreversible strength effects occur due to thermal cycling and high humidity, whereas bonded joints can be.
- No unusual inspection problems for joint quality.
- Disassembly is possible, without destruction of the substrate.

22.2.2 Disadvantages

The disadvantages of mechanical joints can be summarised as:

- Machining of holes is necessary, weakening the component.

- Stress is concentrated at the bearing surfaces, thereby creating stress raisers which can initiate failure.
- Bonded joints are generally stronger, unless mechanical joints are heavy or used for joining thick laminates.
- Mass is added to the joint, reducing the overall joint efficiency.

22.3 Factors affecting design

22.3.1 General

Mechanical fastening of laminated composites is an effective joining technique providing that consideration is given to:

- Tensile and bending stresses of component.
- Strength and flexibility of the fastener.
- Loss of tensile strength in the component due to the drilling.
- Preload in the fastener.
- Shear distribution in the joint.
- Friction between parts.
- Residual stresses.
- Allowable bearing stresses.
- Types of fasteners.
- [Fatigue](#).

Joint selection is based on consideration of:

- Component required strength; both static and fatigue.
- Reliability.
- Ease of fabrication.
- Cost.
- Special joint functions, e.g. removable, replaceable.

All of these variables can be grouped into the categories:

- [Material parameters](#):
 - fibre type and form, i.e. unidirectional or woven fabric.
 - resin type
 - fibre orientation
 - laminate stacking sequence

- fibre volume fraction
- [Fastener parameters](#), [See also: [22.4](#)]
 - fastener type, i.e. bolt or rivet.
 - fastener size
 - clamping force
 - washer size
 - hole size and tolerance
- [Design parameters](#):
 - joint type, e.g. single lap, double lap.
 - laminate thickness and tolerance
 - geometry, e.g. pitch, edge distance, hole pattern.
 - load direction
 - loading rate
 - static or dynamic load
 - failure criteria

22.3.2 Material parameters

The materials considered are carbon and aramid fibre-reinforced epoxies. The majority of composites used in space structures are stacked unidirectional [ply](#) laminates.

Aramid laminates have poorer compressive and interlaminar properties than carbon composites because of the fibrillated structure of aramid fibres. This reduces the bearing strength and so makes mechanical fastening unattractive.

Little published work is available on mechanically-fastened [ARP](#) aramid composites. The use of woven carbon fibre fabric laminates is increasing and these are amenable to mechanical fastening.

As laminate thickness and hence load-bearing demands increase, there is an increasing tendency to consider mechanical fastening over adhesive bonding.

Combined bolted and bonded joints can negate the deficiencies of either one alone, e.g. bolting can restrain [peeling](#) whereas bonding maintains component location, resists [creep](#) or dimensional changes. The combined approach gives a redundant load path, assuming both load paths are designed to withstand the full load.

Optimising stacking sequences can have a significant effect on joint performance, such as:

- The inclusion of $\pm 45^\circ$ plies reduces stress concentration factors around holes in [CFRP](#).
- Optimum tensile properties are obtained with a ratio of 0° to 45° plies of 2:1, whilst optimum shear strength needs a ratio of 1:1.
- For glass fibre-reinforced plastics, Ref. [\[22-5\]](#) recommends putting the 90° fibre on the surface of the laminate.
- The combination of 0° , $\pm 45^\circ$, 90° is an improvement in terms of achieved joint strength to laminate strength.

Figure 22.3.1 summarises the effect of ply configuration on bearing stresses, Ref. [22-4].

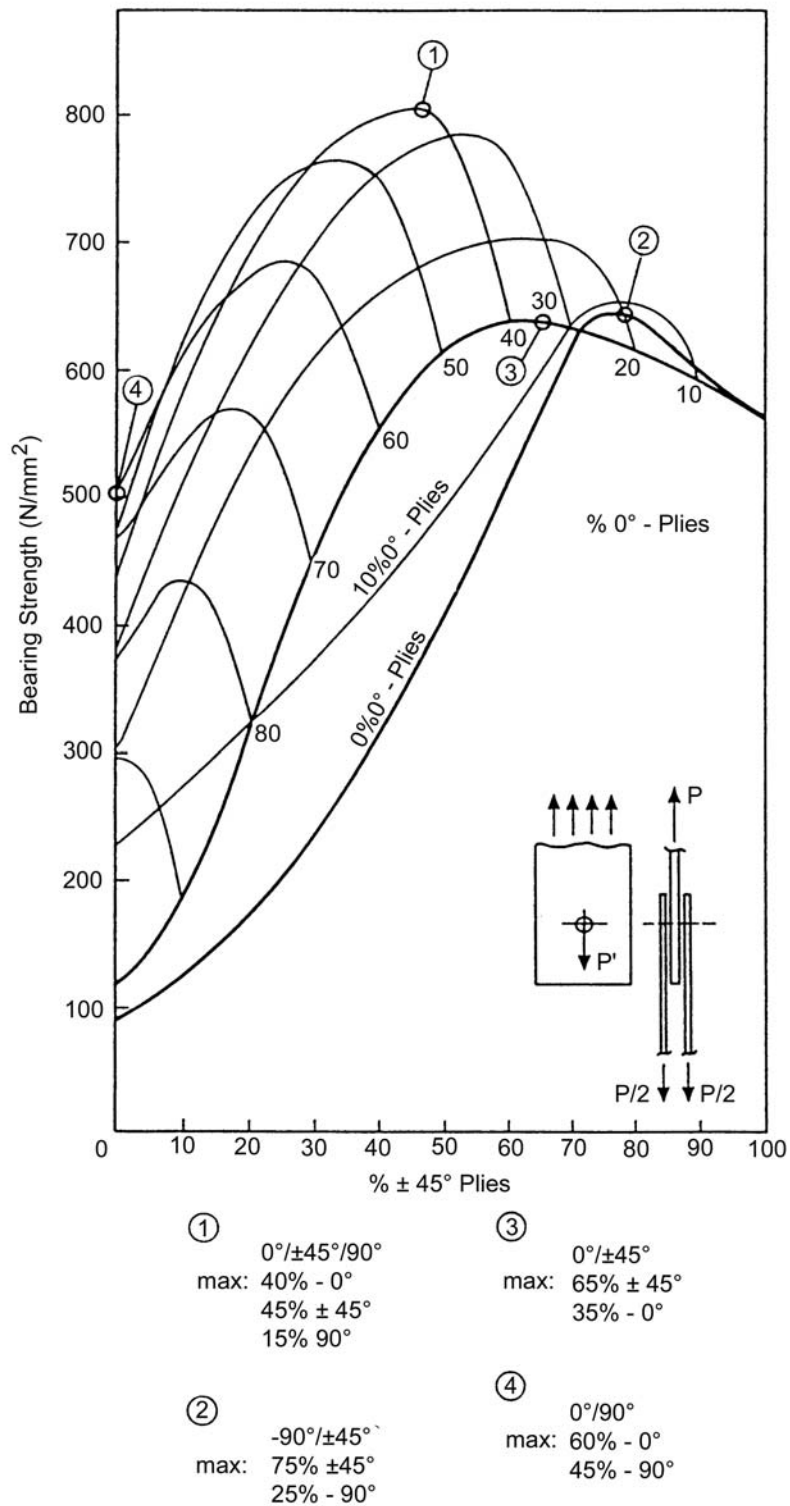


Figure 22.3-1 - Bolted joints: Bearing stresses for various CFRP ply configurations

22.3.3 Fastener parameters

The choice of mechanical fasteners is between:

- Bolts are preferred because they offer the greatest strength of all mechanically fastened joints in composites, [See: [22.4](#)].
- Rivets, where joints have adequate strength in high duty [CFRP](#) laminates with thicknesses up to about 3 mm. The type of rivet, [See: [22.6](#)], the use of washers, dimensions of countersink and imposed clamping loads all affect the ultimate strength of the joint. Laminates with fewer than four plies cannot be riveted. Little use of riveted joints is envisaged within space structures, unless very lightly loaded, i.e. secondary or tertiary structures.
- Screws, which cause extensive damage to the laminate.

22.3.4 Design parameters

22.3.4.1 Joint types

The choice of joint type is dependent on the particular application. Some examples are shown in [Figure 22.3.2](#), Ref. [\[22-1\]](#).

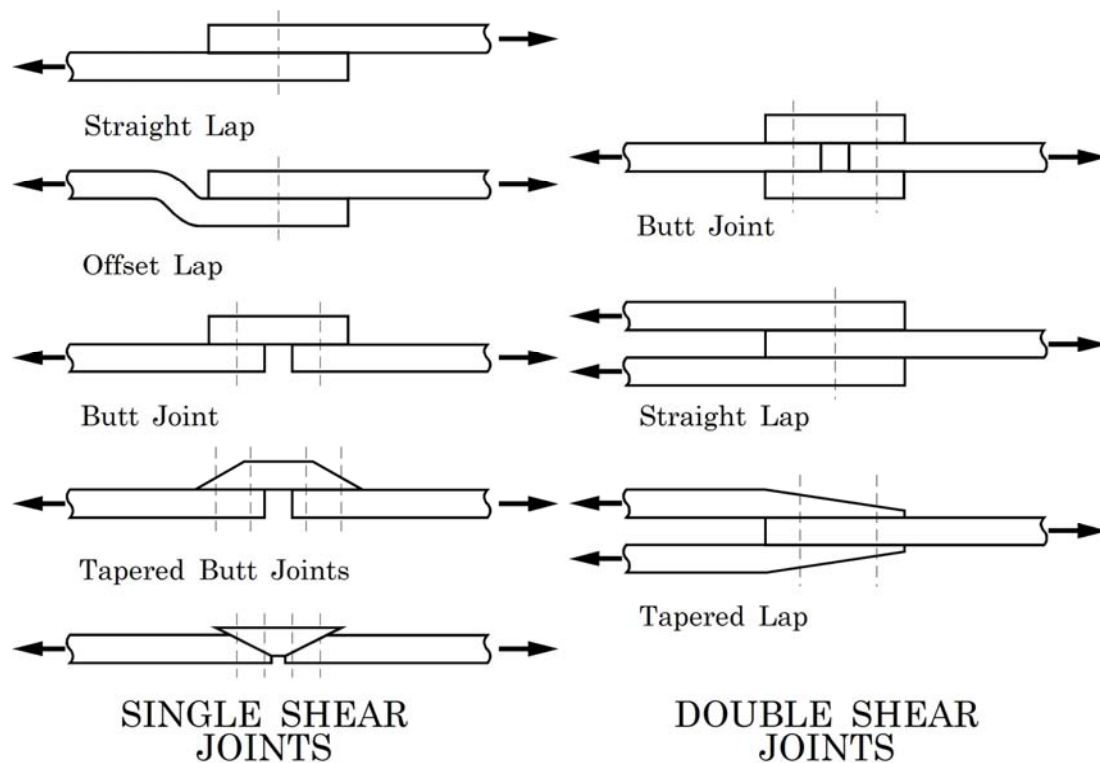


Figure 22.3-2 - Mechanically fastened joints: Examples of configurations

When using experimental data, a close correlation between idealised test joints and the actual configuration being designed is necessary. Likewise, all loading modes and eccentricities should be considered. This usually necessitates considerable testing of bolted specimens to produce design data.

22.3.4.2 End-distance effects

A minimum value of e/d ratio is needed for full bearing strength, [See: [Figure 22.4.1](#)]. The ratio is always greater than 3 for pseudo isotropic $[0^\circ, \pm 45^\circ, 90^\circ, \pm 45^\circ]$ lay ups. For $\pm 45^\circ$ lay ups, it is greater than 5 (this differs from the end-distance ratio of 2.0 recommended by [ECSS-E-HB-32-23](#) for metallic materials).

22.3.4.3 Width effects

From work on single hole specimens, it has been found that $[0^\circ, \pm 45^\circ]$ lay ups in [CFRP](#) need a minimum w/d of 4 (w/d of 8 for all $\pm 45^\circ$), which can probably be equated to minimum pitch distances for multi-hole joints, [See: [Figure 22.4.1](#)]. In $[0^\circ, \pm 45^\circ]$ lay ups the minimum e/d and w/d depend on the relative proportions of 0° and $\pm 45^\circ$ plies.

22.3.4.4 Row and pitch distance

The factors to be considered are:

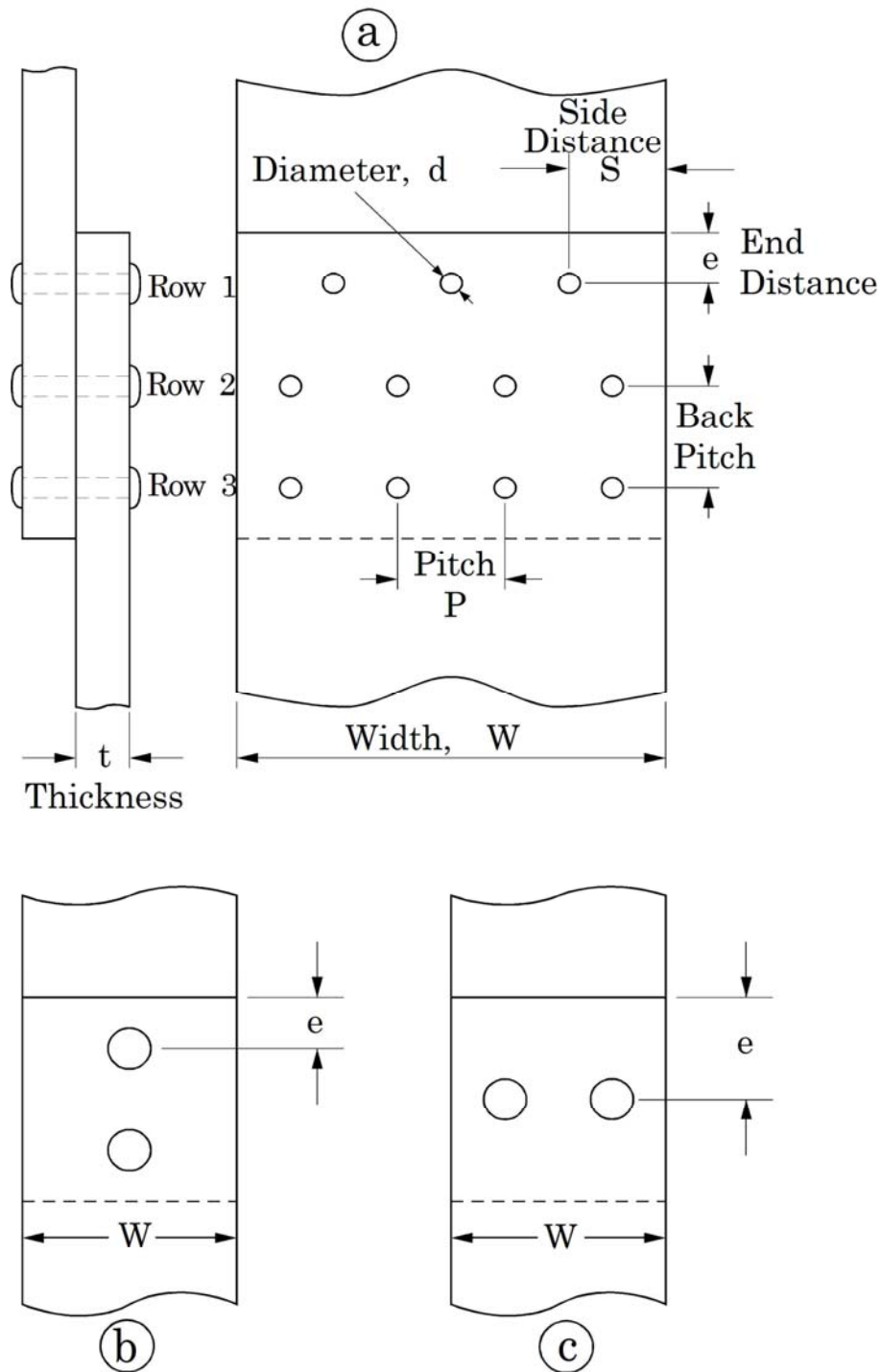
- Hole patterns: A tandem row is preferable to a parallel row, [See: [Figure 22.3.3](#), Ref. [\[22-1\]](#)], and the use of staggered pitch with tandem rows helps.
- Generally, a pitch of $5d$ (5 times the fastener diameter) is acceptable for joints of large safety factors, while $4d$ is a minimum value.
- Multiple rows of fasteners: The pitch on outer rows is greater than that on inner rows, since large tensile loading can thus be tolerated in the joint.

Where eccentricity of the joint is considered, e.g. an unsymmetrical-type fastening produces bending stress in the joint, then multiple rows of fasteners can minimise:

- damage due to bending, but
- axial load carrying capacity.

In such a case, a single row of fasteners displaced every second fastener can be an improvement.

The recommended distance (back pitch) between adjacent rows is no less than $4d$. High back pitch provides the displacement needed to minimise stresses caused by joint eccentricity.



Key:

- a. Row of bolts: Rows 1 and 2 are staggered; Rows 2 and 3 are uniform rectangular pattern.
- b. Two bolts in tandem (line of bolts).
- c. Two bolts in parallel (row of bolts).

Figure 22.3-3 - Mechanically fastened joints: Definition of joint geometry

22.3.4.5 Diameter thickness effect

Extremely thin laminates ($t \sim 0.76$ mm) need to be reinforced to avoid d/t ratio greater than 4.

For [CFRP](#), a d/t ratio ≤ 3 is generally satisfactory for most thicknesses.

22.3.4.6 Failure criteria and modes

The definition of failure varies widely which, in turn, confuses the value of '[design allowable](#)' strengths. A partially accepted failure criterion is based on the deformation of the bolt hole under load. However, agreement on the degree of permanent hole deformation is lacking with values varying from 0.5% to 4% of the hole diameter being suggested. A safety factor of 2 on the ultimate strength appears to be a minimum and is close to the stress at which damage initiates.

Mechanically fastened joints can display a number of failure modes, as shown in [Figure 22.3.4](#). Failure is normally gradual, with progressive damage eventually resulting in complete loss of load-bearing capacity.

The definition of joint strength can become confused, the failure criteria can be:

- The onset of damage,
- Degrees of damage or
- Ultimately, the maximum load-bearing capacity.

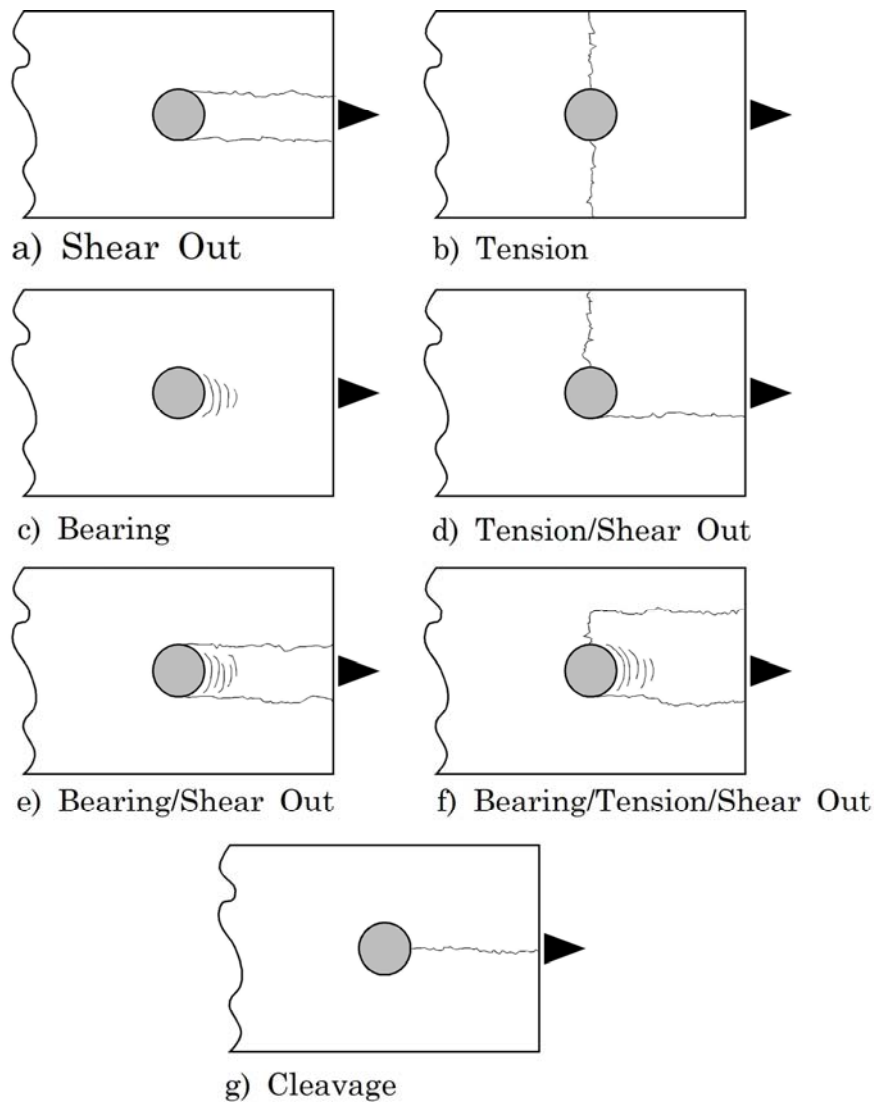


Figure 22.3-4 - Bolted joints: Failure modes

For joints combining composite and metal, each material has its own failure characteristics, e.g.

- Composites have a low strain, brittle mode of failure.
- Metals show greater ductility and plastic deformation than composites; depending on their composition and condition.

For bolted joints, full bearing strength is only developed if failure due to tension and shear, [See: [Figure 22.3.4](#)], is suppressed by providing adequate end distance and width (or pitch), and if sufficient restraint is present to prevent local interlaminar failure.

Simple bolted joints rarely achieve more than 50% of base laminate strength. Higher joint strengths can be obtained by:

- localised reinforcement, and
- modified load distribution.

These techniques reduce joint efficiency in terms of mass and increase production costs.

[Figure 22.3.5](#) shows examples of locally reinforced joints.

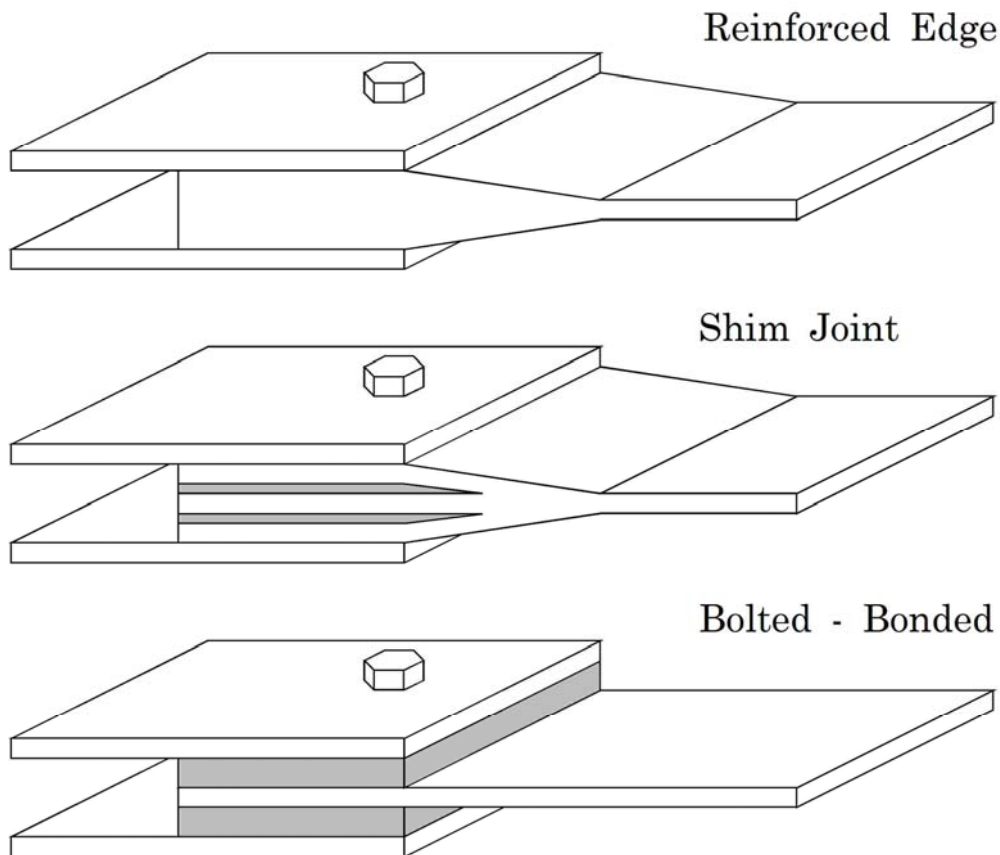


Figure 22.3-5 - Local reinforcements for bolted joints

22.4 Bolted joints

22.4.1 Material parameters

[See: [22.3](#)]

22.4.2 Fastener parameters

Bolts offer the greatest strength for mechanically fastened joints in composites. Unless overtightened, no damage is done to the composite during assembly.

Machining of holes in composites needs care to achieve a repeatable high quality. If machining damages the composite around the hole then joint performance and durability can be impaired.

In terms of optimising strength, the factors to consider are:

- The bolt is a good fit into the (preferably) reamed hole.
- Increasing the bolt tightening torque, and hence clamping force, increases the bearing strength. Optimum levels of clamping exist.
- The hole in the washer (ideally, reamed) is a close fit to the bolt. Washer size can influence strength.

- Beware of [galvanic corrosion](#).

A problem identified with mechanically fastened [CFRP](#) for aircraft constructions is [galvanic corrosion](#), [See: [20.3](#)]. For CFRP and aluminium, it can be particularly acute because their electrochemical potentials are very different.

Titanium fasteners are better, though expensive, for CFRP. Whilst corrosion is not normally a problem for deployed satellites, reusable vehicles and launchers have to operate in Earth's environment, exposing structures to galvanic corrosion problems.

Whilst bolt tightening can be used to increase joint bearing strengths, it is not advisable to rely on this increment of strength when designing constructions. Some relaxation of clamped composites occurs over a period of time and the strength is then lost. The additional strength due to clamping is ignored during design, its presence is an unaccounted safety margin benefit.

[Figure 22.4.1](#) shows the bearing strength of bolted carbon fibre-reinforced laminates, Ref. [\[22-2\]](#).

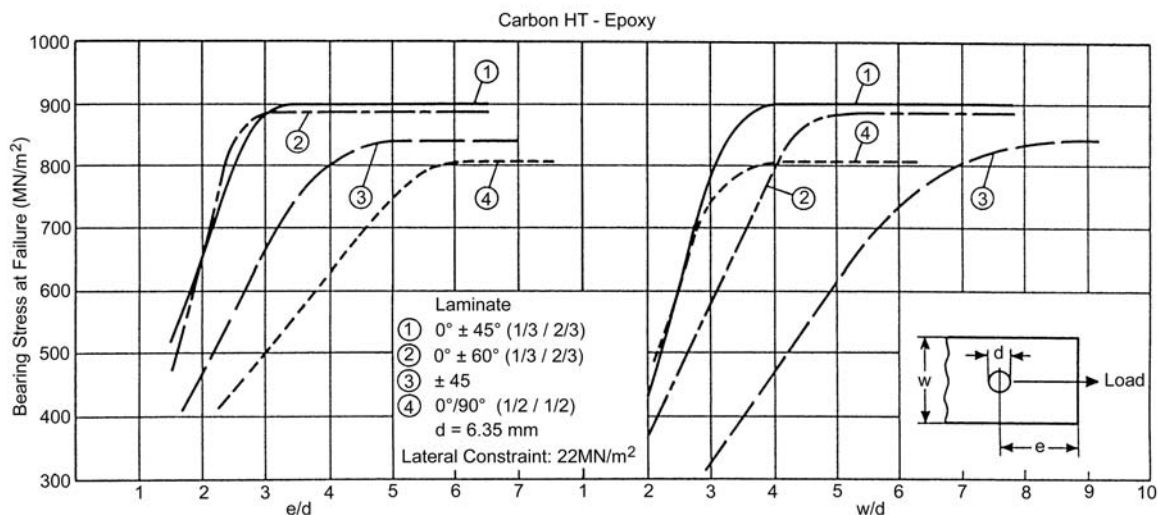


Figure 22.4-1 - Bearing strength of bolted carbon fibre reinforced laminates

There are many different bolts applicable to composites, included in these are countersunk variants which need additional composite machining which in turn affects strength and failure modes. A short review of fasteners for composites was published based experiences within the American aircraft manufacturers'; and identifies several sources of fasteners.

[See: [22.3](#) for comments on other types of mechanical fasteners]

[See: [ECSS-O-ST-70-46](#) for procurement of threaded fasteners]

22.4.3 Design parameters

[See: [22.3](#) - Design parameters]

[See also: [ECSS-E-HB-32-23](#) for guidelines on the design of bolted joints; [ECSS-O-ST-70-46](#) for procurement of threaded fasteners]

22.5 Bolted joint: Analysis

22.5.1 General

Joints in [CFRP](#) elements are normally designed in much the same way as those in metallic structures using mechanical fasteners. Knowledge of the stress distribution and the failure strength is helpful in selecting appropriate joint sizes.

An overview of certain problems and a guideline for the preliminary design of bolted joints is presented.

22.5.2 Analytical methods

22.5.2.1 Two-dimensional analysis

Analytical methods have been developed for calculating the strength of bolted joints on the basis of two-dimensional analysis methods, Ref. [\[22-6\]](#), [\[22-7\]](#), [\[22-8\]](#), [\[22-9\]](#), but they ignore several effects, including:

- free edge effects at open holes
- clamping effects when joints are bolted
- influence of delamination on load distribution (plastification).

22.5.2.2 Three-dimensional analysis

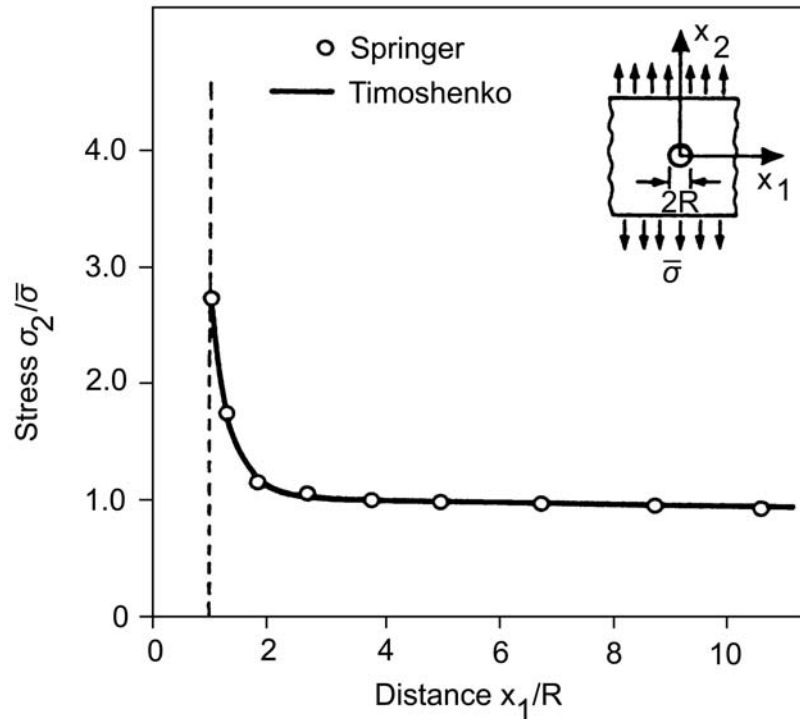
Highly sophisticated [FE](#) computer codes, Ref. [\[22-10\]](#), have been used to perform three-dimensional analyses which are in good accordance with experimental results.

22.5.3 Stress distribution

22.5.3.1 Infinite isotropic plate containing a circular unloaded hole

An analytical solution for the stress distribution in an infinite isotropic plate, containing an unloaded hole, from Ref. [\[22-11\]](#), and calculated with the aid of a computer program, Ref. [\[22-7\]](#).

The stress distributions are shown in [Figure 22.5.1](#).

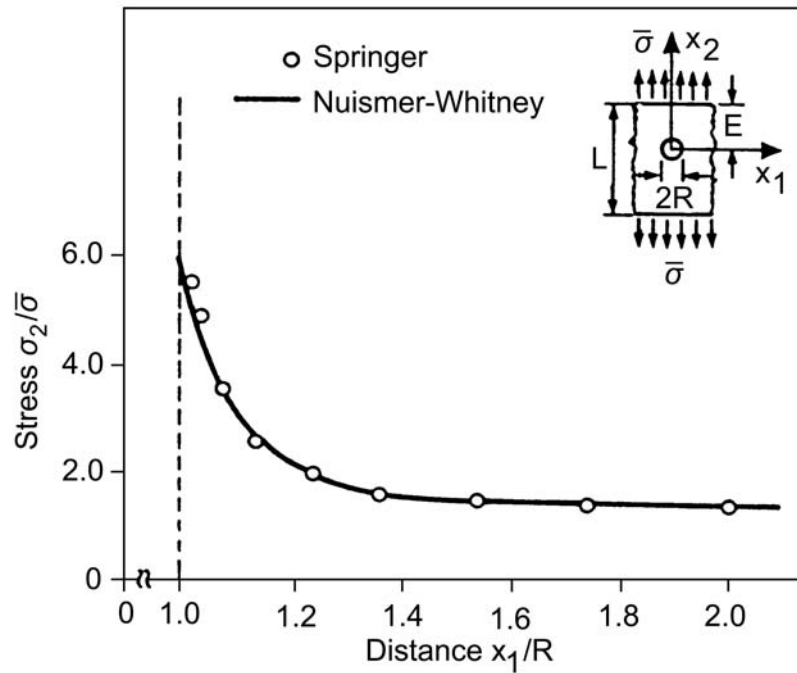


Comparison of Springer, Ref. [22-7] with the theoretical results given by Timoshenko, Ref. [22-11]:

Figure 22.5-1 – Stress σ_2 along the x_1 -axis in an isotropic infinite plate containing an unloaded circular hole

22.5.3.2 Infinite orthotropic plate containing a circular unloaded hole

For comparison, [Figure 22.5.2](#) gives the stress distribution in an orthotropic plate $[0^\circ/90^\circ]$. This diagram is based on the solution given in Ref. [22-7], [22-8].



Comparison of Springer, Ref. [22-7] with the theoretical results obtained by Nuismer Whitney, Ref. [22-8].

Figure 22.5-2 - Stress σ_2 along the x_1 -axis in an orthotropic infinite plate $[0^\circ/90^\circ]$ containing an unloaded circular hole

22.5.3.3 Finite width isotropic plate containing a circular loaded hole

Figure 22.5.3 presents the stress distribution in an isotropic plate containing a loaded hole. This diagram is based on the solution methods presented in Ref. [22-7], [22-9].

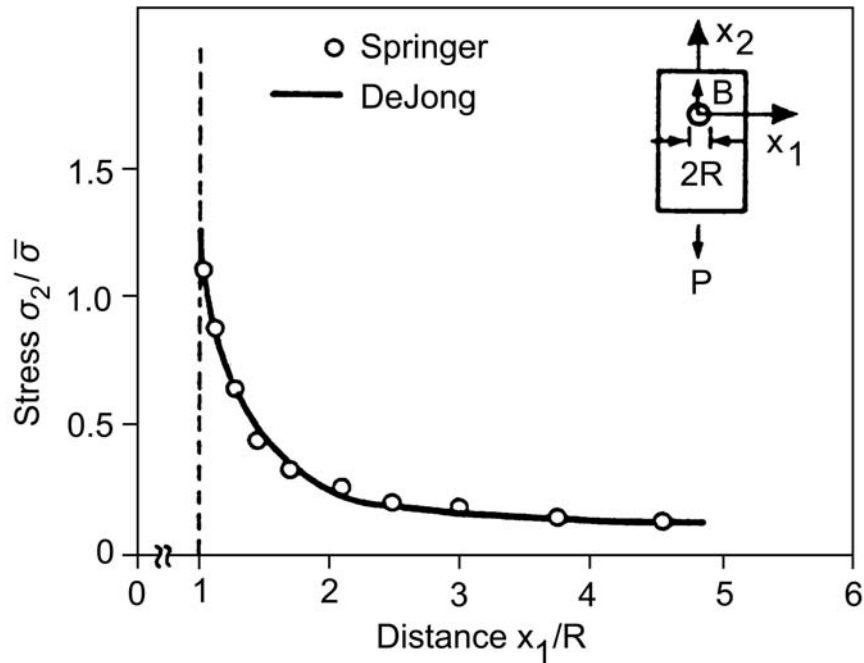


Figure 22.5-3 - Stress σ_2 along the x_1 -axis in an isotropic plate of finite width containing a loaded hole

22.5.4 Failure prediction

22.5.4.1 General

Numerous failure criteria have been developed for laminated composites. The ESAcomp software documentation explains many of the criteria that are commonly used in the European space industry, Ref. [22-18]. These criteria are generally expressed in the form of 'far-field' strain or stress levels that cannot be exceeded (i.e. the strength of the laminate without any load concentrations). When applying such criteria to bolted joints, it is recommended that local effects around the loaded hole are accounted for by using the [Whitney/Nuismer failure hypothesis](#). This hypothesis is used in conjunction with one of the far-field failure criterion such as the Yamada criterion.

22.5.4.2 Yamada failure criterion

This criterion is based on the assumption that failure occurs when every ply has failed as a result of cracks along the fibres, Ref. [22-12].

Conditions which are met in any one of the plies are:

$$\left(\frac{\sigma_1}{R_1^{tu}}\right)^2 + \left(\frac{\tau_{12}}{R_{12}^{su}}\right)^2 = e^2 \quad \begin{array}{l} e < 1: \text{ no failure} \\ e \geq 1: \text{ failure} \end{array} \quad [22.5-1]$$

where:

σ_1 and τ_{12} are the longitudinal and shear stresses in a ply (x and y being the co-ordinates parallel and normal to the fibres in the ply),

R_1''' is the longitudinal tensile strength of the ply, and

R_{12}''' is the shear strength of a symmetric, cross-ply laminate that has the same number of plies as the laminate under consideration.

22.5.4.3 Whitney/Nuismer failure hypothesis

This hypothesis, Ref. [22-13], is used with an appropriate failure criterion, e.g. Yamada, and proposes that failure occurs when in any one of the plies of a laminate stresses satisfy this criterion on a characteristic curve around the loaded hole. This characteristic curve is shown in [Figure 22.5.4](#) and can be calculated by:

$$r_c(\theta) = D/2 + R_{ot} + (R_{oc} - R_{ot})\cos\theta \quad [22.5-2]$$

where:

$$-\frac{\pi}{2} \leq \theta \leq \frac{\pi}{2} \quad [22.5-3]$$

R_{ot} and R_{oc} are characteristic lengths for tension and compression. These parameters can be determined experimentally by measuring the tensile and compressive strengths of notched laminates.

R_{ot} and R_{oc} depend only on the material. Therefore, the co-ordinates of the characteristic curve also depend only on the material and are independent of the geometry and the stress distribution.

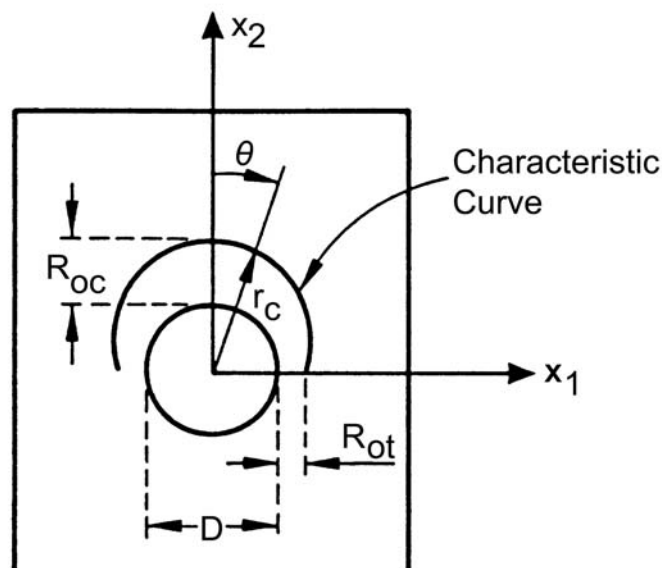


Figure 22.5-4 - Whitney/Nuismer failure hypothesis: Characteristic curve

When this hypothesis is used together with the Yamada criterion, failure occurs when:

$$e \geq 1 \text{ at } r = r_c$$

at any point on the characteristic curve.

This hypothesis is general and not restricted to Yamada's criterion. Any other criterion can be used.

22.5.5 Experimental data

22.5.5.1 Shear load carrying capabilities of bolts in CFRP facings

The samples were tested statically (tension and compression) up to fracture load using the test device shown in [Figure 22.5.5](#), Ref. [\[22-14\]](#).

The tests were performed with:

- different fibre orientations of the facing
- different materials ([HT](#) and [HM CFRP](#)).
- laminate thickness 0.25 mm and 0.375 mm.

The test results are shown in [Table 22.5.1](#) for 914C-T300 composite and in [Table 22.5.1](#) for 914C-HM composite, Ref. [\[22-14\]](#).

[Figure 22.5.6](#) compares the bearing stresses at the failure point, Ref. [\[22-14\]](#).

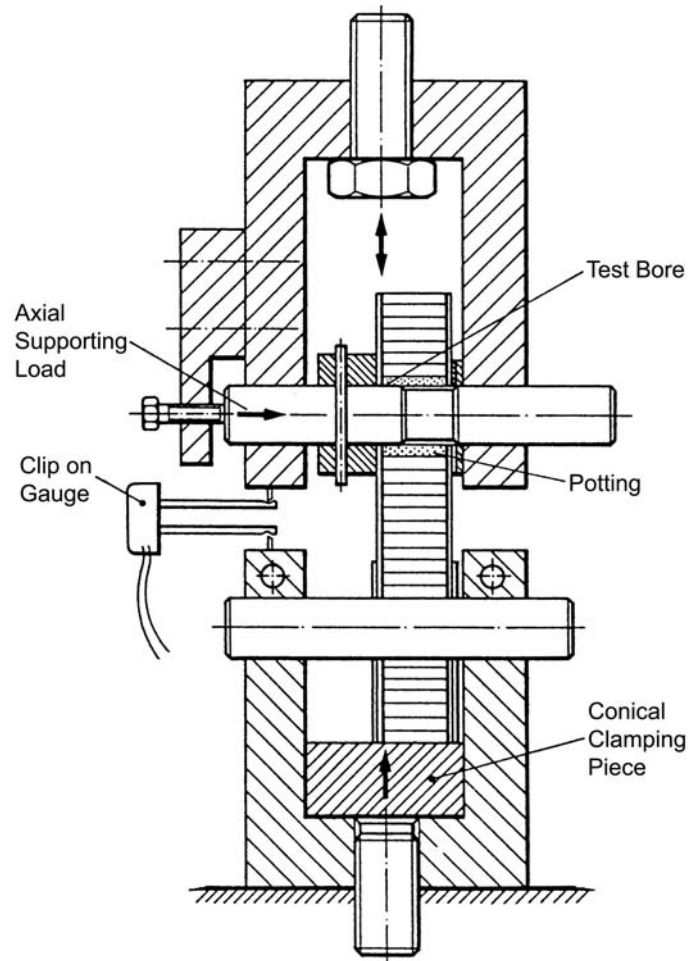


Figure 22.5-5 - Bolted joints: Test device and configuration for in- plane face sheet loading

Table 22.5-1 - Bolted joints: Results of static test on material 914C T300

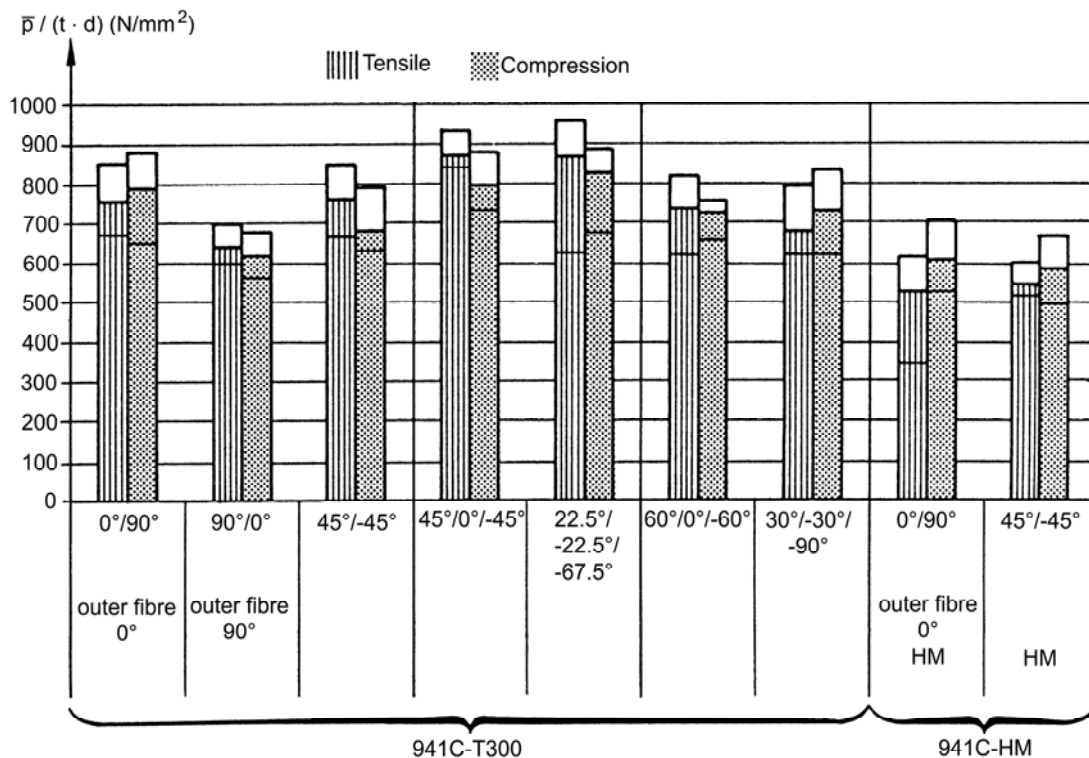
Lay-up	0°/90°		90°/0°		45°/-45°		45°/0°/-45°		22.5°/-22.5°/-67.5°		60°/60°/-60°		30°/-30°/-90°	
Tf	0.25		0.25		0.25		0.375		0.375		0.375		0.375	
Sample No.	Load [N]		Load [N]		Load [N]		Load [N]		Load [N]		Load [N]		Load [N]	
	Tensile	Comp.	Tensile	Comp.	Tensile	Comp.	Tensile	Comp.	Tensile	Comp.	Tensile	Comp.	Tensile	Comp.
1	2639	2656	2383	2355	2360	2225	4444	4409	4500	4578	4212	4005	3554	3693
2	2944	2717	(2625)†	2236	2766	2253	4534	4260	5072	4401	3273	3523	4180	4401
3	2465	3067	2442	2188	2830	2475	4620	3994	4991	4645	(4887) <i>f</i>	5042	3499	3787
4	2621	2289	2166	2197	(1779)‡	1686	4450	3731	4273	4036	(4410) <i>f</i>	4252	3258	3921
5	2919	2905	2140	1981	2940	2764	4901	4621	4600	4555	3738	3996	3499	3783
6	2326	2736	2135	2039	2564	2251	4774	3868	5007	4386	4275	4107	3856	4257
7	2660	2952	-	-	2474	2318	4851	4261	3276	3406	3854	3437	3380	3159
p	2653	2760	2253	2166	2660	2381	4653	4163	4531	4315	3870	3813	3604	3858
S.D.	223	254	147	136	232	208	190	313	630	373	404	309	313	405
p/(t·d) Nmm ⁻²	758	789	643	618	760	680	886	793	863	822	737	726	686	735
Failure mode	buckling under 0°	buckling under 0°	buckling under 0°	buckling under 0°	bearing + 45° shear	bearing + 3x45° buckling	bearing	bearing	bearing	bearing	bearing	bearing	bearing 1 x buckling	bearing

Key: †: Very high load speed ‡: Without axis clamping *f*: Shimming around hole Tf: Facing Thickness

Table 22.5-2 - Bolted joints: Results of static test on material 914C – HM

Lay-up	0°/90°		45°/-45°	
Facing Thickness (T_f)	0.25		0.25	
Sample No.	Load [N]		Load [N]	
	Tensile	Comp.	Tensile	Comp.
1	2144	2483	1950	2201
2	(1630) ¹	2074	2104	1958
3	(1655) ¹	2022	1860	2165
4	1980	2194	1964	1963
5	1998	2093	1863	2113
6	2061	2249	1962	2355
7	1544	2152	1812	1727
\bar{p}	1825	2128	1931	2069
S.D.	299	169	97	206
$\bar{p}/(t \cdot d)$, Nmm ⁻²	521	608	552	591
Failure mode	tensile + shear out	buckling under 0°	tensile + shear out under 45°	shear out 1 x buckl. under 45°

Key: 1) Sample was influenced by the failure of neighbouring samples.


Figure 22.5-6 - Bolted joints: Bearing stress at failure point of CFRP facings with different lay-ups

22.6 Riveted joints

22.6.1 General

In the initial structural application of composite materials, fasteners and installation procedures that had been optimised for metallic structures were applied. For these applications interference fit and high preload give strength and durability improvements and the use of rivet guns to install rivets leads to cost savings. Experience has shown that using the same fasteners and installation procedures in composite structures can produce unacceptable damage.

The nature of the resulting damage, the fastener implications and types of fasteners are described here.

22.6.2 Installation damage of riveted joints

22.6.2.1 Interference

The low interlaminar strength of composite materials restricts the use of interference fit fasteners. When permanent fasteners are forced into an interference-fit hole, the plies on the back side can [delaminate](#) and split out.

Rivets are usually installed such that they completely fill the hole by expansion of the shank. Experience with fibreglass has shown that such expansion causes [delaminations](#) and [ply](#) buckling. These difficulties have led to the general requirement that only clearance fit (0.000 to $+1.02 \times 10^{-4}$ m) fasteners are appropriate to composite structures, Ref. [\[22-15\]](#). This is not to imply that interference fit is not desirable or that suitable fastener concepts for interference are not available, e.g. increasing the level of interference in a carbon/epoxy joint can increase the fatigue life, Ref. [\[22-15\]](#). Interference is also desirable to:

- increase load sharing in joints with multiple rows of fasteners,
- retard fuel leakage in tank areas, and
- provide the reactive torque needed for one sided installations of 'Hi Lok' fasteners.

22.6.2.2 Impact forces

The propensity of composite structures to delaminate and split out on the back side from the impact forces created by debris or tools is well known. Consequently, the use of rivet guns on composite structures is prohibited.

The pull type fasteners, like the lock-bolt systems, also deliver impact forces in the form of the reaction forces released when the breakneck is severed. However, no damage to the laminate, attributable to this type of impact, has been observed.

22.6.2.3 Preload

Preload is the force exerted on the sheets being joined by the following:

- Nut torquing,
- Collar swaging
- Tail formation.

With the low compressive strength of composites, a high preload results in laminate crushing. The aerospace industry mainly makes use of 'bigfoot' fasteners to overcome this problem, [See: [Footprint](#)]. There is, however, room for some optimisation of the fastener design in the future, e.g. higher preloads can provide longer fatigue lives.

22.6.3 Pull through strength

22.6.3.1 General

The low pull through strength of mechanically fastened composite joints is well known. The prevalence of fasteners with enlarged [footprints](#) and enlarged heads in such structures is evidence of this fact. Modified fasteners have been developed to improve pull-through characteristics.

22.6.3.2 Footprint

The '[footprint](#)' is the bearing area of the nut, collar or tail of an installed fastener. The pull through strength of a fastener is partially determined by the size of the footprint as shown in [Figure 22.6.1](#).

Monogram developed the 'Bigfoot™' fastener, which has the same tail diameter and pull through strength as the 'Hi Loks' used on the opposite surface. The collar for the titanium GPL fasteners (Groove Proportional Lockbolt) also has an enlarged footprint to avoid pull through problems.

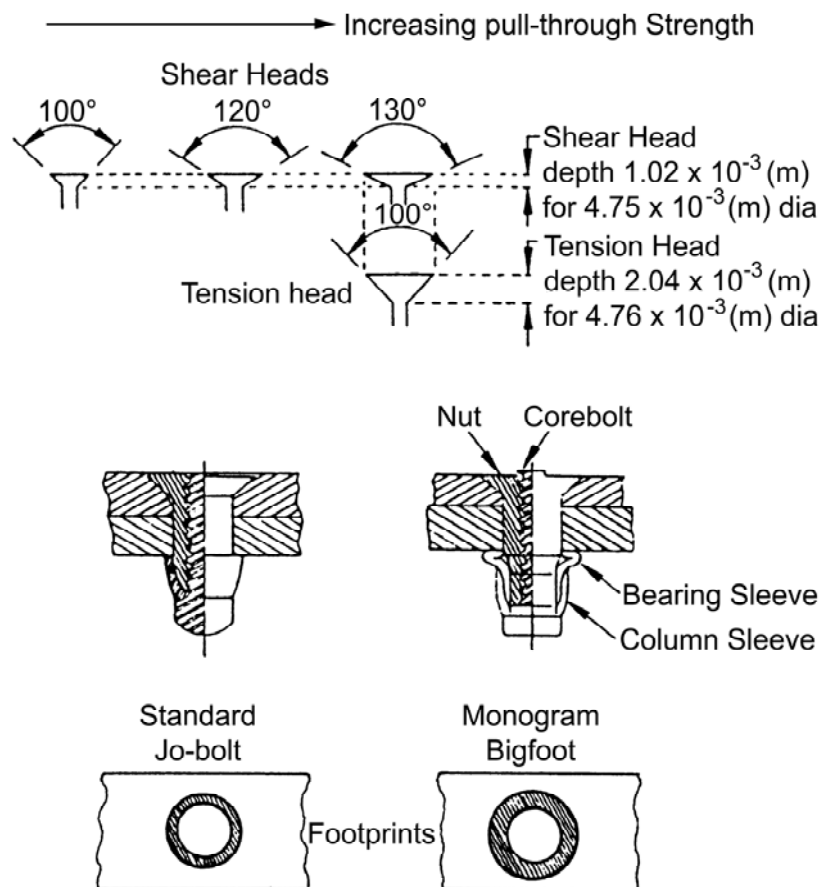


Figure 22.6-1 - Rivets: Improvement in pull-through strength by larger flush head diameter and footprint

22.6.3.3 Flush head configuration

The flush head configurations considered, [See: [Figure 22.6.1](#)], are where the pull through strength is shown to be a function of the head outside diameter. Factors to be considered are:

- Thick composites: The use of tension head fasteners (100°) for thick composite structures is now quite common.
- Thin composites: Fasteners with 130° shear head reportedly supports 30% more load than the 100° shear head. The 120° shear head can also be applicable.

22.6.4 Fasteners used in composite structures

A summary of those fasteners used for aerospace materials is shown in [Table 22.6.1](#), Ref. [22-15].

Table 22.6-1 - Types of fasteners used to join aerospace materials

Load Transfer	Materials Joined	Head Type	Fastener Type
Low	C/E → C/E	Flush	Threaded
	C/E → C/E	Flush	Blind
	C/E → C/E	Protruding	Threaded
Low	C/E → metal	Flush	Blind
	C/E → metal	Flush	Threaded
	C/E → metal	Flush	Rivet
	C/E → metal	Protruding	Threaded
High	C/E → metal	Protruding	Threaded
	C/E → metal	Flush	Threaded
	C/E → metal	Flush	Blind
	C/E → metal	Flush	Swaged

Key: C/E - Carbon fibre/epoxy composite.

22.6.4.1 Types of rivets

Various types of rivets proposed for joining aerospace materials are shown in [Figure 22.6.2](#).

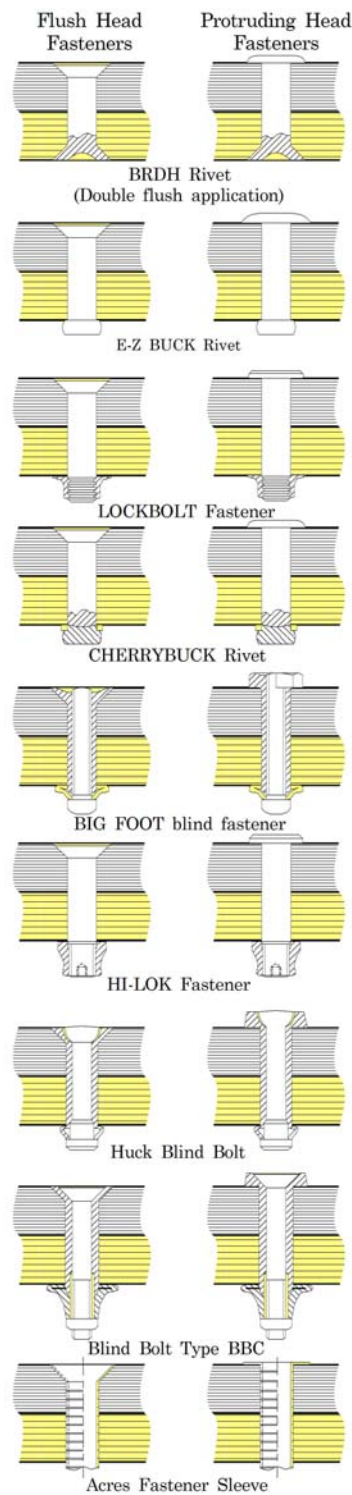


Figure 22.6-2 - Types of rivets for aerospace materials

22.7 References

22.7.1 General

- [22-1] Fulmer Research Laboratories
'Guidelines on basic aspects of jointing technology for advanced fibre reinforced plastics used in space structures'
ESA Contract 5487/83/NL/PB (SC)
- [22-2] T.A. Collings
'The strength of bolted joints in multi directional CFRP laminates'
Composites, January 1977
- [22-3] G. Lubin
'Handbook of Composites'
Von Nostrand Reinhold Company, 1982
- [22-4] J. Bauer
'Gegenüberstellung von Vorhersagewerten und Versuchsergebnissen an Kerben und bolzenbelasteten Bohrungen in CFK Laminaten'
DGLR Symposium, 1984
- [22-5] E.W. Godwin & F.L. Matthews
'A review of strength of joints in fibre reinforced plastics'
Composites, July 1980
- [22-6] C.M.S. Wong & F.L. Matthews
'A finite element analysis of single and two-hole bolted joints in fibre reinforced plastic'
- [22-7] G.S. Springer et al
'Strength of mechanically fastened composite joints'
Journal of Composite Materials, Vol. 16, 1982
- [22-8] R.J. Nuismer & J.M. Whitney
'Uniaxial failure of composite laminate containing stress concentrations'
ASTM STP 593
- [22-9] Th. De Jong
'Stresses around pin loaded holes in composite materials' Mechanics of Composite Materials: Recent Advances
- [22-10] ASKA Computer Code
- [22-11] S. Timoshenko & S. Waimowsky-Krieger
'Theory of Plates and Shells'
McGraw-Hill, New York 1940
- [22-12] S.E. Yamada
'Analysis of laminate strength and its distribution'
Journal of Composite Materials, Vol. 12, 1978
- [22-13] J.M. Whitney & R.J. Nuismer
'Stress fracture criteria for laminated composite containing stress concentrations'

Journal of Composite Materials, Vol. 8, 1974

- [22-14] MBB/ERNO Raumfahrttechnik
'Inserts in nonmetallic sandwich components'
ESA Contract 440/80/NL/AK (SC)

- [22-15] R.T. Cole et al
'Fastener for composite structures'
Composites, July 1982

- [22-16] G.P. Sendeckyj & M.D. Richardson
'Fatigue behaviour of a graphite epoxy laminate loaded through an
interference fit pin'
Proceedings of 2nd Air Force Conference on Fibrous Composites in Flight
Vehicle Design, AFFDL74 103, September 1974

- [22-17] J.M. Hodgkinson, D.L. de Beer & F.L. Matthews
'The strength of bolted joints in Kevlar RP'
Proc Workshop 'Composite Design for Space Applications'
ESTEC Noordwijk, Oct 1985 (ESA SP-243, Feb 1986) p53-61

- [22-18] M. Palaterä: [Componeering Inc.](#) (Finland)
'Theoretical Background of ESAComp Analyses'
Part of ESAComp software documentation, v. 1.5 (April 1999)

22.7.2 ECSS standards

[See: [ECSS](#) website]

ECSS-E-HB-32-23	Threaded fasteners handbook; previously ESA PSS-03-208.
ECSS-Q-ST-70-46	Requirements for manufacturing and procurement of threaded fasteners; previously ESA PSS-01-746